frontiers | Research Topics

Deep subsurface microbiology and energetics

Edited by
Alberto Robador, James Andrew Bradley and William J. Brazelton

Published in
Frontiers in Microbiology

ISSN 1664-8714
ISBN 978-2-8325-6363-2
DOI 10.3389/978-2-8325-6363-2

About Frontiers

Frontiers is more than just an open access publisher of scholarly articles: it is a pioneering approach to the world of academia, radically improving the way scholarly research is managed. The grand vision of Frontiers is a world where all people have an equal opportunity to seek, share and generate knowledge. Frontiers provides immediate and permanent online open access to all its publications, but this alone is not enough to realize our grand goals.

Frontiers journal series

The Frontiers journal series is a multi-tier and interdisciplinary set of open-access, online journals, promising a paradigm shift from the current review, selection and dissemination processes in academic publishing. All Frontiers journals are driven by researchers for researchers; therefore, they constitute a service to the scholarly community. At the same time, the *Frontiers journal series* operates on a revolutionary invention, the tiered publishing system, initially addressing specific communities of scholars, and gradually climbing up to broader public understanding, thus serving the interests of the lay society, too.

Dedication to quality

Each Frontiers article is a landmark of the highest quality, thanks to genuinely collaborative interactions between authors and review editors, who include some of the world's best academicians. Research must be certified by peers before entering a stream of knowledge that may eventually reach the public - and shape society; therefore, Frontiers only applies the most rigorous and unbiased reviews. Frontiers revolutionizes research publishing by freely delivering the most outstanding research, evaluated with no bias from both the academic and social point of view. By applying the most advanced information technologies, Frontiers is catapulting scholarly publishing into a new generation.

What are Frontiers Research Topics?

Frontiers Research Topics are very popular trademarks of the *Frontiers journals series*: they are collections of at least ten articles, all centered on a particular subject. With their unique mix of varied contributions from Original Research to Review Articles, Frontiers Research Topics unify the most influential researchers, the latest key findings and historical advances in a hot research area.

Find out more on how to host your own Frontiers Research Topic or contribute to one as an author by contacting the Frontiers editorial office: frontiersin.org/about/contact

Deep subsurface microbiology and energetics

Topic editors

Alberto Robador — University of Southern California, United States

James Andrew Bradley — UMR7294 Institut Méditerranéen d'océanographie (MIO), France

William J. Brazelton — The University of Utah, United States

Citation

Robador, A., Bradley, J. A., Brazelton, W. J., eds. (2025). *Deep subsurface microbiology and energetics*. Lausanne: Frontiers Media SA.

doi: 10.3389/978-2-8325-6363-2

Articles in this Research Topic are dedicated to commemorating the late Jan Amend, whose pioneering work significantly advanced our understanding of microbial life in deep subsurface environments. Amend's contributions not only challenged existing notions about the limits of life but also provided key insights into the survival strategies of microbes in energy-limited settings, continuing to inspire and guide current research in extreme microbiology.

Table of contents

frontiers | Frontiers in Microbiology

TYPE Editorial
PUBLISHED 07 May 2025
DOI 10.3389/fmicb.2025.1611707

OPEN ACCESS

EDITED AND REVIEWED BY
Andreas Teske,
University of North Carolina at Chapel Hill, United States

*CORRESPONDENCE
Alberto Robador
robadora@usc.edu

RECEIVED 14 April 2025
ACCEPTED 21 April 2025
PUBLISHED 07 May 2025

CITATION
Robador A, Brazelton WJ and Bradley JA (2025) Editorial: Deep subsurface microbiology and energetics. *Front. Microbiol.* 16:1611707. doi: 10.3389/fmicb.2025.1611707

Editorial: Deep subsurface microbiology and energetics

Alberto Robador[1]*, William J. Brazelton[2] and James Andrew Bradley[3]

[1]Department of Biological Sciences, University of Southern California, Los Angeles, CA, United States, [2]School of Biological Sciences, The University of Utah, Salt Lake City, UT, United States, [3]Mediterranean Institute of Oceanography, Marseille, France

KEYWORDS

deep biosphere, microbial energetics, redox zonation, energy-limiting ecosystems, subsurface biogeochemistry

Editorial on the Research Topic
Deep subsurface microbiology and energetics

Introduction

Deep subsurface environments host vast and dynamic ecosystems that challenge conventional paradigms of the rules of microbial life. At the same time, these unusual ecosystems are integral to Earth's biogeochemical cycles. Because these environments are shaped by geological processes and often constrained by extreme energetic limitations, life in the deep subsurface is governed by complex interactions among redox chemistry, spatial structure, and long-term adaptation to energy scarcity. The collection of articles presented in this Research Topic, *"Deep subsurface microbiology and energetics,"* provides an interdisciplinary perspective through which to examine the metabolic potential, ecological organization, and functional resilience of microorganisms inhabiting these remote environments.

Redox zonation and microbial niche partitioning

Microbial metabolism in the deep subsurface is tightly coupled to redox gradients established by the interactions of water, rock and biology. These gradients define not only the thermodynamic constraints for energy conservation but also the spatial partitioning of microbial niches.

In hyperalkaline fluids derived from serpentinization in the Samail Ophiolite, Howells et al. reveal that formate, rather than hydrogen or acetate, provides the most favorable energy source for methanogenesis under CO_2-limiting conditions. This finding highlights the selective pressure exerted by fluid geochemistry on microbial metabolic strategies with the unusual example of CO_2 as the limiting substrate. In a related system, Twing et al. investigate microbial communities within altered ultramafic rocks from the Coast Range Ophiolite. Their results underscore the distinction between rock-hosted and fluid-associated microbial assemblages, with implications for potential spatial isolation and endemism of deep biosphere lineages.

Sedimentological and fracture-hosted systems offer further insights into the persistence of microbial metabolic potential over time. In the sediments of Lake Cadagno,

Rodriguez et al. document the preservation of core metabolic functions across millennia, despite taxonomic shifts in sediment microbial communities. Similarly, Acciardo et al. report stable groundwater microbial and hydrochemical compositions across an Alpine tunnel system, in spite of notable temporary variations corresponding to seismic events. These studies collectively suggest that functional redundancy and environmental buffering contribute to the resilience of deep subsurface microbiomes.

Strategies for survival in energy-limited settings

Adaptation to energy scarcity is a hallmark of deep subsurface systems. Survival in the energy-limited subsurface depends not only metabolic versatility but also regulatory and genomic mechanisms attuned to long-term energy deprivation and survival over long timescales.

Sebastian et al. address this challenge through an experimental evolution framework, demonstrating that *Halomonas* strains isolated from North Pond crustal fluids rapidly lose the genetic capacity for survival in carbon-depleted media when exposed to nutrient-rich laboratory conditions. Their findings point to specific gene products, including lipase-like proteins, as key mediators of nutrient acquisition under oligotrophic conditions.

Complementing this genomic perspective, Feyhl-Buska et al. use microcalorimetry to directly quantify energy metabolism in groundwater samples spanning a range of redox conditions, revealing nutrient limitation in continental subsurface communities. The results provide empirical constraints on microbial power output and underscore the influence of both thermodynamic and ecological parameters on community-level metabolism.

Beyond classical metabolism: novel energetic pathways and functional innovation

Emerging theoretical frameworks and cultivation-based discoveries continue to expand the known boundaries of microbial energetics.

Karnachuk et al. describe the isolation of two novel thermophilic bacterial genera from deep aquifers in Western Siberia. These members of the *Limnochordia* lineage possess the capacity for carbon monoxide and hydrogen oxidation, autotrophic carbon fixation, and aerobic respiration. Their physiological versatility illustrates the metabolic plasticity that may underpin survival in thermally and chemically extreme environments.

A conceptual advance is presented by Marshall, who proposes the existence of Electromicrobiological Concentration Cells (EMCCs). These hypothetical systems rely on conductive matrices to bridge spatially distinct redox reactions, allowing microorganisms to exploit electrochemical disequilibria that would otherwise be inaccessible. The EMCC framework challenges traditional assumptions about the spatial coherence required for microbial energy harvesting and may have relevance for life in both deep terrestrial and extraterrestrial settings.

Coupled biogeochemical cycling and ecosystem regulation

The influence of subsurface microbial communities extends to the regulation of key geochemical processes, including methane production and oxidation, nutrient turnover, and mineral transformation.

Coon et al. demonstrate that the directionality of methane cycling in coastal sediments is modulated by hydrogen availability. In organic-poor settings, syntrophic interactions between fermenters and methanogens or sulfate reducers maintain low hydrogen concentrations, promoting fermentation and anaerobic methane oxidation. Conversely, elevated hydrogen levels in organic-rich sediments destabilize these interactions, favoring methanogenesis.

In the context of engineered subsurface environments, Cheng et al. investigate microbial community dynamics in oil reservoir cores subjected to nutrient amendments. Their findings indicate that nutrient limitation supports greater community diversity and network stability, whereas nutrient enrichment promotes dominance by functionally narrow taxa and reduces ecological resilience.

This theme is extended by Mura et al., who simulate dihydrogen (H_2) co-injection in a natural gas–bearing, low-salinity deep aquifer under controlled laboratory conditions. Using a high-pressure reactor system with native rock and fluid phases, they show that microbial activity leads to sequential reduction processes, including sulfate reduction, acetogenesis, and ultimately methanogenesis, with the latter accounting for the majority of H_2 consumption. While microbial H_2 uptake remained limited—likely due to nutrient depletion—the work reveals that aquifers with low salinity and restricted electron acceptor availability may provide relatively stable reservoirs for H_2 storage. This study further emphasizes the need for site-specific microbial and geochemical assessment when evaluating the feasibility of underground H_2 storage.

Further advancing the discussion on trace element-driven microbial processes, Montoya and Escobar-Briones explore the role of cobalt and vitamin B_{12} (cobalamin) in structuring microbial and metazoan communities associated with ferromanganese crusts and polymetallic nodules. These cobalt-rich habitats host diverse microbial assemblages, including cobalamin-producing prokaryotes such as Thaumarchaeota and Proteobacteria, which support cobalamin-auxotrophic eukaryotes via trophic and symbiotic interactions. The authors argue that the abundance of cobalt in these deep-sea mineral systems may create micronutrient "hotspots" where metabolic interdependencies become intensified. This framework posits cobalt and cobalamin as pivotal drivers of deep-sea microbial ecology and proposes that these mineral-rich habitats offer valuable models for studying micronutrient-based ecological networks and their vulnerability to anthropogenic disturbance.

Integrating the deep subsurface biosphere into planetary systems thinking

A broader systems perspective is articulated by Robador, who conceptualizes the oceanic crustal biosphere as a globally distributed, low-energy biogeochemical reactor. This framework situates subseafloor microbial processes within Earth's carbon cycle and emphasizes the significance of subsurface ecosystems in global redox balance. By drawing parallels between deep biosphere functions and potential analogs on other planetary bodies, the review reinforces the role of subsurface microbiology in astrobiology and Earth system science.

Concluding remarks

The contributions compiled in this Research Topic underscore the multifaceted nature of deep subsurface microbial life. From theoretical advances and empirical discoveries to environmental and engineered system analyses, these studies highlight the central role of microbial subsurface communities in mediating geochemical processes under extreme conditions. As exploration of subsurface environments continues—on Earth and beyond—the principles of microbial energetics, adaptation, and resilience described herein will serve as a foundation for understanding life in one of its most enigmatic domains.

This Research Topic is in memory of Jan Amend, whose work and ideas, mentorship, enthusiasm and leadership not only transformed the field of deep subsurface microbiology but also inspired and guided a generation of scientists that have continued to advance this field.

Author contributions

AR: Conceptualization, Writing – original draft, Writing – review & editing. WB: Writing – review & editing. JB: Writing – review & editing.

Conflict of interest

The authors declare that the research was conducted in the absence of any commercial or financial relationships that could be construed as a potential conflict of interest.

The author(s) declared that they were an editorial board member of Frontiers, at the time of submission. This had no impact on the peer review process and the final decision.

Publisher's note

frontiers | Frontiers in Microbiology

TYPE Original Research
PUBLISHED 31 July 2024
DOI 10.3389/fmicb.2024.1450226

OPEN ACCESS

EDITED BY
Alberto Robador,
University of Southern California,
United States

REVIEWED BY
Han Meng,
Nanjing Normal University, China
Kankan Zhao,
University of California, San Diego,
United States

*CORRESPONDENCE
Yuan Yun
yuanyun@nankai.edu.cn
Ting Ma
tingma@nankai.edu.cn
Guoqiang Li
gqli@nankai.edu.cn

†These authors have contributed equally to this work

RECEIVED 17 June 2024
ACCEPTED 10 July 2024
PUBLISHED 31 July 2024

CITATION
Cheng W, Tian W, Wang W, Lv T, Su T, Wu M, Yun Y, Ma T and Li G (2024) Nutrient availability contributes to structural and functional diversity of microbiome in Xinjiang oilfield.
Front. Microbiol. 15:1450226.
doi: 10.3389/fmicb.2024.1450226

Nutrient availability contributes to structural and functional diversity of microbiome in Xinjiang oilfield

Wei Cheng[1†], Wenzhuo Tian[1†], Weilong Wang[1], Tianhua Lv[1], Tianqi Su[1], Mengmeng Wu[1], Yuan Yun[1*], Ting Ma[1,2*] and Guoqiang Li[1,2*]

[1]Key Laboratory of Molecular Microbiology and Technology, Ministry of Education, College of Life Sciences, Nankai University, Tianjin, China, [2]Tianjin Engineering Technology Center of Green Manufacturing Biobased Materials, Tianjin, China

Indigenous microbial enhanced oil recovery (IMEOR) is a promising alternative way to promote oil recovery. It activates oil recovery microorganisms in the reservoir by adding nutrients to the injected water, utilizing microbial growth and metabolism to enhance recovery. However, few studies have focused on the impact of injected nutrients on reservoir microbial community composition and potential functions. This limits the further strategic development of IMEOR. In this study, we investigated the effects of nutrition on the composition of the reservoir bacterial community and functions in the Qizhong block of Xinjiang Oilfield, China, by constructing a long core microbial flooding simulation device. The results showed that the microbial community structure of the reservoir changed from aerobic state to anaerobic state after nutrient injection. Reducing the nutrient concentration increased the diversity and network stability of the reservoir bacterial community. At the same time, the nitrogen metabolism function also showed the same change response. Overall, these results indicated that nutrition significantly affected the community structure and function of reservoir microorganisms. Injecting low concentrations of nutrients may be more beneficial to improve oil recovery. This study is of great significance for guiding IMEOR technology and saving costs at the field site.

KEYWORDS

IMEOR, community stability, community structure, nutrition, nitrogen cycle

1 Introduction

Indigenous microbial enhanced oil recovery (IMEOR) is a promising and sustainable method for oil recovery. The oil reservoir is a specialized ecological environment of high temperature, high salt, and high pressure that can be analogized to a giant bioreactor. Previous studies have described them as complex ecosystems filled with a variety of microbial entities (Orphan et al., 2001). The sustainability of the oil recovery functions and services provided by such ecosystems depends on a relatively stable microbial system, which is defined as the degree of change or turnover of the microbial community (Griffiths et al., 2008; Tripathi et al., 2018). IMEOR exploits the proliferation and metabolic capacity of microorganisms to increase oil production. The mechanisms of oil recovery mainly include biological blockage of large pores, changes of physical and chemical properties of crude oil, and an increase in the internal pressure of the reservoir. This approach incorporates biotechnology solutions to address the challenges of the oil industry (Sharma et al., 2023).

In the process of microbial oil recovery, nutrients are generally injected into the injection well in the oil field. However, there are often great differences in the microbial community structure and oil augmentation efficiency of different production wells in actual production. 16S rRNA gene analysis was used in a previous study to study the microbial community in a specific block of the North China Oil Field. Different microbial distributions are observed across producing wells in the same block, which correlated with different oil yields (Tang et al., 2012). Crude oil production is closely related to the structure of the reservoir microbial community (Yin et al., 2023). Nutrient injection is the primary means of IMEOR, which stimulates an increase in the abundance of dominant functional bacteria and inhibits harmful microbial species during oil extraction (Gao et al., 2018; Liang et al., 2022). For example, sulfate reducing bacteria (SRB), produce hydrogen sulfide gas which can corrode flood pipes in oil reservoirs and pose health hazards to workers. When the supply of nutrients is stopped, the relative abundance of hydrocarbon degrading bacteria decreased and the relative abundance of anaerobes increased (Wang et al., 2020). In the study of the effect of IMEOR on the microbial community and oil recovery rate in Luliang Oilfield, nutrient injection showed positive effects on aromatic hydrocarbon degradation, resin and asphaltene fractions, and the oil recovery rate increased from 51.2 to 60.7%. The difference in microbial community structure in different wells will lead to different oil recovery. In the field experiment at Shengli Oilfield, the oil recovery is increased by 9.14% by stimulating local bacteria with nutrient injection (Bao et al., 2009). The addition of nutrients to oilfield produced water in the laboratory shows the enhancement of microbial growth, microbial community transfer, and microbial degradation capacity (Li et al., 2020). Studies of individual IMEOR production wells at the field site have shown significant effects of nutrient injection on the diversity, composition and relative abundance of reservoir microbes (Wang et al., 2015). It can be seen that there is a close relationship between nutrition, microbial community structure, and oil recovery function. However, how the structure and function of reservoir microbial communities respond to nutrient injection has not been fully studied. This has a potentially important role in enhancing oil recovery.

The response mechanism of microbial communities to nutrient changes in the environment has been reported in other environments, and nutrient injection has significant effects on microbial communities in soil, wetland and ocean (Han et al., 2012; Li et al., 2019; Bannon et al., 2022). Globally, the addition of nitrogen-containing nutrients significantly affects soil microbial diversity and community structure (Wang et al., 2023). Resource availability is the key to controlling soil microbial diversity and the main factor regulating microbial functional traits (Zhu et al., 2023). In seawater sediments, microorganisms associated with nitrogen, phosphorus, and sulfur cycles show different abundances at different sites, and the metabolism of microorganisms is the main factor affecting the distribution of microbial communities (Lu et al., 2019). When affected by changes in external conditions, the transformation of carbon, nitrogen, phosphorus and sulfur will inevitably disrupt microbial homeostasis and lead to changes in the composition, diversity and metabolic function of the microbiome (Marzocchi et al., 2020). For example, "nitrogen metabolism" and "phosphate metabolism" are special metabolic functions that are critical to community stability (Xun et al., 2021). In oil reservoir ecosystems, the addition of appropriate concentrations of organic phosphorus and nitrogen can promote the production of biosurfactants by oil reservoir microorganisms (Shi et al., 2021). But how specialized metabolic functions in microbial communities change during this dynamic process has not been fully investigated.

To elucidate the response of microbial community structure and function to injected nutrients in a reservoir environment. We constructed a long core microbial flooding simulation device to simulate the whole process of IMEOR in Qizhong block of Xinjiang oil field. We continuously monitored for 60 days and sampled at 7 locations in the core. Based on 16S rRNA sequencing and metagenomic analysis, we studied the response changes of reservoir microorganisms to nutrient injection. And we focused on the link between different injected nutrient concentrations, microbial community stability and function. This study has important implications for cost savings in the field and for improving oil recovery.

2 Materials and methods

2.1 Medium and fluids

All fluids used in this study, including crude oil (the oil phase of the fluid produced in the wells) and produced water (the water phase of the fluid produced in the wells), were obtained from the Qizhong block oil field in Karamay, Xinjiang, China. The extracted water used in the experiment was mixed with formation water from five production wells. The sample well numbers were 72,602, 72,604, 72,605, 72,649, and 72,659. The samples were completely filled into 15 L sterilized drums, which were previously swept with nitrogen to prevent oxygen from diffusing into the samples. The samples were immediately transported to our laboratory. All freshly produced fluids were either used immediately or refrigerated at 4°C for subsequent experiments. The viscosity of the crude oil during the experiments was 5.55 mpa.s (thin oil, 37°C).

2.2 Long core microbial flooding simulation device

The device was constructed according to the previous method, as shown in Supplementary Figure S1 (Cheng et al., 2023). The porous medium in the tube was quartz sand (30–50 μm) with no pores. The measured permeability was 5,839 millidarcy (md). The formation water was fully saturated, with a calculated pore volume (PV) of 6,670 cm^3. The entire process of the oil drive experiment was designed to simulate the entire oil recovery process of the field, including the water saturation stage, oil saturation stage, water drive stage, and microbial drive stage (tertiary oil recovery). The sand-filled tube was first saturated by formation water under vacuum conditions (water-saturated stage). Next, oil was injected into the sand-filled tube until the end of uniform flow of crude oil. After that, formation water was injected for the secondary extraction stage (water drive stage). The injection was stopped when the water content at the end of the sand-filled tube exceeded 98%. This was followed by a simulated microbial oil drive stage. The nutrient solution was injected for microbial oil recovery. All tests were maintained at a constant flow rate of 1 mL/min at 37°C for 60 days.

TABLE 1 Nutrient formulation and concentration for 60 days.

Injection time	Nutrient concentrations (g/L)			
1–40 days	Molasses 3.50	Corn extract powder 1.50	NH_4Cl 4.0	$(NH_4)_2HPO_4$ 3.0
40–60 days	Molasses 1.75	Corn extract powder 1.50	NH_4Cl 2.0	$(NH_4)_2HPO_4$ 1.50

2.3 Sample collection

The nutrient infusion was carried out throughout the study according to the medium recipe in Table 1. The medium in the intermediate vessel was changed twice a day. Samples were taken from seven sampling ports. Each time the sampling port switch was turned on, the stored liquid was drained. Samples were collected in 5 mL centrifuge tubes and centrifuged immediately (12,000 r, 8 min). The precipitate was used for genomic DNA extraction, while the supernatant was used for the determination of nutrient concentrations. DNA extraction was performed using the AxyPre™ Genomic DNA Miniprep Kit (Axygen Biosciences, CA, United States), the procedure of which was detailed in Supplementary material.

2.4 Determination of nutrients

The supernatant of the extract was subjected to determination of nutrient concentrations. Total sugars (TS) were determined by the phenol-sulfuric acid method. Total nitrogen (TN) was determined using the persulfate oxidation method (Lima et al., 1997). Total phosphorus (TP) by the digestion-molybdenum-antimony method. The required kits were provided by Tianjin Hass Water Analytical Instruments Co. Detailed steps for the determination of the three nutrient concentrations were given in Supplementary material.

2.5 High-throughput 16S rRNA gene sequencing

Extract genomic DNA as described earlier (Gao et al., 2018). High-throughput sequencing of 16S rRNA genes was done by Beijing NovoGene Co. Qiime2 (Quantitative Insights into Microbial Ecology 2) was utilized to analyze the raw reads. After quality control, denoising, and chimera removal, sequences with 97% identity were clustered as one OTU. The representative sequence of each feature was compared with the Silva 132 database to ensure its taxonomy and with the NCBI 16S rRNA database to determine their best hits at the species level (Quast et al., 2012). The community structure of each sample was counted at the genus level. The abundance data has been rarefied at depth of 41,051 and samples were analyzed for α-diversity using the qiime diversity function by Qiime2. The prediction of functional genes for nitrogen and phosphorus metabolism was performed by PICRUST (version 1.1.0). The data presented in the study are deposited in the NCBI Sequence Reads Archive repository, accession number PRNA1021155.

2.6 Network construction

In this study, the OTU-OTU co-occurrence networks was initially constructed for 16, 20, 24, and 39 days (high nutrient concentration) and 41, 42, 53, and 58 days (low nutrition concentration). To avoid sparse OTUs affecting correlation analyses, OTUs from all samples were involved in the microbe-microbe interaction assessment after filtering out OTUs with a relative abundance <0.01%. Statistically robust correlations based on Spearman correlation coefficients (ρ) > 0.6 and corresponding p-values <0.01 were included in the network analysis, where each node represented a genus and each edge represented a significant correlation between two nodes (Zhu et al., 2019). The FDR method used for p-value adjustment. Network visualization and topology properties using R v 3.6.3 ('psych' package) and Gephi platform v 0.9.2[1] (Chen et al., 2020). Topological coefficients, including the number of nodes and edges, average degree, graph density and negative correlation were calculated for each network to estimate the complexity of the network. We evaluated network stability at different injected nutrients concentrations by node residual ratio and robustness (Liu et al., 2023). The higher the remaining proportion of nodes in the network, the more robust it was and the more stable the microbial co-occurrence network was. Moreover, we constructed two nutrients-OTU co-occurrence networks to evaluate the relationship between the three nutrients (TS, TN, and TP) and OTU at high injected nutrients concentration and low injected nutrients concentration, respectively. The nodes unrelated to the three nutrients were removed. The method for constructing the nutrients-OTU co-occurrence networks is consistent with the method for constructing OTU–OTU networks.

2.7 Analysis of metabolic functions

We performed metagenomic sequencing on samples from days 7, 20, 39, 42, 48, and 53 of sampling port 10. Sequencing was done by Beijing NovoGene Co. We quantified the functions encoded by the microbial community in each sample according to a stratified search of HUMAnN2 (v 3.7), functionally annotated via the EggNOG (v 6.0) database (Hernández-Plaza et al., 2022), and stratified their relative abundance according to the genes that perform these functions. By applying traditional within-sample (alpha) and between-sample (beta) measures of community diversity to more accurately explore the contribution of species to the function of interest, defined here as the 'diversity of contributions' to the function (Franzosa et al., 2018). All computed gene categories were drawn from the broader categories of metabolic function, genetic information processing, organismal systems, and cellular information processing. Within these types, metabolic functions are further divided into broad metabolic functions and specialized metabolic functions (Xun et al., 2021).

1 https://gephi.org/

Previous studies had shown that the function of "nitrogen metabolism" (nitrification or denitrification) was limited to specific microorganisms (Chen et al., 2016). Narrow distribution of methanogenic and methane-oxidizing bacteria involved in the function of "methane metabolism" due to their aerobic/anaerobic requirements or through coupling with nitrogen and sulfuric metabolism (Zhu et al., 2015). The gene cluster related to "terpene and polyketide metabolism" consisted mainly of *Actinomycetes* and *Bacillus* from the soil microbial community (Crits-Christoph et al., 2018). Specialized metabolic functions in reservoirs included those related to 'sulfuric metabolism,' 'nitrogen metabolism,' and 'methane metabolism,' which had been shown to be restricted to specialized taxa (Yao et al., 2023). In this study, we focused on "nitrogen metabolism" and "phosphorus metabolism," which had been shown that the nitrogen and phosphorus cycles affect the stability of the soil microbiome (Xun et al., 2021).

3 Results

3.1 Changes in nutrient concentrations and microbial communities

Trends in total sugar, total nitrogen, and total phosphorus concentrations were consistent across the seven sampling ports, with a delay in nutrient concentration changes at the back end of the long core, but the delay was not perfectly consistent with the rate of injection (Figure 1). The change in the concentration of total sugars fluctuated more, and the concentration was maintained at 150 mg/L after 17 days (Figure 1C). Total nitrogen and total phosphorus stabilized after day 8 (Figures 1A,B). After 40 days, we lowered the concentration of injected nutrients and nutrient concentrations at each sampling port decreased.

We monitored changes in the microbial community at each sampling port for 60 days (Supplementary Figures S2–S5). When the injected nutrient volume was less than 1PV, the community structure of each sampling port was significantly different. We mainly focused on the changes in the dominant genus, *Exiguobacterium* was first activated after the nutrients reached each sampling port. *Exiguobacterium* belongs to the hydrocarbon oxidizing bacteria, which has the ability to degrade alkanes (Mohanty and Mukherji, 2008). The high growth of aerobic microorganisms may have contributed to the instability of the total sugar concentration in the pre-existing period. *Enterococcus* was a facultative anaerobic bacterium capable of producing organic acids through fermentation (Supplementary Figure S2), which was highly activated on days 6–10 (Schauf et al., 2019). After 12 days, some anaerobic fermenting genera were activated (Supplementary Figures S3, S4), such as *LNR_A2-18* and *Sphaerochaeta*, which were able to ferment to produce acetate, ethanol, hydrogen and CO_2 (Ritalahti et al., 2012). The process of microbial community change was consistent with the results of our previous study (Cheng et al., 2023). This further demonstrated the succession of reservoir microorganisms from aerobic to anaerobic states during the indigenous microbial enhanced oil recovery.

3.2 Analysis of co-occurring network structure

A network analysis of the microbial community at each sampling port after nutrient injection was performed to determine if the

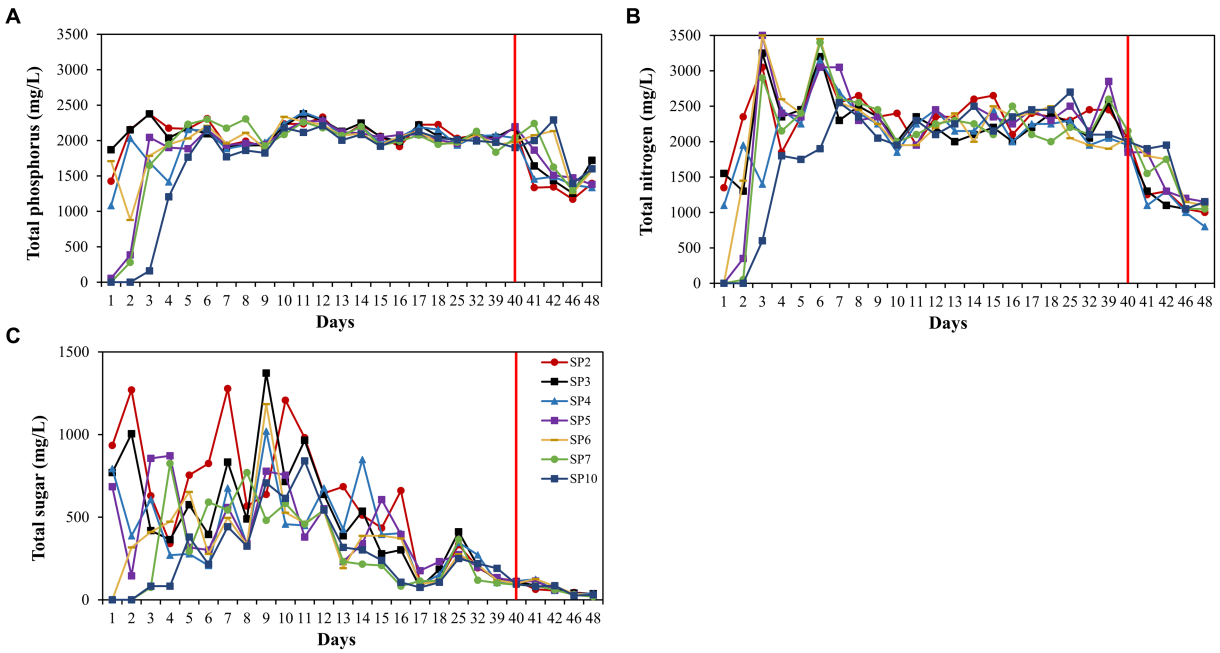

FIGURE 1
Nutrient concentration changes during the 60-day monitoring period. Concentration of total phosphorus **(A)**, concentration of total nitrogen **(B)**, and concentration of total sugar **(C)**. The sampling port 2, 3, 4, 5, 6, 7, and 10 are displayed with lines of different colors. SP2 represents sampling port 2, and so on for others.

microbial co-occurrence patterns changed over time. At the initial nutrient concentration, we performed network visualization of microbial communities on days 16, 20, 34, and 39. After lowering the injected nutrient concentration, we performed network visualization of microbes on days 41, 42, 48, and 53. The topological eigenvalues of microorganisms at both nutrient concentrations are shown in Table 2. Each network had unique topological properties. Overall, the injection of nutrients resulted in more nodes and edges in the microbial networks, higher average degrees, and more complex networks. This suggested that injection of nutrients increases the complexity of reservoir microbial networks. In each co-occurring network, positive interactions were greater than negative interactions.

In addition, we constructed a total network based on OTU-Nutrition (Figure 2). After removing unconnected nodes, the total network at the initial nutrient concentration consisted of 82 nodes and 124 edges (16% of positive edges). Microorganisms connected to TP and TS by microbial annotation of OTUs in the network included Proteobacteria, Firmicutes, Bacteroidota, Cloacimonadota, Spirochaetota, Desulfobacterota, and Thermotogota. Microorganisms connected to TN include *Firmicutes* (Figure 2A).

After reducing the nutrient concentration, the total microbial network consisted of 49 nodes and 68 edges (72% of positive edges) (Figure 2B). Microorganisms linked to TS include Proteobacteria, Firmicutes, Cloacimonadota, Spirochaetota, Desulfobacterota and Thermotogota. Microorganisms linked to TP include Proteobacteria and Bacteroidota. And microorganisms linked to TN include Proteobacteria, Firmicutes, Bacteroidota, Cloacimonadota, Spirochaetota, Desulfobacterota and Thermotogota. The relationship between nutrients and microorganisms together constitutes the ecological network of reservoir microorganisms.

3.3 Stability of co-occurring networks

We counted the proportion of negative correlations in community co-occurrence networks under high (initial nutrient concentration) and "low nutrients," and the microbial network structure showed lower negative interactions after lowering the nutrient (Figure 3B). The results showed that the negative interactions among reservoir microorganisms was weakened after lowering the nutrients. Also our results showed an increase in bacterial diversity after decreasing the injected nutrient concentration (Figure 3A). Low nutrient concentrations may increase the diversity of bacterial communities (Yun et al., 2021). We evaluated the stability of the microbial network before and after nutrient reduction. The proportion of remaining nodes in the network after randomly removing some nodes was calculated (Figure 3C). We also counted the percentage of nodes remaining in the network after randomly deleting 50% of the nodes (Figure 3D). The results all indicated that the network structure of reservoir microbial communities showed higher stability after reducing nutrients.

TABLE 2 Topological eigenvalues of microbial network structure after nutrient injection.

Days	Node	Edge	Average degree	Density	Negative correlation
16	314	811	5.166	0.017	29.47%
20	323	1,114	6.898	0.021	35.73%
24	333	1,308	7.856	0.024	36.47%
39	379	1,275	6.728	0.018	27.06%
41	377	1,227	8.509	0.017	33.58%
42	380	1996	10.505	0.028	12.88%
48	372	3,002	16.14	0.044	38.04%
53	409	1743	8.523	0.021	22.83%

3.4 Changes in the potential functions of reservoir microbial communities

Reduced nutrition had a positive effect on the stability of the reservoir microbial network, but the effect on nitrogen and phosphorus-related metabolic functions in the community was unknown. Therefore, we predicted the abundance changes of related functional genes based on PICRUST. Notably, the abundance of functional genes related to nitrogen metabolism increased after lowering the injected nutrient concentration, especially on days 41, 42, 48, and 53 (Figure 4B). These metabolic processes included nitrogen fixation, nitrite reduction to ammonia, ammonia oxidation, nitrate reduction, dissimilatory nitrate reduction and nitric oxide reduction (Figure 5). Many microorganisms related to nitrogen metabolism have a potential role in improving crude oil recovery, such as NRB and denitrifying bacteria (Niu et al., 2020). Our results suggested that injecting low concentrations of nutrients may be more beneficial for improving oil recovery.

We performed metagenomic sequencing of low and high nutrient samples from sampling port 10, and further analyzed nitrogen metabolism and phosphorus metabolism functions in the samples by performing stratified searches using the HUMAnN2 tool (Franzosa et al., 2018). The total mapped abundance to EggNOG database is within the range of 47.30–61.73% (Supplementary Table S1). The major community composition identified by HuMAnN2 were *Methanocorpusculum*, *Vibrio*, *Methanosarcina*, etc. (Supplementary Table S2). The results showed that the types of metabolic functions were similar in the six samples (Figure 6A). The metabolic types involved in phosphorus metabolism were methylphosphonate degradation I, inosine-5′-phosphate biosynthesis and pentose phosphate pathway, etc. The types of metabolism related to the nitrogen cycle included nitrate reduction (assimilatory) and nitrate reduction (denitrification). Notably, the relative abundance of nitrogen metabolism in the microbiome was higher at high nutrient concentrations compared to low nutrient concentrations (Figure 7). This was consistent with predicted changes in the abundance of functional genes for nitrogen metabolism (Figure 4A).

In addition, we further explored the diversity of contributions in reservoir microbial nitrogen metabolism pathways (functions with broad "unclassified" abundances may be contributed by one or more different species within or between samples, and thus they were excluded from this analysis) (Figure 6B). The genera that made a major contribution to reservoir nitrogen metabolism mainly include *Enterobacter*, *Klebsiella*, *Pantoea*, *Citrobacter*, *Escherichia*, and *Leclercia*. Contributors to nitrogen metabolism were variable across samples, further demonstrating the potential inconsistency between individual functions and community-level diversity. Although

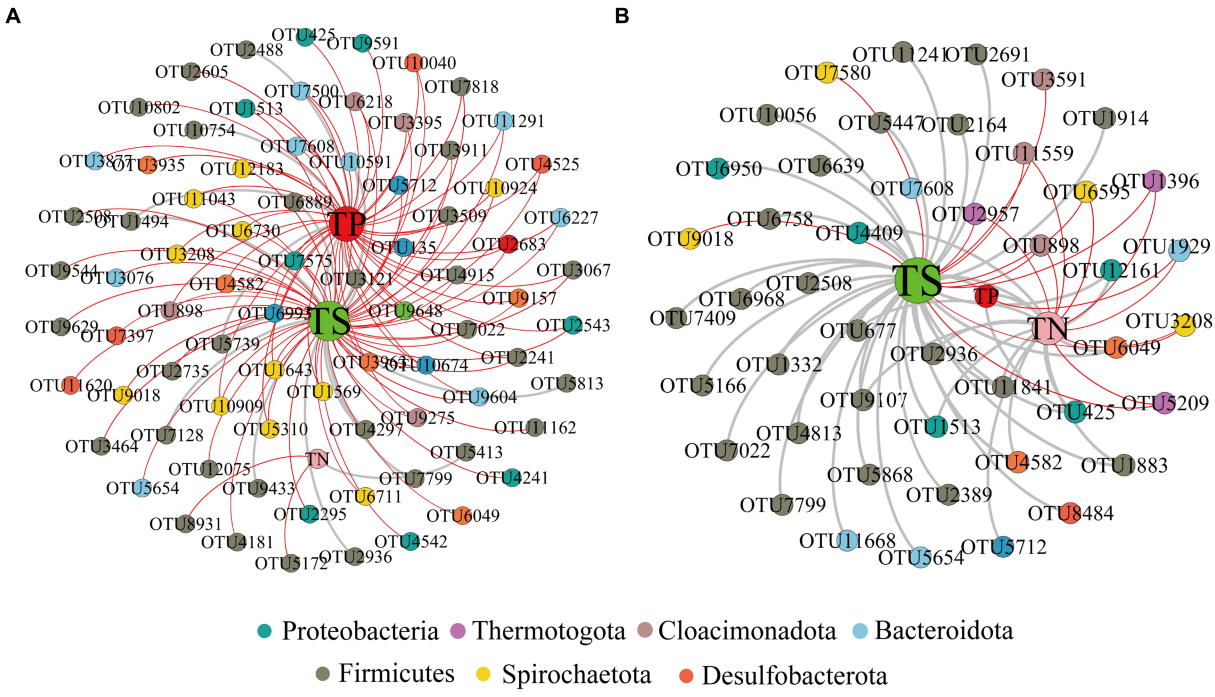

FIGURE 2
Network visualizes the nutrient-OTU interactions between initial nutrient concentration **(A)** and reduced nutrient concentration **(B)**. Positive correlations are shown in gray and negative correlations in red. The size of each node is proportional to the betweenness centrality. The red, green and pink dots marked with TP, TS and TN represent total phosphorus, total sulfur and total nitrogen, respectively.

nitrogen metabolism had complex and variable contributors in each sample, both *Enterobacter* and *Klebsiella*, which were major contributors, belonged to *Proteobacteria* (Carter et al., 2004; Manter et al., 2011).

4 Discussion

In order to explore the response of microbial community structure and function to nutrition. In this study, a long core microbial flooding simulation device was constructed under laboratory conditions and dynamically monitored for 60 days. The effects of nutrition on microbial community composition, network stability and function were explored. At the beginning of the injection of nutrition, the community microorganisms were different from each sampling port due to the delayed nutrition (Supplementary Figure S2). As nutrients gradually arrived at each sampling port, the difference of microbial community structure gradually decreased. This is also the case in oilfield sites, where the interwell connectivity of the reservoir media is complex, and the pore size of different reservoir rocks also has a filtering effect on the injected nutrients (Dong et al., 2023). Injected nutrients may be consumed by the time they reach each well, resulting in differences in microbial community structure between wells. This suggests that the level of nutrient supply may be the main factors affecting the microbial community structure of different production wells in the same block.

We observed changes in the dominant genus and could find that the hydrocarbon oxidizing bacterium (*Exiguobacterium*) would be activated first (Supplementary Figure S2). On days 6–20, *Enterococcus* became the main dominant genus (Supplementary Figure S3). After 20 days, some anaerobic fermenting genera gradually gained some dominance, such as *LNR_A2-18* and *Sphaerochaeta* (Supplementary Figure S4). They belonged to the anaerobic fermenting bacteria, which was consistent with the hypothesis of microbial ecological "food chain" succession in the reservoir, which also tentatively supported the two-step activation theory of the transition from aerobic to anaerobic microorganisms in the reservoir (Cheng et al., 2023).

Network analysis helps to gain insights into the interactions between microbiomes and reveals patterns of co-occurrence between microorganisms. After nutrient injection, topological features showed that the network became more complex, suggesting that nutrient injection led to stronger connections among microorganisms. The positive interaction among reservoir microorganisms was dominant. Secondly, the microbial community structure showed higher bacterial diversity and lower competition after lowering the injected nutrient concentration (Figures 3A,B). During oil recovery, only a few groups of bacteria with specialized functions are enriched, such as hydrocarbon oxidizing and nitrate-reducing bacteria, other bacteria with broad functions or smaller numbers are reduced or even disappear, which can lead to fewer species and lower α-diversity in the ecosystem (Yun et al., 2021). Increasing bacterial diversity improves the functional redundancy of the reservoir microbiome, which is conducive to increasing oil recovery potential. In the gut microbial system, loss of bacterial diversity had been observed to enable microbial community shifts and associated loss of metabolic functions (Shang et al., 2021).

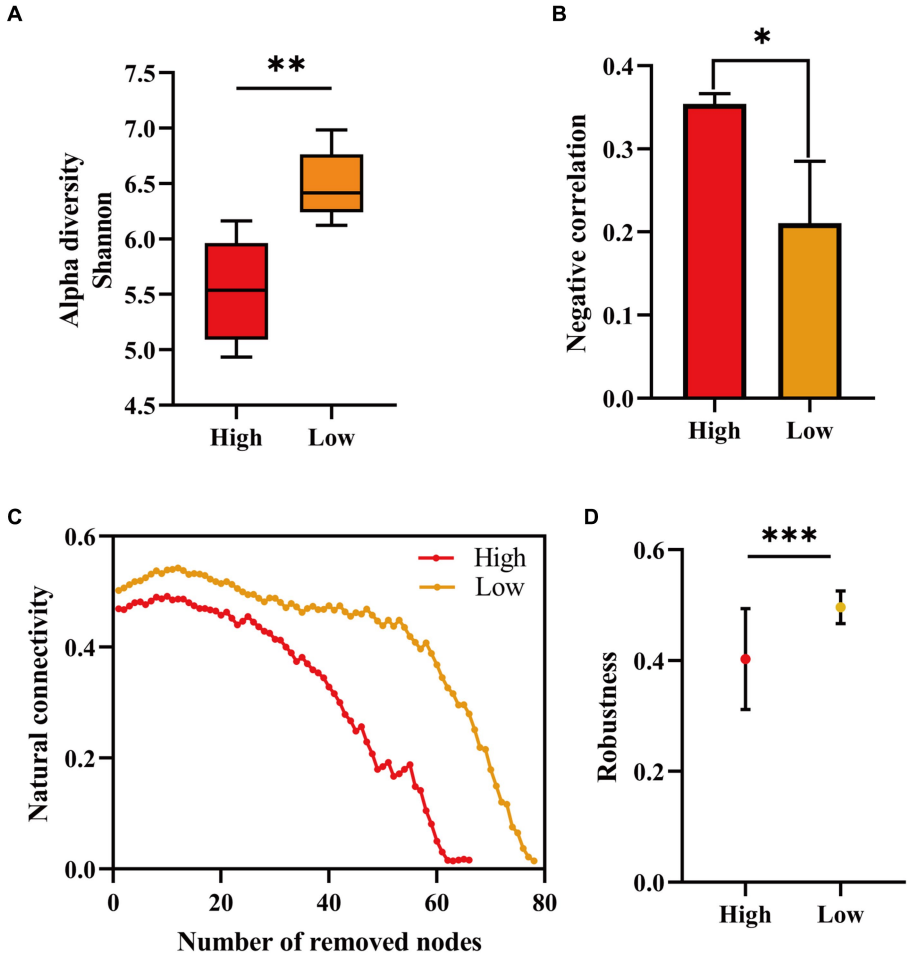

FIGURE 3
Microbial α-diversity at different injected nutrient concentrations **(A)**, proportion of negative correlation in the co-occurring network **(B)**, proportion of remaining nodes in the network after randomly deleting some nodes **(C)**, and proportion of remaining nodes in the network after randomly deleting 50% **(D)**. Initial injected nutrient concentration stage (high) and reduced injected nutrient concentration stage (low). Alpha diversity, negative correlation, and robustness are significant at different stages of injected nutrient concentration (*$p < 0.05$, **$p < 0.01$ and ***$p < 0.001$).

Microbiome stability can be defined in terms of community resilience (the ability of the community to return to a relatively stable state) or resistance (the ability of the community to resist external disturbances) (Allison and Martiny, 2008). We provided valuable insights into the stability of microbial communities by assessing the efficiency of reservoir microbial networks and the loss of nodes after simulating nutrient injection. Although most previous studies had not directly examined stability, less connected network structures were thought to reduce microbial community stability (Mougi and Kondoh, 2012; Zhang et al., 2023). We assessed the stability of the network by randomly removing nodes, and the microbial network showed higher stability after reducing the nutrient concentration (Figures 3C,D). The level of nutrient availability influenced the stability of microbial communities, and "high nutrients" seemed to negatively affect the stability of reservoir microbiomes. These results suggested that in reservoir microbial systems, high nutrient concentrations may increase negative interactions between bacteria, leading to a loss of bacterial diversity and a decrease in microbial community stability, which may affect reservoir microbial oil recovery capacity (Wang et al., 2023). Therefore, in the oilfield field, the selection of the concentration of injected nutrients is particularly important. If a suitable low-nutrient formulation is selected for injection and extraction, it will improve the crude oil recovery and reduce the cost investment at the same time.

It has been suggested that unstable microbial network structures reduce the number of functions provided by the community (Wei et al., 2015). In soil ecosystems, nitrogen metabolism has been found to be closely related to the stability of microbial networks (Xun et al., 2021). By predicting the abundance of nitrogen cycle-related genes at the 16 s level, which were dominated by nitrate reduction (Figures 4A, 5). This phenomenon was beneficial for oil recovery because nitrate-reducing bacteria can control acidification and protect metal pipelines through biocompetitive rejection of SRBs in reservoirs (Duque et al., 2004). Increased abundance of genes functioning in nitrogen metabolism after reduced nutrition (Figure 4). An elevated abundance of associated nitrogen metabolism was also observed in the metagenomic results (Figure 7). Previous studies suggested that nitrogen metabolism may be a key metabolic function in maintaining microbial community stability (Xun et al., 2021). Our results also showed that nitrogen metabolism and related functional genes showed the same response to changes in microbiome network stability. The diversity of contributions to key functions of "nitrogen metabolism"

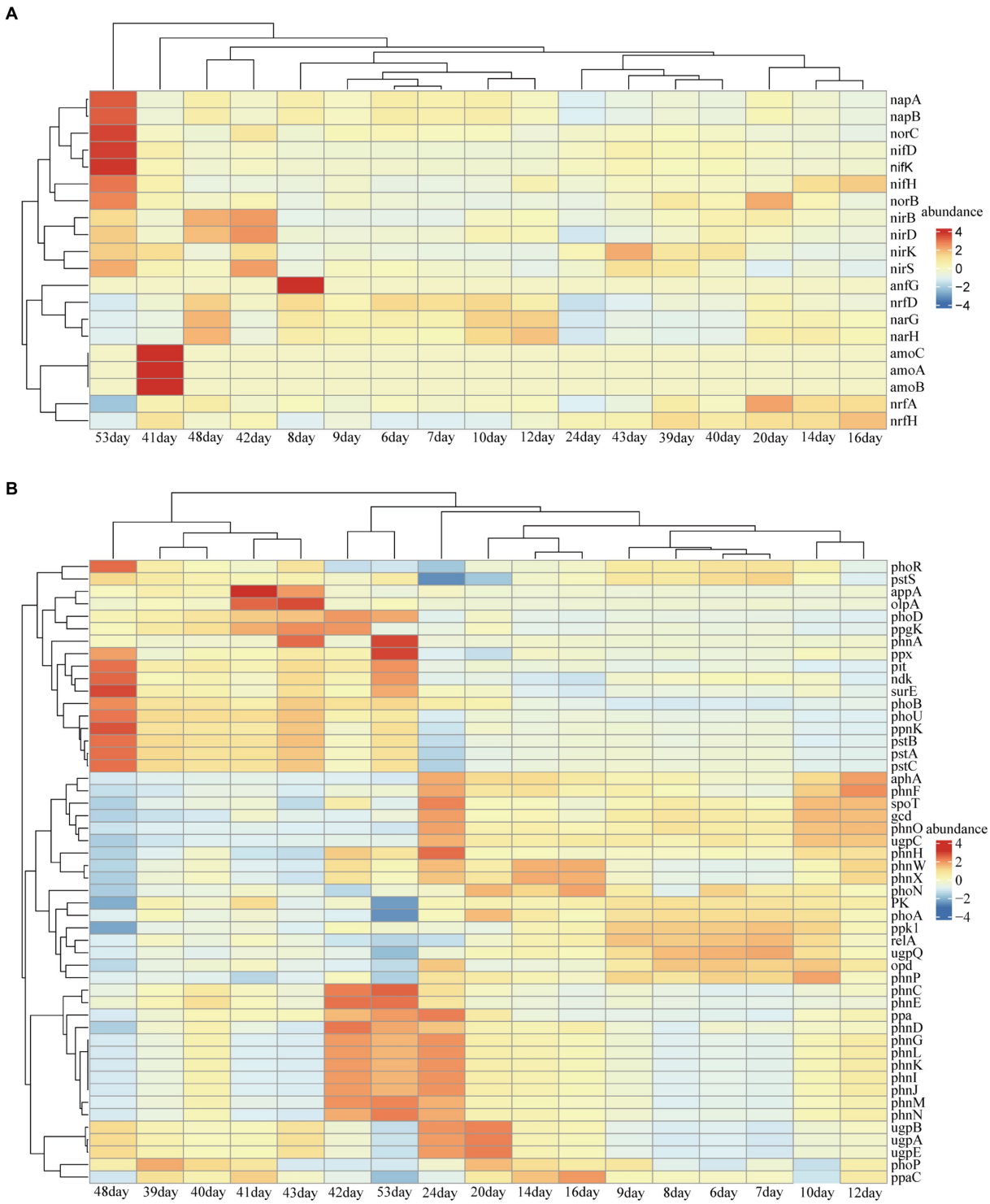

FIGURE 4
Predicted abundance of functional genes for nitrogen **(A)** and phosphorus **(B)** metabolism obtained from PICRUSt results. Less than 1% of functional genes and unclassified functional genes were removed.

suggested that some of the major bacterial genera (*Enterobacter* and *Klebsiella*) were the main microbes involved in nitrogen metabolism (Figure 6B). They may be key species associated with microbiome stability. *Enterobacter* and *Klebsiella* belong to the Proteobacteria, a group of nitrogen-fixing bacteria. In the results of the total network of OTU-nutrition, microorganisms connected to TN were also found to contain *Proteobacteria* (Figure 2). Previous studies based on network analysis of 16S rRNA gene amplicon sequencing data had shown that most of the key taxa of bacteria belonged to *Proteobacteria* (Ma et al., 2016). Not surprisingly, specialized metabolic functions of nitrogen

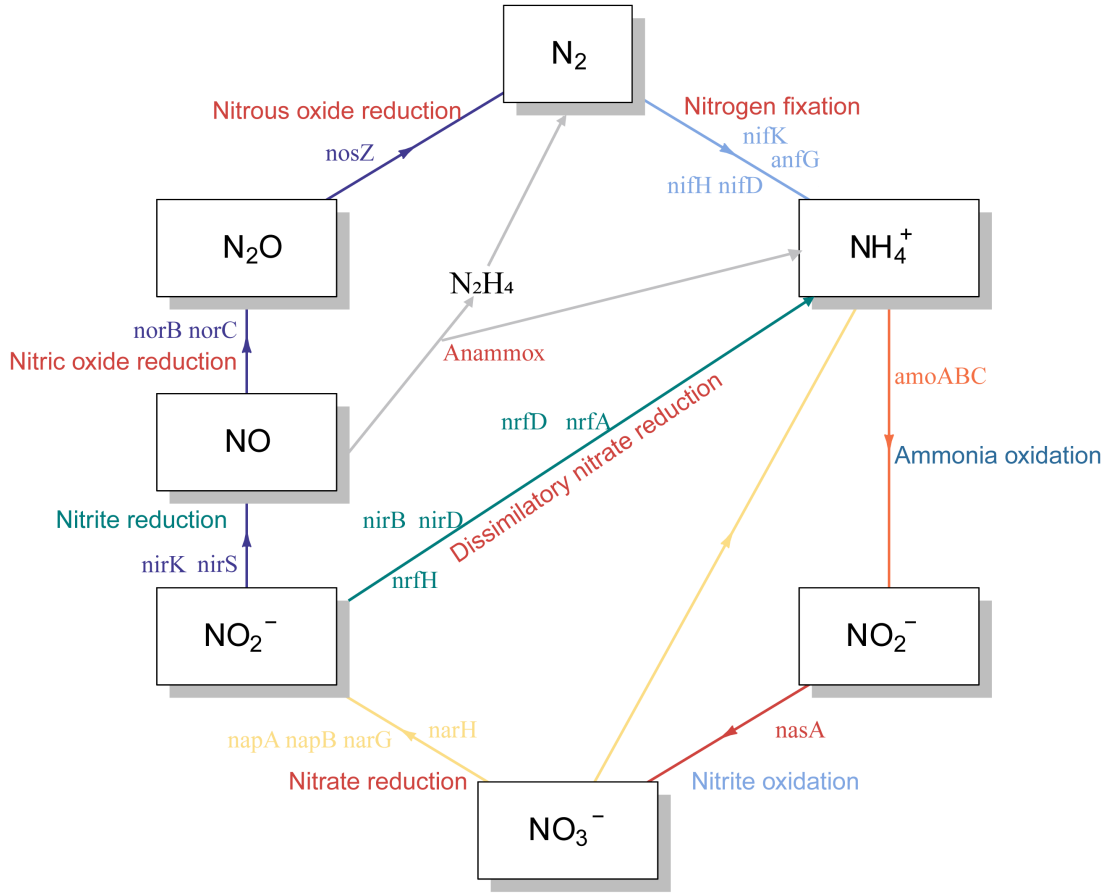

FIGURE 5
Predictions of nitrogen cycle metabolic pathways from PICRUSt results.

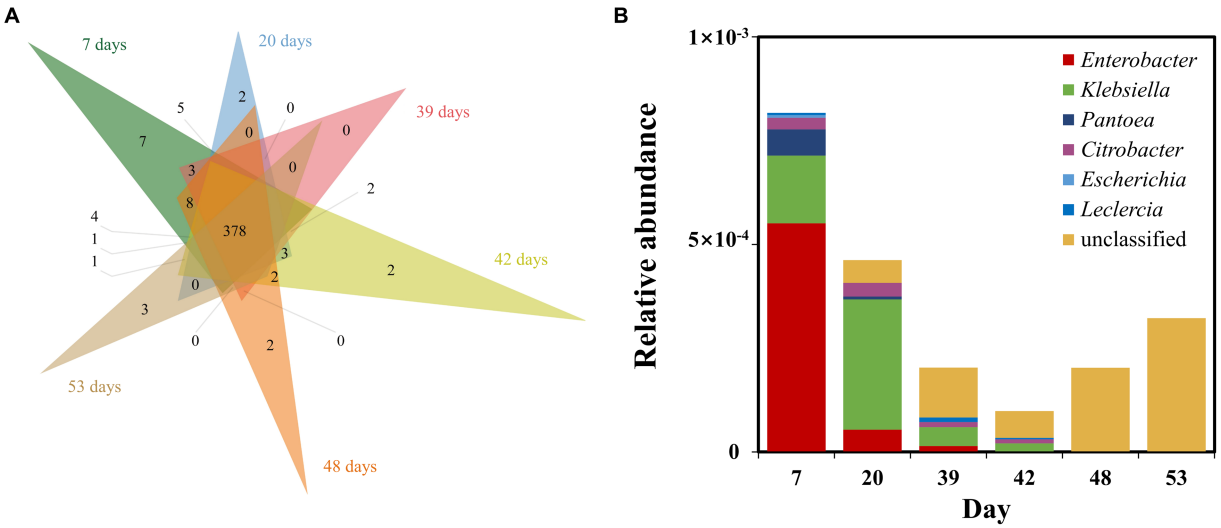

FIGURE 6
Venn diagram showing the types of microbial metabolism detected at different stages of injected nutrient concentration at sampling port 10 **(A)**. Diversity of contributions within samples of nitrogen metabolism and phosphorus metabolism pathways **(B)**.

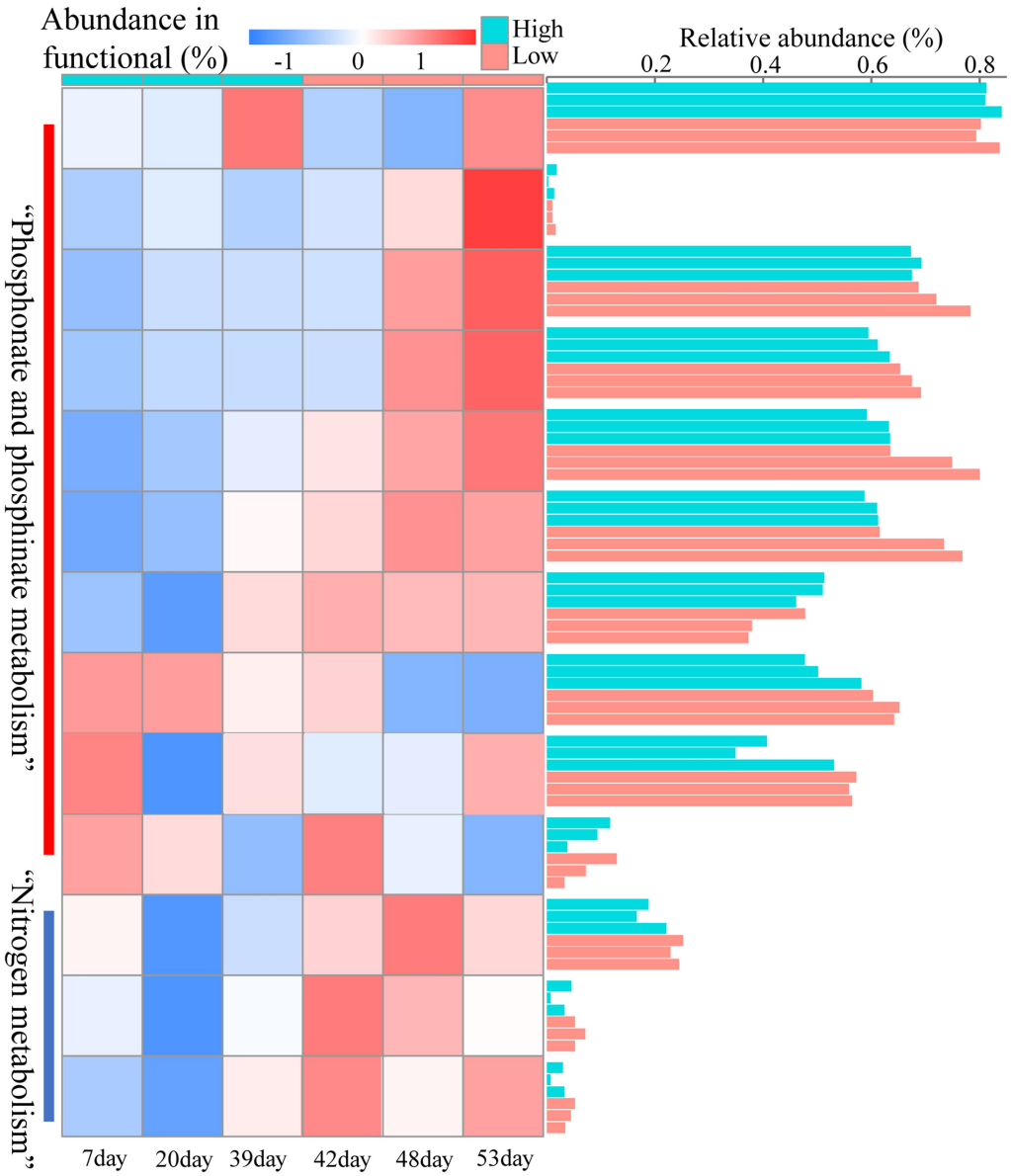

FIGURE 7
Heatmaps of the relative abundance of nitrogen metabolism and phosphorus metabolism at different injected nutrient concentrations obtained based on metagenomic results.

metabolism in reservoirs may be related to reservoir microbial community stability, containing a key group of microorganisms belonging to *Proteobacteria*. Many genera of *Proteobacteria* have the ability to enhance crude oil recovery (Yao et al., 2023). Therefore, the nutrient concentration, microbial community stability, and functional oil recovery bacteria that are intrinsically linked to each other should be focused on in future research.

In this study, the effect of nutrients on the structure and function of reservoir microbial communities was investigated by a long core microbial flooding simulation device. This provides new insights into the concentration selection of nutrients injected into the field, and injecting low concentration nutrients may be more beneficial to improve oil recovery and save oil field costs. Since reservoir microorganisms in specific blocks were selected in this study, it does not represent the overall changes in microbial communities in all oilfields. In addition, we mainly explore the nitrogen metabolism function in reservoir microorganisms, and more extensive research is needed in the future for other functions (carbon metabolism, sulfur metabolism, and methanogenesis), especially for the understanding of reservoir microbial communities and functional adaptations. This will facilitate a better understanding of the effects of nutrition on reservoir microbial community structure and function during microbial oil recovery.

5 Conclusion

In this study, we investigated the effects of nutrient injection on the structure and function of reservoir microbial communities by constructing a long core microbial flooding simulation device. The

study showed that the injection of nutrients made the microbial network structure more complex, the microbial community structure underwent obvious turnover, and the reservoir microbial community transitioned from aerobic to anaerobic states. Reducing the injected nutrient concentration increased the diversity, network stability, and functional abundance related to nitrogen metabolism in the reservoir bacterial community. Overall, nutrient availability significantly affects the composition and function of the reservoir microbiome. In the field, the injection of low concentrations of nutrients may be more beneficial to improve oil recovery. Future studies should continue to explore the relationship between nutrient concentration and oil recovery function and elucidate the changes in microbial community function after nutrient injection. This study provides new insights into reservoir microbiota and ecosystem functions as well as guidance for field applications in oil fields.

Data availability statement

The data presented in the study are deposited in the NCBI repository, BioProject accession number PRJNA1131017.

Author contributions

WC: Conceptualization, Data curation, Investigation, Methodology, Software, Writing – original draft. WT: Formal analysis, Methodology, Project administration, Supervision, Validation, Writing – review & editing. WW: Data curation, Methodology, Writing – review & editing. TL: Methodology, Project administration, Supervision, Writing – review & editing. TS: Formal analysis, Methodology, Supervision, Writing – review & editing. MW: Methodology, Supervision, Writing – review & editing. YY: Conceptualization, Formal analysis, Investigation, Project administration, Validation, Writing – review & editing. TM: Funding acquisition, Resources, Visualization, Writing – review & editing. GL: Funding acquisition, Resources, Visualization, Writing – review & editing.

Funding

The author(s) declare that financial support was received for the research, authorship, and/or publication of this article. This work was supported by National Key Research and Development Program of China (No. 2020YFC1808600), Tianjin Synthetic Biotechnology Innovation Capacity Improvement Project (No. TSBICIP-KJGG-015-04), and National Natural Science Foundation of China (Grant No. U2003128).

Conflict of interest

The authors declare that the research was conducted in the absence of any commercial or financial relationships that could be construed as a potential conflict of interest.

Publisher's note

Supplementary material

The Supplementary material for this article can be found online at: https://www.frontiersin.org/articles/10.3389/fmicb.2024.1450226/full#supplementary-material

References

Allison, S. D., and Martiny, J. B. H. (2008). Resistance, resilience, and redundancy in microbial communities. *Proc. Natl. Acad. Sci.* 105, 11512–11519. doi: 10.1073/pnas.0801925105

Bannon, C., Rapp, I., and Bertrand, E. M. (2022). Community interaction co-limitation: nutrient limitation in a marine microbial community context. *Front. Microbiol.* 13:846890. doi: 10.3389/fmicb.2022.846890

Bao, M. T., Kong, X., Jiang, G. C., Wang, X. L., and Li, X. M. (2009). Laboratory study on activating indigenous microorganisms to enhance oil recovery in Shengli oilfield. *J. Pet. Sci. Eng.* 66, 42–46. doi: 10.1016/j.petrol.2009.01.001

Carter, H. D., Svetlov, V., and Artsimovitch, I. (2004). Highly divergent RfaH orthologs from pathogenic proteobacteria can substitute for *Escherichia coli* RfaH both in vivo and in vitro. *J. Bacteriol.* 186, 2829–2840. doi: 10.1128/JB.186.9.2829-2840.2004

Chen, Y., Pan, J., Yun, Y., Zhi, B., Li, G. Q., Li, M., et al. (2020). Halomonas plays a central role in the syntrophic community of an alkaline oil reservoir with alkali-surfactant-polymer (ASP) flooding. *Sci. Total Environ.* 747:141333. doi: 10.1016/j.scitotenv.2020.141333

Chen, J., Zhou, H. C., Pan, Y., Shyla, F. S., and Tam, N. F. (2016). Effects of polybrominated diphenyl ethers and plant species on nitrification, denitrification and anammox in mangrove soils. *Sci. Total Environ.* 553, 60–70. doi: 10.1016/j.scitotenv.2016.02.052

Cheng, W., Fan, H. Q., Yun, Y., Zhao, X. Q., Su, Z. Y., Tian, X. F., et al. (2023). Effects of nutrient injection on the Xinjiang oil field microbial community studied in a long core flooding simulation device. *Front. Microbiol.* 14:1230274. doi: 10.3389/fmicb.2023.1230274

Crits-Christoph, A., Diamond, S., Butterfield, C. N., Thomas, B. C., and Banfield, J. F. (2018). Novel soil bacteria possess diverse genes for secondary metabolite biosynthesis. *Nature* 558, 440–444. doi: 10.1038/s41586-018-0207-y

Dong, H., Zhu, Q., Wang, L., Yue, X. K., Fang, H. X., Wang, Z. J., et al. (2023). Effects of shale pore size and connectivity on $scCO_2$ enhanced oil recovery, a molecular dynamics simulation investigation. *Langmuir* 39, 6287–6299. doi: 10.1021/acs.langmuir.3c00904

Duque, Z., Chicote, E., Isabel Sarró, M., Diego, A., Moreno, D. A., de Romero, M. M. F., et al. (2004). Corrosivity of H_2S-producing bacteria isolated from formation waters used in secondary crude-oil recovery. *Rev. Téc. Fac. Ing. Univ.* 27, 83–92.

Franzosa, E. A., McIver, L. J., Rahnavard, G., Thompson, L. R., Schirmer, M., Weingart, G., et al. (2018). Species-level functional profiling of metagenomes and metatranscriptomes. *Nat. Methods* 15, 962–968. doi: 10.1038/s41592-018-0176-y

Gao, P. K., Li, G., Le, J., Liu, X. B., Liu, F., and Ma, T. (2018). Succession of microbial communities and changes of incremental oil in a post-polymer flooded reservoir with nutrient stimulation. *Appl. Microbiol. Biotechnol.* 102, 2007–2017. doi: 10.1007/s00253-018-8766-2

Griffiths, B. S., Hallett, P. D., Kuan, H. L., Gregory, A. S., Watts, C. W., and Whitmore, A. P. (2008). Functional resilience of soil microbial communities depends on

both soil structure and microbial community composition. *Biol. Fertil. Soils* 44, 745–754. doi: 10.1007/s00374-007-0257-z

Han, J., Jung, J., Hyun, S., Park, H., and Park, W. (2012). Effects of nutritional input and diesel contamination on soil enzyme activities and microbial communities in Antarctic soils. *J. Microbiol.* 50, 916–924. doi: 10.1007/s12275-012-2636-x

Hernández-Plaza, A., Szklarczyk, D., Botas, J., Cantalapiedra, C. P., Giner-Lamia, J., Mende, D. R., et al. (2022). eggNOG 6.0: enabling comparative genomics across 12 535 organisms. *Nucleic Acids Res.* 51, D389–D394. doi: 10.1093/nar/gkac1022

Li, H., Chi, Z. F., Li, J. L., Wu, H. T., and Yan, B. X. (2019). Bacterial community structure and function in soils from tidal freshwater wetlands in a Chinese delta: potential impacts of salinity and nutrient. *Sci. Total Environ.* 696:134029. doi: 10.1016/j.scitotenv.2019.134029

Li, H. L., Lai, R. Q., Jin, Y. L., Fang, X. X., Cui, K., Sun, S. S., et al. (2020). Directional culture of petroleum hydrocarbon degrading bacteria for enhancing crude oil recovery. *J. Hazard. Mater.* 390:122160. doi: 10.1016/j.jhazmat.2020.122160

Liang, K. Q., Liu, M. M., Liang, Q. S., Yang, H., Li, J., Yao, Z., et al. (2022). Shifts in bacterial and archaeal community composition in low-permeability oil reservoirs by a nutrient stimulation for enhancing oil recovery. *Appl. Sci.* 12:8075. doi: 10.3390/app12168075

Lima, J. L. F. C., Rangel, A. O. S. S., Souto, M. R. S., and Zagatto, E. A. G. (1997). Turbidimetric flow-injection determination of total nitrogen and potassium in vegetables. *Anal. Chim. Acta* 356, 259–265. doi: 10.1016/S0003-2670(97)00555-2

Liu, L., Zhang, Z., Wang, X., Zhang, R., Wang, M., Wurzburger, N., et al. (2023). Urbanization reduces soil microbial network complexity and stability in the megacity of Shanghai. *Sci. Total Environ.* 893:164915. doi: 10.1016/j.scitotenv.2023.164915

Lu, M. Q., Luo, X., Jiao, J. J., Li, H. L., Wang, X. J., Gao, J. Y., et al. (2019). Nutrients and heavy metals mediate the distribution of microbial community in the marine sediments of the Bohai Sea, China. *Environ. Pollut.* 255:113069. doi: 10.1016/j.envpol.2019.113069

Ma, B., Wang, H., Dsouza, M., He, Y., Dai, Z. M., Brookes, P. C., et al. (2016). Geographic patterns of co-occurrence network topological features for soil microbiota at continental scale in eastern China. *ISME J.* 10, 1891–1901. doi: 10.1038/ismej.2015.261

Manter, D. K., Hunter, W. J., and Vivanco, J. M. (2011). *Enterobacter soli* sp. nov., a lignin-degrading γ-Proteobacteria isolated from soil. *Curr. Microbiol.* 62, 1044–1049. doi: 10.1007/s00284-010-9809-9

Marzocchi, U., Palma, E., Rossetti, S., Aulenta, F., and Scoma, A. (2020). Parallel artificial and biological electric circuits power petroleum decontamination, the case of snorkel and cable bacteria. *Water Res.* 173:115520. doi: 10.1016/j.watres.2020.115520

Mohanty, G., and Mukherji, S. (2008). Biodegradation rate of diesel range n-alkanes by bacterial cultures *Exiguobacterium aurantiacum* and *Burkholderia cepacia*. *Int. Biodeterior. Biodegrad.* 61, 240–250. doi: 10.1016/j.ibiod.2007.06.011

Mougi, A., and Kondoh, M. (2012). Diversity of interaction types and ecological community stability. *Science* 337, 349–351. doi: 10.1126/science.1220529

Niu, J., Liu, Q., Lv, J., and Peng, B. (2020). Review on microbial enhanced oil recovery, mechanisms, modeling and field trials. *J. Pet. Sci. Eng.* 192:107350. doi: 10.1016/j.petrol.2020.107350

Orphan, V. J., Hinrichs, K. U., Ussler, W., Paul, C. K., Taylor, L. T., Sylva, S. P., et al. (2001). Comparative analysis of methane-oxidizing archaea and sulfate-reducing bacteria in anoxic marine sediments. *Appl. Environ. Microbiol.* 67, 1922–1934. doi: 10.1128/AEM.67.4.1922-1934.2001

Quast, C., Pruesse, E., Yilmaz, P., Gerken, J., Schweer, T., Yarza, P., et al. (2012). The SILVA ribosomal RNA gene database project, improved data processing and web-based tools. *Nucleic Acids Res.* 41, D590–D596. doi: 10.1093/nar/gks1219

Ritalahti, K. M., Justicia-Leon, S. D., Cusick, K. D., Ramos-Hernandez, N., Rubin, M., Dornbush, J., et al. (2012). *Sphaerochaeta globosa* gen. Nov., sp. nov. and *Sphaerochaeta pleomorpha* sp. nov., free-living, spherical spirochaetes. *Int. J. Syst. Evol. Microbiol.* 62, 210–216. doi: 10.1099/ijs.0.023986-0

Schauf, S., Nakamura, N., and Castrillo, C. (2019). Effect of Calsporin® (*Bacillus subtilis* C-3102) addition to the diet on faecal quality and nutrient digestibility in healthy adult dogs. *J. Appl. Anim. Nutr.* 7:e3. doi: 10.1017/jan.2019.2

Shang, J. H., Zhang, W. L., Chen, X. Q., Li, Y., Niu, L. H., Wang, L. F., et al. (2021). How environmental stress leads to alternative microbiota states in a river ecosystem, a new insight into river restoration. *Water Res.* 203:117538. doi: 10.1016/j.watres.2021.117538

Sharma, N., Lavania, M., Kukreti, V., Rana, D. P., and Lal, B. (2023). Enhanced oil recovery using indigenous microbiome of high temperature oil reservoirs. *Curr. Microbiol.* 80:179. doi: 10.1007/s00284-023-03272-6

Shi, Z., Usman, M., He, J., Chen, H. H., Zhang, S. C., and Luo, G. (2021). Combined microbial transcript and metabolic analysis reveals the different roles of hydrochar and biochar in promoting anaerobic digestion of waste activated sludge. *Water Res.* 205:117679. doi: 10.1016/j.watres.2021.117679

Tang, Y. Q., Li, Y., Zhao, J. Y., Chi, C. Q., Huang, L. X., Dong, H. P., et al. (2012). Microbial communities in long-term, water-flooded petroleum reservoirs with different in situ temperatures in the Huabei oilfield, China. *PLoS One* 7:e33535. doi: 10.1371/journal.pone.0033535

Tripathi, B. M., Stegen, J. C., Kim, M., Dong, K., Adams, J. M., and Lee, Y. K. (2018). Soil pH mediates the balance between stochastic and deterministic assembly of bacteria. *ISME J.* 12, 1072–1083. doi: 10.1038/s41396-018-0082-4

Wang, G., Duan, L. S., Han, F., Wang, R., Liu, S. S., Lei, X. Y., et al. (2020). Research on the change rule of microbial community in the microbial flooding process of Baolige oilfield. *IOP Conf. Ser. Mater. Sci. Eng.* 729:012040. doi: 10.1088/1757-899X/729/1/012040

Wang, X. D., Feng, J. G., Ao, G. K. L., Qin, W. K., Han, M. G., Shen, Y. W., et al. (2023). Globally nitrogen addition alters soil microbial community structure, but has minor effects on soil microbial diversity and richness. *Soil Biol. Biochem.* 179:108982. doi: 10.1016/j.soilbio.2023.108982

Wang, X. B., Xue, Y. F., Yuan, S. Q., Huang, Z. Y., and Ma, Y. H. (2015). Influences of microbial community structures and diversity changes by nutrients injection in Shengli oilfield, China. *J. Pet. Sci. Eng.* 133, 421–430. doi: 10.1016/j.petrol.2015.06.020

Wei, Z., Yang, T., Friman, V. P., Xu, Y. C., Shen, Q. R., and Jousset, A. (2015). Trophic network architecture of root-associated bacterial communities determines pathogen invasion and plant health. *Nat. Commun.* 6:8413. doi: 10.1038/ncomms9413

Xun, W. B., Liu, Y. P., Li, W., Ren, Y., Xiong, W., Xu, Z. H., et al. (2021). Specialized metabolic functions of keystone taxa sustain soil microbiome stability. *Microbiome* 9, 1–15. doi: 10.1186/s40168-020-00985-9

Yao, S., Jin, T., Zhang, L., Zhang, Y., Chen, R., Wang, Q., et al. (2023). N/S element transformation modulating lithospheric microbial communities by single-species manipulation. *Microbiome* 11:107. doi: 10.1186/s40168-023-01553-7

Yin, J., Wei, X. X., Hu, F. T., Cheng, C. K., Zhuang, X. L., Song, M. Y., et al. (2023). Halotolerant *Bacillus velezensis* sustainably enhanced oil recovery of low permeability oil reservoirs by producing biosurfactant and modulating the oil microbiome. *Chem. Eng. J.* 453:139912. doi: 10.1016/j.cej.2022.139912

Yun, Y., Gui, Z. Y., Chen, Y., Tian, X. F., Gao, P. K., Li, G. Q., et al. (2021). Disentangling the distinct mechanisms shaping the subsurface oil reservoir bacterial and archaeal communities across northern China. *Sci. Total Environ.* 789:148074. doi: 10.1016/j.scitotenv.2021.148074

Zhang, L. Y., Delgado-Baquerizo, M., Hotaling, S., Li, Y., Sun, X. X., Xu, Y. F., et al. (2023). Bacterial diversity and co-occurrence patterns differ across a world-wide spatial distribution of habitats in glacier ecosystems. *Funct. Ecol.* 37, 1520–1535. doi: 10.1111/1365-2435.14317

Zhu, L. Y., Chen, Y., Sun, R. B., Zhang, J. B., Hale, L., Dumack, K., et al. (2023). Resource-dependent biodiversity and potential multi-trophic interactions determine belowground functional trait stability. *Microbiome* 11:95. doi: 10.1186/s40168-023-01539-5

Zhu, H. Z., Zhang, Z. F., Zhou, N., Jiang, C. Y., Wang, B. J., Cai, L., et al. (2019). Diversity, distribution and co-occurrence patterns of bacterial communities in a karst cave system. *Front. Microbiol.* 10:1726. doi: 10.3389/fmicb.2019.01726

Zhu, G. B., Zhou, L. L., Wang, Y., Wang, S. Y., Guo, J. H., Long, X. E., et al. (2015). Biogeographical distribution of denitrifying anaerobic methane oxidizing bacteria in Chinese wetland ecosystems. *Environ. Microbiol. Rep.* 7, 128–138. doi: 10.1111/1758-2229.12214

frontiers | Frontiers in Microbiology

TYPE Original Research
PUBLISHED 31 July 2024
DOI 10.3389/fmicb.2024.1439866

OPEN ACCESS

EDITED BY
William J. Brazelton,
The University of Utah, United States

REVIEWED BY
Noura Eddaoui,
UMR7327 Institut des sciences de la Terre d'Orléans (ISTO), France
Gion Strobel,
Clausthal University of Technology, Germany

*CORRESPONDENCE
Anthony Ranchou-Peyruse
✉ anthony.ranchou-peyruse@univ-pau.fr

RECEIVED 28 May 2024
ACCEPTED 17 July 2024
PUBLISHED 31 July 2024

CITATION
Mura J, Ranchou-Peyruse M, Guignard M, Ducousso M, Larregieu M, Isaure M-P, Le Hécho I, Hoareau G, Poulain M, Buruti MdS, Chiquet P, Caumette G, Petit A, Cézac P and Ranchou-Peyruse A (2024) Experimental simulation of H_2 coinjection via a high-pressure reactor with natural gas in a low-salinity deep aquifer used for current underground gas storage.
Front. Microbiol. 15:1439866.
doi: 10.3389/fmicb.2024.1439866

Experimental simulation of H_2 coinjection via a high-pressure reactor with natural gas in a low-salinity deep aquifer used for current underground gas storage

Jean Mura[1], Magali Ranchou-Peyruse[1,2,3], Marion Guignard[2], Marion Ducousso[1,3], Marie Larregieu[2], Marie-Pierre Isaure[2], Isabelle Le Hécho[2,3], Guilhem Hoareau[4], Marie Poulain[1,3], Mateus de Souza Buruti[1], Pierre Chiquet[3,5], Guilhem Caumette[3,6], Anélia Petit[7], Pierre Cézac[1,3] and Anthony Ranchou-Peyruse[2,3]*

[1]LaTEP, E2S UPPA, Université de Pau et des Pays de l'Adour, Pau, France, [2]IPREM, CNRS, E2S UPPA, Université de Pau et des Pays de l'Adour, Pau, France, [3]Joint Laboratory SEnGA, E2S UPPA, Pau, France, [4]LFCR, CNRS, E2S UPPA, Université de Pau et des Pays de l'Adour, Pau, France, [5]Geosciences Department, Teréga, Pau, France, [6]Environment Department, Teréga, Pau, France, [7]Geosciences Department, Storengy, Bois-Colombes, France

If dihydrogen (H_2) becomes a major part of the energy mix, massive storage in underground gas storage (UGS), such as in deep aquifers, will be needed. The development of H_2 requires a growing share of H_2 in natural gas (and its current infrastructure), which is expected to reach approximately 2% in Europe. The impact of H_2 in aquifers is uncertain, mainly because its behavior is site dependent. The main concern is the consequences of its consumption by autochthonous microorganisms, which, in addition to energy loss, could lead to reservoir souring and alter the petrological properties of the aquifer. In this work, the coinjection of 2% H_2 in a natural gas blend in a low-salinity deep aquifer was simulated in a three-phase (aquifer rock, formation water, and natural gas/H_2 mix) high-pressure reactor for 3 months with autochthonous microorganisms using a protocol described in a previous study. This protocol was improved by the addition of protocol coupling experimental measures and modeling to calculate the pH and redox potential of the reactor. Modeling was performed to better analyze the experimental data. As in previous experiments, sulfate reduction was the first reaction to occur, and sulfate was quickly consumed. Then, formate production, acetogenesis, and methanogenesis occurred. Overall, H_2 consumption was mainly caused by methanogenesis. Contrary to previous experiments simulating H_2 injection in aquifers of higher salinity using the same protocol, microbial H_2 consumption remained limited, probably because of nutrient depletion. Although calcite dissolution and iron sulfide mineral precipitation likely occurred, no notable evolution of the rock phase was observed after the experiment. Overall, our results suggested that H_2 can be stable in this aquifer after an initial loss. More generally, aquifers with low salinity and especially low electron acceptor availability should be favored for H_2 costorage with natural gas.

KEYWORDS

dihydrogen, UGS, deep aquifer, microbial community, gas storage, methanogens, sulfate reducers

1 Introduction

Shifting toward carbon-free renewable fuels is essential for facing global warming and resource depletion. Dihydrogen (H_2) could be a coherent alternative to fossil fuels, as it can be produced by electrolyzers using renewable electricity and does not produce greenhouse gases during its combustion. Thus, excess renewable energy could be used to produce H_2 (power-to-gas), which could be stored until use in periods of high demand (Pastore et al., 2022). To achieve carbon neutrality, substantial storage capacity will be needed. In France, most seasonal gas storage is assured by underground gas storage (UGS) in deep aquifers, which could provide a large storage capacity for H_2 in large-scale production. The development of H_2 production implies that blends of H_2 and natural gas will flow in the gas grid and will need to be stored in deep aquifers. The H_2 percentage in these blends is expected to reach 2%. Feasibility and site selection studies of H_2 storage in porous rock reservoirs and aquifers have been conducted based on the structural characteristics of H_2 storage, such as porosity, cap rock, and permeability (Aghaei et al., 2023; Bo et al., 2023; Buscheck et al., 2023; Harati et al., 2023; Lysyy et al., 2023; Wang et al., 2023). Many researchers have investigated the injection/withdrawal cycles of H_2 in aquifers (Heinemann et al., 2021; Chai et al., 2023; Pan et al., 2023; Jadhawar and Saeed, 2023a,b; Izadi Amiri et al., 2024; Saeed and Jadhawar, 2024), enabling the determination of optimal strategies for site exploitation. One of the major challenges of massive H_2 storage in deep aquifers is its interaction with indigenous microorganisms (Šmigáň et al., 1990; Dopffel et al., 2021; Haddad et al., 2022b; Mura et al., 2024). Indeed, H_2 is a reactive molecule that can be used as an energy source and an electron donor by autochthonous lithoautotrophic microorganisms, so called hydrogenotrophs (Šmigáň et al., 1990; Dopffel et al., 2021; Haddad et al., 2022b; Mura et al., 2024). Based on town gas storage experience (Šmigáň et al., 1990; Buzek et al., 1994; Liebscher et al., 2016; Stolten and Emonts, 2016; Pichler, 2019; Tremosa et al., 2023) and experimental studies (Haddad et al., 2022b; Dohrmann and Krüger, 2023; Mura et al., 2024; Vasile et al., 2024), the major reactions to be expected are sulfate reduction, methanogenesis (Vítězová et al., 2023), and acetogenesis with acetate and formate production. The electron acceptors of these reactions (sulfate, CO_2, and bicarbonates; Ebrahimiyekta, 2017) can be naturally present at various concentrations in deep aquifers and can be found in aquifers hosting UGS storages. In addition to energy loss through H_2 consumption, microbial reactions and growth can cause multiple drawbacks to H_2 storage. Biofilm development can lead to pore clogging (Eddaoui et al., 2021) and has been shown to influence sandstone wettability and liquid/gas transfer (Stewart, 2003; Ali et al., 2023). Sulfate reduction produces sulfide and can lead to souring. Physicochemical changes induced by microbial reactions could lead to precipitation and dissolution by equilibrium displacement (Ulrich et al., 2003; Dupraz et al., 2009) or lasting changes in water physicochemistry (i.e., low sulfate concentration; Ranchou-Peyruse et al., 2019). An induced decrease in porosity would lower the storage performance, whereas an increase in porosity could harm the storage integrity. However, microbial activity can be inhibited by inappropriate pH or a lack of nutrients (Dopffel et al., 2023; Mura et al., 2024). The abiotic effects of H_2 could also be expected, as H_2S could be produced by pyrite reduction (Šmigáň et al., 1990). However, microbial activity could also benefit storage, as microorganisms such as sulfate reducers are known to attenuate aromatic molecules (Mancini et al., 2003).

Despite the development of new experimental studies (Haddad et al., 2022b; Dohrmann and Krüger, 2023; Dopffel et al., 2023; Liu et al., 2023; Mura et al., 2024; Vasile et al., 2024), the feasibility of H_2 storage in porous reservoirs remains unclear, mainly because of site-dependent phenomena related notably to its pressure and temperature conditions and its mineralogy. While microorganisms are expected to be present in deep aquifers, their taxonomic diversity and cell concentration could change depending on the studied site. Moreover, there is variability in the physicochemistry and hydrology between aquifers (Fillinger et al., 2023), and temperature and mineralogy can influence microbial activity (Dohrmann and Krüger, 2023; Muller et al., 2023). Thus, site-specific microbiological and geochemical analyses are needed to evaluate the feasibility of H_2 coinjection in deep aquifers (Dopffel et al., 2021). For experimental approaches, the modeling of H_2 storage in porous rocks has increased (Amid et al., 2016; Hagemann et al., 2016; Hogeweg et al., 2022; Veshareh et al., 2022; Gelencsér et al., 2023; Maniglio et al., 2023; Strobel et al., 2023; Tremosa et al., 2023; Wu et al., 2023). Conceptual kinetic modeling of microbial growth and reactions was performed on various systems ranging from near atmospheric pressure laboratory experiments to reservoir-scale modeling. Both experimental and modeling approaches underscore the need for additional experimental studies and data to better understand the intricate phenomena of H_2 in underground storage.

In recent works (Haddad et al., 2022b; Ranchou-Peyruse et al., 2023; Mura et al., 2024), a multidisciplinary protocol to recreate deep aquifers in a three-phase high-pressure reactor was developed and applied to four French aquifers hosting natural gas storages. In this work, a similar approach was applied to another UGS in a deep aquifer to investigate the feasibility of H_2 coinjection at this site. The formation water and rock phase were sampled from the studied aquifer, and a gas mixture representing the natural gas storage (with 1% CO_2) was added with a final pressure of 60 bar. Two percent H_2 was added to the gas phase to simulate its injection in the aquifer. The extent of the reactions was computed based on physicochemical parameters and microbial taxonomic diversity to model the amount of H_2 consumed by each microbial reaction. To better quantify the *in situ* pH and redox potential in the high-pressure reactor, the initial protocol was upgraded with a new sampling protocol coupled with modeling using PHREEQC. Briefly, dissolved gases were quantified at atmospheric pressure to account for their acido-basic and redox effects. The Materials and Methods section describes the experimental protocol and the modeling approach. The outcomes of the experiment and modeling results are presented in the Results section and analyzed and compared in the Discussion section.

2 Materials and methods

2.1 Simulated site characteristics and sampling procedure

The UGS studied in this work is a previously studied deep aquifer operated for seasonal natural gas storage, referred to as Ab_L in the literature (Ranchou-Peyruse et al., 2019, 2024; Haddad et al., 2022a, 2023). This aquifer is in southwestern France and belongs to the South

Aquitaine sedimentary basin (582 m depth; Haddad et al., 2022a). The formation water was sampled from a control well close to the gas bubble, ensuring optimal contact between the liquid phase (i.e., formation water) and the stored natural gas. With 0.8% salinity of seawater, the formation water has a low salinity (Haddad et al., 2022a). The porous rock is mainly composed of quartz (80%) and calcite (12%) and contains small amounts of iron sulfide, clays, and barite (Jacquemet et al., 2020; Haddad et al., 2022a). During the sampling campaign on well Ab_L_1, formation water was collected using two bottom hole samplers (Leutert Bottom Hole Positive Displacement Sampler) to ensure sterile conditions, maintenance of anoxia and pressure until the samples reached the laboratory, according to a protocol (Ranchou-Peyruse et al., 2023). From the samplers, 578 mL and 594 mL were slowly depressurized (<1 bar.min^{-1}) in the laboratory, transferred to sterile and anoxic flasks, and stored at 4°C until use. On the day of sampling, wellhead formation water was also sampled and sterilized by filtration (PES 47 mm membranes, 0.1 µm, Sartorius). All water samples were stored at 4°C in darkness until use. On the day the experiment began, the two flasks were mixed with 778 mL of filtered water collected from the wellhead. The procedure was carried out in an anaerobic chamber (GP Campus, Jacomex). One hundred milliliters were sampled to study the microbial taxonomic diversity. The characteristics and composition of the water mix are detailed in Table 1. The rock phase was composed of infra-molassic sands and was recovered from drilling cuttings from the reservoir studied (Ranchou-Peyruse et al., 2019; Haddad et al., 2022a, 2023).

2.2 Experiment

2.2.1 Experimental protocol

This experiment was carried out in a high-pressure reactor using a protocol to simulate H_2 or O_2 injection in deep aquifers used previously (Haddad et al., 2022a,b, 2023; Mura et al., 2024). This reactor was made of corrosion-resistant Hastelloy C-276 material and was equipped with pressure and temperature sensors. The solid phase was contained in a Teflon basket sitting in the middle of the reactor to represent the water-gas interface in the porous rock of the aquifer. A piston enables the modification of the reactor volume to compensate for the liquid sampling and manage the height of the water-gas interface throughout the experiment. The liquid and gas phases were stirred at 20 rpm. After the solid basket filled with rock was introduced into the reactor, the reactor was sterilized by moist heat with ultrapure water at 110°C for 24 h under low nitrogen (N_2) pressure. Then, the liquid phase was introduced into the reactor previously placed under vacuum from a Teflon bottle prepared in an anaerobic glovebox. A custom gas mixture simulating natural gas (99% CH_4, 1% CO_2, 7.95 ppm benzene, and 3.57 ppm toluene) was injected into the reactor to reach the target pressure. The height of the piston was set to immerse the solid phase fully. After 7 days, the piston was lowered to immerse 1 cm of solid. The pressure loss induced was compensated by injecting a new amount of the initial gas mixture. After validation of the microbial activity, dihydrogen (CAS: 1333-74-0, purity 99.999%) was injected at a gas phase molar fraction of 2%. The microbial activity was validated by sulfate consumption and cell count (data not shown) based on previous experiments (Haddad et al., 2022a,b, 2023; Mura et al., 2024). Immediately after H_2 injection, additional filtered formation water was injected into the reactor to extend the duration of the experiment, which was limited by the quantity of water available to the sample. Each week, the composition of the liquid and gas phases was monitored, and more detailed chemical and biological analyses (qPCR, taxonomic diversity, and benzene/toluene quantification) were performed for key events. Water samples were taken regularly to monitor changes in the taxonomic and functional diversities of the microbial community. Filtered formation water was added to the reactor on day 17 of the experiment to extend its duration. At the end of the experiment, the remaining liquid phase and the solid basket were maintained under anoxic conditions and recovered for further analysis (Haddad et al., 2022a).

TABLE 1 Characteristics and composition of the formation water sampled from the studied UGS aquifers.

Experiment parameters	Value	Unit
Water composition		
pH	8.3	
Redox potential	−20	mV
Chloride	0.23	mM
Nitrate	<0.0016	mM
Nitrite	<0.0004	mM
Sulfate	0.09	mM
Carbonate	<1	mM
Bicarbonate	3.44	mM
Calcium	1.37	mM
Total iron	9.24	µM
Magnesium	0.30	mM
Potassium	0.15	mM
Sodium	0.50	mM

Analyses were carried out at atmospheric pressure by UT$_2$A (Pau, France).

2.2.2 Physico-chemical analyses

The anions (fluoride, acetate, formate, chloride, sulfate) were analyzed by ionic chromatography (Dionex Integrion HPIC, Thermo Fisher Scientific) with ±5% precision. The dissolved inorganic carbon, including carbonate, bicarbonate, and dissolved CO_2, was quantified using a dedicated chromatography system (ICS-900, Dionex) equipped with an ICE-AS1 IC column. The precision of this measure was ±5%. The metal concentrations (sodium, iron, barium, magnesium, potassium, and calcium) in the liquid samples were determined during all the experiments via inductively coupled plasma-optical emission spectroscopy (ICP–OES, Thermo Scientific iCAP6500 Duo). The instrumental conditions for ICP–OES were as follows: RF power of 1,300 W, plasma gas flow rate of 15 L.min^{-1}, nebulizer gas flow rate of 0.65 L.min^{-1}, and auxiliary gas flow rate of 0.5 L.min^{-1}. All the samples were diluted in a 2% HNO_3 solution at a dilution ratio of four. The measurements were performed in triplicate, and the coefficient of variation (relative standard deviation) for each analysis was less than 2% for all measurements.

The gas phase species (H_2, O_2, CH_4, CO_2, H_2S) were quantified using in-line micro gas phase chromatography with 5% precision (GC-mTCD; Micro GC Fusion; Chemlys; France). The pH and redox potential were measured at atmospheric pressure using Inlab

Ultramicro ISM (Mettler Toledo) and Inlab Redox Micro (Mettler Toledo) probes. The specifications of each analysis method were detailed in a previous work (Haddad et al., 2022a).

The use of the compound-specific isotope analysis (CSIA) approach makes it possible to demonstrate or estimate the *in situ* bioattenuation of organic pollutants such as benzene and toluene (Fischer et al., 2016; Ponsin et al., 2017). This method can be used to directly monitor the biodegradation of aromatic hydrocarbons in groundwater by measuring the isotopic fractionation of the remaining contaminant as degradation proceeds (Mancini et al., 2003). CSIA requires an analytical chain composed of a gas chromatograph (GC, Thermo, Trace 1310) coupled via a combustion interface at 1,000°C (CT, Thermo, GC-Isolink) to an isotope ratio mass spectrometer (IRMS, Thermo Delta V Plus). All $\delta^{13}C$ signatures of the analytes were reported relative to Vienna PeeDee Belemnite ($\delta^{13}CVPDB$), and the calibration was achieved by coupling an elemental analyzer (EA, Thermo, Flash 2000) with an isotope ratio mass spectrometer (Berg et al., 2007; Hunkeler et al., 2008). In parallel, the identification and quantification of benzene and toluene in the liquid and gas phases were carried out by coupling gas chromatography to a quadrupole mass spectrometer (MS, Thermo, ISQ). This configuration thus makes it possible to obtain the identification and quantification of benzene/toluene via GC–MS and the determination of isotopic ratios via GC-CT-IRMS during the analysis of a sample, avoiding any problem of correspondence between the CO_2 peak and the compound of interest. Preconcentration of benzene and toluene was performed by SPME with a polydimethylsiloxane/carboxene (PDMS/CAR) fiber, and chromatographic separation was performed with a DB-624 column (Agilent). For each sample, two 10 mL water samples were taken and stored at 4°C. *prior* to the analysis, 90 µL of the 0.5 ppm 1,2,4-trimethylbenzene internal standard was added to each 6.9 g sample. Gas samples were collected in vials at one bar using a needle sampling system controlled by a manometer. The quantification was performed with methane as a reference gas containing 10 mol ppm benzene and toluene (Li et al., 2014; Haddad et al., 2022a).

2.2.3 Molecular biology approaches

2.2.3.1 Nucleic acid extraction and RNA reverse transcription

Aqueous phase samples were used to coextract nucleic acids (DNA and RNA) throughout the experiment. Membrane filters (47 mm PES with 0.1 µm porosity, Sartorius Stedim) were used to filter aqueous samples directly from the reactor. The filters with the samples were kept at −80°C until use. The filters were then ground in liquid nitrogen, and a Fast RNA Prosoil Direct kit (MP BIO) was used to recover the nucleic acids. An AllPrep RNA/DNA kit (Qiagen) was used to separate the DNA and RNA. A Quant-it™ dsDNA HS kit (Invitrogen) and a Quant-it™ RiboGreen kit (Invitrogen) were used to quantify the extracted DNA and RNA, respectively. A BioTEK SYNERGY HTX microplate reader was used to measure the extracted DNA and RNA. M-MLV reverse transcriptase (Invitrogen™) was used to reverse transcribe RNA and obtain complementary DNAs (cDNAs).

2.2.3.2 Polymerase chain reaction, qPCR, and sequencing

The primer pairs 515F-928R (V4-V5 region), dsr2060F-dsr4R, and mlasF-mcrAR (Wagner et al., 1998; Geets et al., 2006; Steinberg and Regan, 2008, 2009; Wang and Qian, 2009) were used to target the *16S rRNA*, *dsrB* and *mcrA* genes from the obtained DNA and cDNA, respectively. The addition of bovine serum albumin (BSA, NEV-B9200S) to PCR at a concentration of 1 $mg.mL^{-1}$ reduced the inhibition. A Taq PCR kit (Roche) was used to amplify the *16S rRNA* and *dsrB* genes, while a Fidelio® Hot Start PCR kit (Ozyme) was used to amplify the *mcrA* gene. Amplifications were obtained using a 2700 Thermal Cycler (Applied Biosystems). Haddad et al. (2022a) described the procedures in greater detail. The quantification of genes, their transcripts and associated standards was performed by quantitative PCR (qPCR; Bio-Rad CFX Connect) and 41 Takyon NO ROX SYBR 2X MasterMix blue dTTP (Eurogentec), as described by Haddad et al. (2022a). The primer pairs used in this work were synthesized with the adaptors GTGYCAGCMGCCGCGGTA (forward) and CCCCGYCAATTCMTTTRAGT (reverse). The raw sequencing data are publicly accessible on the NCBI SRA with bioproject ID PRJNA1117242. The MiSeq sequencing data were processed with QIIME 2 (Bolyen et al., 2019; version 2022.11) to analyze taxonomic diversity. Amplicon sequence variants (ASVs) were obtained with DADA2 (Callahan et al., 2016) after demultiplexing, filtering, denoising, trimming of any eliminating chimera sequences and excluding singletons. The SILVA v138 database (Quast et al., 2012; Yilmaz et al., 2014) was used for taxonomic affiliation. The same treatment was applied to the *mcrA* and *dsrB* sequences, as well as the *16S rDNA* sequences. For *mcrA*, the Yang et al. (2014) database was used for ASV affiliation, while for *dsrB*, we used our own database (Ranchou-Peyruse et al., 2024). Calculations and analyses in R.Studio (version 4.2.2) were performed with the Phyloseq (McMurdie and Holmes, 2013) and ggplot 2 (Wickham, 2016) packages. The ComplexHeatmap package (Gu et al., 2016; Gu, 2022) was used to generate heatmaps, and the Corrplot (Wei and Simko, 2017), FactoMineR (Lê et al., 2008) and factoExtra (Kassambara and Mundt, 2020) packages were used for PCA and PCoA. Bray–Curtis was used for PCoA distance calculations, and covariance analysis was used for PCA.

2.2.4 X-ray diffraction

X-ray diffraction (XRD) was performed to characterize the crystallized mineralogical phases before and after the experiment. At ambient temperature in the anaerobic glove box, samples were collected from the basket at three different depths (surface 0–1 cm, middle 2–5 cm, and bottom 6–7.5 cm). The samples were then dried with N_2 gas flux, manually ground, and sieved to <100 µm into a homogeneous powder in the anaerobic chamber to limit oxidation. Solid powders were then mounted on holders and directly analyzed by XRD. The analyses were performed using a Bruker D2 Phaser powder diffractometer equipped with a Cu Kα radiation source. XRD patterns were recorded over a 5° to 90° 2Θ range with a 0.02° step and a 0.5 s counting time per step. DIFFRAC.EVA software was used to identify the mineral phases.

2.2.5 Scanning electron microscopy

Aliquots of the same samples collected at three different depths were subjected to a petrographic study using scanning electron microscopy coupled with energy dispersive spectroscopy (SEM–EDS). Solid pieces were directly mounted on PIN stubs and coated with carbon. Observations and mineral identification were performed with a JEOL JSM 7800F Prime SEM-FEG instrument equipped with an Oxford Instruments AZtecEnergy EDS SDD X-Max 80 mm^2 detector at Centre Castaing, Toulouse, France.

2.2.6 Biochemical modeling

To better identify microbial reactions and quantify their effect on H_2 consumption, the extent of reactions was computed. The sulfate reduction (van Houten et al., 1994; Reitenbach et al., 2015; Hemme and Van Berk, 2018; Eq. 1), acetogenesis (Gregory et al., 2019; Rabii et al., 2019; Eq. 2), formate production (Logroño et al., 2022; Eq. 3), and methanogenesis (Panfilov, 2010; Hemme and Van Berk, 2018; Thaysen et al., 2021; Eq. 4) reactions were chosen based on literature mechanisms and used in agreement with microbiology analyses. These reactions were combined with the acido-basic reaction of the CO_2/HCO_3^- couple to consider the buffering of H^+ ion consumption/production. The stoichiometric coefficients of HS^- and H_2S were calculated based on sulfide speciation (Daumas et al., 1993; Mura et al., 2024). The extent of each reaction was determined from the quantification over time of selected species. The extents of sulfate reduction, acetogenesis, formate production, and methanogenesis were calculated based on the experimental changes in the quantities of sulfate, acetate, formate, and CO_2, respectively.

$$SO_4^{2-} + 4H_2 + 1.93\,CO_2 \rightarrow 0.93H_2S + 0.07\,HS^- + 1.93\,HCO_3^- + 2.07\,H_2O \quad (1)$$

$$CO_2 + HCO_3^- + 4H_2 \rightarrow CH_3COO^- + 3H_2O \quad (2)$$

$$HCO_3^- + H_2 \rightarrow HCOO^- + H_2O \quad (3)$$

$$CO_2 + 4H_2 \rightarrow CH_4 + 2H_2O \quad (4)$$

To consider the evolution of dissolved gas, the liquid–gas equilibrium was modeled with PHREEQC version 3 software (Parkhurst and Appelo, 2013) using the phreeqc.dat database. This database uses the Peng Robinson equation of state (Peng and Robinson, 1976) to consider the gas phase's nonideality. Gas solubility was calculated based on the fugacity of gases in the gas phase and the hypothesis of thermodynamic equilibrium between the two phases. This modeling procedure was detailed in a previous work (Mura et al., 2024).

The standard Gibbs energy of reaction (ΔG_r^0) of formate production (Eq. 3) was computed using the NBS Tables of Chemical Thermodynamics (Wagman, 1982), considering standard conditions of 298.15 K and 1 bar (Eq. 7). Activities were computed using the PHREEQC data from the *in situ* characterization protocol (section 0.). The Gibbs energy of reaction at the temperature of the experiment [$\Delta G_r^0(T)$] (36°C) was computed using the Gibbs-Helmoltz equation (Eq. 8). The theoretical equilibrium concentration of formate in the reactor was obtained by computing the activity of formate at equilibrium with dissolved H_2 and bicarbonate using the formate production mass action law (Eq. 9). The theoretical equilibrium concentration of formate at atmospheric pressure was calculated considering the activity of dissolved H_2 in equilibrium with a gas phase containing the molar fraction of H_2 measured on day 21 at 1 bar.

2.2.7 *In situ* characterization protocol

In this work, a protocol combining experimental measures and modeling was developed to determine the *in situ* pH and redox potential of a reactor. A 10 mL liquid sample was collected from the reactor in a gas-tight glass syringe (SGE, 50 mL) closed by a manual valve to retain the gases that were degassed due to a change in pressure. The total released gas quantity was quantified by directly reading its volume via syringe graduation. The uncertainty of this measure was ±5% compared to a reference value measured by a manual gasometer (results not shown; VINCI Technologies). The sample temperature was measured by a CheckTemp thermometer (± 0.2°C; HANNA instruments). Both the liquid and gas phases were injected into a rubber-sealed vial placed under an N_2 atmosphere for analysis. The gas composition in the vial was determined using the micro gas chromatography setup described in section 2.2.2. It was assumed that the gas composition did not change between the syringe and the vial, except for the dilution in N_2. The liquid phase was analyzed using the methods described in section 2.2.2.

The *in situ* conditions were then modeled using PHREEQC with the BRGM database Thermoddem (Blanc et al., 2012). This database was modified by removing redox couples linked by slow redox reactions (carbon, nitrogen, and sulfur) to model redox disequilibrium in solution (Gelencsér et al., 2023; Tremosa et al., 2023). This modeling was composed of three steps. First, the liquid and the released gas at atmospheric pressure were modeled using experimentally collected data. Using the ideal gas law, each gas quantity was computed from the gas composition, pressure, temperature, and volume. It was assumed that the sample in the syringe was at atmospheric pressure. In the second step, the thermodynamic equilibrium between the gas and liquid phases in the syringe was modeled using the composition of the syringe gas phase to quantify the dissolved gas concentrations in the syringe. At this stage, the calculated and measured pH values were close. Finally, the pressurization of the two phases at the reactor pressure and temperature was modeled to return to the reactor conditions.

The pH under these conditions was determined by the default PHREEQC calculations, assuming acido-basic equilibrium among all acid–base species in the solution. In the absence of redox equilibrium in solution, it is possible to only compute the theoretical Nernst potential of each redox couple (Lindberg and Runnells, 1984; Stefánsson et al., 2005; Ioka et al., 2011). Using Thermoddem.dat parameters, the redox potentials of the H^+/H_2 and CO_2/CH_4 couples were calculated (Eqs. 5, 6):

$$E_{H^+/H_2} = \left(\log\left(K_{H^+/H_2}\right) + \log\left(\frac{1}{a_{H_2}}\right) - 2pH \right) \ln(10) \frac{RT}{2F} \quad (5)$$

$$E_{CO_2/CH_4} = \left(\log\left(K_{CO_2/CH_4}\right) + \log\left(\frac{a_{CO_2}}{a_{CH_4} a_{H_2O}^2}\right) - 8pH \right) \ln(10) \frac{RT}{8F} \quad (6)$$

with

E_i: Redox potential of couple i relative to the standard hydrogen electrode (V).

$\log(K_i)$: Equilibrium constant of the half equation of couple i.

a: activity of species i.

R: gas constant (8.314 kg m^2 s^{-2} mol^{-1} K^{-1}).
T: temperature (K).
F: Faraday constant (9.6485•10^4 A s mol^{-1}).

$$\Delta G_r^0 = \sum_i \nu_i \Delta G_{fi}^0 \quad (7)$$

$$\Delta G_r^0(T) = \frac{\Delta G_r^0}{T_{ref}} + \Delta H_r^0 \left(\frac{1}{T} - \frac{1}{T_{ref}} \right) \quad (8)$$

$$K(T) = \frac{a_{HCOO^-_{(aq)}} a_{H_2O_{(aq)}}}{a_{H_{2(aq)}} a_{HCO^-_{3\,(aq)}}} = \frac{e^{\Delta G_r^0(T)}}{RT} \quad (9)$$

with

ν_i: Stoichiometric coefficient of species i in the reaction.
ΔG_{fi}^0 : Standard Gibbs energy of formation of species i.
T_{ref}: Standard state temperature.
T: Temperature of the experiment.
ΔH_r^0 : Standard enthalpy of reaction.
$K(T)$: Equilibrium constant.
a_i: Activity of species i.

3 Results

3.1 Physicochemical monitoring of the gas phase evolution during the experiment

The CH_4-CO_2-benzene/toluene gas mixture was first injected to a total pressure of 62.0 ± 0.6 bar at 36°C, corresponding to 4.54 ± 4.5•10^{-2} moles of CH_4 (results not shown) and 4.58•10–2 ± 4.6•10–4 moles of CO_2 (Figure 1A). After 7 days, mainly due to solubilization, the CO_2 quantity decreased to 3.1•10^{-2} ± 1.5•10^{-3} mol, while the CH_4 quantity remained within the error margin due to its low solubility. On day 7, the piston was lowered to immerse only 1 cm of the solid basket. To compensate for the pressure drop caused by the increase in the cell volume, the initial gas was injected again, resulting in a total quantity of 4.7 ± 2.3•10^{-1} moles of CH_4 and 3.3•10^{-2} ± 1.7•10^{-3} moles of CO_2. Dihydrogen was injected on day 9, with a molar fraction of 2.2 ± 0.1%, corresponding to 1.06•10^{-1} ± 5.3•10^{-3} moles (Figure 1A). On day 17, 353 g of formation water was added to the reactor to prolong the experiment. Following this injection, on day 21, only CO_2 solubilization was significant (2.7•10^{-2} ± 1.4•10^{-3} moles). From day 21 to the end of the experiment (day 105), the H_2 and CO_2 concentrations slowly decreased to 7.6•10^{-2} ± 3.8•10^{-3} and 1.95•10^{-2} ± 9.8•10^{-4} mole, respectively. No significant evolution of CH_4 was noted.

3.2 Physicochemical monitoring of the liquid phase evolution during the experiment

Before injection into the reactor, the formation water contained mostly bicarbonate (2.4•10^{-3} ± 1.2•10^{-4} mol.kg^{-1}) and calcium (Figure 1B; 1.31•10^{-3} ± 6.5•10^{-5} mol.kg^{-1}). Sodium (6.0•10^{-4} ± 3.0•10^{-5} mol.kg^{-1}), magnesium (4.4•10^{-4} ± 2.2•10^{-5} mol.kg^{-1}), chloride (3.0•10^{-4} ± 1.5•10^{-5} mol.kg^{-1}), and sulfate (Figure 1C; 7.0•10^{-4} ± 3.5•10^{-5} mol.kg^{-1}) were also present initially at lower concentrations. Iron and barium were detected at trace levels (6.5•10^{-6} ± 3.2•10^{-7} mol.kg^{-1} and 1.0•10^{-6} ± 5.0•10^{-7} mol.kg^{-1}, respectively). Acetate and formate were not detected. On day 3, after contact between the liquid and solid phases, significant increases in bicarbonate (3.1•10^{-3} ± 1.5•10^{-4} mol.kg^{-1}), calcium (2.88•10^{-3} ± 1.4•10^{-4} mol.kg^{-1}), chloride (1.97•10^{-3} ± 9.84•10^{-5} mol.kg^{-1}) and sulfate (5.9•10^{-4} ± 2.9•10^{-5} mol.kg^{-1}) concentrations were observed. Acetate was first detected on this day (1.82•10^{-4} ± 9•10^{-6} mol.kg^{-1}). From days 3 to 9, before H_2 injection, sulfate molality decreased to 3.7•10^{-4} ± 1.8•10^{-5} mol.kg^{-1}. Furthermore, the bicarbonate, calcium, and acetate concentrations increased to 4.9•10^{-3} ± 2.4•10^{-4} mol.kg^{-1}, 4.1•10^{-3} ± 2.1•10^{-4} mol.kg^{-1}, and 7.0•10^{-4} ± 3.5•10^{-5} mol.kg^{-1}, respectively. The other ion concentrations remained within the margin of error.

After H_2 injection, sulfate molality continued to decrease until total consumption on day 15. On day 21, after the addition of the formation water, several ion molalities increased: Bicarbonate (6.6•10^{-3} ± 3.3•10^{-4} mol.kg^{-1}), calcium (4.8•10^{-3} ± 2.4•10^{-4} mol.kg^{-1}), acetate (1.08•10^{-3} ± 5.4•10^{-5} mol.kg^{-1}) and formate (1.12•10^{-3} ± 5.6•10^{-5} mol.kg^{-1}). After day 21, the bicarbonate and calcium concentrations continued to increase until they reached a plateau on day 28 (7.1•10^{-2} ± 3.6•10^{-4} mol.kg^{-1} and 4.9•10^{-3} ± 2.4•10^{-4} mol.kg^{-1}, respectively). From detection on day 14,

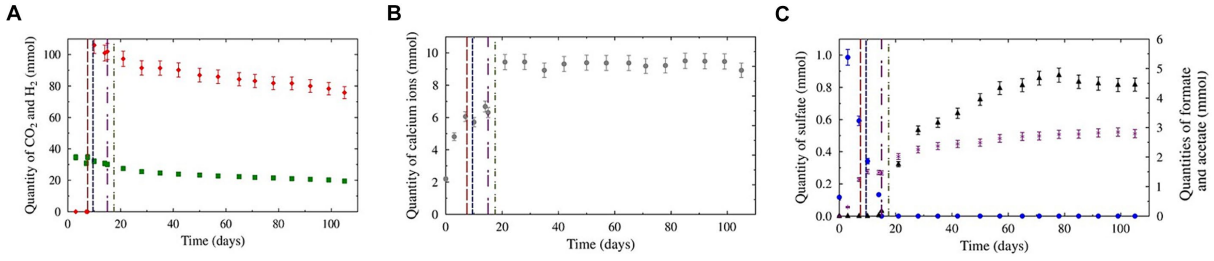

FIGURE 1
Evolution of the aqueous and gaseous phase compositions during the experiments. The red, blue, purple, and green dotted lines represent $CH_4 + CO_2$ gas reinjection, H_2 injection, total sulfate consumption, and formation water addition, respectively. Panel **(A)** represents the evolution of H_2 (red diamonds) and CO_2 (green squares) in the gas phase. Panel **(B)** represents the evolution of sulfate (blue dots), formate (black triangles), and acetate (purple crosses) in the liquid phase. Panel **(C)** represents the evolution of calcium ions in the liquid phase.

10.3389/fmicb.2024.1439866

formate molality steadily increased to a maximum molality of $3.4•10^{-3} \pm 1.7•10^{-4}$ mol.kg^{-1} before slightly decreasing at the end of the experiment ($3.1•10^{-3} \pm 1.5•10^{-4}$ mol.kg^{-1}). Acetate production continued after H_2 injection but at a diminishing rate. At the end of the experiment, the acetate molality stabilized at $1.74•10^{-3} \pm 8.7•10^{-5}$ mol.kg^{-1}. The iron and barium concentrations steadily increased during the experiment, reaching $1.83•10^{-4} \pm 9.14•10^{-6}$ mol.kg^{-1} and $1.95•10^{-5} \pm 9.7•10^{-7}$ mol.kg^{-1}, respectively, at the end of the experiment.

3.3 Benzene and toluene evolution

The quantities of benzene and toluene measured followed the same trends. Benzene and toluene levels in the gases slightly decreased over the first 21 days ($-7•10^{-3} \pm 4•10^{-3}$ mmol between day 3 and day 21 for both benzene and toluene; Figure 2). Afterward, the concentrations obtained were held constant, considering the standard deviations. In the liquid phase, the quantities measured were constant throughout the experiment, considering the standard deviations. A closer look at the behavior of benzene and toluene in the aqueous phase shows that the carbon isotope values for benzene and toluene did not vary within the standard deviations (Table 2). From day 21 onward, the carbon isotope ratios of benzene and toluene slightly changed compared with those determined between day 3 and day 15, when benzene and toluene were enriched by gaseous inputs.

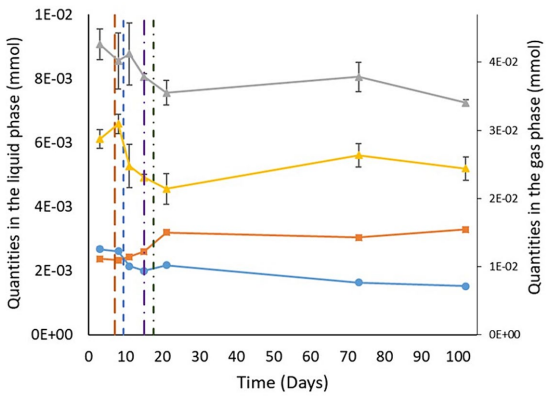

FIGURE 2
Variations in benzene and toluene quantities in the liquid and gas phases. The gray and yellow curves show the evolution of the quantity of benzene and toluene in the gas phase, respectively. The light blue and orange curves correspond to the quantity of benzene and toluene in the liquid phase, respectively. The brown, blue, purple, and green vertical lines indicate $CH_4 + CO_2$ injection, H_2 injection, sulfate total consumption, and formation water reinjection, respectively.

3.4 Microbial community evolution during the experiment

During the experiment, the prokaryotic concentration increased from $2.4•10^4 \pm 4.3•10^3$ copies of *16S rRNA* genes.mL^{-1} at the beginning of the experiment to a maximum of $7.4•10^5 \pm 2.2•10^5$ copies of *16S rRNA* genes.mL^{-1} after 21 days of incubation (Figure 3A). After 105 days of incubation, the average concentration of *16S rRNA* genes was $2.7•10^5 \pm 8.8•10^4$ copies.mL^{-1}. Based on the results of the *dsrB* gene quantification, sulfate reducers were present throughout the experiment despite the total sulfate consumption after day 20. A complementary experiment using *Desulforamulus profundi* Bs107 as a model sulfate reducer demonstrated *dsrB* gene expression even in the absence of sulfate (data not shown). After H_2 injection on day 9, the concentration of sulfate-reducers continuously increased from $4.4•10^2 \pm 6.0•10^1$ (day 9) to $1.0•10^5 \pm 3.1•10^4$ copies of the *dsrB* genes. mL^{-1} (day 43). Based on the *mcrA* gene, methanogens began to be detected on day 10 (1 day after H_2 injection), with $1.8•10^1 \pm 7.7•10^0$ copies of the *mcrA* gene.mL^{-1}. The concentrations of these archaea remained quite low until day 21 (<2.4 10^1 copies of the *mcrA* gene. mL^{-1}). Then, they reached a maximum on day 71, with $1.0•10^4 \pm 3.3•10^3$ copies of the *mcrA* gene.mL^{-1}. Their concentrations remained stable until the end of the experiment. Microbial activity decreased throughout the incubation period (Figure 3B), as did the sulfate-reducing activity. From day 43 onward, methanogens showed increased activity within the microbial community.

The taxonomic diversity of the microbial community was monitored during the experiment by high-throughput sequencing of the *16S rRNA* gene (Figure 4). Initially, the microbial community was dominated by the *Peptococcaceae* (54% relative representativeness), *Gracilibacteraceae* (30%), *Rhizobiaceae* (4%), and *Tannerallaceae* (2%) families (Figure 4A). Just before H_2 injection (day 9) and 1 day after, the largely dominant family was *Peptococcaceae*, with 95% and 94% relative

TABLE 2 Isotopic ratios of benzene and toluene during the experiment.

Day of experiment	$\delta^{13}C/^{12}C$ Isotopic ratio (‰)			
	Liquid phase		Gas phase	
	Benzene	Toluene	Benzene	Toluene
3	−28.4 ± 0.3	−27.25 ± 0.05	−25.9 ± 0.3	−25.94 ± 0.09
8	−28.0 ± 0.6	−27.1 ± 0.1	−26.6 ± 0.4	−25.0 ± 0.2
11	−27.86 ± 0.07	−27.14 ± 0.06	−25.1 ± 0.9	−25.6 ± 0.7
15	−28.0 ± 0.1	−27.2 ± 0.1	−26.1 ± 0.6	−25.88 ± 0.02
21	−27.80 ± 0.06	−27.08 ± 0.09	−26.5 ± 0.5	−25.0 ± 0.2
73	−27.6 ± 0.2	−26.6 ± 0.2	−25.6 ± 0.2	−26.3 ± 0.2
102	−27.5 ± 0.2	−26.5 ± 0.1	−25.5 ± 0.8	−25.3 ± 0.4

10.3389/fmicb.2024.1439866

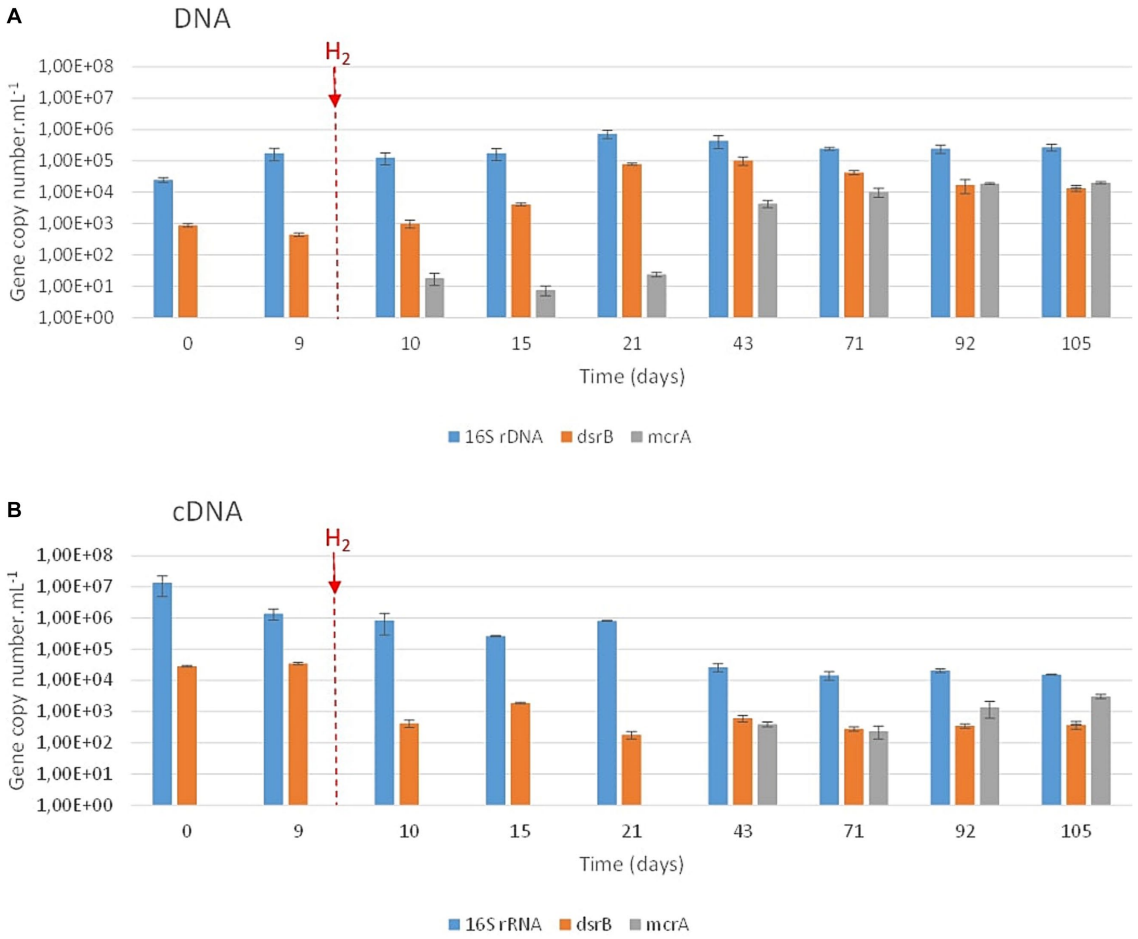

FIGURE 3
qPCR quantification of prokaryotes, sulfate reducers and methanogens over incubation time. The various microbial groups were targeted via the *16S rRNA* (prokaryotes; in blue), *dsrB* (sulfate reducers; in orange) and *mcrA* (methanogens; in gray) genes **(A)** and their transcripts **(B)**. H_2 injection is indicated by the vertical red hatched line.

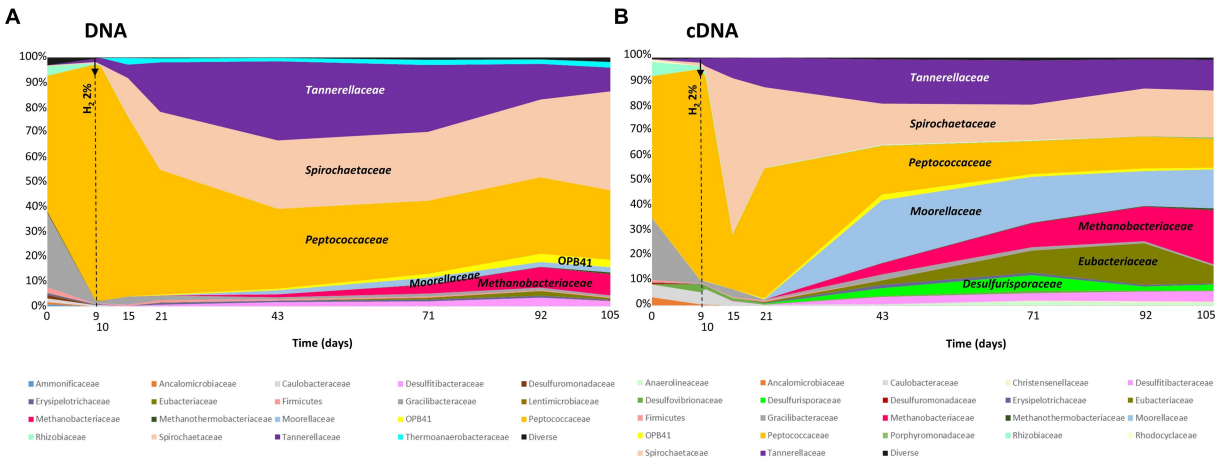

FIGURE 4
Monitoring the taxonomic diversity of microorganisms evolving in the high-pressure reactor during simulated H_2 injection in a deep aquifer used as a UGS. **(A)** Analysis of prokaryotic diversity based on the *16S rRNA* gene; **(B)** Analysis of prokaryotic diversity based on transcripts of the same gene. The results are expressed as relative proportions. The vertical hatched line indicates the day of H_2 injection. The names of the major families are indicated in the figures.

representativeness, respectively. After 21 days of incubation, i.e., 12 days after H_2 injection, the microbial community was dominated by the *Peptococcaceae* (50%), *Spirochaetaceae* (fermentative bacteria; 23%) and *Tannerellaceae* (20%) families. Among the *Spirochaetaceae*, the most abundant ASV could be affiliated with *Rectinema cohabitans* HM (100% identity on 366 nt). By day 43, members of three other families began to grow until day 105: *Anaerosomataceae* (OPB41; 3%), *Moorellaceae* (2%) and *Methanobacteriaceae* (8%). The *Peptococcaceae* family was almost exclusively represented by sulfate-reducing bacteria close to the *Desulforamulus reducens* species until day 10. From day 15, the detection of formate led us to analyze the microbial diversity to identify the producer of this molecule. At this time, bacteria affiliated with a second taxonomic group of *Peptococcaceae* began to grow. This group is phylogenetically close to a strain previously isolated from the same aquifer, Ab_L_15_s1 (377 nt; 100% identity), which has not been described and whose closest genus is *Phosphitispora* (1,348 nt; 94%; personal communication). As incubation progresses, these bacteria became dominant within *Peptococcaceae*, representing 44 to 81% of the sequences affiliated with this family. Finally, a third group of *Peptococcaceae*, close to the sulfate-reducing species *Desulforamulus profundi* Bs107 (377 nt; 100%), developed from day 21 and represented 9 to 13% of the representatives of this family until the end of incubation. Regarding active microorganisms (Figure 4B), in addition to the described families, there were two other families active after H_2 injection: *Tannerellaceae* (fermentative bacteria), *Spirochaetaceae* (fermentative bacteria), *Peptococcaceae* (sulafe reducers and fermenters), *Moorellaceae* (acetogens), *Eubacteriaceae* (fermentative bacteria) and *Desulfurisporaceae* (sulfate reducers). Throughout the experiment, the microbial community was largely dominated by bacteria, and methanogenic archaea accounted for only 8% of the relative representativeness at the end of incubation. Most members of the *Methanobacteriaceae* family are affiliated with the species *Methanobacterium flexile* (381 nt; 100%; accession #NR_116276).

3.5 Solid phase evolution during the experiment

XRD revealed quartz in the initial rock (80%) with calcite (12%), muscovite (4%), and clay minerals, including illite and kaolinite, as well as traces of iron sulfite (marcasite; Figure 5). At the end of the experiment, the same phases were detected. Note that illite clay minerals seemed to increase slightly at the bottom of the basket, while iron sulfides increased in the middle.

SEM–EDS observations showed that the solid phase was mainly composed of quartz (Figure 6). The grains were variably coated with micritic calcite and, to a lesser extent, clays, with both phases commonly mixed. The molding of former micrite grains on the surface of several quartz grains indicated an episode of quartz overgrowth after micrite emplacement. Other minerals presented in trace amounts included iron sulfides and, more rarely, K-rich silicates (identified as muscovite by XRD), barite, rutile, and iron oxides. All these phases were observed as parts of the coatings. Although the well-preserved euhedral morphology of the micrites might have suggested authigenic growth, most of the iron sulfide grains were interpreted as being of detrital origin. No marked changes could be observed before or after the experiment.

3.6 Biochemical modeling

To calculate the extent of each metabolic reaction, the reactions cited in section 2.2.6 were considered during the periods when the microorganisms used were detected. Sulfate reduction, acetogenesis, formate production, and methanogenesis were considered from days 9 to 15, 9 to 105, 9 to 105, and 35 to 105, respectively. From H_2 injection on day 9 to total sulfate consumption, H_2 was consumed only by sulfate reducers ($3.5 \bullet 10^{-3} \pm 1.8 \bullet 10^{-4}$ mol; Figure 7). From day 15, H_2

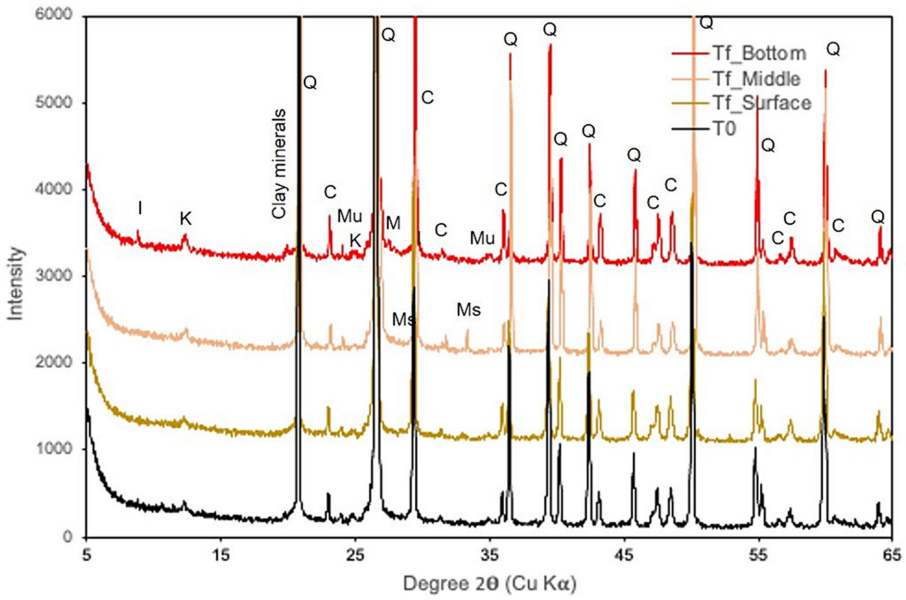

FIGURE 5
X-ray diffraction patterns of samples collected at the beginning (T_0) and at the end of the experiment (T_f) at various reactor depths. I, illite; K, kaolinite; Q, quartz; C, calcite; Mu, muscovite; Ms., Marcasite.

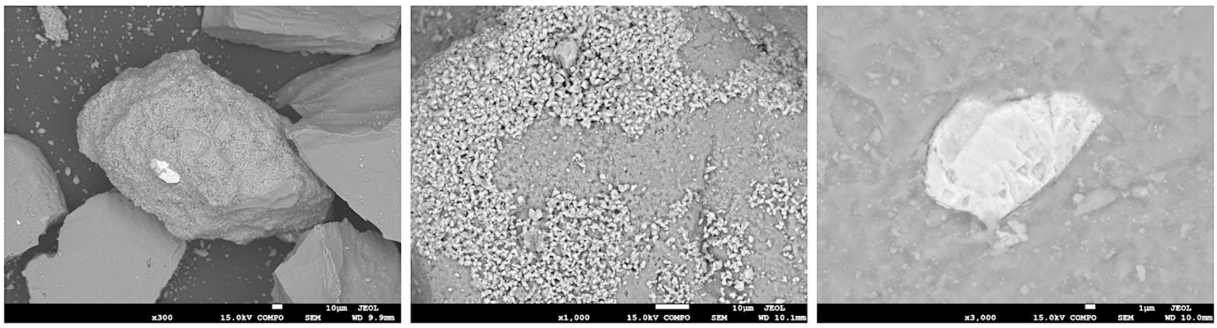

FIGURE 6
SEM image of variably coated quartz grains. Note the presence of an iron sulfide grain in white (left). Close-up of micrite grains forming a quartz grain coating, with molds of former micrite grains on the quartz surface (middle). Close-up of an iron sulfide grain of detrital origin partially embedded in quartz (right).

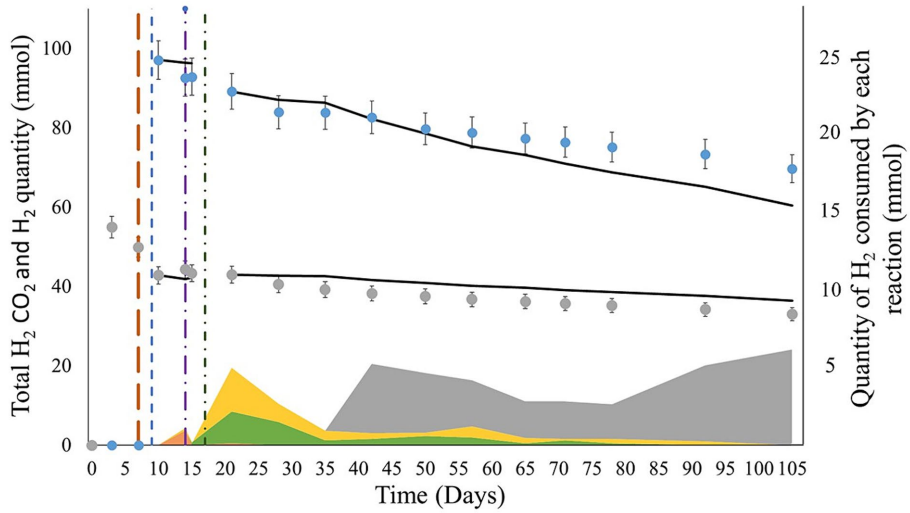

FIGURE 7
Comparison of the evolution of the experimental and modeled H_2 and CO_2 quantities during the experiments. The blue and gray dots represent the evolution of the total experimental quantities of H_2 and CO_2 (liquid + gas phase), respectively. The black curves show the quantities of H_2 and CO_2 modeled by calculating the extent of the reaction. The brown, blue, purple, and green vertical lines indicate the $CH_4 + CO_2$ gas mix reinjection, H_2 injection, total sulfate consumption, and formation water reinjection, respectively. The orange, yellow, green, and gray areas correspond to the H_2 quantities consumed by sulfate reduction, acetogenesis, formate production, and methanogenesis, respectively, between each measuring point.

was consumed through acetogenesis ($5.4 \bullet 10^{-3} \pm 2.7 \bullet 10^{-4}$ mol) and formate production ($4.5 \bullet 10^{-3} \pm 2.2 \bullet 10^{-4}$ mol). From day 35 to the end of the experiment, methanogenesis explained most of the H_2 consumption ($2.5 \bullet 10^{-2} \pm 5.0 \bullet 10^{-3}$ mol). Overall, methanogenesis was the primary source of H_2 consumption. While H_2S was not detected in the gas phase, based on sulfate reduction after day 9, $8.8 \bullet 10^{-4} \pm 4.4 \bullet 10^{-4}$ mol of sulfide should have been produced.

3.7 *In situ* characterization protocol

On the first sampling with this protocol, on day 28, the pH obtained was 6.0 (Figure 8). This value did not significantly evolve throughout the experiment, as the evolution of the solution composition was slow. All the pH values were between 6.0 and 6.1. The values measured at atmospheric pressure were between 6.6 and 7.2. Gas solubilization caused acidification of the solution. The carbon and hydrogen Nernst potentials were distinct, directly showing the lack of equilibrium among the redox couples. For pH, the values were stable for each potential. The carbon and hydrogen ranged from −439 to −430 mV and −577 and −572 mV, respectively. The uncertainty of these values was calculated with the combined uncertainties of the measures used in this protocol. The uncertainty of the pH was ±0.1 and was mainly due to the uncertainty in the quantity of CO_2 and bicarbonate. The uncertainty of the Nernst potential was ±10 mV, which was caused mainly by the uncertainty of the pH.

4 Discussion

The H_2 geological storage simulated in this experiment has the particularity of targeting a low-salt aquifer (Ab_L_1) with sulfate

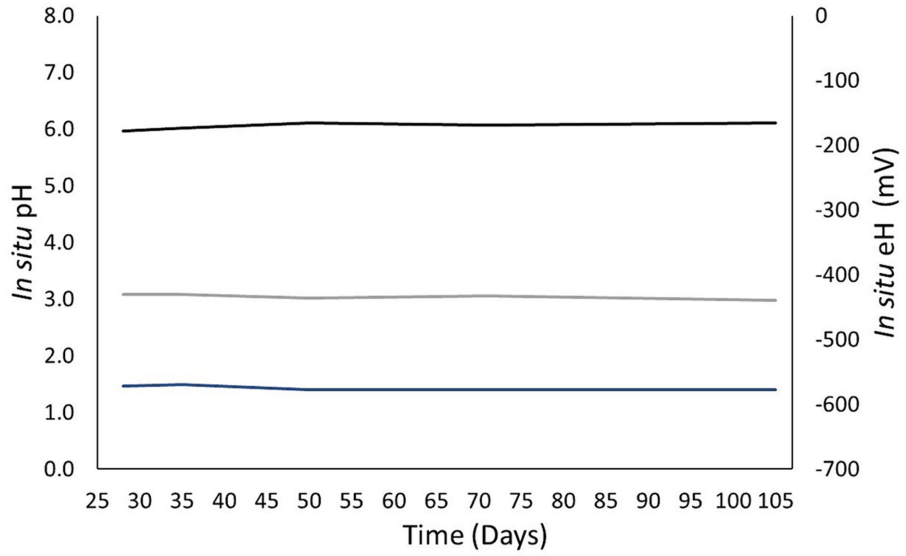

FIGURE 8
Evolution of the *in situ* pH and oxidoreduction potential computed with the *in situ* characterization protocol developed in this work. The black curve represents the calculated pH. The gray and blue curves correspond to the carbon and hydrogen redox potentials calculated by the Nernst equation.

concentrations below 7 mg. L^{-1} (Haddad et al., 2022a, 2023). At the beginning of incubation, the gas phase consisted of 99% CH_4, 1% CO_2, 7.95 ppm benzene, and 3.57 ppm toluene at a pressure of 60 bar and a temperature of 36°C. Some of the CO_2 rapidly solubilized in water. Storage of the aquifer formation water containing the microorganisms most certainly resulted in an evolution in its taxonomic composition, although the sample was kept at 4°C to slow metabolism.

4.1 Sulfate and acetate evolution

In the formation water, sulfate was the main external electron acceptor available to microorganisms and was most certainly depleted, explaining why, at the beginning of the experiment, the microbial community was largely dominated by bacteria capable of fermenting the organic molecules present or necromass. Among these microorganisms, the amplicon sequence variants (ASVs) grouped in the *Peptococcaceae* family were, for the most part, affiliated with the sulfate-reducing *Desulforamulus reducens* species, described as being capable of fermenting simple compounds, such as pyruvate (Visser et al., 2016). At the beginning of incubation, the microbial community returned to conditions close to those *in situ* (temperature, pressure, rock, etc.) with a gas phase simulating natural gas storage. *D. reducens* was the main sulfate reducer present, completely consuming 0.99 mmol of sulfate in just 15 days. This sulfate reducer likely operated mainly heterotrophically prior to H_2 injection. This species has been shown to incompletely oxidize organic molecules serving as carbon sources (Visser et al., 2016) and could therefore be one of the sources of acetate. Furthermore, the measured sulfate consumption (0.6 mmol) and acetate production (1.2 mmol) between days 3 and 10 are consistent with this metabolic stoichiometry (Daumas et al., 1993). This metabolic activity could also partly explain bicarbonate production in the incubation phase. Members of the *Gracillibacteriaceae* and *Spirochaetaceae* (i.e., *Rectinema cohabitans*) families also participate in acetate production via fermentation (Lee et al., 2006; Haddad et al., 2022b). As soon as sulfate was depleted, the relative abundance of *D. ramulus* species declined sharply from almost 100% of the relative abundance of *Peptococcaceae* to 7%.

4.2 Formate evolution

Formate began to be detected on day 15, i.e., 6 days after H_2 injection. Previous studies have shown that formate appears very quickly after H_2 addition under conditions similar to those in our experiment (Haddad et al., 2022b; Mura et al., 2024). In this study, however, sulfate was depleted by day 15. Based on the work of Visser and collaborators (2016), we hypothesize that *D. reducens* can use formate produced between days 9 and 15 as a carbon source as long as sulfate is present as an electron acceptor. This would explain the apparent delay in formate production in this experiment and the sharp increase between days 15 and 21. For the formate source, *Peptococcaceae*, close to strain Ab_L_15_s1, developed from day 15 and remained active until the end of incubation. As hypothesized, pressure incubation with CO_2 is thought to promote formate production during acetogenesis (Haddad et al., 2022b; Mura et al., 2024). The *Peptococcaceae* strain Ab_L_15_s1 could therefore be a good candidate in the search for the microorganism responsible for formate production in this study. The low equilibrium constant for formate production (Stams, 1994) could explain why formate was not observed in near atmospheric pressure experiments. Formate production at high pressure could be triggered by equilibrium displacement due to high H_2 partial pressure. Under the conditions of this study, the calculated equilibrium molality of formate enabled by thermodynamic equilibrium just after H_2 injection (day 14) was 6.7 mmol.kg^{-1}, whereas this value would be negligible for the same H_2 molar fraction at atmospheric pressure (0.1 mmol.kg^{-1}). This could explain why formate is not detected in near atmospheric pressure experiments. The decrease

in the formate production rate observed at the end of the experiment could be caused by thermodynamic constraints as the reaction approaches equilibrium (Jin and Bethke, 2005). Finally, the species *Methanobacterium flexile*, family *Methanobacteriaceae*, has been described to utilize H_2/CO_2 or formate (Zhu et al., 2011). Moreover, methanogenesis is an alkalinity-producing metabolic process. It was previously described that H_2 or formate utilization in *Methanococcus thermolithotrophicus* was pH dependent, with formate utilization favored at higher pH (Belay et al., 1986). However, pH monitoring in the bulk appeared to be constant throughout the experiment (pH 6.0–6.1). Different pH values cannot be ruled out in microniches with different rock porosities, but this cannot be verified. Another hypothesis could be that formate consumers need time to adapt. Notably, the members of the OPB41 taxon (family *Anaerosomataceae*), detected from day 43 onward, have been shown to grow lithotrophically on H_2 or formate (Khomyakova et al., 2022).

4.3 Evolution of CO_2, H_2, CH_4, and H_2S

The physicochemical monitoring of CO_2, H_2, CH_4 and H_2S throughout the experiment revealed no substantial changes. Although it was not possible to measure the production of CH_4 and H_2S, it is nevertheless certain that these molecules were produced by microbial metabolism. Fermentation products include CO_2, H_2, and organic acids such as acetate. Furthermore, the modeled H_2 consumption based on sulfate-reduction, methanogenesis, acetogenesis and formate production extents of reaction was overestimated, which could support the fact that fermenters produced H_2. Methanogens produced methane, as the calculated extent of acetogenesis was insufficient to explain the global CO_2 consumption. As for methanogens, they obviously produced methane, as the calculated acetogenesis extent of reaction was insufficient to explain the global CO_2 consumption. Extents of reaction calculations suggest that methanogenesis was responsible for the major part of H_2 consumption. As in a study (Haddad et al., 2022b) with a similar sulfate concentration before H_2 injection (1.2 mM), H_2S was not detected in the gas phase. The low but continuous release of iron during the experiment and the detection of a potentially greater amount of marcasite at the end of the experiment suggest the attenuation of sulfide by iron sulfide precipitation. We hypothesize that this release could occur by partial dissolution of iron-bearing minerals, possibly aluminosilicates and/or clays.

4.4 Calcite dissolution

Calcium and bicarbonate release in the aqueous phase occurred only during the incubation phase, implying that calcite dissolution was triggered by the equilibration of the formation water with the rock. Indeed, the calculated *in situ* pH was two units lower than the measured pH of the initial water mix at atmospheric pressure, mainly because of CO_2 degassing during the depressurization of the bottom hole samplers. We hypothesize that calcite precipitated during formation water sampling and dissolved after the initial CO_2 injection. Thus, this phenomenon was not linked to H_2 injection and should not lead to porosity changes in the reservoir. Globally, changes in mineralogy remain small and do not indicate a risk of variation in the petrological properties during storage.

4.5 Benzene and toluene evolution

Benzene and toluene were added to the gas phase to obtain conditions similar to those in the field (Aüllo et al., 2016). These monoaromatic compounds are also present in water due to thermodynamic equilibrium. These compounds were monitored in both the liquid and gas phases. The variations observed during the first few days could be caused by adsorption on the solid surface and the liquid–vapor equilibrium. The isotopic values of carbon fluctuate around -27.9 ± 0.3 ‰ and -27.0 ± 0.3 ‰ for benzene and toluene, respectively, in water, which does not indicate enrichment or depletion. The conditions of the experiment (duration and addition of water and gas containing benzene and toluene) impact the evidence of biodegradation, as the concentration of benzene and toluene in the water depends on the thermodynamic equilibrium with the gas phase (Darracq et al., 2009). The experiment did not last long enough to demonstrate biodegradation, as benzene degradation by sulfate-reducing bacteria is slow compared to other metabolic processes (Mancini et al., 2003).

4.6 Fate of a UGS coinjected with 2% H_2

In this study, the scenario tested was the coinjection of 2% H_2 with a gas mixture simulating natural gas (99% CH_4, 1% CO_2, traces of BT). Without an anomaly, the storage site we experimentally simulated is in a low-salt water and, therefore, has a very low sulfate concentration. Deep aquifers are oligotrophic, and the presence of natural gas in the vicinity has been shown to increase microbial activity, particularly sulfate reduction, due to the dissolved organic molecules of the gas in the formation water, even if some of these molecules are recalcitrant to biodegradation (Ranchou-Peyruse et al., 2019). Thus, even the sulfate renewed by the slow recharge of water could not compensate for the decrease in its concentration over the years. During massive H_2 injection, it is therefore expected that the only two electron acceptors will be sulfate and CO_2. In view of the results presented here, it seems likely that sulfate will be depleted very quickly since there are few sulfated minerals (Figure 1). A nonnegligible proportion of the sulfide will remain trapped in the rock as iron sulfide (Figure 6). This means that the last available electron acceptor remaining, and therefore a limiting growth factor, will be CO_2. Dihydrogen and CO_2 are then consumed by acetogenic and methanogenic microorganisms. In our case, this consumption appeared to be limited over the incubation period of approximately 3 months. There are other limiting nutrients that slow microbial development and seem to prevent it from exceeding a maximum concentration of microorganisms (Figure 3). The low metabolic efficiency of sulfate reduction, acetogenesis, and methanogenesis observed here contrasts with results for other UGSs simulated in high-pressure reactors and showing alkalinization phenomena (Haddad et al., 2023; Mura et al., 2024).

5 Conclusion

In this study, the injection of a natural gas/H_2 blend (98% / 2%) in a low-salinity aquifer was simulated in a high-pressure reactor. This work provides more data for understanding H_2 behavior in deep aquifers and helps researchers understand the parameters affecting site variations. Overall, this experiment suggested that H_2

coinjection with natural gas in this UGS could be viable due to several factors:

- Contrary to experiments using the same protocol, while sulfate reducers and methanogens were active, only a minor amount of H_2 was consumed over the 3 months of the experiment. This probably occurred due to a lack of nutrients.
- Dissolution and precipitation of minerals likely occurred but were not formally detected. As for other experiments, the impact of H_2 on the aquifer porous rock is negligible, as no significant changes were observed in the XRD and SEM analyses.
- After initial CO_2 solubilization from the injected CH_4/CO_2/benzene/toluene gas mixture, no significant changes in the reactor *in situ* pH or redox potential were observed due to low microbial activity. Thus, calcium or magnesium carbonate precipitation was prevented.

Although we identified key parameters for viable H_2 costorage in deep aquifers, quantitative extrapolation of these results to the reservoir remains a challenge due to scale effects. Notably, the conditions simulated in the reactor represent those encountered near the gas bubble, but due to transport phenomena, the conditions far from the gas bubble could be very different. Thus, the modeling of pilot-scale studies will be essential for accurate feed reservoir simulations of H_2 costorage in aquifers.

Data availability statement

The datasets presented in this study can be found in online repositories. The names of the repository/repositories and accession number(s) can be found at: https://www.ncbi.nlm.nih.gov/, PRJNA1117242.

Author contributions

JM: Writing – review & editing, Writing – original draft, Visualization, Software, Methodology, Investigation, Formal analysis, Data curation. MR-P: Writing – review & editing, Writing – original draft, Visualization, Validation, Supervision, Methodology, Investigation, Formal analysis, Data curation, Conceptualization. MG: Writing – original draft, Methodology, Investigation, Formal analysis, Data curation. MD: Writing – original draft, Supervision, Methodology, Data curation. ML: Writing – original draft, Methodology, Investigation, Data curation. M-PI: Writing – review & editing, Writing – original draft, Visualization, Validation, Methodology, Investigation, Data curation. IH: Writing – review & editing, Writing – original draft, Validation, Methodology, Investigation, Data curation. GH: Writing – review & editing, Writing – original draft, Validation, Methodology, Investigation, Data curation. MP: Writing – original draft, Methodology, Investigation, Data curation. MdSB: Writing – original draft, Methodology, Investigation, Data curation. PCh: Writing – original draft, Validation, Resources, Funding acquisition, Conceptualization. GC: Writing – original draft, Validation, Resources, Funding acquisition, Conceptualization. AP: Writing – original draft, Validation, Resources, Investigation, Funding acquisition, Conceptualization. PCe: Writing – review & editing, Writing – original draft, Validation, Supervision, Resources, Project administration, Methodology, Investigation, Funding acquisition, Conceptualization. AR-P: Writing – review & editing, Writing – original draft, Visualization, Validation, Supervision, Resources, Project administration, Methodology, Investigation, Funding acquisition, Formal analysis, Conceptualization.

Funding

The author(s) declare that financial support was received for the research, authorship, and/or publication of this article. MR-P salary was supported by E2S-UPPA.

Acknowledgments

Teréga and Storengy are acknowledged for funding this research project. We are grateful to the Genotoul platform (genotoul.fr) for the sequencing analyses.

Conflict of interest

PCh, GC, and AP were employed by two French companies specialized in geological natural gas storage which are Teréga and Storengy.

The remaining authors declare that the research was conducted in the absence of any commercial or financial relationships that could be construed as a potential conflict of interest.

Publisher's note

References

Aghaei, H., Al-Yaseri, A., Toorajipour, A., Shahsavani, B., Yekeen, N., and Edlmann, K. (2023). Host-rock and caprock wettability during hydrogen drainage: implications of hydrogen subsurface storage. *Fuel* 351:129048. doi: 10.1016/j.fuel.2023.129048

Ali, M., Arif, M., Sedev, R., Sánchez-Román, M., Keshavarz, A., and Iglauer, S. (2023). Underground hydrogen storage: the microbiotic influence on rock wettability. *J. Energy Storage* 72:108405. doi: 10.1016/j.est.2023.108405

Amid, A., Mignard, D., and Wilkinson, M. (2016). Seasonal storage of hydrogen in a depleted natural gas reservoir. *Int. J. Hydrogen Energy* 41, 5549–5558. doi: 10.1016/j.ijhydene.2016.02.036

Aüllo, T., Berlendis, S., Lascourrèges, J.-F., Dessort, D., Duclerc, D., Saint-Laurent, S., et al. (2016). New bio-indicators for long term natural attenuation of Monoaromatic compounds in deep terrestrial aquifers. *Front. Microbiol.* 7:122. doi: 10.3389/fmicb.2016.00122

Belay, N., Sparling, R., and Daniels, L. (1986). Relationship of formate to growth and methanogenesis by *Methanococcus thermolithotrophicus*. *Appl. Environ. Microbiol.* 52, 1080–1085. doi: 10.1128/aem.52.5.1080-1085.1986

Berg, M., Bolotin, J., and Hofstetter, T. B. (2007). Compound-specific nitrogen and carbon isotope analysis of nitroaromatic compounds in aqueous samples using solid-phase microextraction coupled to GC/IRMS. *Anal. Chem.* 79, 2386–2393. doi: 10.1021/ac0622577

Blanc, P., Lassin, A., Piantone, P., Azaroual, M., Jacquemet, N., Fabbri, A., et al. (2012). Thermoddem: a geochemical database focused on low temperature water/rock interactions and waste materials. *Appl. Geochem.* 27, 2107–2116. doi: 10.1016/j.apgeochem.2012.06.002

Bo, Z., Boon, M., Hajibeygi, H., and Hurter, S. (2023). Impact of experimentally measured relative permeability hysteresis on reservoir-scale performance of underground hydrogen storage (UHS). *Int. J. Hydrogen Energy* 48, 13527–13542. doi: 10.1016/j.ijhydene.2022.12.270

Bolyen, E., Rideout, J. R., Dillon, M. R., Bokulich, N. A., Abnet, C. C., Al-Ghalith, G. A., et al. (2019). Reproducible, interactive, scalable and extensible microbiome data science using QIIME 2. *Nat. Biotechnol.* 37, 852–857. doi: 10.1038/s41587-019-0209-9

Buscheck, T. A., Goodman, A., Lackey, G., De Toledo Camargo, J., Huerta, N., Haeri, F., et al. (2023). Underground storage of hydrogen and hydrogen/methane mixtures in porous reservoirs: influence of reservoir factors and engineering choices on deliverability and storage operations. *Int. J. Hydrogen Energy* 49, 1088–1107. doi: 10.1016/j.ijhydene.2023.07.073

Buzek, F., Onderka, V., Vancura, P., and Wolf, I. (1994). Carbon isotope study of methane production in a town gas storage reservoir. *Fuel* 73, 747–752. doi: 10.1016/0016-2361(94)90019-1

Callahan, B. J., McMurdie, P. J., Rosen, M. J., Han, A. W., Johnson, A. J. A., and Holmes, S. P. (2016). DADA2: high-resolution sample inference from Illumina amplicon data. *Nat. Methods* 13, 581–583. doi: 10.1038/nmeth.3869

Chai, M., Chen, Z., Nourozieh, H., and Yang, M. (2023). Numerical simulation of large-scale seasonal hydrogen storage in an anticline aquifer: a case study capturing hydrogen interactions and cushion gas injection. *Appl. Energy* 334:120655. doi: 10.1016/j.apenergy.2023.120655

Darracq, G., Couvert, A., Couriol, C., Amrane, A., and Le Cloirec, P. (2009). Absorption and biodegradation of hydrophobic volatile organic compounds: determination of Henry's constants and biodegradation levels. *Water Sci. Technol.* 59, 1315–1322. doi: 10.2166/wst.2009.124

Daumas, S., Magot, M., and JL, C. (1993). Measurement of the net production of acidity by a sulphate-reducing bacterium: experimental checking of theoretical models of microbiaily influenced corrosion. *Res. Microbiol.* 144, 327–332.

Dohrmann, A. B., and Krüger, M. (2023). Microbial H2 consumption by a formation fluid from a natural gas Field at high-pressure conditions relevant for underground H2 storage. *Environ. Sci. Technol.* 57, 1092–1102. doi: 10.1021/acs.est.2c07303

Dopffel, N., Jansen, S., and Gerritse, J. (2021). Microbial side effects of underground hydrogen storage – knowledge gaps, risks and opportunities for successful implementation. *Int. J. Hydrogen Energy* 46, 8594–8606. doi: 10.1016/j.ijhydene.2020.12.058

Dopffel, N., Mayers, K., Kedir, A., Alagic, E., An Stepec, B., Djurhuus, K., et al. (2023). Microbial hydrogen consumption leads to a significant pH increase under high-saline-conditions: implications for hydrogen storage in salt caverns. *Sci. Rep.* 13:10564. doi: 10.1038/s41598-023-37630-y

Dupraz, S., Parmentier, M., Ménez, B., and Guyot, F. (2009). Experimental and numerical modeling of bacterially induced pH increase and calcite precipitation in saline aquifers. *Chem. Geol.* 265, 44–53. doi: 10.1016/j.chemgeo.2009.05.003

Ebrahimiyekta, A. (2017). Characterization of geochemical interactions and migration of hydrogen in sandstone sedimentary formations: Application to geological storage. (Doctoral dissertation, Université d'Orléans)

Eddaoui, N., Panfilov, M., Ganzer, L., and Hagemann, B. (2021). Impact of pore clogging by Bacteria on underground hydrogen storage. *Transp. Porous Media* 139, 89–108. doi: 10.1007/s11242-021-01647-6

Fillinger, L., Griebler, C., Hellal, J., Joulian, C., and Weaver, L. (2023). "Chapter 9—microbial diversity and processes in groundwater" in Groundwater ecology and evolution. eds. F. Malard, C. Griebler and S. Rétaux. *2nd* ed (San Diego: Academic Press), 211–240.

Fischer, A., Manefield, M., and Bombach, P. (2016). Application of stable isotope tools for evaluating natural and stimulated biodegradation of organic pollutants in field studies. *Curr. Opin. Biotechnol.* 41, 99–107. doi: 10.1016/j.copbio.2016.04.026

Geets, J., Borremans, B., Diels, L., Springael, D., Vangronsveld, J., van der Lelie, D., et al. (2006). DsrB gene-based DGGE for community and diversity surveys of sulfate-reducing bacteria. *J. Microbiol. Methods* 66, 194–205. doi: 10.1016/j.mimet.2005.11.002

Gelencsér, O., Árvai, C., Mika, L., Breitner, D., Leclair, D., Szabo, C., et al. (2023). Effect of hydrogen on calcite reactivity in sandstone reservoirs: experimental results compared to geochemical modeling predictions. *J. Energy Storage* 61:106737. doi: 10.1016/j.est.2023.106737

Gregory, S. P., Barnett, M. J., Field, L. P., and Milodowski, A. E. (2019). Subsurface microbial hydrogen cycling: natural occurrence and implications for industry. *Microorganisms* 7:53. doi: 10.3390/microorganisms7020053

Gu, Z. (2022). Complex heatmap visualization. *iMeta* 1:e43. doi: 10.1002/imt2.43

Gu, Z., Eils, R., and Schlesner, M. (2016). Complex heatmaps reveal patterns and correlations in multidimensional genomic data. *Bioinformatics* 32, 2847–2849. doi: 10.1093/bioinformatics/btw313

Haddad, P. G., Mura, J., Castéran, F., Guignard, M., Ranchou-Peyruse, M., Sénéchal, P., et al. (2022a). Biological, geological and chemical effects of oxygen injection in underground gas storage aquifers in the setting of biomethane deployment. *Sci. Total Environ.* 806:150690. doi: 10.1016/j.scitotenv.2021.150690

Haddad, P. G., Ranchou-Peyruse, M., Guignard, M., Mura, J., Casteran, F., Ronjon-Magand, L., et al. (2022b). Geological storage of hydrogen in deep aquifers – an experimental multidisciplinary study. *Energ. Environ. Sci.* 15, 3400–3415. doi: 10.1039/D2EE00765G

Haddad, P. G., Ranchou-Peyruse, M., Guignard, M., Mura, J., Castéran, F., Sénéchal, P., et al. (2023). Physicochemical and microbiological effects of geological biomethane storage in deep aquifers: introduction of O_2 as a cocontaminant. *Environ. Sci. Adv.* 2, 1727–1738. doi: 10.1039/D3VA00086A

Hagemann, B., Rasoulzadeh, M., Panfilov, M., Ganzer, L., and Reitenbach, V. (2016). Hydrogenization of underground storage of natural gas: impact of hydrogen on the hydrodynamic and bio-chemical behavior. *Comput. Geosci.* 20, 595–606. doi: 10.1007/s10596-015-9515-6

Harati, S., Rezaei Gomari, S., Ramegowda, M., and Pak, T. (2023). Multi-criteria site selection workflow for geological storage of hydrogen in depleted gas fields: a case for the UK. *Int. J. Hydrogen Energy*. doi: 10.1016/j.ijhydene.2023.10.345

Heinemann, N., Scafidi, J., Pickup, G., Thaysen, E. M., Hassanpouryouzband, A., Wilkinson, M., et al. (2021). Hydrogen storage in saline aquifers: the role of cushion gas for injection and production. *Int. J. Hydrogen Energy* 46, 39284–39296. doi: 10.1016/j.ijhydene.2021.09.174

Hemme, C., and Van Berk, W. (2018). Hydrogeochemical modeling to identify potential risks of underground hydrogen storage in depleted gas fields. *Appl. Sci.* 8:2282. doi: 10.3390/app8112282

Hogeweg, S., Strobel, G., and Hagemann, B. (2022). Benchmark study for the simulation of underground hydrogen storage operations. *Comput. Geosci.* 26, 1367–1378. doi: 10.1007/s10596-022-10163-5

Hunkeler, D., Meckenstock, R. U., Sherwood Lollar, B., Schmidt, T. C., Wilson, J. T., Schmidt, T., et al. (2008). Report NO: EPA 600/R-08/148. A guide for assessing biodegradation and source identification of organic ground water contaminants using compound specific isotope analysis (CSIA): US EPA Ada.

Ioka, S., Sakai, T., Igarashi, T., and Ishijima, Y. (2011). Long-term continuous in situ potentiometrically measured redox potential in anoxic groundwater with high methane and iron contents. *Environ. Earth Sci.* 64, 143–149. doi: 10.1007/s12665-010-0830-x

Izadi Amiri, I., Zivar, D., Ayatollahi, S., and Mahani, H. (2024). The effect of gas solubility on the selection of cushion gas for underground hydrogen storage in aquifers. *J. Energy Storage* 80:110264. doi: 10.1016/j.est.2023.110264

Jacquemet, N., Chiquet, P., and Grauls, A. (2020). Hydrogen reactivity with (1) a well cement-PHREEQC geochemical thermodynamics calculations. In: *1st geoscience & engineering in energy transition conference. Vol. 2020* European Association of Geoscientists & Engineers. 1–5.

Jadhawar, P., and Saeed, M. (2023a). Mechanistic evaluation of the reservoir engineering performance for the underground hydrogen storage in a deep North Sea aquifer. *Int. J. Hydrogen Energy* 50, 558–574. doi: 10.1016/j.ijhydene.2023.07.272

Jadhawar, P., and Saeed, M. (2023b). Optimizing the operational efficiency of the underground hydrogen storage scheme in a deep North Sea aquifer through compositional simulations. *J. Energy Storage* 73:108832. doi: 10.1016/j.est.2023.108832

Jin, Q., and Bethke, C. M. (2005). Predicting the rate of microbial respiration in geochemical environments. *Geochim. Cosmochim. Acta* 69, 1133–1143. doi: 10.1016/j.gca.2004.08.010

Kassambara, A., and Mundt, F. (2020). factoextra: Extract and Visualize the Results of Multivariate Data Analyses. Available at: https://cran.r-project.org/web/packages/factoextra/index.html (Accessed 30 January 2024).

Khomyakova, M. A., Zavarzina, D. G., Merkel, A. Y., Klyukina, A. A., Pikhtereva, V. A., Gavrilov, S. N., et al. (2022). The first cultivated representatives of the actinobacterial lineage OPB41 isolated from subsurface environments constitute a novel order Anaerosomatales. *Front. Microbiol.* 13:1047580. doi: 10.3389/fmicb.2022.1047580

Lê, S., Josse, J., and Husson, F. (2008). FactoMineR: An *R* package for multivariate analysis. *J. Stat. Softw.* 25:i01. doi: 10.18637/jss.v025.i01

Lee, Y.-J., Romanek, C. S., Mills, G. L., Davis, R. C., Whitman, W. B., and Wiegel, J. (2006). *Gracilibacter thermotolerans* gen. Nov., sp. nov., an anaerobic, thermotolerant bacterium from a constructed wetland receiving acid sulfate water. *Int. J. Syst. Evol. Microbiol.* 56, 2089–2093. doi: 10.1099/ijs.0.64040-0

Li, Z., Wang, X., Li, L., Zhang, M., Tao, M., Xing, L., et al. (2014). Development of new method of δ13C measurement for trace hydrocarbons in natural gas using solid phase

micro-extraction coupled to gas chromatography isotope ratio mass spectrometry. *J. Chromatogr. A* 1372, 228–235. doi: 10.1016/j.chroma.2014.10.089

Liebscher, A., Wackerl, J., and Streibel, M. (2016). "Geologic storage of hydrogen—fundamentals, processing, and projects" in Hydrogen science and engineering: Materials, processes, systems and technology. eds. D. Stolten and B. Emonts (USA: Wiley), 629–658.

Lindberg, R. D., and Runnells, D. D. (1984). Ground water redox reactions: An analysis of equilibrium state applied to eh measurements and geochemical modeling. *Science* 225, 925–927. doi: 10.1126/science.225.4665.925

Liu, N., Kovscek, A. R., Fernø, M. A., and Dopffel, N. (2023). Pore-scale study of microbial hydrogen consumption and wettability alteration during underground hydrogen storage. *Front. Energy Res.* 11:1124621. doi: 10.3389/fenrg.2023.1124621

Logroño, W., Nikolausz, M., Harms, H., and Kleinsteuber, S. (2022). Physiological effects of 2-Bromoethanesulfonate on Hydrogenotrophic pure and mixed cultures. *Microorganisms* 10:355. doi: 10.3390/microorganisms10020355

Lysyy, M., Fernø, M. A., and Ersland, G. (2023). Effect of relative permeability hysteresis on reservoir simulation of underground hydrogen storage in an offshore aquifer. *J. Energy Storage* 64:107229. doi: 10.1016/j.est.2023.107229

Mancini, S. A., Ulrich, A. C., Lacrampe-Couloume, G., Sleep, B., Edwards, E. A., and Lollar, B. S. (2003). Carbon and hydrogen isotopic fractionation during anaerobic biodegradation of benzene. *Appl. Environ. Microbiol.* 69, 191–198. doi: 10.1128/AEM.69.1.191-198.2003

Maniglio, M., Rivolta, G., Elgendy, A., Panfili, P., and Cominelli, A. (2023). Evaluating the impact of biochemical reactions on H2 storage in depleted gas fields., (OnePetro). In: *Paper presented at the SPE Annual Technical Conference and Exhibition*, San Antonio, Texas, USA

McMurdie, P. J., and Holmes, S. (2013). Phyloseq: An R package for reproducible interactive analysis and graphics of microbiome census data. *PLoS One* 8:e61217. doi: 10.1371/journal.pone.0061217

Muller, E., Julia, G., Sissmann, O., Tafit, A., and Poirier, S. (2023). Changes in hydrogen conversion kinetics and microbial response to variations in temperature and mineralogy., in *Goldschmidt 2023 Conference*, (GOLDSCHMIDT).

Mura, J., Ranchou-Peyruse, M., Guignard, M., Haddad, P. G., Ducousso, M., Casteran, F., et al. (2024). Comparative study of three H2 geological storages in deep aquifers simulated in high-pressure reactors. *Int. J. Hydrogen Energy* 63, 330–345. doi: 10.1016/j.ijhydene.2024.02.322

Pan, B., Liu, K., Ren, B., Zhang, M., Ju, Y., Gu, J., et al. (2023). Impacts of relative permeability hysteresis, wettability, and injection/withdrawal schemes on underground hydrogen storage in saline aquifers. *Fuel* 333:126516. doi: 10.1016/j.fuel.2022.126516

Panfilov, M. (2010). Underground storage of hydrogen: in situ self-organisation and methane generation. *Transp. Porous Media* 85, 841–865. doi: 10.1007/s11242-010-9595-7

Parkhurst, D. L., and Appelo, C., and others (2013). Description of input and examples for PHREEQC version 3—a computer program for speciation, batch-reaction, one-dimensional transport, and inverse geochemical calculations. US Geol. Surv. Tech. Methods 6:497.

Pastore, L. M., Lo Basso, G., Quarta, M. N., and de Santoli, L. (2022). Power-to-gas as an option for improving energy self-consumption in renewable energy communities. *Int. J. Hydrogen Energy* 47, 29604–29621. doi: 10.1016/j.ijhydene.2022.06.287

Peng, D.-Y., and Robinson, D. B. (1976). A new two-constant equation of state. *Ind. Eng. Chem. Fundam.* 15, 59–64. doi: 10.1021/i160057a011

Pichler, M. (2019). "Underground sun storage results and outlook" in EAGE/DGMK joint workshop on underground storage of hydrogen (Celle, Germany: European Association of Geoscientists & Engineers), 1–4.

Ponsin, V., Buscheck, T. E., and Hunkeler, D. (2017). Heart-cutting two-dimensional gas chromatography–isotope ratio mass spectrometry analysis of monoaromatic hydrocarbons in complex groundwater and gas-phase samples. *J. Chromatogr. A* 1492, 117–128. doi: 10.1016/j.chroma.2017.02.060

Quast, C., Pruesse, E., Yilmaz, P., Gerken, J., Schweer, T., Yarza, P., et al. (2012). The SILVA ribosomal RNA gene database project: improved data processing and web-based tools. *Nucleic Acids Res.* 41, D590–D596. doi: 10.1093/nar/gks1219

Rabii, A., Aldin, S., Dahman, Y., and Elbeshbishy, E. (2019). A review on anaerobic co-digestion with a focus on the microbial populations and the effect of multi-stage digester configuration. *Energies* 12:1106. doi: 10.3390/en12061106

Ranchou-Peyruse, M., Auguet, J.-C., Mazière, C., Restrepo-Ortiz, C. X., Guignard, M., Dequidt, D., et al. (2019). Geological gas-storage shapes deep life. *Environ. Microbiol.* 21, 3953–3964. doi: 10.1111/1462-2920.14745

Ranchou-Peyruse, M., Guignard, M., Chiquet, P., Caumette, G., Cézac, P., and Ranchou-Peyruse, A. (2024). Assessment of the in situ biomethanation potential of a deep aquifer used for natural gas storage. *FEMS Microbiol. Ecol.* 100:66. doi: 10.1093/femsec/fiae066

Ranchou-Peyruse, M., Guignard, M., Haddad, P. G., Robin, S., Boesch, F., Lanot, M., et al. (2023). A deep continental aquifer downhole sampler for microbiological studies. *Front. Microbiol.* 13:1012400. doi: 10.3389/fmicb.2022.1012400

Reitenbach, V., Ganzer, L., Albrecht, D., and Hagemann, B. (2015). Influence of added hydrogen on underground gas storage: a review of key issues. *Environ. Earth Sci.* 73, 6927–6937. doi: 10.1007/s12665-015-4176-2

Saeed, M., and Jadhawar, P. (2024). Optimizing underground hydrogen storage in aquifers: the impact of cushion gas type. *Int. J. Hydrogen Energy* 52, 1537–1549. doi: 10.1016/j.ijhydene.2023.08.352

Šmigáň, P., Greksák, M., Kozánková, J., Buzek, F., Onderka, V., and Wolf, I. (1990). Methanogenic bacteria as a key factor involved in changes of town gas stored in an underground reservoir. *FEMS Microbiol. Lett.* 73, 221–224. doi: 10.1016/0378-1097(90)90733-7

Stams, A. J. M. (1994). Metabolic interactions between anaerobic bacteria in methanogenic environments. *Antonie Van Leeuwenhoek* 66, 271–294. doi: 10.1007/BF00871644

Stefánsson, A., Arnórsson, S., and Sveinbjörnsdóttir, Á. E. (2005). Redox reactions and potentials in natural waters at disequilibrium. *Chem. Geol.* 221, 289–311. doi: 10.1016/j.chemgeo.2005.06.003

Steinberg, L. M., and Regan, J. M. (2008). Phylogenetic comparison of the methanogenic communities from an acidic, oligotrophic fen and an anaerobic digester treating municipal wastewater sludge. *Appl. Environ. Microbiol.* 74, 6663–6671. doi: 10.1128/AEM.00553-08

Steinberg, L. M., and Regan, J. M. (2009). mcrA-targeted real-time quantitative PCR method to examine methanogen communities. *Appl. Environ. Microbiol.* 75, 4435–4442. doi: 10.1128/AEM.02858-08

Stewart, P. S. (2003). Diffusion in biofilms. *J. Bacteriol.* 185, 1485–1491. doi: 10.1128/JB.185.5.1485-1491.2003

Stolten, D., and Emonts, B. (2016). Hydrogen science and engineering, 2 volume set: Materials, processes, systems, and technology Weinheim, Germany: John Wiley & Sons.

Strobel, G., Hagemann, B., Lüddeke, C. T., and Ganzer, L. (2023). Coupled model for microbial growth and phase mass transfer in pressurized batch reactors in the context of underground hydrogen storage. *Front. Microbiol.* 14:1150102. doi: 10.3389/fmicb.2023.1150102

Thaysen, E., McMahon, S., Strobel, G. J., Butler, I., Heinemann, N., Ngwenya, B., et al. (2021). Estimating microbial growth and hydrogen consumption in hydrogen storage in porous media. *Renew. Sustain. Energy Rev.* 151:111481. doi: 10.1016/j.rser.2021.111481

Tremosa, J., Jakobsen, R., and Le Gallo, Y. (2023). Assessing and modeling hydrogen reactivity in underground hydrogen storage: a review and models simulating the Lobodice town gas storage. *Front. Energy Res.* 11:978. doi: 10.3389/fenrg.2023.1145978

Ulrich, G. A., Breit, G. N., Cozzarelli, I. M., and Suflita, J. M. (2003). Sources of sulfate supporting anaerobic metabolism in a contaminated aquifer. *Environ. Sci. Technol.* 37, 1093–1099. doi: 10.1021/es011288a

van Houten, R. T., Pol, L. W. H., and Lettinga, G. (1994). Biological sulphate reduction using gas-lift reactors fed with hydrogen and carbon dioxide as energy and carbon source. *Biotechnol. Bioeng.* 44, 586–594. doi: 10.1002/bit.260440505

Vasile, N. S., Bellini, R., Bassani, I., Vizzarro, A., Abdel Azim, A., Coti, C., et al. (2024). Innovative high pressure/high temperature, multi-sensing bioreactors system for microbial risk assessment in underground hydrogen storage. *Int. J. Hydrogen Energy* 51, 41–50. doi: 10.1016/j.ijhydene.2023.10.245

Veshareh, J., Thaysen, E. M., and Nick, H. M. (2022). Feasibility of hydrogen storage in depleted hydrocarbon chalk reservoirs: assessment of biochemical and chemical effects. *Appl. Energy* 323:119575. doi: 10.1016/j.apenergy.2022.119575

Visser, M., Stams, A. J. M., Frutschi, M., and Bernier-Latmani, R. (2016). Phylogenetic comparison of Desulfotomaculum species of subgroup 1a and description of Desulfotomaculum reducens sp. nov. *Int. J. Syst. Evol. Microbiol.* 66, 762–767. doi: 10.1099/ijsem.0.000786

Vítězová, M., Onderka, V., Urbanová, I., Molíková, A., Hanišáková, N., Buriánková, I., et al. (2023). In situ field experiment shows the potential of methanogenic archaea for biomethane production from underground gas storage in natural rock environment. *Environ. Technol. Innov.* 32:103253. doi: 10.1016/j.eti.2023.103253

Wagman, D. D. (1982). The NBS tables of chemical thermodynamic properties selected values for inorganic and C1 and C2 organic substances in SI units. *J. Phys. Chem. Ref. Data Monogr.* 11, 2–391.

Wagner, M., Roger, A. J., Flax, J. L., Brusseau, G. A., and Stahl, D. A. (1998). Phylogeny of dissimilatory sulfite reductases supports an early origin of sulfate respiration. *J. Bacteriol.* 180, 2975–2982. doi: 10.1128/JB.180.11.2975-2982.1998

Wang, Y., and Qian, P.-Y. (2009). Conservative fragments in bacterial 16S rRNA genes and primer design for 16S ribosomal DNA amplicons in metagenomic studies. *PLoS One* 4:e7401. doi: 10.1371/journal.pone.0007401

Wang, J., Wu, R., Wei, M., Bai, B., Xie, J., and Li, Y. (2023). A comprehensive review of site selection, experiment and numerical simulation for underground hydrogen storage. *Gas Sci. Eng.* 118:205105. doi: 10.1016/j.jgsce.2023.205105

Wei, T., and Simko, V. (2017). R Package "Corrplot": Visualization of a Correlation Matrix (Version 0.84). Available at: https://github.com/taiyun/corrplot

Wickham, H. (2016). ggplot2: Elegant graphics for data analysis. *2nd* Edn. Cham: Springer International Publishing: Imprint: Springer.

Wu, L., Hou, M. Z., Luo, Z., Huang, L., Xiong, Y., Mehmood, F., et al. (2023). Efficiency assessment of underground biomethanation with hydrogen and carbon dioxide in depleted gas reservoirs: a biogeochemical simulation. *Energy* 283:128539. doi: 10.1016/j.energy.2023.128539

Yang, S., Liebner, S., Alawi, M., Ebenhöh, O., and Wagner, D. (2014). Taxonomic database and cut-off value for processing mcrA gene 454 pyrosequencing data by MOTHUR. *J. Microbiol. Methods* 103, 3–5. doi: 10.1016/j.mimet.2014.05.006

Yilmaz, P., Parfrey, L. W., Yarza, P., Gerken, J., Pruesse, E., Quast, C., et al. (2014). The SILVA and "all-species living tree project (LTP)" taxonomic frameworks. *Nucleic Acids Res.* 42, D643–D648. doi: 10.1093/nar/gkt1209

Zhu, J., Liu, X., and Dong, X. (2011). *Methanobacterium movens* sp. nov. and *Methanobacterium flexile* sp. nov., isolated from lake sediment. *Int. J. Syst. Evol. Microbiol.* 61, 2974–2978. doi: 10.1099/ijs.0.027540-0

frontiers | Frontiers in Microbiology

TYPE Hypothesis and Theory
PUBLISHED 21 August 2024
DOI 10.3389/fmicb.2024.1407868

OPEN ACCESS

EDITED BY
William J. Brazelton,
The University of Utah, United States

REVIEWED BY
Lina Joana Bird,
National Research Council, United States
Tori Hoehler,
National Aeronautics and Space Administration (NASA), United States
Annette Ruth Rowe,
University of Cincinnati, United States

*CORRESPONDENCE
Ian P. G. Marshall
ianpgm@bio.au.dk

RECEIVED 27 March 2024
ACCEPTED 05 August 2024
PUBLISHED 21 August 2024

CITATION
Marshall IPG (2024) Electromicrobiological concentration cells are an overlooked potential energy conservation mechanism for subsurface microorganisms.
Front. Microbiol. 15:1407868.
doi: 10.3389/fmicb.2024.1407868

Electromicrobiological concentration cells are an overlooked potential energy conservation mechanism for subsurface microorganisms

Ian P. G. Marshall*

Center for Electromicrobiology, Department of Biology, Aarhus University, Aarhus, Denmark

Thermodynamics has predicted many different kinds of microbial metabolism by determining which pairs of electron acceptors and donors will react to produce an exergonic reaction (a negative net change in Gibbs free energy). In energy-limited environments, such as the deep subsurface, such an approach can reveal the potential for unexpected or counter-intuitive energy sources for microbial metabolism. Up until recently, these thermodynamic calculations have been carried out with the assumption that chemical species appearing on the reactant and product side of a reaction formula have a constant concentration, and thus do not count towards net concentration changes and the overall direction of the reaction. This assumption is reasonable considering microorganisms are too small (~1 μm) for any significant differences in concentration to overcome diffusion. However, recent discoveries have demonstrated that the reductive and oxidative halves of reactions can be separated by much larger distances, from millimetres to centimetres via conductive filamentous bacteria, mineral conductivity, and biofilm conductivity. This means that the concentrations of reactants and products can indeed be different, and that concentration differences can contribute to the net negative change in Gibbs free energy. It even means that the same redox reaction, simultaneously running in forward and reverse, can drive energy conservation, in an ElectroMicrobiological Concentration Cell (EMCC). This paper presents a model to investigate this phenomenon and predict under which circumstances such concentration-driven metabolism might take place. The specific cases of oxygen concentration cells, sulfide concentration cells, and hydrogen concentration cells are examined in more detail.

KEYWORDS

concentration cells, cable bacteria, microbial ecology, metabolism, electromicrobiology

1 Introduction

Microbial communities inhabit spatially heterogeneous and complex environments that resist simple understanding. While most of our understanding of microbial physiology is the result of more than a century of cultivating and isolating pure cultures of microorganisms, this approach has proven inadequate for understanding all microbial diversity, with 22–87% of archaeal and bacterial genera remaining uncultivated depending on the environment

(Lloyd et al., 2018). Spatially heterogeneous environments such as sediment, the terrestrial subsurface, and soil contain the highest fractions of uncultivated taxa (Lloyd et al., 2018). Such spatially heterogeneous environments contain concentration gradients of microbial substrates, such as O_2, sulfide, and H_2. It has recently been shown that certain microorganisms can link metabolic reactions taking place across these gradients via long-distance electron transport between microbial cells, thus allowing them to better exploit optimal substrate concentrations than a single cell. One example of this is the cable bacteria *Electronema* and *Electrothrix* (Trojan et al., 2016; Plum-Jensen et al., 2024), which were discovered through careful measurement of chemical microprofiles in aquatic sediment (Pfeffer et al., 2012). Cable bacteria are filamentous bacteria that couple the oxidation of sulfide in deep, anoxic sediment to the reduction of oxygen in shallow sediment. They conduct electricity over several centimetres through as-yet uncharacterized conductive structures in their periplasm. This discovery changed our conception of what living organisms are capable of – we previously thought that oxidative and reductive halves of an organism's metabolism had to exist in the same cell, cable bacteria demonstrated that it is possible to oxidize an electron donor in one cell and use that electron to reduce an electron acceptor in another cell, possibly centimetres away, by transporting that electron through a conductive biological wire much faster than diffusion could transport an electron carrier molecule. Similarly, it has been shown that microorganisms can transfer electrons centimetre distances via networks of dissolved organic matter and organo-mineral associations (Bai et al., 2023), or across millimetre distances in biofilms (Li et al., 2016).

There is also increasing evidence that some anaerobic microorganisms can reverse their metabolism depending on the surrounding chemical environment. For example, acetogens have been shown to oxidize acetate in a H_2-consuming co-culture (Hattori et al., 2005). Obviously, a single-celled microorganism cannot conserve energy through the simultaneous oxidation and reduction of the same compound – this reaction would not be exergonic. However, if we combine this concept with the long-distance transport of electrons one can imagine two distant, yet electrically connected, bacterial cells in different chemical environments – one environment with a higher concentration of electron donor favouring the forward reaction and the other with a higher concentration of the oxidized form of the substrate favouring the reverse reaction. The metabolism of these microorganisms would be powered by an electrochemical concentration cell.

An electrochemical concentration cell is an electrochemical system where a single redox reaction, run both in forward and reverse directions, can result in an electrical current between two different concentration regimes (Foulkes, 2012). Such concentration cells are well known in some fields, such as the contribution of oxygen concentration cells to metal corrosion (Iverson, 1987). Traditionally, concentration cells have not been seen as relevant for individual microorganisms, as a ~1 μm cell is much too small to span multiple concentration regimes. However, the discovery of long-distance electron transport in heterogeneous subsurface environments by cable bacteria, conductive minerals, and biofilms makes this topic newly relevant. Concentration differences could drive microbial metabolism in the subsurface in a way that has not been previously recognized, in what could be called an ElectroMicrobiological Concentration Cell (EMCC). The energy yields would be small, and turnover rates may be small compared to other processes driving the concentration differences, but the energy-starved subsurface has previously shown to be homes for such low-energy-yield metabolisms, like anaerobic methane oxidation (Knab et al., 2008) or acetogenesis (Lever, 2012), and low metabolic rates are also common in subsurface environments (Jørgensen and Marshall, 2016). As long as steep concentration gradients exist, for example at geochemical transition zones or boundaries between sediments or rocks of different chemical compositions, then EMCCs are thermodynamically possible. The minimum energy requirement to support oxidative phosphorylation is thought to be as low as −10 kJ/mol (Hoehler et al., 2001). At least one microbial cell involved in the reaction would have to conserve energy at any given time, and if multiple cells conserved energy simultaneously this would multiply energy needs. There may also be situations where such concentration cells do not support microbial energy conservation, but their activity still may impact geochemical element cycling.

The goal of this paper is to develop a theoretical framework for understanding microbial metabolism through concentration cells. I will present three concentration-cell scenarios based on H_2O/O_2, SO_4^{2-}/S^{2-}, and H^+/H_2.

2 Model

We will assume that this reaction takes place in two distant yet electrically connected cells, one in a more reducing environment and one in a more oxidizing environment.

The reaction at the cell in the reduced compartment is the following:

$$XH_n \rightarrow X + nH^+ + ne^-$$

Where X is the oxidized form of the substrate, XH_n is the reduced form of the substrate, n is the number of electrons transferred, and H^+ indicates a proton. The electrons from this reaction are transferred onto a conductor, leading to one or more cells in the oxidized compartment where the reverse reaction takes place:

$$ne^- + nH^+ + X \rightarrow XH_n$$

These two reactions can be combined to show the sum of both reactions across the reducing and oxidizing environments in a galvanic cell. Subscripts "*ox*" and "*red*" will be used to keep track of where each chemical species is produced or consumed (not whether it is reduced or oxidized). Electrons do not appear in this equation, as electrons produced on the left-hand side are the consumed on the right hand side.

$$XH_{n,red} + nH^+_{ox} + X_{ox} \rightarrow XH_{n,ox} + nH^+_{red} + X_{red}$$

The next step is to determine whether this reaction can proceed exergonically, and what the Gibbs free energy is. While there is no change in Gibbs free energy from the substrates to the products, as the total Gibbs free energy of formation remains unchanged with identical

chemical species as substrates and products, the change in energy is purely driven by concentration differences between the reducing and oxidizing environment:

$$\Delta G = RT\ln\left(\frac{\left[XH_{n,ox}\right]\left[H^{+}_{red}\right]^{n}\left[X_{red}\right]}{\left[XH_{n,red}\right]\left[H^{+}_{ox}\right]^{n}\left[X_{ox}\right]}\right)$$

Where ΔG is the change in Gibbs free energy, R is the gas constant, T is temperature in kelvin, and *ln* indicates the natural logarithm. A negative ΔG will result in an exergonic reaction, which means, generally speaking, that as long as the numerator is less than the denominator in the above equation the reaction can proceed. For simplicity, all models in this paper will only alter the value of a single chemical species between the reducing and oxidizing environment. These concentration differences (and similarities) must be maintained by other biological, chemical, or physical processes for the reaction to proceed. Differences in pH between the two environments can be critical for whether the reaction can proceed.

There is one final element to add to this model, and that is energy loss between the reducing and oxidizing environment as a result of resistance. We assume a linear drop in potential with distance:

$$\Delta G = RT\ln\left(\frac{\left[XH_{n,ox}\right]\left[H^{+}_{red}\right]^{n}\left[X_{red}\right]}{\left[XH_{n,red}\right]\left[H^{+}_{ox}\right]^{n}\left[X_{ox}\right]}\right) + nFED$$

Where n is the number of electrons transferred per reaction, F is Faraday's constant, E is the expected voltage drop per unit distance, and D is the distance. E has been estimated for cable bacteria to be 12.3–14.6 ± 3.8–4.1 mV mm^{-1} (Bjerg et al., 2018), so I use a value of 13 mV mm^{-1} in this paper. Other conductors, such as biofilms or organo-mineral associations, may have different values.

Another way of expressing this model is as a function of potentials for the reactions where XH is oxidized and where X is reduced:

$$\Delta E = E_{red} + E_{ox} - E_{loss}$$

Each chemical species contributes to the overall potential change, along with the loss of some potential in along the conductor. Each of these has a standard potential modified by the local concentrations of all products and substrates. This is where XH is oxidized:

$$E_{ox} = -E^{0} - \left(\frac{RT}{nF}\right)\ln\left(\frac{\left[H^{+}_{red}\right]^{n}\left[X_{red}\right]}{\left[XH_{n,red}\right]}\right)$$

And where X is reduced:

$$E_{red} = E^{0} - \left(\frac{RT}{nF}\right)\ln\left(\frac{\left[XH_{n,ox}\right]}{\left[H^{+}_{ox}\right]^{n}\left[X_{ox}\right]}\right)$$

Let us take an example of an O_2/H_2O EMCC, where the O_2 concentration at the oxidized end is 300 µM, at the reduced end is 1 nM, and where pH is a constant 7. E^0 for O_2 reduction to H_2O is 818 mV for O_2 in an aqueous solution (Thauer et al., 1977). The pH is 7 at both ends, and water is not included in the reaction quotient as this is already taken into account by the standard potential for an aqueous solution. For the oxidation reaction, the standard potential needs to be made negative to show its reversal relative to the reduction reaction. There is 2 mm of conductor between the two points.

$$E_{ox} = -0.818 - \left(\frac{(8.314)(293)}{(4)(96485.3)}\right)\ln\left(\frac{\left(10^{-7}\right)^{4}\left(10^{-9}\right)}{1}\right)$$

$$E_{ox} = -1.276\ \text{V}$$

$$E_{red} = 0.818 - \left(\frac{(8.314)(293)}{(4)(96485.3)}\right)\ln\left(\frac{1}{\left(10^{-7}\right)^{4}(0.0003)}\right)$$

$$E_{red} = 1.356\ \text{V}$$

$$E_{loss} = 0.013 * 2\text{mm}$$

$$E_{loss} = 0.026\text{V}$$

$$\Delta E = 1.356\text{V} - 1.276\text{V} - 0.026\text{V}$$

$$\Delta E = 0.054\ \text{V}$$

$$\Delta G = -nF\Delta E$$

$$\Delta G = (-4)(96485.3)(0.054)$$

$$\Delta G = -20.8\ \text{kJ / mol}$$

To model these electromicrobiological concentration cells (EMCCs), I assume that one reaction takes place in a single point in one-dimensional space and then calculate ΔG for cells electrically connected to this point. The idea that one half of the reaction takes place in a very small area and the other half over a larger area is consistent with our current understanding of cable bacteria, where oxygen reduction is restricted to <10% of the filament (Scilipoti et al., 2021).

Real-world pH and O_2 microprofile data was obtained from the Pangaea database from studies on freshwater lake sediment (Fiskal

et al., 2019a,b), and marine sediment (Lichtschlag et al., 2011, 2013; Grünke et al., 2012; Felden et al., 2013). These data were filtered to include only depths below 0 mm, and measurements of 0 μM O_2 were modified to 1 nM to permit the calculation of ΔG without an infinite value. In the case of data from the Nordic Margin (Lichtschlag et al., 2011), the O_2 concentration never reached a stable zero, hovering around 0–2 μM even below several centimetres of sediment depth. I interpreted this as a technical error, and set the concentration to 1 nM from the depth where the concentration was consistently at its minimum (2.7 cm depth). For the Amon Mud Volcano dataset, the pH data missing from the deepest measurement in one dataset was set to 7.98, to assume that the relatively stable downcore trend would have continued had measurements been made.

Code for the model is available at https://github.com/ianpgm/EMCC_models.

3 Results and discussion

3.1 A general description of electromicrobiological concentration cells (EMCC)

The EMCC concept, outlined in Figure 1, can seem counter intuitive at first: a reaction where substrates and products are the same is usually understood to result in no net changes in any chemical concentrations and therefore no possibility for an organism to conserve energy. However, the key here is that the substrates and products are in fact not the "same" as they exist in areas with different substrate and product concentrations. The reaction is driven forward by coupling the two reactions together through electrical conductivity, allowing the concentration difference to drive the reaction and permit energy conservation. This concentration difference would have to be maintained by some other biotic or abiotic process to keep the EMCC running, as the EMCC will diminish this concentration difference over time. This is just like any other chemotrophic microorganism—substrates are used up over time, leading to the cessation of metabolism if substrates are not replenished.

Figure 2 presents a generalised model for this process, showing how different variables can affect the ΔG. The assumption is that the electron acceptor varies in concentration over a distance of 1 millimetre, with the lowest concentration being 1 nM and the highest concentration being a number of orders of magnitude above 1 nM. This electron acceptor is reduced by a certain number of electrons to make an electron donor. The calculated Gibbs free energy is for the difference between the concentration at 0 mm and the concentration at the indicated depth. The energy conservation itself does not necessarily occur at the indicated depth, but the indicated ΔG shows the total free energy available for an EMCC extending over that depth. The exact energy yield at each depth would depend on whether the energy was conserved in cells carrying out the oxidation reaction or the reduction reaction.

Figure 2 provides several key insights into the EMCC concept. Firstly, order-of-magnitude changes in concentration differences lead to linear changes in Gibbs free energy. Secondly, the number of electrons transferred change the nFED term in the ΔG calculation and thus alter the slope in the linear part of the calculation. Fewer transferred electrons mean less energy loss along the conductor,

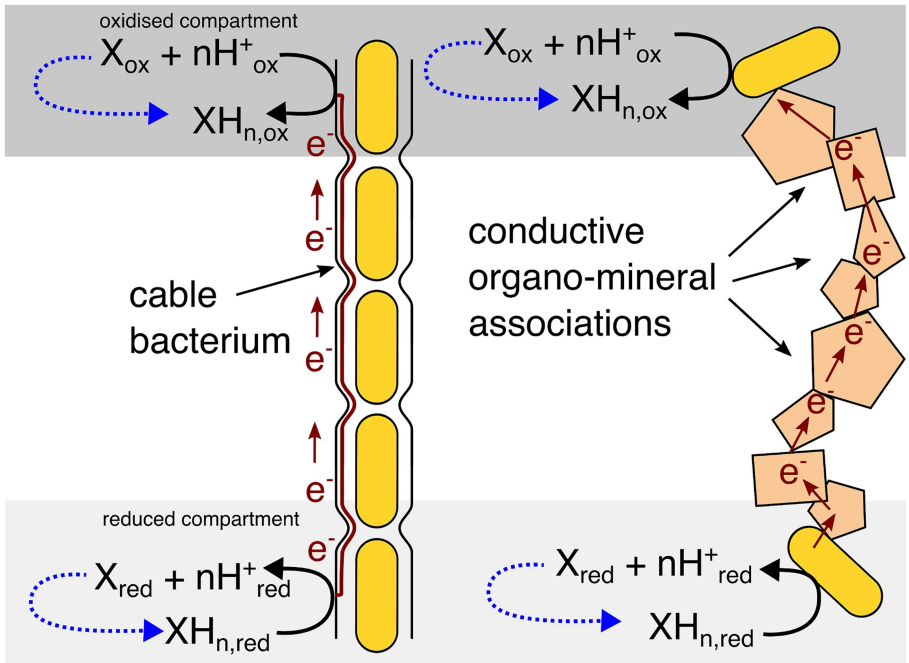

FIGURE 1
Generic overview of the electromicrobiological concentration cell model. The oxidized and reduced compartments may be a consequence of a concentration gradient (as the examples in this paper show) or a physical conductive barrier preventing diffusion from one compartment to the other. Dotted blue lines show that some other abiotic or biotic process will need to maintain the concentration difference for an EMCC to remain energetically favourable over time.

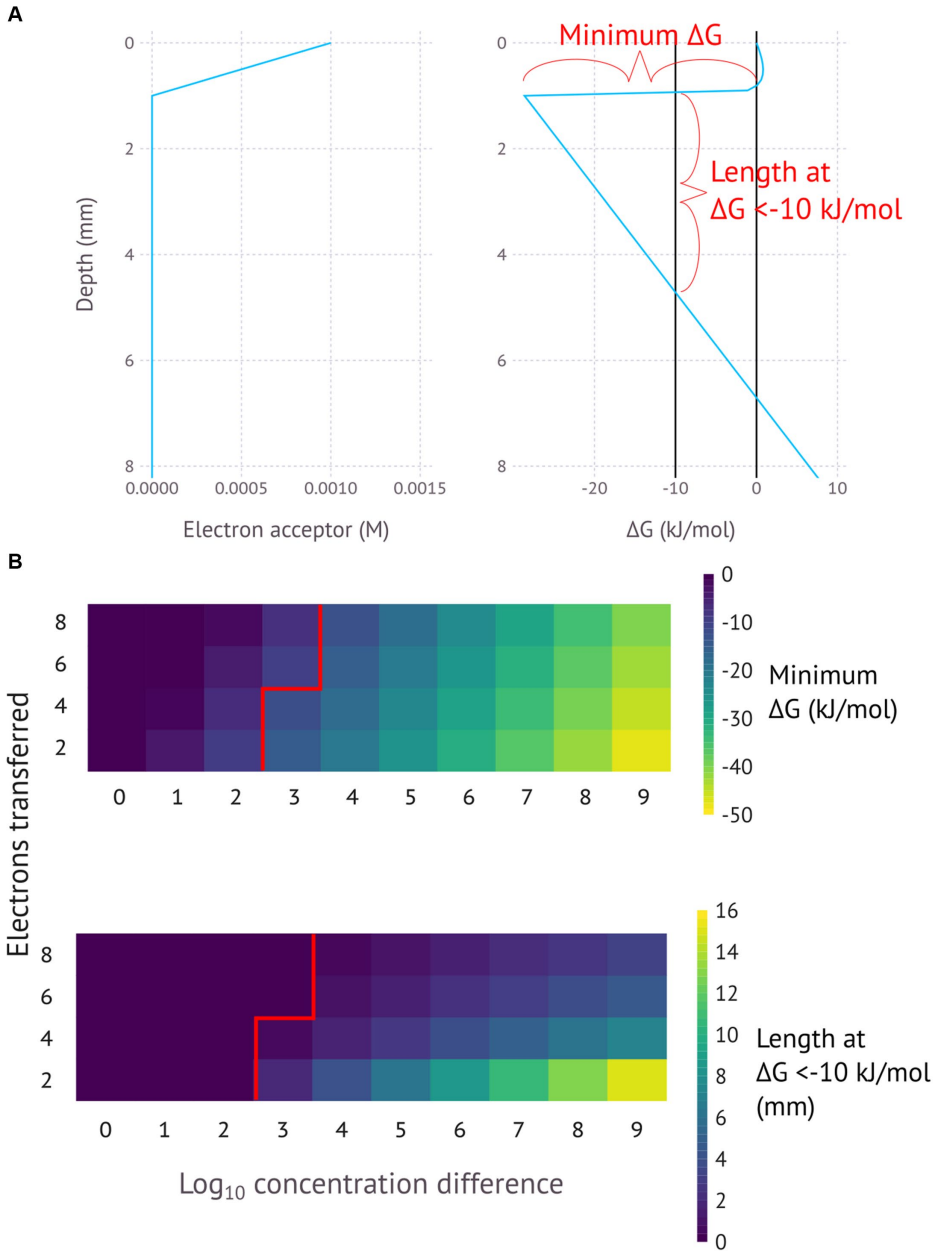

FIGURE 2
(A) General model for an electromicrobiological concentration cell for a 4-electron reaction with 6 orders of magnitude concentration difference, with a minimum. **(B)** General models for a range of different electron numbers and concentration differences, with the minimum Gibbs free energy and distance at <−10 kJ/mol (the assumed minimum necessary for ATP production) shown for reactions with different numbers of electrons transferred and different concentration ranges. pH is assumed to be constant.

resulting in a longer distance that a favourable ΔG can be maintained. This difference in energy loss rate reflects the fact that higher currents result in higher potential loss according to Ohm's law (V = IR)—assuming a constant substrate turnover rate and resistance, redox reactions transferring more electrons will have a proportionally higher current that results in a higher loss in potential. Put together this means that the most energetically favourable EMCCs involve high concentration differences and low numbers of electrons transferred.

The model for EMCCs in Figures 1, 2 is best understood when applied to certain specific scenarios, some where the model may help to explain certain difficult to understand observations. Figures 3–5 illustrate models for EMCCs based on O_2, H_2S and H_2 gradients, with the concentration of all other chemical species assumed as constant. These gradients transition from maximum concentration to minimum concentration linearly across a given penetration depth. Penetration depths and maximum substrate concentrations were chosen based on observed literature values (Jørgensen et al., 1979; Nielsen et al., 2015). Supplementary Figures show ΔG calculated from real-world microprofiles for O_2, S^{2-}, and pH – this is a small selection of possible models based on publicly available data, and should not be interpreted as representative of all real-world possibilities. No suitable publicly available H_2/pH microprofile datasets were found. Choosing a

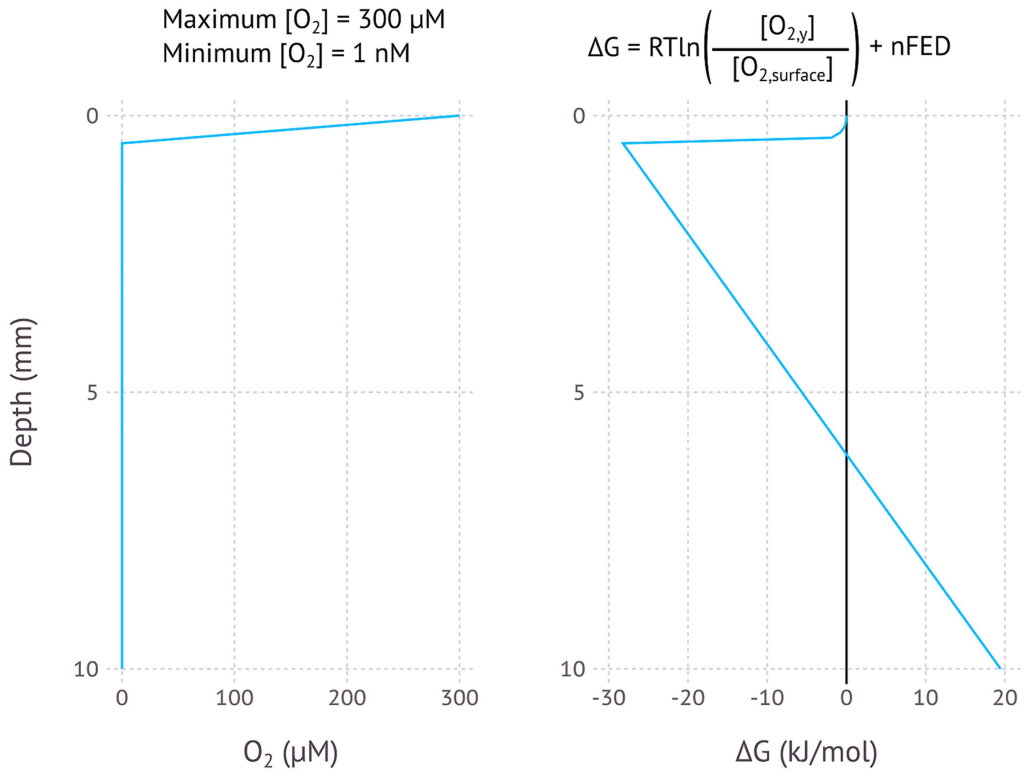

FIGURE 3
Modelled EMCC based on an O_2 concentration gradient, assuming an oxygen penetration depth of 0.5 mm, a maximum O_2 concentration of 300 µM and a minimum concentration of 1 nM. pH is assumed to be constant.

minimum substrate concentration presented an interesting challenge – setting this to 0 µM would make the ΔG impossible to calculate, as the logarithm of zero is infinite. We therefore need to choose an arbitrarily low number for our minimum substrate concentration, but how low this arbitrarily low number is will have a big impact on the resulting ΔG – each order of magnitude change in the minimum concentration could lower the ΔG by up to −5.6 kJ/mol. For each model I have chosen to set the minimum concentration to 1 nM, which is below the 2–20 nM detection limit for the current most sensitive microscale detection methods for O_2 (Revsbech et al., 2009), H_2S (e.g., https://unisense.com/products/h2s-microsensor/), and H_2 (Nielsen et al., 2015) and therefore our best understanding of "zero" at present.

One interesting aspect of EMCCs is the large impact of pH on the resulting ΔG. Protons are produced where oxidation takes place, and consumed where reduction takes place. Multiple protons lead to exponents on the proton concentration in the ΔG calculation, leading to exponential impacts on the overall calculation: an O_2/H_2O EMCC involves the transfer of 4 electrons and thus 4 protons, with $[H^+]^4$ then appearing in the numerator and denominator of the reaction quotient. The H_2S/SO_4^{2-} EMCC involves 8 protons and the H_2/H^+ EMCC involves 2 protons. This means that the pH concentration profile of an environment has a large impact on whether an EMCC is possible. A lower pH at the reducing environment than the oxidizing environment will inhibit an EMCC, while a higher pH in the reducing environment will make an EMCC more likely to be exergonic. Figure 2 and the other theoretical models in this study assume a constant pH, but the models based on real-world data (Supplementary Figures) take pH differences into account and show that in many cases the reaction could still be thermodynamically favourable even when the reducing end of the EMCC has a lower pH. As an EMCC runs, more protons are produced at the reducing end and consumed at the oxidizing end, making the pH profile less favourable for an EMCC as time goes on, with the rate of this degradation in ΔG a function of how well buffered the system is. In a poorly buffered system, the pH difference will render the reaction unfavourable before the other system components due to the higher exponents.

The calculated changes in Gibbs free energy closest to the zero position are a function of whether the chemical species at the zero position is consumed (O_2 and H_2) or produced (H_2S), with consumption resulting in a concave curve and production in a convex curve. The linear part of the curve starts where the concentration becomes constant – here the energy change is a function of the distance and the number of electrons transferred, with more electrons resulting in a steeper slope (Figures 2–5).

3.2 Oxygen reduction coupled to water splitting

$$2H_2O_{red} + 4H^+_{ox} + O_{2,ox} \rightarrow 2H_2O_{ox} + 4H^+_{red} + O_{2,red}$$

$$\Delta G = RT \ln \left(\frac{\left[H^+_{red}\right]^4 \left[O_{2,red}\right]}{\left[H^+_{ox}\right]^4 \left[O_{2,ox}\right]} \right) + nFED$$

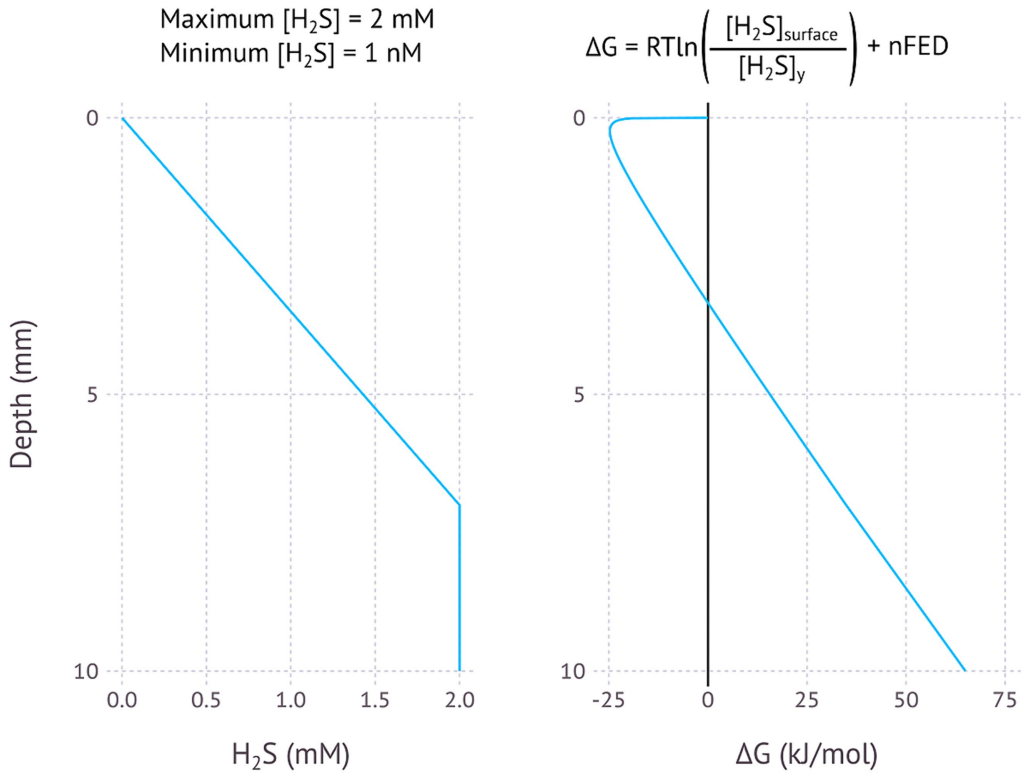

FIGURE 4
Modelled EMCC based on a H_2S concentration gradient, assuming most sulfide is removed in the upper 7 millimetres, a maximum H_2S concentration of 2 mM and a minimum concentration of 1 nM. pH is assumed to be constant.

The oxic/anoxic interface in aquatic sediments is a possible environment where EMCCs may occur, as shown by the theoretical model used here (Figure 3) and the models based on O_2 and pH microprofiles from freshwater and marine environments (Supplementary Figures SF1–F6). Oxygen from the water column is consumed by aerobic microorganisms, often in the uppermost millimetre of sediments with ample electron donor. This creates a steep O_2 gradient in the sediment, meaning that a conductive structure could connect O_2-reducing and H_2O-oxidizing processes on either end of this gradient without losing too much potential.

The steepness of the O_2 gradient appears to be critical for whether or not an EMCC will be possible – O_2 penetration depths of about 1–2 mm as found in Lake Baldegg (Supplementary Figure SF1), Lake Greifen (Supplementary Figure SF2), the shallow part of Lake Lucerne (Supplementary Figure SF3), Lake Zug (Supplementary Figure SF4), and Amon Mud Volcano (Supplementary Figure SF5) result in ΔG values below −10 kJ/mol, while O_2 penetration depths of about 1 cm or more found in the two deep cores from Lake Lucerne (SF3) and the Nordic Margin (SF6) result in positive ΔG values. This is because the potential difference lost over the longer O_2 penetration depth is greater than the potential difference created by the concentration difference. The fact that steeper gradients are more likely to produce EMCCs introduces an interesting paradox – O_2 is depleted rapidly by aerobic microorganisms oxidizing organic matter, and more organic matter (such as in the eutrophic lakes Baldegg, Greifen, and Zug) results in a steeper decline in O_2 concentration than environments with less organic matter, like Lake Lucerne. However, higher organic matter concentrations will also mean that an EMCC microorganism is more likely to be outcompeted by an aerobic chemoorganotroph in the oxic sediment layer. The EMCC organism could only become established if there was some factor preventing direct competition for oxygen, such as physically extending further into the oxic zone above the sediment surface. Similar processes have been observed in cable bacteria emerging from the sediment under conditions of oxygen limitation (Burdorf et al., 2018).

Cable bacteria form conductive structures from the oxic layer to the anoxic layer, allowing an exergonic production of O_2 from water in the uppermost part of the anoxic layer. Such O_2 production may explain the observation of so-called "flocking" bacteria, microorganisms capable of aerobic respiration that flock around cable bacteria in the anoxic zone of a slide designed to reproduce O_2 gradients as in sediment (Bjerg et al., 2023; Lustermans et al., 2023). These flocking bacteria would consume O_2 produced by the cable bacteria, keeping the O_2 concentration in the anoxic sediment low and allowing the O_2-producing reaction to continue to proceed. In a way this would extend the influence of O_2 several millimetres below the oxic/anoxic interface, even allowing O_2-dependent reactions such as aerobic methane and ammonium oxidation to proceed. There is currently no direct evidence for such cryptic O_2 production in sediment, only some evidence of O_2 production by cable bacteria filament sheaths in an *in vitro* concentration cell (Digel et al., 2023), but the model presented here shows that such a process is thermodynamically possible.

These thoughts about O_2 production in cable bacteria come amid an increasing wave of interest in trace amounts of O_2 produced in ostensibly anoxic environments and making aerobic respiration

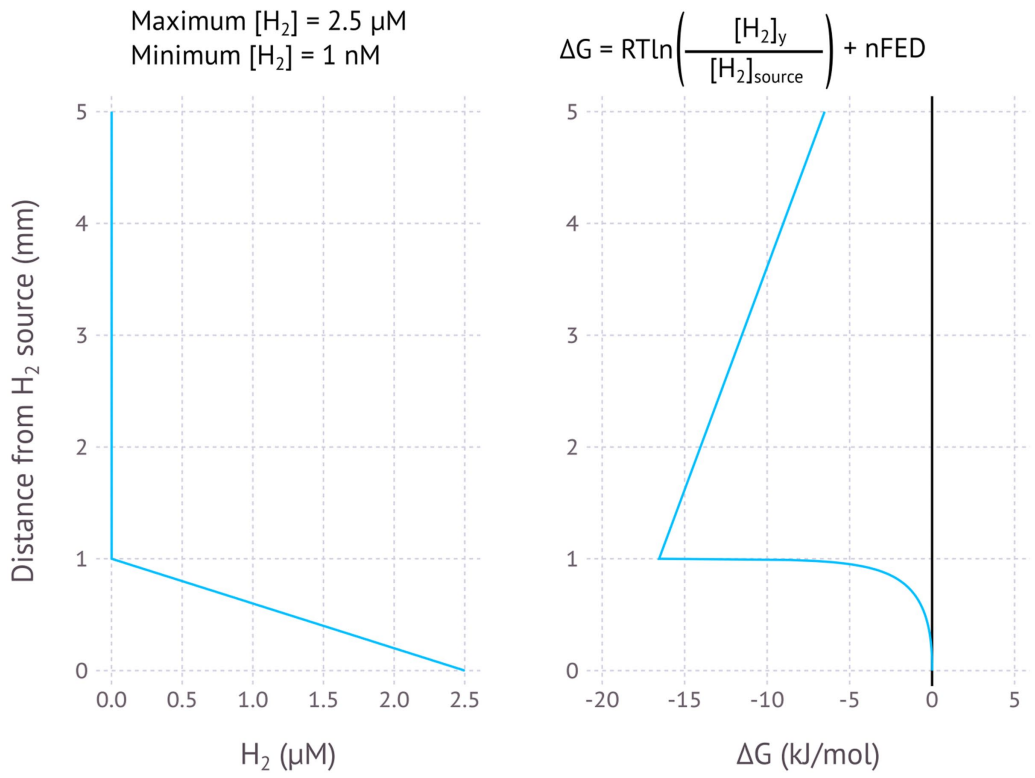

FIGURE 5
Modelled EMCC based on a H_2 gradient, assuming H_2 is produced and concentration diminishes within 1 mm of the production surface. Maximum H_2 concentration is 2.5 µM, minimum H_2 concentration is 1 nM.

possible (Berg et al., 2022; Kraft et al., 2022; Ruff et al., 2023). While EMCCs cannot explain many of the observations made until now, especially in the water column, the potential for such concentration-driven production of O_2 ought to be considered a possible explanation for some otherwise difficult-to-explain aerobic metabolism.

3.3 Sulfate reduction coupled to sulfide oxidation

$$4H_2O_{red} + H_2S_{red} + 8H^+_{ox} + SO^{2-}_4{}_{ox} \rightarrow 4H_2O_{ox} + H_2S_{ox} + 8H^+_{red} + SO^{2-}_4{}_{red}$$

$$\Delta G = RT \ln\left(\frac{\left[H_2S_{ox}\right]\left[H^+_{red}\right]^8\left[SO^{2-}_4{}_{red}\right]}{\left[H_2S_{red}\right]\left[H^+_{ox}\right]^8\left[SO^{2-}_4{}_{ox}\right]}\right) + nFED$$

Sulfate reduction is a strong candidate for EMCCs, as the dissimilatory sulfite reduction (DSR) pathway is already known to be able to run in reverse, oxidizing sulfide or reducing sulfate. It used to be thought that microorganisms using the oxidative DSR pathway were phylogenetically distinct from sulfate-reducing organisms (Müller et al., 2015), but sulfide-oxidizing organisms with a *dsrAB* genes that belong to sulfate-reducing clades have since been found. These include cable bacteria (Kjeldsen et al., 2019) and *Desulfurivibrio alkaliphilus* (Thorup et al., 2017). Similarly, many sulfate-reducing bacteria have been shown to oxidize sulfide while reducing O_2, albeit without observed growth (Dannenberg et al., 1992). While a single organism capable of energy conservation using either sulfate reduction and sulfide oxidation has not yet been observed, it has not been ruled out yet either, especially not using an electrode as electron donor or acceptor rather than a chemical substrate. One could imagine a situation where an organism capable of both sulfide oxidation and sulfate reduction could couple these two processes together electrically from an environment with high sulfide concentration to low sulfide concentration (Figure 4). An examination of sulfide and pH gradients in nature shows that in at least one case such a sulfide-driven EMCC would be exergonic (Supplementary Figure SF7).

One interesting consequence of this model would be that abiotic consumption of sulfide could enable an EMCC to use alternative electron donors indirectly. For example, cable bacteria are not known to reduce metal oxides or organic matter, and nor do they have any clear indications in their genome that such electron acceptors could be used (Kjeldsen et al., 2019). However, metal oxide minerals (Peiffer et al., 1992) and organic matter (Yu et al., 2015) can abiotically oxidize sulfide, creating a low sulfide zone around their surfaces. A cable bacteria EMCC could drive its metabolism using this area around a mineral with a lower sulfide concentration against a relatively constant sulfate concentration background, thus indirectly accessing alternative electron acceptors with abiotic sulfide/sulfate cycling as an intermediate. Cable bacteria activity results in iron oxide near the sediment surface (Seitaj et al., 2015), could these iron oxides support cable bacteria survival during annual bottom water hypoxia?

A laboratory analogue to such sulfur-mediated use of alternative electron acceptors may already have been observed. There have been several observations of cable bacteria being attracted to and potentially growing on graphite anodes in the place of other electron acceptors (Reimers et al., 2017; Li et al., 2021; Bonné et al., 2024). Could these graphite electrodes be abiotically oxidizing sulfide released from the sediment, creating a low-sulfide zone around the electrode that can enable the coupling of sulfate reduction close to the electrode to the oxidation of sulfide distant from the electrode? Abiotic sulfide oxidation at graphite electrodes has been observed before (Ateya and Al-Kharafi, 2002). The observed increase in current compared to cable-free controls could be explained by the cable bacteria increasing the effective surface area of the electrode. This explanation would avoid the need for any direct-interspecies electron transfer to the electrodes by cable bacteria.

3.4 Proton reduction coupled to hydrogen consumption

$$H_{2,red} + 2H^+_{ox} \rightarrow H_{2,ox} + 2H^+_{red}$$

$$\Delta G = RT \ln \left(\frac{\left[H_{2,ox}\right]\left[H^+_{red}\right]^2}{\left[H_{2,red}\right]\left[H^+_{ox}\right]^2} \right) + nFED$$

Hydrogen metabolism is widespread amongst prokaryotes, with both H_2 oxidation and H_2 production by H^+ reduction coupled to many other redox reductive processes. Several types of hydrogenases exist to mediate these reactions, and [NiFe]-hydrogenases are known to catalyse both the oxidation of H_2 and the reduction of H^+ (Vignais and Billoud, 2007). H_2 as an electron donor for microorganisms can be produced geologically (Nealson et al., 2005). One could imagine a subsurface source of H_2 where the H_2 diffuses away, creating a high-H_2 to low-H_2 gradient, ideal for an electromicrobiological concentration cell driven by the H_2 concentration difference, assuming that pH remains relatively constant (Figure 5).

The idea of an H_2 EMCC is particularly interesting in the context of the earliest forms of metabolism in the early Earth or other planets. One challenge for the first life forms was the absence of electron acceptors—the early Earth atmosphere was very reduced (Shaw, 2008), and the first life has often been thought to use nitrogen oxides (Mancinelli and McKay, 1988) or carbon dioxide (Walker, 1985). But a H_2-based concentration cell gives us another possible electron acceptor for early life: H^+, coupled to the oxidation of H_2. In this way early life would not have had to find a way to couple energy conservation to CO_2 fixation all at once (as in the complex methanogenesis pathway), but could have had an alternative energy source from the beginning. One key advantage for early life would be that a single reversible proto-hydrogenase could function both to oxidize the electron donor and reduce the electron acceptor, limiting the complexity for a minimal metabolism to work. Extracellular H_2 oxidation produces a higher H^+ concentration outside the cell, generating a proton motive force that could have driven the first metabolism with a single catalyst. This is not the first suggestion that concentration gradients could have helped drive metabolism in the earliest life (e.g., Ooka et al., 2019), but it is striking how simple the earliest life form could be if concentration cells are taken into account.

4 Perspectives

While it seems clear that electromicrobiological concentration cells are theoretically possible, and that there are some experimental observations which may be explained by the model described in this paper, experimental tests of this theory will be the next logical step.

Identifying environments where EMCCs may be found can be done based on fine-scale chemical characterisation of heterogeneous aquatic environments. Competition with other members of the microbial community is an important factor in determining whether an EMCC will be established – if other electron donors or acceptors are present in the area where substrates are consumed, other microorganisms may outcompete EMCC microbes. For example, a conventional aerobic organotroph will likely outcompete an O_2-reducing EMCC at an oxic/anoxic interface with plenty of organic matter available as an electron donor. Or a sulfide-oxidizing EMCC will be outcompeted by a conventional nitrate-reducing sulfide-oxidizer if nitrate is present. The best place to find EMCCs are therefore environments with steep changes in substrate concentration but without too many alternative electron donors or acceptors to use these substrates. Such environments are rare – steep gradients are typically a result of high metabolic rates driven by non-EMCC metabolic processes that will typically outcompete the EMCC organisms, but there are certain situations that have been covered in this paper that would circumvent this problem: EMCC structures that extend beyond the edge of the gradients to an area with less competition, for example, or gradients driven by physical or chemical processes rather than metabolism. EMCCs based on chemical gradients produced by other microbes will likely have a minimal impact on overall geochemical cycles, as the processes producing these gradients will be operating at higher rates. While the observation of chemical gradients at the micrometre to millimetre scale has improved vastly over recent decades with microsensors, optodes, and other technologies, there are still many environments, particularly at geochemical transition zones in the deep subsurface, that have not been well characterised on the micro-scale for logistical reasons.

Once potential EMCC environments are identified, the next step would be to identify possible microorganisms involved. While cultivation and isolation has been the most effective method of understanding microbial physiology for over a 100 years, it is obvious why no EMCC-organism has ever been isolated: most cultivation systems are homogeneous and mixed, and the relatively few microbiologists who have carried out gradient-based enrichment and isolation (for example for the cultivation of colourless sulfur bacteria) have used opposing gradients of different electron donors and acceptors, rather than a gradient of the same chemical species from its oxidized to its reduced form. Such EMCC gradient systems would be even more challenging to operate than traditional gradient systems, so either a great deal of effort or some technical innovation (probably both) would be necessary for this to work. Perhaps bioelectrochemical systems similar to the sediment microbial fuel cells described above for cable bacteria could be the way forward for enrichment and cultivation.

If enrichment and isolation of EMCC microorganisms is difficult, could their direct observation in the environment or laboratory microcosms be the way forward? Electrochemical and optical sensing is improving constantly and may provide new opportunities for measuring gradients at the millimetre to centimetre scale. The electric potential microelectrode (Damgaard et al., 2014) has proven vital for cable bacteria research, and EMCCs ought to produce an electric field just as conventional cable bacteria metabolism does, so the electric potential microelectrode could play a similar role. Other forms of sensing, such as stable-isotope based methods and living biosensors, could also be important. With observations of EMCCs, more accurate models than those presented here will become possible. For example, the energy loss along the conductor, critical for determining whether en EMCC is exergonic or not, is a function of the current through the conductor – if this current can be estimated, then more accurate predictions could be made. EMCCs operating at very low rates could be exergonic for much longer distances than the predictions made in this study.

5 Conclusion

Electromicrobiological concentration cells are fascinating theoretical constructs which, if found to exist in the real world, could greatly impact our understanding of microbial element cycling, physiology, and the origin of life on Earth and elsewhere. I hope that other scientists will be inspired by this paper to explore this concept further, both theoretically and experimentally.

Data availability statement

The original contributions presented in the study are included in the article/Supplementary material, further inquiries can be directed to the corresponding author.

Author contributions

IM: Conceptualization, Funding acquisition, Investigation, Methodology, Visualization, Writing – original draft, Writing – review & editing.

Funding

The author(s) declare that financial support was received for the research, authorship, and/or publication of this article. This work was funded by the Villum Foundation (Villum Experiment grant 40808) and the Danish National Research Foundation DNRF136.

Acknowledgments

IM would like to acknowledge all colleagues at the Center for Electromicrobiology who have discussed this theory over the past years, and to the reviewers whose comments have resulted in an improved paper.

Conflict of interest

The author declares that the research was conducted in the absence of any commercial or financial relationships that could be construed as a potential conflict of interest.

Publisher's note

All claims expressed in this article are solely those of the authors and do not necessarily represent those of their affiliated organizations, or those of the publisher, the editors and the reviewers. Any product that may be evaluated in this article, or claim that may be made by its manufacturer, is not guaranteed or endorsed by the publisher.

Supplementary material

The Supplementary material for this article can be found online at: https://www.frontiersin.org/articles/10.3389/fmicb.2024.1407868/full#supplementary-material

References

Ateya, B., and Al-Kharafi, F. (2002). Anodic oxidation of sulfide ions from chloride brines. *Electrochem. Commun.* 4, 231–238. doi: 10.1016/s1388-2481(02)00254-0

Bai, Y., Sun, T., Mansor, M., Joshi, P., Zhuang, Y., Haderlein, S. B., et al. (2023). Networks of dissolved organic matter and Organo-mineral associations stimulate Electron transfer over centimeter distances. *Environ. Sci. Technol. Lett.* 10, 493–498. doi: 10.1021/acs.estlett.3c00172

Berg, J. S., Ahmerkamp, S., Pjevac, P., Hausmann, B., Milucka, J., and Kuypers, M. M. M. (2022). How low can they go? Aerobic respiration by microorganisms under apparent anoxia. *FEMS Microbiol. Rev.* 46:fuac006. doi: 10.1093/femsre/fuac006

Bjerg, J. T., Boschker, H. T. S., Larsen, S., Berry, D., Schmid, M., Millo, D., et al. (2018). Long-distance electron transport in individual, living cable bacteria. *Proc. Natl. Acad. Sci. USA* 115, 5786–5791. doi: 10.1073/pnas.1800367115

Bjerg, J. J., Lustermans, J. J. M., Marshall, I. P. G., Mueller, A. J., Brokjær, S., Thorup, C. A., et al. (2023). Cable bacteria with electric connection to oxygen attract flocks of diverse bacteria. *Nat. Commun.* 14:1614. doi: 10.1038/s41467-023-37272-8

Bonné, R., Marshall, I. P. G., Bjerg, J., Marzocchi, U., Manca, J., Nielsen, L. P., et al. (2024). Interaction of living cable bacteria with carbon electrodes in bioelectrochemical systems. *Appl. Environ. Microbiol.* e00795-24. doi: 10.1128/aem.00795-24

Burdorf, L. D. W., Malkin, S. Y., Bjerg, J. T., van Rijswijk, P., Criens, F., Tramper, A., et al. (2018). The effect of oxygen availability on long-distance electron transport in marine sediments. *Limnol. Oceanogr.* 63, 1799–1816. doi: 10.1002/lno.10809

Damgaard, L. R., Risgaard-Petersen, N., and Nielsen, L. P. (2014). Electric potential microelectrode for studies of electrobiogeophysics. *J. Geophys. Res. Biogeo.* 119, 1906–1917. doi: 10.1002/2014jg002665

Dannenberg, S., Kroder, M., Dilling, W., and Cypionka, H. (1992). Oxidation of H2, organic compounds and inorganic sulfur compounds coupled to reduction of O2 or nitrate by sulfate-reducing bacteria. *Arch. Microbiol.* 158, 93–99. doi: 10.1007/BF00245211

Digel, L., Mierzwa, M., Bonné, R., Zieger, S., Pavel, I., Ferapontova, E., et al. (2023). Cable Bacteria skeletons as catalytically active electrodes. *Angew. Chem. Int. Ed.* 63:e202312647. doi: 10.1002/anie.202312647

Felden, J., Lichtschlag, A., Wenzhöfer, F., de Beer, D., Feseker, T., Pop Ristova, P., et al. (2013). Limitations of microbial hydrocarbon degradation at the Amon mud volcano (Nile deep-sea fan). *Biogeosciences* 10, 3269–3283. doi: 10.5194/bg-10-3269-2013

Fiskal, A., Deng, L., Michel, A., Eickenbusch, P., Han, X., Lagostina, L., et al. (2019b). Effects of eutrophication on sedimentary organic carbon cycling in five temperate lakes. *Biogeosciences* 16, 3725–3746. doi: 10.5194/bg-16-3725-2019

Fiskal, A., Deng, L., Michel, A., Eickenbusch, P., Han, X., Lagostina, L., et al. (2019a). Porewater and sediment geochemistry of five temperate Swiss lakes. *PANGAEA Data Publisher for Earth & Environmental Science*. doi: 10.1594/PANGAEA.908543

Foulkes, F. R. (2012). Physical chemistry for engineering and applied sciences. Raton, FL: Taylor & Francis Group.

Grünke, S., Lichtschlag, A., de Beer, D., Felden, J., Salman, V., Ramette, A., et al. (2012). Mats of psychrophilic thiotrophic bacteria associated with cold seeps of the Barents Sea. *Biogeosciences* 9, 2947–2960. doi: 10.5194/bg-9-2947-2012

Hattori, S., Galushko, A. S., Kamagata, Y., and Schink, B. (2005). Operation of the CO dehydrogenase/acetyl coenzyme a pathway in both acetate oxidation and acetate formation by the syntrophically acetate-oxidizing bacterium *Thermacetogenium phaeum*. *J. Bacteriol.* 187, 3471–3476. doi: 10.1128/JB.187.10.3471-3476.2005

Hoehler, T. M., Alperin, M. J., Albert, D. B., and Martens, C. S. (2001). Apparent minimum free energy requirements for methanogenic Archaea and sulfate-reducing bacteria in an anoxic marine sediment. *FEMS Microbiol. Ecol.* 38, 33–41. doi: 10.1111/j.1574-6941.2001.tb00879.x

Iverson, W. P. (1987). "Microbial corrosion of metals" in Advances in applied microbiology. eds. G. M. Gadd and S. Sariaslani (Amsterdam: Elsevier).

Jørgensen, B. B., and Marshall, I. P. G. (2016). Slow microbial life in the seabed. *Annu. Rev. Mar. Sci.* 8, 311–332. doi: 10.1146/annurev-marine-010814-015535

Jørgensen, B. B., Revsbech, N. P., Blackburn, T. H., and Cohen, Y. (1979). Diurnal cycle of oxygen and sulfide microgradients and microbial photosynthesis in a cyanobacterial mat sediment. *Appl. Environ. Microbiol.* 38, 46–58. doi: 10.1128/aem.38.1.46-58.1979

Kjeldsen, K. U., Schreiber, L., Thorup, C. A., Boesen, T., Bjerg, J. T., Yang, T., et al. (2019). On the evolution and physiology of cable bacteria. *Proc. Natl. Acad. Sci.* 116, 19116–19125. doi: 10.1073/pnas.1903514116

Knab, N. J., Dale, A. W., Lettmann, K., Fossing, H., and Jørgensen, B. B. (2008). Thermodynamic and kinetic control on anaerobic oxidation of methane in marine sediments. *Geochim. Cosmochim. Acta* 72, 3746–3757. doi: 10.1016/j.gca.2008.05.039

Kraft, B., Jehmlich, N., Larsen, M., Bristow, L. A., Könneke, M., Thamdrup, B., et al. (2022). Oxygen and nitrogen production by an ammonia-oxidizing archaeon. *Science* 375, 97–100. doi: 10.1126/science.abe6733

Lever, M. A. (2012). Acetogenesis in the energy-starved deep biosphere - a paradox? *Front. Microbiol.* 2:284. doi: 10.3389/fmicb.2011.00284

Li, C., Lesnik, K. L., Fan, Y., and Liu, H. (2016). Millimeter scale electron conduction through exoelectrogenic mixed species biofilms. *FEMS Microbiol. Lett.* 363:fnw153. doi: 10.1093/femsle/fnw153

Li, C., Reimers, C. E., and Alleau, Y. (2021). Using oxidative electrodes to enrich novel members in the Desulfobulbaceae family from intertidal sediments. *Microorganisms* 9:2329. doi: 10.3390/microorganisms9112329

Lichtschlag, A., Boetius, A., and de Beer, D. (2013). High resolution in situ microsensor measurements of Amon mud volcano sediments measured at station M70/2b_805_PROF-2. Santa Barbara, CA: DataONE.

Lichtschlag, A., de Beer, D., and Boetius, A. (2011). In situ microsensor measurement in Nordic margin seep sediments VKGD272/MIC-2. Santa Barbara, CA: DataONE.

Lloyd, K. G., Steen, A. D., Ladau, J., Yin, J., and Crosby, L. (2018). Phylogenetically novel uncultured microbial cells dominate earth microbiomes. *mSystems* 3:e00055-18. doi: 10.1128/mSystems.00055-18

Lustermans, J. J. M., Bjerg, J. J., Burdorf, L. D. W., Nielsen, L. P., Schramm, A., and Marshall, I. P. G. (2023). Persistent flocks of diverse motile bacteria in long-term incubations of electron-conducting cable bacteria, Candidatus Electronema aureum. *Front. Microbiol.* 14:1008293. doi: 10.3389/fmicb.2023.1008293

Mancinelli, R. L., and McKay, C. P. (1988). The evolution of nitrogen cycling. *Origins of Life and Evolution of the Biosphere.* 18, 311–325. doi: 10.1007/bf01808213

Müller, A. L., Kjeldsen, K. U., Rattei, T., Pester, M., and Loy, A. (2015). Phylogenetic and environmental diversity of DsrAB-type dissimilatory (bi)sulfite reductases. *ISME J.* 9, 1152–1165. doi: 10.1038/ismej.2014.208

Nealson, K. H., Inagaki, F., and Takai, K. (2005). Hydrogen-driven subsurface lithoautotrophic microbial ecosystems (SLiMEs): do they exist and why should we care? *Trends Microbiol.* 13, 405–410. doi: 10.1016/j.tim.2005.07.010

Nielsen, M., Larsen, L. H., Ottosen, L. D. M., and Revsbech, N. P. (2015). Hydrogen microsensors with hydrogen sulfide traps. *Sensors Actuators B Chem.* 215, 1–8. doi: 10.1016/j.snb.2015.03.035

Ooka, H., McGlynn, S. E., and Nakamura, R. (2019). Electrochemistry at Deep-Sea hydrothermal vents: utilization of the thermodynamic driving force towards the autotrophic origin of life. *ChemElectroChem* 6, 1316–1323. doi: 10.1002/celc.201801432

Peiffer, S., Dos Santos Afonso, M., Wehrli, B., and Gaechter, R. (1992). Kinetics and mechanism of the reaction of hydrogen sulfide with lepidocrocite. *Environ. Sci. Technol.* 26, 2408–2413. doi: 10.1021/es00036a011

Pfeffer, C., Larsen, S., Song, J., Dong, M., Besenbacher, F., Meyer, R. L., et al. (2012). Filamentous bacteria transport electrons over centimetre distances. *Nature* 491, 218–221. doi: 10.1038/nature11586

Plum-Jensen, L. E., Schramm, A., and Marshall, I. P. G. (2024). First single-strain enrichments of Electrothrix cable bacteria, description of *E. aestuarii* sp. nov. and E. Rattekaaiensis sp. nov., and proposal of a cable bacteria taxonomy following the rules of the SeqCode. *Syst. Appl. Microbiol.* 47:126487. doi: 10.1016/j.syapm.2024.126487

Reimers, C. E., Li, C., Graw, M. F., Schrader, P. S., and Wolf, M. (2017). The identification of cable Bacteria attached to the anode of a benthic microbial fuel cell: evidence of long distance extracellular Electron transport to electrodes. *Front. Microbiol.* 2010:pdb.prot5366. doi: 10.1101/pdb.prot5366

Revsbech, N. P., Larsen, L. H., Gundersen, J., Dalsgaard, T., Ulloa, O., and Thamdrup, B. (2009). Determination of ultra-low oxygen concentrations in oxygen minimum zones by the STOX sensor. *Limnol. Oceanogr. Methods* 7, 371–381. doi: 10.4319/lom.2009.7.371

Ruff, S. E., Humez, P., de Angelis, I. H., Diao, M., Nightingale, M., Cho, S., et al. (2023). Hydrogen and dark oxygen drive microbial productivity in diverse groundwater ecosystems. *Nat. Commun.* 14:3194. doi: 10.1038/s41467-023-38523-4

Scilipoti, S., Koren, K., Risgaard-Petersen, N., Schramm, A., and Nielsen, L. P. (2021). Oxygen consumption of individual cable bacteria. *Sci. Adv.* 7:eabe1870. doi: 10.1126/sciadv.abe1870

Seitaj, D., Schauer, R., Sulu-Gambari, F., Hidalgo-Martinez, S., Malkin, S. Y., Burdorf, L. D. W., et al. (2015). Cable bacteria generate a firewall against euxinia in seasonally hypoxic basins. *Proc. Natl. Acad. Sci. USA* 112, 13278–13283. doi: 10.1073/pnas.1510152112

Shaw, G. H. (2008). Earth's atmosphere – hadean to early Proterozoic. *Geochemistry* 68, 235–264. doi: 10.1016/j.chemer.2008.05.001

Thauer, R. K., Jungermann, K., and Decker, K. (1977). Energy conservation in chemotrophic anaerobic bacteria. *Bacteriol. Rev.* 41, 100–180. doi: 10.1128/br.41.1.100-180.1977

Thorup, C., Schramm, A., Findlay, A. J., Finster, K. W., and Schreiber, L. (2017). Disguised as a sulfate reducer: growth of the Deltaproteobacterium *Desulfurivibrio alkaliphilus* by sulfide oxidation with nitrate. *MBio* 8:8. doi: 10.1128/mBio.00671-17

Trojan, D., Schreiber, L., Bjerg, J. T., Bøggild, A., Yang, T., Kjeldsen, K. U., et al. (2016). A taxonomic framework for cable bacteria and proposal of the candidate genera Electrothrix and Electronema. *Syst. Appl. Microbiol.* 39, 297–306. doi: 10.1016/j.syapm.2016.05.006

Vignais, P. M., and Billoud, B. (2007). Occurrence, classification, and biological function of hydrogenases: an overview. *Chem. Rev.* 107, 4206–4272. doi: 10.1021/cr050196r

Walker, J. C. G. (1985). Carbon dioxide on the early earth. *Orig. Life Evol. Biosph.* 16, 117–127. doi: 10.1007/bf01809466

Yu, Z.-G., Peiffer, S., Göttlicher, J., and Knorr, K.-H. (2015). Electron transfer budgets and kinetics of abiotic oxidation and incorporation of aqueous sulfide by dissolved organic matter. *Environ. Sci. Technol.* 49, 5441–5449. doi: 10.1021/es505531u

frontiers | Frontiers in Microbiology

TYPE Original Research
PUBLISHED 23 September 2024
DOI 10.3389/fmicb.2024.1441865

OPEN ACCESS

EDITED BY
James Andrew Bradley,
UMR7294 Institut Méditerranéen d'océanographie (MIO), France

REVIEWED BY
Sonia Tiquia-Arashiro,
University of Michigan–Dearborn, United States
Sophie Holland,
Monash University, Australia

*CORRESPONDENCE
Olga V. Karnachuk
✉ olga.karnachuk@green.tsu.ru

RECEIVED 31 May 2024
ACCEPTED 27 August 2024
PUBLISHED 23 September 2024

CITATION
Karnachuk OV, Lukina AP, Avakyan MR, Kadnikov VV, Begmatov S, Beletsky AV, Vlasova KG, Novikov AA, Shcherbakova VA, Mardanov AV and Ravin NV (2024) Novel thermophilic genera *Geochorda* gen. nov. and *Carboxydochorda* gen. nov. from the deep terrestrial subsurface reveal the ecophysiological diversity in the class *Limnochordia*. *Front. Microbiol.* 15:1441865. doi: 10.3389/fmicb.2024.1441865

Novel thermophilic genera *Geochorda* gen. nov. and *Carboxydochorda* gen. nov. from the deep terrestrial subsurface reveal the ecophysiological diversity in the class *Limnochordia*

Olga V. Karnachuk[1]*, Anastasia P. Lukina[1], Marat R. Avakyan[1], Vitaly V. Kadnikov[2], Shahjahon Begmatov[2], Alexey V. Beletsky[2], Ksenia G. Vlasova[1], Andrei A. Novikov[3], Viktoria A. Shcherbakova[4], Andrey V. Mardanov[2] and Nikolai V. Ravin[2]

[1]Laboratory of Biochemistry and Molecular Biology, Tomsk State University, Tomsk, Russia, [2]Institute of Bioengineering, Research Centre of Biotechnology of the Russian Academy of Sciences, Moscow, Russia, [3]Gubkin University, Moscow, Russia, [4]Skryabin Institute of Biochemistry and Physiology of Microorganisms, Federal Research Center Pushchino Center for Biological Research of the Russian Academy of Sciences, Moscow, Russia

The class *Limnochordia* harbors a single cultivated member, the mesophilic *Limnochorda pilosa,* which was isolated from a meromictic lake. Despite numerous molecular signatures reported in various ecosystems, the ecophysiological versatility of this deeply branched lineage of *Firmicutes (Bacillota)* remains poorly understood. The objective of this study was to use targeted cultivation, based on metagenome-assembled genomes from a deep terrestrial aquifer in Western Siberia, to isolate two new thermophilic members of the class. These isolates, described as *Geochorda subterranea* gen. nov. sp. nov. and *Carboxydochorda subterranea* gen. nov. sp. nov. within the *Geochordaceae* fam. nov., were capable of both anaerobic and aerobic respiration using fumarate and O_2, respectively, with simple sugars as electron donors. The cultivated *Geochordaceae* have demonstrated fermentative growth and degradation of various polymers, including starch, maltose, maltodextrin, xylan, and chitin. The carboxydotrophic *C. subterranea* sp. nov. exhibited autotrophic growth via the Calvin–Benson–Bassham cycle, using CO, H_2, and formate as electron donors and O_2 as an electron acceptor, adding metabolic flexibility to the bacterium in the nutrient-depleted "deep biosphere" and supporting the possibility of aerobic metabolism in the deep subsurface. The broad physiological potential deciphered from physiological experiments and comparative genomic data explains the widespread distribution of uncultivated members of the class *Limnochordia* in various ecosystems, where they can oxidize complex organic substrates through both aerobic and anaerobic respiration, as well as pursue a chemolithotrophic lifestyle through the oxidation of H_2 or CO.

KEYWORDS

deep terrestrial subsurface, *Limnochordia*, thermophiles, carboxydotrophs, aerobic respiration, didermic cell wall

1 Introduction

It is widely accepted that cultivated bacteria and archaea represent only a small portion of the uncultivated majority of the prokaryotic world, known to us through environmental DNA sequences. The cultivation of microorganisms is not only necessary to validate novel taxa but also provides the basis for deciphering a growing number of microbial proteins with unknown functions. Careful consideration of metabolic pathways in metagenome-assembled genomes (MAGs) from uncultivated prokaryotes provides essential clues to their cultivation. The class *Limnochordia*, representing a distant phylogenetic lineage in the phylum *Firmicutes* (recently renamed *Bacillota*), is an example of a higher-ranking bacterial taxon with only one cultivated species. This class was created to accommodate the mesophilic *Limnochorda pilosa* HC45^T, isolated from meromictic lake sediments in Japan (Watanabe et al., 2015). The isolate was distantly related to the genera *Simbiobacterium*, *Thermaerobacter*, and *Sulfobacillus* and had a number of specific characteristics that distinguish the strain from the canonical *Firmicites*, including a high DNA G+C content, a high percentage of GTC start codons, and the absence of several conserved genes involved in cell division (Watanabe et al., 2016). Later, metagenomic analysis revealed *Limnochordia* in various surface biotopes, including thermophilic compost (Braga et al., 2021), cattle manure enrichment hydrolyzing carboxymethyl cellulose (Scheffer et al., 2021), aged refuse soil (Hou et al., 2021), pit mud used for the production of Chinese beverage Baijiu (Shoubao et al., 2023), and mice cadaver brain immersed in fresh water (Wang et al., 2022). *Limnochordia* was also one of the main components of the microbial consortium applied for lignocellulose degradation (Liu et al., 2021).

A recent phylogenetic analysis of uncultivated *Firmicutes* from the uncultured bacteria and archaea (UBA) dataset of Parks et al. (2017) placed *Limnochordia* as the second-deepest-branching lineage after the *Halanaerobiales* (Taib et al., 2020). One unique characteristic of the *Limnochordia* is the presence of an outer membrane and a diderm (Gram-negative) character of the cell envelope. Phylogenomic analysis of the outer membrane markers in *Limnochordia*, *Negativicutes*, and *Halanaerobiales* has led the authors to hypothesize a two-membrane cell envelope in the ancestor of all *Firmicutes* and the multiple loss of the outer membrane during the diversification of the phylum (Taib et al., 2020). A recent rooted bacterial phylogeny has confirmed the diderm character of the last bacterial common ancestor (LBCA) (Coleman et al., 2021). Most of the 46 unclassified UBA genomes of uncultivated *Limnochordia* used for phylogenomic analysis by Taib et al. (2020) were assembled from anaerobic mud and digester samples. Until now, *L. pilosa* remained the only cultivated species in the class *Limnochordia,* and the ecophysiological versatility of this group remains largely understudied due to the lack of cultivated representatives.

A characteristic feature of deep terrestrial subsurface biotopes is the scarcity of energy sources for microbial life. There is a general consensus that deep subsurface environments are nutrient-depleted, oligotrophic, and energy-constrained (Purkamo et al., 2017; Westmeijer et al., 2022). The absence of light precludes photosynthetic production. The chemosynthetic production of organic carbon in the deep subsurface is highly variable due to the lack of a clear, constant supply of inorganic electron donors, including CH_4, HS^-, or Fe(II), as occurs in marine hydrothermal vents. Dihydrogen is the most common electron donor in the deep terrestrial biosphere (Ruff et al., 2023). Serpentinization produces H_2 as a result of the reaction of olivine and pyroxene minerals with water (Onstott et al., 2019). Molecular hydrogen is also generated by water radiolysis, which also produces sulfate, an electron acceptor, via the oxidation of sulfides by radiolytically produced H_2O_2 (Lefticariu et al., 2006). A possible source of organic carbon for heterotrophic microorganisms in deep terrestrial biotopes is microbial necromass formed by chemolithotrophs. They can also use the mostly recalcitrant organic carbon associated with oil-, gas-, or coal-endowed sedimentary rocks (Kadnikov et al., 2020).

From an electron acceptor perspective, the deep environmental conditions below the Earth's surface have traditionally been considered anoxic and anaerobic (Lovley and Chapelle, 1995; Kieft et al., 2005; Liebensteiner et al., 2014). Sulfate, carbonate, iron, and manganese oxides were considered the most common electron acceptors (Onstott et al., 2019). However, a recent study demonstrated the presence of dissolved oxygen at concentrations of 0.52 ± 0.12 mg L^{-1} in multiple groundwater monitoring well samples (<250 m depth) located in 14 aquifers in Canada (Ruff et al., 2023). It was assumed that the so-called "dark oxygen" formed in the absence of light arises from microbial dismutation of chlorite, nitric oxide, or H_2O_2, which is reflected in the isotopic composition of oxygen.

Metagenomic shotgun sequencing of water from a deep terrestrial aquifer in Mesozoic sediments at a depth of 2.0 km in Western Siberia revealed a plethora of organothrophic prokaryotes possessing aerobic respiratory pathways (Kadnikov et al., 2020). One of the MAG, designated as Ch19 and containing genes for cytochrome *c* oxidase, a marker of oxygen respiration, belonged to the class *Limnochordia*. The MAG made up 0.37% of the metagenome. In this study, we applied targeted isolation of the Ch19 bacterium using specific electron donors whose potential metabolism was inferred from the Ch19 MAG. Following the successful isolation of the Ch19 bacterium, another member of *Limnochordia* was isolated from a geographically distinct deep terrestrial aquifer in the Altay region based on the use of genomic information on the metabolism of *Limnochordia*. Here we report the isolation and characterization of two novel cultivated members of the class *Limnochordia* derived from different deep terrestrial thermal aquifers, capable of both aerobic and anaerobic respiration. One of the isolates exhibits a dual mode of life—heterotrophic by degradation of organic compounds and autotrophic by oxidation of CO and H_2 using oxygen as an external electron acceptor.

2 Materials and methods

2.1 Deep water sampling and the initial enrichments set up

The geographical location, geology, and water characteristics of the deep boreholes used for cultivation have been previously described in detail (Kadnikov et al., 2017, 2018a, 2020; Lukina

et al., 2023). Briefly, borehole 5P, which contains MAG Ch19 (Kadnikov et al., 2020), is a former oil-exploration artesian well located near the small village of Chazhemto in the Tomsk region of Western Siberia (58.0758 N, 82.8374 E). On July 11, 2019, water samples were collected from a sampling line at the wellhead for use in *Limnochordia* enrichments and subsequent pure culture isolation. Cells from 5 L of borehole water were collected on 0.22 μm cellulose nitrate membrane (Sartorius, Germany) using a Sartorius filtration unit.

Borehole 4E is located in the small town of Belokurikha in the Altay region (51.988832 N, 84.969378 E). The water from the borehole is used to supply mineral water to a local spa. On August 8, 2019, water samples for cultivation were collected from the wellhead of the 4E borehole. Both boreholes are classified as artesian wells; water flows from them under pressure, which minimizes the possibility of contamination from the surface. Water was not sampled until its physiochemical characteristics (temperature, pH, and Eh) were stable while flowing.

Water temperature, pH, and Eh were measured at the wellhead using a pH-meter HI 8314 (Hanna Instruments, Vöhringen, Germany) equipped with appropriate electrodes. The water sample was fixed with 2.4% Zn-acetate in a 1:5 proportion for hydrogen sulfide determination. H_2S was measured colorimetrically in triplicate using a Smart Spec Plus spectrophotometer (Bio-Rad Laboratories, Hercules, CA) and the methylene blue method (Cline, 1969).

2.2 Pure culture isolation and characterization

Initial enrichments were prepared on-site. Cells from the water sample of the 5P borehole (Chazhemto) were concentrated by filtration through a 0.22 μm sterile filter (Sartorius, Germany). The total volume of filtered water was 5 L, and the filter was aseptically cut into 16 pieces, with each piece placed into a 500 ml serum bottle filled with cultivation medium. Initial enrichments were prepared in the modified spirochete basal medium (Karnachuk et al., 2021). The medium contained 2.0 g $NaNO_3$, 1.0 g K_2HPO_4, 0.5 g $MgSO_4$, 0.5 g KCl, 0.01 g $FeSO_4$, 1.0 g yeast extract, and 1.0 g glucose per liter. It was also supplemented with 2 mL of vitamin solution (Widdel and Bak, 1992), 1 mL of selenite–tungsten solution (Widdel and Bak, 1992), and 1 mL of trace element solution (DSMZ141). $Na_2S{\cdot}9H_2O$ (96 g/L, 2 mL/L of basal medium) was used as a reducing agent, and each culture flask received an iron wire (100% Fe) as described previously (Karnachuk et al., 2019). Enrichments were incubated at 50°C. No preliminary cell concentration on the filter was used for the 4E (Belokurikha) borehole water sample. Instead, the 500-ml serum bottles with the modified spirochete medium were inoculated with approximately 50 ml of thermal water drawn directly from the borehole wellhead. Glucose was substituted with starch (1%). The pure culture was created using the serial dilution-to-extinction method. The purity of the cultures was determined through microscopic examination of bacterial morphology and genome sequencing. The 16S rRNA gene was amplified using the primer pairs 27F and 1492R (Lane, 1991) and sequenced commercially by Syntol Co. (Moscow, Russia) using the Sanger method.

Cell morphology was examined using both phase contrast microscopy (Axio Imager A1 microscope) and transmission electron microscopy (TEM) of ultra-thin sections, as described previously by Ikkert et al. (2013). Briefly, for TEM, cells from 500 ml serum bottles were harvested by centrifugation at 11,000 x g for 40 min and then washed with 1 x PBS buffer. Fixation of pelletized samples with glutaraldehyde, staining with osmium tetroxide, and dehydration with ethanol have been described previously by Ikkert et al. (2013). Ultra-thin sections (60–100 nm) were prepared using an ultramictome (Ultratome III, LKB, Stockholm, Sweden) and viewed with a JEM-100 CXII electron microscope (JEOL, Tokyo, Japan) at a voltage of 80 kV.

Growth experiments were conducted on a spirochete basal medium supplemented with vitamin, microelement, and selenite–tungsten solutions. Growth was tested at temperatures ranging from 28°C to 80°C and pH levels ranging from 5.0 to 10.0, and the pH was adjusted to the desired experimental pH values using 0.5 M H_2SO_4 or 2 M NaOH. The optimal salinity for growth was determined to be 0% to 2.5% NaCl. To test growth substrates for the LN^T strain, a modified DSMZ 963 medium was used, which contained (per liter): 0.78 g K_2HPO_4, 0.75 g KH_2PO_4, 0.04 g Na3 EDTA, 0.01 g $FeSO_4{\cdot}7\ H_2O$, 0.25 g $MgSO_4{\cdot}7\ H_2O$, 0.03 g $CaCl_2{\cdot}2\ H_2O$, 0.20 g NaCl, 0.050 g NH_4Cl, 0.10 g yeast extract, 10 ml of Wolin's vitamin solution, 10 ml of DSMZ 318 trace element solution, and 5 ml of $Na_2S{\cdot}9\ H_2O$ solution (Widdel and Bak, 1992). To test growth substrates for the $L945^T$ strain, a modified Widdel-Bak (WB) medium (Widdel and Bak, 1992) was used, which contained (per liter): 0.15 g Na_2SO_4, 0.2 g KH_2PO_4, 0.25 g NH_4Cl, 1.0 g NaCl, 0.4 g $MgCl_2{\cdot}6H_2O$, 0.5 g KCl, 0.113 g $CaCl_2$, 0.10 g yeast extract, 10 ml of Wolin's vitamin solution, 10 ml of DSMZ 318 trace element solution, and 2 ml of $Na_2S{\cdot}9\ H_2O$ solution (Widdel and Bak, 1992). The strain growth was tested under anaerobic conditions with the following substrates: sucrose (2 mM), glucose (5 mM), fructose (5 mM), arabinose (10 mM), rhamnose (10 mM), maltose (10 mM), lactose (10 mM), mannose (10 mM), galactose (2 mM), sorbitol (10 mM), glycerol (10 mM), ethanol (20 mM), propanol (17 mM), formate (7.5 mM), pyruvate (7 mM), butyrate (7 mM), succinate (4.5 mM), lactate (7.3 mM), propionate (13.5 mM), acetate (10 mM), fumarate (10 mM), malate (7.5 mM), starch (1%), dextrin (1%), maltodextrin (1%), peptone (1%), gelatin (1%), chitin (2%), chitosan (2%), and microcrystalline cellulose (2%) (all Sigma-Aldrich). Fumarate (10 mM) was used as an electron acceptor. Insoluble substrates were added before autoclaving, and soluble substrates were then filtered through a 0.2 μm-pore-size filter and added into a sterilized medium. If growth was detected, the culture was sub-cultivated at least five times in the presence of each substrate to ensure proper utilization. For anaerobic cultivations, cultures were grown in liquid media in sealed culture vials with no headspace and incubated at the optimal temperature (65°C and 55°C for strains LN^T and $L945^T$, respectively). Aerobic growth was assessed using pyruvate (7 mM) for strain LN^T and glucose (5 mM) for strain $L945^T$. CO-fed cultures were grown in WB medium with N_2 headspace using CO (1%−10%) as the sole electron donor. For aerobic cultivations, cultures were grown in 50-ml serum bottles with 70% gas phase under continuous agitation.

For the analysis of cellular fatty acids, biomass was harvested from cells grown in pyruvate (7 mM)- and fumarate-enriched (10 mM) spirochete basal medium until exponential growth phase, and 5 mg of freeze-dried cell material was treated with anhydrous 3N HCl/MeOH in PTFE-lined screw-cap borosilicate glass vial at 70°C for 2 h for conversion to fatty acid methyl ester. Cellular fatty acids (CFA) were determined by GC–MS (Thermo Scientific Trace GC Ultra DSQ II; CP-Sil 88 50 m × 250 μm × 0.20 μm highly polar cyanopropyl column; injection with a split ratio of 1:20; helium gas flow 1.2 mL/min; with a temperature program 5 min at 140°C, then 10 K/min to 220°C, then hold 22 min at 220°C; transfer line at 280°C EI 70 eV; mass scanning from 50 to 550 m/z at 0.25 scans/s) as a percentage of the total ion flow area.

2.3 Genome sequencing and analysis

Genomic DNA was isolated from strains LN^T and L945^T using a DNeasy PowerSoil DNA isolation kit (Mo Bio Laboratories, Carlsbad, CA, USA) and sequenced using Illumina and Oxford Nanopore technologies. For Illumina sequencing, the shotgun genome library was prepared using the NEBNext Ultra II DNA library prep kit (New England Biolabs, Ipswich, MA, USA) and sequenced on an Illumina MiSeq in a paired reads mode (2 × 300 nt). A total of 2,877,132 (1.3 Gb) and 3,786,751 (2.0 Gb) read pairs were generated for strains LN^T and L945^T, respectively. Both genomes were additionally sequenced on a MinION instrument (Oxford Nanopore Technologies, Oxford, UK) using the ligation sequencing kit 1D and FLOMIN110 cells. A total of 663 Mb and 882 Mb of Nanopore sequences were obtained for strains LN^T and L945^T, respectively.

The complete circular genome of strain LN^T was assembled from Nanopore reads with Flye v.2.8.2 (Kolmogorov et al., 2019). The consensus sequence of the assembled circular contig was corrected using Illumina reads and two iterations of Pilon v.1.22 (Walker et al., 2014). To obtain the complete circular genome of strain L945^T, the hybrid assembly of Illumina and Nanopore reads was performed using SPAdes v.3.13.0 (Bankevich et al., 2012).

Gene search and annotation were carried out using the NCBI Prokaryotic Genome Annotation Pipeline (Tatusova et al., 2016) and the RAST server 2 (Brettin et al., 2015). AAI between the genomes was determined using the aai.rb script from the enveomics collection (Rodriguez-R and Konstantinidis, 2016). Prediction and comparative analysis of the metabolic capabilities of MAGs and genomes of isolates was performed using the Distilled and Refined Annotation of Metabolism (DRAM) tool (Shaffer et al., 2020). CheckM2 v.1.0.1 (Chklovski et al., 2023) was used to evaluate the completeness and contamination values of genomes. Genomes were taxonomically classified according to the genome-based taxonomic system (Parks et al., 2018) using the Genome Taxonomy Database Toolkit (GTDB-Tk) v.2.4.0 (Chaumeil et al., 2022) and Genome Taxonomy Database (GTDB), release 09-RS220.

For genome-based phylogenetic analysis, genes from all analyzed genomes were clustered using Blastclust v.2.2.26 of the BLAST package, with a minimum threshold of 40% alignment identity over 90% length of a shorter gene. One hundred and eighty single-copy genes presented in at least 24 of 29 genomes were selected based on the results of clustering. The alignment for the tree construction was created by concatenating alignments of each single-copy gene using MAFFT v.7 (Katoh and Standley, 2013). The concatenated alignment was additionally trimmed using ClipKit (Steenwyk et al., 2020) to remove errors and phylogenetically uninformative sites. A maximum-likelihood tree was computed by PhyML v. 3.3 (Guindon et al., 2010) using default parameters (LG amino acid substitution model, four substitution rate categories modeled by discrete gamma distribution with estimated shape parameter, and branch support values calculated using the approximate Bayes method). The default settings were used for all software unless specifically stated otherwise.

3 Results

3.1 5P and 4E boreholes water chemistry

The detailed water chemistry of the 5P and 4E boreholes has been reported in our previous studies (Kadnikov et al., 2017, 2018a; Lukina et al., 2023). Briefly, the 5P (Chazhemto) water temperature at the outflow varied from 14.5°C to 20.8°C, the water was anoxic (Eh from −329 to −480 mV), and the pH was circumneutral (7.5–7.6). At the time of sampling for cultivation on July 11, 2019, the temperature was 14.5°, the pH was 7.5, and the Eh was −420 mV. The H_2S concentration was 3.46 ± 0.47 mg/l. The 4E (Belokurikha) thermal water was slightly anoxic and alkaline. At the time of sampling for cultivation on 8 August 2019 the temperature was 38.0°C, pH −9.12 and Eh −40 mV.

3.2 MAG-based isolation of uncultivated *Limnochordia*

Microscopic observation of the set of enrichments from the 5P (Chazhemto) borehole revealed different morphotypes, including vibrios, rods, filamentous cells, and long rods with pointed ends (Supplementary Figure S1). Based on the previous reports on the cell morphology of *L. pilosa* (Watanabe et al., 2015, 2016), it was suggested that the long rods may represent the Ch19 *Limnochordia* bacterium, which MAG has been previously assembled from the 5P (Chazhemto) borehole water (Kadnikov et al., 2020). This MAG provided a clue for the enrichment and selection of the Ch19 bacterium. The sorbitol degradation pathway was present in the genome, making sorbitol the chosen growth substrate for the *Limnochordia* bacterium pure culture isolation. The pure culture was obtained using the serial dilution-to-extinction method on the modified spirochete medium with sorbitol (10 mM). The strain was designated LN^T, and its 16S rRNA gene sequence analysis showed that it represented a distinct lineage with a sequence similarity with that of only 85.2% to that of *L. pilosa* HC45^T.

Considering the amylolytic potential predicted by analysis of the Ch19 bacterium MAG (Kadnikov et al., 2020), starch (1%) was chosen as the growth substrate for the isolation of the *Limnochordia* bacterium from another deep thermal borehole, 4E in Belokurikha. *Limnochorda*-like morphotypes were observed in the enrichment culture with starch, and the bacteria formed spherical bodies. Given the small width of the *Limnochordia*-like morphotypes, filtration

through a 0.22 μm filter was chosen for further enrichment. After a series of dilutions, a pure culture isolate was obtained and designated strain L945^T. The 16S rRNA gene sequence showed that *L. pilosa* was the closest cultivated and validly described species with a sequence similarity of 87.05%.

3.3 Morphology, growth conditions and physiology of *Geochorda subterranea* gen. nov. sp. nov. LN^T and *Carboxydochorda subterranea* gen. nov. sp. nov. L945^T

Cells of strain LN^T were curved rods, 1.5–9.0 μm long and 0.15–0.20 μm wide (Figure 1). The cells were immotile under all studied culture conditions, despite the presence of a set of genes necessary for flagellar motility and chemotaxis in the genome. TEM micrographs of ultra-thin sections of cells revealed filamentous electron-transparent structures (Figure 2). The cells had a didermic (Gram-negative) wall containing an outer membrane (Figure 2) and formed spherical bodies (Figure 3A). In cells and spherical bodies grown with pyruvate (9 mM) and fumarate (1 mM) for 9 days, an S-layer was observed (Figure 3B). The genome of the strain LN^T contains an S-layer homology domain-containing protein, which is an amino acid sequence that shares only 27.4% identity with that of *L. pilosa* but 50.1% with uncultivated *Limnochordales* MAGs binned from burning coal seams (Bu05) (Kadnikov et al., 2023). Electron-lucent granules were also observed in cells grown with pyruvate and fumarate for 7 days (Figure 1).

Strain L945^T cells reached lengths of 1.5 to 7.0 μm and widths of 0.15–0.30 μm (Figure 4). The strain formed round bodies of up to 2 μm in size. The cell wall of the strain was didermic (Gram-negative), containing an outer membrane and S-layer, which was visible in old cultures grown for 50 days (Figure 5). However, no S-layer proteins were found in the genome.

Strain LN^T had a relatively wide pH growth range of pH 6.0 to 9.5, with an optimum of 7.5–8.0 and necessary NaCl for growth. The optimal NaCl range for growth varied from 0.1% to 2.0% (w/v), with an optimum of 1.0%−1.5% (w/v). The temperature range for the strain growth was 45°−70° with an optimum of 65°. The highest growth rate was observed when strain LN^T was grown with pyruvate and fumarate. Fumarate respiration was also observed with a narrow range of sugars, including fructose, glucose, sucrose, galactose, and propionate. The strain was able to hydrolyze starch, dextrin, maltodextrin, xylan, chitin, and chitosan in the presence of fumarate in the medium. Slow growth was observed when sorbitol and malate were used as electron donors for fumarate respiration. The strain was unable to use arabinose, rhamnose, maltose, lactose, mannose, glycerol, ethanol, propanol, formate, butyrate, succinate, lactate, acetate, peptone, gelatin, tryptone, soytone, or microcrystalline cellulose for fumarate respiration. Strain LN^T did not use any of the tested inorganic electron acceptors for anaerobic respiration, including sulfate, sulfite, thiosulfate, elemental sulfur, nitrate, nitrite, or Fe–NTA. Surprisingly, strain LN^T, isolated from the deep subsurface, was able to grow aerobically respiring with O_2 using glucose, fructose, or sucrose as electron donors. However, the strain could not grow on glucose, lactate, or pyruvate without adding fumarate to the medium. No autotrophic growth was observed with formate or CO as the electron donor and fumarate or O_2 as the electron acceptor. Also, the strain did not grow with H_2 and CO_2.

The fatty acid profile of the LN^T strain cell wall indicated that the major proportion (>10%) comprised iso-C15:0 (23.1%), anteiso-C17:0 (18.4%), iso-C16:0 (16.3%), anteiso-C15:0 (15.0%), and C16:0 (13.6%) (Supplementary Table S1).

Strain L945^T could grow at pH 6.5–9.0, with an optimum of 7.0–7.5. The optimal growth was observed without NaCl addition to the growth medium. The strain could tolerate up to 1% NaCl. The temperature range for strain L945^T was 37°−60° with an optimum of 55°. Similar to strain LN^T, strain L945^T utilized pyruvate, fructose, glucose, sucrose, and galactose with fumarate as an electron acceptor. The strain was unable to hydrolyze dextrin and maltodextrin in the presence of fumarate in the medium. Slow growth with chitin occurred in the presence of fumarate in the medium. The strain did not use arabinose, rhamnose, maltose, lactose, mannose, glycerol, ethanol, propanol, butyrate, succinate, lactate, propionate, acetate, peptone, gelatin, or microcrystalline cellulose for fumarate respiration. Similar to strain LN^T, L945^T grew under aerobic conditions using glucose, fructose, and sucrose as electron donors for aerobic respiration with O_2. In addition to organic electron donors, L945^T was capable of autotrophic growth with CO (2%) or formate with O_2 as an electron acceptor. CO was also used as an electron donor for fumarate respiration. Sulfate, sulfite, thiosulfate, nitrate, nitrite, or Fe–NTA were not used by the strain as electron acceptors. However, strain L945^T actively grew by sulfur respiration with glucose as an electron donor.

Lipid analysis indicated that similar to *L. pilosa* (Watanabe et al., 2015), the major fatty acids (>10%) present in strain L945^T cell wall were anteiso-C15:0 (46.1%) and iso-C15:0 (28.3%) (Supplementary Table S1).

3.4 Genome-based phylogenetic placement of strains LN^T and L945^T

Taxonomic assignment of strains LN^T and L945^T was determined by searching against the Genome Taxonomy database (GTDB) (Parks et al., 2018), placing them in the phylum *Firmicutes (Bacillota),* class *Limnochordia,* order *Limnochordales*, and family Bu05. To further characterize the phylogeny of the class *Limnochordia*, we constructed a phylogenetic tree based on the concatenated sequences of 180 conserved marker genes, including the LN^T and L945^T genomes, 13 other genomes from the order *Limnochordales*, and 13 genomes representing other candidate orders of *Limnochordia* (Figure 6). All lineages recognized by the GTDB within the *Limnochordia* were represented by distinct monophyletic branches.

The average amino acid sequence identity between the LN^T and L945^T genomes was 67.13%, which is above the proposed genera delineation threshold (65%, Konstantinidis et al., 2017). However, their 16S rRNA gene sequences were 93.51% identical, suggesting that they represent different genera. The closest relative of L945^T, with an AAI of 97.13%, is an uncultivated *Limnochordaceae* bacterium Bu05 (GCA_014896295.1), obtained from the coal-fire heated soil in Eastern Siberia

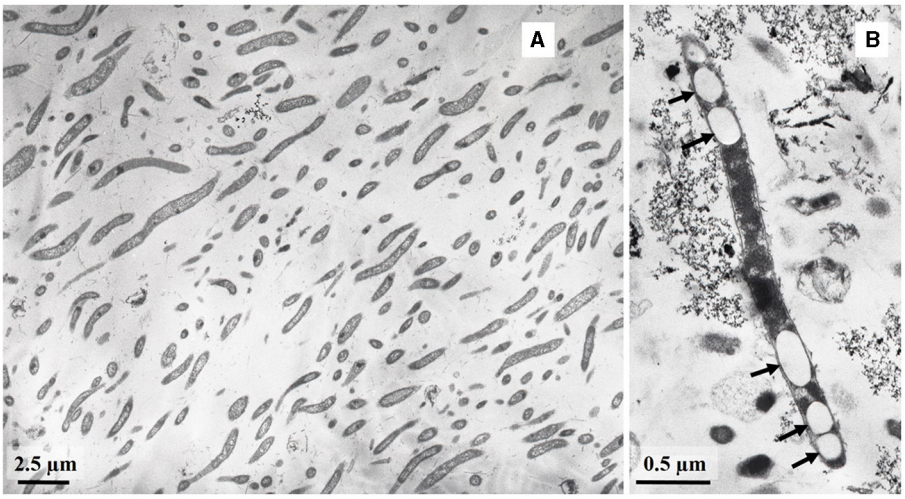

FIGURE 1
TEM micrographs of ultra-thin sections of strain LN^T cells **(A)** and cells containing electron-transparent granules (shown by arrows) **(B)**.

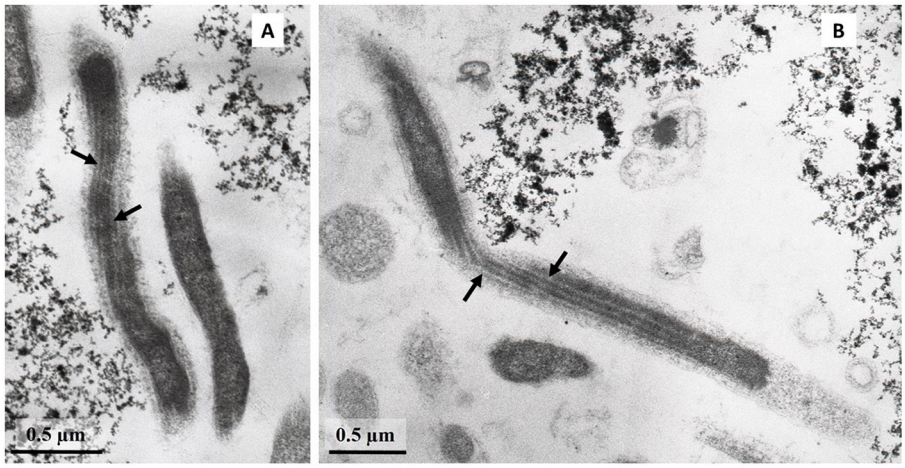

FIGURE 2
(A, B) TEM micrographs of ultra-thin sections of strain LN^T with filamentous electron-transparent structures (shown by arrows).

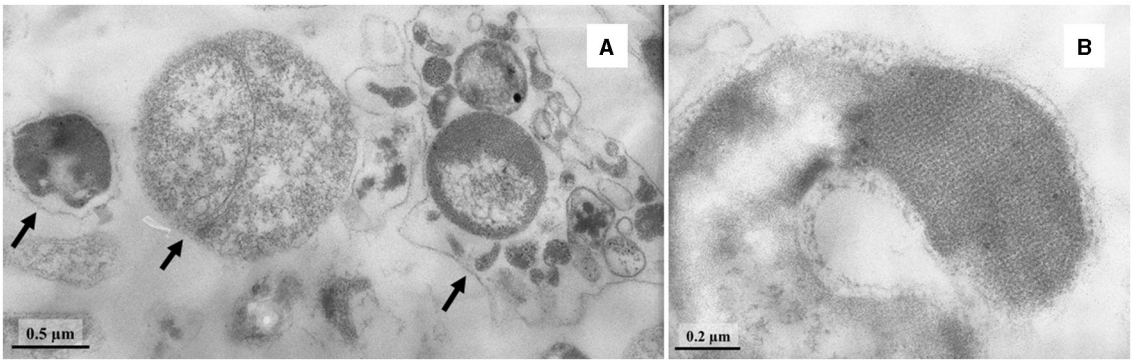

FIGURE 3
TEM micrographs of ultra-thin sections of round bodies (shown by arrows) **(A)** and S-layer **(B)** of strain LN^T.

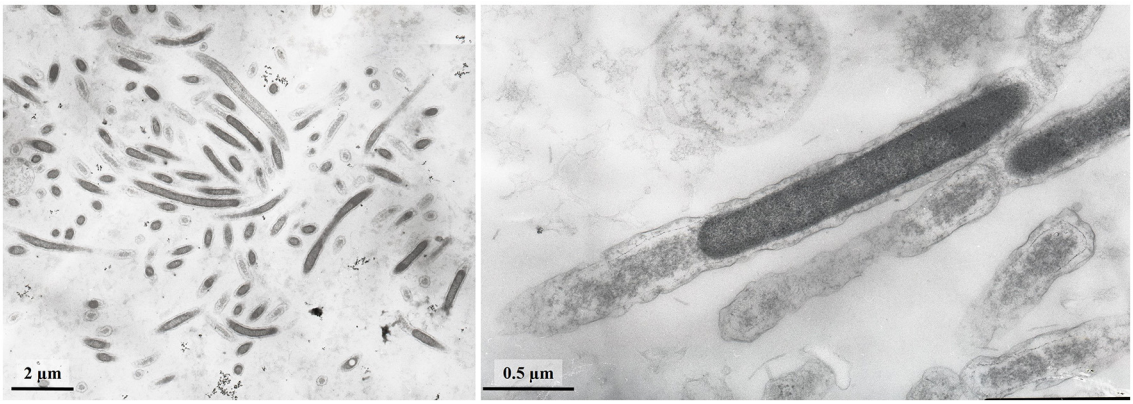

FIGURE 4
TEM micrographs of ultra-thin sections of strain L945^T cells.

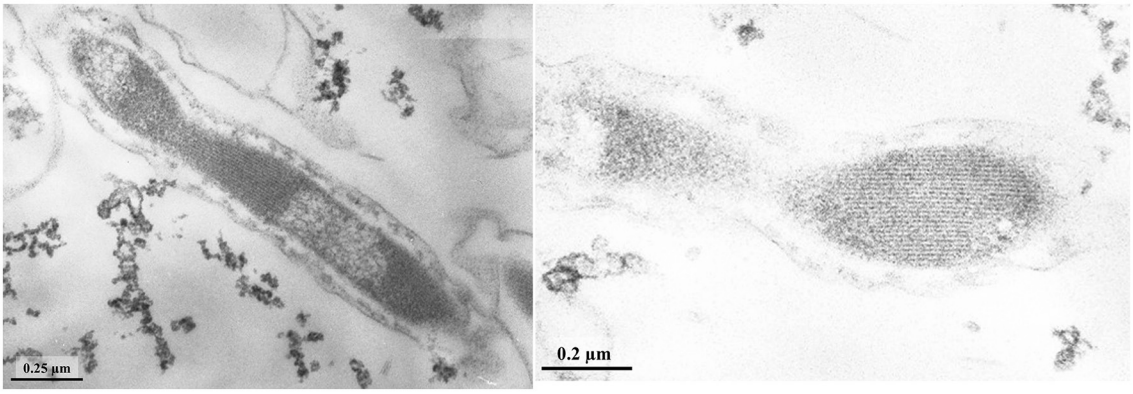

FIGURE 5
TEM micrographs of ultra-thin sections of strain L945^T cells with S-layer.

(Kadnikov et al., 2023). Apparently, these bacteria belong to the same species.

3.5 Main metabolic pathways

Analysis of the LN^T and L945^T genomes revealed the presence of a complete set of genes encoding enzymes for the Embden–Meyerhof glycolytic pathway, gluconeogenesis, and the tricarboxylic acid (TCA) cycle (Figure 7). Both genomes also contain genes encoding the malic enzyme, which decarboxylates malate to pyruvate, and the phosphoenolpyruvate carboxylase, which catalyzes the addition of bicarbonate to phosphoenolpyruvate to form oxaloacetate. The strain L945^T genome encodes the pentose phosphate pathway, including both oxidative and non-oxidative branches, while only the latter is encoded in the LN^T strain. Pyruvate produced in the glycolysis could be decarboxylated to acetyl coenzyme A (CoA) by pyruvate:ferredoxin oxidoreductase or converted to lactate by lactate dehydrogenase. The formation of acetate as a fermentation product can be enabled by acetyl-CoA synthetase (ADP-forming).

All major components of the aerobic respiratory chain are encoded in both genomes, including the proton-translocating NADH:quinone oxidoreductase, membrane-linked succinate dehydrogenase, cytochrome *bc* complex III, and terminal oxidases. Both genomes also encode two proton-translocating cytochrome *c* oxidases, and the L945^T genome additionally harbors genes for cytochrome *bd* ubiquinol oxidase. Physiological experiments confirmed the ability of both strains to respire O_2. The ability of both bacteria to grow aerobically is consistent with the presence of superoxide dismutase and catalase participating in protection against oxidative stress in aerobes.

Genome analysis revealed no known reductases for dissimilatory reduction of sulfate and other sulfur compounds, nitrate, and arsenate, in consistent with the observed lack of growth with SO_4^{2-} and NO_3^-. In addition to fumarate reductase, which enables anaerobic respiration with fumarate, the other terminal reductases for anaerobic respiration are the nitric-oxide reductase, found in genomes, copper-containing nitrite reductase in strain LN^T, and nitrous-oxide reductase in strain L945^T. However, we

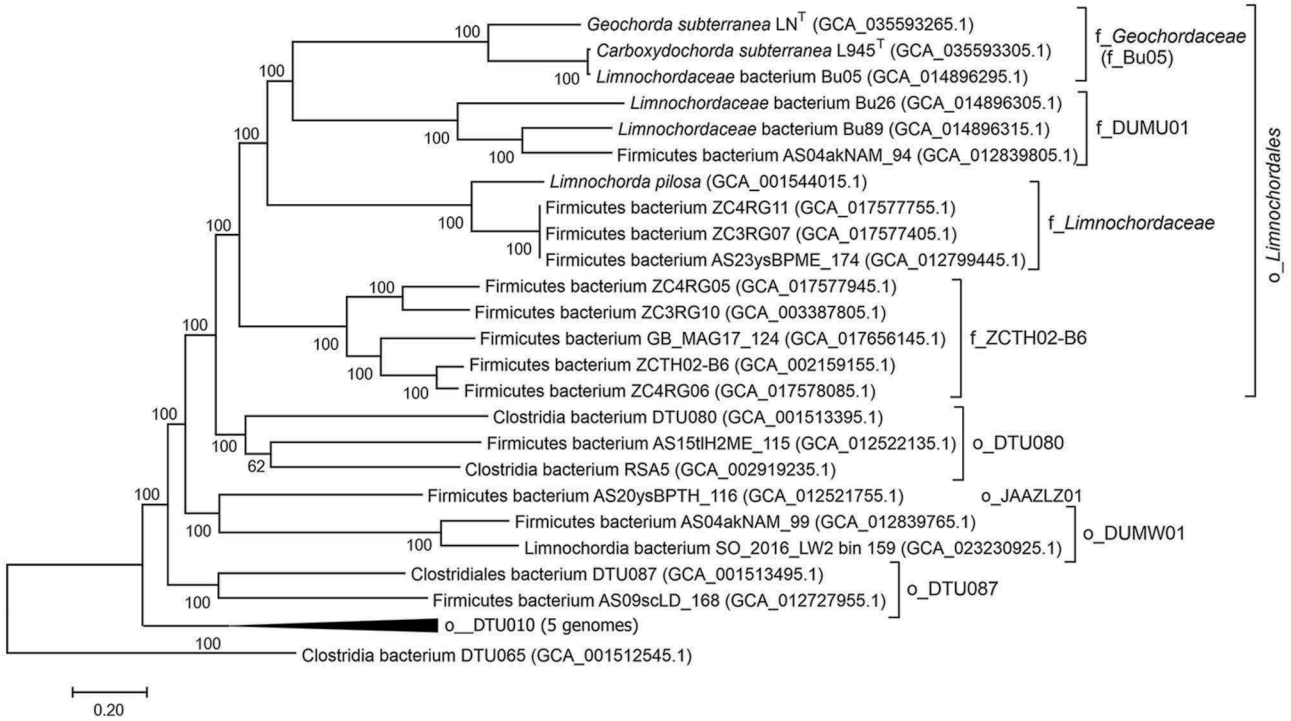

FIGURE 6
Genome-based phylogeny of *Limnohordia*. The level of support for internal branches was assessed using the Bayesian test in PhyML. Taxonomy is shown according to the GTDB release R207 (o, order; f, family). The genome of Clostridia bacterium DTU065 representing a sister class DTU065 in the candidate phylum Firmicutes G was used to root the tree.

were unable to grow LN^T and L945^T with nitrite. Additionally, the strain L945^T genome was found to contain genes for the complex iron–sulfur molybdoenzyme oxidoreductase of the Psr/Phs family, which could perform the reduction of sulfur and/or tetrathionate. Consistently, strain L945^T showed active growth with elemental sulfur.

The transmembrane proton gradient generated by respiratory chains may be used for ATP synthesis by an F_0F_1-type ATPase. Both bacteria have an additional mechanism to generate a transmembrane ion gradient that can be used for ATP synthesis, namely the ion-transporting complex Rnf (*rnfCDEAB* genes). In *Firmicutes*, this membrane-linked complex acts catabolically as a ferredoxin: NAD+ oxidoreductase, moving sodium ions or protons across the membrane out of the cell (Biegel et al., 2011).

One important difference between strains LN^T and L945^T is the presence of key genes involved in the Calvin–Benson–Bassham cycle for autotrophic carbon fixation in the latter, including ribulose bisphosphate carboxylase and phosphoribulokinase. The Wood–Ljungdahl pathway was not found in both genomes, as well as reductive TCA, as evidenced by the absence of citrate lyase. Thus, CO_2 fixation in L945^T growth experiments with H_2 and CO_2 presumably occurs via the Calvin–Benson–Bassham cycle.

The genome of strain L945^T also contains the genes for membrane-bound formate dehydrogenase and a membrane-linked [NiFe] group 1d hydrogenase, which enable hydrogenotrophic respiration using O_2 or fumarate as terminal electron acceptors (Greening et al., 2016). These oxygen-tolerant hydrogenases are commonly found in *Firmicutes*. Aerobic carbon monoxide dehydrogenase genes were also found in the genome of this strain, which is consistent with its observed ability to grow autotrophically on CO in the presence of oxygen. These traits were absent in strain LN^T.

In the search for potentially secreted glycosyl hydrolases that could enable the utilization of polysaccharides, a limited set of enzymes containing N-terminal secretion signal peptides was found. Both genomes contain genes for the utilization of chitin and N-acetyl-D-glucosamine (GlcNAc), including GH18 family chitinases and GH3 family beta-N-acetylglucosaminidases. These enzymes carry N-terminal secretion signals, suggesting their extracellular operation in the hydrolysis of chitin and chitooligosaccharides. The coordinated activity of these enzymes could result in the hydrolysis of chitin into oligomers and the production of GlcNAc monomers, which may be imported by ATP-binding cassette (ABC)-type transporters. In the cytoplasm, GlcNAc may be phosphorylated by *N*-acetylglucosamine kinase. Then, GlcNAc-6-P could be deacetylated by *N*-acetylglucosamine-6-phosphate deacetylase to form glucosamine-6-phosphate. The latter is then converted by glucosamine-6-phosphate deaminase into fructose-6-P, which enters the Embden–Meyerhof pathway (Beier and Bertilsson, 2013).

Consistent with the observed ability of strain LN^T to hydrolyze starch, its genome comprises an operon including genes for secreted GH57 family alpha-amylase, maltodextrin ABC transporter, and maltodextrin glucosidase of the GH13 family. Strain L945^T also harbors a similar operon, but it lacks GH57 alpha-amylase. Both genomes also encode

10.3389/fmicb.2024.1441865

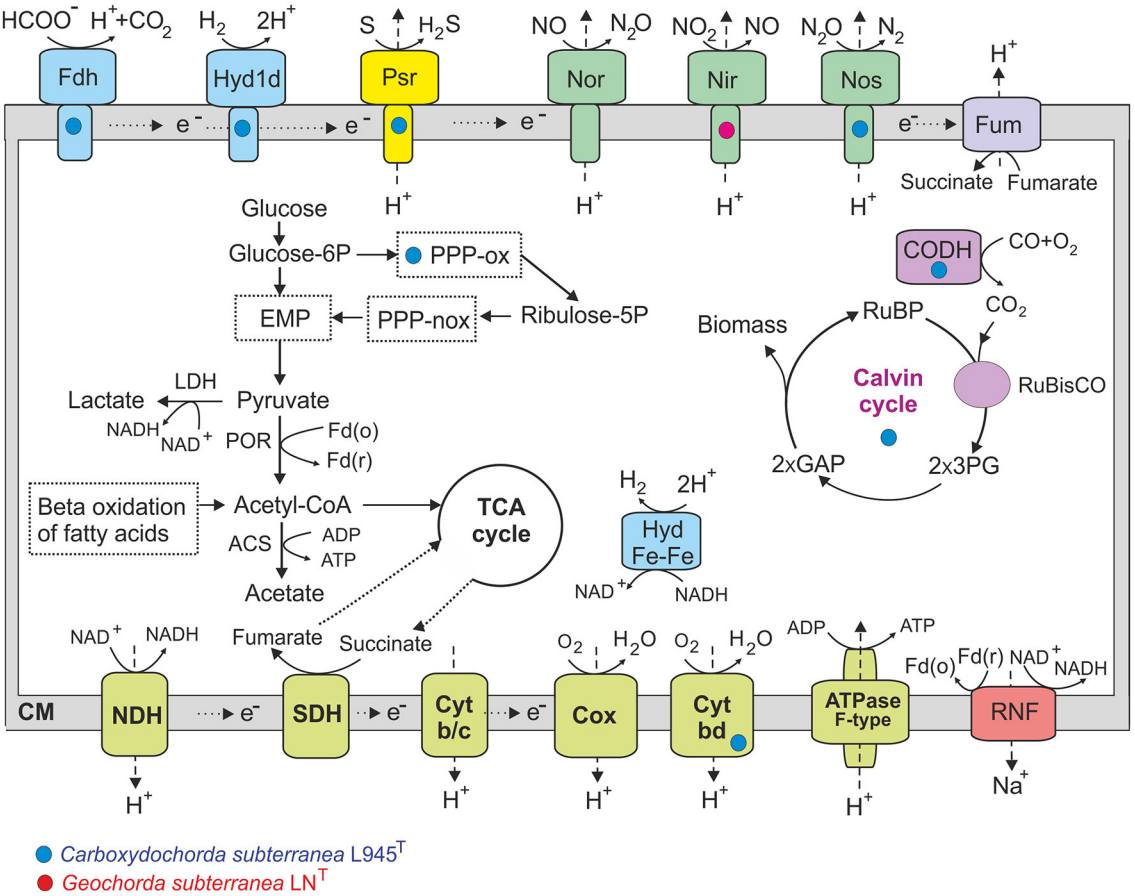

FIGURE 7
An overview of metabolic pathways of *Geochorda subterranea* LN^T and *Carboxydochorda subterranea* 945^T. Genes/pathways present only in one strain are marked by red (in LN^T) or blue (in 945^T) circles, other traits were found in both genomes. EMP, Embden–Meyerhof pathway; PPP-ox and PPP-nox, oxidative and non-oxidative phases of the pentose phosphate pathway; POR, pyruvate ferredoxin oxidoreductase; ACS, acetyl-CoA synthetase; LDH, lactate dehydrogenase; NDH, NADH dehydrogenase; SDH, succinate dehydrogenase; Cyt b/c, cytochrome *b/c* complex; Cox, cytochrom *c* oxidase; Cyt bd, quinol oxidase *bd* complex; Fdh, formate dehydrogenase; Hyd1d, membrane-bound [NiFe] group 1d uptake hydrogenase; Hyd Fe-Fe, cytoplasmic [Fe-Fe] group A hydrogenase; Psr, polysulfide/tetrathionate reductase; Nor, nitric-oxide reductase; Nir, nitrite reductase; Nos, nitrous-oxide reductase; Fum, fumarate reductase; CODH, carbon monoxide dehydrogenase; Glucose-6P, glucose 6-phosphate; Ribulose-5P, ribulose 5-phosphate; RuBP, ribulose-1,5-bisphosphate; 3PG, 3-phosphoglycerate; GAP, glyceraldehydes-3-phosphate; Fd(o)/Fd(r), ferredoxin, oxidized and reduced form.

several other GH13 and GH57 hydrolases that lack N-terminal signal peptides.

The LN^T genome encodes an endo-1,4-beta-xylanase of the GH10 family and an enzyme of the GH16 family with different activities, including endo-xyloglucanase and endo-β-1,3-glucanase/laminarinase. This genome also contains genes for ABC transporters of beta-xylosides and xylose, as well as intracellular enzymes involved in xylan metabolism, such as GH39 family beta-xylosidase, xylose isomerase, and xylulose kinase. Growth of the strain with xylan was observed under anaerobic conditions in the presence of fumarate in physiological experiments. However, strain L945^T lacked extracellular xylanolytic enzymes. On the contrary, both genomes encode numerous ABC-type transporters for the import of simple sugars, including galactose, maltose, maltodextrin, and alpha-glucosides, as well as transporters for amino acids, oligo-, and dipeptides. The presence of an L-rhamnose ABC transporter, L-rhamnose isomerase, and rhamnulokinase in the strain L945^T genome suggests that it can utilize rhamnose. However, this was not confirmed in physiological experiments.

In addition to transporters for sugars and amino acids, both genomes contain several transport systems that enable the uptake of di- and tricarboxylates of the TCA cycle. These include the tripartite tricarboxylate transporters TctABC for citrate (Rosa et al., 2018) and the TRAP-type C4-dicarboxylate transport system, enabling the symport of C4-dicarboxylates (succinate, fumarate, and malate) and aspartate with sodium ions or protons (Janausch et al., 2002). Both strains appear to be able to use fatty acids as growth substrates, as evidenced by the presence of a fatty acid beta-oxidation pathway. This includes genes for long-chain fatty acid-CoA ligases, acyl-CoA dehydrogenases, enoyl-CoA hydratases, 3-hydroxyacyl-CoA dehydrogenases, and 3-ketoacyl-CoA thiolases.

3.6 Description of *Geochorda* gen. nov.

Geochorda (Ge.o.chor′da. Gr. fem. n. *gê* the Earth; L. fem. n. *chorda*, chord, string; N.L. fem. n. *Geochorda* Earth string).

Cells are curved rods 0.15–0.20 μm in diameter and up to 9.0 μm long. These cells stain Gram-negative, have a didermic cell wall, and form round bodies up to 1.5 μm in diameter. They are facultatively anaerobic, thermophilic, and chemoorganoheterotrophic and are capable of hydrolyzing polysaccharides, including starch, dextrin, maltodextrin, and xylan. They are also free-living.

The type species is *Geochorda subterranea*.

3.7 Description of *Geochorda subterranea* sp. nov.

Geochorda subterranea (sub.ter.ra′ne.a. L. prep. *sub*, below underneath; L. fem. n. *terra*, soil; L. fem. adj. *subterranea* below the terrestrial ground, referring to the place of isolation).

Exhibit the following properties in addition to those listed in the genus description. The temperature range for growth is 45°C−70°C, with an optimum of 65°C. The pH range for growth is 6.0 to 9.5, with an optimum of 7.5–8.0. NaCl is necessary for growth, with an optimal concentration of 1.0%−1.5% (w/v). Fructose, glucose, sucrose, galactose, and propionate serve as electron donors during fumarate respiration. Hydrolyzes starch, dextrin, maltodextrin, xylan, chitin, and chitosan in the presence of fumarate in the medium. Glucose, fructose, or sucrose are used as electron donors for aerobic respiration. Arabinose, rhamnose, maltose, lactose, mannose, glycerol, ethanol, propanol, formate, butyrate, succinate, lactate, acetate, peptone, gelatin, or microcrystalline cellulose are not used as electron donors. Sorbitol and malate support slight growth, with fumarate as an electron acceptor. Sulfate, sulfite, thiosulfate, elemental sulfur, nitrate, nitrite, or Fe–NTA do not serve as electron acceptors. The major fatty acids are iso-$C_{15:0}$, anteiso-$C_{17:0}$, iso-$C_{16:0}$, anteiso-$C_{15:0}$, and $C_{16:0}$. The species description is based on the properties of strain LN^T (=VKM B-3703^T = JCM 39508) isolated from a deep subsurface aquifer in Chazhemto (Tomsk region, Russia). The DNA G+C content is 70.96 mol% (genome).

3.8 Description of *Carboxydochorda* gen. nov.

Carboxydochorda (Car.bo.xy.do.chor′da. N.L. neut. N. *carboxydum* carbon monoxide; L. fem. n. *chorda* chord, string; N.L. fem. n. *Carboxydochorda* carbon monoxide using string).

Cells are curved rods measuring 0.15–0.30 μm in diameter and up to 7.0 μm in length. Gram-negative cells have a didermic cell wall and round bodies measuring 0.7–1.5 μm in diameter. These are facultatively anaerobic, moderately thermophilic, and chemoorganoheterotrophic or chemolithoautotrophic. CO acts as an electron donor during fumarate or aerobic respiration. They are also free-living.

The type species is *Carboxydochorda subterranea*.

3.9 Description of *Carboxydochorda subterranea* sp. nov.

Carboxydochorda subterranea (sub.ter.ra′ne.a. L. prep. *sub*, below, underneath; L. fem. n. *terra*, soil; L. fem. adj. subterranea below the terrestrial ground, referring to the place of isolation).

Exhibit the following features in addition to those specified in the genus description. The temperature range for growth is 37°C−60°C, with an optimum of 55°C. The pH range for growth is 6.5–9.0, with an optimum of 7.0–7.5. This does not require NaCl for growth. Fructose, glucose, sucrose, and galactose are used as electron donors for fumarate respiration. Glucose, fructose, sucrose, H_2, CO, and formate are used as electron donors for aerobic respiration. Arabinose, rhamnose, maltose, lactose, mannose, glycerol, ethanol, propanol, formate, butyrate, succinate, lactate, acetate, peptone, gelatin, dextrin, maltodextrin, and microcrystalline cellulose are not used as electron donors. This hydrolyzes chitin and chitosan in the presence of fumarate. Sulfate, sulfite, thiosulfate, nitrate, nitrite, or Fe–NTA do not serve as electron acceptors. Elemental sulfur is used as an electron acceptor in the presence of glucose in the medium. The main fatty acids are anteiso-$C_{15:0}$ and iso-$C_{15:0}$. The species description is based on the properties of strain L945^T (= VKM B-3704^T = JCM 39509), which was isolated from a deep subsurface aquifer in Belokurikha (Altay region, Russia). The DNA G+C content is 69.48 mol% (genome).

3.10 Description of *Geochordaceae* fam. nov.

Geochordaceae (Ge.o.chor'da.ce'ae. N.L. fem. n. *Geochorda*, a bacterial genus; *–aceae*, ending to denote a family; N.L. fem. pl. n. *Geochordaceae*, the family of *Geochorda* genus).

Cells are curved rods, stain Gram-negative, have didermic cell walls, and form round bodies. These are facultatively anaerobic, thermophilic, and chemoorganoheterotrophic or chemolithoautotrophic. They are also capable of hydrolyzing polysaccharides, including starch, dextrin, maltodextrin, xylan, and chitin. They are also free-living.

The family belongs to the *Limnochordales* order.

The type genus is *Geochorda* gen. nov.

3.11 Comparative genomics of *Limnochordales*

At present, in addition to *L. pilosa*, strains LN^T and L945^T, the order *Limnochordales* comprises nine uncultivated species defined on the basis of the corresponding genomes (Figure 6). In order to gain insights into the lifestyle of *Limnochordales*, we conducted a comparative genomic analysis of its representatives and analyzed the presence of important metabolic pathways using the DRAM tool. Since only three genomes derived from cultivated isolates (*L. pilosa*, strains LN^T and L945^T) were assembled as closed circular chromosomes and are assumed to be complete the absence of certain genes/pathways in the remaining MAGs should be

considered with caution, as it may be due to their incompleteness. The completeness and contamination of the genomes, according to the CheckM2 estimates, are shown in Supplementary Table S2.

All members of *Limnochordales* possess most of the genes of the Embden–Meyerhof pathway and the non-oxidative stage of the pentose phosphate pathway, while the Entner–Doudoroff pathway is absent (Figure 8). Cytochrome c oxidases were found in all genomes except for three MAGs representing the family DUMU01. All these enzymes are low-affinity *aa3*-type oxidases; the high-affinity *cbb3*-type enzymes were not found. Additionally, DUMU01 genomes also lacked genes enabling anaerobic respiration and the complete TCA cycle, indicating that DUMU01 bacteria are devoted to a fermentative lifestyle.

Some members of *Limnochordales* possess genes enabling anaerobic respiration with nitrogen compounds, such as NO-forming nitrite reductase (*nirK*), nitrous-oxide reductase, and nitric-oxide reductase, which were found in five, two, and four genomes, respectively. However, genes for dissimilatory nitrate reductase and ammonia-forming cytochrome c nitrite reductase (*nrfAH*) were not found in any of the genomes. The ability to perform dissimilatory reduction of oxidized sulfur compounds appears to be rare. None of the genomes encodes the dissimilatory sulfate reduction pathway. Tetrathionate and thiosulfate reductases were identified in two (including strain L945^T) and one genome, respectively.

The ribulose bisphosphate carboxylase and phosphoribulokinase genes, which are hallmarks of the Calvin cycle for autotrophic carbon fixation, were found in the genomes of *L. pilosa*, strain L945^T and the MAG Bu05. All three genomes also contain genes for formate dehydrogenase and [NiFe] group 1d hydrogenase, while aerobic carbon monoxide dehydrogenase genes were only found in strains L945 ^{T} and *L. pilosa*. These genes are absent in other *Limnochordales* genomes. Probably only these three members of *Limnochordales* are capable of chemolithoautotrophic growth. Furthermore, the ribulose bisphosphate carboxylase and phosphoribulokinase from these three bacteria are more similar to each other in amino acid sequences than to proteins from other microorganisms, indicating that the Calvin cycle genes were acquired by the common ancestor of *Limnochordales* through a single horizontal transfer event and were subsequently lost in most lineages. The absence of the Calvin cycle in strain LN^T, the closest relative of the strain L945^T/Bu05 group, supports this hypothesis well.

Thus, the ability for heterotrophy and aerobic respiration is likely the most common and ancestral trait in the *Limnochordales*. Respiratory capacities were lost only in family DUMU01. The ability for autotrophic CO_2 fixation and the use of hydrogen and CO as energy sources were apparently acquired later and then lost in most phylogenetic lineages.

4 Discussion

Until now, the class *Limnochordia* was represented by a single cultivated member, *L. pilosa*, isolated from meromictic lake sediments (Watanabe et al., 2015), and our knowledge of this phylogenetic group was based on the uncultivated majority, primarily from sludge samples (Taib et al., 2020). Using high-throughput sequencing, we discovered the presence of a member of this class in water samples from the deep subsurface thermal aquifer, broached by borehole 5-P (Chazhemto), where the *Limnochordia* phylotype (MAG Ch19) was not abundant and constituted <1% of the prokaryotic community (Kadnikov et al., 2020). The metabolic features of *Limnochordia* inferred from genomic data were also used to enrich and isolate a cultivated representative of the class from a geographically distant deep thermal aquifer, broached by borehole 4E in Belokurikha (Altay Region). The latter deep thermal water was previously distinguished by the simultaneous presence of both cultivated anaerobic and aerobic prokaryotes (Lukina et al., 2023). The boreholes sampled in this study, 5-P in Chazhemto and 4E in Belokurikha, are artesian wells with pressurized water outflow, which minimizes the possibility of surface contamination. Targeted isolation from the water of geographically distant deep thermal aquifers in Chazhemto (Tomsk Region) and Belokurikha (Altay Region) resulted in the isolation of two new representatives of the class *Limnochordia*, described as *G. subterranea* gen. nov. sp. nov. and *C. subterranea* gen. nov. sp. nov. The deciphered metabolism of these two isolates suggests that *Geochordaceae* fam. nov. primarily live a heterotrophic life in the deep subsurface, respiring or fermenting simple sugars, fatty acids, and macromolecules derived from necromass or fossilized organic carbon from sedimentary rocks as electron donors.

C. subterranea L945^T, unlike *G. subterranea* LN^T, has limited ability to degrade polymers other than chitin and starch, but its metabolic flexibility is enhanced by the ability to grow lithoautotrophically on either H_2 or CO. H_2 is a common electron donor in the deep subsurface (Brazelton et al., 2012; Ruff et al., 2023). CO-based metabolism is well-recognized in hot springs and deep-sea volcanic vents (Robb and Techtmann, 2018), but the presence of carbon monoxide has also been postulated in subsurface environments with serpentinization under alkaline conditions (Brazelton et al., 2012). It is worth noting that the deep thermal waters of Belokurikha, from which the carboxydotrophic strain L945^T was isolated, have an alkaline reaction with a pH of 9.12. Chapelle and Bradley (2007) found that dissolved CO concentrations in shallow groundwater aquifers ranged from 0.0056 to 0.56 μg/L. It is also conceivable that the bacterium may use biogenic CO produced by sulfate-reducing and methanogenic prokaryotes, which are common inhabitants of the deep biosphere. For example, the sulfate-reducing *Desulfovibrio vulgaris* (recently reclassified as *Nitratidesulfovibrio vulgaris*) has been shown to produce a high amount of CO during the stationary growth phase (Voordouw, 2002). Thus, members of the *Geochordaceae* fam. nov. can switch from fermentation to anaerobic or aerobic respiration with organic or inorganic electron donors to optimize their performance under changing environmental conditions in the deep subsurface, where low energy fluxes are limited.

Of particular interest is the active aerobic respiration with O_2 observed in both *Geochordaceae* strains. The co-existence of the strictly anaerobic sulfate-reducing *Thermodesulfovbrio* and aerobic *Meiothermus* was earlier demonstrated for reduced water from borehole 4E in Chazhemto (Lukina et al., 2023), which was used for the isolation of *C. subterranea* L945^T, described in this study. Cultivation revealed both anaerobic sulfate reducers and heterotrophic aerobes in fracture water samples from the

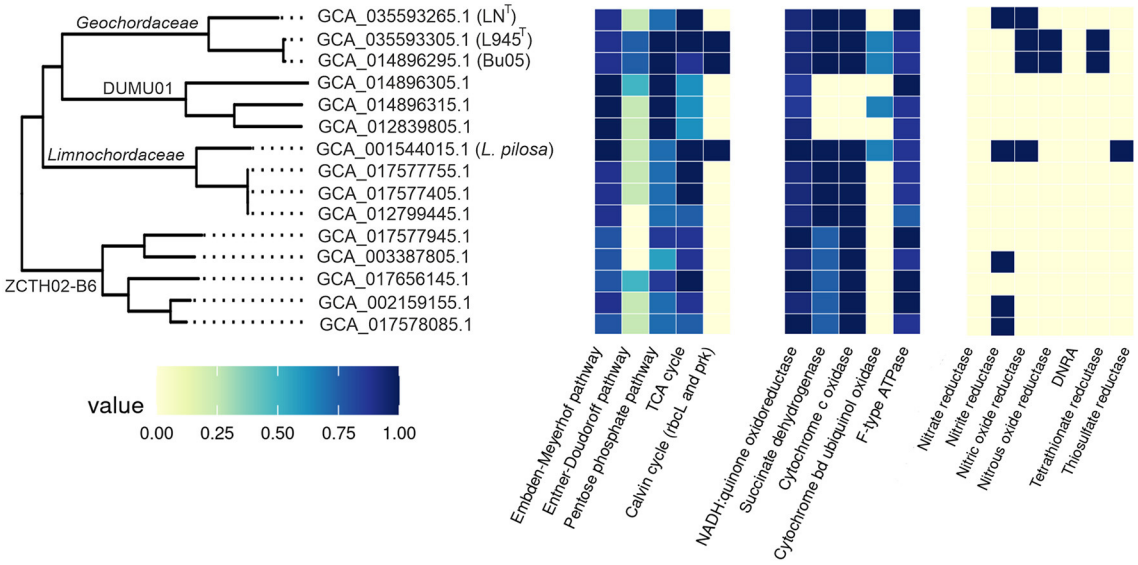

FIGURE 8
Comparative analysis of the main metabolic pathways along the *Limnochordales* (shaded in blue) and Limnochordales_A (shaded in green) using the DRAM tool. Strain/MAG names discussed in the text are shown after genome accession numbers. DNRA, ammonia-forming cytochrome c nitrite reductase.

Thompson mine (Manitoba, Canada), collected approximately 1 km below the surface (Song et al., 2024). The heterogeneous conditions of the water-rock system in deep aquifers can result in special compartmentalization and the formation of toxic microzones. The traditional view of deep subterranean environments as devoid of oxygen and aerobic life (Onstott et al., 2019) has recently changed. Gaseous oxygen and oxygen-respiring prokaryotes have been found in deep terrestrial aquifers, which has been linked to the influx of oxygenated meteoric waters (An et al., 2013; Frank et al., 2016; Kadnikov et al., 2018a, 2019). Dissolved oxygen concentration reached 0.42–2.3 ml/L in fracture water from a deep gold mine in South Africa (Weinstein et al., 2019), from which the underground nematode *Halicephalobus mephisto* was isolated (Borgonie et al., 2011). Significant dissolved oxygen concentrations (0.52 ± 0.12 mg L^{-1}) were recorded in geochemically mature groundwater samples collected from 138 groundwater monitoring wells in Alberta, Canada (Ruff et al., 2023). This amount of oxygen was suggested by the authors would be sufficient to support aerobic metabolisms in subsurface ecosystems on an unprecedented scale. *In-situ* production of molecular oxygen was confirmed by molecular oxygen (O_2) isotope analysis and attributed to the microbial dismutation of chlorite and nitric oxide. In addition to the biological production of so-called "dark oxygen," geochemical and geological processes like water radiolysis (Lin et al., 2005) and stress-induced generation via silicate mineral water interactions (He et al., 2021) may contribute to the appearance of oxygen in the deep subsurface. Thus, the growing evidence for aerobic metabolism, such as *Geochodaceae* fam. nov., should be considered when studying the deep biosphere.

The most active growth of both *Geochordaceae* strains in the laboratory cultures was observed when fumarate was used as an electron acceptor. Interestingly, there are reports of fumarate-respiring bacteria originating from the deep biosphere, despite the lack of clear evidence for the fumarate occurrence in these environments, including the strictly fumarate-respiring *Thermoanaerosceptrum fracticalcis*, isolated from an aquifer in fractured Paleozoic carbonate rocks at 863–923 meters below land surface in Nevada (Hamilton-Brehm et al., 2019). The only substrate supporting the growth of the bacterium was fumarate, whereas it was absent in the water sample used to isolate the strain. The source of fumarate in the subsurface remains unclear (Hamilton-Brehm et al., 2019 and references therein). Borehole drilling agents have been reported to be a source of fumarate (Borchardt, 1989). It is also conceivable that laboratory culture growth is not necessarily a model of bacterial metabolism in the environment. Bacteria can ferment organic substrates derived from decomposed fossil organics or necromass as hydrogen-scavenging community members reduce H_2 pressure in the ecosystem. In the absence of an H_2-scavenger, both *Geochordaceae* strains grew very slowly under fermentation conditions. Similarly, fumarate may promote optimal growth in the laboratory but does not affect the metabolism of the bacteriua in the environment.

Despite the fact that all cultivated members of the *Limnochordia* class have been isolated from water bodies, the majority of uncultivated members of the class in public databases originate from sludge and manure samples. A metagenome-based analysis of relative MAG abundance in digestors of a full-scale biogas plant revealed that *Limnochordia* was the most abundant MAG in all three digestors operating differently (Hassa et al., 2023). *Limnochordales* was the most frequent order revealed among MAGs binned from thermophilic composting cells at the São Paulo Zoo containing a mixture of lignocellulose and animal waste (Braga et al., 2021). The dominance of *Limnochrdia* phylotypes has been reported in sewage sludge (Shekhurdina et al., 2023) and digested cattle manure (Zhuravleva et al., 2022), where it was suggested that the MBA03 group of *Limnochordia* has syntrophic relationships with methanogenic archaea and is involved in direct interspecies electron transfer (DIET). This group

also dominated the enrichment culture derived from microbial fuel cell cathodes inoculated with bovine and swine wastewater (Rago et al., 2018). The co-existence of the *Limnochordia* MBA03 group and *Methanosarcina* has been proposed to ensure DIET in full-scale methanogenic reactors (Calusinska et al., 2018). The transmission of electrical currents is known for the so-called cable bacteria, which are long filamentous multicellular members of the *Desulfobulbaceae* family (Cornelissen et al., 2018). The cell envelope of cable bacteria contains cell filaments that are continuous across the cell-to-cell junction. It is conceivable that the filamentous structures that we observed on the cell envelope of L945^T and LN^T strains (Figure 2) may be involved in electron transport and electroactivity of *Limnochordia* as occurs in cable bacteria.

Carboxydotrophic representatives of *Limnochordia* may constitute a notable share of the microbial community in ecosystems characterized by the presence of CO. An example of such an environment is the burning wastes of coal mining, where CO is the main gaseous product of incomplete combustion of coal (Karnachuk et al., 2023). MAG Bu05 belonging to *C. subterranea* was obtained from the coal-fire heated soil in Eastern Siberia (Kadnikov et al., 2023). Uncultivated members of the class *Limnochordia* were detected by 16S rRNA gene profiling in samples of burning lignite seams at Chagan-Uzun in the Altay Mountains during a long-term study (Kadnikov et al., 2018b; Karnachuk et al., 2023). Over a 6-year sampling period, its presence in the microbial community of heated rocks and soils of Chagan-Uzun ranged between 0.01% and 4.39%. *Limnochordales* phylotypes were discovered in heated rock samples from an abandoned coal mine near Kiselevsk, Kuzbass coal basin (Kadnikov et al., 2021a). The share of *Limnochordales* in the microbial community of thermal wastes from another Kuzbass coal mine ranged from 0.01% to 2.39% (Kadnikov et al., 2021b). CO is a common gas produced when organic waste and litter decompose, and it could be a potential substrate for carboxydothrophic *Geochordaceae*. CO concentrations of 120 μM were found in green waste compost and reached up to 10 mM in livestock waste composts (Hellebrand and Schade, 2008). In addition, carboxydotrophic bacteria have the potential to be used in biotechnological applications via syngas, a mixture of CO_2, CO, and H_2, produced as a byproduct of incomplete fossil fuel production (Alves et al., 2020).

Until now, *L. pilosa* was the only cultivated member of the class *Limnochordia* and the only option to verify the didermic (Gram-negative) character of the cell wall in this phylogenetic group. By screening 1,639 genomes of uncultivated *Firmicutes*, Taib et al. (2020) revealed outer membrane (OM) signatures in *Limnochordia*, strengthening their hypothesis of a didermic ancestor of *Firmicutes* and subsequent multiple OM losses in the phylum. The OM cluster of gene markers combined by Taib et al. (2020) was found in all 46 UBA *Limnochordia* genomes analyzed by the authors. A recent rooted bacterial phylogeny has confirmed the didermic character of the LBCA (Coleman et al., 2021). The OM of the cell wall of *G. subterreanea* sp. nov. and *C. subterreanea* sp. nov. clearly demonstrate the didermic (Gram-negative) character of the cell envelope of the novel cultivated representatives of the class *Limnochordia*.

Our study shows that careful consideration of genomic information may provide clues to obtaining laboratory cultures of yet-to-be-cultivated organisms. It is assumed that the lack of cultivated *Limnochordia* is due to overgrowth by other organotrophic bacteria in laboratory cultures when standard organic substrates are abundant. The discovery of less common metabolic pathways in the genome, such as the use of sorbitol in the case of *Geochorda subterranea* gen. nov. sp. nov., may result in the isolation of new microbes in the laboratory. Thus, genome availability may be an important prerequisite for cultivation. It is anticipated that novel *Limnochordia* isolates from sludge and agricultural waste, whose genomes are already available in UBA, will be cultured in the near future.

Data availability statement

The data presented in the study are deposited in the NCBI GenBank, accession numbers CP141614.1 (*Geochorda subterranea* LNT genome), CP141615.1 (*Carboxydochorda subterranea* L945T genome), PP660922.1 (16S rRNA gene of *Geochorda subterranea* LNT), and PP660921.1 (16S rRNA gene of *Carboxydochorda subterranea* L945T). The data can be found here: https://www.ncbi.nlm.nih.gov/nuccore/CP141614.1; https://www.ncbi.nlm.nih.gov/nuccore/CP141615.1; https://www.ncbi.nlm.nih.gov/nuccore/PP660922.1; https://www.ncbi.nlm.nih.gov/nuccore/PP660921.1.

Author contributions

OK: Conceptualization, Funding acquisition, Project administration, Resources, Supervision, Writing – original draft, Writing – review & editing. AL: Investigation, Methodology, Writing – review & editing. MA: Data curation, Investigation, Visualization, Writing – review & editing. VK: Investigation, Resources, Writing – review & editing. SB: Investigation, Writing – review & editing. AB: Data curation, Investigation, Writing – review & editing. KV: Investigation, Writing – review & editing. AN: Investigation, Writing – review & editing. VS: Validation, Writing – review & editing. AM: Investigation, Writing – review & editing. NR: Data curation, Project administration, Writing – original draft, Writing – review & editing.

Funding

The author(s) declare financial support was received for the research, authorship, and/or publication of this article. This study was supported by the Russian Science Foundation (Project No. 24-14-00396 to OK; cultivation and physiological experiments and Project No. 22-14-00178 to NR; genome sequencing and analysis). AL thanks the scholarship (No. SP-3706.2021.1; strain LN^T isolation). The study by AN at Gubkin University (lipid extraction and analysis) was supported by the Russian Science Foundation (Project No. 20-79-10388).

Acknowledgments

We thank Maria Chuvochina for her help with Latin etymology.

Conflict of interest

The authors declare that the research was conducted in the absence of any commercial or financial relationships

that could be construed as a potential conflict of interest.

The author(s) declared that they were an editorial board member of Frontiers, at the time of submission. This had no impact on the peer review process and the final decision.

Publisher's note

All claims expressed in this article are solely those of the authors and do not necessarily represent those of their affiliated organizations, or those of the publisher, the editors and the reviewers. Any product that may be evaluated in this article, or claim that may be made by its manufacturer, is not guaranteed or endorsed by the publisher.

Supplementary material

The Supplementary Material for this article can be found online at: https://www.frontiersin.org/articles/10.3389/fmicb.2024.1441865/full#supplementary-material

References

Alves, J. I., Visser, M., Arantes, A. L., Nijsse, B., Plugge, C. M., Alves, M. M., et al. (2020). Effect of sulfate on carbon monoxide conversion by a thermophilic syngas-fermenting culture dominated by a *Desulfofundulus* species. *Front. Microbiol.* 11:588468. doi: 10.3389/fmicb.2020.588468

An, D., Caffrey, S. M., Soh, J., Agrawal, A., Brown, D., Budwill, K., et al. (2013). Metagenomics of hydrocarbon resource environments indicates aerobic taxa and genes to be unexpectedly common. *Environ. Sci. Technol.* 47, 10708–10717. doi: 10.1021/es4020184

Bankevich, A., Nurk, S., Antipov, D., Gurevich, A. A., Dvorkin, M., Kulikov, A. S., et al. (2012). SPAdes: A new genome assembly algorithm and its applications to single-cell sequencing. *J. Comput. Biol.* 19, 455–477. doi: 10.1089/cmb.2012.0021

Beier, S., and Bertilsson, S. (2013). Bacterial chitin degradation-mechanisms and ecophysiological strategies. *Front. Microbiol.* 4:149. doi: 10.3389/fmicb.2013.00149

Biegel, E., Schmidt, S., González, J. M., and Müller, V. (2011). Biochemistry, evolution and physiological function of the Rnf complex, a novel ion-motive electron transport complex in prokaryotes. *Cell. Mol. Life Sci.* 68, 613–634. doi: 10.1007/s00018-010-0555-8

Borchardt, J. K. (1989). *Chemicals Used in Oil-Field Operations*. Houston, TX: Westhollow Research Center, Shell Development Company. doi: 10.1021/bk-1989-0396.ch001

Borgonie, G., García-Moyano, A., Litthauer, D., Bert, W., Bester, A., van Heerden, E. (2011). Nematoda from the terrestrial deep subsurface of South Africa. *Nature* 474, 79–82. doi: 10.1038/nature09974

Braga, L. P. P., Pereira, R. V., Martins, L. F., Moura, L. M. S., Sanchez, F. B., Patané, J. S. L., et al. (2021). Genome-resolved metagenome and metatranscriptome analyses of thermophilic composting reveal key bacterial players and their metabolic interactions. *BMC Gen.* 22:652. doi: 10.1186/s12864-021-07957-9

Brazelton, W. J., Nelson, B., and Schrenk, M. O. (2012). Metagenomic evidence for h(2) oxidation and h(2) production by serpentinite-hosted subsurface microbial communities. *Front. Microbiol.* 2:268. doi: 10.3389/fmicb.2011.00268

Brettin, T., Davis, J. J., Disz, T., Edwards, R. A., Gerdes, S., Olsen, G. J., et al. (2015). RASTtk: a modular and extensible implementation of the RAST algorithm for building custom annotation pipelines and annotating batches of genomes. *Sci. Rep.* 5:8365. doi: 10.1038/srep08365

Calusinska, M., Goux, X., Fossépré, M., Muller, E. E. L., Wilmes, P., and Delfosse, P. (2018). A year of monitoring 20 mesophilic full-scale bioreactors reveals the existence of stable but different core microbiomes in bio-waste and wastewater anaerobic digestion systems. *Biotechnol. Biofuels* 11:196. doi: 10.1186/s13068-018-1195-8

Chapelle, F. H., and Bradley, P. M. (2007). Hydrologic significance of carbon monoxide concentrations in ground water. *Ground Water* 45, 272–280. doi: 10.1111/j.1745-6584.2007.00284.x

Chaumeil, P. A., Mussig, A. J., Hugenholtz, P., Parks, D. H., (2022). GTDB-Tk v2: memory friendly classification with the genome taxonomy database. *Bioinformatics*. 38, 5315–5316. doi: 10.1093/bioinformatics/btac672

Chklovski, A., Parks, D. H., Woodcroft, B. J., and Tyson, G. W. (2023). CheckM2: a rapid, scalable and accurate tool for assessing microbial genome quality using machine learning. *Nat. Methods* 20, 1203–1212. doi: 10.1038/s41592-023-01940-w

Cline, J. D. (1969). Spectrophotometric determination of hydrogen sulfide in natural waters. *Limnol. Oceanogr.* 14:454458. doi: 10.4319/lo.1969.14.3.0454

Coleman, G. A., Davín, A. A., Mahendrarajah, T. A., Szánthó, L. L., Spang, A., Hugenholtz, P., et al. (2021). A rooted phylogeny resolves early bacterial evolution. *Science* 372:eabe0511. doi: 10.1126/science.abe0511

Cornelissen, R., Bøggild, A., Thiruvallur Eachambadi, R., Koning, R. I., Kremer, A., Hidalgo-Martinez, S., et al. (2018). The cell envelope structure of cable bacteria. *Front. Microbiol.* 9:3044. doi: 10.3389/fmicb.2018.03044

Frank, Y. A., Kadnikov, V. V., Gavrilov, S. N., Banks, D., Gerasimchuk, A. L., Podosokorskaya, O. A., et al. (2016). Stable and variable parts of microbial community in Siberian deep subsurface thermal aquifer system revealed in a long-term monitoring study. *Front. Microbiol.* 7:2101. doi: 10.3389/fmicb.2016.02101

Greening, C., Biswas, A., Carere, C. R., Jackson, C. J., Taylor, M. C., Stott, M. B., et al. (2016). Genomic and metagenomic surveys of hydrogenase distribution indicate H2 is a widely utilised energy source for microbial growth and survival. *ISME J.* 10, 761–777. doi: 10.1038/ismej.2015.153

Guindon, S., Dufayard, J. F., Lefort, V., Anisimova, M., Hordijk, W., and Gascuel, O. (2010). New algorithms and methods to estimate maximum-likelihood phylogenies: assessing the performance of PhyML 3.0. *Syst. Biol.* 59, 307–321. doi: 10.1093/sysbio/syq010

Hamilton-Brehm, S. D., Stewart, L. E., Zavarin, M., Caldwell, M., Lawson, P. A., Onstott, T. C., et al. (2019). Thermoanaerosceptrum fracticalcis gen. nov. sp. nov., a novel fumarate-fermenting microorganism from a deep fractured carbonate aquifer of the US Great Basin. *Front. Microbiol.* 10:2224. doi: 10.3389/fmicb.2019.02224

Hassa, J., Tubbesing, T. J., Maus, I., Heyer, R., Benndorf, D., Effenberger, M., et al. (2023). Uncovering microbiome adaptations in a full-scale biogas plant: insights from MAG-centric metagenomics and metaproteomics. *Microorganisms* 11:2412. doi: 10.3390/microorganisms11102412

He, H., Wu, X., Xian, H., Zhu, J., Yang, Y., Lv, Y., et al. (2021). An abiotic source of Archean hydrogen peroxide and oxygen that pre-dates oxygenic photosynthesis. *Nat. Commun.* 12:6611. doi: 10.1038/s41467-021-26916-2

Hellebrand, H. J., and Schade, G. W, (2008). Carbon monoxide from composting due to thermal oxidation of biomass. *J. Environ. Qual.* 37, 592–598. doi: 10.2134/jeq2006.0429

Hou, F., Du, J., Yuan, Y., Wu, X., and Zhao, S. (2021). Analysis of microbial communities in aged refuse based on 16S sequencing. *Sustainability* 13:4111. doi: 10.3390/su13084111

Ikkert, O. P., Gerasimchuk, A. L., Bukhtiyarova, P. A., Tuovinen, O. H., and Karnachuk, O. V. (2013). Characterization of precipitates formed by H_2S-producing, Cu-resistant Firmicute isolates of *Tissierella* from human gut and *Desulfosporosinus* from mine waste. *Antonie Van Leeuwenhoek* 103, 1221–1234. doi: 10.1007/s10482-013-9900-x

Janausch, I. G., Zientz, E., Tran, Q. H., Kröger, A., and Unden, G. (2002). C4-dicarboxylate carriers and sensors in bacteria. *Biochim. Biophys. Acta* 1553, 39–56. doi: 10.1016/S0005-2728(01)00233-X

Kadnikov, V. V., Frank, Y. A., Mardanov, A. V., Beletsky, A. V., Ivasenko, D. A., Pimenov, N. V., et al. (2017). Variability of the composition of the microbial community of the deep subsurface thermal aquifer in Western Siberia. *Microbiology* 86, 765–772. doi: 10.1134/S002626171706008X

Kadnikov, V. V., Mardanov, A. V., Beletsky, A. V., Banks, D., Pimenov, N. V., Frank, Y. A., et al. (2018a). A metagenomic window into the 2-km-deep terrestrial subsurface aquifer revealed multiple pathways of organic matter decomposition. *FEMS Microbiol. Ecol.* 94:fiy152. doi: 10.1093/femsec/fiy152

Kadnikov, V. V., Mardanov, A. V., Beletsky, A. V., Grigoriev, M. A., Karnachuk, O. V., and Ravin, N. V. (2021a). Thermophilic *Chloroflexi* dominate in the microbial community associated with coal-fire gas vents in the Kuznetsk Coal Basin, Russia. *Microorganisms* 9:948. doi: 10.3390/microorganisms9050948

Kadnikov, V. V., Mardanov, A. V., Beletsky, A. V., Karnachuk, O. V., and Ravin, N. V. (2020). Microbial life in the deep subsurface aquifer illuminated by metagenomics. *Front. Microbiol.* 11:572252. doi: 10.3389/fmicb.2020.572252

Kadnikov, V. V., Mardanov, A. V., Beletsky, A. V., Karnachuk, O. V., and Ravin, N. V. (2021b). Metagenomic analysis of the microbial community in the underground coal fire area (Kemerovo Region, Russia) revealed predominance of thermophilic

members of the phyla *Deinococcus-Thermus*, *Aquificae*, and *Firmicutes*. *Microbiology*, 90, 578–587. doi: 10.1134/S0026261721050088

Kadnikov, V. V., Mardanov, A. V., Beletsky, A. V., Karnachuk, O. V., and Ravin, N. V. (2023). Prokaryotic life associated with coal-fire gas vents revealed by metagenomics. *Biology* 12:723. doi: 10.3390/biology12050723

Kadnikov, V. V., Mardanov, A. V., Beletsky, A. V., Rakitin, A. L., Frank, Y. A., Karnachuk, O. V., et al. (2019). Phylogeny and physiology of candidate phylum BRC1 inferred from the first complete metagenome-assembled genome obtained from deep subsurface aquifer. *Syst. Appl. Microbiol.* 42, 67–76. doi: 10.1016/j.syapm.2018.08.013

Kadnikov, V. V., Mardanov, A. V., Ivasenko, D. A., Antsiferov, D. V, Beletsky, A. V., Karnachuk, O. V., et al. (2018b). Lignite coal burning seam in the remote Altai Mountains harbors a hydrogen-driven thermophilic microbial community. *Sci. Rep.* 8:6730. doi: 10.1038/s41598-018-25146-9

Karnachuk, O. V., Frank, Y. A., Lukina, A. P., Kadnikov, V. V., Beletsky, A. V., Mardanov, A. V., et al. (2019). Domestication of previously uncultivated *Candidatus* Desulforudis audaxviator from a deep aquifer in Siberia sheds light on its physiology and evolution. *ISME J.* 13, 1947–1959. doi: 10.1038/s41396-019-0402-3

Karnachuk, O. V., Lukina, A. P., Kadnikov, V. V., Sherbakova, V. A., Beletsky, A. V., Mardanov, A. V., et al. (2021). Targeted isolation based on metagenome-assembled genomes reveals a phylogenetically distinct group of thermophilic spirochetes from deep biosphere. *Environ. Microbiol.* 23, 3585–3598. doi: 10.1111/1462-2920.15218

Karnachuk, O. V., Rusanov, I. I., Panova, I. A., Kadnikov, V. V., Avakyan, M. R., Ikkert, O. P., et al. (2023). The low-temperature germinating spores of the thermophilic *Desulfofundulus* contribute to an extremely high sulfate reduction in burning coal seams. *Front. Microbiol.* 14:1204102. doi: 10.3389/fmicb.2023.1204102

Katoh, K., and Standley, D. M. (2013). MAFFT multiple sequence alignment software version 7: improvements in performance and usability. *Mol. Biol. Evol.* 30, 772–780. doi: 10.1093/molbev/mst010

Kieft, T. L., McCuddy, S. M., Onstott, T. C., Davidson, M., Lin, L.-H., Mislowack, B., et al. (2005). Geochemically generated, energy-rich substrates and indigenous microorganisms in deep, ancient groundwater. *Geomicrobiol. J.* 22, 325–335. doi: 10.1080/01490450500184876

Kolmogorov, M., Yuan, J., Lin, Y., and Pevzner, P. A. (2019). Assembly of long, error-prone reads using repeat graphs. *Nat. Biotechnol.* 37, 540–546. doi: 10.1038/s41587-019-0072-8

Konstantinidis, K. T., Rosselló-Móra, R., and Amann, R. (2017). Uncultivated microbes in need of their own taxonomy. *ISME J.* 11, 2399–2406. doi: 10.1038/ismej.2017.113

Lane, D. J. (1991). "16S/23S rRNA sequencing," in *Nucleic Acid Techniques in Bacterial Systematics,* eds. E. Stackebrandt and M. Goodfellow (New York: Wiley), 115–175.

Lefticariu, L., Pratt, L. M., and Ripley, E. M. (2006). Mineralogic and sulfur isotopic effects accompanying oxidation of pyrite in millimolar solutions of hydrogen peroxide at temperatures from 4 to 150 degrees C. *Geochim. Cosmochim. Acta* 70, 4889–4905. doi: 10.1016/j.gca.2006.07.026

Liebensteiner, M. G., Tsesmetzis, N., Stams, A. J., and Lomans, B. P. (2014). Microbial redox processes in deep subsurface environments and the potential application of (per)chlorate in oil reservoirs. *Front. Microbiol.* 5:428. doi: 10.3389/fmicb.2014.00428

Lin, L.-H., Slater, G. F., Lollar, B. S., Lacrampe-Couloume, G., and Onstott, T. C. (2005). The yield and isotopic composition of radiolytic H_2, a potential energy source for the deep subsurface biosphere. *Geochim. Cosmochim. Acta* 69, 893–903. doi: 10.1016/j.gca.2004.07.032

Liu, H., Zhang, L., Sun, Y., Xu, G., Wang, W., Piao, R., et al. (2021). Degradation of lignocelluloses in straw using AC-1, a thermophilic composite microbial system. *PeerJ.* 9:e12364. doi: 10.7717/peerj.12364

Lovley, D. R., and Chapelle, F. H. (1995). Deep subsurface microbial processes. *Rev. Geophys.* 33, 365–381. doi: 10.1029/95RG01305

Lukina, A. P., Kadnikov, V. V., Rusanov, I. I., Avakyan, M. R., Beletsky, A. V., Mardanov, A. V., et al. (2023). Anaerobic *Thermodesulfovibrio* and aerobic *Meiothermus* coexist in deep thermal water. *Microbiology* 92, 324–333. doi: 10.1134/S0026261723600234

Onstott, T. C., Ehlmann, B. L., Sapers, H., Coleman, M., Ivarsson, M., Marlow, J. J., et al. (2019). Paleo-rock-hosted life on Earth and the search on Mars: a review and strategy for exploration. *Astrobiology*,19, 1230–1262. doi: 10.1089/ast.2018.1960

Parks, D. H., Chuvochina, M., Waite, D. W., Rinke, C., Skarshewski, A., Chaumeil, P. A., et al. (2018). A standardized bacterial taxonomy based on genome phylogeny substantially revises the tree of life. *Nat. Biotechnol.* 36, 996–1004. doi: 10.1038/nbt.4229

Parks, D. H., Rinke, C., Chuvochina, M., Chaumeil, P. A., Woodcroft, B. J., Evans, P. N., et al. (2017). Recovery of nearly 8,000 metagenome-assembled genomes substantially expands the tree of life. *Nat. Microbiol.* 2, 1533–1542. doi: 10.1038/s41564-017-0012-7

Purkamo, L., Bomberg, M., Nyyssönen, M., Ahonen, L., Kukkonen, I., and Itävaara, M. (2017). Response of deep subsurface microbial community to different carbon sources and electron acceptors during ~2 months incubation in microcosms. *Front. Microbiol.* 8:232. doi: 10.3389/fmicb.2017.00232

Rago, L., Zecchin, S., Marzorati, S., Goglio, A., Cavalca, L., Cristiani, P., et al. (2018). A study of microbial communities on terracotta separator and on biocathode of air breathing microbial fuel cells. *Bioelectrochemistry* 120, 18–26. doi: 10.1016/j.bioelechem.2017.11.005

Robb, F. T., and Techtmann, S. M. (2018). Life on the fringe: microbial adaptation to growth on carbon monoxide. *F1000Res.* 7:F1000–1981. doi: 10.12688/f1000research.16059.1

Rodriguez-R., L. M., and Konstantinidis, K. T. (2016). The enveomics collection: a toolbox for specialized analyses of microbial genomes and metagenomes. *PeerJ* 4:e1900v1. doi: 10.7287/peerj.preprints.1900v1

Rosa, L. T., Bianconi, M. E., Thomas, G. H., and Kelly, D. J. (2018). Tripartite ATP-independent periplasmic (TRAP) transporters and tripartite tricarboxylate transporters (TTT): From uptake to pathogenicity. *Front. Cell. Infect. Microbiol.* 8:33. doi: 10.3389/fcimb.2018.00033

Ruff, S. E., Humez, P., de Angelis, I. H., Diao, M., Nightingale, M., Cho, S., et al. (2023). Hydrogen and dark oxygen drive microbial productivity in diverse groundwater ecosystems. *Nat. Commun.* 14:3194. doi: 10.1038/s41467-023-38523-4

Scheffer, G., Berdugo-Clavijo, C., Sen, A., and Gieg, L. M. (2021). Enzyme biotechnology development for treating polymers in hydraulic fracturing operations. *Microb. Biotechnol.* 14, 953–966. doi: 10.1111/1751-7915.13727

Shaffer, M., Borton, M. A., McGivern, B. B., Zayed, A. A., La Rosa, S. L., Solden, L. M., et al. (2020). DRAM for distilling microbial metabolism to automate the curation of microbiome function. *Nucleic Acids Res.* 48, 8883–8900. doi: 10.1093/nar/gkaa621

Shekhurdina, S., Zhuravleva, E., Kovalev, A., Andreev, E., Kryukov, E., Loiko, N., et al. (2023). Comparative effect of conductive and dielectric materials on methanogenesis from highly concentrated volatile fatty acids. *Bioresour. Technol.* 377:128966. doi: 10.1016/j.biortech.2023.128966

Shoubao, Y., Yonglei, J., Qi, Z., Shunchang, P., and Cuie, S. (2023). Bacterial diversity associated with volatile compound accumulation in pit mud of Chinese strong-flavor baijiu pit. *AMB Expr.* 3:3. doi: 10.21203/rs.3.rs-2214824/v1

Song, M., Warr, O., Telling, J., and Sherwood Lollar, B. (2024). Hydrogeological controls on microbial activity and habitability in the Precambrian continental crust. *Geobiology* 22:e12592. doi: 10.1111/gbi.12592

Steenwyk, J. L., Buida, T. J., Li, Y., Shen, X. X., and Rokas,. A. (2020). ClipKIT: a multiple sequence alignment trimming software for accurate phylogenomic inference. *PLoS Biol.* 18:e3001007. doi: 10.1371/journal.pbio.3001007

Taib, N., Megrian, D., Witwinowski, J., Adam, P., Poppleton, D., Borrel, G., et al. (2020). Genome-wide analysis of the *Firmicutes* illuminates the diderm/monoderm transition. *Nat. Ecol. Evol.* 4, 1661–1672. doi: 10.1038/s41559-020-01299-7

Tatusova, T., DiCuccio, M., Badretdin, A., Chetvernin, V., Nawrocki, E. P., Zaslavsky, L., et al. (2016). NCBI prokaryotic genome annotation pipeline. *Nucleic Acids Res.* 44, 6614–6624. doi: 10.1093/nar/gkw569

Voordouw, G. (2002). Carbon monoxide cycling by *Desulfovibrio vulgaris* Hildenborough. *J Bacteriol.* 184, 5903–5911. doi: 10.1128/JB.184.21.5903-5911.2002

Walker, B. J., Abeel, T., Shea, T., Priest, M., Abouelliel, A., Sakthikumar, S., et al. (2014). Pilon: an integrated tool for comprehensive microbial variant detection and genome assembly improvement. *PLoS ONE* 9:e112963. doi: 10.1371/journal.pone.0112963

Wang, L., Zhang, F., Zeng, K., Dong, W., Yuan, H., Wang, Z., et al. (2022). Microbial communities in the liver and brain are informative for postmortem submersion interval estimation in the late phase of decomposition: a study in mouse cadavers recovered from freshwater. *Front. Microbiol.* 13:1052808. doi: 10.3389/fmicb.2022.1052808

Watanabe, M., Kojima, H., and Fukui, M. (2015). Limnochorda pilosa gen. nov., sp. nov., a moderately thermophilic, facultatively anaerobic, pleomorphic bacterium and proposal of Limnochordaceae fam. nov., Limnochordales ord. nov. and Limnochordia classis nov. in the phylum Firmicutes. *Int. J. Syst. Evol. Microbiol.* 65, 2378–2384. doi: 10.1099/ijs.0.000267

Watanabe, M., Kojima, H., and Fukui, M. (2016). Complete genome sequence and cell structure of *Limnochorda pilosa*, a Gram-negative spore-former within the phylum Firmicutes. *Int. J. Syst. Evol. Microbiol.* 66, 1330–1339. doi: 10.1099/ijsem.0.000881

Weinstein, D. J., Allen, S. E., Lau, M. C. Y., Erasmus, M., Asalone, K. C., Walters-Conte, K., et al. (2019). The genome of a subterrestrial nematode reveals adaptations to heat. *Nat. Commun.* 10:5268. doi: 10.1038/s41467-019-13245-8

Westmeijer, G., Mehrshad, M., Turner, S., Alakangas, L., Sachpazidou, V., Bunse, C., et al. (2022). Connectivity of Fennoscandian Shield terrestrial deep biosphere microbiomes with surface communities. *Commun. Biol.* 5:37. doi: 10.1038/s42003-021-02980-8

Widdel, F. F., and Bak, R. (1992). "Gram-negative mesophilic sulfate-reducing bacteria," in *The Prokaryotes: a handbook on the biology of bacteria: ecophysiology, isolation, identification, applications,* eds. A. Balows, H. G. Truper, M. Dworkin, W. Harder, K. H. Schleifer (Berlin: Springer), *3352*–78. doi: 10.1007/978-1-4757-2191-1_21

Zhuravleva, E. A., Shekhurdina, S. V., Kotova, I. B., Loiko, N. G., Popova, N. M., Kryukov, E., et al. (2022). Effects of various materials used to promote the direct interspecies electron transfer on anaerobic digestion of low-concentration swine manure. *Sci. Total Environ.* 839:156073. doi: 10.1016/j.scitotenv.2022.156073

frontiers | Frontiers in Microbiology

TYPE Original Research
PUBLISHED 12 November 2024
DOI 10.3389/fmicb.2024.1455857

OPEN ACCESS

EDITED BY
William J. Brazelton,
The University of Utah, United States

REVIEWED BY
Jens Kallmeyer,
GFZ German Research Centre for Geosciences, Germany
Christopher H. House,
The Pennsylvania State University, United States

*CORRESPONDENCE
Karen G. Lloyd
lloydk@usc.edu

RECEIVED 27 June 2024
ACCEPTED 22 October 2024
PUBLISHED 12 November 2024

CITATION
Coon GR, Williams LC, Matthews A, Diaz R, Kevorkian RT, LaRowe DE, Steen AD, Lapham LL and Lloyd KG (2024) Control of hydrogen concentrations by microbial sulfate reduction in two contrasting anoxic coastal sediments.
Front. Microbiol. 15:1455857.
doi: 10.3389/fmicb.2024.1455857

Control of hydrogen concentrations by microbial sulfate reduction in two contrasting anoxic coastal sediments

Gage R. Coon[1], Leketha C. Williams[1], Adrianna Matthews[1], Roberto Diaz[1], Richard T. Kevorkian[1], Douglas E. LaRowe[2], Andrew D. Steen[1,2,3,4], Laura L. Lapham[5] and Karen G. Lloyd[1,2]*

[1]Department of Microbiology, The University of Tennessee, Knoxville, Knoxville, TN, United States, [2]Department of Earth Sciences, University of Southern California, Los Angeles, CA, United States, [3]Department of Earth and Planetary Sciences, The University of Tennessee, Knoxville, Knoxville, TN, United States, [4]Department Marine and Environmental Biology, University of Southern California, Los Angeles, CA, United States, [5]Chesapeake Biological Laboratory, University of Maryland Center for Environmental Science, Solomons, MD, United States

Introduction: Molecular hydrogen is produced by the fermentation of organic matter and consumed by organisms including hydrogenotrophic methanogens and sulfate reducers in anoxic marine sediment. The thermodynamic feasibility of these metabolisms depends strongly on organic matter reactivity and hydrogen concentrations; low organic matter reactivity and high hydrogen concentrations can inhibit fermentation so when organic matter is poor, fermenters might form syntrophies with methanogens and/or sulfate reducers who alleviate thermodynamic stress by keeping hydrogen concentrations low and tightly controlled. However, it is unclear how these metabolisms effect porewater hydrogen concentrations in natural marine sediments of different organic matter reactivities.

Methods: We measured aqueous concentrations of hydrogen, sulfate, methane, dissolved inorganic carbon, and sulfide with high-depth-resolution and 16S rRNA gene assays in sediment cores with low carbon reactivity in White Oak River (WOR) estuary, North Carolina, and those with high carbon reactivity in Cape Lookout Bight (CLB), North Carolina. We calculated the Gibbs energies of sulfate reduction and hydrogenotrophic methanogenesis.

Results: Hydrogen concentrations were significantly higher in the sulfate reduction zone at CLB than WOR (mean: 0.716 vs. 0.437 nM H_2) with highly contrasting hydrogen profiles. At WOR, hydrogen was extremely low and invariant (range: 0.41–0.52 nM H_2) in the upper 15 cm. Deeper than 15 cm, hydrogen became more variable (range: 0.312–2.56 nM H_2) and increased until methane production began at ~30 cm. At CLB, hydrogen was highly variable in the upper 15 cm (range: 0.08–2.18 nM H_2). Ratios of inorganic carbon production to sulfate consumption show AOM drives sulfate reduction in WOR while degradation of organics drive sulfate reduction in CLB.

Discussion: We conclude more reactive organic matter increases hydrogen concentrations and their variability in anoxic marine sediments. In our AOM-dominated site, WOR, sulfate reducers have tight control on hydrogen via consortia with fermenters which leads to the lower observed variance due to

interspecies hydrogen transfer. After sulfate depletion, hydrogen accumulates and becomes variable, supporting methanogenesis. This suggests that CLB's more reactive organic matter allows fermentation to occur without tight metabolic coupling of fermenters to sulfate reducers, resulting in high and variable porewater hydrogen concentrations that prevent AOM from occurring through reverse hydrogenotrophic methanogenesis.

KEYWORDS

hydrogen, methane, AOM, methanogenesis, sulfate reduction, thermodynamics, organic matter, marine sediment

1 Introduction

Methane is a potent greenhouse gas that has more than doubled in the atmosphere since the pre-industrial era (Etheridge et al., 1998; US Department of Commerce, N, 2023). Therefore, it is important to understand what controls its sources and sinks, both natural and anthropogenic. Of the ~85 Tg/yr of methane produced in marine sediments, only about one-tenth of this methane is released into the overlying water column, because most of it is removed with sulfate-dependent anaerobic oxidation of methane (AOM) (Reeburgh, 2007), a microbially mediated process whereby upward-diffusing methane is oxidized to carbon dioxide while sulfate is reduced to sulfide in anoxic marine sediments. AOM communities can also use other electron acceptors like nitrate, nitrite, and metal ions to consume methane (Beal et al., 2009; Haroon et al., 2013; Muyzer and Stams, 2008; Timmers et al., 2017; Zhang et al., 2022), although these alternatives have not been shown to be quantitatively important in anoxic sulfate-rich marine sediments.

Hydrogen is a key electron donor that controls the fluxes of important compounds like methane and sulfate in anoxic marine sediments. Hydrogen is produced, along with volatile fatty acids, through the fermentation of a wide range of organic carbon molecules (LaRowe et al., 2020b). The most prevalent methanogenesis pathway in marine sediments—hydrogenotrophic methanogenesis—uses this hydrogen to reduce carbon dioxide to methane (Liu and Whitman, 2008). AOM in marine sediments has been shown to occur through a reversal of hydrogenotrophic methanogenesis with the direction controlled by hydrogen concentrations due to the power of four effect on the energetics in the reversible Equation 1 (Coon et al., 2023; Hoehler et al., 1994, 1998; Timmers et al., 2017):

$$CO_2 + 4H_2 \leftrightarrow CH_4 + 2H_2O \quad (1)$$

The formation of syntrophic partnerships between fermenters and sulfate reducers that use metabolic byproducts to prevent the buildup of inhibitory end products can keep hydrogen concentrations low enough to promote the favorability of both fermentation and AOM (Morris et al., 2013). For example, uncultured anaerobic methanotrophic archaea (*ANME*) form consortia with sulfate reducing bacteria (SRB) where the sulfate reducers gain the electrons which promotes the oxidation of methane by *ANME* through net Equation 2:

$$CH_4 + SO_4^{2-} \rightarrow HCO_3^- + HS^- + H_2O \quad (2)$$

This reaction is the reverse of reaction 1 (or reaction 6, which more accurately reflects that the system uses bicarbonate) but written as the net reaction including sulfate reduction to reflect the consortia dynamics (Hoehler and Alperin, 1996). AOM through reverse hydrogenotrophic methanogenesis creates hydrogen as an intermediate that can be used by SRB as an electron donor (Hoehler et al., 1994; Knittel and Boetius, 2009). Therefore, if SRB form tight consortia with hydrogen-producing fermenters, they can theoretically keep hydrogen concentrations consistently low, preventing methanogenesis and enabling AOM. However, if hydrogen production via fermentation exceeds its consumption via sulfate reduction, hydrogen can accumulate, preventing AOM through reverse hydrogenotrophic methanogenesis. In environments with a high content of labile organic matter, such as anaerobic sludge reactors, hydrogen concentrations can even be high enough to support simultaneous methane production and sulfate reduction (Lovley et al., 1982; Santegoeds et al., 1999; Timmers et al., 2015). Another way to reduce sulfate is through organoclastic sulfate reduction (OSR), the fermentation of organics, through the simplified net Equation 3:

$$2CH_2O + SO_4^{2-} \rightarrow 2HCO_3^- + HS^- + H^+ \quad (3)$$

We can test if sulfate reduction is carried out through syntrophic relationships with AOM or through OSR since the amount of dissolved inorganic carbon (DIC) produced is different for each process (Yang et al., 2008). Thus, $\Delta DIC:\Delta SO_4^{2-}$ increases with a 1:1 ratio for AOM and a 2:1 ratio for OSR assuming the nominal oxidation state of organic carbon (NOSC) is 0 (see LaRowe and Van Cappellen, 2011). However, if the organic matter has a non-neutral NOSC, then the ratios will be slightly different. The use of just hydrogen to reduce sulfate does not yield DIC, and therefore is not considered. AOM can also be demonstrated by an upward-curved profile of methane concentrations with depth; a linear increase in methane with depth instead signifies no net AOM or methanogenesis (Martens and Goldhaber, 1978).

The Gibbs energy function can be used to calculate the thermodynamic favorability of metabolic reactions based on the surrounding environment—(see Amend and LaRowe, 2019). It has been proposed that the generated energy of a reaction must be at least one-third to one-fifth of the energy needed to convert ADP into ATP depending on the number of ion binding sites on the ATP synthases *c* ring (Mayer and Müller, 2014; Müller and Hess, 2017). The minimum Gibbs energy change, ΔG_{min}, for this minimum biological energy quantum (BEQ) is often quoted as −20 kJ/mol (Schink, 1997), though

this value has been proposed to be lower for substrate level phosphorylation (Müller and Hess, 2017). In anoxic sediment, apparent ΔG_{min} values have been calculated as −19.1 kJ/mol SO_4^{2-} for sulfate reducers and −10.6 kJ/mol CO_2 for hydrogenotrophic methanogenic archaea (Hoehler et al., 2001). ΔG_r values greater than the ΔG_{min} (more positive than −10 to −20 kJ/mol) would inhibit microbial catalysis of catabolic reactions in either direction. In the case of Reaction 1, this means ΔG_r values > −10 kJ/mol theoretically prevent biological production of methane (Hoehler et al., 1994).

Despite the critical importance of hydrogen concentrations, few studies measure it because it cannot be preserved from natural samples as easily as other dissolved gases (Hoehler et al., 1998, 2001; Lin et al., 2012; Lovley, 1985; Lovley et al., 1982). This is because hydrogen reacts so quickly that by the time a sediment sample is placed into a gas impermeable vial and capped, the hydrogen concentrations have already changed. The solution is to place sediment, avoiding disturbance and maintaining sediment structure as much as possible, into a glass serum vial, capping with a thick butyl stopper, purging the head space with an anoxic gas like N_2, letting the hydrogen concentrations re-equilibrate over a few days, and then measuring the hydrogen partial pressure in the headspace (Hoehler et al., 1994).

To understand whether organic-rich marine sediments have higher hydrogen concentrations, preventing AOM through ΔG_r limitations, we collected cores from two sites: Cape Lookout Bight, NC, (CLB, organic-rich) and White Oak River estuary, NC (WOR, organic-poor). CLB has been shown to have more labile organic matter than WOR via a higher sedimentation rate—0.25 cm/yr. for WOR (Benninger and Martens, 1983) vs. 10.3 cm/yr in CLB (Martens and Klump, 1984) and via reactive organic carbon input values—67 mol/m^{2*}yr for CLB vs. 2.7 mol/m^{2*}yr for WOR (Martens et al., 1998). Previous work has shown that methane removal through AOM does not occur in the upper sulfate-rich sediments of organic-rich CLB, whereas it does occur in the upper sulfate-rich sediments of organic-poor WOR (Hoehler et al., 1994; Lloyd et al., 2011; Martens et al., 1998). We therefore hypothesize that hydrogen concentrations would be higher in CLB than in WOR. We further hypothesize that these differences do not correspond to the presence or absence of uncultured clades of microbes called *ANME* that have been shown to mediate AOM, since they are commonly found in sediments and enrichments that produce methane as well as those that consume methane (Kevorkian et al., 2021, 2022; Lloyd et al., 2011; Yoshinaga et al., 2014).

2 Methods

2.1 Field sampling

Three duplicate cores were collected from Cape Lookout Bight (CLB), North Carolina, USA, 34° 37′ 01.1" N, 76° 32′ 54.4" W on June 7th, 2023. A fourth core was collected in October of 2013 from the same site. Sediment was 6.25 m below the water surface at an assumed pressure of ~1 atm. The CLB collection site salinity was assumed to be 35‰ and surface water temperature was measured as 24°C. Previously measured pH of the sediment was 7.2 (Hoehler et al., 1994, 1998). A sediment core from White Oak River (WOR) estuary, North Carolina, USA, was collected from 34° 44′ 29.4" N, 77° 7′ 26.4" W in May 2019. The collection site salinity varies tidally; 18.9‰ and a temperature of 28.5°C was used for calculations from Kelley et al. (1990). Cores were sectioned in 2 cm intervals for CLB and 1 cm intervals for WOR, with subsamples from each layer removed in the ways described below for different measurements. Of these measurements, only methane concentration, hydrogen, and porosity were measured for the WOR, since the other measurements have been published from similar cores from this site over many years (Kelley et al., 1990; Martens et al., 1998; Lloyd et al., 2011; Lloyd et al., 2020; Kevorkian et al., 2021). These studies show consistent shapes of the geochemical downcore curves over time, such that knowing the depth of methane increase in a core allows the estimation of the other parameters based on previous measurements.

For microscopy, 1 mL of fresh sediment was taken in a syringe and added to 2 mL O-ring cap tubes with 500 µL of 3–4% paraformaldehyde (PFA) diluted in phosphate-buffered saline (PBS). The sediments were weighed and stored at 4°C. For porosity, 3 mL of sediment was placed in pre-weighed glass serum vials and the wet mass was recorded. Porewater was collected by centrifuging 15 mL of sediment for 5 min and filtering through a 0.2 µm syringe filter. For sulfate, 0.7 µL of porewater was stored in 100 µL of 10% HCl. For sulfide, 1 mL of porewater was stored in 250 µL of 1% $ZnCl_2$. The remaining porewater was stored in pre-weighed and evacuated glass serum vials for measuring DIC. The mass of DIC porewater was recorded. For methane concentration and δ^{13}C-CH_4, 3–4 mL of sediment was added to a glass serum vial containing 1 mL of 0.1 M KOH (enough to make pH ~ 8), capped with rubber stoppers, shaken, and stored upside down at room temperature. For hydrogen, 3 mL of sediment was collected while trying to preserve the layering and orientation of the sediment and added to an empty glass serum vial, capped with squishy butyl rubber stoppers (Rubber BV, Hilversum, NL, USA) to minimize hydrogen loss, and evacuated until flushed with O_2-scrubbed N_2 gas once back to the University of Tennessee, Knoxville, 2 days later.

2.2 Porosity

Sediment water content was calculated by drying the uncapped vials at 55°C for 2 weeks. The water loss was normalized as a fraction of the wet sediment mass. Porosity (Φ) was calculated from Equation 4:

$$\Phi = \frac{w * \rho_{sm}}{\rho_{sm} * w + (1 - w) * \rho_{pw}} \quad (4)$$

where w is sediment water content, ρ_{sm} is solid matter density, and ρ_{pw} is the porewater density; ρ_{sm} and ρ_{pw} were assumed to be 2.5 and 1.025 g/cm^3, respectively.

For depths 0–33 cm, outliers were identified if greater than the third quartile plus 1.5 times the interquartile range or if less than the first quartile minus 1.5 times the interquartile range ($n = 5$). The average of the three adjacent values replaced the outlying porosity value. For depths 33–51 cm, outliers were identified if they were greater than three standard deviations from the average of the surrounding depths. If so, the average of the surrounding depths replaced the outlying porosity value. Supplementary Table S1 lists the porosity outliers that were recalculated to give porosity values used in further calculations.

2.3 Methane

Methane was measured with a gas chromatograph (GC) equipped with a flame ionized detector (GC – Agilent 7890 Network). Replicate standards ranged ±8.9% at values around the average measured ppm. Vials were shaken for at least 1 min prior to headspace sampling. 0.5 mL of headspace was injected with triplicate runs per sample. Aqueous methane concentrations [$CH_{4\,aq}$] were calculated in mM using Equation 5:

$$\left[CH_{4_{aq}}\right] = \frac{CH_{4\,g} * V_h}{R * T * \Phi * V_s * 1000} \quad (5)$$

where $CH_{4\,g}$ is the methane gas concentration in ppm converted from peak area with the standard curve, V_h is the headspace volume, R is the universal gas constant in L*atm/mol*K, T is the temperature in K, Φ is the porosity, V_s is the sediment volume, and 1,000 is the conversion factor for mM.

2.4 $\delta^{13}CH_4$

$\delta^{13}CH_4$ was measured from the same vials as methane using a cavity ringdown spectrometer (Picarro G2201i). Vials were injected with 5 mL of zero air and shaken for 2 min prior to injection. Headspace CH_4 was diluted (5 mL headspace: 135 mL zero air) and injected directly into the spectrometer. Instrument precision was ±1‰.

2.5 Hydrogen

Saturation concentrations for *in situ* hydrogen was calculated as 671.8 µM for CLB and 704.9 µM for WOR to convert ppm into aqueous concentrations (Crozier and Yamamoto, 1974). Serum vials were capped and flushed with O_2-scrubbed N_2 gas and left to incubate at room temperature for at least 4 days. The use of squishy (easy to depress between the fingers) stoppers was tested to ensure hydrogen remains trapped in the headspace. We found that H_2 was lost after 9 days of incubation, so we stopped all incubations at this 9 day mark (Supplementary Figure S1). After incubation, a glass syringe and metal needle were used to collect equilibrated air from the headspace without shaking the vial. Hydrogen was measured with a GC [Peak Performer 1 reducing compound photometer (RCP)]. This instrument has a precision of ±10% of the reading. Triplicates were measured except deeper than 47 cm in WOR cores due to shortage of vials in the field.

2.6 Microscopy

Dilutions [with phosphate-buffered saline (PBS)] of the refrigerated sediment ranged from 1:20 for 0–2 cm, 1:10 for 2–30 cm, and 1:5 for 30+ cm. 20 µL of the diluted samples were added to 5 mL of PBS with 500 µL of 5× SYBR Gold and left to incubate at room temperature in the dark for 10 min. Samples were filtered onto a 0.2 µm filter until dry then mounted with VECTASHIELD. Slides were stored at −20°C for up to 2 weeks. The slides were excited with the 38 HE GFP filter set and counted at 30 random locations on the slide with a ZEISS Axio Imager M2. The average cells counted was extrapolated for the cell concentration of the entire filter, corrected for the dilution used and original mass of sediment collected. The sum of cell counts on a control slide (just PBS) was subtracted from each slide's counts to correct for contamination.

2.7 Sulfate

Sulfate was measured via ion chromatography (IC) equipped with a 4 mm × 250 mm IonPac AS18 hydroxide-selective anion-exchange column (Dionex ICS-2100). Replicate standards averaged ±0.01% at 20 mM. KOH was used as the eluent with each sample's retention time set at 24 min. Chloride peaks were also measured with this method, and no abnormalities were observed.

2.8 Sulfide

Hydrogen sulfide, the sum of H_2S, HS^-, and S^{2-}, was measured with an adapted Cline assay to react porewater hydrogen sulfide with Fe^{3+} and diamine to create methylene blue (Cline, 1969). The samples incubated at room temperature for at least 20 min in the dark before a NanoDrop 2000C spectrophotometer measured the absorbance at 667 nm. This instrument has a ± 3% absorbance accuracy.

2.9 DIC/ΣCO_2

Dissolved inorganic carbon (DIC), the sum of CO_2, HCO_3^-, and CO_3^{2-}, was measured only on CLB cores 1–3 using a cavity ringdown spectrometer (Picarro G2201i) at the Chesapeake Biological Laboratory, Maryland. Instrument precision was ±1‰. Samples were acidified with 0.1 mL of 10% HCl so DIC was converted to CO_2. Vials were injected with 5 mL of zero air and shaken for 2 min, assuming 96.9% of CO_2 was extracted based on the CO_2 solubility (Weiss, 1974). Headspace CO_2 was diluted (5 mL headspace: 135 mL zero air) and injected directly into the spectrometer. If out of the instrument's range (~2,000 ppm CO_2), samples were further diluted (35 mL original dilution: 105 mL zero air). Due to the high sulfide concentrations in the porewater, we verified that there was no interference with the CO_2 signal using a copper trap (Malowany et al., 2015). If no DIC was measured for a sample, the average concentration of the sample above and below was used for thermodynamic calculations.

2.10 DIC: sulfate ratios

Ratios of DIC to sulfate were calculated from our measured DIC and sulfate for CLB and from a WOR dataset of two 2013 cores from the same location as our cores, Station H (Steen, 2016). The ratio uses the change in DIC compared to the overlying water column for WOR or 12 cmbsf concentrations for CLB versus the absolute value of the change in sulfate compared to the overlying water column for WOR or 12 cmbsf for CLB. Only depths deeper than the bioirrigation zone where sulfate is held near constant (>12 cmbsf for CLB, >0 cmbsf for WOR) but also in the sulfate reducing zone (<40 cmbsf for CLB, <47

cmbsf for WOR) were used for determination of the slope of the DIC to sulfate stoichiometric ratio. A 2:1 ratio of ΔDIC to ΔSO_4^{2-} represents OSR and a 1:1 ratio represents sulfate reduction via AOM.

2.11 Gibbs energy calculations

The Gibbs energy of reaction, ΔG_r, was calculated for hydrogenotrophic methanogenesis, Equation 6,

$$HCO_3^- + 4H_2 + H^+ \rightarrow CH_4 + 3H_2O \quad (6)$$

and sulfate reduction, Equation 7,

$$SO_4^{2-} + 4H_2 + H^+ \rightarrow HS^- + 4H_2O \quad (7)$$

using Equation 8:

$$\Delta G_r = \Delta G_r^\circ + RTlnQ_r \quad (8)$$

where ΔG°_r refers to the standard-state Gibbs energy of reaction and Q_r is the reaction quotient. It is calculated using Equation 9:

$$Q_r = \prod_i a_i^{v_i} \quad (9)$$

where a_i refers to the activity and v_i is the stoichiometric coefficient of the ith species.

The concentrations of CH_4, H_2, and DIC were measured in this study as noted above. Since DIC was not measured for WOR, values were used from Kelley et al. (1990). The ratio of bicarbonate to carbon dioxide was calculated to be 0.94 from calculated *in situ* equilibrium constants (Roy et al., 1993). Activity coefficients of CH_4 and H_2 were assumed to be 1 and was calculated for bicarbonate as 0.661 in CLB and 0.660 in WOR based on assumed ionic strength of 0.7 M using the CHNOSZ package for R (Dick, 2019), which implements the revised HKF equation of state for Gibbs energies (Shock et al., 1992; Tanger and Helgeson, 1988) and the extended Debye-Hückel equation for activity coefficients (Helgeson, 1969). Values of ΔG°_r for hydrogenotrophic methanogenesis at CLB ($T = 24°C$, $p = 1$ atm) and WOR ($T = 28.5°C$, $p = 1$ atm) were calculated to be −229.59 kJ/mol and −238.98 kJ/mol, respectively, using the CHNOSZ package.

2.12 DNA extraction and sequencing

DNA was extracted using QIAGEN's RNeasy Powersoil Total RNA Kit with the RNeasy Powersoil DNA Elution Kit, since this kit has been shown to remove co-extracted humic acids, even if the goal is not RNA extraction (Lloyd et al., 2010). All steps in the protocols were followed, using 2 g of sediment, with the following modifications: four freeze thaw steps at 65°C were conducted after step 2. During step 9, samples were incubated at room temperature using a hybridization oven kept at slow rotation, followed by an overnight incubation at 8°C. The V4 region of the 16S rRNA gene was amplified using the Earth Microbiome Project (EMB) 16S Illumina amplicon protocol and the Caporaso 515F and 806R primers. Samples were prepared with the Illumina DNA prep kit and sequenced with an Illumina MiSeq at the Genomics Core at the University of Tennessee.

2.13 Data analysis

16S rRNA gene assays were analyzed in R (R Core Team, 2021; RStudio Team, 2020) with version 1.16 of the Divisive Amplicon Denoising Algorithm (DADA2) pipeline (Callahan et al., 2016). Poor read quality samples were removed along with ASVs with less than 5 reads. Contaminants were removed from analysis if eukaryotic or previously identified as contaminants (Sheik et al., 2018). Taxonomy was assigned with version 138.1 of SILVA reference sequences (Quast et al., 2013; Yilmaz et al., 2014). No species level identification was assigned. The resulting loss per each step of analysis is shown in Supplementary Table S2.

The phyloseq package was used for beta diversity and handling of the large data frame (McMurdie and Holmes, 2013). Plots were created primarily with the ggplot2 package (Wickham, 2016). Raw sequences have been reposited in the ENA bank under project ID PRJEB74703. All code is on GitHub at https://github.com/gagecoon/clb23, with the various helper packages used throughout all data analysis listed as imported libraries in the code.

3 Results

3.1 Geochemistry and Gibbs energy in White Oak River estuary

Methane remains low (<0.1 mM) in the upper 30 cm of sediment until it increases and remains between 0.25 and 1 mM between 36 and 62 cm (Figure 1A). The upward curvature of the methane concentrations signifies methane removal through AOM as methane diffuses upward through the core, as has been consistently observed previously (Kevorkian et al., 2021; Lloyd et al., 2011; Martens et al., 1998). Hydrogen remains low (range = 0.41–0.52 nM H_2) and constant (variance = 0.00081 nM H_2) for the 15 measurements in the upper 15 cm. Below the upper 15 cm, hydrogen concentrations increase to a range of 0.31–2.56 nM between 20 and 62 cm, showing increased variability (variance = 0.203 nM) (Figure 1B). Hydrogen increases 15 cm above the point where methane begins to accumulate. AOM via Reaction 6 is exergonic in the upper 20 cm while methanogenesis is exergonic from 20 to 40 cm (Figure 1C). Below this point, values are not consistently exergonic in either direction.

3.2 Geochemistry and Gibbs energy changes in Cape Lookout Bight

Sulfate depletion depths in the Cape Lookout Bight sediments range from 30 to 40 cm, as has been observed previously (Coon et al., 2023; Hoehler et al., 1994), except for the 2013 core which has shallower sulfate depletion. In all CLB cores, methane increases linearly with depth and is not prevented from accumulating in the sulfate-rich upper ~30 cm, suggesting no net removal or production,

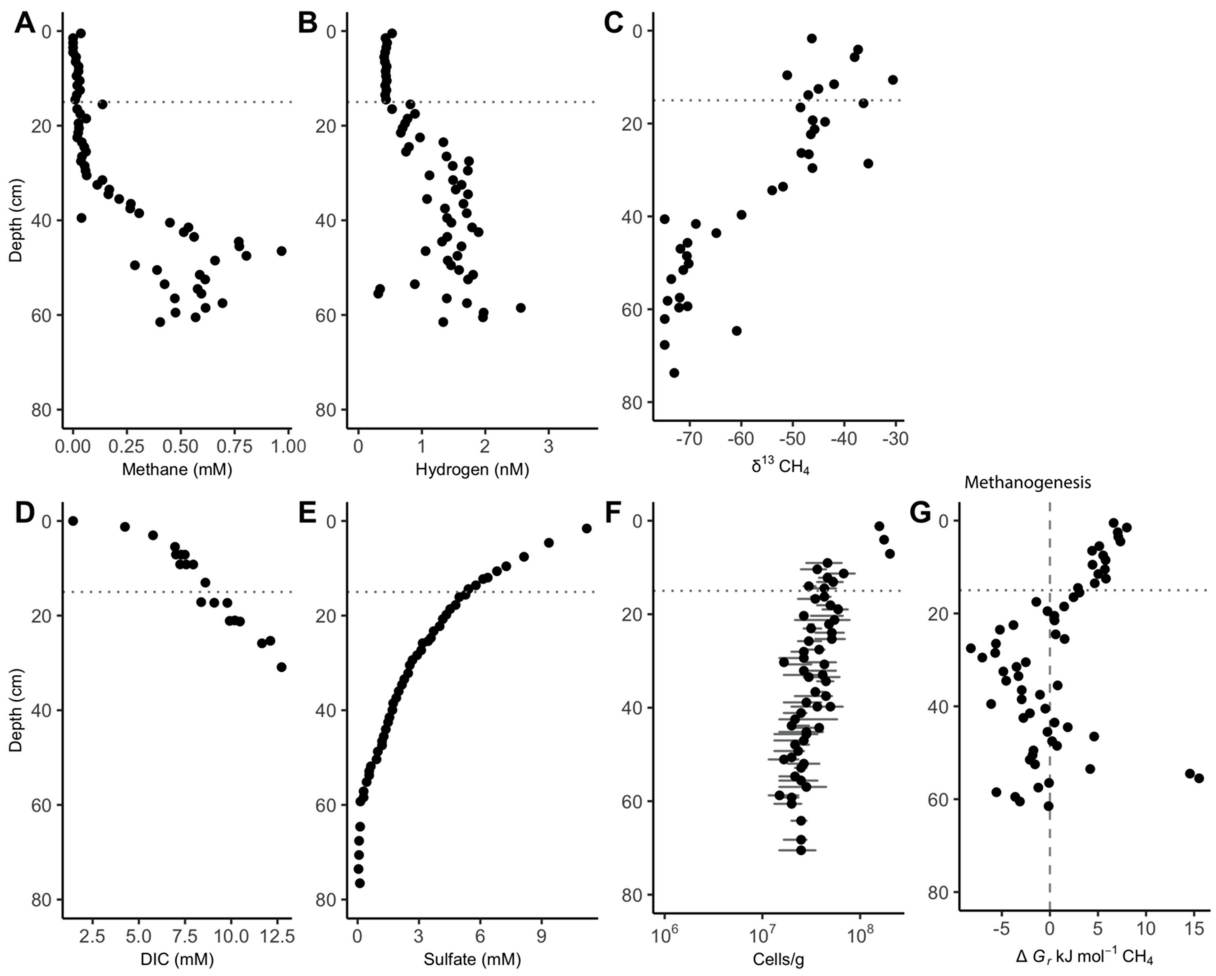

FIGURE 1
White Oak River estuary's downcore porewater concentrations of **(A)** methane and **(B)** hydrogen, **(C)** δ13CH4, **(D)** dissolved inorganic carbon (DIC), **(E)** sulfate, **(F)** cells, and **(G)** Gibbs energy values for hydrogenotrophic methanogenesis, ΔGr, (Reaction 6). The dashed vertical line at 0 kJ/mol delineates equilibrium for Reaction 6, where neither the forward nor reverse reaction is exergonic. The horizontal dotted line at 15 cm is the depth where hydrogen begins to accumulate. Positive values of ΔGr indicate that AOM via reverse methanogenesis is exergonic while negative values show that hydrogenotrophic methanogenesis is exergonic. Data for subplots C, E, and F is from Kevorkian et al. (2021), and data for subplot D is from Kelley et al. (1990). Cell abundance error bars represent the standard deviation of 30 random counts.

in agreement with previous geochemical studies at CLB (Hoehler et al., 1994; Martens et al., 1998). Methane concentrations increase to more than 1 mM in 2023 core 3, reaching full saturation (~1.5 mM, Figure 2A). Hydrogen is highly variable, peaking around 2 nM in the upper few cm, and decreasing to less than 1 nM below 10 cm (Figure 2B). $\delta^{13}CH_4$ values range from −60‰ to −66‰ (Figure 2C), decreasing with depth below 24 and 30 cm in 2023 cores 1 and 3, respectively, suggesting deep AOM that does not occur in the upper sections where sulfate and methane are both abundant. The highly negative isotope ratios show upward-diffusing methane is likely methanogenic in origin. The DIC concentrations (Figures 2D,E), which increase linearly with depth to more than 100 mM, are much higher than values measured previously at WOR (Kelley et al., 1990), as expected for having more labile organic matter at CLB. Sulfate decreases with depth from 24 mM to near 0 mM by 10 cm in 2013's core and at 30–40 cm for 2023's cores (Figure 2F). Sulfide increases with depth until about 30 cm (Figure 2G). Cell abundance ranges from 10^6 to 10^8 for 2023's cores and slightly decreases with depth in all cores (Figure 2H). Porosity is mostly between 0.7 and 0.85 and decreases slightly with depth in all cores (Supplementary Figure S2).

Below a few centimeters sediment depth in CLB cores, Gibbs energies are only exergonic for reverse hydrogenotrophic methanogenesis, Reaction 6 (Figure 3A–D). Sulfate reduction, Reaction 7, is exergonic at most depths, ranging mostly from −40 to −10 kJ/mol (Figure 3E-G).

3.3 DIC: sulfate ratios

The ratio of ΔDIC to ΔSO_4^{2-} shows slopes of 2.38 for CLB and 0.629 for WOR (Figure 4). This suggests that organic matter drives sulfate reduction in CLB and AOM drives sulfate reduction in WOR.

3.4 Microbial diversity and composition in Cape Lookout Bight

Of the 10,232 observed amplicon sequence variants (ASVs), 84.5% are Bacteria, while 15.5% are Archaea. Non-metric multidimensional

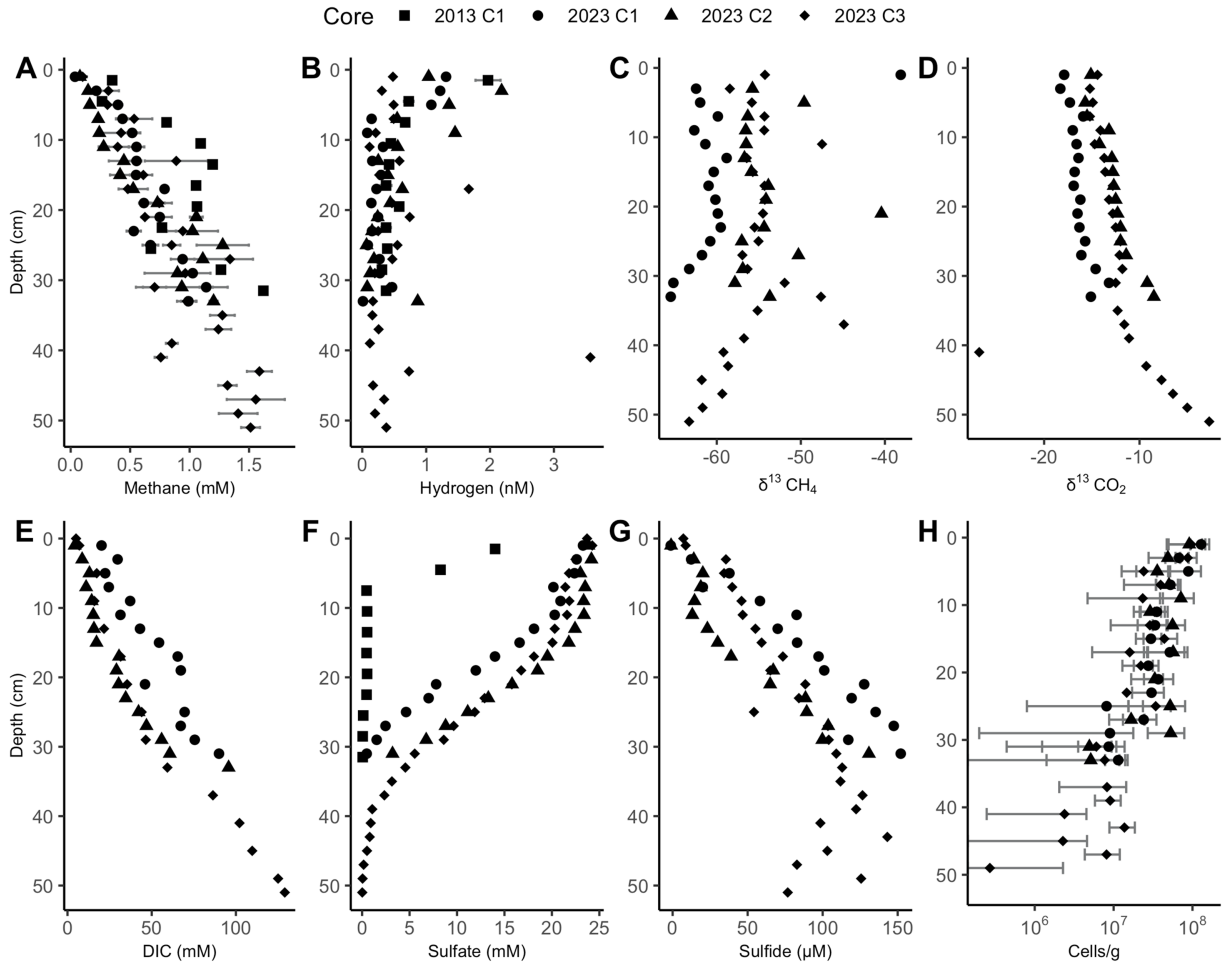

FIGURE 2
Cape Lookout Bight sediment downcore concentrations of **(A)** methane, **(B)** hydrogen, **(C)** δ13CH4, **(D)** δ13CO2, **(E)** dissolved inorganic carbon (DIC), **(F)** sulfate, **(G)** sulfide, and **(H)** cells. Methane and hydrogen error bars represent triplicate measurements of the same sample. Cell abundance error bars represent the standard deviation of 30 random counts. Only a subset of these measurements was performed for the 2013 core.

scaling (NMDS), principal coordinates analysis (PCoA), and canonical correspondence analysis (CCA) ordination of Bray–Curtis dissimilarity distances show depth is a driving factor in the diversity of microbial life in CLB sediments (Supplementary Figures S3, S4), in accordance with what has been found previously (Coon et al., 2023).

Methane-cycling archaea like *ANME-1b*, *Methanofastidiosales*, *Methanomassiliicoccales*, *Methanomicrobiales*, and *Methanosarciniales* are present throughout the cores (Figure 5), in agreement with previous results (Coon et al., 2023). There is a higher relative abundance of *ANME-1b* than other methane-cycling archaea at the lowest depths (29–31 cm) where sulfate is low (~1.5–3.2 mM) (Figure 5). This sharp increase in ANME-1 near the depth of sulfate depletion has been observed previously (Coon et al., 2023) and matches the pattern observed in the White Oak River estuary (Lloyd et al., 2011; Kevorkian et al., 2021). In sulfate-rich sediments, methanogens capable of using methylated compounds are abundant, *Methanofastidiosales* and *Methanomassiliicoccales* (Figure 5). The majority of likely SRB are *Desulfobacteria*, ranging from 4 to 18% of total abundance (Figure 6). Overall, SRB slightly decrease in abundance with depth as previously observed (Coon et al., 2023).

4 Discussion

4.1 Molecular hydrogen from fermentation controls the net direction of methane cycling through consortia between SRB and fermentative microbes

Downcore profiles of hydrogen concentration differ greatly between the relatively organic-poor White Oak River estuary and the relatively organic-rich Cape Lookout Bight. In WOR sediments, hydrogen is tightly controlled in the 15 measurements made in the upper 15 cm (variance = 0.00081 nM H_2). Since this is the depth range where sulfate reduction rates are highest (as shown by the greatest rate of sulfate decrease with depth), a feature that is consistent across years and seasons (Kelley et al., 1990; Lloyd et al., 2011; Martens et al., 1998), these concentrations are likely the result of consistent syntrophy between sulfate reducing microbes and fermentative microbes. Given the consistency of the hydrogen control, it is likely that this is an obligate syntrophy driven by maintaining thermodynamic yields for fermenters degrading recalcitrant lignin-derived compounds dominating the WOR site (Martens et al., 1998). As sulfate is depleted with depth, hydrogen

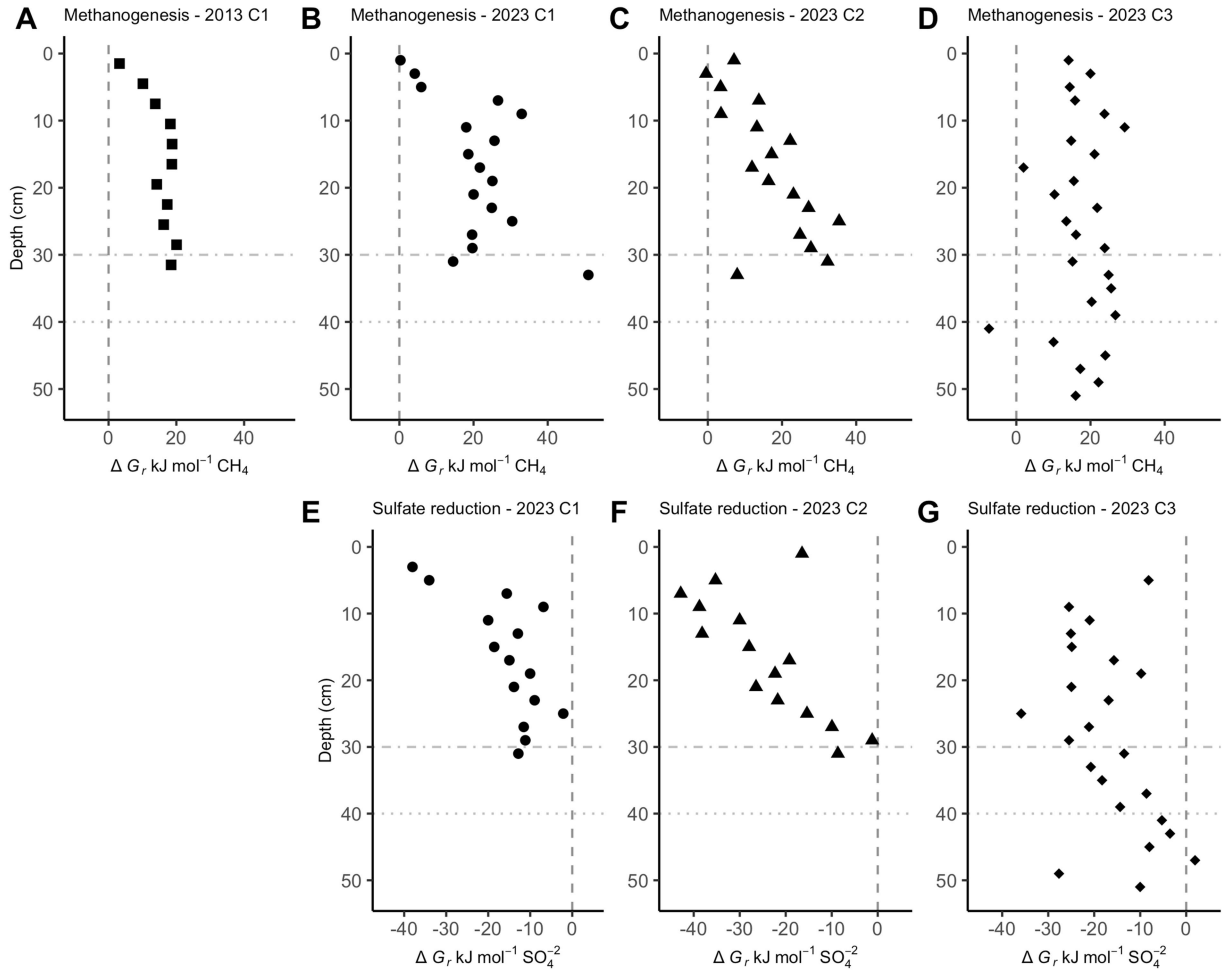

FIGURE 3
Gibbs energies of reaction, Δ*Gr*, for hydrogenotrophic methanogenesis (**A–D**, Reaction 6) and sulfate reduction (**E–G**, Reaction 7) in Cape Lookout Bight sediments. Values left of the dashed vertical lines at 0 kJ/mol show where these reactions begin to be exergonic. Horizontal dot-dash and dotted lines are where sulfate is depleted in core 1 and core 3, respectively.

concentrations increase and become highly variable over the 41 measurements made below 20 cm (range = 0.31–2.56 nM H_2, variance = 0.203 nM H_2), likely because sulfate becomes diffusion-limited, so sulfate reducers are no longer a reliable syntrophic partner with fermenters. Notably, this occurs well above the depth where net methane production occurs. It coincides with a small gradual increase in methane with depth indicative of net removal of methane diffusing up from below. This was also observed in incubations of WOR sediment where hydrogen increased before methanogenesis started (Kevorkian et al., 2022). It is only when hydrogen concentrations stabilize at a still variable but slightly higher value (1.49 nM $H_2 \pm 0.44$ nM H_2) below 30 cm that net methane production occurs. This is the mechanism commonly assumed to occur in anoxic marine sediments; sulfate reducers keep hydrogen concentrations low through syntrophy with fermenters when sulfate is plentiful but lack syntrophy when sulfate is depleted, allowing for higher and more variable hydrogen concentrations and therefore methanogenesis. The only surprising part is that sulfate's control of hydrogen is released well before net methanogenesis occurs and well within the AOM zone. This agrees with observations of long-term incubations from the same site where hydrogen increases before methanogenesis occurs (Kevorkian et al., 2022).

CLB has a very different hydrogen profile; hydrogen concentrations are never well-controlled (variance = 0.2285 nM H_2 for 0–30 cm), suggesting a lack of a well-developed obligate syntrophy between sulfate reducers and fermenters. This lack of widespread syntrophy is likely due to the plentiful and highly reactive organic matter in CLB, as has been found previously (Martens et al., 1998). Here, we show that hydrogen concentrations are significantly higher in the upper 10 cm than below it (0.876 nM H_2 vs. 0.410 nM H_2, t-value = −2.8945, *p*-value = 0.0077, df = 25.604), which implies that the most labile organic matter—toward the surface—supports the highest hydrogen concentrations. This hydrogen profile with higher abundances at the surface has also been observed in the highly reactive organic matter of the Namibian coast (Lin et al., 2012). Sulfide concentrations validate the observed sulfate profile via the opposite trends; these are further used for the Gibbs energy calculations. In CLB, evidence for net AOM only appears deeper than 35 cm (as seen in the $\delta^{13}CH_4$ and $\delta^{13}CO_2$ profiles), suggesting that labile organic matter needs to be depleted so hydrogen concentrations can decrease and AOM can occur.

Evidence for the difference in reliance on consortia between CLB and WOR appears in the $\Delta DIC{:}\Delta SO_4^{2-}$ values, where WOR stoichiometric coefficients reflect sulfate-dependent AOM, and CLB

10.3389/fmicb.2024.1455857

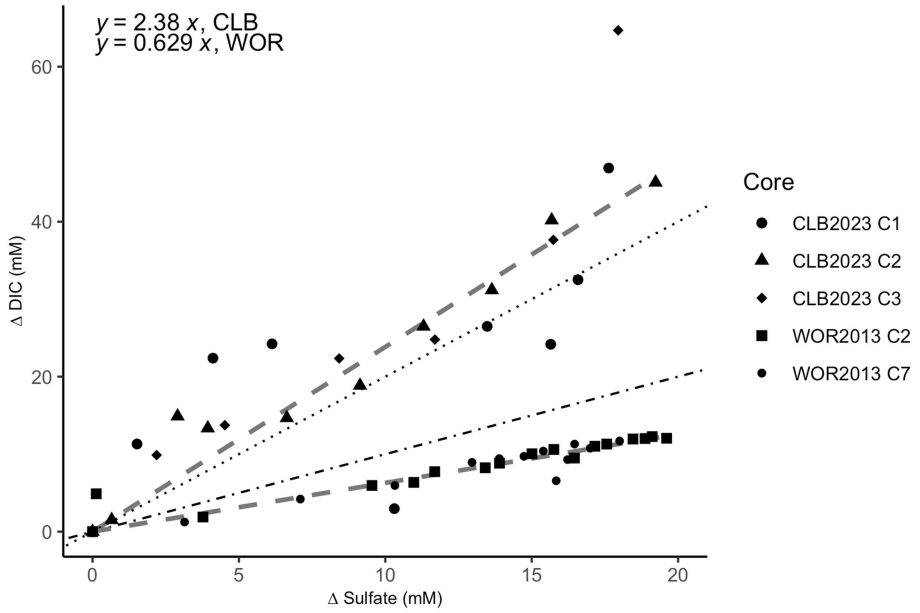

FIGURE 4
Stoichiometric ratios of the change (Δ) in dissolved inorganic carbon (DIC) vs. sulfate in pore fluids from the sulfate reducing zone in Cape Lookout Bight (12–40 cm; circle, triangle, and diamond shapes) and White Oak River estuary (0–47 cm; square and small circle shapes). The change (Δ) in DIC vs. sulfate has a ratio of 2.38 for CLB and 0.629 for WOR calculated from linear fits. The dotted line represents the 2:1 ratio of organoclastic sulfate reduction (OSR) while the dot-dashed line represents the 1:1 ratio of AOM via sulfate reduction.

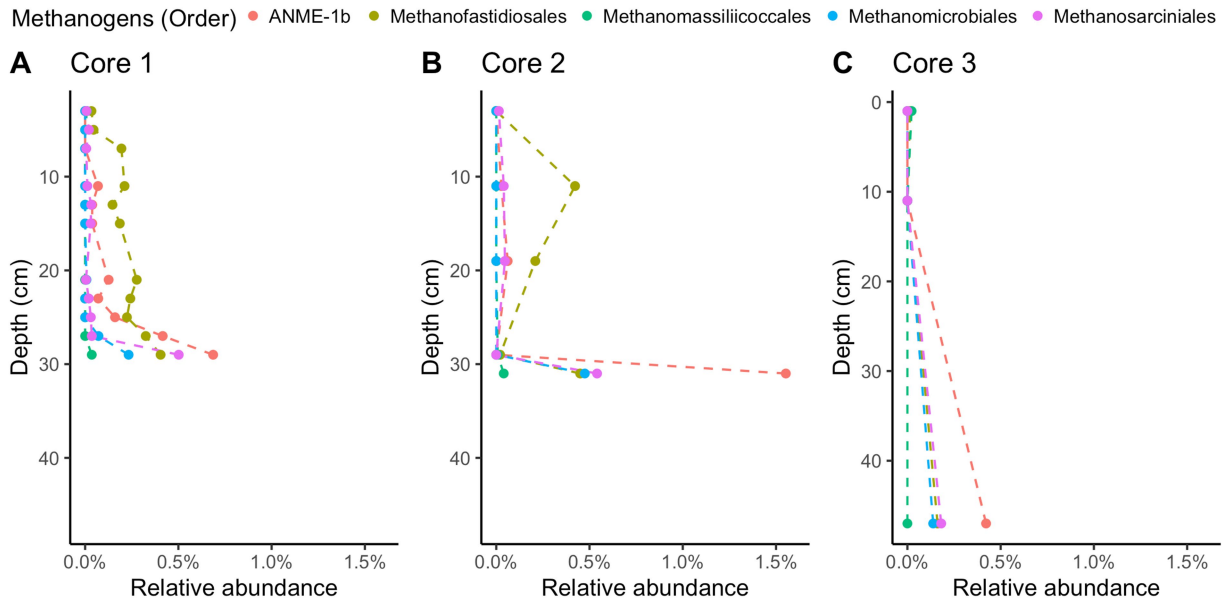

FIGURE 5
16S rRNA gene amplicon relative abundances for likely methane-cycling archaea in Cape Lookout Bight 2023 cores **(A)** 1, **(B)** 2, and **(C)** 3. Dashed lines are intended to guide the eye.

shows organic matter powers sulfate reduction via OSR (Figure 4). The ratio values slightly higher than 2:1 in CLB may reflect excess DIC production via anaerobic heterotrophy and values slightly lower than 1:1 for WOR may reflect net autochthonous carbonate precipitation in WOR. The oxidation state of the organics being non-neutral could also explain the non-integer ratios (LaRowe and Van Cappellen, 2011). Other studies have shown low organic matter lability, like in WOR, promotes sulfate dependent AOM (Pohlman et al., 2013). The OSR in CLB may decrease the favorability of consortia formation between SRB and fermenters since organic matter is more labile. Additionally, with the lack of hydrogen usage, there is the potential for higher and more variable hydrogen concentrations in the organic-rich marine sediment. This would lead to the perceived "messiness" observed in downcore hydrogen measurements that is especially prevalent in the shallowest and most organic-rich depths.

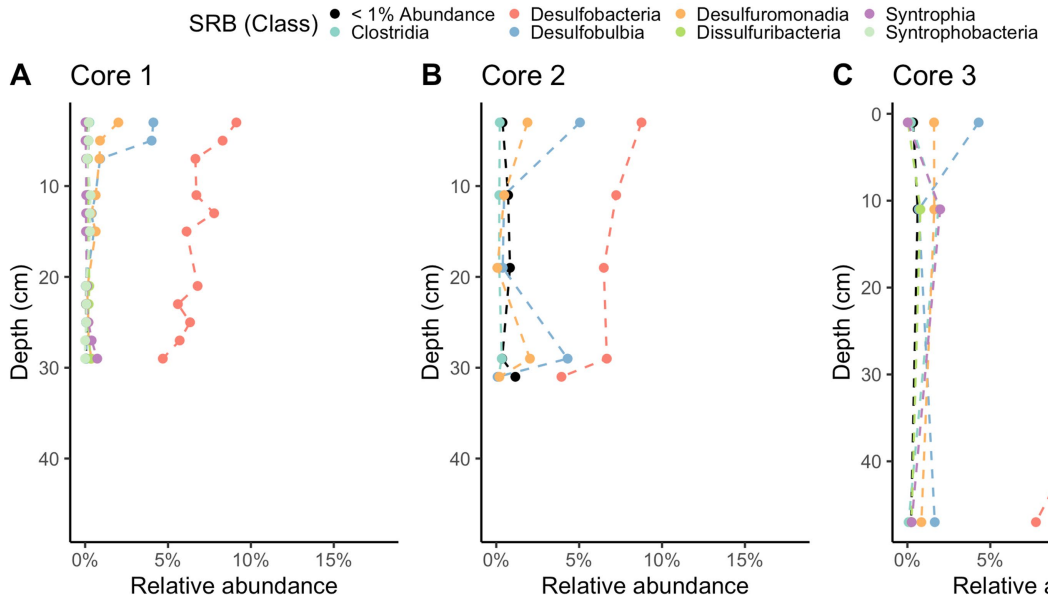

FIGURE 6
16S rRNA gene amplicon relative abundances for likely sulfate-reducing bacteria (SRB) in Cape Lookout Bight 2023 cores **(A)** 1, **(B)** 2, and **(C)** 3. Dashed lines are intended to guide the eye.

Hydrogen profiles in WOR are consistent with the net AOM observed. WOR has clear removal of methane from AOM [shown via the concave up methane profile, the 1:1 $\Delta DIC:\Delta SO_4^{2-}$ slope, previous $\delta^{13}C$ ratios and modeling (Kevorkian et al., 2021, 2022; Lloyd et al., 2011; Martens et al., 1998)]. CLB hydrogen profiles are consistent with the lack of net AOM observed in the upper sulfate-rich sediment (shown via the linear methane profile, the 2:1 $\Delta DIC:\Delta SO_4^{2-}$ slope, the $\delta^{13}C$ ratios, and previous studies) (Hoehler et al., 1994; Martens et al., 1998), and AOM below ~35 cm (shown via the $\delta^{13}C$ ratios and ΔG_r). We conclude that hydrogen does control the net direction of methane-cycling and this hydrogen is controlled by organic matter reactivity. Further, it seems that hydrogen concentrations are controlled by the presence or lack of syntrophy between SRB and fermenters. This has important implications for our understanding of methane cycling from biotic sources in anoxic marine sediment—highly reactive organic matter sites may not have significant methane removal through AOM (Lapham et al., in review; Hoehler et al., 1994, 1998).

4.2 Differences in geochemical processes between these two sites are not due to different microbial communities

The difference in metabolic processes between these two sites is likely not due to the presence of different microbial communities. The microbial communities at each site have many of the same key taxa despite their different geochemistry. Compared to previously published 16S rRNA gene sequence abundances from WOR (Kevorkian et al., 2021), the two sites have similar communities of sulfate reducing bacteria, dominated by *Desulfobacteria*. In comparing the methane-cycling archaea, both have a rapid increase of *ANME-1* in the deepest sampled depths where sulfate is at its lowest. There are some *Methanofastidiosales* in WOR, but they are not as consistent in abundance as at CLB. The similarity in microbial composition patterns in the WOR and CLB suggest that the quality of the organic matter has a larger effect on the respiratory processes than the microbial taxa that are present. However, additional methanol sources may promote methylotrophic methanogenesis in CLB, as plant decay and phytoplankton both supply methanol to marine sediments (Bates et al., 2021; Mincer and Aicher, 2016), which may account for the methylotrophic methanogens in our 16S rRNA libraries in CLB.

4.3 Observed ΔG_r values underestimate favorability assuming a ΔG_{min}

The Gibbs energy calculations shown in Figure 1 reveal that sulfate driven AOM and methanogenesis often yield less energy than the ΔG_{min} of −10 kJ/mol in WOR. However, the geochemical data gathered and analyzed in this study strongly suggests that these processes are occurring where there is not enough energy to satisfy the presumed ΔG_{min}. It has been shown that metabolic reactions via syntrophic associations have been shown to occur close to thermodynamic equilibrium ($\Delta G \approx 0$ kJ/mol) which could allow for these reactions to be exergonic without reaching the −20 to −10 kJ/mol threshold (Jackson and McInerney, 2002). One explanation is that a ΔG_{min} does not exist in these sediments, rather life is limited by the rate at which this energy is delivered, or power (LaRowe et al., 2012; LaRowe and Amend, 2015a, 2015b, 2020). It is intuitive that the rate of energy delivery is more important for life rather than the size of the energetic package, since even 10 kJ/mol would be insufficient to support life if only one mole of a reactant were processed over the lifetime of an organism, as an extreme example.

As a though experiment, suppose that a microbially catalyzed reaction could yield 10 kJ/mol (i.e., $\Delta G_r = -10$ kJ/mol) and the ΔG_{min} term is more negative than this. According to Equation 10, quantifying the Gibbs energy of the proton motive force (*pmf*),

$$\Delta G_{pmf} = -nF\Delta\Psi + 2.303RT\Delta pH \quad (10)$$

0.63 moles of protons could be translocated across energy-transducing membranes (solving for n for typical values of the other parameters in this equation, $\Delta\Psi = 120\,mV$, $\Delta pH = -0.5$ at 25°C). The assumption that a ΔG_{min} must be overcome means that despite this large flux of protons, not a single molecule of ATP could be made from the microbes catalyzing this hypothetical reaction, despite the 3.79×10^{23} protons (N_A * 0.63 mol H^+) passing through their membranes. If this ΔG_{min} were not assumed to exist, 10 kJ per reaction turnover could, if maximally utilized, yield about 0.17 *moles* of ATP under the specified conditions, which is a clearly sufficient amount of ATP to sustain life.

The ΔG_{min} was first stated as an unreferenced assumption that has been perpetuated as conventional wisdom (Hoehler, 2004; Hoehler et al., 2001; Schink, 1990, 1997, 2002; Schink and Stams, 2006; Schink and Thauer, 1988). In the original paper exploring the energetics of anaerobic sludge degradation, (Schink and Thauer, 1988), observed that (a) butyrate fermentation yields "20–25 kJ per mol partial reaction," (b) 75 kJ are required to synthesize 1 mol of ATP and (c) three protons must pass through an energy-transducing membrane to make *one molecule* of ATP. They combine this information, to state, "[t]hus, the equivalent of 1 transported proton is the smallest amount of energy which can be converted into biologically useful energy, meaning: into ATP synthesis." Not only are the values of ΔG_{ATP} production at least 25% higher than what is accepted today [75 vs. 60 kJ (mol ATP)$^{-1}$, though they are variable given the particular temperature, pressure, and compositional conditions—(Larowe and Helgeson, 2007)], the authors have assumed that the energy from fermentation is split evenly between the three groups of organisms involved in butyrate fermentation, despite the fact that the energetics of the intermediate reactions being catalyzed are not equal. The work of many others have addressed an alternative to ΔG_{min} by using a minimum maintenance energy over time, i.e., power, to describe minimum energy thresholds for microbial life (Hoehler and Jørgensen, 2013; Tijhuis et al., 1993). Power has been used instead of just ΔG_r to better constrain the lower limits of energy usage in natural settings (Bradley et al., 2020, 2022; LaRowe et al., 2020a; Zhao et al., 2021). These works show power is a more apt metric for determining energy limits for microbial life. Our data from WOR suggest that a ΔG_{min} does not exist because the direction of methane production or consumption changes with the sign of ΔG, rather than the crossing of a −10 kJ/mol threshold, which is also supported by theory (LaRowe et al., 2012) and the lack of a consensus ΔG_{min} in the literature.

CLB sediment has been shown to lack AOM in the presence of sulfate through radiotracers, geochemical profiles, and stable carbon isotope ratios (Hoehler et al., 1994; Martens et al., 1998, and this paper), yet our Gibbs energy changes predict AOM occurring even in the shallow sediment even though it clearly does not occur there (Figure 3). We hypothesize that the large amounts of labile organic matter at CLB mean that the values we measure do not represent the instantaneous values experienced by methane-cycling archaea in close proximity to hydrogen-producing fermenters over small spatial scales.

5 Conclusion

We measured hydrogen concentrations in two sites (WOR and CLB) with different organic matter reactivity and found these values to be useful for understanding the methane cycle in anoxic marine sediment (summarized in Figure 7). Hydrogen concentrations are tightly controlled by sulfate reducers in the presence of poorly reactive organic matter in WOR, allowing AOM in sulfate-rich sediments while hydrogen concentrations are higher and more variable with the highly reactive organic matter of CLB, preventing AOM in sulfate- and methane-rich sediments. However, the concentrations of species in the reactions describing hydrogenotrophic methanogenesis did not always yield values of ΔG_r that exceed what is thought to be a minimum catabolic energy yield that acts as a thermodynamic limit on life, ΔG_{min}. We have concluded that, in the face of concentration profiles and stable carbon isotopes, that the ΔG_{min} is not a prerequisite for a lower energetic limit of life, other than the obvious fact that ΔG_{min} mut be less than 0. As has been discussed elsewhere, perhaps a minimum power limit for life is a more apt metric for determining the energy limits for life. In the context of our samples shown here, ΔG_r is useful for predicting reaction favorability in controlled sites like WOR, assuming there is no ΔG_{min}. Samples from CLB have higher hydrogen concentrations than WOR; we hypothesize this is due to consortia disruption from the presence of highly reactive organic matter. Due to the difference in organic matter reactivity, CLB and WOR have vastly different hydrogen concentrations and variability with comparable microbial communities. This means that in areas of highly reactive organic matter, net removal of methane through AOM does not occur because the high and variable hydrogen concentrations prevent reverse hydrogenotrophic methanogenesis.

Data availability statement

The datasets presented in this study can be found in online repositories. The names of the repository/repositories and accession number(s) can be found in the article/Supplementary material.

Author contributions

GC: Conceptualization, Data curation, Formal analysis, Investigation, Methodology, Software, Validation, Visualization, Writing – original draft, Writing – review & editing. LW: Data curation, Investigation, Methodology, Writing – review & editing. AM: Conceptualization, Data curation, Formal analysis, Investigation, Methodology, Software, Writing – review & editing. RD: Data curation, Investigation, Methodology, Writing – review & editing. RK: Data curation, Investigation, Methodology, Writing – review & editing. DL: Conceptualization, Methodology, Writing – original draft, Writing – review & editing. AS: Funding acquisition, Project administration, Resources, Supervision, Writing – review & editing. LL: Data curation, Formal analysis, Investigation, Methodology, Software, Validation, Writing – review & editing. KL: Conceptualization, Funding acquisition, Project administration, Resources, Supervision, Writing – original draft, Writing – review & editing.

Funding

The author(s) declare financial support was received for the research, authorship, and/or publication of this article. This project was funded by NSF Chemical Oceanography grant #OCE-1948720, NSF Biological Oceanography grant #OCE-2145434, and US Department of Energy, Office of Science, Office of Biological and Environmental Research, Genomic Science Program (DE-SC0020369).

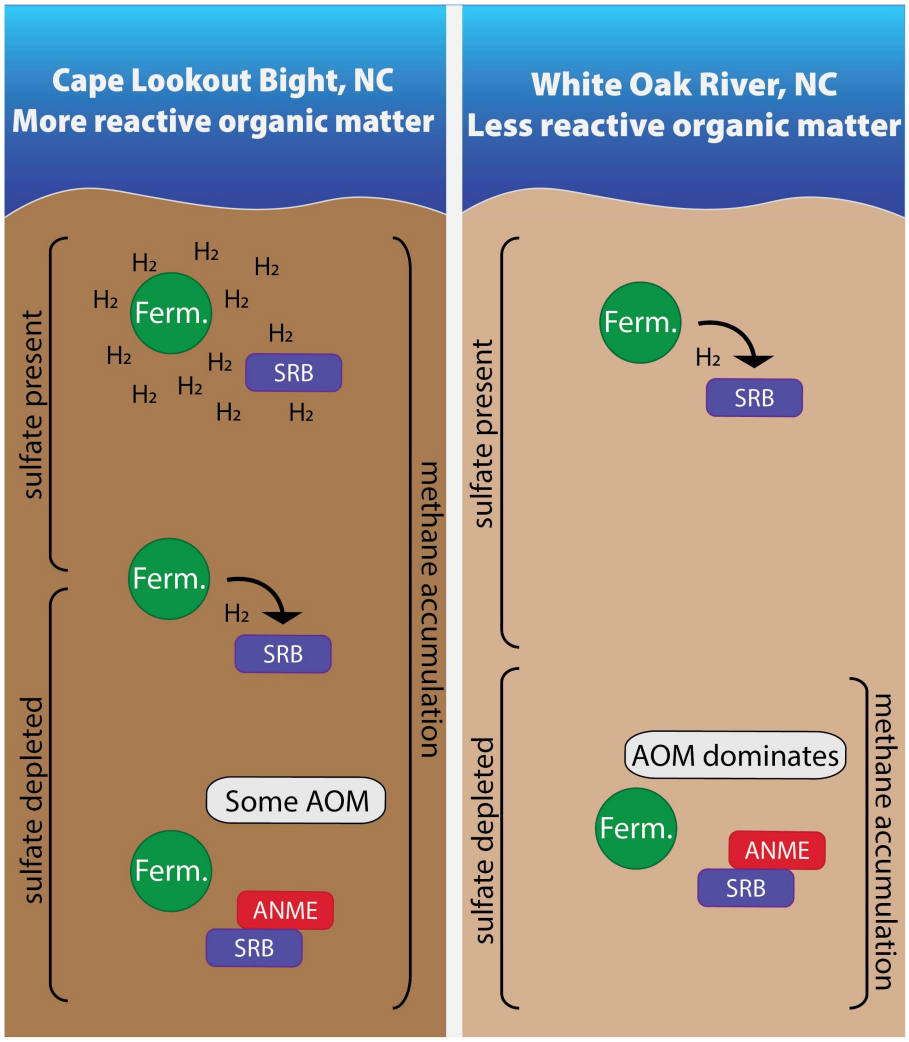

FIGURE 7
In sites with more reactive organic matter, hydrogen accumulates due to high fermentation rates in shallow areas. As the most labile organic matter is depleted with depth, fermentative microbes and sulfate reducing bacteria energetically rely on one another. Once sulfate is depleted, some AOM occurs in these sites with more reactive organic matter while AOM dominates in the site with less reactive organic matter. Areas are not to scale.

DL acknowledges financial support from the NASA Habitable Worlds program under grant 80NSSC20K0228, the NASA Exobiology program under grant NNH22ZDA001N, and the University of Southern California. This is UMCES contribution # 6397.

Acknowledgments

We thank Zachary W. Hudspeth, John Baldridge, Kami Kalhor, Fumnanya Abuah, Joy Buongiorno, and Lovell Smith for help collecting sediment samples, Niels Lindquist for the use of his lab space at UNC Institute for Marine Sciences, Frank Löffler for the use of his ion and gas chromatographs, Maureen Strauss for her help with DIC and carbon isotope ratios, and Marc Alperin for his help with ΔG calculations.

Conflict of interest

The authors declare that the research was conducted in the absence of any commercial or financial relationships that could be construed as a potential conflict of interest.

The author(s) declared that they were an editorial board member of Frontiers, at the time of submission. This had no impact on the peer review process and the final decision.

Publisher's note

All claims expressed in this article are solely those of the authors and do not necessarily represent those of their affiliated organizations, or those of the publisher, the editors and the reviewers. Any product that may be evaluated in this article, or claim that may be made by its manufacturer, is not guaranteed or endorsed by the publisher.

Supplementary material

The Supplementary material for this article can be found online at: https://www.frontiersin.org/articles/10.3389/fmicb.2024.1455857/full#supplementary-material

References

Amend, J. P., and LaRowe, D. E. (2019). Minireview: demystifying microbial reaction energetics. *Environ. Microbiol.* 21, 3539–3547. doi: 10.1111/1462-2920.14778

Bates, K. H., Jacob, D. J., Wang, S., Hornbrook, R. S., Apel, E. C., Kim, M. J., et al. (2021). The global budget of atmospheric methanol: new constraints on secondary, oceanic, and terrestrial sources. *J. Geophys. Res. Atmos.* 126:e2020JD033439. doi: 10.1029/2020JD033439

Beal, E. J., House, C. H., and Orphan, V. J. (2009). Manganese- and iron-dependent marine methane oxidation. *Science* 325, 184–187. doi: 10.1126/science.1169984

Benninger, L. K., and Martens, C. S. (1983). *Sources and fates of sedimentary organic matter in the White Oak and Neuse River Estuaries.* Water Resources Research Institute of the University of North Carolina.

Bradley, J. A., Arndt, S., Amend, J. P., Burwicz, E., Dale, A. W., Egger, M., et al. (2020). Widespread energy limitation to life in global subseafloor sediments. *Sci. Adv.* 6:eaba0697. doi: 10.1126/sciadv.aba0697

Bradley, J. A., Arndt, S., Amend, J. P., Burwicz-Galerne, E., and LaRowe, D. E. (2022). Sources and fluxes of organic carbon and energy to microorganisms in global marine sediments. *Front. Microbiol.* 13:910694. doi: 10.3389/fmicb.2022.910694

Callahan, B. J., McMurdie, P. J., Rosen, M. J., Han, A. W., Johnson, A. J. A., and Holmes, S. P. (2016). DADA2: high-resolution sample inference from Illumina amplicon data. *Nat. Methods* 13, 581–583. doi: 10.1038/nmeth.3869

Cline, J. (1969). Spectrophotometric determination of hydrogen sulfide in natural waters. *Limnol. Oceanogr.* 14, 454–458. doi: 10.4319/lo.1969.14.3.0454

Coon, G. R., Duesing, P. D., Paul, R., Baily, J. A., and Lloyd, K. G. (2023). Biological methane production and accumulation under sulfate-rich conditions at Cape Lookout bight, NC. *Front. Microbiol.* 14:1268361. doi: 10.3389/fmicb.2023.1268361

Crozier, T. E., and Yamamoto, S. (1974). Solubility of hydrogen in water, sea water, and sodium chloride solutions. *J. Chem. Eng. Data* 19, 242–244. doi: 10.1021/je60062a007

Dick, J. M. (2019). CHNOSZ: thermodynamic calculations and diagrams for geochemistry. *Front. Earth Sci.* 7:180. doi: 10.3389/feart.2019.00180

Etheridge, D. M., Steele, L. P., Francey, R. J., and Langenfelds, R. L. (1998). Atmospheric methane between 1000 A.D. and present: evidence of anthropogenic emissions and climatic variability. *J. Geophys. Res. Atmos.* 103, 15979–15993. doi: 10.1029/98JD00923

Haroon, M. F., Hu, S., Shi, Y., Imelfort, M., Keller, J., Hugenholtz, P., et al. (2013). Anaerobic oxidation of methane coupled to nitrate reduction in a novel archaeal lineage. *Nature* 500, 567–570. doi: 10.1038/nature12375

Helgeson, H. C. (1969). Thermodynamics of hydrothermal systems at elevated temperatures and pressures. *Am. J. Sci.* 267, 729–804. doi: 10.2475/ajs.267.7.729

Hoehler, T. M. (2004). Biological energy requirements as quantitative boundary conditions for life in the subsurface. *Geobiology* 2, 205–215. doi: 10.1111/j.1472-4677.2004.00033.x

Hoehler, T. M., and Alperin, M. J. (1996). "Anaerobic methane oxidation by a methanogen-sulfate reducer consortium: geochemical evidence and biochemical considerations" in Microbial growth on C1 compounds: Proceedings of the 8th international symposium on microbial growth on C1 compounds, held in San Diego, U.S.A., 27 August – 1 September 1995. eds. M. E. Lidstrom and F. R. Tabita (Netherlands: Springer Netherlands), 326–333.

Hoehler, T. M., Alperin, M. J., Albert, D. B., and Martens, C. S. (1998). Thermodynamic control on hydrogen concentrations in anoxic sediments. *Geochim. Cosmochim. Acta* 62, 1745–1756. doi: 10.1016/S0016-7037(98)00106-9

Hoehler, T. M., Alperin, M. J., Albert, D. B., and Martens, C. S. (2001). Apparent minimum free energy requirements for methanogenic Archaea and sulfate-reducing bacteria in an anoxic marine sediment. *FEMS Microbiol. Ecol.* 38, 33–41. doi: 10.1111/j.1574-6941.2001.tb00879.x

Hoehler, T. M., Alperin, M. J., Albert, D. B., and Martins, C. S. (1994). Field and laboratory studies of methane oxidation in an anoxic marine sediment: evidence for a methanogen-sulfate reducer consortium. *Glob. Biogeochem. Cycles* 8, 451–463. doi: 10.1029/94GB01800

Hoehler, T. M., and Jørgensen, B. B. (2013). Microbial life under extreme energy limitation. *Nat. Rev. Microbiol.* 11, 83–94. doi: 10.1038/nrmicro2939

Jackson, B. E., and McInerney, M. J. (2002). Anaerobic microbial metabolism can proceed close to thermodynamic limits. *Nature* 415:6870. doi: 10.1038/415454a

Kelley, C. A., Martens, C. S., and Chanton, J. P. (1990). Variations in sedimentary carbon remineralization rates in the white oak. *Limnol. Oceanogr.* 35, 372–383. doi: 10.4319/lo.1990.35.2.0372

Kevorkian, R. T., Callahan, S., Winstead, R., and Lloyd, K. G. (2021). ANME-1 archaea may drive methane accumulation and removal in estuarine sediments. *Environ. Microbiol. Rep.* 13, 185–194. doi: 10.1111/1758-2229.12926

Kevorkian, R. T., Sipes, K., Winstead, R., Paul, R., and Lloyd, K. G. (2022). Cryptic methane-cycling by methanogens during multi-year incubation of estuarine sediment. *Front. Microbiol.* 13:847563. doi: 10.3389/fmicb.2022.847563

Knittel, K., and Boetius, A. (2009). Anaerobic oxidation of methane: progress with an unknown process. *Ann. Rev. Microbiol.* 63, 311–334. doi: 10.1146/annurev.micro.61.080706.093130

LaRowe, D. E., and Amend, J. P. (2015a). Catabolic rates, population sizes and doubling/replacement times of microorganisms in natural settings. *Am. J. Sci.* 315, 167–203. doi: 10.2475/03.2015.01

LaRowe, D. E., and Amend, J. P. (2015b). Power limits for microbial life. *Front. Microbiol.* 6:718. doi: 10.3389/fmicb.2015.00718

LaRowe, D. E., and Amend, J. P. (2020). "Energy limits for life in the subsurface" in Whole earth carbon: past to present. eds. B. N. Orcutt, I. Daniel and R. Dasgupta (Cambridge: Cambridge University Press), 585–619.

LaRowe, D. E., Arndt, S., Bradley, J. A., Burwicz, E., Dale, A. W., and Amend, J. P. (2020a). Organic carbon and microbial activity in marine sediments on a global scale throughout the quaternary. *Geochim. Cosmochim. Acta* 286, 227–247. doi: 10.1016/j.gca.2020.07.017

LaRowe, D. E., Arndt, S., Bradley, J. A., Estes, E. R., Hoarfrost, A., Lang, S. Q., et al. (2020b). The fate of organic carbon in marine sediments—new insights from recent data and analysis. *Earth Sci. Rev.* 204:103146. doi: 10.1016/j.earscirev.2020.103146

LaRowe, D. E., Dale, A. W., Amend, J. P., and Van Cappellen, P. (2012). Thermodynamic limitations on microbially catalyzed reaction rates. *Geochim. Cosmochim. Acta* 90, 96–109. doi: 10.1016/j.gca.2012.05.011

Larowe, D. E., and Helgeson, H. C. (2007). Quantifying the energetics of metabolic reactions in diverse biogeochemical systems: electron flow and ATP synthesis. *Geobiology* 5, 153–168. doi: 10.1111/j.1472-4669.2007.00099.x

LaRowe, D. E., and Van Cappellen, P. (2011). Degradation of natural organic matter: a thermodynamic analysis. *Geochim. Cosmochim. Acta* 75, 2030–2042. doi: 10.1016/j.gca.2011.01.020

Lin, Y.-S., Heuer, V. B., Goldhammer, T., Kellermann, M. Y., Zabel, M., and Hinrichs, K.-U. (2012). Towards constraining H2 concentration in subseafloor sediment: a proposal for combined analysis by two distinct approaches. *Geochim. Cosmochim. Acta* 77, 186–201. doi: 10.1016/j.gca.2011.11.008

Liu, Y., and Whitman, W. B. (2008). Metabolic, phylogenetic, and ecological diversity of the methanogenic archaea. *Ann. N. Y. Acad. Sci.* 1125, 171–189. doi: 10.1196/annals.1419.019

Lloyd, K. G., Alperin, M. J., and Teske, A. (2011). Environmental evidence for net methane production and oxidation in putative ANaerobic MEthanotrophic (ANME) archaea. *Environ. Microbiol.* 13, 2548–2564. doi: 10.1111/j.1462-2920.2011.02526.x

Lloyd, K. G., Bird, J. T., Buongiorno, J., Deas, E., Kevorkian, R., Noordhoek, T., et al. (2020). Evidence for a growth zone for deep-subsurface microbial clades in near-surface anoxic sediments. *Appl. Environ. Microbiol.* 86:e00877-20. doi: 10.1128/AEM.00877-20

Lloyd, K. G., MacGregor, B. J., and Teske, A. (2010). Quantitative PCR methods for RNA and DNA in marine sediments: maximizing yield while overcoming inhibition. *FEMS Microbiol. Ecol.* 72, 143–151. doi: 10.1111/j.1574-6941.2009.00827.x

Lovley, D. R. (1985). Minimum threshold for hydrogen metabolism in methanogenic bacteria. *Appl. Environ. Microbiol.* 49, 1530–1531. doi: 10.1128/aem.49.6.1530-1531.1985

Lovley, D. R., Dwyer, D. F., and Klug, M. J. (1982). Kinetic analysis of competition between sulfate reducers and methanogens for hydrogen in sediments. *Appl. Environ. Microbiol.* 43, 1373–1379. doi: 10.1128/aem.43.6.1373-1379.1982

Malowany, K., Stix, J., Van Pelt, A., and Lucic, G. (2015). H_2S interference on CO_2 isotopic measurements using a Picarro G1101-i cavity ring-down spectrometer. *Atmos. Meas. Tech.* 8, 4075–4082. doi: 10.5194/amt-8-4075-2015

Martens, C. S., Albert, D. B., and Alperin, M. J. (1998). "Biogeochemical processes controlling methane in gassy coastal sediments-part 1. A model coupling organic matter flux to gas production, oxidation and transport" in Continental shelf research, vol. 18, 1741–1770.

Martens, C. S., and Goldhaber, M. B. (1978). Early diagenesis in transitional sedimentary environments of the white Oak River estuary, North Carolina 1. *Limnol. Oceanogr.* 23, 428–441. doi: 10.4319/lo.1978.23.3.0428

Martens, C. S., and Klump, J. V. (1984). Biogeochemical cycling in an organic-rich coastal marine basin 4. An organic carbon budget for sediments dominated by sulfate reduction and methanogenesis. *Geochimica et Cosmochimica Acta* 48, 1987–2004. doi: 10.1016/0016-7037(84)90380-6

Mayer, F., and Müller, V. (2014). Adaptations of anaerobic archaea to life under extreme energy limitation. *FEMS Microbiol. Rev.* 38, 449–472. doi: 10.1111/1574-6976.12043

McMurdie, P. J., and Holmes, S. (2013). Phyloseq: an R package for reproducible interactive analysis and graphics of microbiome census data. *PLoS One* 8:e61217. doi: 10.1371/journal.pone.0061217

Mincer, T. J., and Aicher, A. C. (2016). Methanol production by a broad phylogenetic array of marine phytoplankton. *PLoS One* 11:e0150820. doi: 10.1371/journal.pone.0150820

Morris, B. E. L., Henneberger, R., Huber, H., and Moissl-Eichinger, C. (2013). Microbial syntrophy: interaction for the common good. *FEMS Microbiol. Rev.* 37, 384–406. doi: 10.1111/1574-6976.12019

Müller, V., and Hess, V. (2017). The minimum biological energy quantum. *Front. Microbiol.* 8:2019. doi: 10.3389/fmicb.2017.02019

Muyzer, G., and Stams, A. J. M. (2008). The ecology and biotechnology of sulphate-reducing bacteria. *Nat. Rev. Microbiol.* 6:Article 6. doi: 10.1038/nrmicro1892

Pohlman, J. W., Riedel, M., Bauer, J. E., Canuel, E. A., Paull, C. K., Lapham, L., et al. (2013). Anaerobic methane oxidation in low-organic content methane seep sediments. *Geochim. Cosmochim. Acta* 108, 184–201. doi: 10.1016/j.gca.2013.01.022

Quast, C., Pruesse, E., Yilmaz, P., Gerken, J., Schweer, T., Yarza, P., et al. (2013). The SILVA ribosomal RNA gene database project: improved data processing and web-based tools. *Nucleic Acids Res.* 41, D590–D596. doi: 10.1093/nar/gks1219

R Core Team (2021). R: A language and environment for statistical computing. Vienna, Austria: R Foundation for Statistical Computing.

Reeburgh, W. S. (2007). Oceanic methane biogeochemistry. *Chem. Rev.* 107, 486–513. doi: 10.1021/cr050362v

Roy, R. N., Roy, L. N., Vogel, K. M., Porter-Moore, C., Pearson, T., Good, C. E., et al. (1993). The dissociation constants of carbonic acid in seawater at salinities 5 to 45 and temperatures 0 to 45°C. *Mar. Chem.* 44, 249–267. doi: 10.1016/0304-4203(93)90207-5

RStudio Team (2020). RStudio: Integrated Development for R. RStudio, PBC. Available at: http://www.rstudio.com/

Santegoeds, C. M., Damgaard, L. R., Hesselink, G., Zopfi, J., Lens, P., Muyzer, G., et al. (1999). Distribution of sulfate-reducing and methanogenic bacteria in anaerobic aggregates determined by microsensor and molecular analyses. *Appl. Environ. Microbiol.* 65, 4618–4629. doi: 10.1128/AEM.65.10.4618-4629.1999

Schink, B. (1990). Conservation of small amounts of energy in fermenting bacteria. *Biotechnol. Focus* 2, 63–89.

Schink, B. (1997). Energetics of syntrophic cooperation in methanogenic degradation. *Microbiol Mol Biol Rev* 61, 262–280. doi: 10.1128/mmbr.61.2.262-280.1997

Schink, B. (2002). Synergistic interactions in the microbial world. *Antonie Van Leeuwenhoek* 81, 257–261. doi: 10.1023/A:1020579004534

Schink, B., and Stams, A. J. M. (2006). Syntrophism among prokaryotes. Available at: http://kops.uni-konstanz.de/handle/123456789/7281

Schink, B., and Thauer, R. K. (1988). Energetics of syntrophic methane formation and the influence of aggregation. *Granular Anaerobic Sludge*, 5–17. Available at: https://edepot.wur.nl/318089

Sheik, C. S., Reese, B. K., Twing, K. I., Sylvan, J. B., Grim, S. L., Schrenk, M. O., et al. (2018). Identification and removal of contaminant sequences from ribosomal gene databases: lessons from the census of deep life. *Front. Microbiol.* 9:840. doi: 10.3389/fmicb.2018.00840

Shock, E. L., Oelkers, E. H., Johnson, J. W., Sverjensky, D. A., and Helgeson, H. C. (1992). Calculation of the thermodynamic properties of aqueous species at high pressures and temperatures. Effective electrostatic radii, dissociation constants and standard partial molal properties to 1000°C and 5 kbar. *J. Chem. Soc. Faraday Trans.* 88, 803–826. doi: 10.1039/FT9928800803

Steen, A. D. (2016). Dataset: porewater geochemistry (sulfate, methane, and DIC) from sediments of the White Oak River (WOR), NC, Station H in 2013 (SEDpep project) | BCO-DMO. Available at: https://www.bco-dmo.org/dataset/640333

Tanger, J. C., and Helgeson, H. C. (1988). Calculation of the thermodynamic and transport properties of aqueous species at high pressures and temperatures; revised equations of state for the standard partial molal properties of ions and electrolytes. *Am. J. Sci.* 288, 19–98. doi: 10.2475/ajs.288.1.19

Tijhuis, L., Van Loosdrecht, M. C. M., and Heijnen, J. J. (1993). A thermodynamically based correlation for maintenance gibbs energy requirements in aerobic and anaerobic chemotrophic growth. *Biotechnol. Bioeng.* 42, 509–519. doi: 10.1002/bit.260420415

Timmers, P. H. A., Gieteling, J., Widjaja-Greefkes, H. C. A., Plugge, C. M., Stams, A. J. M., Lens, P. N. L., et al. (2015). Growth of anaerobic methane-oxidizing Archaea and sulfate-reducing Bacteria in a high-pressure membrane capsule bioreactor. *Appl. Environ. Microbiol.* 81, 1286–1296. doi: 10.1128/AEM.03255-14

Timmers, P. H. A., Welte, C. U., Koehorst, J. J., Plugge, C. M., Jetten, M. S. M., and Stams, A. J. M. (2017). Reverse Methanogenesis and respiration in Methanotrophic Archaea. *Archaea* 2017:e1654237. doi: 10.1155/2017/1654237

US Department of Commerce, N (2023). Global monitoring laboratory—carbon cycle greenhouse gases. Available at: https://gml.noaa.gov/ccgg/trends_ch4/

Weiss, R. F. (1974). Carbon dioxide in water and seawater: the solubility of a non-ideal gas. *Mar. Chem.* 2, 203–215. doi: 10.1016/0304-4203(74)90015-2

Wickham, H. (2016). ggplot2: elegant graphics for data analysis. New York: Springer-Verlag.

Yang, T., Jiang, S.-Y., Yang, J.-H., Lu, G., Wu, N.-Y., Liu, J., et al. (2008). Dissolved inorganic carbon (DIC) and its carbon isotopic composition in sediment pore waters from the Shenhu area, northern South China Sea. *J. Oceanogr.* 64, 303–310. doi: 10.1007/s10872-008-0024-2

Yilmaz, P., Parfrey, L. W., Yarza, P., Gerken, J., Pruesse, E., Quast, C., et al. (2014). The SILVA and "all-species living tree project (LTP)" taxonomic frameworks. *Nucleic Acids Res.* 42, D643–D648. doi: 10.1093/nar/gkt1209

Yoshinaga, M. Y., Holler, T., Goldhammer, T., Wegener, G., Pohlman, J. W., Brunner, B., et al. (2014). Carbon isotope equilibration during sulphate-limited anaerobic oxidation of methane. *Nat. Geosci.* 7, 190–194. doi: 10.1038/ngeo2069

Zhang, Z., Zhang, C., Yang, Y., Zhang, Z., Tang, Y., Su, P., et al. (2022). A review of sulfate-reducing bacteria: metabolism, influencing factors and application in wastewater treatment. *J. Clean. Prod.* 376:134109. doi: 10.1016/j.jclepro.2022.134109

Zhao, R., Mogollón, J. M., Roerdink, D. L., Thorseth, I. H., Økland, I., and Jørgensen, S. L. (2021). Ammonia-oxidizing archaea have similar power requirements in diverse marine oxic sediments. *ISME J.* 15, 3657–3667. doi: 10.1038/s41396-021-01041-6

frontiers | Frontiers in Microbiology

TYPE Mini Review
PUBLISHED 27 November 2024
DOI 10.3389/fmicb.2024.1495895

OPEN ACCESS

EDITED BY
Mark Alexander Lever,
The University of Texas at Austin,
United States

REVIEWED BY
Michael Hügler,
Technologiezentrum Wasser, Germany

*CORRESPONDENCE
Alberto Robador
✉ robadora@usc.edu

RECEIVED 13 September 2024
ACCEPTED 13 November 2024
PUBLISHED 27 November 2024

CITATION
Robador A (2024) The subseafloor crustal biosphere: Ocean's hidden biogeochemical reactor.
Front. Microbiol. 15:1495895.
doi: 10.3389/fmicb.2024.1495895

The subseafloor crustal biosphere: Ocean's hidden biogeochemical reactor

Alberto Robador*

Department of Biological Sciences, University of Southern California, Los Angeles, CA, United States

Underlying the thick sediment layer in ocean basins, the flow of seawater through the cracked and porous upper igneous crust supports a previously hidden and largely unexplored active subsurface microbial biome. Subseafloor crustal systems offer an enlarged surface area for microbial habitats and prolonged cell residence times, promoting the evolution of novel microbial lineages in the presence of steep physical and thermochemical gradients. The substantial metabolic potential and dispersal capabilities of microbial communities within these systems underscore their crucial role in biogeochemical cycling. However, the intricate interplay between fluid chemistry, temperature variations, and microbial activity remains poorly understood. These complexities introduce significant challenges in unraveling the factors that regulate microbial distribution and function within these dynamic ecosystems. Using synthesized data from previous studies, this work describes how the ocean crustal biosphere functions as a continuous-flow biogechemical reactor. It simultaneously promotes the breakdown of surface-derived organic carbon and the creation of new, chemosynthetic material, thereby enhancing element recycling and ocean carbon productivity. Insights gained from the qualitative analysis of the extent of biogeochemical microbial activity and diversity across the temperature and chemical gradients that characterize these habitats, as reviewed herein, challenge traditional models of global ocean carbon productivity and provide the development of a new conceptual framework for understanding the quantitative metabolic potential and broad dispersal of the crustal microbial biome.

KEYWORDS

subseafloor biosphere, crustal microbiology, biogeochemical cycling, hydrothermal circulation, carbon productivity

Introduction

The biogeochemical role of microbes deeply buried beneath the seafloor is far more important than presumed possible 80 years ago (Zobell and Anderson, 1936; Zobell, 1938). Over the past decades, comprehensive studies of subseafloor sedimentary microbes have revealed not only cell abundances that match previous estimates in seawater and in surface sediments (Kallmeyer et al., 2012) but most importantly, have demonstrated the viability of these microbes (Morono et al., 2011; Trembath-Reichert et al., 2017; Imachi et al., 2019) and their essential role in operating and maintaining global biogeochemical cycles (Parkes et al., 2014). We now understand that beneath the sediment layer, fluids moving through the basaltic ocean crust hold a similar amount of organic carbon, stored within living prokaryotic biomass (~1.6 Gt C, Bar-On et al., 2018). The volume of the ocean crust biosphere represents nearly 2% of the volume of the oceans (Johnson and Pruis, 2003). Conditions along the active fluid flow paths that characterize this habitat indicate that the crustal biosphere is the most favorable of deep-subsurface habitats and is likely a very active site of element cycling (Johnson et al., 2006). Furthermore, this aquifer is hydrothermally active and interactions with the overlaying

sediments and ocean seawater facilitate the free exchange of fluid, chemicals, biological material, and heat, which likely have a large impact on the variability of seawater chemical composition and global biogeochemical cycling (Edwards et al., 2011).

The upper crustal reservoir as a sub-surface microbial biosphere

Basaltic ocean crust is formed at the axis of spreading mid-ocean ridges (MORs, Figure 1). As new ocean floor is formed and moves away from the spreading center, it is cooled by the interaction with seawater. Aging crustal porewaters remain generally isolated within buried upper oceanic basement, subjected to increasing temperatures as plates move away from spreading ridges. The accumulation of overlaying sediments on the MOR flanks and ocean basins prevents continued advective heat loss and results in strong hydrothermal gradients, which drive the rapid—on the order of m/day (Neira et al., 2016)—and largely lateral flow of low temperature (~5–65°C) fluids. Local circulation patterns are largely controlled by differences in pressure between cool (recharging) bottom seawater and warm (discharging) crustal fluids occurring at permeable igneous outcrops that penetrate the thick sediment cover (Winslow and Fisher, 2015; Winslow et al., 2016; Lauer et al., 2018). In contrast to the diffusion-dominated overlying sediments, the advective flow of hydrothermal fluids within the basaltic crust provides a pathway for the fast transport of solutes and particles including microbial cells, carbon and nutrients and generates small-scale variability in conditions supporting crustal biomes (Edwards et al., 2012a). The microbial biosphere, presumably located within the uppermost part of the igneous crust (Heberling et al., 2010), has likely been present since microbes first inhabited the oceanic crust around 3.5 billion years ago (Furnes et al., 2004). Quantitative knowledge of the extent of its metabolic potential and contribution to active global biogeochemical cycling, however, remains largely speculative (Orcutt et al., 2011b), as direct access to uncontaminated fluids in old ocean crust remains a major challenge.

Access "windows" to crustal biosphere

The active circulation of hydrothermal fluids between open surfaces of the reservoir and overlying seawater provides multiple access "windows" to the subseafloor biosphere and, therefore, the opportunity to obtain high integrity samples from this challenging environment (Figure 1, #1–4). Most studies of subseafloor crustal microbiology (Figure 1, #1) have focused on MOR spreading areas, i.e., hydrothermal vents (Thorseth et al., 2001; Edwards et al., 2003;

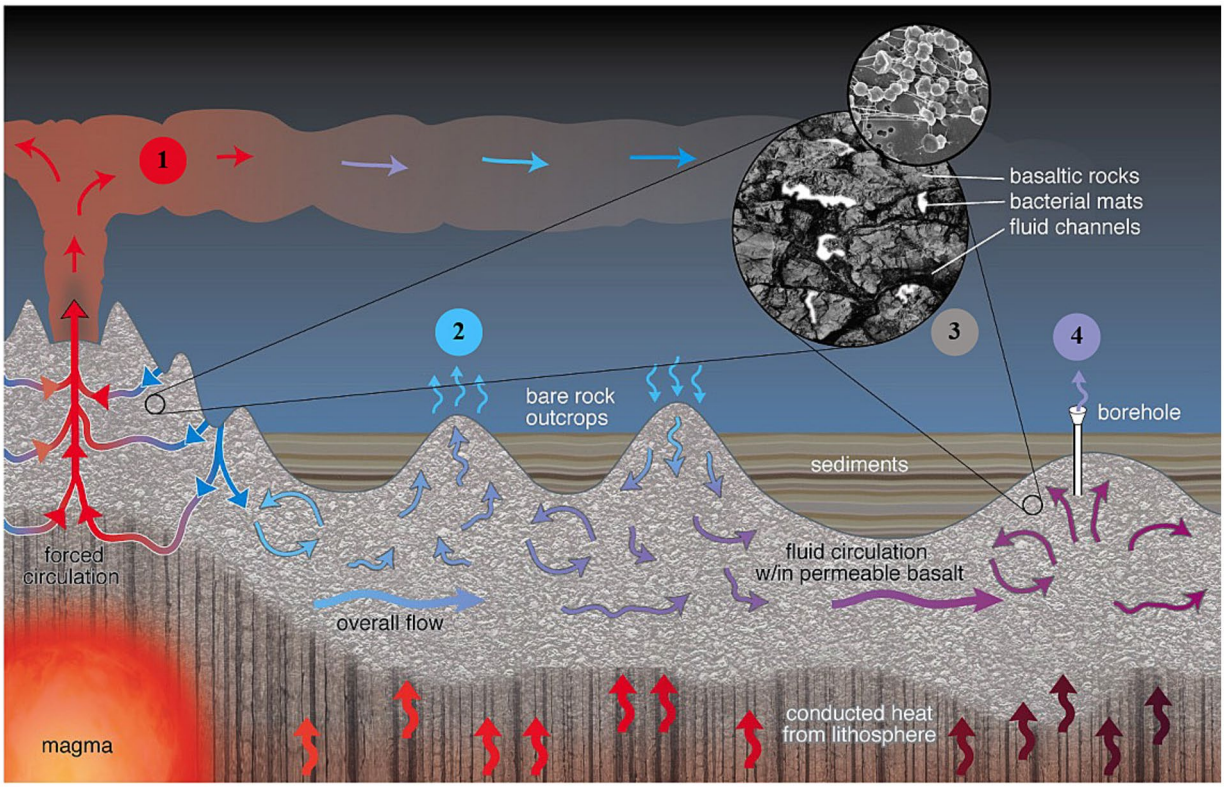

FIGURE 1
Several key access "windows" provide entry points to the crustal biosphere: ❶ Hydrothermal vents at mid-ocean ridges (MORs), featuring both diffuse and focused high-temperature flows (up to ~400°C) and event plumes associated with seafloor eruptions; ❷ Warm water seeps (<150°C) found at exposed rocky discharge zones on seamounts; ❸ Borehole cores extracted from sediment and basement rock layers; and ❹ Borehole CORK (Circulation Obviation Retrofit Kit) observatories, installed in boreholes, which offer the most precise control over sample placement, depth, and quality. These observatories provide unparalleled access to discrete depths in deep basement environments, enabling *in situ* sampling and experimentation with the highest degree of accuracy.

Lysnes et al., 2004), event plumes associated with seafloor eruptions (Meyer et al., 2013), and other settings where volcanism occurs (Fisk et al., 2003; Santelli et al., 2008). Active subseafloor microbial communities in venting fluids from MOR spreading axes are indicative of their local geologic setting and resultant geochemistry (Trembath-Reichert et al., 2019). These communities, however, do not reflect conditions in other crustal environments. The high-temperature focused fluid flows that characterized these MOR field sites tap the deepest and hottest (400°C) sub-crustal zone and can be considered end members with respect to the range of conditions that determine the nature of subseafloor crustal biomes (Elderfield et al., 1999). Most of the upper oceanic crust remains relatively cool, with temperatures below 150°C (Mottl and Wheat, 1994). Additionally, MOR flanks contribute more substantially to the global output of the upper crustal reservoir compared to the hotter axial regions, which play a comparatively minor role (Mottl, 2003). Recent research supports this disparity, showing that while axial zones release high-temperature fluids from hydrothermal activity near magma chambers, the ridge flanks exhibit a significantly greater overall heat flux through widespread low-temperature hydrothermal circulation (Urabe et al., 2015).

Exposed rocky discharge seamounts along MOR flanks in the other hand, are characterized by warm (<150°C) diffuse water seeps (Wheat et al., 2017) and offer an alternative access to the near surface basement biosphere (Figure 1, #2). Important surveys in exiting fluids of both heat and chemical fluxes as well as microbial communities have shown a high diversity of microorganisms in a continuum of near seafloor to deep subsurface biosphere communities (Hara et al., 2005; Huber et al., 2006; Lee et al., 2015). However, due in part to their generally diffuse flow there is a high mixing rate with overlying sediments (Meyers et al., 2014; Zinke et al., 2018) and, consequently, these sites have been studied to relatively limited extent.

At present, drilling represents the only access into the upper crustal reservoir for older, heavily sedimented crust (Figure 1, #3). Reports on the phylogenetic distribution of microbial communities within drilled marine basalts have revealed a cosmopolitan community with many members but vastly different from that in crustal fluids (Mason et al., 2007, 2009, 2010; Lever et al., 2013; Goordial et al., 2021). The extraction of borehole rock cores has no control over the placement, depth and quality of the samples (Lever, 2013), which leaves open the possibility of seawater or sediment contamination.

The best opportunities for co-located and simultaneous microbiological in situ sampling and experimentation have been provided by Borehole Circulation Obviation Retrofit Kit (CORK) observatories installed at Ocean Drilling Program (ODP/IODP) boreholes (e.g. Edwards et al., 2014; Fisher et al., 2005; Fisher et al., 2011) (Figure 1, #4). CORK's critical attributes include the ability to penetrate through sediments into basement and isolate different horizons within the borehole, e.g., depth, degree of fracturing and differential flow rates. CORK observatories allow permanent access to samples through individual CORK installations as well as arrays of CORKs. Furthermore, *in situ* sampling and experimentation is possible using both downhole and seafloor fluid sampling systems. In downhole applications, flow-through osmotic pumping systems (FLOCS) represent an important technological advancement, providing a reliable fluid sampling solution. FLOCS are powerful steadfast osmotic pumps operating without any moving parts or electronics by bringing a reservoir of super-saturated salt solution to equilibrium (Orcutt et al., 2010; Edwards et al., 2012b). They are highly versatile and provide the pumping power to collect samples in manipulative experiments, such as colonization chambers that integrate various relevant mineral and control surfaces into the in-line flow path of the osmo-samplers (Orcutt et al., 2011a). On the other hand, technological advancements on seafloor applications, such as the GeoMICROBE sled (Cowen et al., 2012), represent significant progress in the ability to conduct long-term monitoring and in-depth analysis of microbial and chemical processes deep beneath the ocean floor. This innovative autonomous sensor and accompanying fluid sampling systems were designed to extract large volumes of fluid from crustal aquifers for surface analysis, highlighting a leap forward in crustal research capabilities (Lin et al., 2020). This article emphasizes investigations into the microbial community in the crustal subseafloor using borehole CORK observatories because they have yielded the most extensive knowledge on the crustal microbial biosphere (Orcutt et al., 2020) and stablished the foundation for present studies on the microbial community's metabolic potential and role in global biogeochemical cycles.

Emerging crustal microbiology

Microbial communities in crustal fluids exhibit spatial heterogeneity (Jungbluth et al., 2013) and inter-annual variability (Jungbluth et al., 2014) reflecting the dynamic and diverse environments that characterize the hydrogeological active upper igneous crust. Shared distinct microbial lineages, however, are consistent with the inferred hydrogeologic connectivity of these systems and the idea of permanent residency in the crustal subseafloor (Jungbluth et al., 2016). When analyzing datasets from different crustal habitats, the nature of the crustal environment (distinguished by either planktonic communities or mineral-attached communities), the prevailing redox conditions, and the geochemical evolution of these habitats collectively reveal patterns of global biogeographic distribution (Smith et al., 2016; Zhang et al., 2016b; Ramírez et al., 2019; Orcutt et al., 2021). Time-course studies of the genetic makeup and evolutionary trajectories of recovered metagenome-assembled genomes (MAGs) in subsurface crustal fluids (Anderson et al., 2022) have shown rapid allele frequency shifts linked to gene flow and recombination between microbial populations, which are mainly associated with stochastic events such as dispersal and mixing of populations throughout the aquifer. Despite this dynamism, however, temporal and spatial trends reconstructed from MAGs (Tully et al., 2018) have shown a significant amount of functional redundancy in the subseafloor microbial populations, which do not correspond to changes in the composition of the community over time. This implies global microbial functional stability in the ubiquitous crustal subseafloor biosphere.

Driven by geochemical redox gradients created by the continued interaction of seawater with the basaltic rock at different spatial and temporal scales, microbes in these crustal environments have developed physiological and metabolic strategies to exploit the specific conditions of their environment. In young, oxic, and low-temperature crustal environments –key to most global hydrothermal fluid circulation in the ocean—the metabolic reconstruction of recovered

MAGs (Tully et al., 2018) has revealed microorganisms representative of heterotrophic and autotrophic lifestyles. These versatile microbes, however, are also poised to exploit hypoxic and anoxic conditions with alternative electron acceptors, i.e., nitrate and sulfate. Furthermore, complementary time-series metatranscriptomic data have confirmed that microbial communities in this environment are populated by motile mixotrophic and organotrophic bacteria active under both oxic and anoxic conditions (Seyler et al., 2021). In old, anoxic, and warm crustal environments –representative of situations that are common in all ocean basins where hydrothermal circulation is isolated from the deep ocean– the MAG of a versatile heterotrophic microbial population has been recovered capable of oxidizing reduced carbon species with nitrate, iron, and sulfur compounds as potential electron acceptors (Boyd et al., 2019). Comparative analysis of single-amplified genomes (SAGs) representative of other persistent lineages also suggests the heterotrophic potential of anaerobic crustal communities to respire organic carbon with sulfate and nitrate (Carr et al., 2019) and other external terminal electron acceptors such as iron and sulfur oxides consistent with the mineralogy of these environments (Booker et al., 2023). Further genomic evidence has also identified MAGs representative of chemosynthetic microbial communities residing in mineral biofilms (Smith et al., 2019). These communities are sustained by water-rock reactions in a process involving the use molecular hydrogen to convert inorganic carbon from seawater into organic matter, with additional energy supplementation derived from amino acids or peptides present in the mineral-attached biofilms (Smith et al., 2021). Altogether, this suggests the presence of highly dynamic microbial communities capable of rapid adaptation to varying redox conditions within the basaltic crustal fluids. Moreover, the transcription of genes related to biofilm formation and motility suggests an adaptation for spatial relocation in response to environmental shifts, crucial for accessing diverse nutrient and energy sources.

The subseafloor crustal system as a continuous-flow biogeochemical reactor

The biogeochemical state of the subseafloor crustal reservoir is influenced by several factors. The age of the crust affects the geochemical extent of water-rock interaction, while the thermal state of the aquifer determines the nature and scale of metabolic reactions that can occur. Fluids along the flow paths of the hydrogeologically active upper oceanic crust exhibit a geochemical reaction consistent with a decline in the redox potential of oxidants and concentrations of organic material (Lin et al., 2012). By leveraging compositional geochemical data of basement fluids relative to bottom seawater, comprehensive thermodynamic modeling of diverse redox reactions has shown a geochemical shift toward lower free energy availability with increasing residence time and temperature (Robador et al., 2015). Despite this energetic constraint, direct heat measurements indicative of the change in enthalpy associated with total microbial activity have demonstrated the high metabolic potential of microbes to respire under oxic and anoxic conditions (Robador et al., 2016). This is observed in fluids characteristic of both young, oxygenated, and warm, highly reacted end-member areas of the upper oceanic crust, respectively. Furthermore, extensive studies have demonstrated the widespread potential of microbial activity in crustal fluids, with high rates of autotrophy and heterotrophy comparable to those found in surface environments (Meyer et al., 2016; Robador et al., 2016; Zhang et al., 2016a; Trembath-Reichert et al., 2021). These findings suggest that the upper crustal reservoir, functioning as a subsurface microbial biosphere, may be as metabolically active as the overlying ocean.

Additionally, the rate at which fluid flows through the crust influences the replenishment of reactants and the removal of byproducts, thus affecting the concentration of chemical species. During the geochemical evolution of fluids, redox species are removed, further shaping the chemical composition. This geochemical evolution of crustal fluids strongly suggests *in situ* microbial consumption within the basement (Orcutt et al., 2013; Robador et al., 2015). However, sediment pore water data from near sediment-basement interface (Elderfield et al., 1999) indicate that deep sediments must also serve as a sink for basement electron acceptors, which diffuse into the overlaying depleted sediments. This dynamic exchange supplies essential electron acceptors, such as oxygen and sulfate, to deeper sediment layers, which is crucial for sustaining microbial metabolisms within the sediment. Deep sediment porewater profiles demonstrate that oxygen diffuses upward from the underlying basalt and nitrate accumulates in the overlying sediments (Ziebis et al., 2012). This observation strongly implicates the process of nitrification as both an autotrophic sink of porewater oxygen and a source of nitrate, which, in turn, may support heterotrophy via denitrification where oxygen is absent and, potentially, autotrophic growth via methanogenesis. Furthermore, diffusion of sulfate from crustal fluids into overlying sediments, can form a transition zone where sulfate meets *in situ*-produced methane, thereby stimulating microbial heterotrophic respiration, i.e., anaerobic methane oxidation coupled to sulfate reduction (Engelen et al., 2008; Fichtel et al., 2012, 2015). These microbial processes, in turn, accelerate the breakdown of organic carbon deposits. Concurrently, the sediments supply electron donors, including dissolved organic carbon (DOC), to the basement ecosystem. Higher sediment pore water DOC likely diffuses into the basement, making it a sink for both seawater and sediment DOC. This reciprocal exchange results in the alteration of DOC compounds with respect to seawater (LaRowe et al., 2017) and underscores the complex interplay between geochemical processes and microbial life in deep subsurface crustal environments, driving both the degradation and the recycling of organic materials (Shah Walter et al., 2018; Lin et al., 2019). The ocean crustal biosphere, therefore, functions to simultaneously degrade surface-derived organic carbon and to export new, chemosynthetic material (McCarthy et al., 2011; Lin et al., 2015). As such, the ocean crustal biosphere acts as a biogeochemical reactor, facilitating the transformation and transport of elements through various states and locations. By breaking down organic carbon from surface sources and synthesizing new materials through chemosynthesis, it promotes element recycling and enhances ocean carbon productivity. Given that the entire volume of seawater is estimated to cycle through the ocean crust approximately every 100,000 years (Johnson and Pruis, 2003), this continuous-flow biogeochemical reactor plays a crucial role in driving the cycling of key elements, supporting diverse microbial communities, and sustaining essential ecological processes in the ocean. The complex interactions and metabolic activities within the ocean crustal

biosphere underscore its critical role in maintaining the balance of both oceanic and global biogeochemical cycles.

Conclusion

The subseafloor crustal system plays a crucial role in the biogeochemical cycling within mid-ocean ridge flanks by redistributing mass and energy between deep sediments and basement aquifers and back into the ocean. Although quantitative estimates of microbial contributions to global biogeochemical cycles are limited by difficult access and sparse sampling, the widespread metabolic potential of this biosphere suggests that incorporating the crustal system into current global biogeochemical models will be crucial for accurately representing the full ocean carbon cycle. The ocean crustal biosphere plays a dual role, capturing the intricate processes of carbon degradation and synthesis occurring beneath the ocean floor. Recognizing its impact on global biogeochemical cycles will allow for a more comprehensive understanding of carbon mineralization and recycling, enhancing the accuracy of predictions related to ocean productivity and ecological dynamics. Moreover, studying the ocean crustal biosphere has significant implications for astrobiology, as it serves as an analog for potential life on other planetary bodies (Jones et al., 2018). Understanding how microbial life thrives in these extreme conditions on Earth offers valuable insights into the potential for life in similar environments elsewhere in the solar system and beyond. This connection highlights the broader importance of studying these systems, not only to improve our biogeochemical models but also to advance our search for life beyond Earth.

Author contributions

AR: Writing – original draft, Writing – review & editing.

Funding

The author(s) declare that no financial support was received for the research, authorship, and/or publication of this article.

Conflict of interest

The author declares that the research was conducted in the absence of any commercial or financial relationships that could be construed as a potential conflict of interest.

The author(s) declared that they were an editorial board member of Frontiers, at the time of submission. This had no impact on the peer review process and the final decision.

Publisher's note

References

Anderson, R., Graham, E., Huber, J., and Tully, B. (2022). Microbial populations are shaped by dispersal and recombination in a low biomass subseafloor habitat. *MBio* 13:e0035422. doi: 10.1128/mbio.00354-22

Bar-On, Y. M., Phillips, R., and Milo, R. (2018). The biomass distribution on earth. *Proc. Natl. Acad. Sci. USA* 115, 6506–6511. doi: 10.1073/pnas.1711842115

Booker, A. E., D'angelo, T., Adams-Beyea, A., Brown, J. M., Nigro, O., Rappé, M. S., et al. (2023). Life strategies for Aminicenantia in subseafloor oceanic crust. *ISME J.* 17, 1406–1415. doi: 10.1038/s41396-023-01454-5

Boyd, J. A., Jungbluth, S. P., Leu, A. O., Evans, P. N., Woodcroft, B. J., Chadwick, G. L., et al. (2019). Divergent methyl-coenzyme M reductase genes in a deep-subseafloor Archaeoglobi. *ISME J.* 13, 1269–1279. doi: 10.1038/s41396-018-0343-2

Carr, S. A., Jungbluth, S. P., Eloe-Fadrosh, E. A., Stepanauskas, R., Woyke, T., Rappé, M. S., et al. (2019). Carboxydotrophy potential of uncultivated Hydrothermarchaeota from the subseafloor crustal biosphere. *ISME J.* 13, 1457–1468. doi: 10.1038/s41396-019-0352-9

Cowen, J. P., Copson, D. A., Jolly, J., Hsieh, C. C., Lin, H. T., Glazer, B. T., et al. (2012). Advanced instrument system for real-time and time-series microbial geochemical sampling of the deep (basaltic) crustal biosphere. *Deep-Sea Res. I Oceanogr. Res. Pap.* 61, 43–56. doi: 10.1016/j.dsr.2011.11.004

Edwards, K. J., Bach, W., and Rogers, D. R. (2003). Geomicrobiology of the ocean crust: a role for chemoautotrophic Fe-bacteria. *Biol. Bull.* 204, 180–185. doi: 10.2307/1543555

Edwards, K., Fisher, A., and Wheat, C. G. (2012a). The deep subsurface biosphere in igneous ocean crust: frontier habitats for microbiological exploration. *Front. Microbiol.* 3:8. doi: 10.3389/fmicb.2012.00008

Edwards, K.J., Wheat, C.G., Orcutt, B.N., Hulme, S., Becker, K., and Jannasch, H., and Al., E. (2012b). "Design and deployment of borehole observatories and experiments during IODP expedition 336 mid-Atlantic ridge flank at north pond" in *Proc. IODP, 336*. (eds.) K.J. Edwards, W. Bach, A. Klaus & E. Scientists. Integrated Ocean Drilling Program Management International, Inc., Tokyo, Japan.

Edwards, A. T., Bach, T., Klaus, K., and the IODP Expedition 336 Scientific Party. (2014). Mid-Atlantic Ridge microbiology: initiation of long-term coupled microbiological, geochemical, and hydrological experimentation within the seafloor at North Pond, western flank of the Mid-Atlantic Ridge. *IODP Prel. Rept.* 336. doi: 10.2204/iodp.pr.336.2012

Edwards, K. J., Wheat, C. G., and Sylvan, J. B. (2011). Under the sea: microbial life in volcanic oceanic crust. *Nat. Rev. Microbiol.* 9, 703–712. doi: 10.1038/nrmicro2647

Elderfield, H., Wheat, C. G., Mottl, M. J., Monnin, C., and Spiro, B. (1999). Fluid and geochemical transport through oceanic crust: a transect across the eastern flank of the Juan de Fuca ridge. *Earth Planet. Sci. Lett.* 172, 151–165. doi: 10.1016/s0012-821x(99)00191-0

Engelen, B., Ziegelmueller, K., Wolf, L., Kopke, B., Gittel, A., Cypionka, H., et al. (2008). Fluids from the oceanic crust support microbial activities within the deep biosphere. *Geomicrobiol J.* 25, 56–66. doi: 10.1080/01490450701829006

Fichtel, K., Logemann, J., Fichtel, J., Rullkötter, J., Cypionka, H., and Engelen, B. (2015). Temperature and pressure adaptation of a sulfate reducer from the deep subsurface. *Front. Microbiol.* 6:1078. doi: 10.3389/fmicb.2015.01078

Fichtel, K., Mathes, F., Koenneke, M., Cypionka, H., and Engelen, B. (2012). Isolation of sulfate-reducing bacteria from sediments above the deep-subseafloor aquifer. *Front. Microbiol.* 3:65. doi: 10.3389/fmicb.2012.00065

Fisher, A. T., Wheat, C. G., Becker, K., Davis, E. E., Jannasch, H., Schroeder, D., et al. (2005). Scientific and technical design and deployment of long-term, subseafloor observatories for hydrogeologic and related experiments, IODP Expedition 301, eastern flank of Juan de Fuca Ridge. *In* Fisher, A.T., Urabe, T., Klaus, A., and the Expedition 301 Scientists, *Proc. IODP*, 301: College Station TX (Integrated Ocean Drilling Program Management International, Inc.). doi: 10.2204/iodp.proc.301.103.2005

Fisher, A. T., Tsuji, T., Petronotis, K., and the Expedition 327 Scientists. (2011). Site U1362. *Proc. IODP*, 327: Tokyo (Integrated Ocean Drilling Program Management International, Inc.). doi: 10.2204/iodp.proc.327.103.2011

Fisk, M. R., Storrie-Lombardi, M. C., Douglas, S., Popa, R., Mcdonald, G., and Di Meo-Savoie, C. (2003). Evidence of biological activity in Hawaiian subsurface basalts. *Geochem. Geophys. Geosyst.* 4:1103. doi: 10.1029/2002GC000387

Furnes, H., Banerjee, N., Muehlenbachs, K., Staudigel, H., and Wit, M. J. (2004). Early life recorded in Archean pillow lavas. *Science* 304, 578–581. doi: 10.1126/science.1095858

Goordial, J., D'angelo, T., Labonté, J. M., Poulton, N. J., Brown, J. M., Stepanauskas, R., et al. (2021). Microbial diversity and function in shallow subsurface sediment and oceanic lithosphere of the Atlantis massif. *MBio* 12, e0049021–e0000421. doi: 10.1128/mBio.00490-21

Hara, K., Kakegawa, T., Yamashiro, K., Maruyama, A., Ishibashi, J.-I., Marumo, K., et al. (2005). Analysis of the archaeal sub-seafloor community at Suiyo seamount on the Izu-Bonin arc. *Adv. Space Res.* 35, 1634–1642. doi: 10.1016/j.asr.2005.04.111

Heberling, C., Lowell, R. P., Liu, L., and Fisk, M. R. (2010). Extent of the microbial biosphere in the oceanic crust. *Geochem. Geophys. Geosyst.* 11. doi: 10.1029/2009gc002968

Huber, J. A., Johnson, H. P., Butterfield, D. A., and Baross, J. A. (2006). Microbial life in ridge flank crustal fluids. *Environ. Microbiol.* 8, 88–99. doi: 10.1111/j.1462-2920.2005.00872.x

Imachi, H., Tasumi, E., Takaki, Y., Hoshino, T., Schubotz, F., Gan, S. C., et al. (2019). Cultivable microbial community in 2-km-deep, 20-million-year-old subseafloor coalbeds through similar to 1000 days anaerobic bioreactor cultivation. *Sci. Rep.* 9:2305. doi: 10.1038/s41598-019-38754-w

Johnson, H. P., Baross, J. A., and Bjorklund, T. A. (2006). On sampling the upper crustal reservoir of the NE Pacific Ocean. *Geofluids* 6, 251–271. doi: 10.1111/j.1468-8123.2006.00151.x

Johnson, H. P., and Pruis, M. J. (2003). Fluxes of fluid and heat from the oceanic crustal reservoir. *Earth Planet. Sci. Lett.* 216, 565–574. doi: 10.1016/s0012-821x(03)00545-4

Jones, R. M., Goordial, J. M., and Orcutt, B. N. (2018). Low energy subsurface environments as extraterrestrial analogs. *Front. Microbiol.* 9:1605. doi: 10.3389/fmicb.2018.01605

Jungbluth, S. P., Bowers, R. M., Lin, H.-T., Cowen, J. P., and Rappé, M. S. (2016). Novel microbial assemblages inhabiting crustal fluids within mid-ocean ridge flank subsurface basalt. *ISME J.* 10, 2033–2047. doi: 10.1038/ismej.2015.248

Jungbluth, S. P., Grote, J., Lin, H.-T., Cowen, J. P., and Rappe, M. S. (2013). Microbial diversity within basement fluids of the sediment-buried Juan de Fuca ridge flank. *ISME J.* 7, 161–172. doi: 10.1038/ismej.2012.73

Jungbluth, S., Lin, H.-T., Cowen, J., Glazer, B. T., and Rappe, M. (2014). Phylogenetic diversity of microorganisms in subseafloor crustal fluids from boreholes 1025C and 1026B along the Juan de Fuca ridge flank. *Front. Microbiol.* 5:119. doi: 10.3389/fmicb.2014.00119

Kallmeyer, J., Pockalny, R., Adhikari, R. R., Smith, D. C., and D'hondt, S. (2012). Global distribution of microbial abundance and biomass in subseafloor sediment. *Proc. Natl. Acad. Sci. USA* 109, 16213–16216. doi: 10.1073/pnas.1203849109

Larowe, D. E., Koch, B. P., Robador, A., Witt, M., Ksionzek, K., and Amend, J. P. (2017). Identification of organic compounds in ocean basement fluids. *Org. Geochem.* 113, 124–127. doi: 10.1016/j.orggeochem.2017.07.017

Lauer, M. R., Fisher, A., and Winslow, D. M. (2018). Three-dimensional models of hydrothermal circulation through a seamount network on fast-spreading crust. *Earth Planet. Sci. Lett.* 501, 138–151. doi: 10.1016/j.epsl.2018.08.025

Lee, M. D., Walworth, N. G., Sylvan, J. B., Edwards, K. J., and Orcutt, B. N. (2015). Microbial communities on seafloor basalts at dorado outcrop reflect level of alteration and highlight global lithic clades. *Front. Microbiol.* 6:1470. doi: 10.3389/fmicb.2015.01470

Lever, M. A. (2013). Functional gene surveys from ocean drilling expeditions a review and perspective. *FEMS Microbiol. Ecol.* 84, 1–23. doi: 10.1111/1574-6941.12051

Lever, M. A., Rouxel, O., Alt, J. C., Shimizu, N., Ono, S. H., Coggon, R. M., et al. (2013). Evidence for microbial carbon and sulfur cycling in deeply buried ridge flank basalt. *Science* 339, 1305–1308. doi: 10.1126/science.1229240

Lin, H.-T., Amend, J. P., Larowe, D. E., Bingham, J.-P., and Cowen, J. P. (2015). Dissolved amino acids in oceanic basaltic basement fluids. *Geochim. Cosmochim. Acta* 164, 175–190. doi: 10.1016/j.gca.2015.04.044

Lin, H. T., Cowen, J. P., Olson, E. J., Amend, J. P., and Lilley, M. D. (2012). Inorganic chemistry, gas compositions and dissolved organic carbon in fluids from sedimented young basaltic crust on the Juan de Fuca ridge flanks. *Geochim. Cosmochim. Acta* 85, 213–227. doi: 10.1016/j.gca.2012.02.017

Lin, H.-T., Hsieh, C.-C., Repeta, D. J., and Rappé, M. S. (2020). Sampling of basement fluids via circulation obviation retrofit kits (CORKs) for dissolved gases, fluid fixation at the seafloor, and the characterization of organic carbon. *MethodsX* 7:101033. doi: 10.1016/j.mex.2020.101033

Lin, H.-T., Repeta, D. J., Xu, L., and Rappé, M. S. (2019). Dissolved organic carbon in basalt-hosted deep subseafloor fluids of the Juan de Fuca ridge flank. *Earth Planet. Sci. Lett.* 513, 156–165. doi: 10.1016/j.epsl.2019.02.008

Lysnes, K., Thorseth, I. H., Steinsbu, B. O., Ovreas, L., Torsvik, T., and Pedersen, R. B. (2004). Microbial community diversity in seafloor basalt from the Arctic spreading ridges. *FEMS Microbiol. Ecol.* 50, 213–230. doi: 10.1016/j.femsec.2004.06.014

Mason, O. U., Di Meo-Savoie, C. A., Van Nostrand, J. D., Zhou, J. Z., Fisk, M. R., and Giovannoni, S. J. (2009). Prokaryotic diversity, distribution, and insights into their role in biogeochemical cycling in marine basalts. *ISME J.* 3, 231–242. doi: 10.1038/ismej.2008.92

Mason, O. U., Nakagawa, T., Rosner, M., Van Nostrand, J. D., Zhou, J. Z., Maruyama, A., et al. (2010). First investigation of the microbiology of the deepest layer of ocean crust. *PLoS One* 5:e15399. doi: 10.1371/journal.pone.0015399

Mason, O. U., Stingl, U., Wilhelm, L. J., Moeseneder, M. M., Di Meo-Savoie, C. A., Fisk, M. R., et al. (2007). The phylogeny of endolithic microbes associated with marine basalts. *Environ. Microbiol.* 9, 2539–2550. doi: 10.1111/j.1462-2920.2007.01372.x

Mccarthy, M. D., Beaupre, S. R., Walker, B. D., Voparil, I., Guilderson, T. P., and Druffel, E. R. M. (2011). Chemosynthetic origin of C-14-depleted dissolved organic matter in a ridge-flank hydrothermal system. *Nat. Geosci.* 4, 32–36. doi: 10.1038/ngeo1015

Meyer, J. L., Akerman, N. H., Proskurowski, G., and Huber, J. A. (2013). Microbiological characterization of post-eruption "snowblower" vents at axial seamount, Juan de Fuca Ridge. *Front. Microbiol.* 4:153. doi: 10.3389/fmicb.2013.00153

Meyer, J. L., Jaekel, U., Tully, B., Glazer, B. T., Wheat, C. G., Lin, H. T., et al. (2016). A distinct and active bacterial community in cold oxygenated fluids circulating beneath the western flank of the mid-Atlantic ridge. *Sci. Rep.* 6:22541. doi: 10.1038/srep22541

Meyers, M. E. J., Sylvan, J. B., and Edwards, K. J. (2014). Extracellular enzyme activity and microbial diversity measured on seafloor exposed basalts from Loihi seamount indicate the importance of basalts to global biogeochemical cycling. *Appl. Environ. Microbiol.* 80, 4854–4864. doi: 10.1128/AEM.01038-14

Morono, Y., Terada, T., Nishizawa, M., Ito, M., Hillion, F., Takahata, N., et al. (2011). Carbon and nitrogen assimilation in deep subseafloor microbial cells. *Proc. Natl. Acad. Sci. USA* 108, 18295–18300. doi: 10.1073/pnas.1107763108

Mottl, M. J. (2003). "Partitioning of energy and mass fluxes between mid-ocean ridge axes and flanks at high and low temperature" in Energy and Mass Transfer in Marine Hydrothermal Systems. eds. P. Halbach, V. Tunnicliffe and J. R. Hein (Berlin: Dahlem University Press), 271–286.

Mottl, M. J., and Wheat, C. G. (1994). Hydrothermal circulation through mid ocean ridge flanks: fluxes of heat and magnesium. *Geochim. Cosmochim. Acta* 58, 2225–2237. doi: 10.1016/0016-7037(94)90007-8

Neira, N. M., Clark, J. F., Fisher, A. T., Wheat, C. G., Haymon, R. M., and Becker, K. (2016). Cross-hole tracer experiment reveals rapid fluid flow and low effective porosity in the upper oceanic crust. *Earth Planet. Sci. Lett.* 450, 355–365. doi: 10.1016/j.epsl.2016.06.048

Orcutt, B. N., Bach, W., Becker, K., Fisher, A. T., Hentscher, M., Toner, B. M., et al. (2011a). Colonization of subsurface microbial observatories deployed in young ocean crust. *ISME J.* 5, 692–703. doi: 10.1038/ismej.2010.157

Orcutt, B., D'angelo, T., Jungbluth, S.P., Huber, J.A., and Sylvan, J.B. (2020). "Microbial life in oceanic crust". OSF [Preprint]. doi: 10.31219/osf.io/2wxe6

Orcutt, B. N., D'angelo, T., Wheat, C. G., and Trembath-Reichert, E. (2021). Microbe-mineral biogeography from multi-year incubations in oceanic crust at north pond, mid-Atlantic ridge. *Environ. Microbiol.* 23, 3923–3936. doi: 10.1111/1462-2920.15366

Orcutt, B. N., Sylvan, J. B., Knab, N. J., and Edwards, K. J. (2011b). Microbial ecology of the Dark Ocean above, at, and below the seafloor. *Microbiol. Mol. Biol. Rev.* 75, 361–422. doi: 10.1128/mmbr.00039-10

Orcutt, B., Wheat, C. G., and Edwards, K. J. (2010). Subseafloor Ocean crust microbial observatories: development of FLOCS (FLow-through Osmo colonization system) and evaluation of borehole construction materials. *Geomicrobiol J.* 27, 143–157. doi: 10.1080/01490450903456772

Orcutt, B. N., Wheat, C. G., Rouxel, O., Hulme, S., Edwards, K. J., and Bach, W. (2013). Oxygen consumption rates in subseafloor basaltic crust derived from a reaction transport model. *Nat. Commun.* 4:2539. doi: 10.1038/ncomms3539

Parkes, R. J., Cragg, B., Roussel, E., Webster, G., Weightman, A., and Sass, H. (2014). A review of prokaryotic populations and processes in sub-seafloor sediments, including biosphere: geosphere interactions. *Mar. Geol.* 352, 409–425. doi: 10.1016/j.margeo.2014.02.009

Ramírez, G. A., Garber, A. I., Lecoeuvre, A., D'angelo, T., Wheat, C. G., and Orcutt, B. N. (2019). Ecology of subseafloor crustal biofilms. *Front. Microbiol.* 10:1983. doi: 10.3389/fmicb.2019.01983

Robador, A., Jungbluth, S. P., Larowe, D. E., Bowers, R., Rappe, M., Amend, J. P., et al. (2015). Activity and phylogenetic diversity of sulfate-reducing microorganisms in low-temperature subsurface fluids within the upper oceanic crust. *Front. Microbiol.* 5:748. doi: 10.3389/fmicb.2014.00748

Robador, A., Larowe, D. E., Jungbluth, S. P., Lin, H. T., Rappe, M. S., Nealson, K. H., et al. (2016). Nanocalorimetric characterization of microbial activity in deep subsurface oceanic crustal fluids. *Front. Microbiol.* 7:454. doi: 10.3389/fmicb.2016.00454

Santelli, C. M., Orcutt, B. N., Banning, E., Bach, W., Moyer, C. L., Sogin, M. L., et al. (2008). Abundance and diversity of microbial life in ocean crust. *Nature* 453, 653–656. doi: 10.1038/nature06899

Seyler, L. M., Trembath-Reichert, E., Tully, B. J., and Huber, J. A. (2021). Time-series transcriptomics from cold, oxic subseafloor crustal fluids reveals a motile, mixotrophic microbial community. *ISME J.* 15, 1192–1206. doi: 10.1038/s41396-020-00843-4

Shah Walter, S. R., Jaekel, U., Osterholz, H., Fisher, A. T., Huber, J. A., Pearson, A., et al. (2018). Microbial decomposition of marine dissolved organic matter in cool oceanic crust. *Nat. Geosci.* 11, 334–339. doi: 10.1038/s41561-018-0109-5

Smith, A. R., Fisk, M. R., Thurber, A. R., Flores, G. E., Mason, O. U., Popa, R., et al. (2016). Deep crustal communities of the Juan de Fuca ridge are governed by mineralogy. *Geomicrobiol J.* 34, 147–156. doi: 10.1080/01490451.2016.1155001

Smith, A. R., Kieft, B., Mueller, R., Fisk, M. R., Mason, O. U., Popa, R., et al. (2019). Carbon fixation and energy metabolisms of a subseafloor olivine biofilm. *ISME J.* 13, 1737–1749. doi: 10.1038/s41396-019-0385-0

Smith, A. R., Mueller, R., Fisk, M. R., and Colwell, F. S. (2021). Ancient metabolisms of a thermophilic subseafloor bacterium. *Front. Microbiol.* 12:764631. doi: 10.3389/fmicb.2021.764631

Thorseth, I. H., Torsvik, T., Torsvik, V., Daae, F. L., and Pedersen, R. B. (2001). Diversity of life in ocean floor basalt. *Earth Planet. Sci. Lett.* 194, 31–37. doi: 10.1016/S0012-821X(01)00537-4

Trembath-Reichert, E., Butterfield, D. A., and Huber, J. A. (2019). Active subseafloor microbial communities from Mariana back-arc venting fluids share metabolic strategies across different thermal niches and taxa. *ISME J.* 13, 2264–2279. doi: 10.1038/s41396-019-0431-y

Trembath-Reichert, E., Morono, Y., Ijiri, A., Hoshino, T., Dawson, K. S., Inagaki, F., et al. (2017). Methyl-compound use and slow growth characterize microbial life in 2-km-deep subseafloor coal and shale beds. *Proc. Natl. Acad. Sci. USA* 114, E9206–E9215. doi: 10.1073/pnas.1707525114

Trembath-Reichert, E., Shah Walter, S. R., Ortiz, M. A. F., Carter, P. D., Girguis, P. R., and Huber, J. A. (2021). Multiple carbon incorporation strategies support microbial survival in cold subseafloor crustal fluids. *Sci. Adv.* 7:eabg0153. doi: 10.1126/sciadv.abg0153

Tully, B. J., Wheat, C. G., Glazer, B. T., and Huber, J. A. (2018). A dynamic microbial community with high functional redundancy inhabits the cold, oxic subseafloor aquifer. *ISME J.* 12, 1–16. doi: 10.1038/ismej.2017.187

Urabe, T., Ishibashi, J.-I., Sunamura, M., Okino, K., Takai, K., and Suzuki, K. (2015) In: Subseafloor biosphere linked to hydrothermal systems: TAIGA concept, edited by J.-I. Ishibashi, K. Okino and M. Sunamura. Springer Japan 2015.

Wheat, C. G., Fisher, A. T., Mcmanus, J., Hulme, S. M., and Orcutt, B. N. (2017). Cool seafloor hydrothermal springs reveal global geochemical fluxes. *Earth Planet. Sci. Lett.* 476, 179–188. doi: 10.1016/j.epsl.2017.07.049

Winslow, D. M., and Fisher, A. T. (2015). Sustainability and of outcrop-to-outcrop hydrothermal circulation. *Nat. Commun.* 6:7567. doi: 10.1038/ncomms8567

Winslow, D. M., Fisher, A. T., Stauffer, P. H., Gable, C. W., and Zyvoloski, G. A. (2016). Three-dimensional modeling of outcrop-to-outcrop hydrothermal circulation on the eastern flank of the Juan de Fuca ridge. *J. Geophys. Res. Solid Earth* 121, 1365–1382. doi: 10.1002/2015jb012606

Zhang, X., Fang, J., Bach, W., Edwards, K. J., Orcutt, B. N., and Wang, F. (2016a). Nitrogen stimulates the growth of subsurface basalt-associated microorganisms at the Western flank of the mid-Atlantic ridge. *Front. Microbiol.* 7:633. doi: 10.3389/fmicb.2016.00633

Zhang, X., Feng, X., and Wang, F. (2016b). Diversity and metabolic potentials of subsurface crustal microorganisms from the Western flank of the mid-Atlantic ridge. *Front. Microbiol.* 7:363. doi: 10.3389/fmicb.2016.00363

Ziebis, W., Mcmanus, J., Ferdelman, T., Schmidt-Schierhorn, F., Bach, W., Muratli, J., et al. (2012). Interstitial fluid chemistry of sediments underlying the North Atlantic gyre and the influence of subsurface fluid flow. *Earth Planet. Sci. Lett.* 323-324, 79–91. doi: 10.1016/j.epsl.2012.01.018

Zinke, L. A., Reese, B. K., Mcmanus, J., Wheat, C. G., Orcutt, B. N., and Amend, J. P. (2018). Sediment microbial communities influenced by cool hydrothermal fluid migration. *Front. Microbiol.* 9:1249. doi: 10.3389/fmicb.2018.01249

Zobell, C. E. (1938). Studies on the bacterial flora of marine bottom sediments. *J. Sediment. Res.* 8, 10–18. doi: 10.1306/d4268fd6-2b26-11d7-8648000102c1865d

Zobell, C. E., and Anderson, D. Q. (1936). Vertical distributionof bacteria in marine sediments. *Bull. Am. Assoc. Pet. Geol.* 20, 258–269. doi: 10.1306/3D932DB2-16B1-11D7-8645000102C1865D

frontiers | Frontiers in Microbiology

TYPE Original Research
PUBLISHED 23 December 2024
DOI 10.3389/fmicb.2024.1455594

OPEN ACCESS

EDITED BY
Andreas Teske,
University of North Carolina at Chapel Hill, United States

REVIEWED BY
Axel Schippers,
Federal Institute for Geosciences and Natural Resources, Germany
Thore Rohwerder,
Helmholtz Association of German Research Centres (HZ), Germany

*CORRESPONDENCE
Jayme Feyhl-Buska
✉ feyhlbus@usc.edu

†PRESENT ADDRESSES
Fabai Wu,
School of Life Sciences, College of Science, Eastern Institute of Technology, Ningbo, China
Isaiah E. Smith,
GeoZentrum Nordbayern, Friedrich-Alexander-Universität Erlangen-Nürnberg, Erlangen, Germany

‡Deceased

RECEIVED 27 June 2024
ACCEPTED 04 December 2024
PUBLISHED 23 December 2024

CITATION
Feyhl-Buska J, Wu F, Smith IE, LaRowe DE, Robador A, Kruger B, Osburn MR and Amend JP (2024) Calorimetric measurement of energy and nutrient stimulation of microorganisms from the continental deep subsurface. *Front. Microbiol.* 15:1455594. doi: 10.3389/fmicb.2024.1455594

Calorimetric measurement of energy and nutrient stimulation of microorganisms from the continental deep subsurface

Jayme Feyhl-Buska[1]*, Fabai Wu[1†], Isaiah E. Smith[1†], Douglas E. LaRowe[1], Alberto Robador[2], Brittany Kruger[3], Magdalena R. Osburn[4] and Jan P. Amend[1,2‡]

[1]Department of Earth Sciences, University of Southern California, Los Angeles, CA, United States, [2]Department of Biological Sciences, University of Southern California, Los Angeles, CA, United States, [3]Division of Hydrologic Sciences, Desert Research Institute, Las Vegas, NV, United States, [4]Department of Earth and Planetary Sciences, Northwestern University, Evanston, IL, United States

Microbial activity in the deep continental subsurface is difficult to measure due to low cell densities, low energy fluxes, cryptic elemental cycles and enigmatic metabolisms. Nonetheless, direct access to rare sample sites and sensitive laboratory measurements can be used to better understand the variables that govern microbial life underground. In this study, we sampled fluids from six boreholes at depths ranging from 244 m to 1,478 m below ground at the Sanford Underground Research Facility (SURF), a former goldmine in South Dakota, United States. The heat produced by microorganisms in these samples was measured in a nanocalorimeter as a proxy for activity. Heat flow measurements on unamended groundwater samples from five of the six boreholes comprising the Deep Underground Microbial Observatory (DeMMO) fell below the limit of detection, suggesting very low metabolic rates. Fluid samples from the borehole that registered a heat signal (DeMMO 6) from 1,478 m deep, were amended with a series of electron donors, electron acceptors, and amino acids before being introduced into the calorimeter. The addition of formate resulted in more than a ~500 nW increase in heat flow relative to the signal for unamended fluids during the first 100 h of incubation while the next highest heat flow arose from nitrate and acetate co-addition, at ~125 nW. Notably, both amendment conditions led to a ~1.5 orders of magnitude increase in cell density without causing major changes to community composition, suggesting that these electron donors and acceptors may be exploited by these communities *in-situ*. The addition of ~0.4 mM casamino acids resulted in a total heat flow of 2.25 μW within 35 h and a more than three orders of magnitude increase in cell density. In these experiments, *Hydrogenophaga* grew to dominate the amino acid amended borehole fluids. The strong microbial response to amino acid addition indicates a deep continental surface community that is limited by the availability of amino acids. A high potential for amino acid metabolism was proposed in genomic studies from this and similar sites but has not been shown in actively growing communities.

KEYWORDS

calorimetry, deep biosphere, Sanford Underground Research Facility, nutrient limitation, microbial activity

1 Introduction

Despite being Earth's largest microbial habitat, the subsurface remains understudied due to its inaccessibility (Whitman et al., 1998; Amend and Teske, 2005; Kallmeyer et al., 2012; Edwards et al., 2012; Colwell and D'Hondt, 2013; McMahon and Parnell, 2014). Microbes in the deep continental subsurface respire orders of magnitude slower than their surface-dwelling analogs (Onstott et al., 1999; Price and Sowers, 2004), and catabolize up to a million times slower than laboratory cultures grown in nutrient-rich media (Hoehler and Jørgensen, 2013). This leads to calculated doubling times, ranging from hundreds to thousands of years (Phelps et al., 1994; Jørgensen and D'Hondt, 2006; Lin et al., 2006).

Determining the catabolic reactions catalyzed by such slow-growing microbes is challenging, as many typical metabolic rate measurements are not designed to detect extremely low levels of activity. For example, measuring microbial turnover rates during incubations (Hoehler and Jørgensen, 2013) is not applicable to the extremely slow metabolic processes characteristic of subsurface systems (Parkes et al., 2005). Furthermore, interpreting the results of such lab-based experiments is often complicated by shifts in the community resulting from selective growth under incubation conditions. Metatranscriptomic analysis of the microbial community RNA provides an alternative option to assess microbial activity in the subsurface. This approach, however, is hampered by difficulties with RNA extraction (Schippers et al., 2005; Biddle et al., 2006; Orsi et al., 2013; Urich et al., 2014; Pachiadaki et al., 2016; Zinke et al., 2017) and limited by the quantity of *in-situ* activity.

To overcome these limitations, we used a nanocalorimeter to measure the heat associated with microbial activity in underground samples collected from the Sanford Underground Research Facility (SURF). Calorimetry allows for the agnostic measurement of heat flow and therefore records the total change in enthalpy for all reactions occurring in a system, biotic and abiotic. Additionally, this technique boasts a low detection limit, ~1.2 nW/mL (Braissant et al., 2010). Nanocalorimetry can measure potential bacterial heat production in cell cultures of approx. $1 \times 10^{2-3}$ cells/mL (Higuera-Guisset et al., 2005; Braissant et al., 2010; Robador et al., 2018) and natural samples of $1 \times 10^{3-4}$ cells/mL (Robador et al., 2016). Cell densities in SURF samples are well within this range, between 1×10^3 cells/mL and 4×10^5 cells/mL. Furthermore, the sum of the total heat over time was complemented with concentration measurements of products and reactants evolving during the experiment to thermodynamically constrain the reactions being catalyzed. For example, Robador et al. (2018) used this technique to identify microbial lactate oxidation as the key reaction in a system where multiple microbial metabolic pathways could be employed. Prior studies at SURF revealed discrepancies in metabolic predictions at identical boreholes, noting that while sulfate and nitrate reduction pathways were frequently identified, they were not the most energetically advantageous (Osburn et al., 2014; Momper et al., 2017). Further analysis of functional genes across DeMMO sites by Momper and colleagues in 2023 showed that genomic potential did not align with the predominant geochemical species at each location. However, the 2023 study also reported ubiquitous potential for the metabolism of small organic molecules, such as amino acids and acetate. This study aims to identify which metabolic pathways are actively employed by microbes, focusing on their actual metabolic activities instead of their potential capabilities.

2 Materials and methods

2.1 Sample collection and geochemical characterization

Samples were collected from all the Deep Mine Microbial Observatory (DeMMO; Osburn et al., 2019) at the Sanford Underground Research Facility (SURF) in Lead, South Dakota, United States. SURF is located within the former Homestake Gold Mine and DeMMO accesses groundwater from six separate areas within SURF, ranging in depth from 244 m to 1,478 m beneath the surface. Prior research utilizing the DeMMO infrastructure has developed a geochemical and biological time series (Osburn et al., 2019; Osburn et al., 2020), and explored the metabolic capabilities at SURF through *in-situ* cultivation and studies on energetics and metagenomics (Osburn et al., 2014; Momper et al., 2017; Casar et al., 2021a; Casar et al., 2021b; Momper et al., 2021; Momper et al., 2023).

The samples retrieved for this study were obtained in tandem with those of long-term monitoring for geochemical and biological variability within the DeMMO network (Osburn et al., 2019). All six DeMMO boreholes were sampled (DeMMO 1–6) during two expeditions, on December 5–10th, 2016, and September 9–14th, 2018. Data from the time of sampling is available in Table 1. Detailed sampling procedures for geochemical and community analysis are available in companion studies (Osburn et al., 2019; Osburn et al., 2020). As described in these studies, geochemical analysis was performed on samples either directly at the field site or after being prepared and shipped to the laboratory for more comprehensive processing. At the field, temperature, pH, redox-sensitive ions, oxidation reduction potential (ORP), and conductivity were measured using a Hach field testing kit (Hach, Loveland, CO, United States) and a Myron Ultrameter II (Myron L Company, Carlsbad, CA, United States). Additional geochemical analyses were carried out in other academic or commercial labs: major dissolved cations and anions (ACZ Laboratories, Steamboat Springs, CO, United States), dissolved organic carbon (DOC; Anatek Labs, Moscow, ID, United States) and dissolved inorganic carbon (DIC; Northwestern Stable Isotope Biogeochemistry Laboratory, Evanston, IL, United States). Dissolved gasses were measured via gas chromatography on a Shimadzu GC-2014 using FID and TCD detectors and referenced to Scott analytical standards (Air Liquide, Paris, France). Cells from field samples were fixed with paraformaldehyde and stored at −20°C prior to staining with DAPI (4′,6-diamidino-2-phenylindole) and concentration onto a 0.22 μm black polycarbonate filter (Millipore, Burlington, MA).

2.2 Calorimetry

Groundwater samples for calorimetry were collected in sterile, anaerobic, glass serum bottles. Prior to fieldwork, the bottles were combusted at 400°C for 4 h, closed with butyl stoppers and seals, then flushed with nitrogen gas until anaerobic. The anaerobic combusted bottles were autoclaved at 121°C for 30 min, prior to being evacuated to maximum achievable negative pressure. In the field, the tops of the prepared serum bottles were sterilized with 70% isopropanol wipes, and Viton® tubing (DuPont Performance Elastomers LLC, Wilmington, DE, United States) and needles were used to

TABLE 1 Geochemical concentrations at six DeMMO boreholes during two sampling trips.

Date of Sampling	Borehole	Depth (m)	Temperature (°C)	pH	ORP (mV)	Conductivity (uS)	Total Dissolved Solids (ppm)	Nitrate (mg/L)	Ammonia (mg/L)	Ferrous Iron (mg/L)	Sulfide (ug/L)	Sulfate (mg/L)	Dissolved Oxygen (mg/L)	Dissolved Organic Carbon (mg/L)
December, 2016	1	244	10	7.37	−96	956.1	688.7	0.2	0.07	2.27	0	297	0	0.4
	2	244	12.5	7.72	−93	626.5	443.5	0.1	0.03	0.31	29	156	0.54	0.387
	3	610	16.2	7.27	−30	3,036	2,313	0.2	0.28	2.92	0	1,540	0.147	0.259
	4	1,250	22.6	8.88	−278	1774	1,296	1	1.56	0.01	537	262	0.043	0.174
	5	1,478	31.4	9.07	−233	1,540	1,109	0.7	0.46	0	329	80.3	0.058	BDL
	6	1,478	24.6	8.64	−205	7,978	6,685	0.4	0.08	1.23	55	4,370	0.09	0.136
September, 2018	1	244	10.6	NA	−78	980.3	701.1	0.3	0.08	2.68	0	360	0.042	0.42
	2	244	12.3	NA	−49	623.8	440.6	0.2	0.03	0.31	0	97.4	NA	0.381
	3	610	16.2	NA	−77	3,112	2,370	0.2	0.17	1.8	17	1740	0.009	0.244
	4	1,250	22.4	NA	−207	1781	1,302	0.9	1.36	0	780	291	0.032	0.181
	5	1,478	31.4	NA	−185	1,537	1,105	0.9	0.46	0	334	173	0.121	0.173
	6	1,478	21.5	NA	−194	7,873	6,561	0.3	0.12	0.88	38	4,380	0	0.252

"BDL" indicates that the constituent was "below detection limit," "NA" indicates that the measurement is not available from that date.

anaerobically and aseptically transfer fluids from the boreholes to the bottles. For each borehole, at least one serum bottle was filled with borehole water that first passed through a 0.2 μm filter. A few weeks after samples were returned to the lab, these filtered borehole water samples were stained with acridine orange and collected onto a 0.22 μm black polycarbonate filter (Millipore, Burlington, MA) prior to visualization on a Zeiss Axiovision Epifluorescent Microscope to inspect for growth indicative of contamination, but no cells were observed in any of the filtered water bottles.

All borehole fluids were kept at 4°C following sample collection until placed in the calorimeter. Samples for calorimetry were prepared as described by Robador et al. (2016), with slight modifications. Briefly, 4 mL TA Instruments ampules were sealed with aluminum foil and combusted at 400°C for 4 h (TA Instruments, New Castle, DE, United States). Combusted ampules were then autoclaved at 121°C for 30 min. Groundwater was aseptically and anaerobically removed from the serum bottles collected in the field and 2 mL was transferred into each ampule in a Coy Laboratories anaerobic chamber (Grass Lake, MI, United States) at <5 ppm oxygen. Ampules were sealed with a crimp top cap, which includes a built-in rubber stopper. For the experiments that included amendments, the added chemical was mixed with the groundwater aseptically in the anaerobic chamber prior to being transferred into the calorimetric ampule.

For all calorimetric analyses, a TAM III thermal activity monitor (TA Instruments-Waters LLC, New Castle, DE, United States) equipped with two nanocalorimeters was equilibrated to 28°C prior to the start of experiments. Reference ampules, calorimetric samples identical in chemical composition to the groundwater sample ampules, but with biomass removed via a 0.1 μm filter, were loaded into the reference position in each calorimeter prior to the beginning of each new experiment. Once the reference ampules equilibrated with the calorimeters, samples were lowered into the sample slots on each calorimeter, allowing for thermal equilibration halfway through the lowering process into measuring position.

Due to the high system sensitivity, it is necessary to adjust the experimental data to compensate for the heat produced when lowering experimental ampules into the calorimeter's measuring position. In this manuscript, two methods were utilized for the removal of perturbation signal. For low total-signal samples (such as in Figures 1–3), the "synchronization method" was used, which involved synchronizing the heat signals across all experiments to make the initial disruption in each experiment's heat curve easily recognizable. Only data collected after this initial surge of heat are presented; any data collected before this convergence point are deemed artifacts resulting from the insertion process and are thus disregarded. In the amino acid amended experiments (such as in Figures 4, 5), microbial activity generated a significant heat signal, allowing for the use of the less human-biased "power function method." This permitted the use of a power function ($f(x) = a*xb + c$) to model the artificial heat effects. The function helped identify the initial and final data segments as background noise due to disturbances resulting from the insertion of the sample, which were then excluded from the analysis. An illustration of this method can be found in Supplementary Figure 1. A variety of negative controls were tested to subtract out the potential confounding factors in quantification. To assess whether the 0.1 μm filtered borehole fluid in the reference ampule was not, in fact, sterile, reference ampules were prepared with borehole fluid autoclaved once, twice, and once with additional 0.1 μm filtration. Different methods

to reduce baseline heat signal introduced during sample-insertion process were also tested. The duration of time that the sample was allowed to equilibrate during lowering was varied, as was the time the sample was given to return to 28°C after storage at 4°C. Based on this test work, the methodology described earlier in this section for reference and sample ampule handling was selected.

Amendments to the calorimetric samples were prepared as concentrated, anaerobic, sterile solutions. Borehole water samples and amendment solutions were combined aseptically in an anaerobic chamber, at a final concentration of 10 mM for all additions except the amino acid and ammonium additions. Casamino Acids (Amresco Bacterological Grade) were utilized for the amino acid addition experiments and amended into the borehole fluids as a sterile anerobic solution at varying percentages. These percentages were later converted into molarities using the average molecular weight for casamino acids, 539.583 g/mol, given by the manufacturer. It should be noted that all "amino acid" concentrations reported here are a combination of free amino acids and small peptides that result from the digestion of casein. Therefore, tryptophan is not present in this mixture, and the remaining amino acids are not present in equal abundances. Electron donor (ED) and acceptor (EA) additions were predominantly conducted individually, with the assumption that the amended ED or EA would be coupled with a redox partner from the borehole fluid. Exceptions to this method were made for the co-addition of acetate and nitrate, while three potential EDs were added simultaneously with lactate, citrate, and pyruvate. Following the conclusion of all calorimetric experiments, ampules were closely examined for cracks in the glass and gaps in the seal, to ensure that vial integrity was maintained throughout the experiment.

2.3 DNA and RNA processing

While in the field, samples for genomic DNA and RNA extraction were collected onto 2–4 sterile replicate housing-encased 0.1 µm Supor filters per borehole. Based on cell enumeration from fluids and fluid rates, a minimum of 10^6 cells were captured onto each filter, with samples collected in <1 h (Table 2). Most filtration was completed within 40 min, and two filters contained 10^9 cells. Collected cells were immediately frozen at −80°C and kept at this temperature until extraction.

Initial DNA and RNA extractions from the filters employed a modified version of the protocol in Momper et al. (2017), which was used for genomic DNA extraction from the same sample site. In short, filters were subjected to physical and chemical lysis through a combination of bead beating, freeze/thaw cycles, and sequential exposure to an extraction buffer (Tris and EDTA) and a TESC buffer. Following cell lysis, proteins, humic acids, and other contaminants were removed via 24:1 chloroform:isoalcohol precipitation. The resulting pellet was cleaned using 100% ethanol, prior to being dried and re-suspended in TE buffer. Following DNA and RNA extraction,

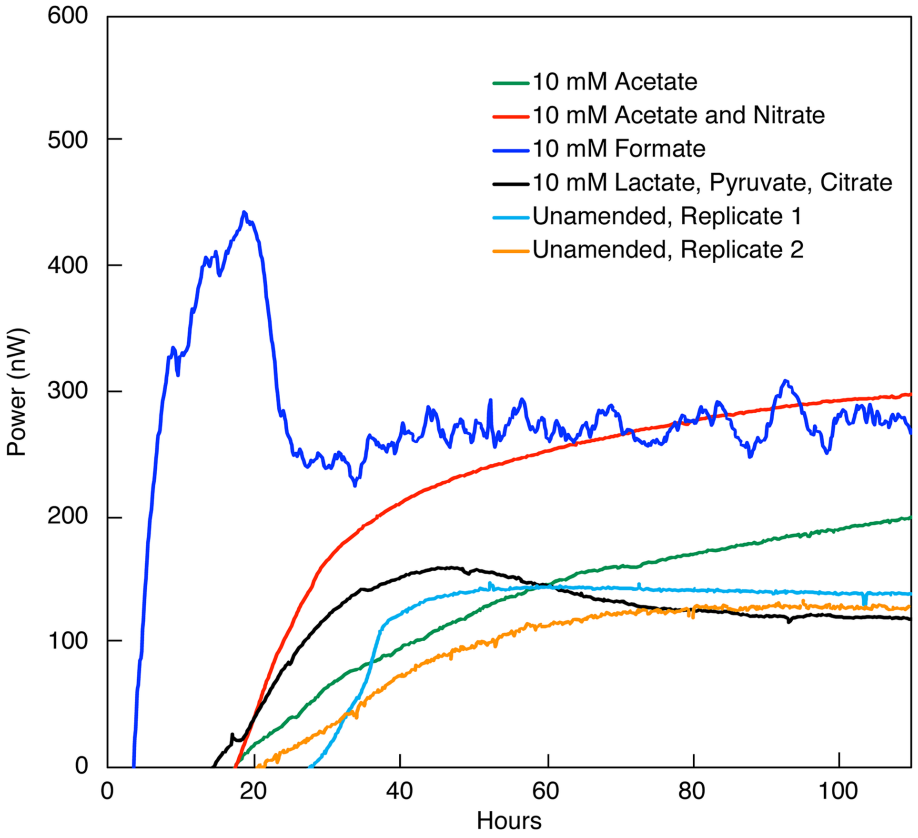

FIGURE 1
Heat flow (Power) from the indicated amendments to DeMMO 6 borehole fluid. The baseline heat flow signal has been corrected using the synchronization method.

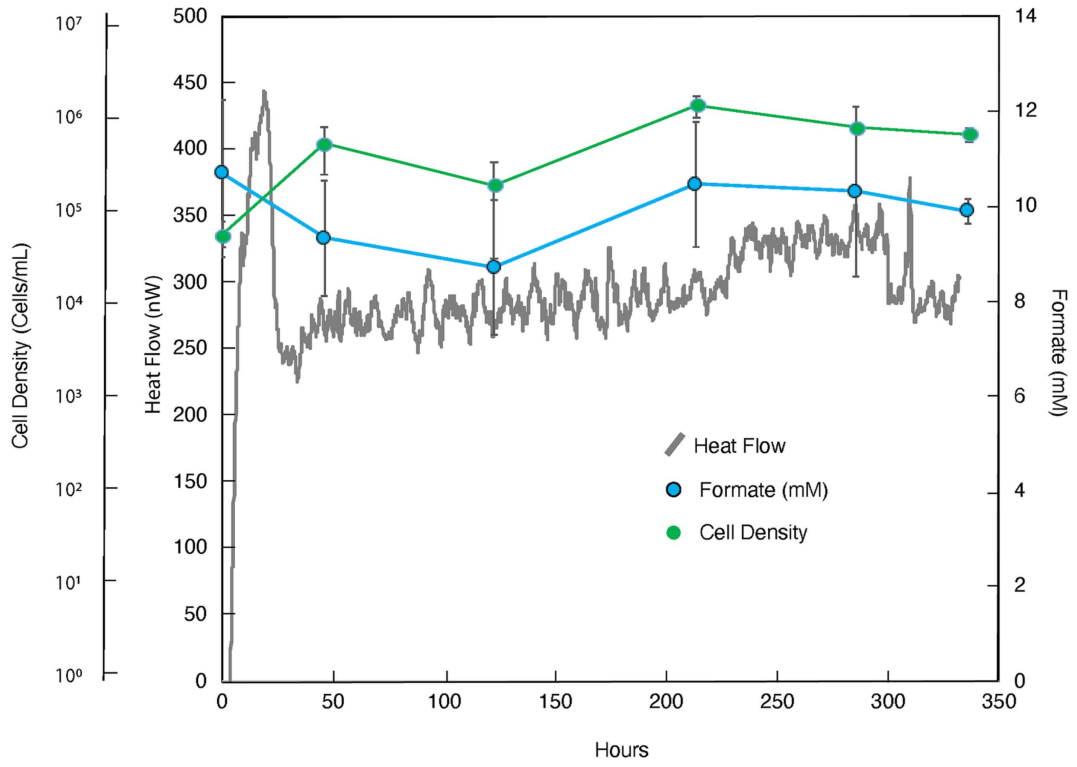

FIGURE 2
Heat flux (Power), cell density and formate concentration as a function of time for the amendment experiment in which formate (10 mM) was added to borehole fluids from DeMMO 6. The baseline heat flow signal has been corrected using the synchronization method.

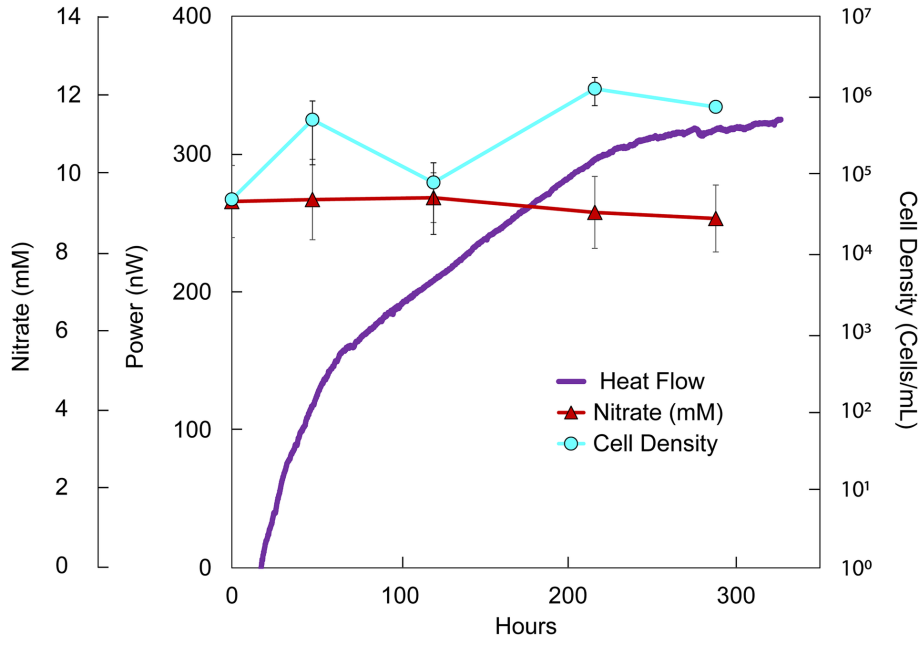

FIGURE 3
Heat flux (Power), cell density and nitrate concentration over time in DeMMO 6 fluids amended with nitrate (10 mM) and acetate (10 mM). The baseline heat flow signal has been corrected using the synchronization method.

eluents were divided in half, and in one aliquot, DNA was quantified on a Qubit 2.0 Flurometer (Invitrogen, Carlsbad, CA) using a Qubit dsDNA HS kit. In the other aliquot, RNasein (Promega, Madison, WI, United States) was added to prevent RNA degradation, and TURBO

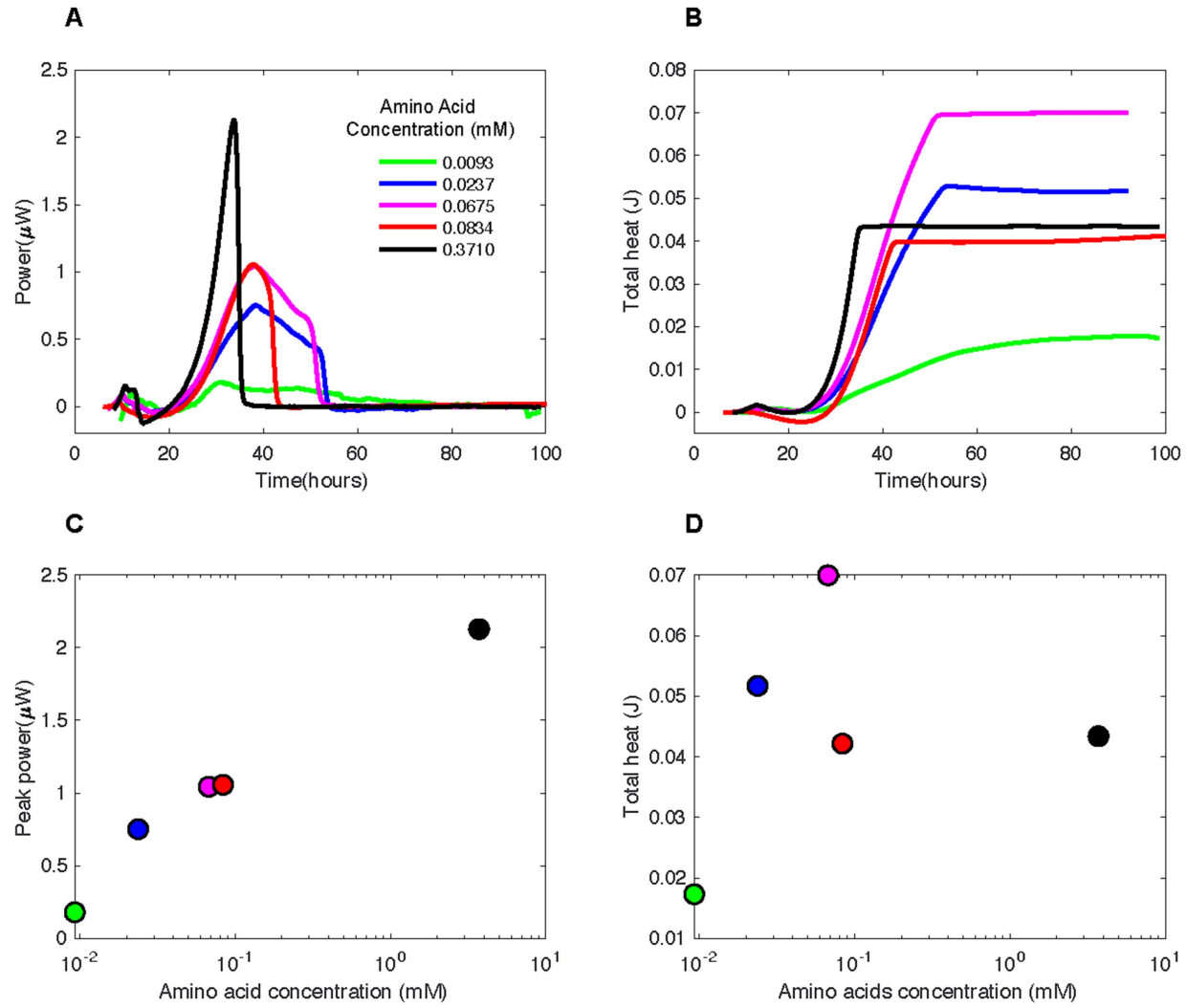

FIGURE 4
(A) Heat flux (Power) and **(B)** cumulative heat as a function of time and **(C)** peak power and **(D)** total heat as a function of amino acid concentrations associated with experiments in which various concentrations of casamino acids were added to borehole fluids from DeMMO 6. The baseline heat flow signal has been corrected using the power function method.

DNase (Invitrogen, Carlsbad, CA, United States) was utilized to remove genomic DNA. RNA was then quantified using a Qubit RNA HS kit. cDNA synthesis was accomplished with SuperScript III First-Strand Synthesis SuperMix (Invitrogen, Carlsbad, CA) using random hexamers, according to manufacturer protocols.

RNA was also extracted using a RNeasy PowerBiofilm Kit (Qiagen, Hilden, Germany), following manufacturer protocols, except that DNase 1 solution was not added to the reactions until after the protocol was completed, allowing for simultaneous DNA and RNA extraction. Once extracted, RNA resulting from this procedure was treated in the same manner as RNA resulting from the procedure noted above.

DNA for 16S rRNA gene community comparisons between the calorimetric experiments was extracted using a DNEasy Power Biofilm Kit (Qiagen, Hilden, Germany), following manufacturer protocols, and quantified with a Qubit dsDNA HS kit. 16S rRNA gene amplification utilized the 515F/926R primer pair (Parada et al., 2016) and GoTaq reaction mix (Promega, Madison, WI, United States), while in a Veriti 96 Well Thermal Cycler for the following steps: 95°C for 3 min, 30 cycles of 95°C for 45 s, 50°C for 45 s, and 72°C for 1 min 30 s. The presence and quality of PCR products was confirmed via gel electrophoresis. PCR products were shipped to Molecular Research DNA (Shallowater, TX, United States) for indexing, purification with Ampure XP beads, normalization and pooling prior to paired end sequencing of the 16S rRNA gene on an Illumina MiSeq platform. The resulting reads were pre-processed in the FASTq Processor (Molecular Research DNA) to remove barcodes, linker primers, and reverse primers. QIIME2, running in R 4.0.1, demultiplexed reads (Bolyen et al., 2019) and the Divisive Amplicon Denoising Algorithm 2 (DADA2) denoised reads (Callahan et al., 2016). This process produced Amplicon Sequence Variants (ASVs), which were compared to the sequences listed in the Ribosomal Database Project's SILVA v138 Database (Quast et al., 2013; Yilmaz et al., 2014). Relative abundance and diversity plots were made in the phyloseq and ggplot2 packages, running in R (McMurdie and Holmes, 2013; Wickham, 2016).

2.4 Viral and prokaryotic quantification

Prokaryotic cells were counted using a Zeiss Axiovision Epifluorescent Microscope. Cells were fixed with paraformaldehyde and stored at −20°C, then stained with acridine orange and collected onto a 0.22 µm black polycarbonate filter (Millipore, Burlington, MA). Viral particles were quantified following Haas et al., 2014. In brief, samples were fixed with paraformaldehyde, filtered onto a 0.02 µm Whatman Anodisc 25 filter, and stained with SYBR Gold. After dye incubation, the excess SYBR Gold was removed and the filter was mounted to a slide using a filtered ascorbic acid/phosphate buffered saline/glycerol mixture. Viral and prokaryotic cells were visualized using a cyan filter and the Image-Pro Plus 7.0 program. 25 micrographs were taken at random and the viral and prokaryotic quantities counted manually.

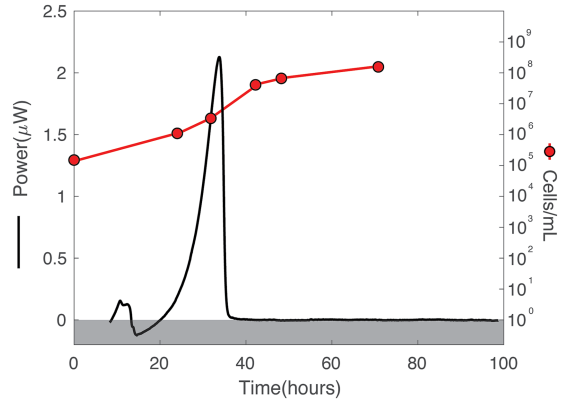

FIGURE 5
Heat flux (Power) and cell density over time in DeMMO 6 fluids amended with 0.3710 mM amino acids. The baseline heat flow signal has been corrected using the power function method. A gray box covers all data below 0 to facilitate ease of understanding for the cell/mL axis, which only starts above 0.

2.5 Parallel experiments

Incubation experiments identical to those carried out in the calorimeter were carried out in parallel in a darkened incubator to determine how the concentrations of cells, anions, organic acids and gases changed with time (samples cannot be removed from the calorimeter during an experiment without significant loss of data). Cell densities and gas concentrations were determined as described above. Anion concentrations were measured on a Metrohm Ion Chromatograph (Metrohm, Riverview, FL, United States) equipped with an anion separation column. Organic acid measurements were made on an Agilent 1,100 Series HPLC (Santa Clara, CA, United States) utilizing an Agilent Hi-Plex H column.

2.6 Thermodynamic calculations

Standard state enthalpies of reaction, ΔH_r^0, were calculated at 28°C and 1 bar using the revised HKF equations of state (Helgeson et al., 1981; Tanger and Helgeson, 1988; Shock et al., 1992), the SUPCRT92

TABLE 2 Total cells collected on filters from the six DeMMO (Deep Mine Microbial Observatory) boreholes considered in this study.

Borehole	Filter	Total filtered (mL)	Duration of filtration (min)	Cell density at borehole (cells/mL)	Total cells on filter
1	1	7,286	40	1.10×10^3	8.03×10^6
	2	10,615	40	1.10×10^3	1.17×10^7
2	1	6,077	40	5.63×10^3	3.42×10^7
	2	1,282	40	5.63×10^3	7.22×10^6
3	1	1,241	40	3.13×10^3	3.88×10^6
	2	520	40	3.13×10^3	1.63×10^6
	3	780	40	3.13×10^3	2.44×10^6
4	1	1,240	40	6.06×10^3	7.51×10^6
	2	640	40	6.06×10^3	3.88×10^6
	3	820	40	6.06×10^3	4.97×10^6
5	1	1,320	40	5.60×10^3	7.40×10^6
	2	3,640	40	5.60×10^3	2.04×10^7
	3	160	40	5.60×10^3	8.96×10^5
	4	10,000	40	5.60×10^3	5.60×10^7
6	1	900	20	4.03×10^5	3.63×10^8
	2	2,720	20	4.03×10^5	1.10×10^9
	3	100	20	4.03×10^5	4.03×10^7
	4	6,844	20	4.03×10^5	2.76×10^9

Borehole water can be split into spigots of variable flow rate; here, flow rate was measured every 10 min and has been averaged to determine the "Total Filtered" water for each borehole. The total cells on filter are calculated from the cell densities and the total fluids filtered.

software package (Johnson et al., 1992) and thermodynamic data taken from a number of sources (Amend and Helgeson, 1997; Dick et al., 2006). For the reactions in which the identities of the amino acids were not known, i.e., when Casamino acids were used, a weighted average of ΔH_r^0 for the 20 common naturally-occurring amino acids in the proportion that they are found in *E. coli* (Neidhardt, 2005) were used to estimate the enthalpies of amino acid oxidation reactions. This approximation was made since the enthalpy calculation requires knowing the defined proportion of amino acids in solution, but the relative amount of each amino acid in Casamino acids is not known. However, the amino acid composition of *E. coli* has been measured. Values of ΔH_r^0 for the half reactions describing the full oxidation of carbon, but not other elements were combined with values of ΔH_r^0 for half reactions describing the reduction of O_2 to H_2O, SO_4^{2-} to HS^- and NO_3^- to N_2 to calculate values of ΔH_r^0 for the oxidation of a nominal amino acid by these three EAs. The enthalpies of reaction were then used in combination with reaction stoichiometries (mol electron acceptor / mol amino acid) and the total heat produced in the calorimeter (0.0433 J) to determine the number of moles of reactants consumed and CO_2 produced. These results are summarized in Table 3.

3 Results

3.1 Indications of microbial activity in unamended borehole fluids

Heat signal in unamended DeMMO 1–5 borehole fluids was below detection, at a limit of ~1.2 nW/mL and despite incubation for at least 150 h. None of the possible sources of signal interference that were tested (see Methods section) improved the replicability or detectability of heat flow measurements in these samples. Only DeMMO 6 borehole fluid produced a replicable power signal equilibrating at ~100 nW within 40 h (Figure 1) and was further interrogated, as discussed below.

Virus-to-prokaryote ratio (VPR) measurements summarized in Figure 6 correlate with the low heat signals measured on the calorimeter. It can be seen in this figure that VPR linearly scaled with cell density, but not with depth within the mine. The 6 DeMMO boreholes access 4 depths at SURF, with DeMMO 6 accessing a borehole containing ~2 orders of magnitude more cells per milliliter than the other DeMMO boreholes (Table 2). The average VPR across the samples was 2.03, with a high at DeMMO 5 (2.66) and low at DeMMO 6 (1.67). DeMMO 5 and 6 are at the same depth in the mine although access very different fluids (Osburn et al., 2019) while boreholes from 244 m deep had similar VPRs (2.25 and 2.06).

mRNA, another proxy for active microbial functions, was extracted from all DeMMO boreholes, but was not detected at a sufficient level for functional interpretation. This result was noted despite the extraction of ample DNA from the same samples and consistently high mRNA recoveries in the positive controls (see Methods section).

3.2 DeMMO 6 amendments

3.2.1 Electron acceptors and donors

DeMMO 6 borehole fluid samples were amended with EAs and/or EDs/carbon sources to investigate the genomic potential and energetic potential of microorganisms previously described in DeMMO (Momper et al., 2017; Osburn et al., 2014) but exhibited low increases in heat flow relative to unamended samples (Figure 1). By ~50 h, all samples reached a heat flow signal that was maintained consistently for upwards of 300 h (only data through 100 h shown in Figure 1). Of the amendment experiments, formate (dark blue curve in Figure 1) and an acetate/nitrate mixture (orange curve) increased the heat flow above that for unamended borehole waters (light blue and yellow curves) by ~500 nW and ~ 125 nW, respectively. Fluid sample amended with only acetate (green curve) and fluid sample amended with a mixture of citrate, lactate, and pyruvate (black curve) produced no significant change with respect to unamended fluid samples (Figure 6). In borehole waters amended with a combination of citrate, lactate, and pyruvate, heat signal peaked at ~175 nW around 45 h. Cells density increased from 1.16×10^4 cells/mL to 4.84×10^5 cells/mL over a period of 240 h, although the community composition remained very consistent throughout the duration of the experiment (Figure 7; Supplementary Figure 2). At the beginning of the experiment (t_0), no single genus accounted for >25% of the community, with the most abundant genera identified as *Afipia*, *Devosia*, *Hydrogenophaga* and *Limnobacter*. These same genera remained in high abundance at the end of the experiment, both within the calorimetric vials and within the parallel experiments.

The addition of formate as potential ED and carbon source resulted in a more robust and oscillating heat signal, peaking at ~450 nW at ~20 h before sharply dropping to ~225 nW and tapering off at ~100 nW above this value for the duration of the experiment (336 h; Figure 2; replication in Supplementary Figure 3). Concurrently, cell densities per milliliter increased from 3.99×10^4 to 4.18×10^5 in the first 46 h and remained relatively constant throughout the duration of the experiment. A notable size increase in cell radius, as visualized microscopically, was also noted during this time (data not shown). It can be further seen that, within measurement uncertainty, apparent formate concentrations did not change.

The microbial community in the formate addition cultures remained markedly consistent, with almost no variation in structure between any replicates or time points (Figure 8). In both t_0 replicates,

TABLE 3 Summary of reactions considered to be sources of heat in the calorimetry experiments carried out on SURF borehole fluids and the cumulative number of moles of specified reactants and CO_2 in these reactions that would be consumed or produced to generate 0.0433 J of heat, the total amount of heat produced following amendment with 0.371 mM amino acids.

Reaction	Moles consumed	Moles produced (CO_2)
$C_3H_7NO_2 + 2C_2H_5NO_2 + 2H_2O \rightarrow CO_2 + 3CH_3COO^- + 3NH_4^+$	Alanine: 4.27×10^{-7}	4.27×10^{-7}
$O_2 + AA \rightarrow H_2O + CO_2$	O_2: 7.15×10^{-8}	7.15×10^{-8}
$SO_4^{2-} + AA \rightarrow HS^- + CO_2$	SO_4^{2-}: 3.97×10^{-6}	7.94×10^{-6}
$NO_3^- + AA \rightarrow N_2 + CO_2$	NO_3^-: 9.71×10^{-8}	1.21×10^{-7}
$0.5O_{2(aq)} + H_{2(aq)} \rightarrow H_2O$	$H_{2(aq)}$: 1.59×10^{-7}	NA
$SO_4^{2-} + 4H_{2(aq)} + H^+ \rightarrow HS^- + 4H_2O$	$H_{2(aq)}$: 7.91×10^{-7}	NA
$NO_3^- + 2.5H_{2(aq)} + H^+ \rightarrow 0.5N_2 + 3H_2O$	$H_{2(aq)}$: 1.70×10^{-7}	NA

"AA" refers to amino acid and "NA" means not applicable.

the dominant community member was *Leucobacter* (~25% relative abundance), with all other community members present in less than 10% abundance. The community structure after 46 h, t_1, looks very similar to the community at t_0, with a slight increase in the abundance of *Parvibaculum* and a slight decrease in the abundance of *Ignavibacteriales* bacterium SR-FBR-L83. These trends stayed consistent after 336 h, t_F, across all replicates within and outside of the calorimeter. *Leucobacter* continued to dominate the community at ~25% abundance, but a larger percentage of the community was composed of *Parvibaculum* (~10%).

While formate additions resulted in an increase in cell density and a change in heat flow, acetate had a negligible effect on the community, even when combined with nitrate. Simultaneous addition of acetate and nitrate to borehole waters resulted in ~175 nW stronger heat signal than unamended groundwater within 100 h (Figure 3). Over the course of the experiment, nitrate and acetate concentrations remained unchanged at ~10 mM each, while cell densities increased variably from 4.74×10^4 cells/mL to a maximal density of 1.20×10^6 cells/ml at 216 h (Supplementary Figure 4; Figure 3). In all inorganic EA and organic ED amendment experiments, heat signals were < 500 nW, with the majority closer to ~100 nW at 100 h.

3.2.2 Amino acids

All amino acid-amended borehole fluids produced a substantial and highly replicable heat flow signal whose maximal magnitude correlated with amino acid concentration. Amendments with 0.3710 mM casamino acids resulted in a maximal heat flow of ~2.25 μW at ~32.5 h (Figure 4C). Heat flow for the next highest concentration of amino acids, 0.0834 mM (red curve), peaked at ~1.1 μW, approximately 5 h after the 0.3710 mM amendment. The heat flow signal for 0.0675 mM (purple curve) reaches the same peak as that for 0.0834 mM amino acids, but tapers for twice as long. The maximal heat signal for the 0.0237 mM amendment (blue curve) is less than those for 0.0675 mM and 0.0834 mM, but the tapering ends at a similar time as it does for the 0.0675 mM experiment. Amendment with 0.0093 mM amino acids results in a much lower heat flow than those experiments with higher amino concentrations, maximally at ~0.2 μW heat flow.

In many of the amino-amended heat flow signals, a small peak occurs around 10 h, followed by a much larger peak around 30–40 h (Figure 4A). The sharpness of the large peak was directly correlated to amino acid concentration, with higher concentrations resulting in steeper peaks. From the maximal heat flow at the peak, all signals dropped off between ~35 and ~ 55 h, except in the case of 0.0093 mM amino acid amended fluids.

The total heat produced during an amino acid addition experiment was influenced by the length of time that the heat flow signal tapered after the steep drop-off following the peak (Figure 4B). For instance, the largest total heat signal, 0.07 J, was present for 0.0675 mM (Figure 4D) which had the same peak width as the

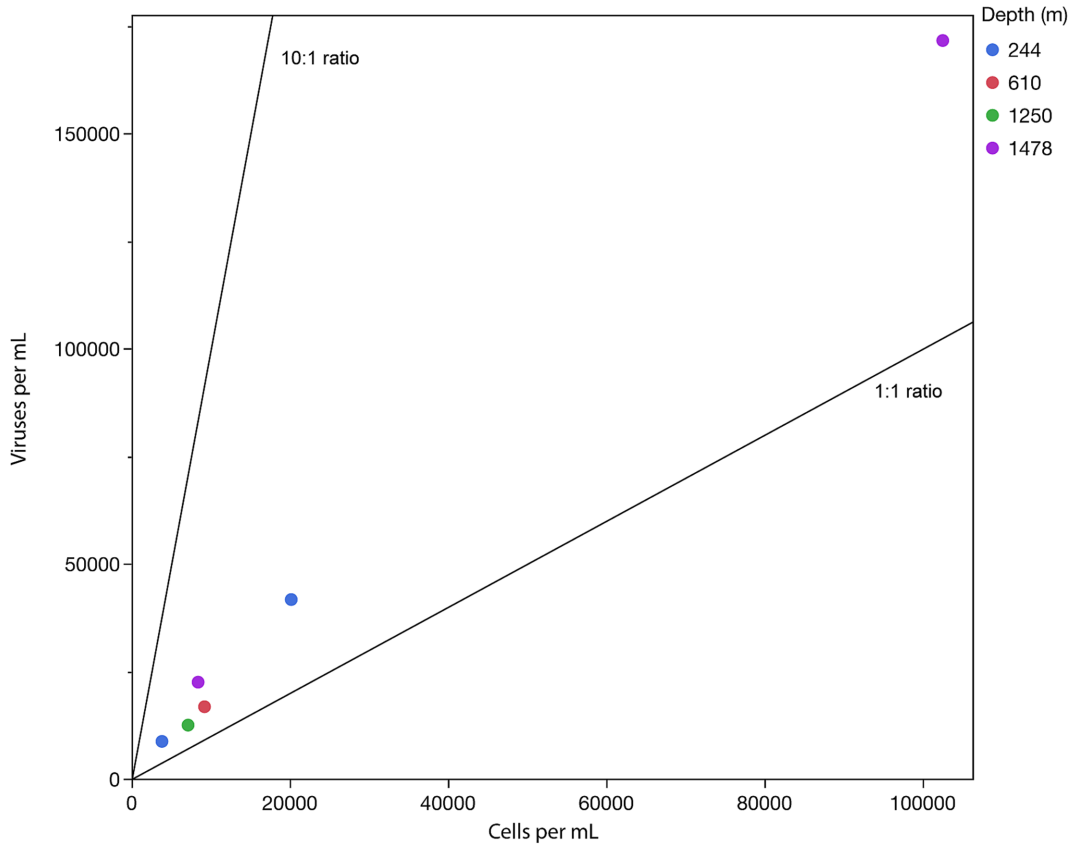

FIGURE 6
Virus-to-prokaryote ratio (VPR) in samples taken from DeMMO boreholes from the indicated depths below the local surface. The black diagonal lines provide a visual guide to specific VPR values with a base of 10.

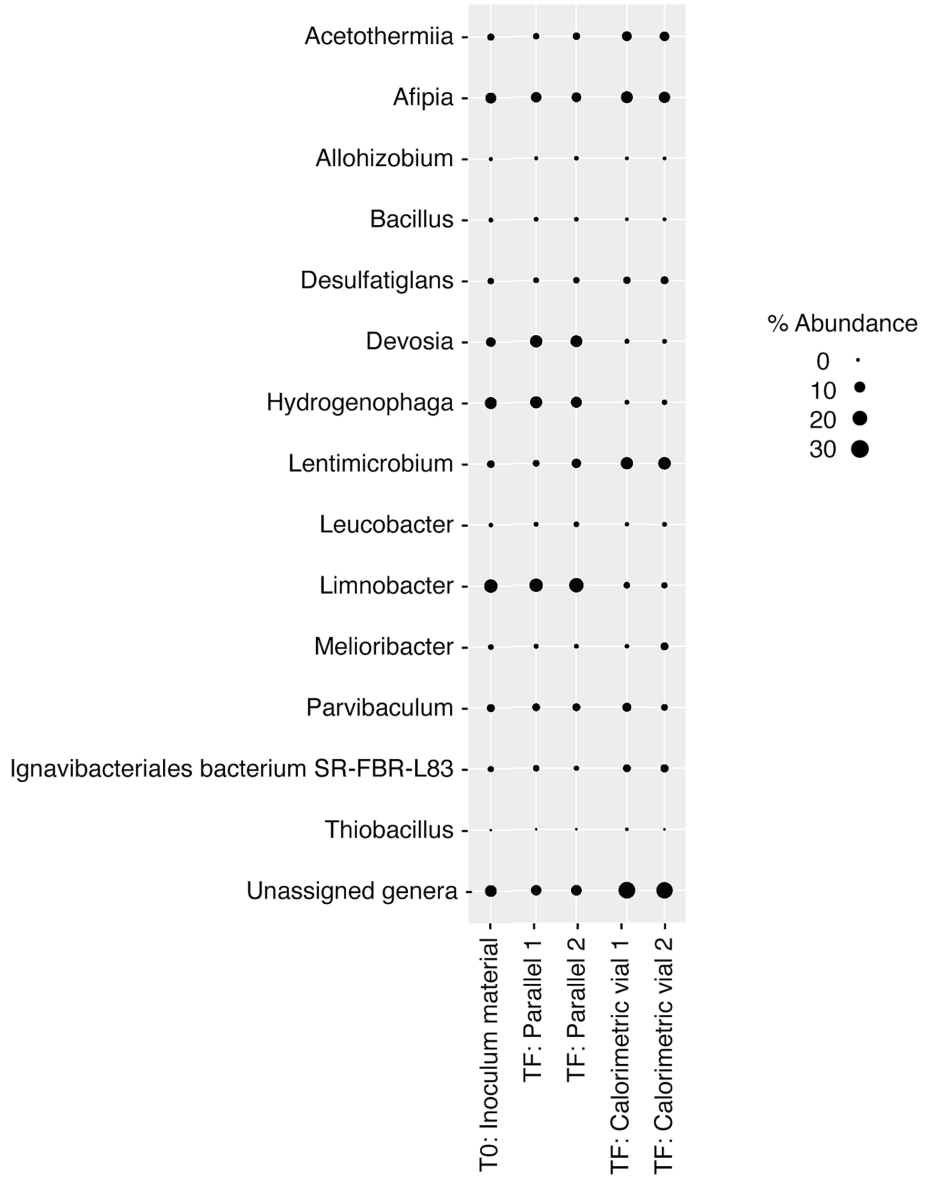

FIGURE 7
Relative abundance of microbial genera in DeMMO 6 borehole fluids before (t_0) and after (t_f) incubations with lactate, citrate, and pyruvate amendments. "Parallel 1" and "Parallel 2" refer to duplicate incubation experiments run outside of the calorimeter and "calorimetric vial 1" and "calorimetric vial 2" correspond to replicate incubations experiments run inside the calorimeter. "Unassigned genera" indicates taxa for which taxonomy could not be assigned at the genus level.

0.0237 mM experiment (Figure 4A). However, the sample with 0.0675 mM casamino acids had a larger maximal heat prior to the tapering period (~1.1 vs. ~0.75 μW). Little heat production occurred after 45 h in most amended samples.

Over the duration of the amino acid amended experiments, the community was dominated by two major taxa that are endemic to the SURF community: *Hydrogenophaga* and *Limnobacter* (Figure 9). In addition to these two taxa, *Allorhizobium* became a major part of the community in the experiments taking place inside the calorimeter. The addition of amino acids slowly changed the community over time, with *Limnobacter* dropping off in abundance from as much as ~75% to as little as ~5%. *Hydrogenophaga* was present at some abundance in all the collected DeMMO 6 groundwater, although it particularly thrived when exposed to more complex organic carbon sources, becoming as much as 75% of the community during amino acid addition. Figure 5 depicts the growth curves corresponding to these data, indicating a cell density increase in the community from 1.16×10^5 cells/mL to 1.41×10^8 cells/mL within 70 h. During this time, sulfate concentrations did not change within the margin of error, while nitrate and oxygen concentrations remained below the detection limit (Supplementary Figure 5). On average, carbon dioxide rose from 1.40×10^{-8} mol/mL to 2.66×10^{-7} mol/mL while hydrogen dropped from 1.03×10^{-6} mol/mL to 2.58×10^{-7} mol/mL.

To test whether the amino acid addition signal results from microbes splitting the ammonia group off the amino acids, amino acids were amended into DeMMO 6 fluids at 0.371 μM and 9.3 μM concentrations. Additionally, 1 M ammonium was added to samples at each of these amino acid concentrations. Only minimal differences

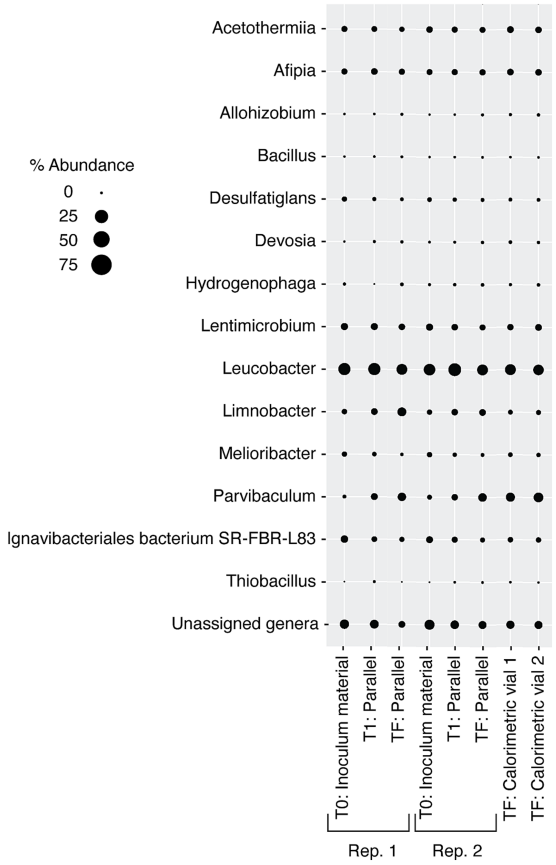

FIGURE 8
Relative abundance of microbial genera in DeMMO 6 fluids before (t_0) and after (t_F) and 46 h into (t_1) incubation with formate. "Parallel" refers to duplicate incubation experiments run outside the calorimeter, and these parallel experiments were replicated (Rep. 1 and Rep. 2). Replicate experiments run inside the calorimeter are noted as "Calorimetric vial 1" and "Calorimetric vial 2". "Unassigned genera" indicates taxa for which taxonomy could not be assigned at the genus level.

were noted between samples amended with amino acids vs. samples amended with amino acids and ammonium (Supplementary Figure 6).

4 Discussion

4.1 *In-situ* activities are low throughout SURF

The investigation into microbial metabolic activity within the SURF borehole fluids from DeMMO 6 reveals a distinct response to nutrient amendments, as evidenced by measured variations in heat flow. Specifically, introducing small concentrations of amino acids (0.3710 mM) stimulated a metabolic reaction that led to the generation of approximately 2.2 μW within a span of 25 h. This indicates a pronounced microbial response to the added substrates, translating into an observable thermodynamic effect. Similarly, the addition of formate and a nitrate/acetate mixture induced significant variations in heat flow, underscoring a substantial metabolic shift compared to the baseline established by unamended borehole fluids. Contrarily, the addition of other substrates such as citrate, lactate, pyruvate, and acetate (in the absence of nitrate) did not manifest in a marked increase in heat flow, suggesting a selective metabolic responsiveness to nutrient types. Despite this apparent lack of response, the results pertaining to these substrates are consistent and exceed the calorimeter's threshold of detection, validating their reliability. Additionally of interest, aging of samples in the laboratory did not result in differences in the maximum heat flow a sample could obtain, but did change the amount of time required for a sample to obtain this heat flow signal. This is evident when comparing the nitrate and acetate co-amendment data in Figures 1, 3, which represent data collected, respectively, within weeks of the sample being collected, and after 3 months. In contrast, unamended fluids from the remaining five DeMMO boreholes failed to yield replicable outcomes, likely attributable to diminished cell densities and inherently low microbial activity within those environments. DeMMO 6 may have increased cell densities and activities relative to the other 5 boreholes resulting from being capped with a steel manifold which inhibits flow. This differential response underscores the complexity of microbial communities' metabolic dynamics and highlights the potential of specific substrates to activate or enhance microbial processes within subsurface ecosystems.

The SURF VPR is another indicator of low microbial activity at this site. Active microbial communities tend to be characterized by a standard ratio of viruses to prokaryotes of about 10:1 (Thingstad, 2000). This ratio is based on the notion that viruses cannot replicate unless their hosts are sufficiently active to utilize their replication machinery. Based on previous studies examining VPR across a variety of environments, the average VPR from SURF, 2.03, is very low. For instance, the average VPR in deep sea environments is 28.45 and for estuaries, it is 11.35 (Parikka et al., 2017). The lowest reported average values across an environment are from waterflow or rivers, at 9.38, although the lowest VPR yet reported (0.0001) was found in deep marine sediments (Yanagawa et al., 2014). These low VPR values may indicate a cost to phage activity, wherein low metabolic rates become necessary for survival *in-situ* (Thingstad et al., 2014). Regardless of the cause of low metabolic rates at SURF, the VPR present across the SURF boreholes is indicative of a dormant or near-dormant metabolic state in the site fluids. It is likely that cell densities and activities are higher in fissures in the source rock, where mineral-associated biofilms provide more hospitable conditions for microbial life (Casar et al., 2021a). However, in the fluids, the case for an inactive microbial community is also supported by the lack of extractable mRNA across all DeMMO boreholes. This trend is of particular interest given that most microbial modeling assumes that microbes are either dead or alive and active, when in fact a state of maintenance may be more applicable in energy-limited systems (Bradley et al., 2018). This study supports the notion of a population that is engaged in very low-energy maintenance activities and provides a variety of potential methods for assessing metabolic rate during dormancy.

The low heat flow rates noted in DeMMO borehole fluids are conspicuously less than those reported for bacteria grown in media but are consistent with environmental values estimated through modeling. Using a reaction transport model and Gibbs energy calculations, it can be determined that, extremely energy-limited cells can exist on 1.5×10^{-8} pW (Bradley et al., 2020). While the enthalpy-based measurements of power employed in this study do not indicate such low activity, heat flow also does not reach the levels described in

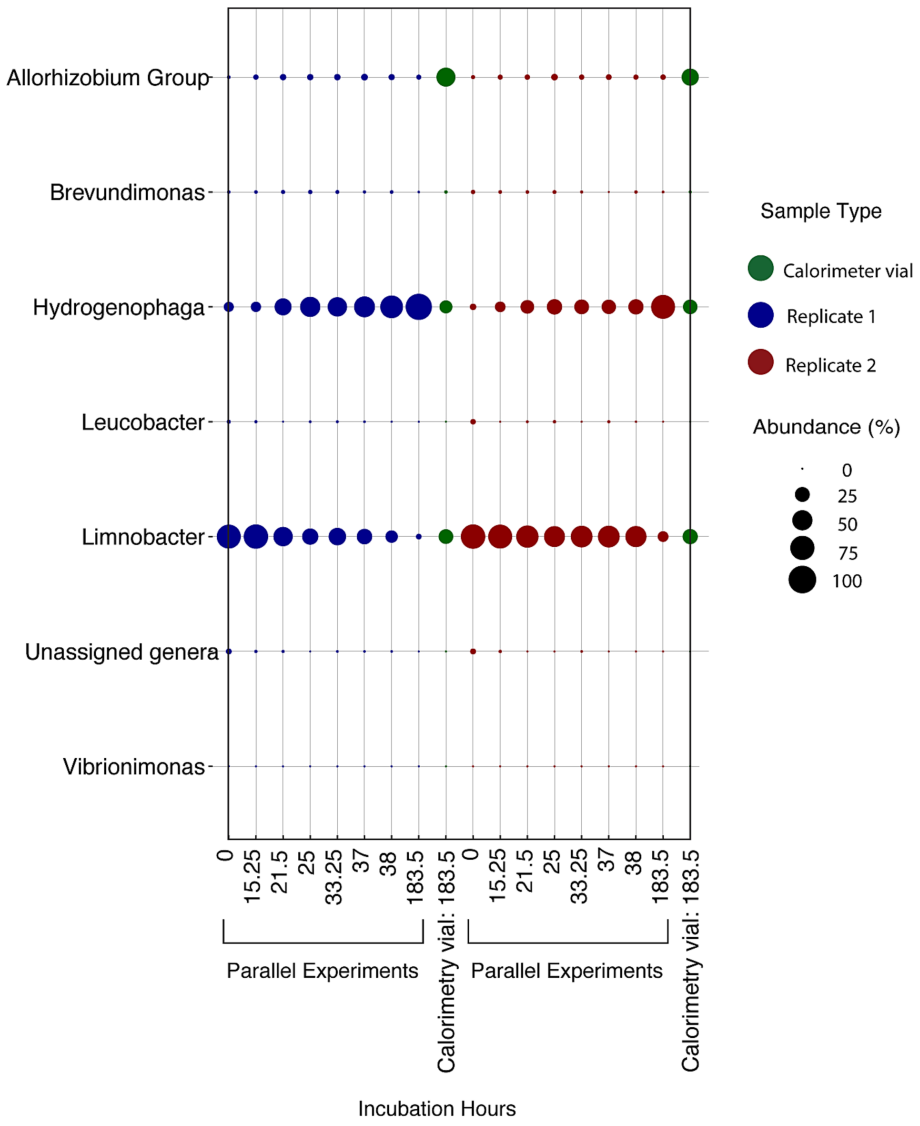

FIGURE 9
Relative abundance of microbial genera in DeMMO 6 fluids amended with 0.371 mM amino acids over various times throughout 183.5 h in two experiments incubated outside of the calorimeter ("parallel experiments") and two replicates incubated inside of the calorimeter ("calorimetry vial"). Calorimetry vial samples were collected at 183.5 h. "Unassigned genera" indicates taxa for which taxonomy could not be assigned at the genus level.

more active communities. For context, a pure culture of *Shewanella oneidensis MR-1* grown under oxygen limitation maximally produces a heat flow of ~24 μW (Robador et al., 2018), a value that is 48 times greater than the maximal heat flow resulting from the SURF borehole water even after amendment with high concentrations of organic acids and EAs. For DeMMO 6, unamended samples produced 100 nW for 5.2×10^5 total cells, indicating that a single cell under those conditions uses around 0.19 pW. This value is in a similar range to that for a single cell in soil (1 pW to 10^{-5} pW), and in the basaltic crust (5.68 pW), and is well above the estimated range for a single cell in marine sediments (10^{-4} pW to 10^{-8} pW; Robador et al., 2016; Bay et al., 2021; Bradley et al., 2022; Zhao et al., 2021), which are based on Gibbs energies, not enthalpies, of reaction. The most straightforward explanation for why consistent heat signals could not be obtained for the other boreholes is that the cell density at those boreholes was too low to generate a replicable signal. The DeMMO 1–5 borehole fluids contain about to a 10^3 cells/mL. Assuming the 0.192 pW of power from DeMMO 6 holds true for the other boreholes, the heat flow for DeMMO 1, at 1.607×10^3 cells/mL would be 0.31 nW. This value is below the detection limit of the calorimeter.

4.2 Energetically favorable or genomically encoded does not mean active

This study tested some of the predictions made by previous papers predicting potential metabolisms at this site (Osburn et al., 2014; Momper et al., 2017; Momper et al., 2023). Nitrate reduction pathways are present at DeMMO 6 and the use of this EA is energetically favorable given the conditions present at this borehole. Although the addition of nitrate to DeMMO 6 borehole fluids did result in a larger heat flow signal than was present in unamended fluids and promoted

cell replication, it failed to produce the large microbially-produced heat signal seen with amino acid addition. Sulfate reduction pathways are also both energetically favorable and commonly encoded at DeMMO 6, but sulfate is abundant at high concentrations (~45 mM) on site, and the supplementation of an additional 10 mM sulfate in calorimetric experiments did not impact heat flow in this study (Supplementary Figure 7).

It has been proposed that organic acids are being produced in the deep subsurface biosphere by fermentative bacteria, and that these organic acids are in turn utilized by organotrophs (Teske, 2005). Acetate has also been shown to stimulate growth in deep subsurface fluid communities from Finland (Miettinen et al., 2018), and genomic studies of other deep subsurface sites have reported abundant genes for heterotrophic processes (Nyyssönen et al., 2014; Nuppunen-Puputti et al., 2022). In the SURF system, acetate, as a proxy for organic matter, was demonstrated to be the most exergonic ED (Osburn et al., 2019). Additionally, genes for acetate and formate oxidation are abundant across the six DeMMO boreholes (Momper et al., 2023). In this study, acetate amendment had a greater impact when co-amended with nitrate, potentially indicating microbial denitrification on site is controlled by the availability of organic acids like acetate. Formate amendment resulted in greater overall heat flows than acetate amendment, although uniquely, this organic acid resulted in an oscillating heat flow indicating potential metabolic shifts. The increase in cell density but lack of concurrent change in community structure noted during this amendment could indicate that all community members are equally sensitive to formate, but another possibility is that the microbes in this community are not doubling so much as becoming more metabolically active and therefore easier to detect. A limit to this study is that all conditions were uniformly tested at a 10 mM concentration, which was selected after lower concentrations of acetate (~1 mM) failed to produce a measurable signal (data not shown). However, 10 mM concentrations of may have introduced inhibitory effects or altered microbial activity patterns. From the previous studies of the genomic potential at SURF, it is difficult to determine which of the many genes for the use of small organic molecules present at DeMMO 6 are actively being transcribed given the environmental conditions the community is experiencing (Momper et al., 2023). The data in this study indicate that organic acids appear to have a lesser impact on catabolic processes than amino acids.

4.3 Deep continental subsurface life is uniquely poised for amino acid metabolism

The amendment of even very low concentrations of casamino acids (0.0093 mM) resulted in an increase in heat flow, total heat, and cell density above that in unamended fluids. A higher amino acid concentration did not necessarily equate to greater total heat. Rather, samples with less amino acids produced a lower but more prolonged peak that produced more total heat. Among the microbial taxa changing most strongly in response to the amendment of amino acids were *Hydrogenophaga* and *Limnobacter*, which were present *in-situ* at the time of sampling and therefore unlikely to be contaminants. In fact, *Hydrogenophaga* was the dominant microbe in the original rock core removed to prepare the DeMMO 6 borehole (Momper et al., 2017), is commonly observed throughout gold mine and continental subsurface environments (Santini et al., 2002; Baker et al., 2003; Nuppunen-Puputti et al., 2022) and has been grown under anaerobic conditions (Duffner et al., 2022). Further, although the marker-gene based community composition of the starting inoculum materials differ slightly between experiments, this is most likely due to the inherent stochasticity of energy-limited deep subsurface environments and is likely to represent the variability that is naturally present in these environments. The preferential growth of *Hydrogenophaga* and other known deep subsurface organisms following nutrient amendment indicate that their responses are relevant to the *in-situ* environment. Although members of the Candidate Phyla Radiation (CPR) group were not reported in this study, it is possible that they are also present in the samples due to the difficulty with which they can be resolved via 16S rRNA analysis.

Growth of the DeMMO 6 communities resulting from amino acid addition could be due to nitrogen limitation, which this study tested with 1 M additional NH_4 supplementation. Although these conditions are not intended to represent a natural environment, they did indicate that additional ammonium failed to produce additional heat signal. Future studies would benefit from supplementation of ammonium at more environmentally relevant concentrations, including during the addition of other substrates. Ammonium has been indicated to be the major source of nitrogen in deep subsurface communities and is generally assimilated via the amino acids glutamine and glutamate (Nyyssönen et al., 2014). At DeMMO 6, the genes for ammonium oxidation are a minor component of the site genomic potential, with oxidative nitrogen metabolisms being rarely encoded across all DeMMO boreholes (Momper et al., 2023). The results of this study suggest that in the conditions tested, microbial activation and the subsequent metabolic processes, as indicated by heat production, are not directly facilitated by or dependent on ammonium as a metabolic substrate.

The Stickland reaction, or the fermentation of amino acids, is a potential catabolic process that could explain the formation of the observed heat flow. However, during the production of 0.0433 J of heat, this reaction produces 3.53×10^{-7} moles of CO_2, an order of magnitude higher than the quantity of CO_2 measured throughout these experiments. It is therefore likely that if the Stickland reaction is being employed by the SURF community, either a portion of the CO_2 is being utilized by the community upon formation (e.g., for biomass production), is being absorbed by the environment (e.g., via carbonate formation), or a secondary reaction is resulting in a proportion of the heat production. These potential secondary reactions include the oxidation of amino acids with NO_3^-, a process that would produce more CO_2 than was measured following these incubations. Moreover, NO_3^- in any concentration was not detected throughout the amino acid addition experiments. The reduction of O_2 with amino acids has the potential to explain the measured heat flow signal, producing approximately the observed amount of CO_2. Throughout these experiments, however, O_2 remained below the detection limit, although only a very low quantity of O_2 (lower than the detection limit of our gas chromatograph) would be required to produce this heat flow signal. The sulfide present in DeMMO 6 fluids is likely to reduce any O_2 originally present in the sample, although sulfide was lower than usual in these samples at the time of collection (Table 1; Momper et al., 2023). Potential evidence in support of the use of O_2 comes from the taxa present in the amino acid amended fluids, which hosts genera containing predominantly aerobic or microaerobic species. It is possible that the *Hydrogenophaga* in the

fluids preferentially reduces O_2 with *in-situ* H_2 or organic matter, and during times of O_2 and organic matter starvation, goes dormant. Additional community members could be engaged in sulfate reduction with H_2. The latter metabolism would consume 7.91×10^{-7} moles of H_2, which is similar to the 6.11×10^{-7} moles of H_2 consumed throughout these experiments, while sulfate reduction with amino acids is unlikely, as this produces 7.93×10^{-6} moles of CO_2, substantially more than what was produced during sulfate addition test work performed during this experiment (Supplementary Figure 7).

Due to the volumes of H_2 consumed and CO_2 produced in SURF fluids following amino acid addition, it seems likely any trace amounts of oxygen were initially consumed by the SURF community alongside amino acids, and perhaps heavily contributing to the measured heat flux. It is worth noting that the trend wherein larger amounts of amino acids produced a sharper heat flow spike, but less total heat production, supports the concept of a community wherein a small quantity of oxygen plus an abundance of amino acids allowed for a spike in activity. When less amino acids were present, the heat signal reached a lower but more sustained peak over time, indicating that a limiting reactant to growth – or potentially simply other metabolic activities – was not so readily exhausted. Perhaps in these experiments and following oxygen exhaustion in the higher concentration amino acid addition experiments, the community shifted toward sulfate reduction with hydrogen, thus explaining the quantity of hydrogen that was consumed over time. The genomic potential for oxygen, hydrogen, and sulfate utilization have all been reported for the DeMMO 6 borehole (Momper et al., 2023). Sulfate reduction is a dominant metabolism in the deep subsurface (Amend and Teske, 2005), and hydrogen is considered a major driver of many subsurface communities (Nealson et al., 2005). At DeMMO 6, the high concentration of sulfate complicated precise measurements of microbially-mediated changes in sulfate (Supplementary Figure 7), and it is possible that taxa with known sulfate reduction metabolisms did not dominate the community 16S rRNA data due to the genes for sulfate reduction being sequestered in CPR taxa, which are not well-resolved via 16S. While no significant consumption of sulfate was noted, the inclusion of amino acids was nonetheless necessary for the large concentration of *in-situ* sulfate to be used.

Future calorimetric work could test the combinative impact of amino acid addition with other substrates, such as organic acids or additional sulfate. Similar studies would also benefit from considering other compounds that are present in deep subsurface environments. Microbial utilization of the sulfur compounds thiosulfate and tetrathionate was investigated via calorimetry in Wentzien et al., 1994, and study of these compounds, in addition to elemental sulfur, helps solidify the story of sulfur cycling at deep subsurface sites. Additionally, it should be noted that calorimetry is occasionally used to assess the degradability of various ores via bioleaching pathways (Schroter and Sand, 1993; Schippers et al., 1995), and as such, future studies would benefit from conducting experiments using solid minerals, such as pyrite. Calorimetric studies investigating the microbial oxidation of pyrite using canonical bioleaching taxa have produced strong signals (Rohwerder et al., 1998), and previous studies from SURF have indicated that pyrite bioleaching may play a significant role in influencing the fluid chemistry onsite (Casar et al., 2021a). Lastly, methane or hydrogen addition would be a particularly attractive target for future work, but precise gas addition was not possible in this experiment without custom modifications to prevent leakage. Based on this study, amino acid addition, whether as a specific organic carbon source or as a building block for proteins, is recommended as a trigger for activity in this community regardless of other nutrient additions.

5 Conclusion

Like many deep continental subsurface environments, SURF appear to exhibit exceptionally low activity. This conclusion is drawn from several observations: only minimal amounts of RNA are transcribed, Virus-to-Prokaryote values suggest cells are in a non-growth state, and ultra-sensitive calorimetry fails to detect any heat signals from catabolic reactions, even after the addition of substrates capable of yielding redox energy. Altogether, these findings indicate a microbial community in a state of dormancy. Despite the low basal activity levels, microorganisms in SURF fluids demonstrate viability, as evidenced by their pronounced metabolic response to casamino acids and more tempered reactions to formate, acetate, and nitrate. This indicates not only the presence of life but also a selective responsiveness to different chemical amendments, highlighting the potential for metabolic activation under specific conditions.

The ability to maintain a low level of activity in a state akin to dormancy follows studies suggesting that in nutrient-limited environments, the fittest organisms in a community are those that can survive times of nutrient limitation, not those which can grow well (Bradley et al., 2019). By characterizing quantitatively and qualitatively the total heat evolved throughout calorimetric experiments, we have shown that the addition of amino acids to the SURF microbial community stimulates microbial growth and metabolic activity. Although samples amended with the highest concentration of amino acids exhibit the highest peak heat flow, it is the samples with a lower amino acid concentration that generate the greatest total amount of heat. Given this trend, measurements of reactants and products, and our calculations of the enthalpy of potential reactions, it is likely that any oxygen is rapidly used in this environment when amino acids are also present. Amino acid addition also appears to allow for the engagement of other catabolic processes, perhaps sulfate reduction with hydrogen or the Stickland reaction. The triggering of metabolic processes following amino acid addition in conjunction with the low heat flow data prior to nutrient amendment indicates that the SURF community is in a form of maintenance until the necessary conditions become available.

Amino acid limitation is commonly due to a lack of microbial amino acid biosynthesis during times of low energy flux (Payne and Wiebe, 1978), a state that certainly describes SURF fluids. Amino acid limitation has been noted in other oligotrophic environments, e.g., in coastal lagoons (Cotner et al., 2000), the subarctic Pacific (Kirchman, 1990), and in the Southern Ocean (Church et al., 2000). Yet, the role of amino acid limitation as a regulatory factor for life in the continental subsurface has not been previously identified.

Data availability statement

The original contributions presented in the study are publicly available in the NCBI repository. This data can be found here: https://www.ncbi.nlm.nih.gov/bioproject, accession number PRJNA1196095.

Author contributions

JF-B: Conceptualization, Data curation, Formal analysis, Funding acquisition, Investigation, Methodology, Visualization, Writing – original draft, Writing – review & editing. FW: Conceptualization, Data curation, Formal analysis, Investigation, Methodology, Supervision, Visualization, Writing – review & editing. IS: Data curation, Formal analysis, Investigation, Methodology, Visualization, Writing – review & editing. DL: Conceptualization, Formal analysis, Investigation, Methodology, Supervision, Visualization, Writing – original draft, Writing – review & editing. AR: Conceptualization, Methodology, Supervision, Writing – review & editing. BK: Investigation, Project administration, Resources, Writing – review & editing. MO: Funding acquisition, Project administration, Resources, Supervision, Writing – review & editing. JA: Conceptualization, Funding acquisition, Project administration, Resources, Supervision, Writing – original draft, Writing – review & editing.

Funding

The author(s) declare that financial support was received for the research, authorship, and/or publication of this article. This work was supported by the NASA Habitable Worlds program under grants 80NSSC20K0228 and 80NSSC24K0076 (DL), the NASA Exobiology program under grant NNH22ZDA001N (DL) and NNX15AM086 (MO), the NASA Astrobiology Institute-Life Underground (NNA13AA92A; DL, JF-B, JA, MO). Additional support came from the NSF Graduate Research Fellowship Program (JF-B) and the University of Southern California (DL, JF-B).

Acknowledgments

Foremost, the authors credit the impact of the late Jan Amend on this publication and on our careers. Amend was heavily involved in this study since its inception, guiding each of the authors through a stage of their respective careers. His role in developing our understanding of the deep subsurface was profound and his advice and mentorship will be sorely missed. Additionally, the authors would like to thank everyone involved with access and sampling at SURF, particularly Jaret Heiss. Discussions with the attendants of 2019 Telluride Science Research Center Workshop in Calorimetry and Microbial Ecology were also essential to this manuscript and the authors recognize the impact of those involved. Lastly, the authors extend their gratitude to Forest Rohwer and Brandie White for their assistance in collecting the VPR data in this study.

Conflict of interest

The authors declare that the research was conducted in the absence of any commercial or financial relationships that could be construed as a potential conflict of interest.

The author(s) declared that they were an editorial board member of Frontiers, at the time of submission. This had no impact on the peer review process and the final decision.

Publisher's note

Supplementary material

The Supplementary material for this article can be found online at: https://www.frontiersin.org/articles/10.3389/fmicb.2024.1455594/full#supplementary-material

References

Amend, J. P., and Helgeson, H. C. (1997). Calculation of the standard Molal thermodynamic properties of aqueous biomolecules at elevated temperatures and pressures part 1L-α-amino acids. *J. Chem. Soc. Faraday Trans.* 93, 1927–1941. doi: 10.1039/A608126F

Amend, J. P., and Teske, A. (2005). Expanding Frontiers in deep subsurface microbiology. *Palaeogeography, Palaeoclimatol. Palaeoecol. Geobiol. Objectives, Concept, Perspec.* 219, 131–155. doi: 10.1016/j.palaeo.2004.10.018

Baker, B. J., Moser, D. P., MacGregor, B. J., Fishbain, S., Wagner, M., Fry, N. K., et al. (2003). Related assemblages of Sulphate-reducing Bacteria associated with Ultradeep gold mines of South Africa and deep basalt aquifers of Washington state. *Environ. Microbiol.* 5, 267–277. doi: 10.1046/j.1462-2920.2003.00408.x

Bay, S. K., Dong, X., Bradley, J. A., Leung, P. M., Grinter, R., Jirapanjawat, T., et al. (2021). Trace gas oxidizers are widespread and active members of soil microbial communities. *Nat. Microbiol.* 6, 246–256. doi: 10.1038/s41564-020-00811-w

Biddle, J. F., Lipp, J. S., Lever, M. A., Lloyd, K. G., Sørensen, K. B., Anderson, R., et al. (2006). Heterotrophic Archaea dominate sedimentary subsurface ecosystems off Peru. *Proc. Natl. Acad. Sci.* 103, 3846–3851. doi: 10.1073/pnas.0600035103

Bolyen, E., Rideout, J. R., Dillon, M. R., Bokulich, N. A., Abnet, C. C., Al-Ghalith, G. A., et al. (2019). Reproducible, interactive, scalable and extensible microbiome data science using QIIME 2. *Nat. Biotechnol.* 37, 852–857. doi: 10.1038/s41587-019-0209-9

Bradley, J. A., Amend, J. P., and LaRowe, D. E. (2018). Bioenergetic controls on microbial ecophysiology in marine sediments. *Front. Microbiol.* 9:180. doi: 10.3389/fmicb.2018.00180

Bradley, J. A., Amend, J. P., and LaRowe, D. E. (2019). Survival of the fewest: microbial dormancy and maintenance in marine sediments through deep time. *Geobiology* 17, 43–59. doi: 10.1111/gbi.12313

Bradley, J. A., Arndt, S., Amend, J. P., Burwicz, E., Dale, A. W., Egger, M., et al. (2020). Widespread energy limitation to life in global subseafloor sediments. *Sci. Adv.* 6:eaba0697. doi: 10.1126/sciadv.aba0697

Bradley, J. A., Arndt, S., Amend, J. P., Burwicz-Galerne, E., and LaRowe, D. E. (2022). Sources and fluxes of organic carbon and energy to microorganisms in global marine sediments. *Front. Microbiol.* 13:910694. doi: 10.3389/fmicb.2022.910694

Braissant, O., Wirz, D., Göpfert, B., and Daniels, A. U. (2010). Use of isothermal microcalorimetry to monitor microbial activities. *FEMS Microbiol. Lett.* 303, 1–8. doi: 10.1111/j.1574-6968.2009.01819.x

Callahan, B. J., McMurdie, P. J., Rosen, M. J., Han, A. W., and Amy Jo, A. (2016). DADA2: high resolution sample inference from Illumina amplicon data. *Nat. Methods* 13, 581–583. doi: 10.1038/nmeth.3869

Casar, C. P., Kruger, B. R., and Osburn, M. R. (2021a). Rock-hosted subsurface biofilms: mineral selectivity drives hotspots for Intraterrestrial life. *Front. Microbiol.* 12:658988. doi: 10.3389/fmicb.2021.658988

Casar, C. P., Momper, L. M., Kruger, B. R., and Osburn, M. R. (2021b). Iron-fueled life in the continental subsurface: deep mine microbial observatory, South Dakota, USA. *ASM J. CD* 87:e0083221. doi: 10.1128/AEM.00832-21

Church, M. J., Hutchins, D. A., and Ducklow, H. W. (2000). Limitation of bacterial growth by dissolved organic matter and Iron in the Southern Ocean. *Appl. Environ. Microbiol.* 66, 455–466. doi: 10.1128/AEM.66.2.455-466.2000

Colwell, F. S., and D'Hondt, S. (2013). Nature and extent of the deep biosphere. *Rev. Mineral. Geochem.* 75, 547–574. doi: 10.2138/rmg.2013.75.17

Cotner, J. B., Sada, R. H., Bootsma, H., Johengen, T., Cavaletto, J. F., and Gardner, W. S. (2000). Nutrient limitation of heterotrophic Bacteria in Florida Bay. *Estuaries* 23, 611–620. doi: 10.2307/1352888

Dick, J. M., LaRowe, D. E., and Helgeson, H. C. (2006). Temperature, pressure, and electrochemical constraints on protein speciation: group additivity calculation of the standard Molal thermodynamic properties of ionized unfolded proteins. *Biogeosciences* 3, 311–336. doi: 10.5194/bg-3-311-2006

Duffner, C., Kublik, S., Fösel, B., Schloter, M., and Schulz, S. (2022). Complete genome sequences of Hydrogenotrophic Denitrifiers. *Microbiol. Resource Announcements* 11, e01020–21. doi: 10.1128/mra.01020-21

Edwards, K. J., Becker, K., and Colwell, F. (2012). The deep, dark energy biosphere: Intraterrestrial life on earth. *Annu. Rev. Earth Planet. Sci.* 40, 551–568. doi: 10.1146/annurev-earth-042711-105500

Haas, A. F., Knowles, B., Lim, Y. W., Somera, T. M. D., Kelly, L. W., Hatay, M., et al. (2014). Unraveling the unseen players in the ocean - a field guide to water chemistry and marine microbiology. *JoVE (J. Visualized Experiments)* 93:e52131. doi: 10.3791/52131

Helgeson, H. C., Kirkham, D. H., and Flowers, G. C. (1981). Theoretical prediction of the thermodynamic behavior of aqueous electrolytes by high pressures and temperatures; IV, calculation of activity coefficients, osmotic coefficients, and apparent Molal and standard and relative partial Molal properties to 600 degrees C and 5kb. *Am. J. Sci.* 281, 1249–1516. doi: 10.2475/ajs.281.10.1249

Higuera-Guisset, J., Rodríguez-Viejo, J., Chacón, M., Muñoz, F. J., Vigués, N., and Mas, J. (2005). Calorimetry of microbial growth using a thermopile based microreactor. *Thermochim. Acta* 427, 187–191. doi: 10.1016/j.tca.2004.09.010

Hoehler, T. M., and Jørgensen, B. B. (2013). Microbial life under extreme energy limitation. *Nat. Rev. Microbiol.* 11, 83–94. doi: 10.1038/nrmicro2939

Johnson, J. W., Oelkers, E. H., and Helgeson, H. C. (1992). SUPCRT92: a software package for calculating the standard Molal thermodynamic properties of minerals, gases, aqueous species, and reactions from 1 to 5000 Bar and 0 to 1000°C. *Comput. Geosci.* 18, 899–947. doi: 10.1016/0098-3004(92)90029-Q

Jørgensen, B. B., and D'Hondt, S. (2006). Ecology - a starving majority deep beneath the seafloor. *Science* 314, 932–934. doi: 10.1126/science.1133796

Kallmeyer, J., Pockalny, R., Adhikari, R. R., Smith, D. C., and D'Hondt, S. (2012). Global distribution of microbial abundance and biomass in subseafloor sediment. *Proc. Natl. Acad. Sci.* 109, 16213–16216. doi: 10.1073/pnas.1203849109

Kirchman, D. (1990). Limitation of bacterial growth by dissolved organic matter in the subarctic Pacific. *Mar. Ecol. Prog. Ser.* 62, 47–54. doi: 10.3354/meps062047

Lin, L.-H., Wang, P.-L., Rumble, D., Lippmann-Pipke, J., Boice, E., Pratt, L. M., et al. (2006). Long-term sustainability of a high-energy, low-diversity crustal biome. *Science* 314, 479–482. doi: 10.1126/science.1127376

McMahon, S., and Parnell, J. (2014). Weighing the deep continental biosphere. *FEMS Microbiol. Ecol.* 87, 113–120. doi: 10.1111/1574-6941.12196

McMurdie, P. J., and Holmes, S. (2013). Phyloseq: an R package for reproducible interactive analysis and graphics of microbiome census data. *PLoS One* 8:e61217. doi: 10.1371/journal.pone.0061217

Miettinen, H., Bomberg, M., and Vikman, M. (2018). Acetate activates deep subsurface fracture fluid microbial communities in Olkiluoto, Finland. *Geosciences* 8:399. doi: 10.3390/geosciences8110399

Momper, Lily, Casar, Caitlin P., and Osburn, Magdalena R.. (2021). A metagenomic view of novel microbial and metabolic diversity found within the deep terrestrial biosphere. *bioRxiv*. doi: 10.1101/2021.05.06.442964

Momper, L., Casar, C. P., and Osburn, M. R. (2023). A metagenomic view of novel microbial and metabolic diversity found within the deep terrestrial biosphere at DeMMO: A microbial Observatory in South Dakota, USA. *Environ. Microbiol.* 25, 3719–3737. doi: 10.1111/1462-2920.16543

Momper, L., Jungbluth, S. P., Lee, M. D., and Amend, J. P. (2017). Energy and carbon metabolisms in a deep terrestrial subsurface fluid microbial community. *ISME J.* 11, 2319–2333. doi: 10.1038/ismej.2017.94

Nealson, K. H., Inagaki, F., and Takai, K. (2005). Hydrogen-driven subsurface Lithoautotrophic microbial ecosystems (SLiMEs): do they exist and why should we care? *Trends Microbiol.* 13, 405–410. doi: 10.1016/j.tim.2005.07.010

Neidhardt, F. C. (2005). "Chemical composition of *Escherichia coli*" in *Escherichia coli* and *Salmonella Typhimurium* cellular and molecular biology. ed. F. C. Neidhardt, vol. *1* (Washington, D.C.: American Society for Microbiology), 3–6.

Nuppunen-Puputti, M., Kietäväinen, R., Raulio, M., Soro, A., Purkamo, L., Kukkonen, I., et al. (2022). Epilithic microbial community functionality in deep oligotrophic continental bedrock. *Front. Microbiol.* 13:826048. doi: 10.3389/fmicb.2022.826048

Nyyssönen, M., Hultman, J., Ahonen, L., Kukkonen, I., Paulin, L., Laine, P., et al. (2014). Taxonomically and functionally diverse microbial communities in deep crystalline rocks of the Fennoscandian shield. *ISME J.* 8, 126–138. doi: 10.1038/ismej.2013.125

Onstott, T. C., Phelps, T. J., Kieft, T., Colwell, F. S., Balkwill, D. L., Fredrickson, J. K., et al. (1999). "A global perspective on the microbial abundance and activity in the deep subsurface" in Enigmatic microorganisms and life in extreme environments. ed. J. Seckbach (Dordrecht: Springer Netherlands), 487–500.

Orsi, W. D., Edgcomb, V. P., Christman, G. D., and Biddle, J. F. (2013). Gene expression in the deep biosphere. *Nature* 499, 205–208. doi: 10.1038/nature12230

Osburn, M. R., Casar, C. P., Kruger, B., Momper, L., Flynn, T. M., and Amend, J. P. (2020). Contrasting variable and stable subsurface microbial populations: An ecological time series analysis from the deep mine microbial observatory. South Dakota, USA: Ecology.

Osburn, M. R., Kruger, B., Masterson, A. L., Casar, C. P., and Amend, J. P. (2019). Establishment of the deep mine microbial observatory (DeMMO), South Dakota, USA, a geochemically stable portal into the deep subsurface. *Front. Earth Sci.* 7:196. doi: 10.3389/feart.2019.00196

Osburn, M. R., LaRowe, D. E., Momper, L. M., and Amend, J. P. (2014). Chemolithotrophy in the continental deep subsurface: Sanford underground research facility (SURF), USA. *Front. Microbiol.* 5:610. doi: 10.3389/fmicb.2014.00610

Pachiadaki, M. G., Rédou, V., Beaudoin, D. J., Burgaud, G., and Edgcomb, V. P. (2016). Fungal and prokaryotic activities in the marine subsurface biosphere at Peru margin and Canterbury Basin inferred from RNA-based analyses and microscopy. *Front. Microbiol.* 7:846. doi: 10.3389/fmicb.2016.00846

Parada, A. E., Needham, D. M., and Fuhrman, J. A. (2016). Every base matters: assessing small subunit RRNA primers for marine microbiomes with mock communities, time series and global field samples. *Environ. Microbiol.* 18, 1403–1414. doi: 10.1111/1462-2920.13023

Parikka, K. J., Le Romancer, M., Wauters, N., and Jacquet, S. (2017). Deciphering the virus-to-prokaryote ratio (VPR): insights into virus–host relationships in a variety of ecosystems. *Biol. Rev.* 92, 1081–1100. doi: 10.1111/brv.12271

Parkes, R. J., Webster, G., Cragg, B. A., Weightman, A. J., Newberry, C. J., Ferdelman, T. G., et al. (2005). Deep sub-seafloor prokaryotes stimulated at interfaces over geological time. *Nature* 436, 390–394. doi: 10.1038/nature03796

Payne, W. J., and Wiebe, W. J. (1978). Growth yield and efficiency in chemosynthetic microorganisms. *Ann. Rev. Microbiol.* 32, 155–183. doi: 10.1146/annurev.mi.32.100178.001103

Phelps, T. J., Murphy, E. M., Pfiffner, S. M., and White, D. C. (1994). Comparison between geochemical and biological estimates of subsurface microbial activities. *Microb. Ecol.* 28, 335–349. doi: 10.1007/BF00662027

Price, P. B., and Sowers, T. (2004). Temperature dependence of metabolic rates for microbial growth, maintenance, and survival. *Proc. Natl. Acad. Sci.* 101, 4631–4636. doi: 10.1073/pnas.0400522101

Quast, C., Pruesse, E., Yilmaz, P., Gerken, J., Schweer, T., Yarza, P., et al. (2013). The SILVA ribosomal RNA gene database project: improved data processing and web-based tools. *Nucleic Acids Res.* 41, D590–D596. doi: 10.1093/nar/gks1219

Robador, A., LaRowe, D. E., Finkel, S. E., Amend, J. P., and Nealson, K. H. (2018). Changes in microbial energy metabolism measured by Nanocalorimetry during growth phase transitions. *Front. Microbiol.* 9:109. doi: 10.3389/fmicb.2018.00109

Robador, A., LaRowe, D. E., Jungbluth, S. P., Lin, H.-T., Rappé, M. S., Nealson, K. H., et al. (2016). Nanocalorimetric characterization of microbial activity in deep subsurface oceanic crustal fluids. *Front. Microbiol.* 7:454. doi: 10.3389/fmicb.2016.00454

Rohwerder, T., Schippers, A., and Sand, W. (1998). Determination of reaction energy values for biological pyrite oxidation by calorimetry. *Thermochim. Acta* 309, 79–85. doi: 10.1016/S0040-6031(97)00352-3

Santini, J. M., Sly, L. I., Wen, A., Comrie, D., De Wulf-Durand, P., and Macy, J. M. (2002). New Arsenite-oxidizing Bacteria isolated from Australian gold mining environments--phylogenetic relationships. *Geomicrobiol J.* 19, 67–76. doi: 10.1080/01490450231724617 4

Schippers, A., Hallmann, R., Wentzien, S., and Sand, W. (1995). Microbial diversity in uranium mine waste heaps. *Appl. Environ. Microbiol.* 61, 2930–2935. doi: 10.1128/aem.61.8.2930-2935.1995

Schippers, A., Neretin, L. N., Kallmeyer, J., Ferdelman, T. G., Cragg, B. A., John Parkes, R., et al. (2005). Prokaryotic cells of the deep sub-seafloor biosphere identified as living Bacteria. *Nature* 433, 861–864. doi: 10.1038/nature03302

Schroter, A. W., and Sand, W. (1993). Estimations on the degradability of ores and bacterial leaching activity using short-time microcalorimetric tests. *FEMS Microbiol. Rev.* 11, 79–86. doi: 10.1111/j.1574-6976.1993.tb00270.x

Shock, E. L., Oelkers, E. H., Johnson, J. W., Sverjensky, D. A., and Helgeson, H. C. (1992). Calculation of the thermodynamic properties of aqueous species at high pressures and temperatures. Effective electrostatic radii, dissociation constants and standard partial Molal properties to 1000 °C and 5 Kbar. *J. Chem. Soc. Faraday Trans.* 88, 803–826. doi: 10.1039/FT9928800803

Tanger, J. C., and Helgeson, H. C. (1988). Calculation of the thermodynamic and transport properties of aqueous species at high pressures and temperatures; revised equations of state for the standard partial Molal properties of ions and electrolytes. *Am. J. Sci.* 288, 19–98. doi: 10.2475/ajs.288.1.19

Teske, A. P. (2005). The deep subsurface biosphere is alive and well. *Trends Microbiol.* 13, 402–404. doi: 10.1016/j.tim.2005.07.004

Thingstad, T. F. (2000). Elements of a theory for the mechanisms controlling abundance, diversity, and biogeochemical role of lytic bacterial viruses in aquatic systems. *Limnol. Oceanogr.* 45, 1320–1328. doi: 10.4319/lo.2000.45.6.1320

Thingstad, T. F., Våge, S., Storesund, J. E., Sandaa, R.-A., and Giske, J. (2014). A theoretical analysis of how strain-specific viruses can control microbial species diversity. *Proc. Natl. Acad. Sci.* 111, 7813–7818. doi: 10.1073/pnas.1400909111

Urich, T., Lanzén, A., Stokke, R., Pedersen, R. B., Bayer, C., Thorseth, I. H., et al. (2014). Microbial community structure and functioning in marine sediments associated with diffuse hydrothermal venting assessed by integrated Meta-omics. *Environ. Microbiol.* 16, 2699–2710. doi: 10.1111/1462-2920.12283

Wentzien, S., Sand, W., Albertsen, A., and Steudel, R. (1994). Thiosulfate and tetrathionate degradation as well as biofilm generation by Thiobacillus intermedius and *Thiobacillus versutus* studied by microcalorimetry, HPLC, and ion-pair chromatography. *Arch. Microbiol.* 161, 116–125. doi: 10.1007/BF00276471

Whitman, W. B., Coleman, D. C., and Wiebe, W. J. (1998). Prokaryotes: the unseen majority. *Proc. Natl. Acad. Sci.* 95, 6578–6583. doi: 10.1073/pnas.95.12.6578

Wickham, H. (2016). *ggplot2: Elegant Graphics for Data Analysis*. New York: Springer-Verlag.

Yanagawa, K., Morono, Y., Yoshida-Takashima, Y., Eitoku, M., Sunamura, M., Inagaki, F., et al. (2014). Variability of subseafloor viral abundance at the geographically and geologically distinct continental margins. *FEMS Microbiol. Ecol.* 88, 60–68. doi: 10.1111/1574-6941.12269

Yilmaz, P., Parfrey, L. W., Yarza, P., Gerken, J., Pruesse, E., Quast, C., et al. (2014). The SILVA and 'all-species living tree project (LTP)' taxonomic frameworks. *Nucleic Acids Res.* 42, D643–D648. doi: 10.1093/nar/gkt1209

Zhao, R., Mogollón, J. M., Roerdink, D. L., Thorseth, I. H., Økland, I., and Jørgensen, S. L. (2021). Ammonia-oxidizing Archaea have similar power requirements in diverse marine Oxic sediments. *ISME J.* 15, 3657–3667. doi: 10.1038/s41396-021-01041-6

Zinke, L. A., Mullis, M. M., Bird, J. T., Marshall, I. P. G., Jørgensen, B. B., Lloyd, K. G., et al. (2017). Thriving or surviving? Evaluating active microbial guilds in Baltic Sea sediment. *Environ. Microbiol. Rep.* 9, 528–536. doi: 10.1111/1758-2229.12578

frontiers | Frontiers in Microbiology

TYPE Original Research
PUBLISHED 31 January 2025
DOI 10.3389/fmicb.2024.1523912

OPEN ACCESS

EDITED BY
Alberto Robador,
University of Southern California,
United States

REVIEWED BY
William J. Brazelton,
The University of Utah, United States
Annette Ruth Rowe,
University of Cincinnati, United States

*CORRESPONDENCE
Alta E. G. Howells
✉ alta.howells@bmsis.org

RECEIVED 06 November 2024
ACCEPTED 23 December 2024
PUBLISHED 31 January 2025

CITATION
Howells AEG, Quinn LM, Silva MG, Akiyama K, Fifer LM, Boyer G, Kashyap S, Robinson K, Broddrick J, Shock EL and Hoehler TM (2025) Energetic and genomic potential for hydrogenotrophic, formatotrophic, and acetoclastic methanogenesis in surface-expressed serpentinized fluids of the Samail Ophiolite.
Front. Microbiol. 15:1523912.
doi: 10.3389/fmicb.2024.1523912

Energetic and genomic potential for hydrogenotrophic, formatotrophic, and acetoclastic methanogenesis in surface-expressed serpentinized fluids of the Samail Ophiolite

Alta E. G. Howells[1,2]*, Lilja M. Quinn[2,3], Miguel G. Silva[2,4], Kylie Akiyama[2,5], Lucas M. Fifer[6,7], Grayson Boyer[8], Srishti Kashyap[9], Kirt Robinson[2,8], Jared Broddrick[1], Everett L. Shock[8] and Tori M. Hoehler[1]

[1]NASA Ames Research Center, Moffett Field, CA, United States, [2]Blue Marble Space Institute of Sciences, San Francisco, CA, United States, [3]Department of Biology, Washington University, St. Louis, MO, United States, [4]Department of Aeronautics and Astronautics, Stanford University, Palo Alto, CA, United States, [5]Department of Bioengineering, University of California, Berkeley, Berkeley, CA, United States, [6]Department of Earth and Space Sciences, University of Washington, Seattle, WA, United States, [7]Astrobiology Program, University of Washington, Seattle, WA, United States, [8]School of Earth and Space Exploration, Arizona State University, Tempe, AZ, United States, [9]Department of Geological Sciences, University of Colorado, Boulder, CO, United States

Serpentinization, the reaction of water with ultramafic rock, produces reduced, hyperalkaline, and H_2-rich fluids that support a variety of hydrogenotrophic microbial metabolisms. Previous work indicates the occurrence of methanogenesis in fluids from the actively serpentinizing Samail Ophiolite in the Sultanate of Oman. While those fluids contain abundant H_2 to fuel hydrogenotrophic methanogenesis ($CO_2 + 4H_2 \rightarrow CH_4 + 2H_2O$), the concentration of CO_2 is very low due to the hyperalkalinity (> pH 11) and geochemistry of the fluids. As a result, species such as formate and acetate may be important as alternative methanogenic substrates. In this study we quantified the impact of inorganic carbon, formate and acetate availability for methanogenic metabolisms, across a range of fluid chemistries, in terms of (1) the potential diffusive flux of substrates to the cell, (2) the Affinity (Gibbs energy change) associated with methanogenic metabolism, and (3) the energy "inventory" per kg fluid. In parallel, we assessed the genomic potential for the conduct of those three methanogenic modes across the same set of fluids and consider the results within the quantitative framework of energy availability. We find that formatotrophic methanogenesis affords a higher Affinity (greater energetic yield) than acetoclastic and hydrogenotrophic methanogenesis in pristine serpentinized fluids and, in agreement with previous studies, find genomic evidence for a methanogen of the genus *Methanobacterium* to carry out formatotrophic and hydrogenotrophic methanogenesis, with the possibility of even using bicarbonate as a supply of CO_2. Acetoclastic methanogenesis is also shown to be energetically favorable in these fluids, and we report the first detection of a potential acetoclastic methanogen of the family *Methanosarcinaceae*, which forms a distinct clade with a genome from the serpentinizing seafloor hydrothermal vent field, Lost City. These results demonstrate the applicability of an energy availability framework for interpreting methanogen ecology in serpentinizing systems.

KEYWORDS
methanogenesis, serpentinization, substrate flux, bioenergetics, genomics

1 Introduction

In the subsurface, where energy from sunlight is not available to life, microorganisms must rely on redox chemical disequilibria as a source of energy. Such disequilibria can result from the reaction of water and rocks. One example is the process of serpentinization, where primary ferrous iron minerals in reduced ultramafic rock from the upper mantle react with water to produce secondary ferric iron minerals and H_2 (McCollom and Bach, 2009). In addition to being H_2-rich, fluids generated through serpentinization are reduced and hyperalkaline. H_2 generated from this process can serve as an electron donor for many microbial metabolisms. When the serpentinized fluid mixes with unreacted fluids rich in electron acceptors, chemical disequilibrium is achieved, and the resulting energy can support life. The energy-rich, habitable zones created in the subsurface by serpentinization are of great interest to astrobiology. Evidence shows that water-rock reactions like serpentinization may occur on the moon of Saturn, Enceladus, and supply H_2 detected in its plumes (Waite et al., 2017). Water-rock reactions may also be a relevant process for Europa, a moon of Jupiter (Vance et al., 2023). Serpentinizing systems on Earth provide a window into the potential habitability of Enceladus, Europa, and possibly other ocean worlds in our outer solar system. Therefore, of the many subsurface processes that can support life through chemical disequilibrium, we are highly motivated to understand how the subsurface process of serpentinization supports microbial life.

While typically thought of as being associated with the ocean floor along ocean-spreading ridges, serpentinization also occurs where the upper mantle has been uplifted and exposed on the continental crust. One example of continental serpentinization is the Samail Ophiolite in the Sultanate of Oman. Because the Samail ophiolite is located in an arid desert, the fluids receive little influence from surrounding vegetation and the fluid chemistry and associated microbiology are predominantly influenced by water-rock reactions.

The geological and physical processes governing fluid chemistry in Oman are well characterized through geochemical modeling and geochemical and mineralogical characterization (Kelemen et al., 2011; Miller et al., 2016; Canovas et al., 2017; Leong et al., 2021; Nothaft et al., 2021a). In Oman, there are two distinct fluid types. Type II fluids—representative of pristine serpentinized fluids—reacted in the deep subsurface (>500 meters). Type II fluids are highly reduced $CaOH_2$ solutions that have high concentrations of H_2, are hyperalkaline (>pH 11), and have low concentrations of dissolved inorganic carbon (DIC). Type I fluids are partially reacted in the shallow subsurface (<50 meters) and are $MgHCO_3^+$ solutions. Type I fluids are circumneutral (pH 7–8), have a lower concentration of H_2 than Type II fluids, and are more oxidized due to the influence from the atmosphere (Leong et al., 2021). The two fluid types can mix in the subsurface and at the surface when expressed through fault lines and fissures to create steep geochemical gradients, making the process of serpentinization in Oman an ideal environment to understand the microbiological response to extreme conditions, namely alkaline pH and carbon limitation.

Methanogenesis, particularly hydrogenotrophic methanogenesis ($4H_2 + CO_2 \rightarrow CH_4 + 2H_2O$), has long been considered as a model for other ocean worlds given that methanogens are deeply rooted in Earth's tree of life and utilize a metabolism that could readily proceed independently of the input of sunlight energy. Given the ample supply of H_2, methanogenesis is an energetically favorable process in serpentinizing systems and a growing body of evidence points to its occurrence therein (Miller et al., 2016; Canovas et al., 2017; Rempfert et al., 2017; Fones et al., 2021; Nothaft et al., 2021a; Nothaft et al., 2021b; Thieringer et al., 2023; Howells et al., 2022). However, serpentinization typically yields fluids that are highly depleted in dissolved inorganic carbon (DIC) and, at high pH, have exceedingly low concentrations of the methanogenic substrate CO_2. The dissolved inorganic carbon concentration in pristine Type II serpentinized fluids can be as low as 20 μM (Howells et al., 2022). For the mesophilic, neutrophilic organism *Methanobacterium congolense*, Chen et al. (2019) report a Monod half-saturation constant for DIC of $K_{S\text{-}DIC}$ = 2.2 mM, meaning that the cell will grow at half of its maximum rate at that DIC concentration. Below that concentration, the growth rate decreases approximately linearly with respect to DIC concentration. The implication of environmental DIC concentrations 100-fold lower than the reported $K_{S\text{-}DIC}$ is, therefore, a 100-fold lower growth rate. The situation is compounded for CO_2, which is indicated by experimental and X-ray crystallographic studies to be the form of DIC that reacts during the first step of methanogenesis (Vorholt and Thauer, 1997) in presently characterized methanogens: based on the pKa of carbonic acid (~6.5) and the pH of the fluids (~11.5) (see modeled CO_2 concentrations in Howells et al., 2022) the difference in CO_2 concentration is eight orders of magnitude. DIC availability may thus significantly limit methanogenesis in serpentinizing systems.

Previous work suggests that DIC availability may indeed be a substantial influence on methanogen ecology for fluids that have undergone the greatest extent of water-rock reaction (Type II). Fones et al. (2021) reported that methanogens of the genus *Methanobacterium*, associated with Type II fluids in the Samail ophiolite, have genomic potential for the uptake of formate and conversion of formate to CO_2 for hydrogenotrophic methanogenesis (Fones et al., 2021). Furthermore, Type II *Methanobacterium* genomes show evidence for loss of H_2 utilization, suggesting that those organisms may rely on formate as an electron donor instead. In parallel, incubations with ^{14}C formate and ^{14}C bicarbonate showed significant methanogenic activity with formate and no activity for bicarbonate in Type II fluids. In contrast *Methanobacterium* genomes from Type I fluids reflect an ability to carry out hydrogenotrophic methanogenesis with H_2 as an electron donor, and methanogenesis from both formate and bicarbonate was observed. In agreement with Fones et al. (2021), Thieringer et al. (2023) observed the distinct Type I and Type II *Methanobacterium* genomes in shotgun metagenome sequencing data from recently drilled bore-hole fluids. However, in addition to formate utilization, they found genomic evidence for acetate uptake by *Methanobacterium* as a carbon source. No studies on serpentinized fluids in Oman have shown evidence for acetoclastic methanogens, namely of the families *Methanosarcinaceae* and *Methanosaetacea*. Potential acetoclastic methanogens of the family *Methanosarcinaceae* have only been detected in the seafloor hydrothermal serpentinized fluids of Lost City (McGonigle et al., 2020; Brazelton et al., 2022) and in no other serpentinizing systems studied to date (Colman et al., 2024).

The energy yield from acetoclastic and formatotrophic methanogenesis is generally lower than from CO_2 reduction with H_2 (Stams and de Sousa, 2019). However, these pathways could become more energetically favorable and support microbial life in

environments where CO_2 is limited but acetate or formate are available. Both acetate and formate can be produced abiotically in serpentinization-driven hydrothermal systems through Fischer-Tropsch-type (FTT) synthesis reactions, which involve the reduction of inorganic carbon (CO or CO_2) with H_2 under high-temperature, high-pressure conditions (McCollom and Seewald, 2007; McDermott et al., 2015) and therefore are a viable carbon source in serpentinizing systems. Both reactions, summarized in Table 1, can produce inorganic carbon, which can feed into the hydrogenotrophic pathways for methanogenesis. Furthermore, serpentinized fluids provide a unique opportunity to examine how low CO_2 concentrations as a product of these reactions influence overall energy availability.

Multiple authors (Fones et al., 2021; Nothaft et al., 2021b; Thieringer et al., 2023; Colman et al., 2022) have pointed to low DIC availability as potentially influencing the microbial ecology of serpentinizing systems in Oman. In this study we quantitatively examine the influence of DIC availability on methanogenesis from three perspectives: (1) potential flux of substrates to the cell, (2) chemical affinity for the methanogenic metabolism, and (3) energy inventory per volume of fluid. Here, we focus on surface expressions of serpentinized fluids which allow ready access to significant chemical diversity (Canovas et al., 2017; Leong et al., 2021; Howells et al., 2022). Surface fluids largely retain both geochemical and biological similarity relative to subsurface fluids, while potentially also allowing us to consider the influence of mixing and atmospheric contact (Leong et al., 2021). For this study we collected and analyzed fluids for the concentration of acetate and formate and combined this new data set with DIC, H_2 and CH_4 values reported in Howells et al. (2022) for quantitative analyses of hydrogenotrophic, formatotrophic and acetoclastic methanogenesis (Table 1). We also performed shotgun metagenome sequencing on Type II fluid microbial communities to assess the genomic potential for these metabolisms. In carrying out a comparative energetic and genomic study, we broaden our understanding of possible metabolic strategies in extreme environments and inform our understanding of habitability.

2 Methods

2.1 Organic acid analysis

In this study, we characterized formate and acetate concentrations in surface-expressed fluids at sites, which are summarized in Table 2. The major ion fluid chemistry of these sites was previously reported on by Leong et al. (2021), and microbial community composition was previously reported by Howells et al. (2022) and Howells et al. (2023). Water samples from surface-expressed fluids were collected using a polytetrafluoroethylene (PTFE) scoop for organic acid analyses. The collected water was transferred to a one-liter Nalgene high-density polyethylene (HDPE) bottle. The bottle had a polypropylene tube inserted through a hole cut into the lid leading to a Covidien 140 mL plastic syringe. All plastic components were rinsed three times with each sample before filtration. This closed-system (albeit not airtight) setup was designed to minimize contamination and loss of volatiles from the sample as it was being apportioned into different types of sample containers.

Water was then filtered through an Acrodisc® Supor® membrane 0.8/0.2 µm filter to remove particulates and cells. Prior to sample collection, >130 mL of sample was rinsed through the filters and not collected for the analyses. Approximately 20 mL of filtered water was then collected for organic acid anion analysis. Samples for organic acid analysis were collected in 20 mL Qorpak amber glass bottles with PTFE cap inserts. Prior to the field expedition, the amber glass bottles and their PTFE cap inserts were first rinsed three times with DI, and then the cap inserts were soaked for 24 h while the glass bottles were muffled in a furnace at 500°C for 24 h in order to remove any potential residual organic carbon. Then, the cap inserts were dried, and these bottles were also closed for transport to the field. Upon return from the field, the amber glass bottles were refrigerated until the time of analysis, which was under 5 weeks for all samples from the time of their collection.

In the lab, organic acid analysis was performed using a Dionex ICS-1500 ion chromatograph equipped with a Dionex IonPac® ICE-AS6 ion exclusion column (9 × 250 mm), a Dionex AMMS-ICE 300 suppressor, a Dionex DS6 heated conductivity cell detector, and a Dionex AS40 autosampler. Samples were spiked with 25 µL of 3.75 M hydrochloric acid prior to analysis so that sample pH was <7 in order for organic acids to speciate into the proper proportions of associated versus dissociated for interaction with the column. Each sample was run twice, and each run consisted of duplicate injections. The first run used 0.60 mM heptafluorobutyric acid (HFBA) as an eluent and was designed to isolate the formate peak from eluting interferences. The second run used 0.15 mM HFBA to isolate the acetate peak. In both cases, the eluent flow rate was set to 1.00 mL/min. The suppressor regenerant was 5.00 mM tetrabutylammonium hydroxide (TBAOH), set to a nitrogen pressure-driven flow of ~3 mL/min. Five-point calibration curves with $R^2 > 0.993$ were generated for formate and acetate using standards purchased from High-Purity Standards. Natural sample peaks were verified in all cases by overlaying sample and standard chromatograms and, in some cases, verified by standard addition. Instrument detection limits for organic acid anions were ~0.2 µM.

TABLE 1 Summary of redox reactions for methanogenic metabolisms examined in this study.

Methanogenic metabolism	Reaction
Hydrogenotrophic	$4H_2 + HCO_3^- + H^+ \rightarrow CH_4 + 3H_2O$
Formatotrophic	$4CHO_2^- + H^+ + H_2O \rightarrow CH_4 + 3HCO_3^-$
Acetoclastic	$C_2H_3O_2^- + H_2O \rightarrow CH_4 + HCO_3^-$

2.2 Energetic calculations

The concentration of major ions and the concentration of Si in this study were previously reported on by Leong et al. (2021) and Howells et al. (2022). For details on methods for fluid sample collection and analyses, please see those studies. Chemical speciation of site fluids to determine chemical activities of reactants and products for methanogenesis reactions summarized in Table 1 were performed on the Water-Organic-Rock-Microbe (WORM) Portal[1] using the AqEquil

1 https://worm-portal.asu.edu

10.3389/fmicb.2024.1523912

TABLE 2 Formate and acetate data collected for this study.

Sample	Fluid location	Fluid	pH	Temp.	Si[a]	% Serp[b]	H_2[a]	DIC[a]	Acetate	Formate
		Type		°C	Molality	Fluid	Molality	Molality	Molality	Molality
140115Z	Al Banah - Suface	Type II	11.3	32.2	1.4E-06	100.0	2.3E-04	3.4E-05	3.2E-06	3.0E-06
140115X	Al Banah - Surface	Type II	11.4	29.5	2.2E-06	99.9	2.3E-04	3.1E-05	4.1E-06	4.3E-06
140115Y	Al Banah - Surface	Type II	11.6	24.5	2.2E-06	99.9	2.1E-05	1.1E-04	2.9E-06	1.7E-06
140114S	Falej North - Surface	Mix	7.7	21	2.0E-04	76.5	1.5E-08	4.4E-03	8.5E-07	
140114U	Falej North - Surface	Type II	11.4	21.7	7.4E-06	99.3	1.7E-08	1.8E-04	2.5E-06	3.3E-06
140114V	Falej North - Surface	Type II	11.4	24.4	2.8E-06	99.8	1.7E-07	2.3E-04		9.8E-07
140114T	Falej North - Surface	Type II	11.4	27.2	1.8E-06	99.9	2.8E-05	4.2E-05	3.0E-06	5.5E-06
140114R	Falej North - Surface	Type II	11.6	21.1	2.4E-06	99.9	1.2E-08	4.2E-05		
140113O	Falej South - Surface	Type II	11.4	28.4	3.7E-06	99.7	3.9E-05	5.7E-05	3.9E-06	4.8E-06
140113P	Falej South - Surface	Type II	11.5	25.9	1.9E-06	99.9	6.6E-05	4.6E-05	2.2E-06	1.6E-06
140111G	Qafifah - Surface	Mix	8.9	22.6	2.8E-04	67.5	2.4E-07	4.1E-03	1.2E-06	
140111H	Qafifah - Surface	Mix	10.2	20.2	1.5E-04	83.0	1.1E-06	1.8E-03	6.6E-07	2.0E-06
140111I	Qafifah - Surface	Mix	10.9	18.8	1.0E-04	88.3	2.1E-06	8.5E-04	9.2E-07	1.3E-06
140111F	Qafifah - Surface	Type II	11.6	23.8	1.1E-05	98.9	2.6E-04	4.1E-05	1.8E-06	1.9E-06
140116B	Shmait - Surface	Mix	7.9	26.5	3.0E-04	64.4	6.2E-08	5.1E-03	1.5E-06	
140116C	Shmait - Surface	Mix	8.7	27.3	2.8E-04	67.2	2.2E-06	4.7E-03	1.6E-06	
140116D	Shmait - Surface	Mix	9.1	27.1	2.6E-04	69.4	1.3E-05	4.0E-03	1.4E-06	
140117J	Shmait - Surface	Mix	11.3	31.6	4.9E-05	94.4	2.2E-04	7.0E-05		5.3E-07
140117I	Shmait - Surface	Type II	11.3	32.3	2.0E-06	99.9	2.3E-04	4.7E-05		4.9E-07
140117G	Shmait - Surface	Type II	11.4	30.5	1.5E-06	100.0	2.8E-06	1.9E-05		1.5E-06
140117F	Shmait - Surface	Type II	11.5	26.2	2.7E-06	99.8	2.7E-04	2.9E-05	1.5E-06	1.2E-06
140117H	Shmait - Surface	Type II	11.5	29.6	1.7E-06	99.9	2.3E-04	2.9E-05		1.1E-06
140110B	Wadi Dima - Surface	Mix	8.4	23.5	1.8E-04	78.5	7.0E-09	3.6E-03		4.4E-07
140112L	Wadi Dima - Surface	Mix	9.8	21.3	1.1E-04	87.0	9.0E-09	1.9E-03		7.4E-07
140110D	Wadi Dima - Surface	Mix	10.4	21.8	9.1E-05	89.3	5.6E-08	8.1E-04		7.5E-07
140112M	Wadi Dima - Surface	Type II	11.4	28.2	5.6E-06	99.5	3.1E-05	5.2E-05		7.4E-07
140112K	Wadi Dima - Surface	Type II	11.4	26.9	3.9E-06	99.7	4.9E-07	3.6E-05	7.9E-07	9.4E-07
140110C	Wadi Dima - Surface	Type II	11.4	27	4.3E-06	99.6	6.4E-06	5.3E-05	1.3E-06	4.2E-06
NSHQ142014	Well*	Type II	11.4	34.9	7.0E-06	99.3	6.7E-04			
NSHQ142015	Well*	Type II	11.3	35.3	5.0E-06	99.6	2.9E-03	1.9E-04	1.2E-06	1.7E-06
NSHQ142016	Well*	Type II	11.2	35.8	5.0E-06	99.6	2.2E-04			
NSHQ212015	Well*	Mix	7.4	33.7	7.8E-04	7.8		2.6E-03	4.9E-07	1.1E-06
NSHQ3B2015	Well*	Mix	8.4	30.1	2.5E-04	71.0		2.5E-03	4.7E-07	1.2E-06
NSHQ42014	Well*	Mix	10.6	35.1	2.0E-04	76.8		2.2E-04	4.4E-06	1.5E-06
NSHQ42015	Well*	Mix	10.5	33.3	1.5E-05	98.4		1.8E-04	1.4E-06	2.3E-06
WAB1032015	Well*	Mix	8.2	30.4	4.8E-04	43.5		2.3E-03	4.3E-07	1.1E-06
WAB1032016	Well*	Type I	8.2	33.8	8.5E-04	0.0				
WAB1042016	Well*	Mix	8.5	33.4	2.1E-04	75.3				
WAB1052016	Well*	Mix	8.3	31.6	4.3E-05	95.1				
WAB1882015	Well*	Mix	8.7	34.2	2.3E-04	72.7		2.3E-03	3.8E-06	1.0E-06
WAB1882016	Well*	Mix	7.6	33	7.9E-04	7.4				
WAB552015	Well*	Type II	9.3	30	6.0E-06	99.4		2.6E-03	2.0E-06	1.4E-06

(Continued)

TABLE 2 (Continued)

Sample	Fluid location	Fluid	pH	Temp.	Si[a]	% Serp[b]	H_2[a]	DIC[a]	Acetate	Formate
WAB552016	Well*	Type II	9.2	34.7	6.0E-06	99.4				
WAB562015	Well*	Type II	10.6	33.3	1.0E-05	99.0	1.8E-04			
WAB712015	Well*	Mix	11.0	33.1	1.7E-05	98.1			6.3E-07	1.5E-06
WAB712016	Well*	Mix	11.1	34.5	2.4E-05	97.3				

[a]Si, H_2, and DIC values from Howells et al. (2022) (surface) and Rempfert et al. (2017) (well).
[b]% Serp. Fluid calculated from Si values in table and the modeled Type II fluid Si concentration reported in Howells et al. (2022).
* Formate and acetate values from Rempfert et al. (2017).

Python package (Boyer et al., 2024) and wrapper for EQ3/6 (Wolery, 2013). During speciation, all redox reactions involving N, C, S, and P were suppressed. The charge balance is set based on pH or Cl^- (or no charge balance), depending on the data available for each sample site. Redox state was set based on O_2 for fluids with greater influence from the atmosphere (Type I and mix) and H_2 for pristine serpentinized fluid (Type II). Chemical affinities and energy supplies for redox reactions were calculated for speciated samples using the calculate_energy function included in AqEquil. This function calculates the chemical affinity of a given reaction, *r*, using the equation published in Shock et al. (2010),

$$A_r \equiv -\left(\frac{\delta \Delta_r G}{\delta \xi_r}\right)_{P,T} \tag{1}$$

which is Gibbs energy change of reaction, *r*, ($\Delta_r G$) with respect to reaction progress (ξ). $\Delta_r G$ is solved by,

$$\Delta_r G = \Delta_r G^\circ + RTlnQ_r \tag{2}$$

with *R* being the universal gas constant, *T* the temperature of the fluid in Kelvin, $\Delta_r G^\circ$ the standard state Gibbs energy of the reaction given by

$$\Delta_r G^\circ = -RTlnK_r \tag{3}$$

and Q_r the activity product given by

$$Q_r = \prod (a_i)^{\nu_{i,r}} \tag{4}$$

Q_r is solved with the chemical activities estimated using the AqEquil package described above where a_i is the activity (*a*) of the given reactant or product (*i*) raised to its stoichiometry in the reaction ($\nu_{i,r}$) (positive for products and negative for reactants). From Equations 1–4 we can solve for affinity,

$$A_r = RTln\left(\frac{K_r}{Q_r}\right) \tag{5}$$

Chemical affinities calculated using Equation 5 were normalized according to the number of moles CH_4 produced (kJ per mole CH_4). Energy supplies for each reaction (E_r) (J per kg fluid) were calculated using equations outlined in Howells et al. (2022). Briefly, affinity (A_r) in J per mole reaction is multiplied by the concentration of the limiting reactant (m_{lim}) and divided by the stoichiometric coefficient of the limiting reactant (ν_{lim}), as summarized below.

$$E_r = \frac{A_r [m_{lim}]}{\nu_{lim}} \tag{6}$$

Using Equation 6, energy supplies were calculated in AqEquil with the parameter as_written set to False to sum all chemical species in equilibrium with a designated substrate. This accounts for the fact that as the substrate is consumed in 1 kg of fluid, the system re-equilibrates to supply more of that substrate. For example, as HCO_3^- is consumed from a pool of inorganic carbon, the system re-equilibrates with other inorganic carbon species ($CO_{2(aq)}$, CO_3^{2-}, $CaHCO_3^+$, etc.) to continuously supply CO_2 until the whole inorganic carbon pool is consumed. The other option in AqEquil is to set the parameter as_written to True, which only uses the concentration of the substrate specified in the reaction and no other (e.g., HCO_3^- and no other forms of DIC), however this option was not used in the current study. The output of AqEquil with all estimated chemical activities can be found in Supplementary Table S1.

2.3 Meta-analysis of 16S rRNA gene amplicon sequencing

For the meta-analysis of microbial diversity in subsurface well and surface-expressed serpentinized fluids we downloaded raw 16S rRNA gene amplicon sequencing data from NCBI Short Read Archive (SRA). For well fluids, we downloaded data from SRA accession SRP092764 (Rempfert et al., 2017). For surface data we downloaded from SRA accession, SRP308538 (Howells et al., 2022). Both sets of data were generated using the EMP primer set (Caporaso et al., 2012) and Illumina MiSeq sequencing platform. Rempfert et al. (2017) used the 2 × 250 Illumina method, Howells et al. (2022) used the 1 × 150 Illumina method. Raw data downloaded from NCBI SRA was processed using programs within the QIIME2 version 2021-4 wrapper following protocol described in Howells et al. (2022). Briefly, sequencing quality was checked using FastQC and trimmed based on a quality score of 25 or lower. Sequences were denoised and resolved to 100% sequence similarity with DADA2 (Callahan

et al., 2016). The resulting amplicon sequence variants (ASVs) were rarefied to 2,500 counts per sample. Alpha diversity analysis carried out in QIIME2 using the q2-diversity plugin. Taxonomic assignment was done using the QIIME2 plugin, q2-feature-classifier with the naïve Bayes method with pre-trained classifier built using the Green Genes 13_8 99 16S rRNA gene database (DeSantis et al., 2006). We acknowledge Green Genes is an older database, however we find that Green Genes produces comparable taxonomic assignments as the more recent SILVA ribosomal RNA gene database (Quast et al., 2012) as shown by Howells et al. (2023). The rarefied ASV table was exported from QIIME2 and beta diversity (NMDS) analysis carried out with the R package, vegan (version 2.5-6) within the R version 3.6.0 (2019-04-26) (R Core Team, 2021). For the NMDS analysis, rarefied frequencies of ASVs at each site were converted to relative abundances and square-root transformed. Bray–Curtis dissimilarity was calculated on the transformed relative abundances. NMDS ordination was conducted with 1,000 permutations and two dimensions. The stress for the NMDS ordination was 0.2. Supplementary Table S2 is the relative abundance of each ASV at each study site and is used for downstream statistical analyses. Supplementary Table S3 relative abundance of ASVs grouped at the genus level (taxonomy included).

2.4 Shotgun metagenome sequencing

Sediments for shotgun metagenome sequencing were collected simultaneously for 16S rRNA gene amplicon sequencing using the same approach described in Howells et al. (2022) from sites 140112K, 140117H, and 140111F. Pictures of the sampling sites and a description of the sediments can be found in Supplementary Figure S1. In the lab, DNA was extracted using the Quick-DNA Miniprep Plus Kit (catalog #D4068) from Zymo. For each Zymo prep, we extracted DNA from ~500 mg (kit protocol recommends 200 mg, but 500 mg was optimal for our sediments) of wet sediment in replicate for each site and pooled the DNA. For site 140112K, 8 replicate DNA extracts were pooled; for site 140117H, 8 replicates were pooled; and for 140111F, 5 replicates were pooled. We implemented the Zymo protocol for "BioFluid + Cell Buffer." Prior to carrying out the extraction protocol provided by Zymo, we conducted freeze/thaw cycles where samples were first thawed at room temperature, then frozen at −80°C for 15 min, heated to 55°C for 15 min three times. We carried out a proteinase K step, adding 10 uL of 20 μg/mL proteinase K per 100 mg of wet sediment and incubated at 55°C for 3 h. From there, the "BioFluid + Cell Buffer" protocol was followed. The quality of the DNA extracts was assessed using a NanoDrop. The A260/A280 of the extracts were between 1.5 and 2. PCR was conducted to ensure extracts were PCR amplifiable. DNA extracts were then pooled. The sequencing facility was provided 35 ng DNA from site 140112K, 30 ng DNA from site 140117H, and 60 ng from site 140111F. Shotgun metagenome sequencing was conducted in the Marine Biological Laboratory at Woods Hole Oceanographic Institute using the Illumina 150 × 2 platform using their standard protocol.

We processed shotgun metagenome sequencing reads in two ways, "by-site" and "co-assembly." For our by-site approach, we processed sequencing data from each site individually. Raw sequencing reads, both forward and reverse, in ".fastq" format were loaded into The Department of Energy Systems Biology Knowledgebase (KBase).[2] In Kbase, the quality of raw sequencing reads was assessed using FastQC v0.12.1.[3] Based on the quality assessment, files were trimmed with the program Trimmomatic v0.36 (Bolger et al., 2014) with a "sliding window size" of 4 and a "sliding window minimum quality" of 25. Once the read files were trimmed, their quality was rechecked using FastQC v0.12.1. Once the quality of the reads was determined to be sufficient, the reads were assembled using metaSPAdes v3.15.3 (Nurk et al., 2017). In MetaSPAdes, the "Minimum Contig Length" parameter was less than or equal to 1,000, with the smallest possible read length being 300. MetaSPAdes produced 32,933 contigs from site 140112K, 68,329 contigs from site 140117H, and 60,294 contigs from site 140111F. The contigs produced were annotated with RASTtk v1.073 using the default KBase parameters.

Contigs were binned using CONCOCT v1.1 (Alneberg et al., 2013) and MetaBAT2 v1.7 (Kang et al., 2019), with the maximum contig length parameter being less than or equal to 2,500 base pairs. The lowest possible contig length for CONCOCT and MetaBAT2 was set to 1,500 base pairs. CONCOCT binned 17,914 contigs from site 140112K, 36,751 contigs from site 140117H, and 41,353 contigs from site 140111F to produce 62, 84, and 87 bins from each site, respectively. MetaBAT2 binned 13,460 contigs from site 140112K, 28,028 contigs from site 140117H, and 32,614 contigs from site 140111F to produce 40, 60, and 49 bins from each site, respectively. We optimized the bin outputs from CONCOCT and MetaBAT2 with DAS Tool v1.1.2 (Sieber et al., 2018) using the default diamond identification tool and default advanced parameters. The bin optimization tool resulted in 22 optimized bins from site 140112K, 41 bins from 140117H, and 36 bins from 140111F.

The quality of the bins produced was assessed with CheckM v1.0.18 (Parks et al., 2015). Following bin assessment, all the bins were extracted as assemblies using Extract Bins as Assemblies from BinnedContigs v1.0.2 in Kbase. Once the bins were extracted, the taxonomy of each bin was classified using GTDB-tk v1.7.0 (Chaumeil et al., 2022), and bins classified as known methanogens were functionally annotated using RASTtk v1.073 (Brettin et al., 2015) using the default KBase parameters.

All quality-checked and trimmed ".fastqc" sequencing files were uploaded into one read file using the program Merge Reads Libraries v1.2.2 in Kbase for the co-assembly approach. From there, contigs were assembled using metaSPAdes. This resulted in 121,536 contigs. Contigs were then binned following the same protocol as the by-site approach. The number of bins resulting from CONCOCT v1.1 was 135 from 121,536 contigs, and the number of bins from MetaBAT2 v1.7 was 96 from 56,113 contigs. Bin optimization was carried out using DAS Tool v1.1.2, resulting in 64 bins. Assemblies were extracted and taxonomically classified using GTDB-tk v1.7.0. Those classified as methanogens were functionally annotated using RASTtk v1.073.

2 https://www.kbase.us

3 http://www.bioinformatics.babraham.ac.uk/projects/fastqc/

The relative frequency of each bin at each site was determined using the program Bowtie2 v2.3.2 (Langmead and Salzberg, 2012) in Kbase with phred33 used as the alignment quality score type, the alignment type set to end-to-end and the maximum fragment length for paired-end alignments set to 500. Bowtie2 maps raw sequence reads against genome assemblies to determine the percentage of reads that align with each assembly at each site.

After assembling and processing the bins, we searched the RASTk annotations for core methanogen metabolism genes using Thieringer et al. (2023) as a guide. We used BLASTp (Camacho et al., 2009) to determine the percent identity with protein sequences of previously characterized methanogen genomes. Supplementary Table S4 contains tables of RASTtk annotations and BLASTp results of amino acid sequences that code for proteins in the core metabolisms of the resolved methanogen genomes.

2.5 Phylogenomic analysis

GToTree was used to construct a phylogenomic tree of methanogens (Lee, 2019). We included several genomes from the Samail Ophiolite isolated by Thieringer et al. (2023), Fones et al. (2019), and those newly published in this study. We also curated and included several high-quality genomes for which environmental metadata was available. Additionally, representative genomes from the genera *Methanobacterium*, *Methanosphaera*, *Methanobrevibacter*, and *Methanosarcina* were included using the "gtt-get-accessions-from-GTDB" functionality with the "--GTDB-representatives-only" flag for each of these taxa. Finally, genomes identified by GTDB-Tk - v2.3.2 as "close relatives" of *Methanocalculus natronophilus*, *Methanobacterium congolense* buetzberg, and the Oman MAGs isolated by Thieringer et al. (2023) and Fones et al. (2019) were also included. However, for genomes identified by GTDB, we removed those that were shown to be redundant in previous maximum parsimony and maximum likelihood trees from the final phylogeny for the sake of clarity. A full table of the genomes used and any associated metadata used in this study is available in Supplementary Table S5.

Once the genomes were collected, GToTree v1.8.8 was run with default parameters, using the hidden Markov model (HMM) target gene set of 76 archaeal marker genes included in the program as the basis for the phylogeny. Genes were predicted within input genomes using Prodigal v2.6.3 (Hyatt et al., 2010); our 76 target genes were then identified within these genes using HMMR v3.4 (Eddy, 2011) and, respectively, aligned using Muscle 5.1 for OS x 64 (Edgar, 2022). These genes were then trimmed via TrimAl v1.5.rev0 (Capella-Gutiérrez et al., 2009) and concatenated to construct the phylogenomic tree. Then, IQ-TREE v2.3.6 (Nguyen et al., 2015) was used to generate a maximum-likelihood phylogeny with 1,000 bootstrap replicates. Subsequently, the tree was visualized in the Interactive Tree of Life online viewer (Letunic and Bork, 2024). Canva was then used to overlay relevant environmental metadata onto the tree and reformat taxon names. Supplementary Table S5 includes optimal growth temperature and pH for genomes of methanogens in culture and the temperature and pH of sampling sites of metagenome-assembled genomes in this study and other studies where relevant.

3 Results and discussion

3.1 Surface-expressed serpentinized fluids, a window into subsurface processes

To illustrate geochemical similarities and differences between surface-expressed and subsurface well fluids, Figure 1 summarizes the concentrations of geochemical constituents reported in Howells et al. (2022) and Rempfert et al. (2017) directly influenced by the process of serpentinization. Leong et al. (2021) describe how the serpentinization process influences pH, Si, Ca, and DIC in detail. Si indicates the extent to which fluids have undergone serpentinization and the extent of mixing between Type I (high Si concentration) and Type II (low Si concentration) fluids. Based on the concentration of Si and pH shown in Figure 1A, there is a high degree of geochemical overlap between surface and subsurface fluids. However, Figure 1B shows a distinction in the concentration of Ca, with more pristine Type II fluids (lowest concentrations of Si) from the subsurface having higher concentrations of Ca. This may be attributed to Ca in surface fluids reacting with inorganic carbon supplied from CO_2 in the atmosphere to form carbonate minerals, which can draw down the Ca concentration in serpentinized fluids. Additionally, in fluids where H_2 was measurable in the Rempfert et al. (2017) study, H_2 is more than an order magnitude higher in concentration than the highest H_2 concentrations from the surface, as shown in Figure 1C. Lower H_2 concentrations in surface fluids may be attributed to the consumption of H_2 by microorganisms or degassing of H_2 from serpentinized fluid along its migration from the subsurface to the surface. Despite these differences, previous energetic calculations show sufficient energy for hydrogenotrophic methanogenesis in more pristine Type II surface-expressed fluids (Canovas et al., 2017; Howells et al., 2022). Energetic observations coupled with the detection of methanogen 16S rRNA gene phylotypes in Howells et al. (2022) suggest that H_2 would not be a limiting factor in many surface-expressed fluids and certainly not in subsurface fluids. The difference in Ca concentration provides insights into factors that may influence inorganic carbon availability in the surface and subsurface.

To examine similarities in microbial community composition and the distribution of *Methanobacterium* in surface-expressed and subsurface well fluids, we conducted a meta-analysis of 16S rRNA gene amplicon sequencing data reported in Howells et al. (2022) (surface-expressed fluids) and Rempfert et al. (2017) (subsurface well fluids). We can do this meta-analysis given that both studies used the Earth Microbiome Primer set (Caporaso et al., 2012) and the same type of sequencing platform (MiSeq 150 × 2). In comparing the alpha diversity, or the number of distinct representative 16S rRNA gene sequences, of surface and subsurface communities, we see in Figure 2A that both surface and subsurface fluid alpha diversity negatively trend with Si. It is worth noting that surface-expressed fluids can have higher alpha diversity than subsurface fluids with <99% serpentinized fluid composition. Both subsurface and surface-expressed Type II fluids have relatively low alpha diversity in comparison to Type I and mixed fluids, which in previous studies is hypothesized to result from the selective pressure of alkaline pH (Rempfert et al., 2017; Fones et al., 2019; Fones et al., 2021).

To assess beta diversity or similarities in community composition, we carried out an NMDS ordination of a Bray–Curtis dissimilarity analysis of square-root transformed 16S rRNA gene

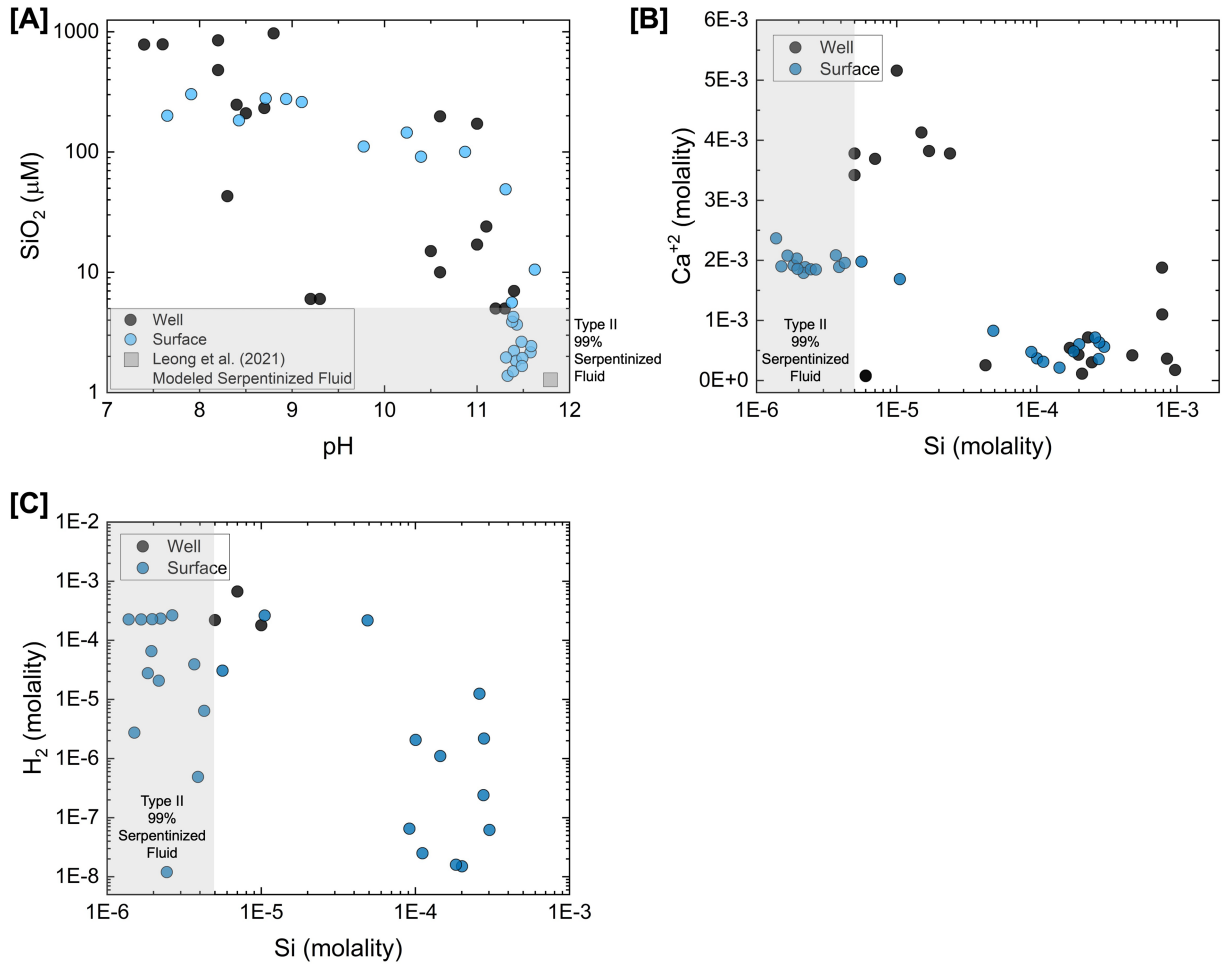

FIGURE 1
Comparison of surface-expressed and subsurface well serpentinized fluid chemistry from the Samail Ophiolite. Chemical constituents plotted are directly influenced by the process of serpentinization as described in Leong et al. (2021). Values for surface-expressed fluid chemistry (blue) are reported in Howells et al. (2022) values from well fluids (black) are reported in Rempfert et al. (2017). This figure is adapted from Howells et al. (2022). **(A)** The concentration of Si in fluids plotted as a function of pH. Si is considered to be an indicator of the extent of serpentinization fluids have undergone and extent Type I and Type II fluids have mixed (Leong et al., 2021). The gray square represents the estimated pH and Si concentration of a pristine serpentinized fluid modeled by Leong et al. (2021). This is used as the Type II end-member fluid for estimating the percent serpentinized fluid composition of fluids using a conservative mixing model with Si as described in Howells et al. (2022). **(B)** Concentration of Ca^{+2} plotted as a function of Si. **(C)** Concentration of H_2 plotted as a function of Si.

ASV relative abundances. Visually, community composition variation along NMDS1 trends with whether the communities are from the surface or the subsurface, as shown in Figure 2B. ANOSIM analysis shows that the communities from the surface and subsurface are significantly different (ANOSIM r statistic = 0.5124, *p*-value = 0.0001, 9,999 permutations); however, Type II fluids from the surface and subsurface fall closer together in ordination than fluids influenced by mixing and Type I fluids. Mixing and Type I fluids are likely dissimilar between the surface and subsurface due to the availability of O_2 and sunlight at the surface. As Howells et al. (2023) reported, surface fluids influenced by mixing are populated by phototrophs and heterotrophs that use O_2 as an electron acceptor. The dissimilarity between the Type II fluid communities may be due to the differences in the relative abundance of *Methanobacterium* and OP1 [also referred to as Acetothermia (Colman et al., 2022)] as shown by the NMDS ordination with OP1 relative abundances overlaid in Supplementary Figure S2. We overlayed the relative abundance of *Methanobacterium* phylotypes onto the NMDS ordination, as shown in Figure 2C. *Methanobacterium* is present in both Type II fluid types; however, it appears to be slightly more prevalent in surface-expressed Type II fluids. Overall, the community analysis shows that while there are significant global differences between surface and subsurface fluids, as may be expected due to differences in the availability of O_2 and sunlight, Type II fluids are surprisingly similar in alpha diversity and community composition. Furthermore, *Methanobacterium* is prevalent in surface-expressed and subsurface Type II fluids.

3.2 Energetic potential for methanogenesis

In this section we quantitatively examine methanogen substrate availability through assessments of substrate flux to the cell, availability of energy in terms of moles CH_4 produced and energy supply per kg of fluid. For these assessments we characterized formate and acetate concentrations shown in Figure 3A in surface-expressed fluids and

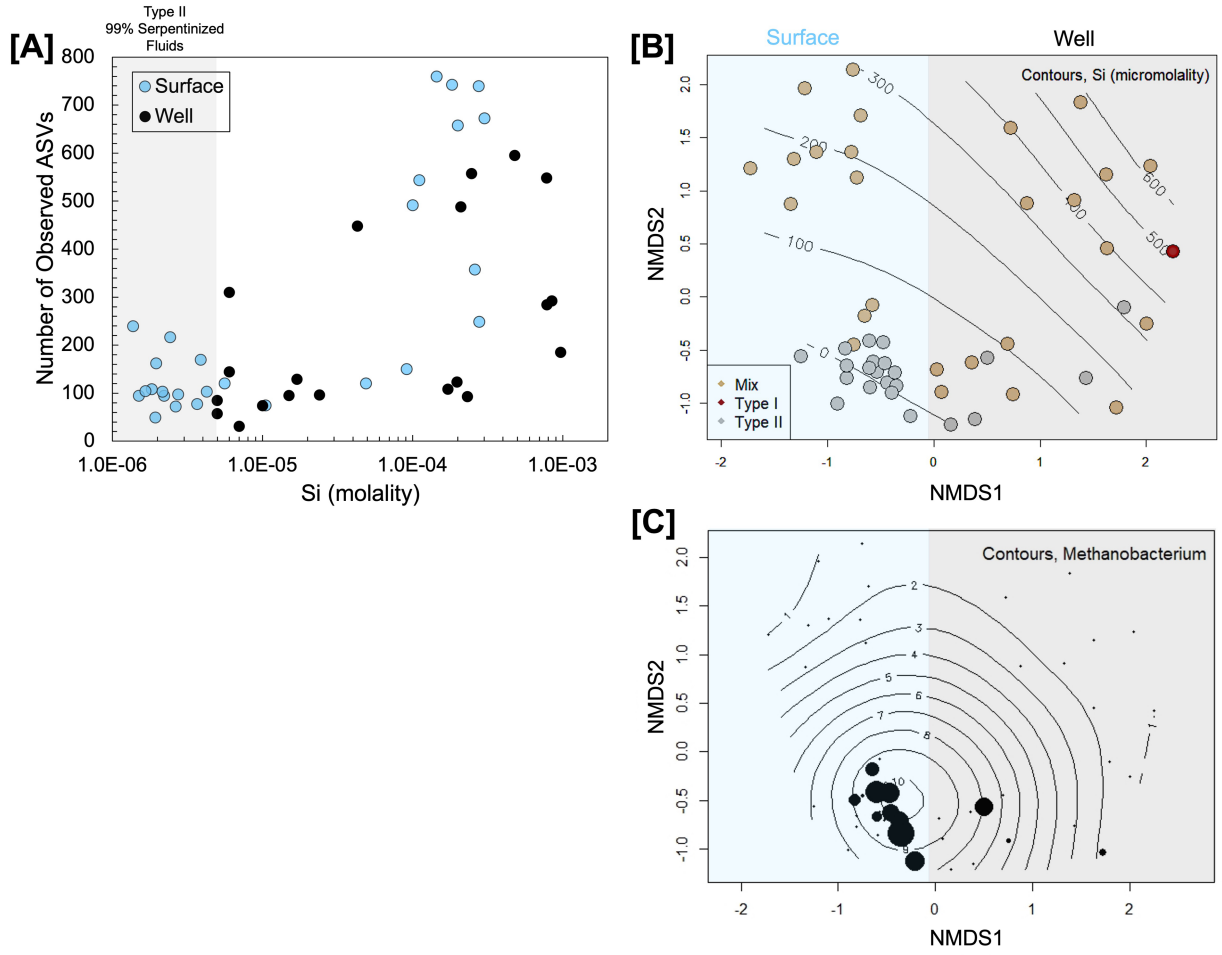

FIGURE 2
Comparison of microbial community diversity in surface-expressed and subsurface well serpentinized fluids of the Samail Ophiolite. 16S rRNA gene amplicon sequencing data from Rempfert et al. (2017) and Howells et al. (2022) were reprocessed to compare the alpha diversity quantified through the number of observed ASVs plotted as a function of Si in **(A)** and the beta diversity assessed through Bray–Curtis dissimilarity analysis of square-root transformed ASV relative abundances visualized through NMDS ordination (stress = 0.2) in **(B)**. Contours in **(B)** are a maximum likelihood fit of the Si concentration at each site and colors indicate fluid type following Table 2. The distribution of 16S rRNA gene amplicon ASVs classified as *Methanobacterium* is shown by the size of circles in **(C)**, which scales with relative abundance and. Contours in **(C)** are a maximum likelihood fit of the relative abundance of *Methanobacterium*.

combine our data with DIC, H_2 and CH_4 concentrations previously reported in Leong et al. (2021) and Howells et al. (2022), which are from the same sites and sampled at the same time. Some well fluids characterized in Rempfert et al. (2017) have measured concentrations of H_2, CH_4, DIC, acetate, and formate allowing comparison between surface and subsurface. Table 2 summarizes the organic acid data collected for this study as well as organic acid data previously reported in Rempfert et al. (2017). Also in Table 2 is an estimation of the percent serpentinized fluid at each study site using the concentration of Si as described in Howells et al. (2022) and a descriptor of the sampling site as Type II (>99% serpentinized fluid), mixed, and our representative Type I surface expressed fluid. As described in the methods, we estimate the chemical activities of dissolved CO_2 and HCO_3^- from measurements of DIC. We account for the effects of major ion concentrations (such as Na^+, Cl^-, Ca^{+2} and Mg^{+2}) and pH on the chemical speciation of DIC and activity of dissolved CO_2 and HCO_3^- using the program EQ3/6 (Wolery, 2013) and program wrapper we developed, AqEquil Python package (Boyer et al., 2024). Given the alkalinity of serpentinized fluids we cannot measure CO_2 through the gas phase as we did with H_2 and CH_4 in Howells et al. (2022). Therefore, estimating dissolved CO_2 in this manner is the best approach for deriving a CO_2 chemical activity. The same approach was used to estimate the chemical activity of formic acid, formate anion, acetic acid and acetate anion from bulk measurements of formate and acetate, respectively. Estimated chemical activities can be found in Supplementary Table S1. We assume chemical activities are approximately equal to molarity for the potential flux calculations described below.

3.2.1 Potential flux

Low concentrations can limit the diffusive flux of substrates to a cell and thereby limit rates of metabolism. We calculated the potential fluxes of methanogenic substrates as follows. The rate of diffusive flux to the surface of a sphere of radius R is given by integrating the general equation relating flux and substrate concentration in spherical coordinates (Crank, 1979) from R to infinity (Hoehler, 2004):

10.3389/fmicb.2024.1523912

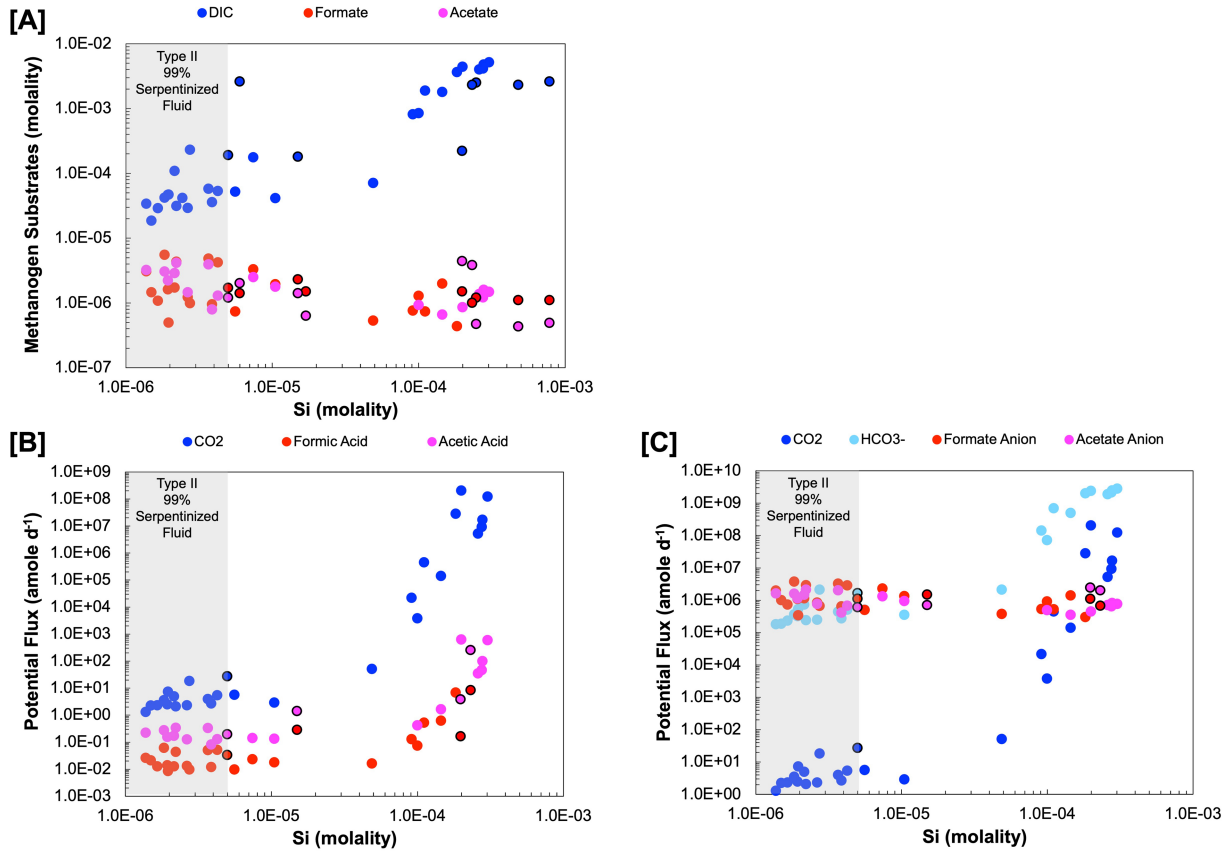

FIGURE 3
Substrate concentration in molality and potential flux in attomoles per day (amole day^{-1}) **(A)** Are the measured concentrations of dissolved inorganic carbon, formate and acetate. **(B)** is the potential flux for the acidic forms, dissolved CO_2 (carbonic acid), formic acid, and acetic acid. **(C)** is the approximation of potential flux for the anion forms HCO_3^-, formate anion and acetate anion. Black outlines indicate subsurface well fluids.

$$J = 4\pi DR \cdot \left(C_\infty - C_R\right) \tag{7}$$

Where J is the diffusive flux, D is the species-specific diffusion coefficient, C_∞ is the substrate concentration at infinite distance from the cell, and C_R is the substrate concentration at the surface of the sphere. In our calculations, R is set to 0.5 μm in order to yield the flux to a spherical surface of cell-like scale. C_∞ is set to the measured bulk solution concentration of a given substrate. In practice, "infinite distance" with respect to a cell consuming substrate at the diffusion limited rate is on the order of tens of microns (Boone et al., 1989), meaning that the substrate concentration at that distance very closely approximates the substrate concentration at true infinite distance. C_R is set to the concentration of substrate that is at equilibrium with respect to the methanogenic metabolism in question, in order to place a lower bound on the possible extent of substrate depletion at the surface of the sphere that could result from metabolic consumption. In practice, C_R would almost certainly be higher because (i) cells can only consume substrates down to concentrations that still support energy conservation, rather than to equilibrium; and (ii) enzymatic substrate consumption at less than the diffusion-limited rate implies that substrate concentrations at the surface of the sphere will be drawn down to only a limited extent. The latter of these considerations is particularly important because most enzymes operate orders of magnitude more slowly than the diffusion-limited rate (Bar-even et al., 2011), and the potential draw down of substrate concentration at R will be limited to the same extent. For these reasons, the calculated fluxes represent physical upper limits on the possible rates of substrate delivery to a cell, and we note this by henceforth referring to them as "potential fluxes."

Separate calculations were performed for potential fluxes of the neutral species CO_2, formic acid, acetic acid, which can potentially diffuse freely across a cell membrane, and the corresponding anionic forms, HCO_3^-, formate, and acetate, which can only transit the cell membrane via facilitated diffusion (e.g., through ion channels) or active transport. The calculated fluxes are specific to a given compound and neglect the potential for resupply by equilibration with protonated or ionic counterparts. For example, calculated fluxes assume that dissolved CO_2 is delivered to the cell surface solely by diffusion from the bulk medium and not via production from bicarbonate in the vicinity of the cell surface. At the length scales considered here, diffusion dominates over the comparatively sluggish kinetics of CO_2 production from bicarbonate (Johnson, 1982), making this approach a good approximation for the DIC system. It is not clear whether the same is true for the potential for formic acid and acetic acid to be formed in the vicinity of the cell by protonation of formate and acetate, respectively, and the potential fluxes of formic and acetic acids could be higher than the calculated values as a consequence. Table 3

TABLE 3 Potential flux values reported in attomoles per day (*a*mole d^{-1}) and the diffusion coefficients in water (*D*) at 25°C, 1 bar for each chemical species used in the calculation.

Sample	SiO_2	CO_2	Formic acid	Acetic acid	HCO_3^-	Formate anion	Acetate anion
	Molality	*a*mole d^{-1}	*a*mole d^{-1}	*a*mole d^{-1}	*a*mole d^{-1}	*a*mole d^{-1}	*a*mole d^{-1}
140115Z	1.4E-06	1.3E+00	2.6E-02	2.2E-01	1.8E+05	2.0E+06	1.6E+06
140115X	2.2E-06	2.1E+00	4.3E-02	3.3E-01	2.4E+05	2.9E+06	2.1E+06
140115Y	2.2E-06	4.9E+00	1.3E-02	1.7E-01	7.3E+05	1.1E+06	1.5E+06
140114S	2.0E-04	2.0E+08		6.2E+02	2.4E+09		4.4E+05
140114U	7.4E-06		2.3E-02	1.4E-01		2.3E+06	1.3E+06
140114V	2.8E-06	1.8E+01	9.5E-03		2.1E+06	6.6E+05	
140114T	1.8E-06	3.5E+00	6.1E-02	2.7E-01	3.6E+05	3.7E+06	1.6E+06
140114R	2.4E-06						
140113O	3.7E-06	3.9E+00	5.0E-02	3.3E-01	4.3E+05	3.2E+06	2.0E+06
140113P	1.9E-06	2.4E+00	1.4E-02	1.5E-01	3.2E+05	1.1E+06	1.1E+06
140111G	2.8E-04	9.1E+06		4.6E+01	2.1E+09		6.3E+05
140111H	1.5E-04	1.4E+05	6.1E-01	1.6E+00	4.9E+08	1.4E+06	3.5E+05
140111I	1.0E-04	3.8E+03	7.3E-02	4.1E-01	7.1E+07	9.0E+05	4.9E+05
140111F	1.1E-05	2.9E+00	1.8E-02	1.3E-01	3.5E+05	1.3E+06	9.3E+05
140116B	3.0E-04	1.2E+08		5.8E+02	2.8E+09		7.5E+05
140116C	2.8E-04	1.7E+07		9.8E+01	2.5E+09		8.1E+05
140116D	2.6E-04	5.2E+06		3.5E+01	1.9E+09		7.0E+05
140117J	4.9E-05	5.1E+01	1.6E-02		2.1E+06	3.7E+05	
140117I	2.0E-06	7.2E+00	8.3E-03		5.2E+05	3.4E+05	
140117G	1.5E-06	2.2E+00	2.1E-02		1.9E+05	9.9E+05	
140117F	2.7E-06	2.3E+00	1.3E-02	1.2E-01	2.5E+05	8.3E+05	7.6E+05
140117H	1.7E-06	2.3E+00	1.3E-02		2.3E+05	7.3E+05	
140110B	1.8E-04	2.8E+07	6.7E+00		2.0E+09	3.0E+05	
140112L	1.1E-04	4.4E+05	5.2E-01		6.9E+08	5.2E+05	
140110D	9.1E-05	2.1E+04	1.3E-01		1.4E+08	5.3E+05	
140112M	5.6E-06	5.6E+00	9.6E-03		5.0E+05	5.0E+05	
140112K	3.9E-06	2.7E+00	1.2E-02	8.0E-02	2.7E+05	6.4E+05	4.1E+05
140110C	4.3E-06	5.3E+00	5.1E-02	1.3E-01	5.0E+05	2.8E+06	6.7E+05
NSHQ212015*	7.8E-04						
WAB1882016*	7.9E-04						
WAB1032015*	4.8E-04						
WAB1032016*	8.5E-04						
WAB1052016*	4.3E-05						
NSHQ3B2015*	2.5E-04						
WAB1042016*	2.1E-04						
WAB1882015*	2.3E-04		8.2E+00	2.5E+02		6.7E+05	2.0E+06
WAB552016*	6.0E-06						
WAB552015*	6.0E-06						
NSHQ42015*	1.5E-05		2.8E-01	1.4E+00		1.5E+06	7.0E+05
NSHQ42014*	2.0E-04		1.6E-01	3.8E+00		1.1E+06	2.4E+06
WAB562015*	1.0E-05						
WAB712015*	1.7E-05						
WAB712016*	2.4E-05						
NSHQ142016*	5.0E-06						
NSHQ142015*	5.0E-06	2.7E+01	3.3E-02	1.9E-01	1.7E+06	1.1E+06	6.0E+05
NSHQ142014*	7.0E-06						
	D at 25°C, 1 bar (m^2 s^{-1})	1.92E-09	1.52E-09	1.19E-09	1.18E-09	1.45E-09	1.09E-09
	Reference	Cussler (2009)	Yaws (2009)	Yaws (2009)	PhreeqC	Vanýsek (1993)	Vanýsek (1993)

* Data used in calculations are from well fluid sites reported in Rempfert et al. (2017).

shows the diffusion coefficients (*D*) used, their references, and the potential fluxes calculated using Equation 7.

Of the acid forms dissolved CO_2 (carbonic acid), formic acid, and acetic acid, dissolved CO_2 has the highest potential flux, as shown in Figure 3B, which can be attributed to the differences in concentration among DIC, formate, and acetate. The anion forms (Figure 3C) have a more nuanced expression of potential flux, particularly in Type II fluids. There are cases where HCO_3^- is more available than the anion forms of formate and acetate and vice versa, making any one of these a viable option for methanogenesis in Type II fluids. Given the orders of magnitude higher potential flux for the anion forms over the acid forms of inorganic carbon, formate, and acetate in Type II fluids, this work suggests it would be at least kinetically more favorable to use these forms if methanogens have a mechanism for taking them up. Indeed, some methanogens have been found to have transporters for formate (White and Ferry, 1992) and acetate anions (Welte et al., 2014). While transporters for HCO_3^- have yet to be characterized in methanogens some bacterial chemolithoautotrophs have been found to have bicarbonate transporters (Scott et al., 2019).

3.2.2 Energy availability, kJ per mole CH_4

Energy availability does not necessarily mean faster growth or prevalence of a microbial population in a system. For example, an organism with a slow maximum growth rate may result in only a fraction of the energy available being utilized. Additionally, in a case where there is sufficient energy available, there may be energetically costly physiological stressors such as alkaline pH. Another possibility is competition for substrates, which can lower the overall experienced energy (Shock and Holland, 2007; Hoehler, 2007; Howells et al., 2022). In a system where energy is limited due to alkaline pH and the system is primarily driven by the geochemistry of the serpentinization reactions, chemical energy availability may have a more considerable impact on biology.

Estimations of energy availability in units of kJ per mole CH_4, shown in Figure 4A and summarized in Table 4, show that formatotrophic methanogenesis would yield the most energy in Type II fluids, followed by acetoclastic methanogenesis and hydrogenotrophic methanogenesis. While the differences in affinity among formatotrophic, acetoclastic and hydrogenotrophic methanogenesis are in some cases less than an order of magnitude, these results emphasize that formatotrophic methanogenesis is just as energy yielding as hydrogenotrophic methanogenesis, which may be surprising given the high H_2 concentrations in serpentinized fluid. Fones et al. (2021) argue that the dependence on formate for methanogenesis by *Methanobacterium* stems from the low concentration of HCO_3^- for hydrogenotrophic methanogenesis, which results in a preference for formate. That said, formate is lower in concentration than DIC, as shown in Figure 3A, which should make it a less viable substrate, especially if the acid form is used (see Figure 3B). However, given that serpentinized fluids have a uniquely low concentration of HCO_3^- and 3 moles of HCO_3^- are produced for every mole of CH_4 produced by the formatotrophic pathway, the low concentration of HCO_3^- as a product (and not a substrate) makes formatotrophic methanogenesis more energetically favorable than hydrogenotrophic methanogenesis. Therefore, the drive to use formate in Type II fluids may be the result of energy availability, not due to the low concentration of HCO_3^- as a substrate, but as a product of formatotrophic methanogenesis.

3.2.3 Energy availability, J per kg of fluid

Another way to examine energy availability is to assess the number of joules of energy that can be supplied to a microbial

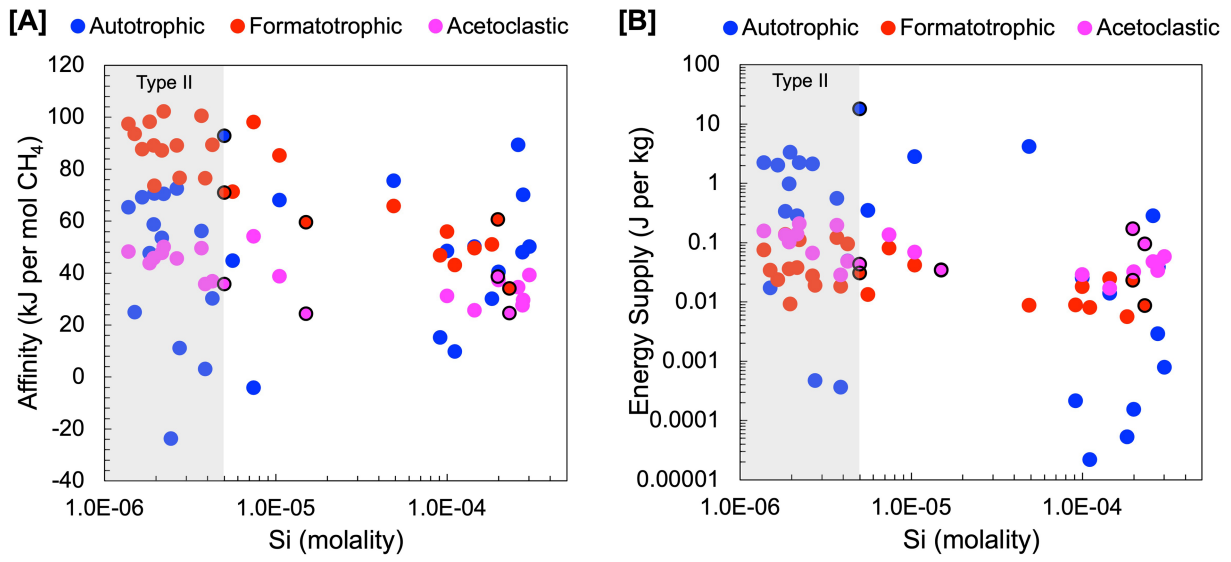

FIGURE 4
Estimations of energy availability for hydrogenotrophic ($4H_2 + HCO_3^- + H^+ \rightarrow CH_4 + H_2O$), formatotrophic ($4CHO_2^- + H^+ + H_2O \rightarrow CH_4 + 3HCO_3^-$) and acetoclastic ($C_2H_3O_2^- + H_2O \rightarrow CH_4 + HCO_3^-$) methanogenesis. Energy availability was estimated in terms of **(A)** kJ per mol of CH_4 and **(B)** kJ per mol of kg of environmental fluid. Black outlines indicate subsurface well fluids.

TABLE 4 Energy availability calculations.

Sample	pH	Si	Hydrogenotrophic	Formatotrophic	Acetoclastic	Hydrogenotrophic	Formatotrophic	Acetoclastic
		Molality	kJ/CH_4	kJ/CH_4	kJ/CH_4	J/kg	J/kg	J/kg
140115Z	11.33	1.38E-06	65.2	97.2	48.1	2.2E+00	7.4E-02	1.5E-01
140115X	11.398	2.22E-06	70.4	102.1	49.9	2.2E+00	1.1E-01	2.1E-01
140115Y	11.579	2.16E-06	53.5	87.1	47.7	2.8E-01	3.7E-02	1.4E-01
140114S	7.65	0.0002	40.3		37.2	1.5E-04		3.2E-02
140114U	11.355	7.43E-06	−4.2	97.9	54.0	0.0E+00	8.0E-02	1.3E-01
140114V	11.407	2.75E-06	11.0	76.6		4.7E-04	1.9E-02	
140114T	11.421	1.84E-06	47.6	98.2	43.7	3.3E-01	1.3E-01	1.3E-01
140114R	11.585	2.44E-06	−23.8			0.0E+00		
140113O	11.43	3.68E-06	56.1	100.4	49.5	5.5E-01	1.2E-01	1.9E-01
140113P	11.49	1.94E-06	58.6	89.0	45.6	9.6E-01	3.6E-02	1.0E-01
140111G	8.936	0.000276	47.9		27.5	2.9E-03		3.3E-02
140111H	10.24	0.000145	50.1	49.4	25.5	1.4E-02	2.4E-02	1.7E-02
140111I	10.87	0.0001	48.4	55.9	31.0	2.5E-02	1.8E-02	2.9E-02
140111F	11.624	1.05E-05	68.0	85.2	38.7	2.8E+00	4.1E-02	6.8E-02
140116B	7.909	0.000303	50.1		39.2	7.8E-04		5.8E-02
140116C	8.714	0.000279	70.0		29.5	3.8E-02		4.7E-02
140116D	9.104	0.00026	89.2		34.4	2.8E-01		4.7E-02
140117J	11.309	4.89E-05	75.4	65.6		4.1E+00	8.7E-03	
140117I	11.313	1.96E-06	70.4	73.5		3.3E+00	9.0E-03	
140117G	11.389	1.50E-06	24.8	93.5		1.7E-02	3.4E-02	
140117F	11.48	2.65E-06	72.4	89.0	45.5	2.1E+00	2.7E-02	6.6E-02
140117H	11.485	1.66E-06	69.1	87.6		2.0E+00	2.3E-02	
140110B	8.425	0.000183	30.0	51.0		5.2E-05	5.5E-03	
140112L	9.774	0.000111	9.6	43.0		2.2E-05	7.9E-03	
140110D	10.394	9.14E-05	15.1	46.7		2.1E-04	8.8E-03	
140112M	11.376	5.60E-06	44.7	71.3		3.4E-01	1.3E-02	
140112K	11.379	3.88E-06	2.9	76.4	35.6	3.6E-04	1.8E-02	2.8E-02
140110C	11.392	4.26E-06	30.1	89.3	36.7	4.8E-02	9.4E-02	4.7E-02
NSHQ142014*	11.4	7.00E-06						

(Continued)

10.3389/fmicb.2024.1523912

TABLE 4 (Continued)

Sample	pH	Si	Hydrogenotrophic	Formatotrophic	Acetoclastic	Hydrogenotrophic	Formatotrophic	Acetoclastic
		Molality	kJ/CH_4	kJ/CH_4	kJ/CH_4	J/kg	J/kg	J/kg
NSHQ142015*	11.3	5.00E-06	92.8	70.8	35.6	1.8E+01	3.0E-02	4.3E-02
NSHQ142016*	11.2	5.00E-06						
NSHQ212015*	7.4	0.000782						
NSHQ3B2015*	8.4	0.000247						
NSHQ42014*	10.6	0.000198		60.5	38.5		2.3E-02	1.7E-01
NSHQ42015*	10.5	1.50E-05		59.4	24.2		3.4E-02	3.4E-02
WAB1032015*	8.2	0.00048						
WAB1032016*	8.2	0.000848						
WAB1042016*	8.5	0.00021						
WAB1052016*	8.3	4.30E-05						
WAB1882015*	8.7	0.000232		34.0	24.5		8.5E-03	9.3E-02
WAB1882016*	7.6	0.000785						
WAB552015*	9.3	6.00E-06						
WAB552016*	9.2	6.00E-06						
WAB562015*	10.6	1.00E-05						
WAB712015*	11	1.70E-05						
WAB712016*	11.1	2.40E-05						

* Data used in calculations are from well fluid sites reported in Rempfert et al. (2017).

10.3389/fmicb.2024.1523912

community in a kg of fluid in Figure 4B. This exemplifies the energy available to microorganisms in a case where 1 kg of fluid is closed off, and all energy is consumed, i.e., the reaction proceeds until the limiting reactant runs out. We can calculate this by multiplying affinity in joules per mole reaction by the concentration of the limiting reactant divided by its stoichiometric coefficient to get J per kg fluid (Equation 6). For the concentration of the limiting reactant, we summed the concentration of the total pool of chemical species the reactant is in equilibrium with; for example, for HCO_3^- we summed the activities of dissolved CO_2, CO_3^{-2}, $CaHCO_3^+$, $MgHCO_3^+$, $CaCO_3$, and $MgCO_3$ in addition to HCO_3^- to calculate energy supply. We do this to account for the fact that as one chemical species is consumed, the system re-equilibrates for a continuous supply of the reactant until the total pool is consumed. Formate and acetate are always the limiting reactant for formatotrophic and acetoclastic methanogenesis, whereas hydrogenotrophic methanogenesis can be either H_2-limited or inorganic carbon-limited depending on their relative concentrations.

Our results show that for energy supply (Figure 4B), hydrogenotrophic methanogenesis tends to yield the most energy, particularly in mixed fluids with the highest energy supply at a site with 99.6% serpentinized fluid. This is because inorganic carbon is the stoichiometrically limiting substrate for hydrogenotrophic methanogenesis in fluids with >70% serpentinized fluid and DIC is higher in concentration than formate and acetate in these fluids. By contrast, in fluids with <70% serpentinized fluids (high Si; mixed and Type I), formatotrophic and acetoclastic methanogenesis yield more energy per kg of fluid than hydrogenotrophic methanogenesis. In mixed and Type I fluids, hydrogenotrophic methanogenesis is stoichiometrically limited by the concentration of H_2. Formate and acetate in these systems are higher in concentration than H_2, and therefore, formatotrophic and acetoclastic methanogenesis yield more energy.

These results suggest that the energy available to methanogens in serpentinized fluids depends on substrate availability and how energy is experienced by the methanogen cell. If methanogens can take up HCO_3^- and the anions of formate and acetate, then, based on our approximation of potential flux, these chemical species are more readily available to methanogens in Type II serpentinized fluids than dissolved CO_2 (Figure 3C). For energy calculations, in terms of moles CH_4 produced, formatotrophic methanogenesis is more energetically favorable than acetoclastic and hydrogenotrophic methanogenesis in Type II fluids (Figure 4A) and may explain why *Methanobacterium* preferentially uses formate in these systems. The observation that hydrogenotrophic methanogenesis can be more energetically yielding per kg fluid suggests that in a case where systems are closed off, methanogens would have a greater supply of energy for hydrogenotrophic methanogenesis and may explain why *Methanobacterium* strains in mixed fluids can use both bicarbonate (with H_2 as an electron donor) and formate for methanogenesis as observed in Fones et al. (2021). While no acetoclastic methanogens have been previously detected in the Samail Ophiolite, energetic calculations suggest this metabolism is viable. However, given that energy availability for acetoclastic methanogenesis is comparable to hydrogenotrophic methanogenesis in Type II fluids, acetoclastic methanogens may be energetically limited. This is also reflected in an assessment of energy available in recently drilled bore-hole fluids from Oman reported in Nothaft et al. (2021b).

3.3 Genomic potential for methanogenesis

To assess the genomic potential for hydrogenotrophic, formatotrophic, and acetoclastic methanogenesis, we conducted shotgun metagenome sequencing on DNA extracts from sediments of three chemically distinct Type II surface-expressed serpentinized fluids. Supplementary Figure S2 includes images of the sampling sites which are pools or streams of surface expressed serpentinized fluids. To acquire enough biological material and minimize system disruption we sampled up to 1 cm depth of sediments that underlie fluids after sampling fluid for chemical characterization. We take the bulk fluid composition that overlies the sediments to be an approximation of what microorganisms experience in the sediments. Given that the sediments are shallow due to the underlying travertine we expect fluid circulation in the sediments. One difference between overlying fluids and the sediment pore fluids may be the concentration of O_2 the microbial communities experience, with the sediment favoring anaerobic metabolisms. Figure 5A summarizes the energetic availability of these three systems. Shotgun metagenomic sequencing revealed that, in agreement with Howells et al. (2022), *Methanobacterium* is present in surface-expressed serpentinized fluids. As summarized in Table 5, we assembled four bins classified as *Methanobacterium*. Bin36 was assembled using our "co-assembly" approach, where reads from all three sites were combined and processed to assemble bins. Bins 5, 9, and 19 were assembled from sites 140112K, 140117H, and 140111F, respectively, using our "by-site" approach where reads from individual sites were used to resolve bins. Bin9 has the highest estimated completeness (87.7%) and lowest estimated contamination (0%) of the assemblies. For the first time in Oman serpentinized fluids, in addition to detecting *Methanobacterium*, we have evidence for a potential acetoclastic methanogen of the class *Methanosarcinaceae*. We assembled two bins, one from the co-assembly approach, Bin50 (completeness 76.14%, contamination 0.65%), and one with the by-site approach, Bin11 (completeness 76.14%, contamination 2.61%), from site 140117H. We could not resolve bins for *Methanosarcinaceae* from sites 140112K and 140111F. *Methanosarcinaceae* bins were classified as JAAXQB01, which is a metagenome-assembled genome in the NCBI genome database (accession #, JAAXQB000000000) resolved from a Lost City serpentinized fluid hydrothermal vent (McGonigle et al., 2020). When examining the nearest neighbors in our classification approach (see methods), Bin50 and Bin11 only share one close relative, that being genome JAAXQB01 (see Supplementary Figure S3), which suggests serpentinized fluid *Methanosarcinaceae* are phylogenetically unique and more work must be done to characterize these novel organisms in serpentinized fluid.

We assessed the relative frequency of the methanogen bins reported in Table 5, focusing on Bin36 (*Methanobacterium*) and Bin50 (*Methanosarcinaceae*) (co-assembled MAGs) in Figure 5B. Among the three sites, *Methanobacterium Bin36* is the most abundant at site 140117H, which is the most H_2-rich and has the highest energy available in terms of kJ per mole CH_4 for formatotrophic and hydrogenotrophic methanogenesis. Bin36 is lowest in abundance at site 140111K, which has the least energy available for hydrogenotrophic and acetoclastic methanogenesis. *Methanosarcinaceae* Bin50 has the highest frequency at site 1401117H, although it is incredibly low (0.4%) when compared to the frequency of *Methanobacterium* Bin36 (9.5%). While we could not characterize energy availability for

10.3389/fmicb.2024.1523912

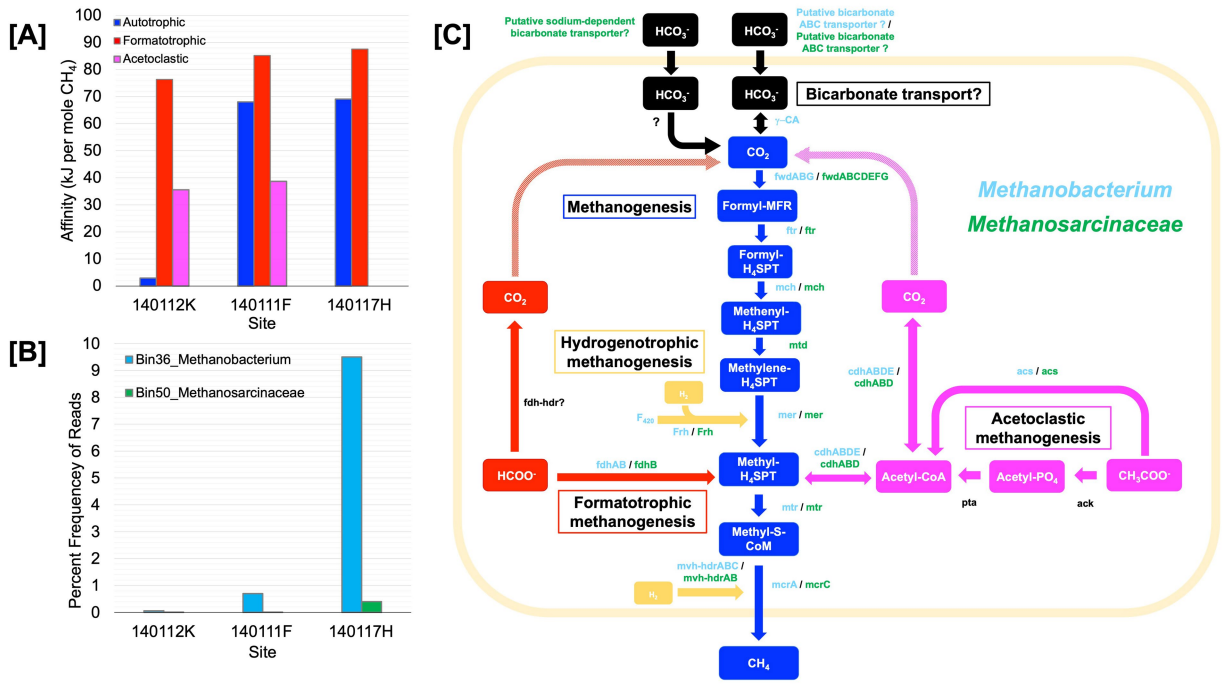

FIGURE 5
Core metabolism summary of methanogen metagenome assembled genomes. **(A)** Energy availability in kJ per mol of CH_4 for methanogenesis reactions at shotgun metagenome sequencing sites. **(B)** Estimated percent frequency of *Methanobacterium Bin36* and *Methanosarcinaceae Bin50* at sequencing sites. **(C)** Portrays the core methanogen metabolic pathways of a *Methanobacterium* and the potential acetolactic methanogen of the genus, *Methanocarcinaceae*. Detected enzymes with >60% sequence identity of cultured methanotroph enzymes are shown in green for *Methanocarcinaceae* and orange for *Methanobacterium*. All enzymes appear next to the arrow between its substrate and product. Carbon substrates and products appear in colored boxes. The meshed arrows indicate the potential pathway in which intracellular CO_2 is generated. Blue colored arrows and boxes indicate Methanogenesis; red indicates Formatotrophic methanogenesis; yellow indicates Hydrogenotrophic methanogenesis, purple indicates Acetoclastic methanogenesis, and black indicates the carbon concentrating mechanism. This figure is inspired by Thieringer et al. (2023). Genes: ɣ-CA, carbonic anhydrase; fwd, formylmethanofuran dehydrogenase; ftr, formylmethanofuran:H4SPT formyltransferase; mch, methenyl-H4SPT cyclohydrolase; mtd, F420-dependent methylene H4SPT dehydrogenase; mer, F420-dependent methyleneH4SPT reductase; mtr, methyl-H4SPT:coenzyme M methyltransferase; mcr, methyl-coenzyme M reductase; ack, acetate kinase; pta, phosphate acetyltransferase; acs, acetyl-CoA synthetase; cdh, carbon monoxide dehydrogenase; fdh, formate dehydrogenase; hdr, heterodisulfide reductase; mvh, methyl viologen-reducing [NiFe]-hydrogenase; frh, coenzyme F420 [NiFe]-hydrogenase; F420, coenzyme F420. Carbon compounds: CO_2, carbon dioxide; formyl-MFR, formyl-methanofuran; formyl-H4SPT, formyl-tetrahydrosarcinapterin; methenyl-H4SPT, methenyl-tetrahydrosarcinapterin; methylene-H4SPT, methylene-tetrahydrosarcinapterin; methyl-H4SPT, methylene-tetrahydrosarcinapterin; methylene-S-CoM, 2-(Methylthio) ethanesulfonate; Acetyl-CoA, acetyl-Coenzyme A; Acetyl-PO4, acetylphosphate; CH_3COO_-, acetate; $HCOO_-$, formate; HCO_3^-, bicarbonate.

acetoclastic methanogenesis at this site due to acetate being below detection, another Type II fluid site in the same sampling location as 1401117H has comparable energy availability as the other two sites in this analysis, 140111K and 140111F. Therefore, the energy availability for acetoclastic methanogenesis may not be a strong determinant for the occurrence of *Methanosarcinaceae* in serpentinizing systems.

Given the estimated completeness of the genomes and the number of contigs that did not pass the binning process at each site (see methods), we take these genomes to be draft genomes. However, valuable insights into methanogen metabolisms can be gained from these assemblies. Figure 5C summarizes the core metabolisms of the *Methanobacterium* and *Methanosarcinaceae* bins. As Figure 5C illustrates, we see the genomic potential for formatotrophic methanogenesis by *Methanobacterium* in surface-expressed Type II fluids with the presence of formate dehydrogenase (fdh). *Methanobacterium* genomes also show evidence for hydrogenotrophic methanogenesis with the presence of methyl viologen reducing hydrogenases (mvh) and CoB-CoM heterodisulfide reductase (hdr) as well as coenzyme F420-reducing hydrogenase (Frh) and membrane bound NiFe hydrogenase (see Supplementary Table S5). As Thieringer et al. (2023) observed, *Methanobacterium* in our study may be able to use acetate as a carbon source with the presence of acetyl-CoA synthetase (acs) and carbon monoxide dehydrogenase (cdh).

In surface-expressed Type II *Methanobacterium* genomes, we also see potential for uptake and utilization of HCO_3^- as a carbon source for hydrogenotrophic methanogenesis. We detect putative ATP-dependent ABC nitrate/sulfonate/bicarbonate transporter in all three *Methanobacterium* bins. While the exact function of this transporter is unknown, it is not out of the realm of possibilities for chemolithotrophs to have functional bicarbonate transporters (Scott et al., 2019), however, bicarbonate transporters have yet to be characterized in methanogens. If *Methanobacterium* has functional bicarbonate transporters, once bicarbonate is transported, it is possible that the gamma carbonic anhydrase detected in *Methanobacterium* bins in this study can convert HCO_3^- to CO_2 for hydrogenotrophic methanogenesis. This process may require some form of a DIC concentrating mechanism, like a carboxysome (an organelle-like structure that traps CO_2 and concentrates carbon in bacteria), but whether or not a carboxysome is required is dependent on the DIC flux required at the in-situ growth rate. Carbon concentrating

TABLE 5 Assembly statistics for metagenome assemble genomes (MAGs) of methanogens and the estimated frequency of the genomes at each sequencing site.

											% Mapped Reads (Bowtie)		
Bin ID	Method	Site/s	Core methane metabolism	Taxonomy (GTDB-Tk)	Est. Compl.	Est. Contam.	GC (%)	Size (bp)	Contig (no.)	CDS	140117H, 99.9%	140112K, 99.1%	140111F, 96.9%
Bin36	Co	All	Formatotrophic/ hydrogenotrophic	Family, *Methanobacteriaceae* Genus, *Methanobacterium*	80.53	0.8	35.4	883,190	227	1,051	9.5	0.06	0.7
Bin9	By site	140117H	Formatotrophic/ hydrogenotrophic	Family, *Methanobacteriaceae* Genus, *Methanobacterium*	87.73	0	35.3	1,123,095	265	1,358	12.8	0.08	0.9
Bin19	By site	140111F	Formatotrophic/ hydrogenotrophic	Family, *Methanobacteriaceae* Genus, *Methanobacterium*	83.04	1.07	35.2	1,245,005	298	1,539	7.8	0.05	0.5
Bin5	By site	140112K	Formatotrophic/ hydrogenotrophic	Family, *Methanobacteriaceae* Genus, *Methanobacterium*	59.11	0.4	35.3	732,008	288	1,046	12.5	0.08	1.0
Bin50	Co	All	Acetoclastic/ hydrogenotrophic	Family, *Methanosarcinaceae* Genus, JAAXQB01	76.14	0.65	33.7	898,440	162	1,006	0.4	0.01	0.01
Bin11	By site	140117H	Acetoclastic/ hydrogenotrophic	Family, *Methanosarcinaceae* Genus, JAAXQB01	76.14	2.61	33.9	949,132	165	1,054	0.4	0	0.02

10.3389/fmicb.2024.1523912

mechanisms have yet to be observed in methanogens and remains a point of exploration, particularly for serpentinized fluids. It is worth noting that carbonic anhydrase was not detected in subsurface *Methanobacterium* genomes characterized in Fones et al. (2021) and Thieringer et al. (2023), making this a unique attribute of surface-expressed serpentinized fluid *Methanobacterium*.

Despite the low estimated completeness of the *Methanosarcinaceae* bins, examining the core metabolism of these genomes reveals that these methanogens have the functional potential to carry out acetoclastic methanogenesis and hydrogenotrophic methanogenesis. The bins of *Methanosarcinaceae* lack the genes that code for acetate kinase (ack) and phosphate acetyltransferase (pta), which together can convert acetate to acetyl-CoA, however they have acetyl-CoA synthetase (acs) which directly converts acetate to acetyl-CoA. Acetoclastic methanogens of the genus *Methanothrix* are known to have acs, which has a higher substrate affinity for acetate than methanogens of the genus *Methanosarcina*, which use ack and pta for acetate activation (Stams et al., 2019). It may be that the overall low organic carbon content of serpentinizing systems selects for acetoclastic methanogens with a high substrate affinity for acetate. It is worth noting that the activation of acetate by acs requires two ATP (Stams et al., 2019). The energetic cost to make 1 ATP from 1 ADP is ~45 kJ per mol CH_4 (Thauer et al., 1977). Based on our affinity calculations there is on average 38 ± 9 kJ per mole CH_4, which is only enough energy for production of 1 ATP and therefore not enough for acetate activation. However, the bins shown evidence for H_2 utilization. If both pools of energy (hydrogenotrophic and acetoclastic) are available to acetoclastic methanogens, then there is more than enough energy for acetate activation. Indeed, some acetoclastic methanogens have been shown to also use H_2 and CO_2 (Welte and Deppenmeier, 2014). It is also worth noting the complete pathway for autotrophy in the *Methanosarcinaceae* bins. It is possible that CO_2 can be supplied through acetate uptake and conversion to CO_2 (with acetyl-CoA as intermediate) by carbon monoxide dehydrogenase (cdh). This may explain why the frequency of Bin11 is highest at 140117H, which has the highest energy availability for hydrogenotrophic methanogenesis as the electron donor among the three sequencing sites.

We carried out a phylogenomic analysis to compare our *Methanobacterium* genomes to those published in Fones et al. (2021) and Thieringer et al. (2023). The resulting maximum likelihood phylogenomic tree shows the pattern of macroevolutionary relationships between Samail Ophiolite *Methanobacterium* and other methanogens, including other *Methanobacterium* species, as well as *Methanosphaera, Methanobrevibacter, Methanocalculus,* and the *Methanosarcinaceae.* Bootstrap values at nodes indicate the percentage of replicate trees in which a given node was observed; these were overwhelmingly close to 100, as can be seen in Figure 6. Genomes for which there was reliable environmental data available were labeled according to environment type. Colored squares were used to indicate pH affinity. The highest observed optimum or environmental pH for each genome was used to assess whether it fell into the following categories: neutrophile: pH 6.5 to 8.5; alkaliphile: pH 8.5 to 10; hyperalkaliphile: pH 10 and above. Colored triangles indicate temperature affinity. Psychrophiles were those with their lowest point in optimum or observed temperature below 20°C; all others were mesophiles. Among genomes from the Samail Ophiolite, colored circles indicate whether genomes were found at the surface or subsurface. The root of the tree is based on Thieringer et al. (2023). An unrooted tree is shown in Supplementary Figure S4.

This analysis shows that *Methanobacterium* bins from surface-expressed fluids share a common ancestor with Type II *Methanobacterium* from the subsurface (Figure 6). The phylogenomic relationship and core metabolism annotation suggest that like Type II *Methanobacterium* from subsurface well fluids (Fones et al., 2021) *Methanobacterium* from the surface may be able to use formate as an electron donor and have maintained functional capability for hydrogenotrophic methanogenesis. The phylogenomic tree also reveals that *Methanobacterium* from Oman form their own clade distinct from neutrophilic *Methanobacterium*. There is one *Methanobacterium* cultivar considered to be an alkaliphile, *M. subterraneum*. However, it is in a clade with other neutrophilic *Methanobacterium* genomes. This suggests that adaptations to serpentinized fluids may extend beyond adaptation to alkaline pH alone. For *Methanobacterium*, this may be attributed to carbon limitation, as described in Fones et al. (2021). The *Methanosarcinaceae* Bin11 and Lost City MAG (JAAXQB01) form their own distinct clade and appear to share a common ancestor with other *Methanosarcina* (see unrooted tree in Supplementary Figure S4). The new serpentinizing system clade are closely relately to methanogens of the genus *Methanocalculus*, some species of which are alkaline soda lake methanogens that can carry out hydrogenotrophic methanogenesis and require acetate for growth (Sorokin et al., 2015). This suggests that alkaline pH may be a selective pressure for evolution of acetoclastic and acetate-utilizing methanogens.

Overall, examining methanogen genomes in surface-expressed Type II fluids shows that hydrogenotrophic methanogenesis with HCO_3^-, formatotrophic methanogenesis, and acetoclastic methanogenesis are genomically possible, even co-occurring in these systems. The genomic potential for formatotrophic methanogenesis by *Methanobacterium* combined with energetic calculations supports the hypothesis that there may be an energetic drive for *Methanobacterium* to carry out formatotrophic methanogenesis, despite the high concentration of H_2 available for hydrogenotrophic methanogenesis. H_2 may may act as an additional electron donor for methanogenesis by *Methanosarcinaceae* in serpentinizing systems after acetate is converted to CO_2 by carbon monoxide dehydrogenase. The first-time detection of genomes in the Samail Ophiolite classified as *Methanosarcinaceae* and their phylogenomic similarity to *Methanosarcinaceae* genomes from Lost City suggest that potential acetoclastic methanogens in serpentinizing systems are unique and beg for deeper characterization.

4 Conclusion

In this study, we found that in the most reduced, hyperalkaline, H_2-rich serpentinized fluids in the Samail Ophiolite, formatotrophic methanogenesis yields more energy than hydrogenotrophic and acetoclastic methanogenesis in terms of kJ per mole CH_4 produced. While these fluids are H_2-rich, they are also depleted of inorganic carbon. Consequently, formatotrophic

10.3389/fmicb.2024.1523912

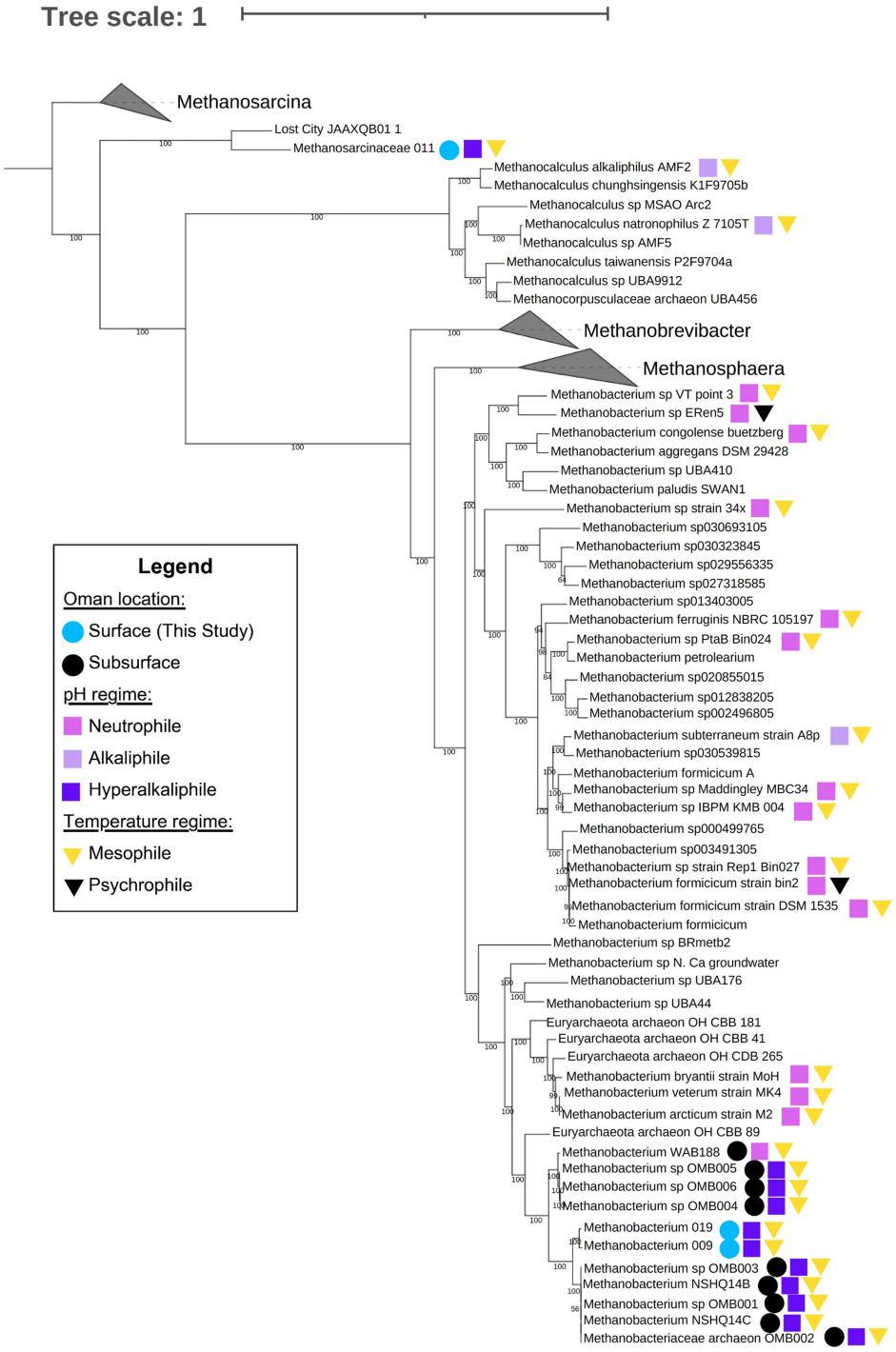

FIGURE 6
Maximum likelihood phylogenomic tree of *Methanobacterium*, *Methanosarcinaceae* and related taxa constructed via GToTree using 76 archaeal marker genes identified by the program. Within GToTree, IQ-TREE was called in order to generate the tree. The program was run with 1,000 bootstrap replicates; bootstrap confidence estimates (out of 100) are shown at nodes. We included 11 genomes from Samail Ophiolite Methanobacterium and 18 genomes from other methanogenic archaea which had satisfactory metadata and genome completeness. Also included were GTDB representative genomes from the genera *Methanobacterium*, *Methanosphaera*, *Methanobrevibacter*, and *Methanosarcina*, as well as genomes identified by GTDB-Tk - v2.3.2 as "close relatives" of *Methanocalculus natronophilus*, *Methanobacterium congolense* buetzberg, and the Oman MAGs isolated by Thieringer et al., 2023 and in this study. Genomes for which relevant metadata was available are marked on the tree. Circles indicate genomes from surface (light blue) and subsurface (teal) environments among methanogens taken from the Samail Ophiolite in Oman. Squares indicate pH affinity, neutrophile (mauve), alkaliphile (lavender), or hyperalkaliphile (dark purple), of all relevant strains; and triangles indicate temperature affinity, mesophile (yellow) or psychrophile (black), of all relevant strains. Neutrophiles were defined as organisms which, whether through environmental or culture-derived data, were determined to thrive between pH 6.5 and 8.5 but no higher; alkaliphiles were defined as those which thrived between pH 8.5 and 10 but no higher; hyperalkaliphiles were those which thrived at pH 10 and above. Similarly, psychrophiles were defined as organisms which, whether through environmental or culture-derived data, were determined to thrive below 20°C; mesophiles were those which thrived between 20 and 50°C but no lower. More information on these genomes and the metadata used to label this tree can be found in Supplementary Table S5.

methanogenesis, a reaction that produces 3 moles of inorganic carbon per mole of CH_4 produced, can be more energetically favorable than hydrogenotrophic methanogenesis with H_2 as the electron donor. This may explain why formatotrophic *Methanobacterium* from Oman characterized in subsurface Type II fluids in Fones et al. (2021) and possibly surface-expressed *Methanobacterium* characterized in this study may preferentially use formate over bicarbonate in Type II fluids. That said, in terms of J per kg of fluid, hydrogenotrophic methanogenesis yields more energy than formatotrophic and acetoclastic methanogenesis, especially in mixed fluids where H_2 is not stoichiometrically limited, and there is a greater supply of inorganic carbon due to fluid mixing. While mixed fluids pose a problem to methanogens at the surface due to the influence of O_2 (Howells et al., 2022), the energy available for hydrogenotrophic methanogenesis in mixed subsurface fluids may explain the ability of *Methanobacterium* (genome Type I) to use inorganic carbon and formate for methanogenesis as reported in Fones et al. (2021).

Our work finds that acetoclastic methanogenesis is energetically favorable in serpentinized fluids in Oman. However, previous studies on the microbial communities in the Samail Ophiolite failed to detect acetoclastic methanogens. In this study, we assembled for the first time a genome classified as belonging to the acetoclastic methanogen family, *Methanosarcinaceae*. Based on phylogenomic analyses, this MAG has only one close relative, a genome of an acetoclastic methanogen of the family *Methanosarcinaceae*, JAAXQB01, resolved from the Lost City serpentinizing hydrothermal vent field (McGonigle et al., 2020). The unique nature of these genomes inspires deeper characterization of a potentially novel methanogen group.

Overall, this work stresses the importance of considering both substrate availability and energy availability when examining factors that influence methanogen distribution and evolution on Earth. For the same reason that hydrogenotrophic methanogenesis is an energetically costly process in serpentinized fluids, formatotrophic methanogenesis is energetically favorable and circumvents the cost of utilizing CO_2 in an inorganic carbon-limited environment. As we look beyond Earth and consider what life may be supported on Enceladus or Europa, this study suggests a broader suite of carbon substrates could support life like methanogens on these moons, particularly given that formate can be produced abiotically under hydrothermal, serpentinizing conditions.

Data availability statement

The original contributions presented in the study are publicly available. This data can be found here: https://www.ncbi.nlm.nih.gov/sra, under the BioProject number PRJNA1207711. The metagenome-assembled genomes presented in this study will be made available by the authors without undue reservation upon request.

Author contributions

AH: Conceptualization, Data curation, Formal analysis, Investigation, Methodology, Project administration, Supervision, Validation, Visualization, Writing – original draft, Writing – review & editing. LQ: Data curation, Formal analysis, Investigation, Methodology, Visualization, Writing – original draft, Writing – review & editing. MS: Data curation, Formal analysis, Investigation, Methodology, Visualization, Writing – original draft, Writing – review & editing. KA: Data curation, Formal analysis, Investigation, Visualization, Writing – original draft, Writing – review & editing. LF: Conceptualization, Data curation, Formal analysis, Investigation, Methodology, Software, Validation, Visualization, Writing – original draft, Writing – review & editing. GB: Data curation, Formal analysis, Investigation, Methodology, Project administration, Software, Supervision, Validation, Visualization, Writing – original draft, Writing – review & editing. SK: Data curation, Formal analysis, Investigation, Methodology, Supervision, Validation, Writing – original draft, Writing – review & editing. KR: Data curation, Formal analysis, Investigation, Methodology, Validation, Writing – original draft, Writing – review & editing. JB: Formal analysis, Funding acquisition, Investigation, Project administration, Resources, Supervision, Writing – original draft, Writing – review & editing. ES: Funding acquisition, Investigation, Project administration, Resources, Supervision, Validation, Writing – original draft, Writing – review & editing. TH: Formal analysis, Funding acquisition, Investigation, Methodology, Project administration, Resources, Supervision, Validation, Writing – original draft, Writing – review & editing.

Funding

The author(s) declare that financial support was received for the research, authorship, and/or publication of this article. Field research was funded by NASA Exobiology Grant NNX12AB38G, the NASA Astrobiology Institute Rock-Powered Life (RPL) project Grant NNA15BB02A, and NSF Grant EAR-1515513. The Water-Organic-Rock-Microbe (WORM) Portal was supported by NSF grants EAR-1949030 and EAR-2149016. Shotgun metagenome sequencing was funded through the Deep Carbon Observatory's Census of Deep Life supported by the Alfred P. Sloan Foundation. We acknowledge support from the NASA Planetary Science Division to the Center for Life Detection ISFM team. The NASA Postdoctoral Program at NASA Ames Research Center funded Alta E. G. Howells postdoctoral fellowship. The University of Washington Astrobiology Program supported Lucas Fifer's involvement in the project. Lilja Quinn, Miguel Silva and Kylie Akiyama completed their portions of this project as part of their participation in the BMSIS Young Scientist Program (YSP) at NASA Ames Research Center under the mentorship of Alta E. G. Howells and Tori M. Hoehler.

Acknowledgments

We acknowledge the contribution of the Exobiology Scholars Program in the Exobiology Branch at NASA Ames Research Center to the internships of Lilja Quinn, Miguel Silva and Kylie Akiyama. We appreciate Sanjoy Som for the helpful insights into methanogenesis and substrate flux in serpentinizing systems. We acknowledge Alexis Templeton and Rock Powered Life for facilitating research in Oman. We thank Peter Kelemen and Jürg Matter for their logistical assistance in the field. We acknowledge the assistance of Michael Kubo in setting up the internships of Lilja Quinn, Kylie Akiyama and Miguel Silva.

We thank Jan Amend for being a source of inspiration and helping lay the foundations of energy supply assessments in this study.

Conflict of interest

The authors declare that the research was conducted in the absence of any commercial or financial relationships that could be construed as a potential conflict of interest.

Generative AI statement

The authors declare that no Gen AI was used in the creation of this manuscript.

Publisher's note

Supplementary material

The Supplementary material for this article can be found online at: https://www.frontiersin.org/articles/10.3389/fmicb.2024.1523912/full#supplementary-material

References

Alneberg, J., Bjarnason, B. S., de Bruijn, I., Schirmer, M., Quick, J., Ijaz, U. Z., et al. (2013). CONCOCT: clustering contigs on coverage and composition. *arXiv:1312.4038*. doi: 10.48550/arXiv.1312.4038

Bar-Even, A., Noor, E., Savir, Y., Liebermeister, W., Davidi, D., Tawfik, D. S., et al. (2011). The moderately efficient enzyme: evolutionary and physicochemical trends shaping enzyme parameters. *Biochemistry* 50, 4402–4410. doi: 10.1021/bi2002289

Bolger, A. M., Lohse, M., and Usadel, B. (2014). Trimmomatic: a flexible trimmer for Illumina sequence data. *Bioinformatics* 30, 2114–2120. doi: 10.1093/bioinformatics/btu170

Boone, D. R., Johnson, R. L., and Liu, Y. (1989). Diffusion of the interspecies electron carriers H2 and formate in methanogenic ecosystems and its implications in the measurement of K m for H2 or formate uptake. *Appl. Environ. Microbiol.* 55, 1735–1741. doi: 10.1128/aem.55.7.1735-1741.1989

Boyer, G., Robare, J., Park, N., Ely, T., and Shock, E. (2024). AqEquil: Python package for aqueous geochemical speciation (v0.19.0). *Zenodo*. doi: 10.5281/zenodo.13530217

Brazelton, W. J., McGonigle, J. M., Motamedi, S., Pendleton, H. L., Twing, K. I., Miller, B. C., et al. (2022). Metabolic strategies shared by basement residents of the lost City hydrothermal field. *Appl. Environ. Microbiol.* 88, e00929–e00922. doi: 10.1128/aem.00929-22

Brettin, T., Davis, J. J., Disz, T., Edwards, R. A., Gerdes, S., Olsen, G. J., et al. (2015). RASTtk: a modular and extensible implementation of the RAST algorithm for building custom annotation pipelines and annotating batches of genomes. *Sci. Rep.* 5, 1–6. doi: 10.1038/srep08365

Callahan, B. J., McMurdie, P. J., Rosen, M. J., Han, A. W., Johnson, A. J. A., and Holmes, S. P. (2016). DADA2: high-resolution sample inference from Illumina amplicon data. *Nat. Methods* 13, 581–583. doi: 10.1038/nmeth.3869

Camacho, C., Coulouris, G., Avagyan, V., Ma, N., Papadopoulos, J., Bealer, K., et al. (2009). BLAST+: architecture and applications. *BMC Bioinformatics* 10:421. doi: 10.1186/1471-2105-10-421

Canovas, P. A. III, Hoehler, T., and Shock, E. L. (2017). Geochemical bioenergetics during low-temperature serpentinization: an example from the Samail ophiolite, Sultanate of Oman. *J. Geophys. Res. Biogeo.* 122, 1821–1847. doi: 10.1002/2017JG003825

Capella-Gutiérrez, S., Silla-Martínez, J. M., and Gabaldón, T. (2009). trimAl: a tool for automated alignment trimming in large-scale phylogenetic analyses. *Bioinformatics* 25, 1972–1973. doi: 10.1093/bioinformatics/btp348

Caporaso, J. G., Lauber, C. L., Walters, W. A., Berg-Lyons, D., Huntley, J., Fierer, N., et al. (2012). Ultra-high-throughput microbial community analysis on the Illumina HiSeq and MiSeq platforms. *ISME J.* 6, 1621–1624. doi: 10.1038/ismej.2012.8

Chaumeil, P. A., Mussig, A. J., Hugenholtz, P., and Parks, D. H. (2022). GTDB-Tk v2: memory friendly classification with the genome taxonomy database. *Bioinformatics* 38, 5315–5316. doi: 10.1093/bioinformatics/btac672

Chen, X., Ottosen, L. D. M., and Kofoed, M. V. W. (2019). How low can you go: methane production of Methanobacterium congolense at low CO2 concentrations. *Front. Bioeng. Biotechnol.* 7:34. doi: 10.3389/fbioe.2019.00034

Colman, D. R., Boyd, E. S., Templeton, A. S., and Spear, J. R. (2024). The microbial ecology of Serpentinites. *bioRxiv*. doi: 10.1101/2024.11.10.622848

Colman, D. R., Kraus, E. A., Thieringer, P. H., Rempfert, K., Templeton, A. S., Spear, J. R., et al. (2022). Deep-branching acetogens in serpentinized subsurface fluids of Oman. *Proc. Natl. Acad. Sci.* 119:e2206845119. doi: 10.1073/pnas.2206845119

Crank, J. (1979). The mathematics of diffusion. New York, United States: Oxford University Press.

Cussler, E. L. (2009). Diffusion: Mass transfer in fluid systems. New York, United States: Cambridge University Press.

DeSantis, T. Z., Hugenholtz, P., Larsen, N., Rojas, M., Brodie, E. L., Keller, K., et al. (2006). Greengenes, a chimera-checked 16S rRNA gene database and workbench compatible with ARB. *Appl. Environ. Microbiol.* 72, 5069–5072. doi: 10.1128/AEM.03006-05

Eddy, S. R. (2011). Accelerated profile HMM searches. *PLoS Comput. Biol.* 7:e1002195. doi: 10.1371/journal.pcbi.1002195

Edgar, R. C. (2022). Muscle5: high-accuracy alignment ensembles enable unbiased assessments of sequence homology and phylogeny. *Nat. Commun.* 13:6968. doi: 10.1038/s41467-022-34630-w

Fones, E. M., Colman, D. R., Kraus, E. A., Nothaft, D. B., Poudel, S., Rempfert, K. R., et al. (2019). Physiological adaptations to serpentinization in the Samail ophiolite, Oman. *ISME J.* 13, 1750–1762. doi: 10.1038/s41396-019-0391-2

Fones, E. M., Colman, D. R., Kraus, E. A., Stepanauskas, R., Templeton, A. S., Spear, J. R., et al. (2021). Diversification of methanogens into hyperalkaline serpentinizing environments through adaptations to minimize oxidant limitation. *ISME J.* 15, 1121–1135. doi: 10.1038/s41396-020-00838-1

Hoehler, T. M. (2004). Biological energy requirements as quantitative boundary conditions for life in the subsurface. *Geobiology* 2, 205–215. doi: 10.1111/j.1472-4677.2004.00033.x

Hoehler, T. M. (2007). An energy balance concept for habitability. *Astrobiology* 7, 824–838. doi: 10.1089/ast.2006.0095

Howells, A. E., De Martini, F., Gile, G. H., and Shock, E. L. (2023). An examination of protist diversity in serpentinization-hosted ecosystems of the Samail ophiolite of Oman. *Front. Microbiol.* 14:1139333. doi: 10.3389/fmicb.2023.1139333

Howells, A. E., Leong, J. A., Ely, T., Santana, M., Robinson, K., Esquivel-Elizondo, S., et al. (2022). Energetically informed niche models of hydrogenotrophs detected in sediments of serpentinized fluids of the Samail ophiolite of Oman. Journal of geophysical research. *Biogeosciences* 127:e2021JG006317. doi: 10.1029/2021JG006317

Hyatt, D., Chen, G. L., LoCascio, P. F., Land, M. L., Larimer, F. W., and Hauser, L. J. (2010). Prodigal: prokaryotic gene recognition and translation initiation site identification. *BMC Bioinformatics* 11:119. doi: 10.1186/1471-2105-11-119

Johnson, K. S. (1982). Carbon dioxide hydration and dehydration kinetics in seawater 1. *Limnol. Oceanogr.* 27, 849–855. doi: 10.4319/lo.1982.27.5.0849

Kang, D. D., Li, F., Kirton, E., Thomas, A., Egan, R., An, H., et al. (2019). MetaBAT 2: an adaptive binning algorithm for robust and efficient genome reconstruction from metagenome assemblies. *PeerJ*, 7:e7359.

Kelemen, P. B., Matter, J., Streit, E. E., Rudge, J. F., Curry, W. B., and Blusztajn, J. (2011). Rates and mechanisms of mineral carbonation in peridotite: natural processes and recipes for enhanced, in situ CO2 capture and storage. *Annu. Rev. Earth Planet. Sci.* 39, 545–576. doi: 10.1146/annurev-earth-092010-152509

Langmead, B., and Salzberg, S. L. (2012). Fast gapped-read alignment with bowtie 2. *Nat. Methods* 9, 357–359. doi: 10.1038/nmeth.1923

Lee, M. D. (2019). GToTree: a user-friendly workflow for phylogenomics. *Bioinformatics* 35, 4162–4164. doi: 10.1093/bioinformatics/btz188

Leong, J. A. M., Howells, A. E., Robinson, K. J., Cox, A., Debes, R. V., Fecteau, K., et al. (2021). Theoretical predictions versus environmental observations on serpentinization

fluids: lessons from the Samail ophiolite in Oman. *J. Geophys. Res. Solid Earth* 126:e2020JB020756. doi: 10.1029/2020JB020756

Letunic, I., and Bork, P. (2024). Interactive tree of life (iTOL) v6: recent updates to the phylogenetic tree display and annotation tool. *Nucleic Acids Res.* 52, W78–W82. doi: 10.1093/nar/gkae268

McCollom, T. M., and Bach, W. (2009). Thermodynamic constraints on hydrogen generation during serpentinization of ultramafic rocks. *Geochim. Cosmochim. Acta* 73, 856–875. doi: 10.1016/j.gca.2008.10.032

McCollom, T. M., and Seewald, J. S. (2007). Abiotic synthesis of organic compounds in deep-sea hydrothermal environments. *Chem. Rev.* 107, 382–401. doi: 10.1021/cr0503660

McDermott, J. M., Seewald, J. S., German, C. R., and Sylva, S. P. (2015). Pathways for abiotic organic synthesis at submarine hydrothermal fields. *Proc. Natl. Acad. Sci.* 112, 7668–7672. doi: 10.1073/pnas.1506295112

McGonigle, J. M., Lang, S. Q., and Brazelton, W. J. (2020). Genomic evidence for formate metabolism by Chloroflexi as the key to unlocking deep carbon in lost City microbial ecosystems. *Appl. Environ. Microbiol.* 86, e02583–e02519. doi: 10.1128/AEM.02583-19

Miller, H. M., Matter, J. M., Kelemen, P., Ellison, E. T., Conrad, M. E., Fierer, N., et al. (2016). Modern water/rock reactions in Oman hyperalkaline peridotite aquifers and implications for microbial habitability. *Geochim. Cosmochim. Acta* 179, 217–241. doi: 10.1016/j.gca.2016.01.033

Nguyen, L. T., Schmidt, H. A., Von Haeseler, A., and Minh, B. Q. (2015). IQ-TREE: a fast and effective stochastic algorithm for estimating maximum-likelihood phylogenies. *Mol. Biol. Evol.* 32, 268–274. doi: 10.1093/molbev/msu300

Nothaft, D. B., Templeton, A. S., Boyd, E. S., Matter, J. M., Stute, M., Paukert Vankeuren, A. N., et al. (2021a). Aqueous geochemical and microbial variation across discrete depth intervals in a peridotite aquifer assessed using a packer system in the Samail ophiolite, Oman. Journal of geophysical research. *Biogeosciences* 126:e2021JG006319. doi: 10.1029/2021JG006319

Nothaft, D. B., Templeton, A. S., Rhim, J. H., Wang, D. T., Labidi, J., Miller, H. M., et al. (2021b). Geochemical, biological, and clumped isotopologue evidence for substantial microbial methane production under carbon limitation in serpentinites of the Samail ophiolite, Oman. *J. Geophys. Res. Biogeosci.* 126:e2020JG006025. doi: 10.1029/2020JG006025

Nurk, S., Meleshko, D., Korobeynikov, A., and Pevzner, P. A. (2017). metaSPAdes: a new versatile metagenomic assembler. *Genome Res.* 27, 824–834. doi: 10.1101/gr.213959.116

Parkhust, D. L., and Appelo, C. A. J. (1999). A computer program for speciation, batch-reaction, one-dimensional transport and inverse geochemical calculations. *USGS Report*.

Parks, D. H., Imelfort, M., Skennerton, C. T., Hugenholtz, P., and Tyson, G. W. (2015). CheckM: assessing the quality of microbial genomes recovered from isolates, single cells, and metagenomes. *Genome Res.* 25, 1043–1055. doi: 10.1101/gr.186072.114

Quast, C., Pruesse, E., Yilmaz, P., Gerken, J., Schweer, T., Yarza, P., et al. (2012). The SILVA ribosomal RNA gene database project: improved data processing and web-based tools. *Nucleic Acids Res.* 41, D590–D596. doi: 10.1093/nar/gks1219

R Core Team (2021). *R: A Language and Environment for Statistical Computing*. R Foundation for Statistical Computing, Vienna, Austria.

Rempfert, K. R., Miller, H. M., Bompard, N., Nothaft, D., Matter, J. M., Kelemen, P., et al. (2017). Geological and geochemical controls on subsurface microbial life in the Samail ophiolite, Oman. *Front. Microbiol.* 8:56. doi: 10.3389/fmicb.2017.00056

Schönheit, P., Moll, J., and Thauer, R. K. (1980). Growth parameters (K s, μmax, Y s) of Methanobacterium thermoautotrophicum. *Arch. Microbiol.* 127, 59–65. doi: 10.1007/BF00414356

Scott, K. M., Leonard, J. M., Boden, R., Chaput, D., Dennison, C., Haller, E., et al. (2019). Diversity in CO2-concentrating mechanisms among chemolithoautotrophs from the genera Hydrogenovibrio, Thiomicrorhabdus, and Thiomicrospira, ubiquitous in sulfidic habitats worldwide. *Appl. Environ. Microbiol.* 85, e02096–e02018. doi: 10.1128/AEM.02096-18

Shock, E. L., and Holland, M. E. (2007). Quantitative habitability. *Astrobiology* 7, 839–851. doi: 10.1089/ast.2007.0137

Shock, E. L., Holland, M., Amend, J. P., Osburn, G. R., and Fischer, T. P. (2010). Quantifying inorganic sources of geochemical energy in hydrothermal ecosystems, Yellowstone National Park, USA. *Geochim. Cosmochim. Acta* 74, 4005–4043. doi: 10.1016/j.gca.2009.08.036

Sieber, C. M., Probst, A. J., Sharrar, A., Thomas, B. C., Hess, M., Tringe, S. G., et al. (2018). Recovery of genomes from metagenomes via a dereplication, aggregation and scoring strategy. *Nat. Microbiol.* 3, 836–843. doi: 10.1038/s41564-018-0171-1

Sorokin, D. Y., Abbas, B., Merkel, A. Y., Rijpstra, W. I. C., Damsté, J. S. S., Sukhacheva, M. V., et al. (2015). Methanosalsum natronophilum sp. nov., and Methanocalculus alkaliphilus sp. nov., haloalkaliphilic methanogens from hypersaline soda lakes. *Int. J. Syst. Evol. Microbiol.* 65, 3739–3745. doi: 10.1099/ijsem.0.000488

Stams, F., and de Sousa, D. M. (2019). Biogenesis of hydrocarbons. Germany: Springer.

Stams, A. J. M., Teusink, B., and Sousa, D. Z. (2019). Ecophysiology of acetoclastic methanogens. In: Biogenesis of Hydrocarbons. Handbook of Hydrocarbon and Lipid Microbiology. Eds. A. Stams, D. Sousa. Cham: Springer.

Thauer, R. K., Jungermann, K., and Decker, K. (1977). Energy conservation in chemotrophic anaerobic bacteria. *Bacteriol. Rev.* 41, 100–180. doi: 10.1128/br.41.1.100-180.1977

Thieringer, P. H., Boyd, E. S., Templeton, A. S., and Spear, J. R. (2023). Metapangenomic investigation provides insight into niche differentiation of methanogenic populations from the subsurface serpentinizing environment, Samail ophiolite, Oman. *Front. Microbiol.* 14:1205558. doi: 10.3389/fmicb.2023.1205558

Vance, S. D., Craft, K. L., Shock, E., Schmidt, B. E., Lunine, J., Hand, K. P., et al. (2023). Investigating Europa's habitability with the Europa clipper. *Space Sci. Rev.* 219:81. doi: 10.1007/s11214-023-01025-2

Vaný́sek, P. (1993). "Ionic conductivity and diffusion at infinite dilution" in CRC handbook of chemistry and physics, vol. 94.

Vorholt, J. A., and Thauer, R. K. (1997). The active species of 'CO2' utilized by formylmethanofuran dehydrogenase from methanogenic Archaea. *Eur. J. Biochem.* 248, 919–924.

Waite, J. H., Glein, C. R., Perryman, R. S., Teolis, B. D., Magee, B. A., Miller, G., et al. (2017). Cassini finds molecular hydrogen in the Enceladus plume: evidence for hydrothermal processes. *Science* 356, 155–159. doi: 10.1126/science.aai8703

Welte, C., and Deppenmeier, U. (2014). Bioenergetics and anaerobic respiratory chains of aceticlastic methanogens. *Biochim. Biophys. Acta Bioenerget.* 1837, 1130–1147. doi: 10.1016/j.bbabio.2013.12.002

Welte, C., Kröninger, L., and Deppenmeier, U. (2014). Experimental evidence of an acetate transporter protein and characterization of acetate activation in aceticlastic methanogenesis of Methanosarcina mazei. *FEMS Microbiol. Lett.* 359, 147–153. doi: 10.1111/1574-6968.12550

White, W. B., and Ferry, J. G. (1992). Identification of formate dehydrogenase-specific mRNA species and nucleotide sequence of the fdhC gene of Methanobacterium formicicum. *J. Bacteriol.* 174, 4997–5004. doi: 10.1128/jb.174.15.4997-5004.1992

Wolery, T. J. (2013). EQ3/6 - software for geochemical modeling, Version 8.0a, LLNL-CODE-2013-683958. Livermore, CA: Lawrence Livermore National Laboratory.

Yaws, C. L. (2009). Chapter 12 - "Diffusion coefficient in water–organic compounds" in Transport properties of chemicals and hydrocarbons (Boston: William Andrew Publishing), 502–593. Available at: https://www.sciencedirect.com/science/article/pii/B978081552039950017X

frontiers | Frontiers in Microbiology

TYPE Original Research
PUBLISHED 03 February 2025
DOI 10.3389/fmicb.2025.1504355

OPEN ACCESS

EDITED BY
Alberto Robador,
University of Southern California,
United States

REVIEWED BY
Carl-Eric Wegner,
Heinrich Heine University of
Düsseldorf, Germany
Jan Kuever,
Bremen Institute for Materials
Testing, Germany

*CORRESPONDENCE
Paula Rodriguez
✉ pramirez@ethz.ch

RECEIVED 30 September 2024
ACCEPTED 06 January 2025
PUBLISHED 03 February 2025

CITATION
Rodriguez P, Berg JS, Deng L, Vogel H, Okoniewski M, Lever MA and Magnabosco C (2025) Persistent functional and taxonomic groups dominate an 8,000-year sedimentary sequence from Lake Cadagno, Switzerland. *Front. Microbiol.* 16:1504355. doi: 10.3389/fmicb.2025.1504355

Persistent functional and taxonomic groups dominate an 8,000-year sedimentary sequence from Lake Cadagno, Switzerland

Paula Rodriguez[1]*, Jasmine S. Berg[2], Longhui Deng[3,4], Hendrik Vogel[5], Michal Okoniewski[6], Mark A. Lever[3,7] and Cara Magnabosco[1]

[1]Department of Earth and Planetary Sciences, ETH Zurich, Zurich, Switzerland, [2]Faculty of Geosciences and Environment, Université de Lausanne, Lausanne, Switzerland, [3]Institute for Biogeochemistry and Pollutant Dynamics, ETH Zurich, Zurich, Switzerland, [4]School of Oceanography, Shanghai Jiao Tong University, Shanghai, China, [5]Oeschger Centre for Climate Change Research, Institute of Geological Sciences, University of Bern, Bern, Switzerland, [6]ID Scientific IT Services, ETH Zurich, Zurich, Switzerland, [7]College of Natural Sciences, Marine Science Institute, University of Texas at Austin, Austin, TX, United States

Most of our knowledge of deep sedimentary life comes from marine environments; however, despite their relatively small volume, lacustrine sediments constitute one of the largest global carbon sinks and their deep sediments are largely unexplored. Here, we reconstruct the microbial functional and taxonomic composition of an 8,000-year Holocene sedimentary succession from meromictic Lake Cadagno (Switzerland) using shotgun metagenomics and 16S rRNA gene amplicon sequencing. While younger sediments (<1,000 years) are dominated by typical anaerobic surface sedimentary bacterial taxa (*Deltaproteobacteria*, *Acidobacteria*, and *Firmicutes),* older layers with lower organic matter concentrations and reduced terminal electron acceptor availability are dominated by taxa previously identified as "persistent populations" within deep anoxic marine sediments (*Candidatus* Bathyarchaeia, *Chloroflexi*, and *Atribacteria*). Despite these dramatic changes in taxonomic community composition and sediment geochemistry throughout the sediment core, higher-order functional categories and metabolic marker gene abundances remain relatively consistent and indicate a microbial community capable of carbon fixation, fermentation, dissimilatory sulfate reduction and dissimilatory nitrate reduction to ammonium. As the conservation of these metabolic pathways through changes in microbial community compositions helps preserve the metabolic pathway connectivity required for nutrient cycling, we hypothesize that the persistence of these functional groups helps enable the Lake Cadagno sedimentary communities persist amidst changing environmental conditions.

KEYWORDS

deep lacustrine sediments, functional potential, microbial communities, biogeochemical cycling, metagenomics

Introduction

Subsurface marine and lacustrine sediments cover approximately 70% of Earth's surface (Oni et al., 2015; Hoshino et al., 2020) and constitute the largest global organic carbon reservoirs (Barber et al., 2017). This substantial habitat hosts a significant fraction of the world's bacterial and archaeal populations (Kallmeyer et al., 2012) and exhibits much slower metabolic rates than their surface sedimentary counterparts (Jorgensen and Marshall, 2016). This is in part due to the low oxygen supply, which often leads to anoxic conditions that promote the preservation of organic matter and environmental signatures in the sediment record (Jessen et al., 2017). Lacustrine sediments are often regarded as time capsules for paleo-reconstructions, as sediment deposition happens continuously and at higher rates, and experiences less reworking, compared to marine sediments (Zolitschka and Enters, 2009). The resulting high-resolution temporal records of environmental change (Zolitschka and Enters, 2009) make lake sediments ideal settings to study the interplay between long-term environmental changes in lake water sheds and biogeochemical processes which slowly alter environmental records after burial (Ariztegui et al., 2015). Despite their unique features, the effects of sediment burial on the community assembly, function, and diversity in deep lacustrine sediments are poorly understood, especially when compared to those of deep marine sediments (Ariztegui et al., 2015). Studies on microbial assemblages in deep lacustrine sediments are thus essential for understanding how the environmental features of lake ecosystems shape sediment microbial communities (Vuillemin et al., 2018).

On a global scale, organic carbon content is one of the main environmental parameters correlated with microbial biogeography patterns in anoxic sediments (Hoshino et al., 2020). In places with high sedimentation rates (e.g., Lake Cadagno, the site of this study), microorganisms living in the water-sediment interface rapidly deplete high-energy terminal electron acceptors (TEAs) such as O_2 and nitrate and degrade the chemically most reactive organic matter pools (Orsi, 2018; D'Hondt et al., 2004; Berg et al., 2022). Below this zone, the utilization of terminal electron acceptors in catabolic reactions generates a vertical gradient in dominant respiration reactions (D'Hondt et al., 2004). Following the same trend, organic matter compositions shift toward increasingly degradation-resistant (refractory) species with sediment age and depth, thus limiting the electron donor pool available for microbial oxidation (Gajendra et al., 2023; Deng et al., 2020; Han et al., 2022).

As a general trend, the shift in sediment communities from freshly deposited sediments (Morono et al., 2020; Hoshino et al., 2020) to older "deeper" sediment communities is accompanied by a steep drop in microbial abundance (Chen et al., 2017; Hoshino et al., 2020). It is proposed that despite a reduction in cell numbers with increasing sediment depth, microorganisms continue to drive elemental cycling in deep sediments (Varliero et al., 2019; D'Hondt et al., 2004) and presumably utilize refractory organic matter (Marshall et al., 2019; Hoshino et al., 2020; Hubert et al., 2009). Under these conditions, it is hypothesized that a fraction of the surface microbial populations becomes predominant with sediment depth (Petro et al., 2017), and these are frequently referred to as "persistent sediment populations" (Starnawski et al., 2017). In anoxic marine sediments, these are commonly representatives from the groups *Atribacteria*, *Candidatus* Bathyarchaeia (also referred to as *Candidatus* Bathyarchaeota), and *Chloroflexi* (Hoshino et al., 2020; Zhou et al., 2018; Lloyd et al., 2013).

Here, we investigated how genome-inferred microbial community composition and metabolic potential relate to the environmental history and organic matter sources of lacustrine sediments from Lake Cadagno, an Alpine meromictic lake in Switzerland with anoxic, sulfidic bottom waters. The high-resolution limnological record of Lake Cadagno reflects these environmental changes, providing an ideal setting to study the co-evolution of anoxic lacustrine sediments and their microbial communities. Our study encompasses deposition throughout the Holocene and after the onset of meromictic conditions in the lake. An initial biological analysis of the sedimentary sequence revealed a weak ($R^2 = 0.35$) correlation between total organic carbon and prokaryotic 16S rRNA gene abundances (Berg et al., 2022); however, the functional and population-level diversity of the microbial communities within these sediments was not investigated. In this study, we combine shotgun metagenomic and 16S rRNA gene sequencing data to investigate the functional and taxonomic microbial community composition across an 8,000-year lacustrine sedimentary covering the period after the establishment of water column stratification and bottom water euxinia in Lake Cadagno.

Methods

Sample collection and study site

Lake Cadagno is a meromictic lake located in the Swiss Alps at 1,921 meters above sea level. The lake basin was formed through glacial erosion into bedrock during the Last Glacial Period with lake conditions being established after the retreat of the glacier from the basin ~12,000 years ago (Wirth et al., 2013). Since its formation and throughout its history it has undergone water column redox transitions that are reflected in the sediment record (Wirth et al., 2013). Today, the water column of the lake is stratified into an oxic epilimnion and an anoxic and sulfidic hypolimnion separated by a 0.5–1.0 m thick chemocline populated by purple sulfur bacteria (PSB) and green sulfur bacteria (GSB) (Philippi et al., 2021). The bottom layer of the water column exhibits a high sulfate concentration (~2 mM) relative to other freshwater systems, and surface sediments are similarly enriched in sulfate (up to 1.5 mM) which is rapidly depleted (<0.05 mM) within the first 20 cm below the lake floor (cmblf) (Berg et al., 2022). In the summer of 2019, a 10 m sediment core was retrieved and an initial 16S rRNA gene-based microbial characterization was performed (Berg et al., 2022). In our current study, a new set of sediment samples from this core were independently analyzed for 16S rRNA gene and shotgun metagenomic analyses. A detailed description of the coring, sampling strategy and geochemistry can be found in Berg et al. (2022). In brief, three sediment cores from Lake Cadagno were collected at a water depth of 21 m (46.55060 N and 8.71201 E) using an UWITEC coring platform (Uwitec, TA) and subsampled

TABLE 1 General information and geochemical data (Berg et al., 2022) for the 13 sediment samples analyzed this study.

Sample depth (cm)	Sediment type	Age mean (Cal BP)	TOC (%)	δ^{13}C-TOC	CH_4 (mmol/l)	S^0 (µml/g dry sed)	C:N	SO_4^{2-} (µmol/l)	NO_3^- (µmol/l)	NH_4^+ (µmol/L)
3	Pelagic	−17.3	17.3	−32.02	0.35	211.4	11.44	1,347.4	0	200
40	Turbidite	221.8	1.7	−27.15	2.23	6.29	13.41	0.09	0	-
153	Turbidite	1,026.6	1.3	−28.19	3.16	1.06	10.24	13.55	0.56	982
187	Turbidite	1,270.1	2.81	−28	4.49	6.75	13.23	12.8	0.26	793
213	Pelagic	1,456.3	2.3	−28.44	4.20	0.36	14.11	24.52	0.32	859
233	Turbidite	1,586.7	2.08	−28.04	4.27	0.57	13.67	51.41	0.37	878
283	Pelagic	1,741.7	1.43	−27.5	2.73	0.6	12.15	26.51	0.88	651
382	Pelagic	2,504.3	1.14	−28.47	2.12	0.34	9.93	10.62	0.19	470
532	Turbidite	3,472.5	1.97	−27.64	1.65	0.06	16.57	11.54	1.66	453
566	Pelagic	3,725.5	4.46	−30.04	4.34	0.28	13.3	-	-	-
582	Turbidite	4,179.5	4.29	−29.93	2.76	0.09	15.02	1.98	0.55	547
693	Turbidite	7,019.8	7.29	−34.67	1.41	0.07	13.1	5.31	0.68	348
738	Turbidite	8,268.6	4.66	−33.8	1.27	8.63	13.97	3.83	0.61	279

Additional geochemical parameters can be found in Supplementary Table 1. Cal BP, calibrated ^{14}C ages expressed in years before present; TOC, Total Organic Carbon, C:N, carbon-nitrogen ratio. Remineralization zones with peaks in phosphate (PO_4^{3-}), ammonium (NH_4^+), iron (Fe^{2+}) and manganese (Mn^{2+}) are highlighted in lime green. For further details on geochemical data, refer to Supplementary Table 1 (extended version).

to biomolecular analytical standards. After retrieval, biomolecular samples were flash-frozen in liquid N_2 and stored at −80°C until the DNA extractions described below.

Sample selection, DNA extraction, and metagenomic sequencing

DNA samples from 13 sediment depths between 0 and 738 cmblf were selected for DNA extraction and metagenomic sequencing (Table 1). Sample selection was based on lithostratigraphic and geochemical parameters to make sure the environmental variability of the sedimentary sequence was well represented. The core exhibits layers of organic matter-rich sediments of lacustrine origin and turbidite layers originating from mass-movement events that vary in porewater (Mn^{2+}, Fe^{2+}, SO_4^{2-}, NO_3^-, PO_4^{3-}, NH_4^+) and solid phase (S^0, TOC, C:N ratio, δ^{13}C-TOC) chemistry (Berg et al., 2022) (Table 1). The 13 samples cover the depositional history of the lake in the last 8,000 years after the onset of water column stratification in the lake during the Holocene, as indicated by age-depth modeling based on ^{14}C radiocarbon dating (Berg et al., 2022; Wirth et al., 2013).

DNA was extracted from three 0.2 g sediment aliquots per sample depth using a modular DNA extraction protocol (Lever et al., 2015) to maximize the DNA yield in deep, old sediments. Briefly, the aliquots were transferred to 2 mL beat-beating tubes and soaked with 10 mM sodium hexametaphosphate solution, and lysis solution I (30 mM Tris-HCl, 30 mM EDTA, 800 mM guanidium hydrochloride, and 0.5% Triton X-100) and then placed in a vortex genie and shaken at maximum speed for 30 s. The samples were then purified using lysis solution II (2% CTAB and 0.1% PVPP) and 24:1 chloroform isoamyl alcohol to remove humic and fluvic acids, residual proteins, and lipids. DNA precipitation was performed using linear polyacrylamide and 70% ethanol. DNA extracts were then purified using magnetic beads (AMPure XP beads 1.0*x*) followed by a final purification and concentration step using the commercial kit ReliaPrep™ DNA Cleanup and Concentration System (Promega, WI, United States).

After extraction and clean-up, the final DNA concentration of samples ranged between 2.44 ng/µL and 17.15 ng/µL (Supplementary Table 1). Samples were normalized to the minimum concentration of 2 ng/µL, which allowed us to perform metagenomic sequencing using the standard NEBnext Ultra II DNA library preparation kit which uses DNA fragmentation by sonication (New England Biolabs, Massachusetts, United States). The NEBnext Ultra II DNA for Illumina library preparation kit requires an initial DNA input of 50 ng and a three-cycle PCR amplification step. This reduced number of PCR cycles minimizes the impact of PCR on gene duplication rates, unequal amplification of genes, and sequencing artifacts (Rochette et al., 2023). Paired-end high-throughput sequencing was performed on a NovSeq 6000 Sequencing System (Illumina, San Diego, CA, USA) at the Functional Genomics Center Zurich (Zurich, Switzerland).

Metagenomic assembly

Sequences were quality-filtered and trimmed using Trimmomatic v.0.35 (Bolger et al., 2014) with the parameters SLIDING WINDOW:4:15 MINLEN:36 and assembled using Spades 3.14.1 (metaSPAdes.py) (Nurk et al., 2017) with k-mer sizes 21, 33,55. Contigs larger than 1,000 bp were retained for further analyses and protein-coding regions were predicted using Prodigal v.2.6.3 (Hyatt et al., 2010). Predicted proteins from all samples

were clustered at a 90% amino acid sequence identity threshold using CD-HIT v.4.6.8 (Li and Godzik, 2006). The representative sequence for each predicted protein cluster was functionally and taxonomically annotated as described below. The taxonomic and functional annotation of each predicted protein cluster's representative protein sequence was then assigned to all sequences within the protein cluster.

Taxonomic and functional gene annotation

Functional annotation of protein clusters within the Clusters of Orthologous Groups (COG) broad metabolic categories was made using eggNOG mapper v.2.1.6 with a likelihood threshold of 1e−5. The functional annotation of METABOLIC-derived marker genes (Zhou et al., 2022) for carbon, sulfur, and nitrogen biogeochemical cycling was performed using HMMER v.3.3.2 (Finn et al., 2011, e-value threshold of 1e−15) and the identity of the marker genes was confirmed using BLAST+ v.2.9.0 (e-value threshold of 1e−30, Camacho et al., 2009) against the NCBI-nr database (February 2024). The taxonomic annotation of the RpS3 marker genes was confirmed using BLAST+ v.2.9.0 (e-value threshold of 1e−30; Camacho et al., 2009) against the NCBI-nr database (January and June 2023). The taxonomy was assigned to the last common ancestor using a consensus vote approach with the top 3 hits of the previously described BLAST*p* search. The functional identities of marker genes involved in nitrogen cycling (*hao*, *narG*, *nifD*, *nifH*, *nifK*, *norB*) and sulfur oxidation (*soxB*) genes were further confirmed, and the taxonomic identities of the sequences were assigned through phylogenetic placement. Briefly, a "reference" phylogenetic tree for each marker gene was constructed by randomly sampling 100 protein sequences from the original METABOLIC marker gene database using seqtk v.1.3. Protein sequence alignments of METABOLIC marker gene and Lake Cadagno sequences were computed using MUSCLE v.3.8.31 (Edgar, 2004) and *de-novo* phylogenetic trees were calculated using FastTree v.2.1.11 (Price et al., 2010) using the Le and Gascuel (LG) model (Le et al., 2008). The placement of Lake Cadagno sequences within these marker gene trees was used for marker gene taxonomic identification.

Functional annotation and analysis of carbohydrate cycling genes

The complete set of protein sequences clustered at 90% amino-acid identity was annotated using the eggNOG mapper v.2.1.6, with a likelihood threshold of 1e−5. Protein clusters within each of the Clusters of Orthologous Groups (COGs) were subsampled for a beta-diversity analysis using complete linkage hierarchical clustering. Based on these results, the category "G" (Carbohydrate transport and metabolism) was selected for an enrichment analysis using the Maaslin2 (Mallick et al., 2021). The enrichment analysis was performed on samples where persistent Amplicon Sequencing Variants (ASVs) from *Ca.* Bathyarchaeia, *Atribacteria*, and *Chloroflexi* constitute more than 10% of the total abundance in the microbial community (samples below 40 cm). Proteins showing significant correlations and anticorrelations to sample depth (q-value < 0.05) were further annotated using BLAST (e-value threshold of 1e−30; Camacho et al., 2009) against the NCBI-nr database (April 2024).

Finally, to identify potential cellulases in the complete metagenomic dataset, protein sequences identified as cellulases based on the eggNOG mapper annotation were selected. The taxonomic and functional annotations of these proteins were further confirmed using BLAST (e-value threshold of 1e−30; Camacho et al., 2009) against the NCBI database (April 2024).

Metabolic pathway completeness assessment

Protein sequences clustered at 90% amino-acid identity were annotated using eggNOG mapper v.2.1.6 with a likelihood threshold of 1e−5. Protein clusters annotated within any of the KEGG categories were further annotated using GhostKOALA (Kanehisa et al., 2016). The resulting output file was used as input for KEGGDecoder (Graham et al., 2018) to generate a functional heatmap illustrating the completeness of the metabolic pathways across different sediment depths for the entire metagenomic dataset. The completeness of the metabolic pathways at any given depth is expressed using scores that range from 0.0 (non-present pathway) to 1.0 (indicating a fully present metabolic pathway).

Phylogenetic analysis of *Candidatus* Bathyarchaeia

A collection of RpS3 protein sequences was obtained from genomes assigned to *Ca.* Bathyarchaeia in GenBank (Benson et al., 2017), reported in the *Ca.* Bathyarchaeia phylogenetic tree of a previous study (Zhou et al., 2018), and identified within the Lake Cadagno metagenomic dataset. A protein sequence alignment was made using MUSCLE (Edgar, 2004). To improve the topological correspondence of our *Ca.* Bathyarchaeia RpS3 tree and previously reported *Ca.* Bathyarchaeia phylogenetic trees (Zhou et al., 2018; Hou et al., 2023), a guide tree was calculated using FastTree v.2.1.11 (Price et al., 2010) using the LG substitution model (Le et al., 2008). A maximum likelihood phylogenetic tree was then calculated using the LG protein substitution model (Le et al., 2008), gamma likelihood optimization and guide tree in RAxML v.8.2.12 (Stamatakis, 2014). Bootstrap analysis with 1,000 replicates was performed to assess the robustness of the tree topology.

16S rRNA targeted gene sequencing

The V4–V5 hypervariable regions of the 16S rRNA gene were amplified using the universal primer pair 515 F (5′-GTG YCA GCM GCC GCG GTA A-3′) and 926 R (5′-CCG YCA ATT YMT TTR AGT TT-3′) (Quince et al., 2011; Parada et al., 2016). This primer pair covers ~500 bp in the V4–V5 hypervariable regions of the bacterial and archaeal 16S rRNA gene and is different from the universal, bacteria-specific and archaea-specific primer

pairs used by Berg et al., 2022 [S-D-Bact-0341-b-S-17/S-D-Bact-0785-a-A-21 (Herlemann et al., 2011) and -D-Arch-0519-a-A-19 (Sørensen and Teske, 2006)/967Rmod (Cadillo-Quiroz et al., 2006)]. Amplicon libraries were prepared using a single-step PCR on the C1000 Touch Thermal Cycler (BioRad, Hercules, California, United States). Samples were run in triplicates, with a reaction volume of 25 μL including 1.0 μL template DNA, 0.5 μL forward primer (10 μM) and reverse primer (10 μM), 10 μL of PlatinumTM Hot Start PCR 2X Master Mix (Thermo Fisher Scientific, Waltham, Massachusetts, United States), and 13 μL of PCR-grade water. The PCR program was run as follows: initial denaturation at 95°C for 3 min, followed by 30 cycles of denaturation at 95°C for 35 s, annealing at 50°C for 45 s, elongation at 68°C for 90 s and a final elongation step at 68°C for 5 min. The DNA amplicons were purified using AMPure XP magnetic beads (Beckman Coulter, Brea, California, United States) at a concentration of 0.8*x*. After purification, the DNA amplicon concentrations were measured using a Qubit and diluted to create a pool with a final concentration of 4 nM. The quality of the 16S rRNA gene library was determined using the D1000 ScreenTape on the Agilent 4150 TapeStation (Agilent Technologies, Santa Clara, California, United States). Paired-end sequencing was performed on a MiSeq sequencer (Illumina Inc., San Diego, California, United States) using the MiSeq Reagent Kit v2 Nano (500 cycles) (Illumina).

16S rRNA gene sequencing data analysis

The quality of the 16S rRNA gene sequences was assessed using FastQC (Andrews, 2010). Data analysis was done using the standard the Qiime2 workflow (Bolyen et al., 2019). In brief, the first six nucleotides of the forward reads and 22 of the reverse reads were trimmed using the –p-trim-left parameter in the denoise-paired function of DADA2 (Callahan et al., 2016). Forward and reverse reads were truncated at 200 and 190 bp, respectively, with the –p-trunc-len function. The 16S rRNA gene feature table was generated and summarized using the qiime feature-table summarize function in Qiime2 (Bolyen et al., 2019). Amplicon sequencing variants (ASVs) related identified within the negative control samples were removed from all samples and excluded from all downstream analyses. Remaining ASVs were annotated using the Silva (Quast et al., 2013) nr database version 138.1.

The OTU table was rarefied to the minimum sample read count using the rrarefy function in the Vegan package (Oksanen et al., 2024) in RStudio to normalize sequencing depth across samples. Richness, defined as the number of unique taxa per sample, was calculated by counting non-zero taxa in the rarefied and non-rarefied data. The Shannon diversity index was calculated for each sample using the diversity function from the Vegan R package.

16S rRNA gene quantification

Abundances of prokaryotic 16S rRNA genes were quantified on a LightCycler 480 II (Roche Life Science, Penzberg, Germany) at ETH Zurich's Genetic Diversity Center (Switzerland) using the universal primer pair 515 F (5′- GTG YCA GCM GCC GCG GTA A−3′) and 926 R (5′- CCG YCA ATT YMT TTR AGT TT−3′) (Quince et al., 2011; Parada et al., 2016). Plasmids of 16S rRNA genes from *Thermoplasma acidophilum*-affiliated archaea and *Holophaga foetida* were used as standards as described in Han et al. (2020). The samples were run in duplicates with a reaction volume of 10 μL including 2 μL of DNA template, 1 μL of water, 1 μL of BSA, 0.5 μL of forward primer (10 μM) and 0.5 μL of reverse primer (10 μM), and 5 μL SYBR green (SsoFast^{TM} EvaGreen® Supermix with Low ROX 2x) (BioRad, Hercules, California, United States). The quantitative PCR (qPCR) reaction was run as follows: activation of the DNA polymerase at 95°C for 5 min, followed by 35 cycles of initial denaturation at 95°C for 10 s, annealing at 50°C for 30 s, extension at 68°C for 15 s and a melting curve (95°C for 15 s and 55°C for 1 min). The standard curve and melt curve for these reactions are provided in Supplementary Figures 1, 2.

Results

Microbial community composition and abundance in Lake Cadagno sediments

The taxonomic composition of the microbial communities from Lake Cadagno sediments was assessed using the 16S rRNA gene and the ribosomal protein S3 (RpS3) predicted protein clusters at 90% amino acid sequence identity ($RpS3_{90\%}$) from targeted and shotgun metagenomic datasets, respectively. At a coarse taxonomic level, the taxonomic profiles reported in this study based on targeted and shotgun metagenomic sequencing data match previously published data, which shows a clear transition from surface sediments dominated by bacteria from groups like *Proteobacteria*, to deeper sediments dominated by *Ca.* Bathyarchaeia and other groups such as *Planctomycetes*, *Chloroflexi* and *Atribacteria* (Berg et al., 2022).

The microbial community composition profiles based on 16S rRNA amplicon and $RpS3_{90\%}$ datasets are generally consistent with the exception of the unique presence of *Candidatus* Atribacteria (formerly OP9) at relatively high abundances (12–33%) in the 16S rRNA gene dataset from 153 cmblf and 582 cmblf (Figure 1, Supplementary File 2) and the dominance (33%) of *Candidatus* Acetothermia (Bipolaricaulota) within the youngest (3 cmblf) sediment sample of the $RpS3_{90\%}$ dataset (Figure 1). Both datasets reveal bacteria-dominated communities composed of *Alphaproteobacteria*, *Gammaproteobacteria*, and *Deltaproteobacteria* with minor populations of *Euryarchaeota* in the two youngest sediment samples (3 cmblf and 40 cmblf). In deeper and older samples (>225 years, >40 cmblf), the bacteria-dominated communities are replaced by *Candidatus* Bathyarchaeia-dominated communities (Figure 1). 16S rRNA gene and $RpS3_{90\%}$ sequences related to *Ca.* Bathyarchaeia, *Ca. Aminicenantes, Deltaproteobacteria, Chloroflexi, Atribacteria, and Planctomycetes* are identified in all samples. Finally, higher alpha-diversity metrics [richness (*S*), Shannon-Wiener Index (*H'*)] are observed within the 16S rRNA gene dataset relative to the $RpS3_{90\%}$ dataset (Table 2). This discrepancy in dataset-derived *S* and *H'* can

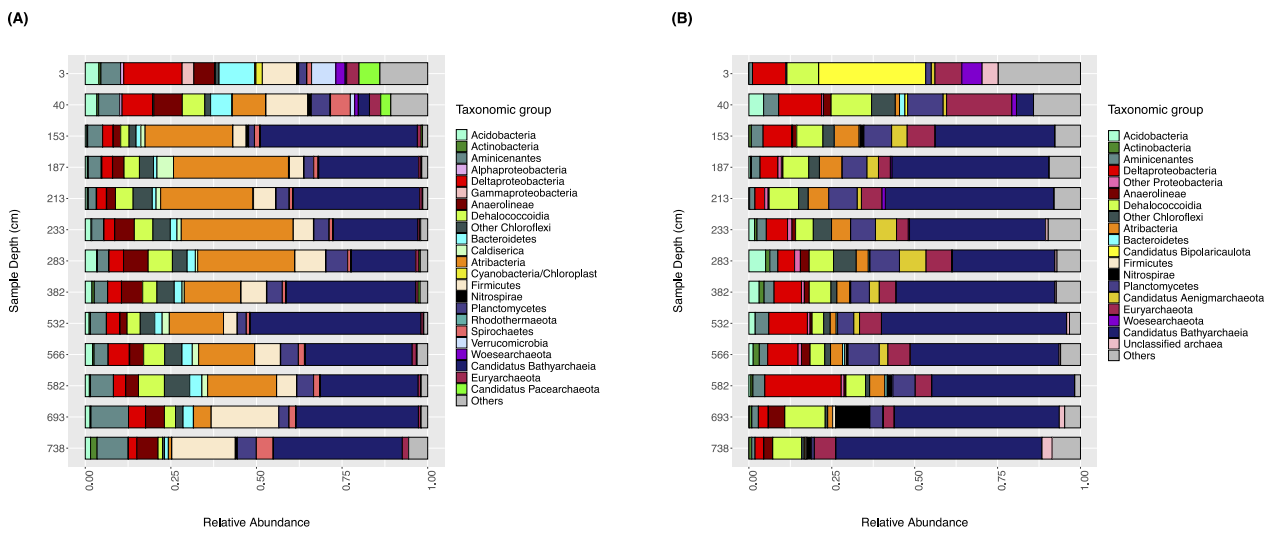

FIGURE 1
Taxonomic characterization of microbial communities from Lake Cadagno with sediment depth. The relative abundance (x-axis) of bacteria and archaea (bar colors) with respect to sediment depth (y-axis) is shown **(A)** for 16S rRNA gene sequences and **(B)** for ribosomal protein S3 ($RpS3_{90\%}$) sequence.

TABLE 2 General sequencing information and diversity metrics per sample depth for the 16S rRNA gene and shotgun metagenomic sequencing datasets.

Sample depth (cm)	16S rRNA targeted sequencing—General metrics					Metagenomic sequencing and $RpS3_{90\%}$ profile—General metrics		
	Number of reads per sample	Richness (ASVs)	Shannon-Wiener Diversity Index (H')	Richness – rarefied table (ASVs)	Shannon-Wiener Diversity Index—rarefied table (H')	Number of reads per sample (millions)	Richness ($RpS3_{90\%}$)	Shannon-Wiener Diversity Index (H')
3	34,343	1,267	6.16	1,138	1.05	52.5	71	3.24
40	39,158	1,407	6.07	1,151	1.04	65.5	109	4.31
153	12,879	230	3.11	230	0.29	49.2	85	3.41
187	57,496	579	3.66	467	0.49	50.6	64	3.02
213	61,388	522	3.36	423	0.45	44.7	73	2.93
233	56,713	717	4.09	564	0.58	54.5	101	3.57
283	59,019	821	4.57	642	0.65	53.9	130	4.15
382	65,587	732	4.12	537	0.56	51.7	72	3.36
532	65,302	512	3.42	397	0.43	38.9	61	2.83
566	39,951	465	4.16	416	0.47	38.4	64	3.35
582	59,423	559	4.05	445	0.48	40.9	41	2.89
693	62,189	480	4.09	392	0.44	63.7	73	3.25
738	39,709	380	4.19	343	0.4	47.9	54	3.12

The community composition profiles and diversity metrics calculations are based on 16S rRNA amplicon sequencing variants (ASVs) and the profile derived from ribosomal protein S3 sequences clustered at 90% amino acid identity ($RpS3_{90\%}$), respectively. The richness is expressed as the total number of ASVs or $RpS3_{90\%}$ per sample. The alpha diversity metrics for the 16S rRNA gene sequencing dataset (ASVs) presented in the table include calculations performed on both the rarefied and non-rarefied ASV tables. The number of reads per sample is expressed in millions for the shotgun metagenomic sequencing dataset. For further details, refer to Supplementary Table 1 (extended version).

be explained by the differences in both the sequencing (targeted vs. untargeted) and bioinformatic approach (Amplicon Sequencing Variant vs. $RpS3_{90\%}$).

In the first 153 cm of sediment, total 16S rRNA gene copy numbers decrease by more than an order of magnitude (2×10^8 to 2×10^7 gene copies per g of wet sediment),

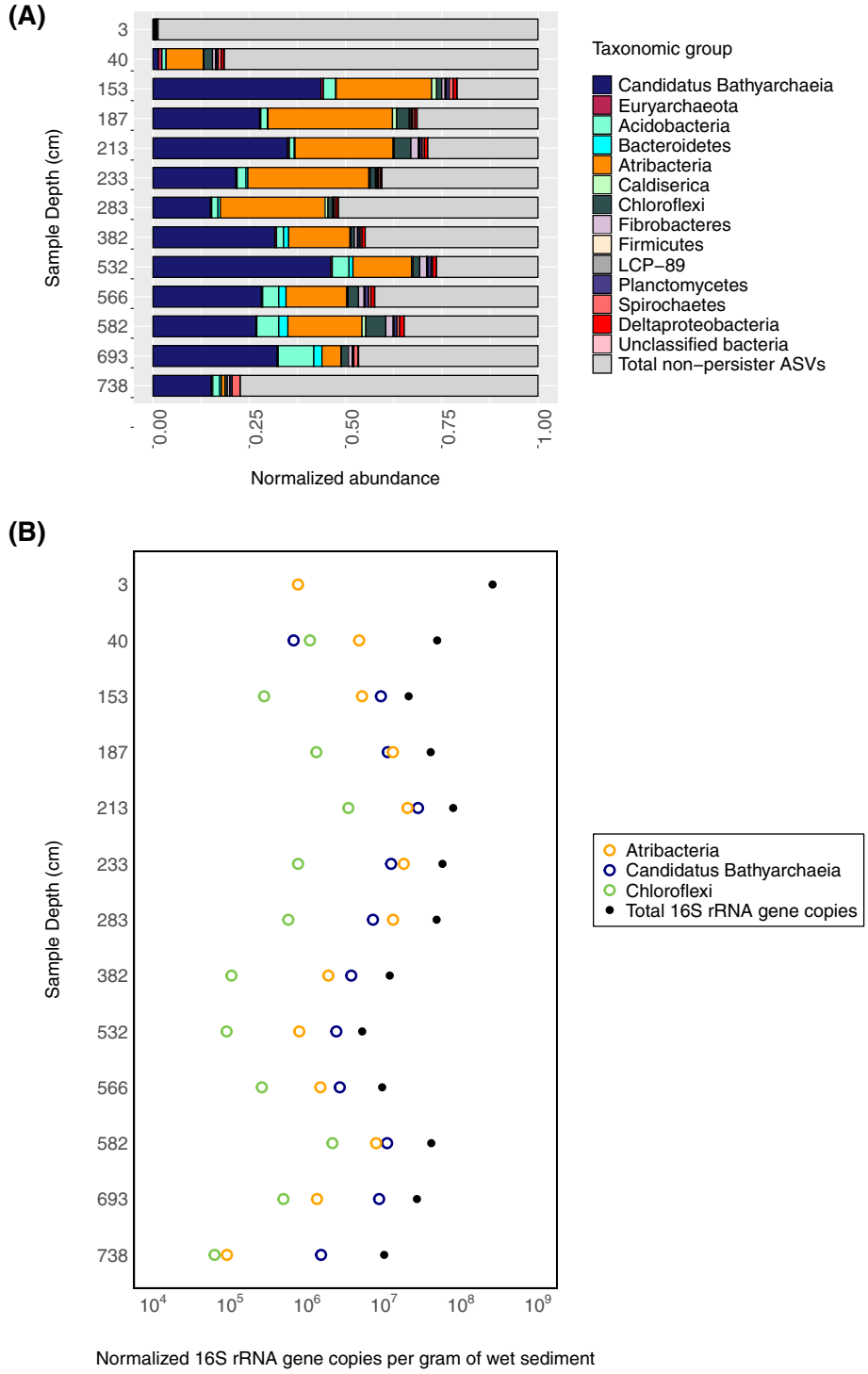

FIGURE 2
Persistent microbial lineages throughout the sedimentary sequence. **(A)** The relative abundance of persistent (present in more than 10 sediment samples) 16S rRNA ASVs and non-persistent ASVs (gray bars) are shown with respect to sediment depth. **(B)** The qPCR-estimated abundance of bacteria and archaea (black dots) relative to estimated persistent *Ca*. Bathyarchaeia (open blue circles), *Atribacteria* (open orange circles), and *Chloroflexi* (open green circles) ASV abundance (x-axis) with depth (y-axis) is shown.

and below this depth, community abundances range from 5 × 10^6 to 8 × 10^7 16S rRNA gene copies per g of wet sediment (Figure 2B). While almost all samples within the 16S rRNA gene dataset are bacteria-dominated, both bacteria- and archaea-specific abundances vary with depth. Two samples (153 cmblf and 532 cmblf) exhibit nearly equal bacteria-to-archaea ratios as reported by Berg et al. (2022) even though their only shared geochemical traits are similarities in sediment type (turbidite) and phosphate concentrations (30.3 μM) (Table 1).

Persistent members of the sediment microbial community

In addition to the changes in Lake Cadagno community composition and abundance, persistent taxonomic groups are also observed throughout the sediment sequence. Persistent groups are generally defined as the members of the community that are present throughout the sediment column (Starnawski et al., 2017). In this study, we define as "persistent groups" the Amplicon Sequencing Variants that are present in more than ten sediment samples in our sedimentary sequence. Out of the 6,148 unique Lake Cadagno Amplicon Sequencing Variants (ASVs), 42 ASVs are observed in at least 11 of the 13 Lake Cadagno sediment sample depths. The persistent ASVs represent a small fraction of the surface sediment community at 3 cmblf (<0.01%) but represent between 33% and 67% of each sample's total 16S rRNA gene-based community below 153 cmblf. The most abundant persistent ASVs are related to *Ca.* Bathyarchaeia (16/42), *Atribacteria* (3/42), and *Chloroflexi* (3/42) (Figure 2B). Additionally, persistent ASVs related to *Acidobacteria* (5/42), *Plantomycetes* (2/42), *Deltaproteobacteria* (2/42), *Fibrobacterota* (1/42) and *Bacteroidota* (1/42) were also identified at >2% (SD = 3.51) average abundance below 153 cm. Among these, the most abundant ASV, at an average abundance of 21% of ASVs in sediments below 153 cm, is related to *Ca.* Bathyarchaeia (ASV_ID= Candidatus Bathyarchaeia ASV 1, Supplementary Figure 3).

Ca. Bathyarchaeia profile based on the metagenomic dataset

Phylogenetic placement of *Ca. Bathyarchaeia* $RpS3_{90\%}$ sequences reveals that the Lake Cadagno sediment RpS3 sequence clusters fall within the newly assigned *Ca.* Bathyarchaeia candidate orders "*Baizomonadales*" ($n = 19$; GTDB o__ B26-1; This Study "Cluster 4" and "Cluster 5"), "*Houtuarculales*" ($n = 4$; GTDB o__40CM-2-53-6; This Study "Cluster 6"), "*Wuzhiqibiales*" ($n = 4$; GTDB o__TCS64; This Study "Cluster 1"), and "*Xuanwuarculales*" ($n = 2$; GTDB o__RBG_16_48_13; This Study "Cluster 2"). The majority of these Lake Cadagno-derived *Ca.* Bathyarchaeia RpS3 sequences are more closely related to other representatives within our sediments, than to other *Ca.* Bathyarchaeia subgroups reported in previous studies (Zhou et al., 2018; Hou et al., 2023). The most abundant persistent *Ca.* Bathyarchaeia ASV (ASV_ID= *Candidatus* Bathyarchaeia ASV 1, Supplementary Figure 3) is significantly correlated to *Ca.* Bathyarchaeia $RpS3_{90\%}$ sequence "Cluster 4A" (Figure 3) ($r = 0.81$, corrected p-value $= 6 \times 10^{-4}$), suggesting that these sequences are derived from the same *Ca.* Bathyarchaeia genome. A dominant and persistent $RpS3_{90\%}$ was also identified for each candidate order of *Ca.* Bathyarchaeia within the Lake Cadagno sedimentary sequence (Figure 3). Noteworthy exceptions appear when two relatively distant $RpS3_{90\%}$ sequence clusters replace the dominant "*Wuzhiqibiales*" sequence cluster at 40 cmblf and the dominant "*Xuanwuarculales*" RpS3 sequence cluster is absent from the 582 cmblf sample.

In our sediments, two *Ca.* Bathyarchaeia populations (expressed as $RpS3_{90\%}$ clusters) exhibit significant correlations (corrected $p < 0.01$) with the δ^{13}C-TOC ratios reported in this study (see Table 1) suggesting their potential involvement in carbon cycling in the sediments. These include negative correlations with δ^{13}C-TOC ratios were observed for "*Baizomonadaceae*" $RpS3_{90\%}$ sequence cluster 4C ($r = -0.84$, corrected $p = 3.4 \times 10^{-4}$) and "*Wuzhiqibiales*" $RpS3_{90\%}$ sequence cluster 1A ($r = -0.71$, corrected $p = 0.006$). The significant negative correlations suggest a link between relatively ^{13}C-depleted organic matter and the presence of these groups.

Microbial functional potential in Lake Cadagno sediments

To evaluate whether specific functional traits are enriched within the Lake Cadagno sediment microbial communities, a characterization of high-order functional categories proposed by the Clusters of Orthologous Genes (COGs) database (Galperin et al., 2021) was performed. Despite the differences in taxonomic composition between samples at 3 cmblf and 40 cmblf compared to sediments below 40 cmblf (Figure 1), the functional profile in terms of COGs remains stable throughout the sediment sequence (Supplementary Figure 4), indicating consistent patterns in the broad functional potential of the microbial community. As biogeochemically relevant gene abundances are more likely to change with changing environmental conditions, a functional profile based on a curated set of biogeochemical marker genes (Zhou et al., 2022) was additionally constructed and analyzed. Within this profile, the per sample carbon-, sulfur-, and nitrogen-cycling marker gene relative abundances are reported as the total coverage of all predicted proteins within a given marker gene protein family ($protein_{tot}$) divided by the total coverage of all ribosomal protein S3 sequences ($RpS3_{tot}$) in a sample (Figure 4).

The COG category for Carbohydrate Transport and Metabolism (COG category "G") was the only category related to nutrient acquisition and metabolism with a significant, positive correlation to sample depth (corrected $p = 0.039$) (Supplementary Table 5). Ten of the "Carbohydrate transport and metabolism" (G COG category) protein clusters were positively enriched with sediment depth (q-value < 0.05, Supplementary File 3). Three of these ten protein clusters are related to *Ca.* Bathyarchaeia (Supplementary Figure 5) and correspond to a phosphoglucosamine mutase (Normalized enrichment score = 0.81, q-value = 0.04), a 6-phosphofructokinase (Normalized enrichment score = 0.41, q-value = 0.038), and a cofactor-independent phosphoglycerate mutase (Normalized enrichment score = 0.34, q-value = 0.03). The remaining seven protein clusters are related to other bacterial groups including *Planctomycetes*, *Deltaproteobacteria*, and *Bacteroidetes*. On the other hand, 30 protein clusters had negative, significant correlations with sample depth. From these, the 10 proteins with the highest enrichment scores are related to bacterial groups such as *Deltaproteobacteria*, *Planctomycetes*, and *Chloroflexi*, and archaeal groups such as *Helarchaeota* and *Methylomirabilis sp.* (Supplementary File 3). Three carbohydrate transport and metabolism predicted proteins derived from

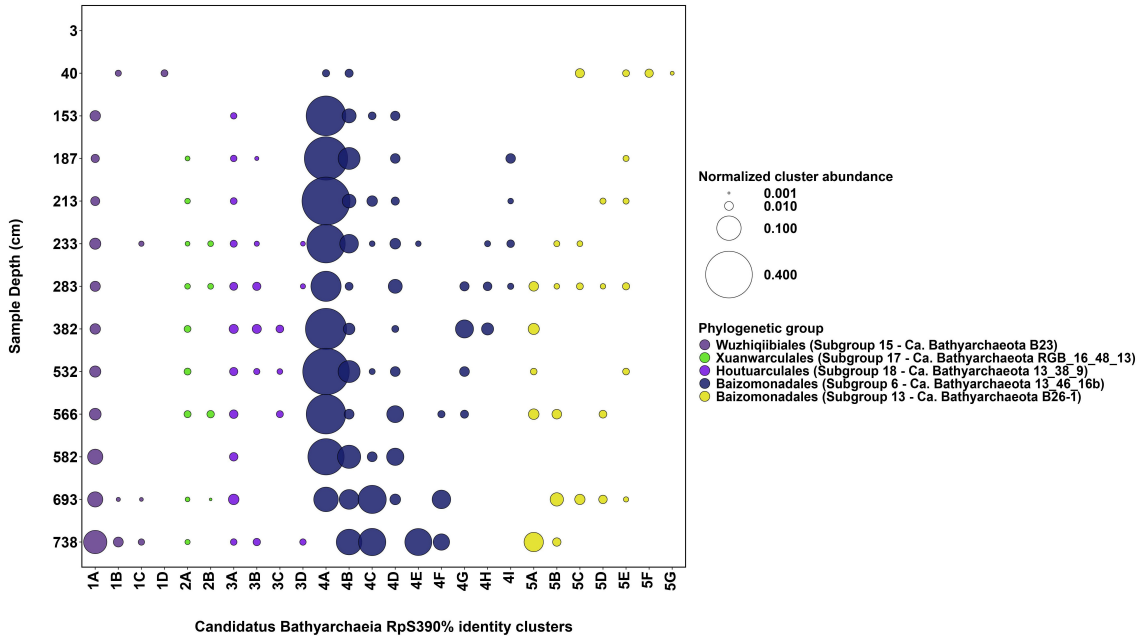

FIGURE 3
Diversity of *Ca*. Bathyarchaeia subgroups in Lake Cadagno sediments. The normalized $RpS3_{90\%}$ cluster abundance (circle size) of the 26 most abundant *Ca*. Bathyarchaeia $RpS3_{90\%}$ clusters (x-axis, 1A–5G) per sediment depth (y-axis) is shown. The digits (1–5) associated with each $RpS3_{90\%}$ cluster ID reflects each cluster's putative phylogenetic clade assignment (circle color).

Ca. Bathyarchaeia were additionally found to be depleted with sample depth (Supplementary Figure 5). These proteins correspond to Major Facilitator Superfamily (MFS) transporters (Normalized enrichment score = −0.33, q-value = 0.04 and Normalized enrichment score = −0.41, q-value = 0.024) and to a Triose Phosphate Isomerase (TIM) barrel protein (Normalized enrichment score = −0.33, q-value = 0.04).

Microbial potential for carbon fixation and methanogenesis

Predicted proteins of the archaeal carbon monoxide dehydrogenase (CdhC) and bacterial carbon monoxide dehydrogenase (AcsA) were used as markers for microbial carbon fixation via the Wood-Ljundahl pathway (WLP). The associated proteins are part of the five-subunit enzyme complex dehydrogenase/acetyl-CoA synthase (CODH/ACS complex) responsible for the formation of Coenzyme A (CoA) to form acetyl-CoA in the WLP (Adam et al., 2018). These genes have been shown to be also involved in the oxidation of CO to CO_2 in methanogenesis and anaerobic oxidation of methane and acetate (Zhou et al., 2022; Bährle et al., 2023) as well as in the reverse direction of the canonical WLP during organo-heterotrophic growth (for a review, see Borrel et al., 2016). A total of 232 unique AcsA and 60 CdhC predicted protein sequence clusters (90% amino acid sequence identity) were observed within the sediments. While a significant anti-correlation between AcsA and CdhC normalized abundances was not observed, the trends indicate that AcsA gene protein cluster abundances decrease below 153 cm and then stabilize, whereas CdhC abundances increase with depth and are linked to a decrease in *Methanomicrobiales*-related CdhC and an increase in *Ca*. Bathyarchaeia-related CdhC (Figure 4; Supplementary Figure 6).

A significant correlation (r = 0.80, corrected p = 0.001) between methanogenic CdhC sequence clusters (sequence clusters belonging to *Methanomicrobiales*) and the methanogenesis marker gene methyl coenzyme M reductase (mcrA) protein cluster abundance was found. In our dataset, McrA protein sequences that are closely related to *Methanomicrobiales* account for 72% of the total protein sequence abundance in samples between 40 cm and 582 cm and between 693 cm and 738 cm, whereas in the depth interval between 532 cm and 566 cm protein sequences associated with *Methanosarcinales* are dominant (40%-80% of the total protein sequence abundance) (Supplementary Figure 7). The results from the metabolic pathway completeness analysis suggest that methanogenesis via acetate may be the predominant metabolic pathway in the sediments, as the completeness values are > 0.99 at all depths except at 3 cm and 738 cm (Supplementary File 4). Methanogenesis via trimethylamine is another potentially preferred pathway in sediments between 40 cm and 532 cm (Supplementary File 4).

Archaeal RuBisCO Type III, mainly found in archaea, is the most abundant archaeal C-cycling marker gene observed within the Lake Cadagno sediment sequence. The presence of this protein is frequently associated to the Calvin-Benson-Bassham cycle (CBB cycle); however, it has also been shown to be involved in other processes such as the Reductive Hexulose-Phosphate Pathway (RHP) and the Pentose Phosphate Pathway (Sato et al., 2007; Kono et al., 2017) (Figure 4). Although calculated for the whole-metagenomic dataset rather than an individual genome, the

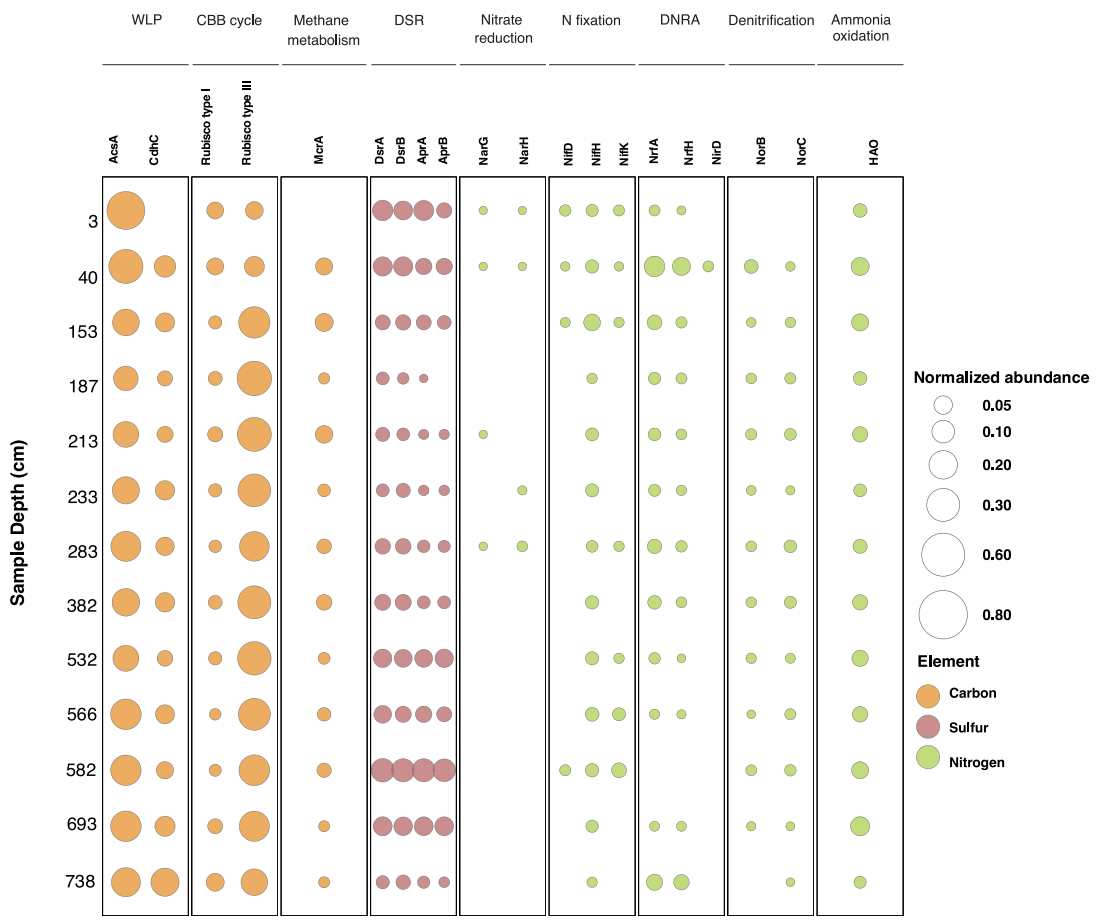

FIGURE 4
Normalized predicted protein abundance for biological carbon, sulfur and nitrogen cycling marker genes with sediment depth. The circles and their respective sizes indicate the normalized marker gene protein cluster relative abundance to the $RpS3_{90\%}$ total abundance at a given depth. The circle colors indicate the cycled elements. WLP, Wood Ljungdahl Pathway; CBB cycle, Calvin-Benson-Bassham Cycle; DSR, Canonical dissimilatory sulfate reduction; DNRA, dissimilatory nitrate reduction to ammonia.

potential prevalence of the CBB cycle in Lake Cadagno sediments is higher (completeness > 0.91) and therefore more likely than the reductive 3-hydroxypropionate (PBP) pathway (completeness < 0.50, Supplementary File 4). A significant anticorrelation in the abundance of Type III RuBisCo and AcsA predicted proteins was also observed ($r = -0.91$, corrected p-value $= 1.4 \times 10^{-5}$) (Supplementary Table 4). In total, 89 Archaeal Type III RuBisCO sequence clusters (90% amino acid sequence identity) were identified with 30 out of 89 of these clusters belonging to *Ca.* Bathyarchaeia and accounting for 80% of the total Type III RuBisCO abundance. Of these sequences, three sequence clusters related to *Ca.* Bathyarchaeia are especially abundant within three distinct depth intervals (Supplementary Figure 8); however, a strong correlation between these Type III RuBisCO abundance patterns and a *Ca.* Bathyarchaeia $RpS3_{90\%}$ sequence cluster was not identified.

Microbial potential for sulfur cycling

Dissimilatory sulfate reduction (DSR) is an energy-yielding process that reduces sulfate to sulfide (Jorgensen et al., 2019), and frequently used DSR marker genes include the dissimilatory sulfite reductase alpha subunit (*dsrA*), dissimilatory sulfite reductase beta subunit (*dsrB*), adenylyl-sulfate reductase alpha subunit (*aprA*), and adenylyl-sulfate reductase beta subunit (*aprB*) (Neukirchen et al., 2023). Throughout the sediment sequence, a strong correlation between the abundance of adenylyl sulfate reductase subunits (AprA and AprB, $r = 0.92$; corrected $p = 4.6 \times 10^{-6}$) and dissimilatory sulfite reduction subunits (DsrA and DsrB, $r = 0.97$; corrected $p = 2.6 \times 10^{-8}$) provides additional support for continuing DSR at depth (Supplementary Table 4), despite the rapid decrease in sulfate concentrations in the first 20 cm of the sediment core (Table 1, Berg et al., 2022). Dissimilatory sulfate reduction to APS and dissimilatory sulfate reduction to sulfide are the two pathways for sulfate reduction that show highest completeness in the sedimentary sequence (Supplementary File 4), this result is consistent with the presence of marker genes for DSR in the complete set of analyzed samples (Figure 4).

A compositional shift in marker genes for DSR is observed with sediment depth. Forty-seven unique DsrB predicted protein sequence clusters (90% amino acid sequence identity) and 42 unique DsrA protein sequence clusters (90% amino acid sequence

identity) were identified, the majority of which are related to *Deltaproteobacteria* (25/47 and 23/42, respectively). In the youngest samples (3 cmblf and 40 cmblf), DsrB predicted protein sequences related to *Chloroflexi*, *Deltaproteobacteria*, and *Desulfobacca acetoxidans* are abundant but *Deltaproteobacteria*-related DsrB dominate depths > 40 cmblf and reach a maximal normalized abundance at 582 cmblf (Figure 4, Supplementary Figures 9, 10). *Nitrospirae*-related DsrB sequences also become prominent in the deepest (693 cm and 738 cm) samples.

Apr is an additional DSR protein that is responsible for catalyzing the oxidative binding of sulfate to AMP to generate APS which is subsequently converted to sulfate by the ATP sulfurylase (Meyer and Kuever, 2007). Although *Deltaproteobacteria*-related Apr are the dominant Apr subtype from 3 cmblf to 582 cmblf, at depths > 693 cmblf, *Nitrospirae*-related AprA and AprB protein sequence clusters represent >70% of the per sample sequence abundance for these genes (Supplementary Figures 11, 12).

Protein-encoding genes involved in the re-oxidation of reduced sulfur species were also identified in Lake Cadagno sediments; however, genes (*soxA*, *soxB*, and *soxC*) which are commonly used for sulfur oxidation (although not limited to this metabolic function) were far less prevalent with SoxA and SoxC predicted protein sequences identified in only 3/13 and 2/13 samples respectively, and SoxB predicted protein sequences identified in only the 3 cmblf sample (Supplementary Figures 13–15). Richness of the Sox predicted proteins was also less than the richness of predicted proteins involved in DSR and most of Sox sequences were related to *Chlorobi*, *Betaproteobacteria*, and *Gemmatimonadetes* (Supplementary Figures 13–15).

Microbial potential for nitrogen cycling

The complete denitrification pathway involves the reduction of nitrate to nitrogen through a series of N-containing intermediates (NO_3^- to NO_2^- to NO to N_2O to N_2). Despite the prevalence of nitric oxide reductase predicted proteins (NorB and NorC) in samples between 40 cm and 693 cm, genomic evidence for the canonical denitrification pathway is sparse (Figure 4). Predicted protein sequences of nitrate reductase subunit alpha (NarG) were identified at relatively low abundances in four of the 13 samples (Figure 4, average $NarG_{tot}/RpS3_{tot} = 0.00241 \pm 0.00023$) and the cytochrome-type dissimilatory nitrite reductase (NirS) was only observed in the 40 cmblf sample ($NirS_{tot}/RpS3_{tot} = 0.00272$). Instead, the enzyme reported to catalyze the reduction of nitrite to ammonia in a process known as denitrification to ammonia (DNRA, Mohan et al., 2004), cytochrome c nitrite reductase (Nrf), was found across all sample depths except 582 cmblf (Figure 4). In total, 50 NrfA predicted protein sequence clusters (90% amino acid sequence identity) and 25 small subunit NrfH predicted protein sequence clusters (90% amino acid sequence identity) were identified at similar abundances and depths (Figure 4). Both predicted proteins show a maximal abundance at 40 cmblf ($NrfA/RpS3_{tot} = 0.15$ and $NrfH/RpS3_{tot} = 0.10$) and are mainly related to *Planctomycetes*, *Chloroflexi*, *Deltaproteobacteria* and *Bacteroidetes* (Supplementary Figures 16, 17).

Microbial cycling of ammonia in the Lake Cadagno sediments may also occur through nitrogen fixation and ammonia oxidation. Although the nitrogenase electron donor subunit (NifH) was identified in the predicted protein pool of all Lake Cadagno sediment samples, the catalytic subunits of nitrogenase, NifD and NifK, were only detected with NifH in four of the thirteen samples (3–158 cmblf and 582 cmblf, Figure 4). The enzyme hydroxylamine oxidoreductase (HAO) which catalyzes the oxidation of NH_2OH to NO_2^- and is a marker gene for ammonia oxidation was detected in all samples with an average $HAO_{tot}/RpS3_{tot}$ of 0.063 ± 0.029. HAO is frequently linked to aerobic ammonia oxidation (Junier et al., 2010) but a variant of the enzyme is also involved in anaerobic ammonium oxidation (anammox) (Sui et al., 2020; Kartal and Keltjens, 2016). Taxonomic assignment of Lake Cadagno HAO predicted proteins revealed a close relationship to *Planctomycetes* and may indicate that anammox occurs within the sediments (Supplementary Figure 18).

Discussion

Despite the drastic changes in sedimentary sources (lacustrine vs. mass-movement deposits) and a transition from bacteria-dominated communities in the top 40 cm to *Ca*. Bathyarchaeia-dominated communities in deeper layers of the 8,000-year sediment sequence of Lake Cadagno (Figure 1), dominant organic matter compositions (Berg et al., 2022; Gajendra et al., 2023) and the metabolic potential of the sediment's *in situ* microbial populations (Figure 4, Supplementary Figure 4) are conserved. Broadly speaking, Lake Cadagno's sedimentary microbial communities have the genomic potential to perform bacterial and archaeal carbon fixation via the Wood-Ljundahl pathway (WLP) and the Calvin-Benson-Bassham cycle (CBB cycle), canonical dissimilatory sulfate reduction (DSR), dissimilatory nitrate reduction to ammonia (DNRA) (Figure 4) and organic matter degradation; however, further studies are needed to confirm the expression and activity of these functions in Lake Cadagno. Interestingly, the taxonomic assignment of persistent marker genes shows strong vertical shifts (Supplementary Figures 6–22) that are not significantly correlated with sediment origin or any of the previously measured environmental parameters for this sedimentary sequence, originally reported in Berg et al. (2022) (Table 1, Supplementary Table 1). Given the absence of significant ecological correlations within this study, we expect that functional taxonomic replacement with depth is most likely driven by neutral processes (Liu et al., 2023), interactions between microbial populations (Martiny et al., 2023), or other non-measured geochemical and physicochemical parameters such as pH, salinity, and porewater content (Hoshino et al., 2020). As previous studies have suggested the preservation of functional traits increases ecosystem stability (Royalty and Steen, 2021), we hypothesize that the stability of functional traits with sediment depth throughout Lake Cadagno likely promotes ecosystem resilience by sustaining the core functions of the community after burial and under energy limitation; however, further activity-based analyses are needed to evaluate this hypothesis.

Although the metagenomic data indicate that a core set of metabolic functions is conserved in the Lake Cadagno sedimentary community, variation within specific metabolic pathways across taxonomic and geochemical gradients is also

observed. In other environments, higher amounts of taxonomic variation within the intermediate steps of major metabolic pathways (e.g., hydrogenotrophic vs. acetoclastic methanogenesis) relative to the metabolic endpoint (e.g., methanogenesis) have also been reported (Louca et al., 2018). In Lake Cadagno, the marker gene for methanogenesis (*mcrA*) is present at relatively similar abundances throughout the sediment core (Figure 4) but a transition between metabolically distinct *Methanomicrobiales* and *Methanosarcinales* archaea is also observed (Supplementary Figure 7). *Methanomicrobiales* persist throughout the sedimentary sequence and typically perform hydrogenotrophic methanogenesis with CO_2 (Zhang et al., 2020) while members of *Methanosarcinales* become the dominant methanogenic group within a local methane peak in Lake Cadagno's sediment (532–566 cmbss, Table 1) and exhibit the potential to perform methylotrophic, hydrogenotrophic and acetoclastic methanogenesis (Evans et al., 2019; Lyautey et al., 2021). Although the complete methanogenesis pathways of Lake Cadagno's methanogens were not recovered in this study, the prevalence of methanogenesis as a core metabolic pathway suggests that it is an essential part of the Lake Cadagno ecological network.

As with the aforementioned methanogens, the vast majority of microbial taxa in our sediments such as *Chloroflexi*, *Proteobacteria*, *Atribacteria*, *Aminicenantes, Ca*. Bathyarchaeia and *Firmicutes* are globally widespread in anoxic subsurface sediments of freshwater and marine environments (e.g., D'Hondt et al., 2004; Orsi, 2018; Yu et al., 2018; Orsi et al., 2020; Vuillemin et al., 2018; Suominen et al., 2021; Han et al., 2020). These similarities in microbial community composition can be partially explained by shared sedimentological properties (Hoshino et al., 2020), terminal electron acceptors, substrates, and metabolic products in deep sedimentary environments (D'Hondt et al., 2004; Vuillemin et al., 2018; Zhang et al., 2020; Dong et al., 2023; Jorgensen et al., 2012; He et al., 2022). Interestingly, a relatively small set of these taxa were identified as "persister populations" throughout the Lake Cadagno sedimentary sequence, appearing in ≥80% of the sampled sediment layers. The most abundant Lake Cadagno persister populations are closely related to the groups *Ca*. Bathyarchaeia, *Chloroflexi*, and *Atribacteria*. These groups dominate the taxonomic profiles of carbon fixation marker genes (Supplementary Figures 6, 8, 19–22), contain genes related to carbohydrate metabolism (Supplementary material 1), and have been identified as potentially versatile mixotrophs in sedimentary environments (Mardanov et al., 2020; Hou et al., 2023; Zhou et al., 2018; Nobu et al., 2016; Dodsworth et al., 2013; Fincker et al., 2020; Lee et al., 2018). Based on the prevalence of these groups throughout Lake Cadagno and other sedimentary environments (Orsi, 2018), we hypothesize that the metabolic versatility of these lineages makes them well-adapted for survival in deep marine and lacustrine sedimentary environments.

At the global scale, organic carbon availability is frequently reported as an important control on the diversity and abundance of sedimentary communities (for a review, see Orsi, 2018) and, therefore, it is also worth noting that changes in the relative functional contribution of persister populations to the organic matter pool are observed across the sediment sequence. In Lake Cadagno, the sedimentary carbohydrate content profile shows an increase in the relative contribution of levosugars with sediment depth and it is hypothesized these are potentially cellulose-derived, but their origin may differ depending on sample depth (surface vs. deep sediments) and sedimentary sources (lacustrine vs. mass-movement deposits) (Gajendra et al., 2023). An enrichment analysis of genes involved in carbohydrate cycling, transport, and metabolism shows that *Chloroflexi*-related gene abundances decrease with sediment depth while deeper sediments are enriched with genes related to *Ca*. Bathyarchaeia and other bacterial groups (Supplementary Figure 5). These results support previous reports that have identified organic matter as an important driver of sedimentary diversity patterns (e.g., Baker et al., 2015; Orsi, 2018) even though a significant correlation between Lake Cadagno's organic carbon pool and microbial diversity was not observed. Taken together, we interpret the observed persistence of microbial community functionality across the different sediment layers with different organic carbon sources (sediment layers of lacustrine vs. turbidite origin) as a sign of ecosystem resilience (Allison and Martiny, 2008) and the persistence of select taxonomic groups throughout sedimentary environments as an indication that specific niches within the sediment are uniquely filled by well-adapted subsurface lineages. However, it is worth noting that only a subset of the populations may be actively performing these specific functions at the time (Louca et al., 2018) and, therefore, single-cell or community-scale activity levels should be assessed by future studies.

Conclusion

Our findings indicate that microbial diversity patterns within Lake Cadagno sediments follow global sediment biodiversity trends such as a decrease in bacterial diversity and abundance and an increase in the relative abundance of persistent archaeal groups with depth. These changes in microbial community composition align with decreases in total organic carbon availability in the sediment; however, energy-transducing functions related to carbon, sulfur, and nitrogen cycling were preserved independently of the taxonomic composition of the sediment samples.

While many studies have reported evidence for a convergence in metabolic features across larger spatial scales (Chen et al., 2022; Royalty and Steen, 2021; Dopheide et al., 2015; Louca et al., 2016; Nelson et al., 2016), this study indicates that shared functionality is also important at more local scales and across sharp geochemical gradients, irrespective of sediment age and organic matter sources. The absence of evidence supporting deterministic selection based on the geochemical parameters considered in this study suggests the taxonomic diversity of groups encoding the selected marker genes is most likely related to stochastic or ecologically neutral processes (Liu et al., 2023) or a more complex combination of ecological factors such as the interactions and feedbacks between individual microbial populations and/or the physiological acclimation of persisting microorganisms after burial (Martiny et al., 2023). Based on these findings we hypothesize that shared functionality across multiple microbial lineages enables Lake Cadagno sediment-hosted microbial communities to survive in energy limitation and preserve the connectivity of metabolic pathways required for biogeochemical cycling.

Data availability statement

The datasets presented in this study can be found in online repositories. The names of the repository/repositories and accession number(s) can be found in the article/Supplementary material.

Author contributions

PR: Conceptualization, Data curation, Formal analysis, Investigation, Methodology, Project administration, Validation, Visualization, Writing – original draft, Writing – review & editing. JB: Conceptualization, Funding acquisition, Investigation, Project administration, Resources, Supervision, Writing – review & editing, Formal analysis. LD: Investigation, Supervision, Validation, Writing – review & editing. HV: Formal analysis, Investigation, Supervision, Writing – review & editing. MO: Data curation, Formal analysis, Writing – review & editing. ML: Conceptualization, Funding acquisition, Investigation, Methodology, Project administration, Resources, Supervision, Writing – review & editing. CM: Conceptualization, Funding acquisition, Investigation, Methodology, Project administration, Resources, Supervision, Validation, Writing – original draft, Writing – review & editing.

Funding

The author(s) declare financial support was received for the research, authorship, and/or publication of this article. This work was supported by ETH start up-funds to CM, the Swiss National Science Foundation (SNSF) grant no. 182096 to ML which covered the cost of the sampling campaign and of work in the Lever Lab. LD was sponsored by the Shanghai Pujiang Program (22PJ1404800). Open access funding by ETH Zurich.

Acknowledgments

We acknowledge the Genomics Diversity Center (GDC) Zurich and the Functional Genomics Center Zurich (FGCZ) for use of their research facilities. We thank Lena Bakker for her support with the protein enrichment analyses, Eleanor Georgiadis for her help proofreading the manuscript and Zhe Wang for his assistance with the nitrogen cycling data interpretation.

Conflict of interest

The authors declare that the research was conducted in the absence of any commercial or financial relationships that could be construed as a potential conflict of interest.

The author(s) declared that they were an editorial board member of Frontiers, at the time of submission. This had no impact on the peer review process and the final decision.

Generative AI statement

The author(s) declare that generative AI was used in the creation of this manuscript. Code was improved in consultation with AI tools. All errors are human.

Publisher's note

Supplementary material

The Supplementary Material for this article can be found online at: https://www.frontiersin.org/articles/10.3389/fmicb.2025.1504355/full#supplementary-material

The scripts used to create the figures in the manuscript, along with the metagenomic sequencing data table and the 16S rRNA gene targeted sequencing OTU table, and Supplementary Data 1 are stored in the GitHub repository https://github.com/PaulaCat/Lake_Cadagno_PFTGLC.git.

References

Adam, P. S., Borrel, G., and Gribaldo, S. (2018). Evolutionary history of carbon monoxide dehydrogenase/acetyl-CoA synthase, one of the oldest enzymatic complexes. *Proc. Natl. Acad. Sci. USA*. 115, E1166–E1173. doi: 10.1073/pnas.1716667115

Allison, S. D., and Martiny, J. B. H. (2008). Resistance, resilience, and redundancy in microbial communities. *Proc. Nat. Acad. Sci.* 105, 11512–11519. doi: 10.1073/pnas.0801925105

Andrews (2010). *FastQC: A Quality Control Tool for High Throughput Sequence Data*. Available at: http://www.bioinformatics.babraham.ac.uk/projects/fastqc/ (accessed April 16, 2021).

Ariztegui, D., Thomas, C., and Vuillemin, A. (2015). Present and future of subsurface biosphere studies in lacustrine sediments through scientific drilling. *Int. J. Earth Sci.* 104, 1655–1665. doi: 10.1007/s00531-015-1148-4

Bährle, R., Böhnke, S., Englhard, J., Bachmann, J., and Perner, M. (2023). Current status of carbon monoxide dehydrogenases (CODH) and their potential for electrochemical applications. *Bioresour. Bioproc.* 10:84. doi: 10.1186/s40643-023-00705-9

Baker, B. J., Lazar, C. S., Teske, A. P., and Dick, G. J. (2015). Genomic resolution of linkages in carbon, nitrogen, and sulfur cycling among widespread estuary sediment bacteria. *Microbiome* 3:6. doi: 10.1186/s40168-015-0077-6

Barber, A., Brandes, J., Leri, A., Lalonde, K., Balind, K., Wirick, S., et al. (2017). Preservation of organic matter in marine sediments by inner-sphere interactions with reactive iron. *Sci. Rep.* 7:366. doi: 10.1038/s41598-017-00494-0

Benson, D. A., Cavanaugh, M., Clark, K., Karsch-Mizrachi, I., Lipman, D. J., Ostell, J., et al. (2017). GenBank. *Nucleic Acids Res.* 45, D37–D42. doi: 10.1093/nar/gkw1070

Berg, J. S., Lepine, M., Laymand, E., Han, X., Vogel, H., Morlock, M. A., et al. (2022). Ancient and modern geochemical signatures in the 13,500-year sedimentary record of Lake Cadagno. *Front Earth Sci (Lausanne)* 9. doi: 10.3389/feart.2021.754888

Bolger, A. M., Lohse, M., and Usadel, B. (2014). Trimmomatic: a flexible trimmer for Illumina sequence data. *Bioinformatics* 30, 2114–2120. doi: 10.1093/bioinformatics/btu170

Bolyen, E., Rideout, J. R., Dillon, M. R., Bokulich, N. A., Abnet, C. C., Al-Ghalith, G. A., et al. (2019). Reproducible, interactive, scalable and extensible microbiome data science using QIIME 2. *Nat. Biotechnol.* 37, 852–857. doi: 10.1038/s41587-019-0209-9

Borrel, G., Adam, P. S., and Gribaldo, S. (2016). Methanogenesis and the wood-ljungdahl pathway: an ancient, versatile, and fragile association. *Genome Biol. Evol.* 8, 1706–1711. doi: 10.1093/gbe/evw114

Cadillo-Quiroz, H., Bräuer, S., Yashiro, E., Sun, C., Yavitt, J., and Zinder, S. (2006). Vertical profiles of methanogenesis and methanogens in two contrasting acidic peatlands in central New York State, USA. *Environ. Microbiol.* 8, 1428–1440. doi: 10.1111/j.1462-2920.2006.01036.x

Callahan, B. J., McMurdie, P. J., Rosen, M. J., Han, A. W., Johnson, A. J. A., and Holmes, S. P. (2016). DADA2: High-resolution sample inference from Illumina amplicon data. *Nat. Methods* 13, 581–583. doi: 10.1038/nmeth.3869

Camacho, C., Coulouris, G., Avagyan, V., Ma, N., Papadopoulos, J., Bealer, K., et al. (2009). BLAST+: Architecture and applications. *BMC Bioinform.* 10:421. doi: 10.1186/1471-2105-10-421

Chen, H., Ma, K., Lu, C., Fu, Q., Qiu, Y., Zhao, J., et al. (2022). Functional redundancy in soil microbial community based on metagenomics across the globe. *Front. Microbiol.* 13:878978. doi: 10.3389/fmicb.2022.878978

Chen, X., Andersen, T. J., Morono, Y., Inagaki, F., Jørgensen, B. B., and Lever, M. A. (2017). Bioturbation as a key driver behind the dominance of Bacteria over Archaea in near-surface sediment. *Sci. Rep.* 7:2400. doi: 10.1038/s41598-017-02295-x

Deng, L., Bölsterli, D., Kristensen, E., Meile, C., Su, C.-C., Bernasconi, S. M., et al. (2020). Macrofaunal control of microbial community structure in continental margin sediments. *Proc. Natl. Acad. Sci. U. S. A.* 117, 15911–15922. doi: 10.1073/pnas.1917494117

D'Hondt, S., Jorgensen, B. B., Miller, D. J., Batzke, A., Blake, R., Cragg, B. A., et al. (2004). Distributions of microbial activities in deep subseafloor sediments. *Science* 306, 2216–2221. doi: 10.1126/science.1101155

Dodsworth, J. A., Blainey, P. C., Murugapiran, S. K., Swingley, W. D., Ross, C. A., Tringe, S. G., et al. (2013). Single-cell and metagenomic analyses indicate a fermentative and saccharolytic lifestyle for members of the OP9 lineage. *Nat. Commun.* 4:2884. doi: 10.1038/ncomms2884

Dong, X., Peng, Y., Wang, M., Woods, L., Wu, W., Wang, Y., et al. (2023). Evolutionary ecology of microbial populations inhabiting deep sea sediments associated with cold seeps. *Nat. Commun.* 14:1127. doi: 10.1038/s41467-023-36877-3

Dopheide, A., Lear, G., He, Z., Zhou, J., and Lewis, G. D. (2015). Functional gene composition, diversity and redundancy in microbial stream biofilm communities. *PLoS ONE* 10:e123179. doi: 10.1371/journal.pone.0123179

Edgar, R. C. (2004). MUSCLE: A multiple sequence alignment method with reduced time and space complexity. *BMC Bioinform.* 5:113. doi: 10.1186/1471-2105-5-113

Evans, P. N., Boyd, J. A., Leu, A. O., Woodcroft, B. J., Parks, D. H., Hugenholtz, P., et al. (2019). An evolving view of methane metabolism in the Archaea. *Nat. Rev. Microbiol.* 17, 219–232. doi: 10.1038/s41579-018-0136-7

Fincker, M., Huber, J. A., Orphan, V. J., Rapp,é, M. S., Teske, A., and Spormann, A. M. (2020). Metabolic strategies of marine subseafloor Chloroflexi inferred from genome reconstructions. *Environ. Microbiol.* 22, 3188–3204. doi: 10.1111/1462-2920.15061

Finn, R. D., Clements, J., and Eddy, S. R. (2011). HMMER web server: Interactive sequence similarity searching. *Nucleic Acids Res.* 39:gkr367. doi: 10.1093/nar/gkr367

Gajendra, N., Berg, J. S., Vogel, H., Deng, L., Wolf, S. M., Bernasconi, S. M., et al. (2023). Carbohydrate compositional trends throughout Holocene sediments of an alpine lake (Lake Cadagno). *Front. Earth Sci.* 11:1047224. doi: 10.3389/feart.2023.1047224

Galperin, M. Y., Wolf, Y. I., Makarova, K. S., Alvarez, R. V., Landsman, D., and Koonin, E. V. (2021). COG database update: focus on microbial diversity, model organisms, and widespread pathogens. *Nucleic Acids Res.* 49, D274–D281. doi: 10.1093/nar/gkaa1018

Graham, E. D., Heidelberg, J. F., and Tully, B. J. (2018). Potential for primary productivity in a globally-distributed bacterial phototroph. *ISME J.* 12, 1861–1866. doi: 10.1038/s41396-018-0091-3

Han, X., Schubert, C. J., Fiskal, A., Dubois, N., and Lever, M. A. (2020). Eutrophication as a driver of microbial community structure in lake sediments. *Environ. Microbiol.* 22, 3446–3462. doi: 10.1111/1462-2920.15115

Han, X., Tolu, J., Deng, L., Fiskal, A., Schubert, C. J., Winkel, L. H. E., et al. (2022). Long-term preservation of biomolecules in lake sediments: potential importance of physical shielding by recalcitrant cell walls. *PNAS Nexus* 1:gac076. doi: 10.1093/pnasnexus/pgac076

He, R., Wang, J., Pohlman, J. W., Jia, Z., Chu, Y.-X., Wooller, M. J., et al. (2022). Metabolic flexibility of aerobic methanotrophs under anoxic conditions in Arctic lake sediments. *ISME J.* 16, 78–90. doi: 10.1038/s41396-021-01049-y

Herlemann, D. P., Labrenz, M., Jürgens, K., Bertilsson, S., Waniek, J. J., and Andersson, A. F. (2011). Transitions in bacterial communities along the 2000 km salinity gradient of the Baltic Sea. *ISME J.* 5, 1571–1579. doi: 10.1038/ismej.2011.41

Hoshino, T., Doi, H., Uramoto, G.-I., Wörmer, L., Adhikari, R. R., Xiao, N., et al. (2020). Global diversity of microbial communities in marine sediment. *Proc. Natl. Acad. Sci. U. S. A.* 117, 27587–27597. doi: 10.1073/pnas.1919139117

Hou, J., Wang, Y., Zhu, P., Yang, N., Liang, L., Yu, T., et al. (2023). Taxonomic and carbon metabolic diversification of Bathyarchaeia during its coevolution history with early Earth surface environment. *Sci Adv.* 9:eadf5069. doi: 10.1126/sciadv.adf5069

Hubert, C., Loy, A., Nickel, M., Arnosti, C., Baranyi, C., Brüchert, V., et al. (2009). A constant flux of diverse thermophilic bacteria into the cold Arctic seabed. *Science* 325, 1541–1544. doi: 10.1126/science.1174012

Hyatt, D., Chen, G.-L., Locascio, P. F., Land, M. L., Larimer, F. W., and Hauser, L. J. (2010). Prodigal: prokaryotic gene recognition and translation initiation site identification. *BMC Bioinform.* 11:119. doi: 10.1186/1471-2105-11-119

Jessen, G. L., Lichtschlag, A., Ramette, A., Pantoja, S., Rossel, P. E., Schubert, C. J., et al. (2017). Hypoxia causes preservation of labile organic matter and changes seafloor microbial community composition (Black Sea). *Sci. Adv.* 3:e1601897. doi: 10.1126/sciadv.1601897

Jorgensen, B. B., Findlay, A. J., and Pellerin, A. (2019). The biogeochemical sulfur cycle of marine sediments. *Front. Microbiol.* 10:849. doi: 10.3389/fmicb.2019.00849

Jorgensen, B. B., and Marshall, I. P. G. (2016). Slow microbial life in the seabed. *Ann. Rev. Mar. Sci.* 8, 311–332. doi: 10.1146/annurev-marine-010814-015535

Jorgensen, S. L., Hannisdal, B., Lanzén, A., Baumberger, T., Flesland, K., Fonseca, R., et al. (2012). Correlating microbial community profiles with geochemical data in highly stratified sediments from the Arctic Mid-Ocean Ridge. *Proc. Natl. Acad. Sci. U. S. A.* 109, E2846–E2855. doi: 10.1073/pnas.1207574109

Junier, P., Molina, V., Dorador, C., Hadas, O., Kim, O. S., Junier, T., et al. (2010). Phylogenetic and functional marker genes to study ammonia-oxidizing microorganisms (AOM) in the environment. *Appl. Microbiol. Biotechnol.* 85, 425–440. doi: 10.1007/s00253-009-2228-9

Kallmeyer, J., Pockalny, R., Adhikari, R. R., Smith, D. C., and D'Hondt, S. (2012). Global distribution of microbial abundance and biomass in subseafloor sediment. *Proc. Natl. Acad. Sci. U. S. A.* 109, 16213–16216. doi: 10.1073/pnas.1203849109

Kanehisa, M., Sato, Y., and Morishima, K. (2016). BlastKOALA and GhostKOALA: KEGG tools for functional characterization of genome and metagenome sequences. *J. Mol. Biol.* 428, 726–731. doi: 10.1016/j.jmb.2015.11.006

Kartal, B., and Keltjens, J. T. (2016). Anammox biochemistry: a tale of Heme c proteins. *Trends Biochem. Sci.* 41, 998–1011. doi: 10.1016/j.tibs.2016.08.015

Kono, T., Mehrotra, S., Endo, C., Kizu, N., Matusda, M., Kimura, H., et al. (2017). A RuBisCO-mediated carbon metabolic pathway in methanogenic archaea. *Nat. Commun.* 8:14007. doi: 10.1038/ncomms14007

Le, S. Q., Gascuel, O., and Quang Le, S. (2008). An improved general amino acid replacement matrix. *Mol. Biol. Evol.* 25, 1307–1320. doi: 10.1093/molbev/msn067

Lee, Y. M., Hwang, K., Lee, J., Kim, M., Hwang, C. Y., Noh, H. J., et al. (2018). Genomic insight into the predominance of candidate phylum Atribacteria JS1 lineage in marine sediments. *Front. Microbiol.* 9:02909. doi: 10.3389/fmicb.2018.02909

Lever, M. A., Torti, A., Eickenbusch, P., Michaud, A. B., Šantl-Temkiv, T., and Jorgensen, B. B. (2015). A modular method for the extraction of DNA and RNA, and the separation of DNA pools from diverse environmental sample types. *Front. Microbiol.* 6:476. doi: 10.3389/fmicb.2015.00476

Li, W., and Godzik, A. (2006). Cd-hit: A fast program for clustering and comparing large sets of protein or nucleotide sequences. *Bioinformatics* 22, 1658–1659. doi: 10.1093/bioinformatics/btl158

Liu, H., Lin, G., Gao, D., Chen, H., He, M., and Lu, J. (2023). Geographic scale influences the interactivities between determinism and stochasticity in the assembly of sedimentary microbial communities on the South China Sea shelf. *Microb. Ecol.* 85, 121–136. doi: 10.1007/s00248-021-01946-x

Lloyd, K. G., Schreiber, L., Petersen, D. G., Kjeldsen, K. U., Lever, M. A., Steen, A. D., et al. (2013). Predominant archaea in marine sediments degrade detrital proteins. *Nature* 496, 215–218. doi: 10.1038/nature12033

Louca, S., Jacques, S. M. S., Pires, A. P. F., Leal, J. S., Srivastava, D. S., Parfrey, L. W., et al. (2016). High taxonomic variability despite stable functional structure across microbial communities. *Nat. Ecol. Evol.* 1:15. doi: 10.1038/s41559-016-0015

Louca, S., Polz, M. F., Mazel, F., Albright, M. B. N., Huber, J. A., O'Connor, M. I., et al. (2018). Function and functional redundancy in microbial systems. *Nat. Ecol. Evol.* 2, 936–943. doi: 10.1038/s41559-018-0519-1

Lyautey, E., Billard, E., Tissot, N., Jacquet, S., and Domaizon, I. (2021). Seasonal dynamics of abundance, structure, and diversity of methanogens and methanotrophs in lake sediments. *Microb. Ecol.* 82, 559–571. doi: 10.1007/s00248-021-01689-9

Mallick, H., Rahnavard, A., McIver, L. J., Ma, S., Zhang, Y., Nguyen, L. H., et al. (2021). Multivariable association discovery in population-scale meta-omics studies. *PLoS Comput. Biol.* 17:e1009442. doi: 10.1371/journal.pcbi.1009442

Mardanov, A. V., Kadnikov, V. V., Beletsky, A. V., and Ravin, N. V. (2020). Sulfur and methane-oxidizing microbial community in a terrestrial mud volcano revealed by metagenomics. *Microorganisms* 8, 1–16. doi: 10.3390/microorganisms8091333

Marshall, I. P. G., Ren, G., Jaussi, M., Lomstein, B. A., Jorgensen, B. B., Roy, H., et al. (2019). Environmental filtering determines family-level structure of sulfate-reducing microbial communities in subsurface marine sediments. *Isme .J* 13, 1920–1932. doi: 10.1038/s41396-019-0387-y

Martiny, J. B. H., Martiny, A. C., Brodie, E., Chase, A. B., Rodríguez-Verdugo, A., Treseder, K. K., et al. (2023). Investigating the eco-evolutionary response of microbiomes to environmental change. *Ecol. Lett.* 26, S81–S90. doi: 10.1111/ele.14209

Meyer, B., and Kuever, J. (2007). Molecular analysis of the distribution and phylogeny of dissimilatory adenosine-5′-phosphosulfate reductase-encoding genes (aprBA) among sulfur-oxidizing. *Microbiology* 153, 3478–3498. doi: 10.1099/mic.0.2007/008250-0

Mohan, S. B., Schmid, M., Jetten, M., and Cole, J. (2004). Detection and widespread distribution of the nrfA gene encoding nitrite reduction to ammonia, a short circuit in the biological nitrogen cycle that competes with denitrification. *FEMS Microbiol. Ecol.* 49, 433–443. doi: 10.1016/j.femsec.2004.04.012

Morono, Y., Ito, M., Hoshino, T., Terada, T., Hori, T., Ikehara, M., et al. (2020). Aerobic microbial life persists in oxic marine sediment as old as 101.5 million years. *Nat. Commun.* 11:1. doi: 10.1038/s41467-020-17330-1

Nelson, M. B., Martiny, A. C., and Martiny, J. B. H. (2016). Global biogeography of microbial nitrogen-cycling traits in soil. *Proc. Natl. Acad. Sci. USA.* 113, 8033–8040. doi: 10.1073/pnas.1601070113

Neukirchen, S., Pereira, I. A. C., and Sousa, F. L. (2023). Stepwise pathway for early evolutionary assembly of dissimilatory sulfite and sulfate reduction. *ISME J.* 17, 1680–1692. doi: 10.1038/s41396-023-01477-y

Nobu, M. K., Dodsworth, J. A., Murugapiran, S. K., Rinke, C., Gies, E. A., Webster, G., et al. (2016). Phylogeny and physiology of candidate phylum "Atribacteria" (OP9/JS1) inferred from cultivation-independent genomics. *ISME J.* 10, 273–286. doi: 10.1038/ismej.2015.97

Nurk, S., Meleshko, D., Korobeynikov, A., and Pevzner, P. A. (2017). MetaSPAdes: a new versatile metagenomic assembler. *Genome Res.* 27, 824–834. doi: 10.1101/gr.213959.116

Oksanen, J., Simpson, G., Blanchet, F., Kindt, R., Legendre, P., Minchin, P., et al. (2024). *vegan: Community Ecology Package. R package version 2.7-0.* Available at: https://github.com/vegandevs/vegan

Oni, O. E., Schmidt, F., Miyatake, T., Kasten, S., Witt, M., Hinrichs, K.-U., et al. (2015). Microbial communities and organic matter composition in surface and subsurface sediments of the Helgoland mud area, North Sea. *Front. Microbiol.* 6:1290. doi: 10.3389/fmicb.2015.01290

Orsi, W. D. (2018). Ecology and evolution of seafloor and subseafloor microbial communities. *Nat. Rev. Microbiol.* 16, 671–683. doi: 10.1038/s41579-018-0046-8

Orsi, W. D., Schink, B., Buckel, W., and Martin, W. F. (2020). Physiological limits to life in anoxic subseafloor sediment. *FEMS Microbiol. Rev.* 44, 219–231. doi: 10.1093/femsre/fuaa004

Parada, A. E., Needham, D. M., and Fuhrman, J. A. (2016). Every base matters: assessing small subunit rRNA primers for marine microbiomes with mock communities, time series and global field samples. *Environ. Microbiol.* 18, 1403–1414 doi: 10.1111/1462-2920.13023

Petro, C., Starnawski, P., Schramm, A., and Kjeldsen, K. U. (2017). Microbial community assembly in marine sediments. *Aquat. Microb. Ecol.* 79, 177–195. doi: 10.3354/ame01826

Philippi, M., Kitzinger, K., Berg, J. S., Tschitschko, B., Kidane, A. T., Littmann, S., et al. (2021). Purple sulfur bacteria fix N2 via molybdenum-nitrogenase in a low molybdenum Proterozoic ocean analogue. *Nat. Commun.* 12:4774. doi: 10.1038/s41467-021-25000-z

Price, M. N., Dehal, P. S., and Arkin, A. P. (2010). FastTree 2 - Approximately maximum-likelihood trees for large alignments. *PLoS ONE* 5:e0009490. doi: 10.1371/journal.pone.0009490

Quast, C., Pruesse, E., Yilmaz, P., Gerken, J., Schweer, T., Yarza, P., et al. (2013). The SILVA ribosomal RNA gene database project: improved data processing and web-based tools. *Nucleic Acids Res.* 41, D590–D596. doi: 10.1093/nar/gks1219

Quince, C., Lanzen, A., Davenport, R. J., and Turnbaugh, P. J. (2011). Removing noise from pyrosequenced amplicons. *BMC Bioinformat.* 12:38. doi: 10.1186/1471-2105-12-38

Rochette, N. C., Rivera-Colón, A. G., Walsh, J., Sanger, T. J., Campbell-Staton, S. C., and Catchen, J. M. (2023). On the causes, consequences, and avoidance of PCR duplicates: Towards a theory of library complexity. *Mol. Ecol. Resour.* 23, 1299–1318. doi: 10.1111/1755-0998.13800

Royalty, T. M., and Steen, A. D. (2021). Functional redundancy in ocean microbiomes controls trait stability. *bioRxiv*. [Preprint]. doi: 10.1101/2021.06.18.448980

Sato, T., Atomi, H., and Imanaka, T. (2007). Archaeal type III RuBisCOs function in a pathway for AMP metabolism. *Science* 315, 1003–1006. doi: 10.1126/science.1135999

Sørensen, K. B., and Teske, A. (2006). Stratified communities of active archaea in deep marine subsurface sediments. *Appl. Environ. Microbiol.* 72, 4596–4603. doi: 10.1128/AEM.00562-06

Stamatakis, A. (2014). RAxML version 8: a tool for phylogenetic analysis and post-analysis of large phylogenies. *Bioinformatics* 30, 1312–1313. doi: 10.1093/bioinformatics/btu033

Starnawski, P., Bataillon, T., Ettema, T. J. G., Jochum, L. M., Schreiber, L., Chen, X., et al. (2017). Microbial community assembly and evolution in subseafloor sediment. *Proc. Natl. Acad. Sci. USA.* 114, 2940–2945. doi: 10.1073/pnas.1614190114

Sui, Q., Wang, Y., Wang, H., Yue, W., Chen, Y., Yu, D., et al. (2020). Roles of hydroxylamine and hydrazine in the in-situ recovery of one-stage partial nitritation-anammox process: Characteristics and mechanisms. *Sci. Total Environm.* 707:135648. doi: 10.1016/j.scitotenv.2019.135648

Suominen, S., van Vliet, D. M., Sánchez-Andrea, I., van der Meer, M. T. J., Sinninghe Damsté, J. S., and Villanueva, L. (2021). Organic matter type defines the composition of active microbial communities originating from anoxic baltic sea sediments. *Front. Microbiol.* 12:628301. doi: 10.3389/fmicb.2021.628301

Varliero, G., Bienhold, C., Schmid, F., Boetius, A., and Molari, M. (2019). Microbial diversity and connectivity in deep-sea sediments of the South Atlantic Polar Front. *Front. Microbiol.* 10:665. doi: 10.3389/fmicb.2019.00665

Vuillemin, A., Ariztegui, D., Horn, F., Kallmeyer, J., Orsi, W. D., Anselmetti, F., et al. (2018). Microbial community composition along a 50 000-year lacustrine sediment sequence. *FEMS Microbiol. Ecol.* 94:fiy029. doi: 10.1093/femsec/fiy029

Wirth, S. B., Gilli, A., Niemann, H., Dahl, T. W., Ravasi, D., Sax, N., et al. (2013). Combining sedimentological, trace metal (Mn, Mo) and molecular evidence for reconstructing past water-column redox conditions: The example of meromictic Lake Cadagno (Swiss Alps). *Geochim. Cosmochim. Acta* 120, 220–238. doi: 10.1016/j.gca.2013.06.017

Yu, T., Wu, W., Liang, W., Lever, M. A., Hinrichs, K. U., and Wang, F. (2018). Growth of sedimentary Bathyarchaeota on lignin as an energy source. *Proc. Natl. Acad. Sci. USA.* 115, 6022–6027. doi: 10.1073/pnas.1718854115

Zhang, C.-J., Pan, J., Liu, Y., Duan, C.-H., and Li, M. (2020). Genomic and transcriptomic insights into methanogenesis potential of novel methanogens from mangrove sediments. *Microbiome* 8:94. doi: 10.1186/s40168-020-00876-z

Zhou, Z., Pan, J., Wang, F., Gu, J. D., and Li, M. (2018). Bathyarchaeota: globally distributed metabolic generalists in anoxic environments. *FEMS Microbiol. Rev.* 42, 639–655. doi: 10.1093/femsre/fuy023

Zhou, Z., Tran, P. Q., Breister, A. M., Liu, Y., Kieft, K., Cowley, E. S., et al. (2022). METABOLIC: high-throughput profiling of microbial genomes for functional traits, metabolism, biogeochemistry, and community-scale functional networks. *Microbiome* 10:8. doi: 10.1186/s40168-021-01213-8

Zolitschka, B., and Enters, D. (2009). "Lacustrine sediments," in *Encyclopedia of Paleoclimatology and Ancient Environments*, ed. V. Gornitz (Dordrecht: Springer Netherlands), 486–488.

frontiers | Frontiers in Microbiology

TYPE Original Research
PUBLISHED 25 February 2025
DOI 10.3389/fmicb.2025.1522714

OPEN ACCESS

EDITED BY
William J. Brazelton,
The University of Utah, United States

REVIEWED BY
Magdalena R. Osburn,
Northwestern University, United States
George Westmeijer,
Umeå University, Sweden
Daniel Gonzalez-Duque,
The Ohio State University, United States

*CORRESPONDENCE
Cara Magnabosco
✉ cara.magnabosco@eaps.ethz.ch

RECEIVED 04 November 2024
ACCEPTED 28 January 2025
PUBLISHED 25 February 2025

CITATION
Acciardo AS, Arnet M, Gholizadeh Doonechaly N, Ceccato A, Rodriguez P, Tran HN, Wenning Q, Zimmerman E, Hertrich M, Brixel B and Magnabosco C (2025) Spatial and temporal groundwater biogeochemical variability help inform subsurface connectivity within a high-altitude Alpine catchment (Riale di Ronco, Switzerland). *Front. Microbiol.* 16:1522714. doi: 10.3389/fmicb.2025.1522714

Spatial and temporal groundwater biogeochemical variability help inform subsurface connectivity within a high-altitude Alpine catchment (Riale di Ronco, Switzerland)

Andrew S. Acciardo[1], Moira Arnet[1], Nima Gholizadeh Doonechaly[1,2], Alberto Ceccato[1], Paula Rodriguez[1], Hoang N.H. Tran[1], Quinn Wenning[1,3], Eric Zimmerman[1], Marian Hertrich[1], Bernard Brixel[1,4] and Cara Magnabosco[1]*

[1]ETH Department of Earth and Planetary Sciences, Zurich, Switzerland, [2]Centre for Hydrogeology and Geothermics (CHYN), Neuchâtel, Switzerland, [3]Deloitte, Zurich, Switzerland, [4]Cantonal Office of the Environment, Geneva, Switzerland

Accessing the deep terrestrial subsurface (greater than 1 km below the surface) presents significant practical challenges, leaving these ecosystems largely uncharacterized despite their extensive presence beneath Earth's landmasses. In this study, we introduce the BedrettoLab Deep Life Observatory (DELOS), a new underground laboratory to study the biogeochemical diversity of groundwater in a high-altitude Alpine catchment tens of meters to 1.6 km underground. Biogeochemical monitoring of DELOS over spatial and temporal scales highlight three dominant ecotypes throughout DELOS: (1) Shallow groundwater with low electrical conductivity enriched in *Leptospirillia*; (2) High-inflow fault zones enriched in ultra-small bacteria and archaea; (3) Bicarbonate-enriched waters that are enriched in *Candidatus* Kryptonia and *Spirochaetota*. Despite a consistent lithology throughout DELOS, groundwater from fractures that are spatially near each other are not always represented by the same ecotype and can be more similar to groundwater emitted from fractures thousands of meters away. Despite this heterogeneity, the biological and hydrochemical compositions of the groundwater of individual fractures remained relatively stable throughout the course of a 1-year monitoring period. An exception to this trend occurred after a series of seismic events near one groundwater-bearing fracture. Here, the microbial community and hydrochemical composition of the groundwater changed after the seismic events but returned to the site's "baseline" composition within 3 weeks. Taken together, these findings provide new insights into the spatial and temporal heterogeneity of deep subsurface ecosystems and the subsurface connectivity of an Alpine subsurface environment.

KEYWORDS

subsurface microbiology, underground laboratory, groundwater, microbial ecology, deep life observatory

1 Introduction

Since the earliest reports of subsurface life in coal beds and oil fields in the 1920s (Bastin et al., 1926; Ginsburg-Karagitscheva, 1926; Lipman, 1928), the field of subsurface geomicrobiology has grown significantly (for a review, see Onstott, 2016) and it is now estimated that more bacteria and archaea reside in the continental subsurface than any other microbial habitat (for a review, see Magnabosco et al., 2018a). All three domains of life and even animals have been found to be capable of surviving hundreds of meters to kilometers underground (Borgonie et al., 2015) and, in many cases, survive exclusively through the utilization of geologically-generated energy sources such as H_2 and CO_2 (for a review, see Magnabosco et al., 2019). Due to the practical challenges of accessing and studying deep (> 500 m) subsurface ecosystems, a variety of subsurface experiments and monitoring programs have been pursued in underground laboratories such as the Äspö Hard Rock Laboratory (Äspö HRL, Sweden) (e.g. Kotelnikova and Pedersen, 1998; Pedersen, 1997; Kyle et al., 2008; Westmeijer et al., 2022), Mizunami Underground Research Laboratory (Japan) (e.g. Fukuda et al., 2010; Ino et al., 2016), Grimsel Test Site (Switzerland) (e.g. Konno et al., 2013), Mont Terri Underground Rock Laboratory (Switzerland) (e.g. Stroes-Gascoyne et al., 2007; Poulain et al., 2008; Bagnoud et al., 2016) and Sanford Underground Research Facility (USA) (e.g. Osburn et al., 2019; Casar et al., 2020; Momper et al., 2023). These research programs have revealed diverse communities of subsurface microorganisms capable of performing a wide range of biogeochemical functions such as methane, nitrogen, sulfur, and iron cycling (e.g. Pedersen, 1997; Fukuda et al., 2010; Konno et al., 2013; Ino et al., 2016; Wu et al., 2017; Lopez-Fernandez et al., 2018, 2023). This study describes the BedrettoLab Deep Life Observatory (DELOS), a new granite-hosted underground laboratory for subsurface microbiology investigations operated by ETH Zürich and located within the Bedretto Tunnel (Switzerland).

The Bedretto Tunnel was originally constructed as an adit for Furka Base Railway Tunnel from 1971 to 1982 and intersects 3 geological units in the Gotthard massif (e.g. Hafner, 1958; Keller and Schneider, 1982; Rast et al., 2022): (1) the Tremola Series from tunnel meter (TM) 0 to TM-434; (2) the Prato Series (TM-434 to TM-1138); and (3) the Rotondo granite (TM-1138 to TM-5218). The metasedimentary Tremola Series is composed of mica-gneiss, amphibolites, schists, calc-silicate rocks, and quartzites (Hafner, 1958; Keller and Schneider, 1982) that change between rock types over meter scales (Labhart, 2005). The Prato Series also exhibits compositional heterogeneity of mica-gneisses, amphibolites, and schists over centimeter to meter scales (Labhart, 2005). A sharp contact between the Prato Series and Rotondo granite occurs at TM-1138 and large amounts of deformation in the granite is observed between TM-1,138 and TM-1,143 (Rast et al., 2022). The Rotondo granite is dissected by brittle faults (Lützenkirchen, 2002) and ductile shear zones (Rast et al., 2022) and is further divided into a biotite-rich porphyritic granite (RG2) in the region of TM-2,800 to TM-3,440 that is surrounded by an equigranular granite (RG1) composed of quartz, alkali feldspar, plagioclase, and biotite (Rast et al., 2022). $^{206}Pb/^{238}U$ Zircon dating of the Rotondo granite indicates intrusion ages of 285 to 319 Ma for RG1 and 280 to 335 Ma RG2. Groundwater residence time estimates based on tritium for natural fractures spanning approximately TM-3,800 to TM-5,218 indicate that glacially-fed fractures experience rapid recharge (1 to 1.5 years) while non-glacially-fed fractures exhibit a much more complex recharge history and contain a sub-modern component (Ofterdinger, 2001). It is worth noting that these hydrochemical measurements are limited to the mineralogically consistent last ~1,500 m of the Bedretto Tunnel due to a tunnel collapse that occurred while the tunnel was left un-maintained from 1982 to 2015 and the residence time of groundwater from TM $0 - 3,800$ is currently unknown.

In 2018, ETH Zürich opened the "Bedretto Underground Laboratory for Geosciences and Geoenergies" (BULGG) between the Bedretto Tunnel's TM-2,000 and TM-2,100 (Ma et al., 2022). The first deep (197–303 m in length) boreholes of the BedrettoLab were drilled in 2019 and ahead of the "Bedretto Reservoir Project" (BRP; May 2021 to July 2023) which executed a series of hydraulic stimulation experiments designed to aid in the development of engineered geothermal systems (Gischig et al., 2020; Ma et al., 2022). In preparation for the BRP hydraulic stimulations, the BedrettoLab Deep Life Observatory (DELOS) was initiated to study the subsurface microorganisms residing within the Gotthard Massif. DELOS was named as an homage to the ancient Athenian island that prohibited death, due to the slow turnover times observed in the continental subsurface (Onstott et al., 2014). Since the majority of the Bedretto Tunnel is not cemented, DELOS is not restricted to the experimental boreholes of BULGG. Instead, inflows from the densely fractured Rotondo granite and gneissic sections of the 5.2 km Bedretto Tunnel can be easily sampled and provide an in-depth view of fractured rock ecosystems from tens to ~1,600 meters below land surface (mbls). This study describes the microbiological and hydrochemical changes throughout the natural fractures of the Bedretto Tunnel over a 1-year period from 2020 to 2021 and captures a period ahead of, during, and after the first hydraulic stimulation experiments within BULGG.

2 Materials and methods

2.1 Area of Study

Surface water from above the Bedretto Tunnel (Figure 1) and groundwater from the BedrettoLab Deep Life Observatory (DELOS) and Grimsel Test site (GTS, https://grimsel.com/) were collected for this study. DELOS is accessed through the Ronco Portal of the Bedretto Tunnel (46.497518°N, 8.494992°E) in the Gotthard Massif (Switzerland, Figure 1) and is part of the Riale di Ronco Alpine catchment. The far end of the Bedretto Tunnel (Furka Portal) intersects the 15 km long Furka Base Tunnel. Only a few sections across the tunnel have been shotcreted or supported by steel arches (structural support is mainly required near the Ronco Portal), providing a unique opportunity to sample groundwater directly from fractures spanning over 5 km (Figure 1, Supplementary Data 1). The GTS is an underground research laboratory located approximately 15 km northwest of DELOS and situated within the granitic rock of the Aarmassif (Keusen et al., 1989). The GTS has been in operation since 1984 and has

supported a variety of field-scale experiments related to radioactive waste disposal and enhanced geothermal systems. The similar geology and proximity of GTS to DELOS provided motivation to collect, analyze, and compare the microbial communities and water composition of GTS boreholes "Pinkel", "ISC Injection 2" and "SB80001".

2.2 Field Measurements And Sampling Strategy

DELOS groundwater samples were obtained from a total of 57 locations. 54 sampling sites were related to natural water inflows along the Bedretto tunnel and 3 sites were connected to tunnel inflows in smaller, uncased boreholes (Ø 10 cm, length unknown) in the tunnel sidewalls (Tunnel Meter (TM)-901, TM-755A and TM-2794, where TM refers to the distance in meters from the Val Bedretto tunnel entrance). Approximately monthly hydrochemical sampling from August 2020 to December 2021 and biological sampling from November 2020 to December 2021 are reported in this study. Additional samples were collected from three boreholes in the Grimsel Test Site in April 2021 and a variety of surface water sources in the DELOS region during the summer of 2021 (Figure 1). Temperature, pH, and electrical conductivity (EC) were directly measured on site using an electronic field probe (EXTECH, multi-parameter PCSTestr 35) that was 3-point calibrated (pH: 4.01, 7.00 and 10.00; EC: 84 μS cm^{-1} , 147 μS cm^{-1} and 1413 μS cm^{-1}). The redox potential (ORP) was measured with a KBM-100 (Voltcraft) field meter. The total alkalinity (carbonate alkalinity) of samples collected from November 2020 to March 2021 was determined through acid titration (Hach®, AL-AP Test) and flow rates (Q) were measured using a bucket-and-stopwatch approach.

2.3 Hydrochemical analyses

For major ion analysis, 2 × 5 mL filtered water samples were collected in the field, transported on ice and stored at 4°C before cation (Mg^{2+}, Ca^{2+}, K^{+}, Na^{+}, NH_4^{+} , Li^{+}, Sr^{2+}) and anion (SO_4^{2-} , Cl^{-},F^{-}, NO_3^{-} , NO_2^{-} , PO_4^{3-}, Br^{-}) analysis via ion chromatography (IC; Dionex DX-120 IC System) at the Institute of Geological Sciences ETH Zürich. Prior to ion analysis, the EC and pH of each sample was measured using the inoLab EC-pH measuring instrument from WTW. Samples that exceeded the IC working range of 0-500 μS cm^{-1} were diluted 10× to ensure ion concentrations were within the ranges of the standards. Water isotope samples were collected and transported to Zürich in 100 mL polyethylene bottles with airtight caps (Semadeni, CH). In Zürich, water isotope samples were filtered using a 0.45 μm filter, sealed in 3 × 2 mL glass autosampler vials and stored at 4°C until water isotope analysis was performed using a Picarro L2130-i analyzer at the Geological Institute of ETH Zürich. Raw measurements were post-processed using the Picarro software ChemCorrect which calculates the isotopic composition as δ^{18}O or δ^{2}H-value with respect to the Vienna Standard Mean Ocean Water (VSMOW). The local meteoric water line of DELOS was estimated from regional isotope data obtained on waterisotopes.org and derived from (Bowen and Revenaugh, 2003).

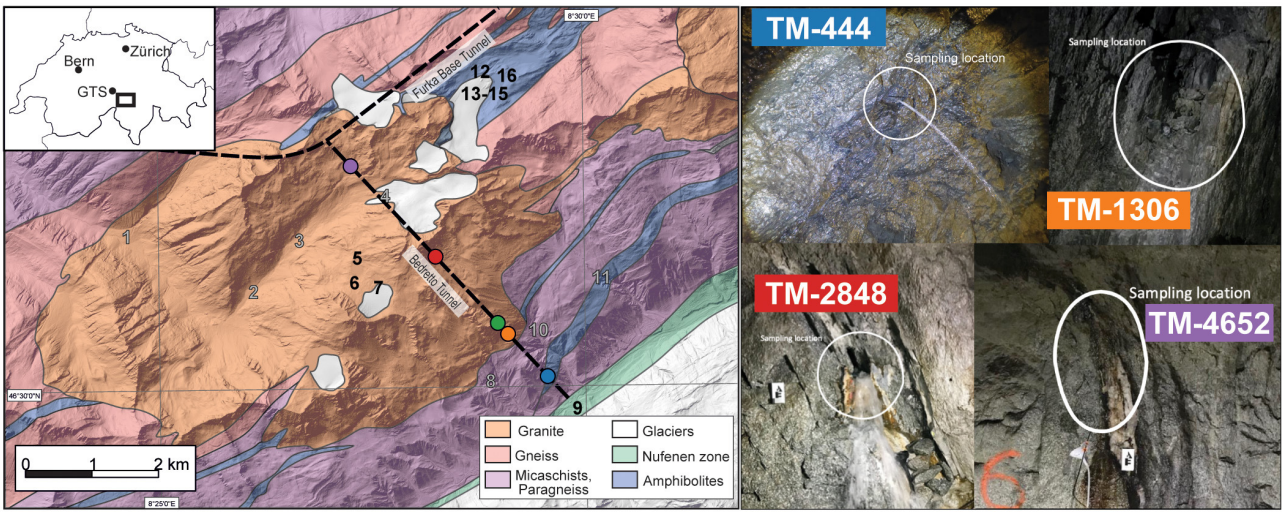

FIGURE 1
A geologic map (modified after Rast et al., 2022) of the BedrettoLab Deep Life Observatory (DELOS) is shown on the left of the figure and overlayed with the location of the Bedretto Tunnel and Furka Base Tunnel (dotted black lines). Tunnel Meter (TM) 0 occurs at the Val Bedretto tunnel entrance. The locations of time series sampling sites TM-444 (blue), TM-1306 (orange), TM-1494 (green), TM-2848 (red), and TM-4562 (purple) within the Bedretto Tunnel are illustrated as circles. Numbers 1–16 on the geologic map indicate surface water sampling sites. Gray numbers indicate locations where hydrochemistry samples were collected and black numbers indicate locations where DNA and hydrochemistry samples were collected. Notable surface DNA sample locations are the Ticino River (9), a high-Alpine spring (7), glacial lakes (5, 6, 12, 16), and the Witenwasseren glacier borehole (13) and flow (14, 15). A map of Switzerland (top left) indicates the locations of DELOS, the Grimsel Test Site (GTS), Zürich, and Bern. Four representative images of groundwater sampling sites are shown on the right. The white circles indicate the groundwater inflow that was sampled for this study. A complete image catalog of sampling sites can be found in Supplementary Data 1.

2.4 DNA extraction, 16S rRNA gene amplification, quantification, and sequencing

Biomass was collected on site by filtering fracture or surface water through 0.22 μm Sterivex filters (SVGPL10RC, Millipore) with a peristaltic pump. Prior to filtration, new sterile tubing was flushed with the fracture water of interest for 3–5 minutes. After filtration, Sterivex filters were stored in sterile, 50 mL falcon tubes, transported on ice to ETH Zürich the same day, and frozen at -80°C until DNA extraction. DNA extractions of samples and extraction blanks were performed following the manufacturer's standard protocol of the DNeasy PowerWater Kit (14900-100-NF, Qiagen). DNA concentrations were quantified by the Qubit 4 Fluorometer (ThermoFisher) and stored in a -80°C freezer for use in downstream applications.

All DNA samples were amplified in triplicate using the Platinum II Hot-Start PCR Master Mix Kit (14000013, Invitrogen) and following a previously defined procedure (McNichol et al., 2021). Briefly, a single-step PCR was performed to amplify a conserved part of the V4-V5 region of the 16S SSU rRNA gene from bacteria and archaea. The region was targeted using Golay-barcoded 515F forward primers (AATGATACGGCGACCACCGAGATCTACACGCT - XXXXXXXXXXXX - TATGGTAATTGT - GTGYCAGCMGCCGCGGTAA, with the X's denoting the variable Golay barcode location) and a 926R PCR reverse primer (CAAGCAGAAGACGGCATACGAGATAGTCAGCCAGGG - CCGYCAATTYMTTTRAGTTT) (Walters et al., 2016). After PCR, triplicates were pooled together and samples were cleaned using Agencourt AMPure XP beads (Beckman Coulter) at a 0.7× ratio and DNA concentrations were measured using the Qubit 4 Fluorometer (ThermoFisher). Using the Qubit measured amplicon concentrations, samples were normalized and pooled. The pooled library was cleaned with AMPure XP beads at a 0.7× ratio and the final, cleaned library was quantified using both the Qubit 4 and 4150 Tapestation (Agilent). The amplicon library was sequenced at the ETH Zürich Genetic Diversity Center on an Illumina MiSeq using a 500-cycle paired end V2 reagent kit (MS-102-2003, Illumina). PhiX was spiked in at a concentration of 8%. The final library loading concentration was 4 pM and custom sequencing primers were used: 515Fseq (TATGGTAATTGTGTGYCAGCMGCCGCGGTAA), 926Rseq (CGGCATACGAGATAGTCAGCCAGGGCCGYCAATTYMTTTRAGTTT), and a modified Illumina index sequence primer (AATGATACGGCGACCACCGAGATCTACACGCT).

16S rRNA gene amplicon copy numbers were quantified using a quantitative PCR (qPCR) with the Lightcycler 480 (Roche). Briefly, a solution containing the V4-V5 forward primer 515F (GTGNCAGCMGCCGCGGTAA, final concentration 0.5 μM), the V4-V5 reverse primer 926R (CCGYCAATTYMTTTRAGTTT, 0.5 μM), 5 μL SsoFast EvaGreen Supermix with Low ROX 2x (1725210, BioRad), and 1 μL Bovine Serum Albumin (10 mg mL^{-1}) were combined with 2 μL of template DNA were prepared in triplicate and loaded onto a 96-well plate for qPCR. 16S rRNA gene standards ranging from 2.088×10^6 to 20.88 16S rRNA gene amplicon copies per μL were prepared using a consensus 16S synthetic construct and serial dilution. The qPCR program included an initialization of 95°C for 300 seconds, 40 cycles of denaturation (10 seconds at 95°C), annealing (30 seconds at 50°C) and elongation (15 seconds at 68°C) with a melting curve of 15 seconds at 95°C and 60 seconds at 55°C and one acquisition per °C from 55°C to 95°C. The fit ($R^2 = 0.99$) and melt curve of the standards are shown in Supplementary Figures 1, 2.

2.5 Biodiversity analyses

The quality of 16S rRNA gene amplicon sequences was assessed using `FastQC` (Babraham Bioinformatics Group). Based on the sequence quality, the first 5 nucleotides of the forward and reverse reads were trimmed using the `FASTX-trimmer`, http://hannonlab.cshl.edu/fastx_toolkit/license.html. Additionally, nucleotides beyond position 230 were removed from the reverse read by the `FASTX-trimmer`. After trimming, `Trimmomatic` (Bolger et al., 2014) was used to quality filter the reads (SLIDINGWINDOW:100:28) and remove adapters. Paired end reads were joined using `fastq-join` (-p 3 -m 20; v-1.04.807), https://github.com/ExpressionAnalysis/ea-utils/blob/wiki/FastqJoin.md. Amplicon sequencing variants (ASVs) were then predicted from joined reads using the "pseudopool" option of `dada2` (Callahan et al., 2016) and annotated using `dada2` and the Silva nr99 v138.2 dataset (Quast et al., 2012; Yilmaz et al., 2014). After annotation, all ASVs found in the control samples were removed from the ASV data table and omitted from all downstream analyses. Biodiversity and statistical analyses were performed in `R` and `python` with ASV data. All code is available via https://github.com/GeobiologyLab/DELOS-2021-time-series.

3 Results

3.1 Seasonal and spatial hydrochemical variability throughout DELOS

DELOS groundwaters exhibit annual mean temperatures from 5°C to 19.5°C and a pH ranging from 8 to 9.6 (Supplementary Data 2), depending on location. Groundwater temperature generally correlates with overburden with the exception of high inflow zones where the largest faults occur around tunnel meter (TM) 1306, TM-2848 and TM-4166 (Figure 2). An additional zone of high inflow is observed in a landslide scarp section between TM 300 – 400, consistent with earlier hydraulic studies (Masset and Loew, 2010; Halter et al., 2024). Nitrate was detected in 22 of the 57 DELOS locations with elevated concentrations observed within the high inflow zones surrounding TM-300, TM-1306, TM-2848, TM-3750, TM-3884 and TM-4166 and a maximum concentration of 3.5 ppm at TM-216 (Figure 2). The average, per-fracture electrical conductivity (EC) in DELOS spans 43.2 μS cm^{-1} (TM-1306) to 931.1 μS cm^{-1} (TM-901; Figure 2). Groundwaters exhibiting an EC in excess of 500 μS cm^{-1} are also enriched with millimolar levels of sulfate. In general, the EC measurements of all groundwater-filled fractures from tunnel meters 4,200 – 5,218 of DELOS exhibit very little

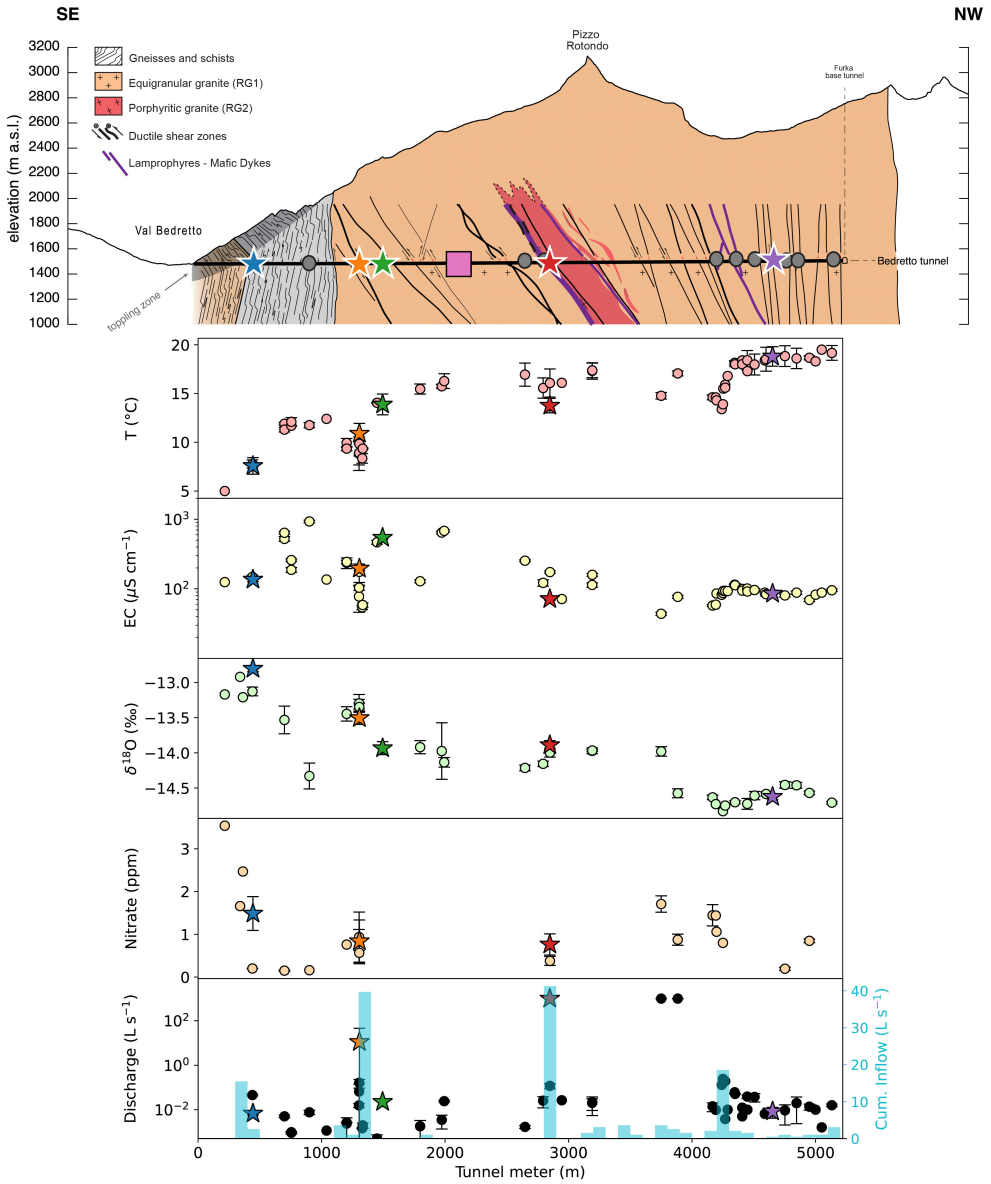

FIGURE 2
Top: A profile of the BedrettoLab Deep Life Observatory (DELOS, horizontal black line) is illustrated with respect to its overburden (modified after Rast et al., 2022). Notable geological features throughout DELOS are described in the panel legend and the Bedretto Underground Laboratory for Geosciences and Geoenergies is indicated by a pink box. Gray circles and colored stars along the tunnel indicate locations where DNA samples were collected as either single samples (gray circles) or as part of the "long-term biological monitoring" program (colored stars). **Lower:** The mean (points) and standard deviation (bars) of temperature (T), electrical conductivity (EC), $\delta^{18}O$, nitrate (samples whose concentrations were below detection are omitted), and discharge (black) measurements of individual fractures throughout a 1-year time series are displayed. Fractures with flow rates above what could be quantified with our measurement protocol were designated as 999 L s^{-1} (TM-2848, TM-3750, TM-3884). To better illustrate tunnel inflow from groundwater-bearing fractures, the cumulative discharge rate binned per 100 m interval is shown (cyan bars, previously reported by Masset and Loew (2010)). m.a.s.l. = meters above sea level.

variation throughout the 16 month hydrochemical monitoring period (mean ± standard deviation: 91 ± 12 μS cm^{-1}). On the other hand, the EC throughout the first 2,000 DELOS tunnel meters is highly variable between fractures but relatively consistent within a fracture throughout the sampling period (Figure 2). Inter-fracture water isotope measurements also exhibit greater variability in the first 2,000 tunnel meters relative to the last 1,000 tunnel meters (Figure 2). It is worth noting that the last 1,000 tunnel meters of DELOS is likely influenced by the drainage effect of the ~15 km long Furka Base Tunnel (Amberg, 1983) and, therefore, the similarities in the hydrochemistry of these sites may be anthropogenically driven.

All DELOS groundwater and DELOS surface waters follow the local meteoric water line (LMWL, Figure 3). With the exception of TM-1494 whose water isotope values are more similar to groundwater from DELOS fractures with over 400 m greater overburden, DELOS groundwater exhibits isotopic depletion as overburden increases (Figure 3). In general, the per-fracture

DELOS groundwater isotope values were relatively stable throughout the monitoring period and did not reveal strong seasonal pattern (Figure 2). Previous water isotope measurements from the Grimsel Test Site (Schneeberger et al., 2017) also follow the DELOS LMWL and are most similar to the shallowest DELOS groundwater sites (Figure 3). It is worth noting that the nearby (< 15 km away), granite hosted Grimsel Test Site (GTS) is located approximately 1,730 m above sea level (masl) (Blechschmidt and Vomvoris, 2015) and the GTS water isotope samples are derived from sampling locations with an overburden of 420 − 520 m (Schneeberger et al., 2017). The surface elevation of DELOS groundwater samples with similar isotopic composition as the GTS samples is approximately 1,760 masl (overburden of 280 m).

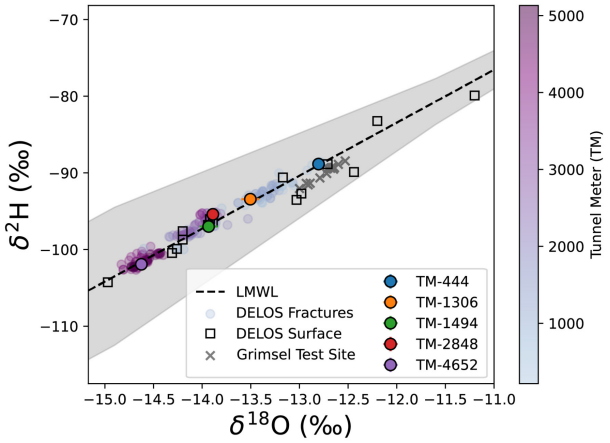

FIGURE 3
The water-derived δ^{18}O (x-axis) and δ^2H (y-axis) of surface waters and snow collected above DELOS (open squares) are shown with respect to an estimated local meteoric water line (LMWL, black dashed line surrounded by a 95% confidence interval illustrated as a gray box). DELOS fracture water samples (circles) are colored according to a blue-to-purple gradient that corresponds to the tunnel meter (TM) in which the sample was collected (see color bar). The 5 "long-term biological monitoring" locations are illustrated according to the site colors used throughout this manuscript. Information on the DELOS surface samples included in this plot are provided in Supplementary Figure 5, Supplementary Data 2.

3.2 DELOS microbial diversity and abundance

14,508 unique amplicon sequencing variants (ASVs) spanning 64 phyla were identified throughout DELOS with the highest richness (2,944 ASVs; Shannon Diversity (H'): 5.8) observed in the November 2021 TM-1306 sample and the lowest richness (267 ASVs; $H' = 4.0$) observed in the December 2020 sampling of TM-4166. DELOS microbial communities are dominated (85 to > 99%) by bacteria. The most abundant bacterial phyla observed within DELOS are related to *Candidatus* Kryptonia (up to 30% at TM-4652), *Nitrospirota* (up to 55% at TM-444), *Pseudomonadota* (previously known as *Proteobacteria*; up to 70% at TM-2647) and *Spirochaetota* (up to 30% at TM-4652) (Supplementary Data 3). A large (> 50%) population of chemolithotrophic *Leptospirillia* from the phylum *Nitrospirota* make the microbial community of the shallow, gneiss-hosted sample from TM-444 an outlier relative to other samples (Figure 4). Rather than *Leptospirillia*, other sites exhibiting large populations of *Nitrospirota* are represented by members of the nitrogen and sulfur cycling class *Thermodesulfovibrionia* (up to 30% at TM-1494, Figure 5). The DPANN archaeal superphylum dominates DELOS archaeal communities and members of this group are most abundant (up to 15% of the total microbial community) in samples from TM-1306, TM-2848 and TM-4447. Ultra-small bacteria within the Candidate Phylum Radiation (*Patescibacteria*) and bacterial class *Omnitrophia* within the *Verrucomicrobiota* phylum are also relatively abundant throughout DELOS, exhibiting their highest relative abundances at TM-4166 (up to 15%) and TM-4447 (up to 23%), respectively.

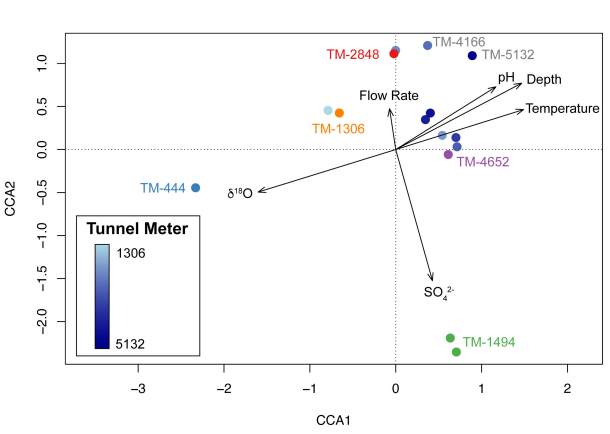

FIGURE 4
Ordination of the amplicon sequencing variant (ASV) taxonomic composition of DELOS fracture water samples collected in November and December 2020 (circles) along environmental gradients (black arrows) are displayed through a canonical correspondence analysis (CCA) plot. With the exception of long-term biological monitoring sites TM-444 (blue label), TM-1306 (orange), TM-1494 (green), TM-2848 (red) and TM-4652 (purple), samples are colored according to a light blue to dark blue gradient that corresponds to the tunnel meter (TM) in which the sample was collected.

Fractures within the gneissic section of DELOS generally exhibit higher concentrations of 16S rRNA gene amplicon copies mL^{-1} ($Q_{25\%}$=7.6 × 10^3, $Q_{75\%}$=3.3 × 10^4) relative to granitic samples ($Q_{25\%}$=1.7 × 10^3, $Q_{75\%}$=6.4 × 10^3) (Supplementary Figure 3). An exception to this trend is observed at the granitic TM-2467 fracture (8.2 ± 2.1 × 10^4 16S rRNA gene amplicon copies mL^{-1}). Here, a visible biofilm surrounds the fracture of TM-2647 (Supplementary Data 1) and may have contributed to the elevated copy numbers in the samples. Large populations of sulfur oxidizing *Pseudomonadota* related to *Sulfurifustis* (35%) and *Thiobacillus* (10%) that, in the case of *Thiobacillus*, have been linked to biofilm formation in the granite-hosted Äspö Hard Rock Laboratory (Lopez-Fernandez et al., 2023), further point to potential biofilm contamination within the TM-2647 sample. On the other hand, the fracture at TM-4652 intersects a quartz vein (Supplementary Data 1) and consistently exhibited the lowest concentrations (931 ± 378) of 16S rRNA gene amplicon

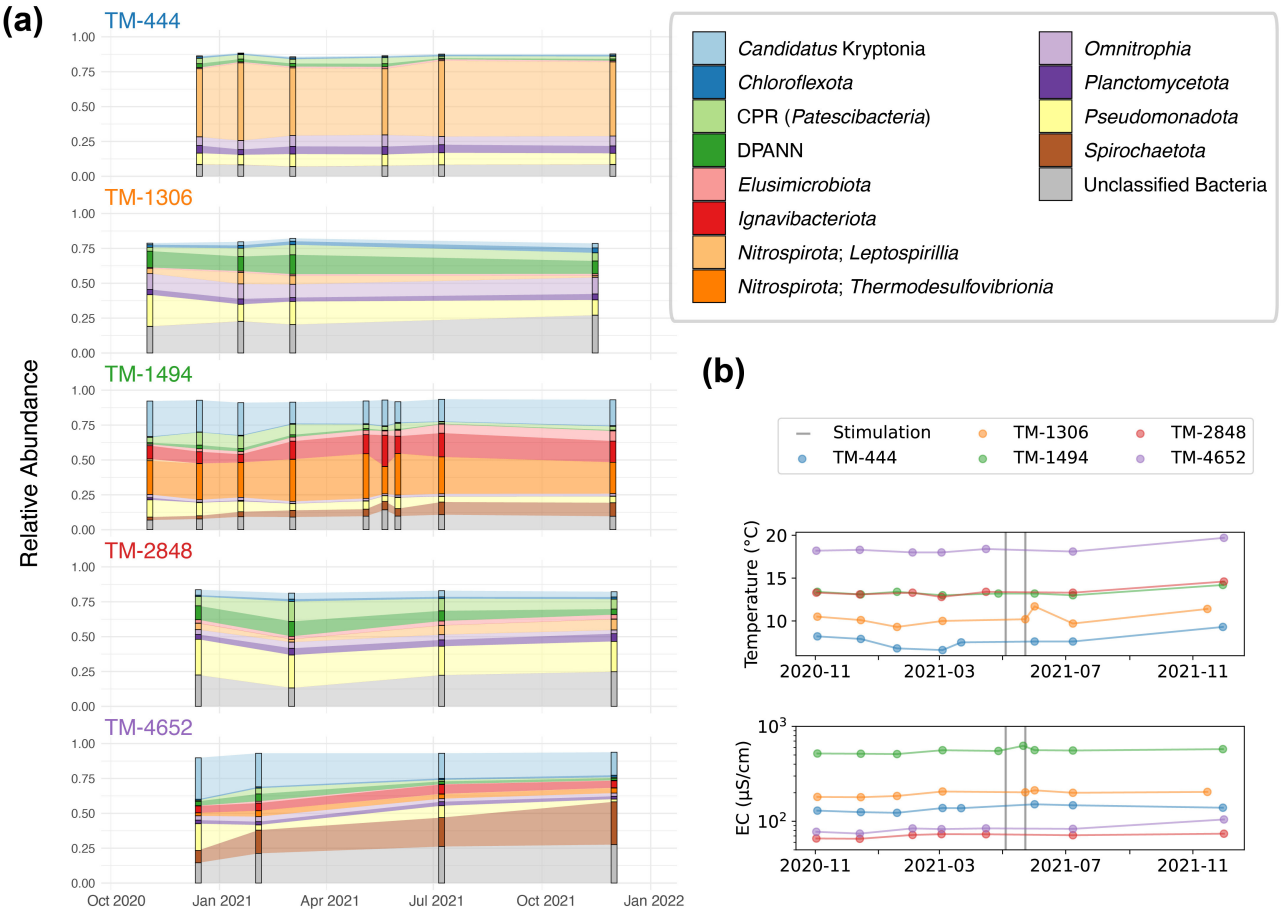

FIGURE 5
(A) The 16S rRNA gene amplicon based community composition of 5 DELOS fractures (TM-444, TM-1306, TM-1494, TM-2848, TM-4652) are shown. Each time point's microbial community is displayed as a bar with the observed change between sampling sites illustrated as the shading between bars. The taxonomic legend is displayed in the top right of the figure. Unfilled space between the top of each bar plot to 1.00 on the y-axis are taxonomic groups that are minor members of the community. **(B)** Changes in temperature (top) and electrical conductivity (EC, bottom) throughout the sampling period are shown for each sampling location. Vertical gray bars indicate the experimental period of 2 hydraulic stimulation experiments associated with the Bedretto Reservoir Project in May 2021.

copies mL^{-1} with a community largely composed of *Candidatus* Kryptonia and *Spirochaetota*.

Canonical correspondence analysis of 16S rRNA gene amplicon sequencing variants (ASVs) and environmental data from DELOS groundwater samples collected in November and December 2020 reveals that DELOS groundwater microbial communities are distributed along a $\delta^{18}O$, depth and temperature gradient that correlates to tunnel meter (Figure 4). As with the DELOS hydrochemical measurements, samples from the last 1,000 m exhibit more similar microbial communities than samples collected throughout the first 3,500 m of the tunnel (Figure 4). An exception to the otherwise tight clustering of samples from the last 1,000 m is a pH 9.0 sample with relatively high abundance (25%) of an uncultivated lineage ("Dadabacteria" also known as *Candidatus* Desulfobacterota) from TM-5132. Further separation of DELOS ecosystem types (ecotypes) are seen in the sulfate- and *Thermodesulfovibrionia*-enriched TM-1494 sample and high flow rate and DPANN/*Patescibacteria*-enriched samples (TM-1306, TM-2848, TM-4166). Together, these findings point to three major ecotypes in the DELOS groundwater system: (1) Shallow groundwater with low electrical conductivity enriched in *Leptospirillia*; (2) High-inflow fault zones enriched in ultra-small bacteria and archaea; (3) Bicarbonate-enriched waters predominantly represented throughout the last 1,000 tunnel meters and that are enriched in *Candidatus* Kryptonia and *Spirochaetota*.

Following the DELOS-wide survey in November and December of 2020, five fractures were selected for seasonal monitoring based on hydrochemical and sampling considerations. 16S rRNA gene analysis reveals that community membership is generally stable and that inter-group differences were significantly greater than intra-group differences (Figure 5, Supplementary Figure 4). TM-4652 exhibits the most phylum-level changes during the 12-month monitoring period, revealing a slow replacement of relatively abundant *Pseudomonadota* and *Patescibacteria* with *Spirochaetota* and *Ignavibacteriota*. A similar change in the abundance of these phyla is observed at TM-1494; however, the most dramatic change in taxonomic composition within this site occurs when the dominant population of *Thermodesulfovibrionia* decreases from

32% to 20% relative abundance from 5 — 21 May 2021. This decrease co-occurs with an increase in the relative abundance of *Ignavibacteriota* and two of unclassified bacterial ASVs that are also observed in TM-1494 throughout the various sampling time points and in TM-4652. This change in community composition follows the first hydraulic stimulation experiment in the Bedretto Reservoir Project's stimulation boreholes (ST, located near TM-2050 of BULGG) on 3–5 May 2021, seismic events near the TM-1494 fracture possibly related to the hydraulic stimulation on 6 May 2021, and seismic events near the TM-1494 fracture associated with heavy rainfall on 10 May 2021 (*personal communication*, BULGG). An increase in electrical conductivity that correlates to an increase in all major ion concentrations except magnesium is additionally observed at TM-1494 between 5 and 21 May 2021. A second hydraulic stimulation experiment that targeted a different depth range (interval) of the aforementioned experimental ST borehole was conducted from 22 — 24 May 2021. This experiment demonstrated a connection between the injection and production wells of the stimulation (Arnet, 2021) but did not result in seismic activity near the TM-1494 fault. The 1 June 2021 sampling of TM-1494 after the 22 — 24 May 2021 stimulation revealed that the fracture's hydrochemical and microbial community composition had recovered to its "baseline" state, indicating that the changes observed on 21 May were relatively short-lived (Figure 5). Interestingly, an increase in electrical conductivity along with an increase in temperature following the 22 — 24 May hydraulic stimulation can be seen in TM-1306 and may indicate that the two Bedretto Reservoir Project stimulation experiments affected two different regions of the Bedretto Reservoir (TM 2000-2100); however, a microbial sample was not collected from TM-1306 during this time period (Figure 5). Together, these observations indicate that both experimentally and naturally induced seismicity contribute to the temporal biodiversity and chemical patterns observed throughout DELOS.

3.3 DELOS groundwater and surface microbial communities exhibit minimal overlap

Three groundwater samples from the granite-hosted Grimsel Test Site (GTS, ~15 km from DELOS) and nine samples from DELOS surface waters (Figure 1) were collected for hydrochemical and microbial community analysis in spring and summer 2021, respectively. These samples represent water from two GTS experimental boreholes ("Pinkel" and "ISC Injection 2"), a GTS monitoring borehole ("SB80001"), the Ticino River, a high-altitude freshwater spring, four glacial lakes, and three samples (one above ice, two below ice) from the Witenwasseren glacier (Supplementary Data 2). Surface samples exhibited a lower mean temperature (6.8 ± 3.5°C) and pH (7.4 ± 0.6) than DELOS and GTS (Table 1). The electrical conductivity of the Ticino River is elevated (EC, 409 μS cm^{-1}) relative to other surface sites, resulting in the high variance in EC across surface sites (Table 1). Groundwater collected from the GTS boreholes exhibit mean temperature, EC and 16S rRNA gene amplicon copies mL^{-1} measurements between the DELOS surface and DELOS groundwater samples (Table 1).

The GTS groundwater samples captured three distinct microbial communities: (1) a *Desulfitobacteriia*-dominated (phylum *Bacillota*) community within the Grimsel *In-Situ* Stimulation and Circulation Experiment experimental borehole (Doetsch et al., 2018, "ISC Injection 2") (2) a *Pseudomonadota*-dominated community composed primarily of *Hydrogenophaga* and *Rhodocyclaceae* in a radionuclide experimental borehole (Quinto et al., 2017, "Pinkel") and (3) a *Pseudomonadota*- and *Thermodesulfovibrionia*-dominated community in the monitoring borehole ("SB80001"). Two Silva-defined bacterial phyla (*Caldisericota* and WS1) were identified in GTS at < 0.2% relative abundance but not DELOS and 29 phyla are found in DELOS but not GTS. On the other hand, 8 Silva-defined bacterial phyla (*Caldisericota*, *Campylobacterota*, *Fusobacteriota*, *Rhodothermota*, *Synergistota*, LCP-89, TX1A-33, and WS4) were identified in the surface samples surrounding DELOS but not DELOS, while 21 bacterial phyla were found in DELOS but not the surface water samples. At the phylum level, surface microbial communities were more similar to each other than DELOS groundwater communities (Figure 6) and there is very little ASV overlap between DELOS fractures, the DELOS surface, and nearby Grimsel Test Site (Figure 7). Furthermore, there is only a small tendency for nearby fractures to have more similar microbial communities (Sørensen Distance-Decay $R^2 = 0.2$) with four of the five DELOS time series fractures exhibiting a greater similarity in community composition with GTS samples than the surrounding surface waters (Figure 8).

4 Discussion

The BedrettoLab Deep Life Observatory (DELOS) provides a unique opportunity to study how hydrogeology affects subsurface

TABLE 1 The mean and standard deviation of temperature, pH, electrical conductivity and 16S rRNA gene amplicon copies per mL collected from DELOS groundwater, Grimsel Test Site groundwater and surface locations surrounding DELOS (DELOS surface).

	DELOS groundwater	Grimsel Test Site	DELOS surface
Temperature (°C)	14.1 ± 3.5	12.9 ± 0.4	6.8 ± 3.5
pH	9.0 ± 0.9	10.3 ± 0.4	7.4 ± 0.6
Electrical Conductivity (μS cm^{-1})	252 ± 250	108 ± 14	72 ± 144
16S rRNA copies (mL^{-1}, $Q_{25\%}$)	2.0×10^3	4.5×10^3	1.0×10^6
16S rRNA copies (mL^{-1}, $Q_{75\%}$)	8.2×10^3	5.0×10^5	4.5×10^6

$Q_{25\%}$ = 25% Quartile. $Q_{75\%}$ = 75% Quartile.

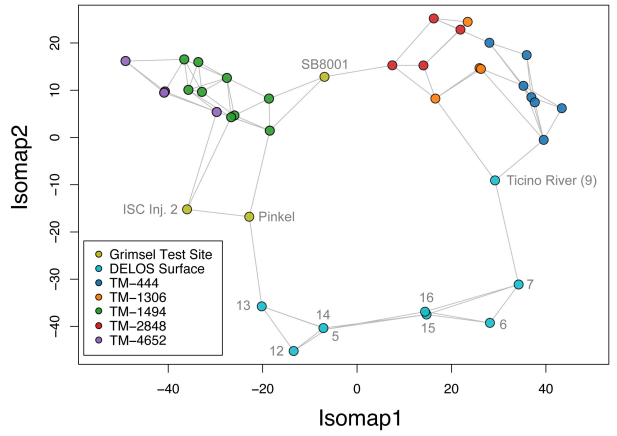

FIGURE 6
A three nearest neighbors isomap embedding of the rarefied phylum-level community composition of samples (points) from the DELOS time series (blue, orange, green, red, purple), surrounding surface waters (light blue), and nearby Grimsel Test Site (olive) is shown. Gray labels indicate sample names from the Grimsel Test Site and DELOS surface as described in the main text and Figure 1. Distances between samples were computed using the robust Aitchison metric and the gray lines illustrate the isomap-constructed neighborhood graph. Points that are connected and within close proximity to one another represent the microbial communities that are more similar.

microbiology. Unlike the majority of underground labs which make use of vertically excavated mines or deep boreholes (e.g. Hallbeck and Pedersen, 2008; Ino et al., 2016; Osburn et al., 2019), DELOS captures a 1,600 meter depth gradient via a horizontally contiguous 5-km long tunnel through 2 main lithologies (gneiss-schist and granite) in the Alps. As with previous subsurface studies (e.g. Hallbeck and Pedersen, 2008; Ino et al., 2016; Osburn et al., 2019), the different geologies (gneiss-schist from TM-0 to TM-1138 and granite from TM-1138 to TM-5218) host hydrochemically and microbially distinct waters; however, within the same lithology, there are also high amounts of hydrochemical and biological variability correlated to depth, recharge, electrical conductivity and flow rate (Figures 2, 4, 6). Calcium- and sulfate-rich waters appear in the high EC sites (Figure 2) while the back half (>TM-2500) of the tunnel tends to have a larger sodium component. High inflow zones of the tunnel are depleted in sulfate and enriched in bicarbonate and nitrate (Figure 2, Supplementary Data 2). These bicarbonate-type waters are most similar to groundwater found in the granite-hosted Korea Atomic Energy Research Institute Underground Research Tunnel (KAERI URT; Ryu et al., 2012), Gotthard Rail Base Tunnel (< 15 km from DELOS; Bucher and Stober, 2010), and Grimsel Test Site (Konno et al., 2013). On the other hand, water from the Mizunami Underground Research Laboratory (Japan; Iwatsuki et al., 2005) and Chalk River Laboratory (Canada; Beaton et al., 2016) uniquely and respectively provide sodium chloride- and sodium bicarbonate-type end members among the granite underground laboratories reported in Figure 9.

Overall, DELOS exhibits a higher degree of hydrochemical diversity than reports of other granite-hosted underground labs (Figure 9) and, within DELOS, this hydrochemical heterogeneity is especially apparent within two granitic inflow zones (TM-1306 and TM-1494) separated by less than 200 m laterally and a difference in overburden of less than 50 m. Water from TM-1494 has a high sulfate concentration and a water isotope signature that is more similar to water encountered in deeper parts of DELOS. On the other hand, the water isotope signature and microbial community of TM-1306 is more similar to shallower parts of the tunnel and the Ticino River (Figure 3, Supplementary Figure 5). As stable water isotopes of oxygen and hydrogen are frequently used to trace groundwater and estimate recharge (Clark and Fritz, 2013; Blasch and Bryson, 2007), the hydrochemical and biological variation within the proximal but isotopically distinct fracture waters supports previous observations of groundwater origin and recharge shaping subsurface ecosystems (e.g. Ben Maamar et al., 2015; Hubalek et al., 2016; Yan et al., 2021). On the other hand, isotopically similar water from TM-1494 and TM-2848 (Figure 3) exhibit extremely different hydrochemical and microbial community compositions (Figure 5) while isotopically distinct water from TM-2848 and TM-4166 exhibit similar hydrochemistry and microbial community compositions (Figure 4, Supplementary Data 2, 3). The similarities between TM-2848 and TM-4166 appear to be correlated to the relatively high flow rates observed at these sites (Figures 2, 4) which also emerge near zones containing biotite-rich lamprophyres (Figure 2). Previous investigations into the microbial diversity of the metasedimentary Deep Mine Microbial Observatory (USA) have shown that mineralogy plays an important role in shaping subsurface hydrochemistry and microbial communities (Casar et al., 2020, 2021). A local enrichment of vanadium in the TM-2848 and TM-4166 groundwater and lamprophyres relative to other locations in DELOS (Supplementary Table 1) is suggestive of a similar connection between mineralogy, hydrochemistry and microbial diversity. As most groundwater vanadium studies surround sites with vanadium concentrations several orders of magnitude higher than DELOS (e.g. Xiao et al., 2017; Zhang et al., 2019, 2020a), additional work is needed to discern whether there is a significant relationship between vanadium and microbial diversity in DELOS.

Fracture flow rate, a proxy for hydraulic conductivity, may play an additional and understudied role in shaping subsurface ecosystems. DELOS fractures TM-1306, TM-2848 and TM-4166 occur within the 3 regions of highest inflow and all show an increased proportion of ultra-small bacteria and archaea relative to other sampling sites throughout DELOS. Previous studies have suggested that smaller cells are transported more easily than larger cells due to mechanical filtration (e.g. Gannon et al., 1991; Abu-Ashour et al., 1994); however, regions of DELOS with a lower flow rate and, thus a lower permeability and higher potential for filtering (Bense et al., 2013), do not exhibit an ultra-small microbial enrichment. Mechanical filtering is, therefore, not sufficient to explain the distribution of ultra-small microorganisms in this region and other factors such as groundwater turbulence may play a role. In shallow groundwater, an increase in the detachment of ultra-small bacteria from soils into groundwater during high infiltration periods has been observed (Herrmann et al., 2019, 2023). If similar processes control the abundance patterns of ultra-small microorganisms in DELOS, the increased turbulence associated within these highly permeable regions may similarly detach populations of ultra-small microorganisms from shallower

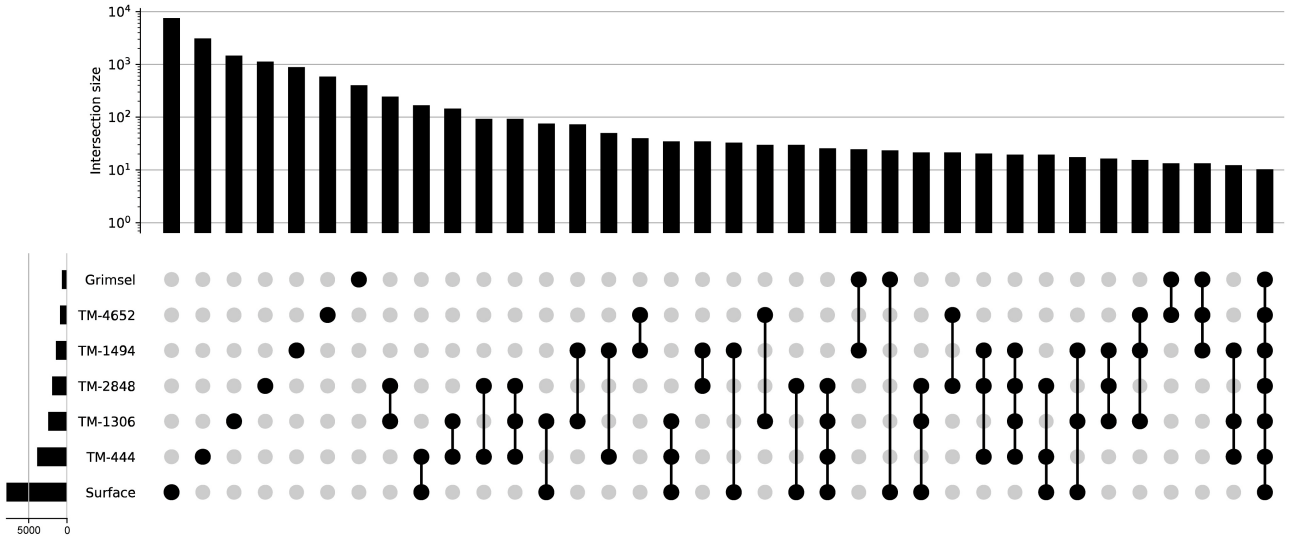

FIGURE 7
UpSet plot displaying the number of unique and shared amplicon sequencing variants (ASVs) between samples collected during the DELOS time series, from surface waters surrounding DELOS, and the Grimsel Test Site (x- and y-axis histograms). Black dots indicate the sampling locations for which the comparison of shared ASVs are being made. Comparisons for which there are less than 10 shared ASVs are not shown.

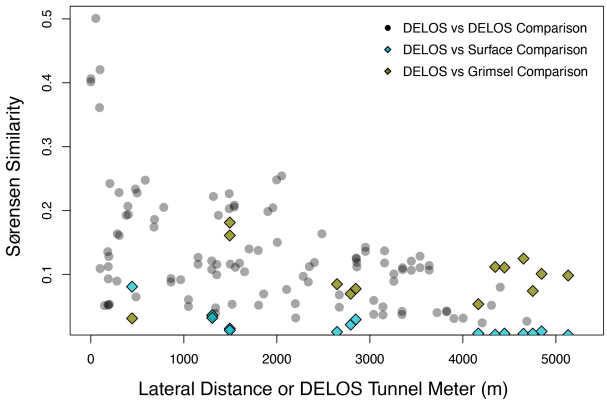

FIGURE 8
The amplicon sequencing variant (ASV)-level Sørensen Similarity (y-axis) between pairs of DELOS samples collected during November and December 2020 (black transparent circles) are shown with respect to the lateral tunnel distance between the pairs (x-axis). As a point of reference, pairwise comparisons between the individual DELOS samples with microbial communities from the monitoring borehole (SB80001) of Grimsel Test Site (olive diamonds) and the Ticino River (blue diamonds) are shown with respect to the tunnel meter in which the DELOS sample was collected (i.e., the far left olive and light blue diamonds represent comparisons between the December 2020 DELOS TM-444 sample and SB80001 and the December 2020 DELOS TM-444 sample and the Ticino River, respectively). SB80001 and the Ticino River were selected for comparison with DELOS since their microbial communities exhibited the greatest community overlap with DELOS samples.

biofilms and/or provide a medium to more easily carry small particles further.

Seasonal observation of DELOS fractures additionally indicates that groundwater mixing and/or alterations in flow paths can occur in DELOS (Figure 5). Research on the "critical zone" has found that changes in land cover and/or land use can change the biological and chemical properties of subsurface ecosystems and that extreme events such as heavy rainfall and earthquakes dominate the transfer of energy and matter from the surface to shallow ($<$ 100 m below land surface) subsurface environments (Küsel et al., 2016; Skelton et al., 2019; Hosono et al., 2020). Seasonal mixing of more oxidizing shallow groundwater with deeper, more reducing fluids have also been observed and shown to introduce new substrates that stimulate the expansion of microorganisms into higher-energy niches (e.g. Magnabosco et al., 2018b; Bochet et al., 2020; Zhang et al., 2023) and human activities, such as tunnel construction and fluid injection, have been shown to alter groundwater flow paths and water chemistry (e.g. Banwart et al., 1996; Dong et al., 2014; Daly et al., 2016; Zhang et al., 2020b, 2022). Throughout the monitoring period, very minor seasonal changes were observed throughout DELOS (Figure 2); however, a measurable change in electrical conductivity and microbial community composition was observed in TM-1494 following a hydraulic stimulation experiment and rainfall-associated seismic events near the main fault sampled at this location. Hydrochemical measurements taken throughout the tunnel during this period (April–June 2021) suggest that these events may have altered the groundwater flow paths (Figure 2; Arnet, 2021). In particular, the increase in electrical conductivity observed at TM-1306 and TM-1494 during this period may be stem from an increase in the contribution of higher EC groundwater from the "badboy" fault (TM-1993, EC $= 707 \pm 64$ μS cm^{-1}) to these fractures. Although biological samples from TM-1993 are not available for comparison, a related experimental strategy, known as a "flow test" involving a 10 month injection of fluids into a deep borehole of the metasedimentary Sanford Underground Research Facility, showed that groundwater can be displaced during injection and result in the replacement of pre-existing communities with new microorganisms via advection (Zhang et al., 2022). Together, these observations suggest that the hydraulic stimulation and/or

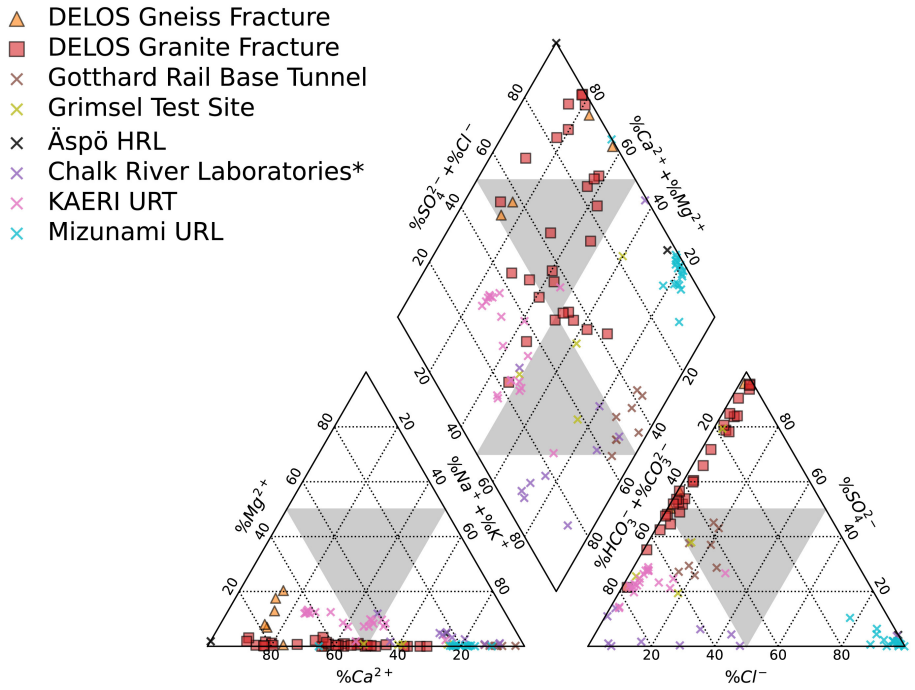

FIGURE 9
The mean annual composition of DELOS groundwaters derived from the gneissic (orange triangles) and granitic (red squares) sections of DELOS is displayed in a Piper diagram. Additional groundwater data from other subsurface laboratories and tunnels hosted in gneiss and/or granite (colored ×'s) are shown. Data is compiled from the Gotthard Rail Base Tunnel (Switzerland) (Bucher and Stober, 2010), Grimsel Test Site (Swizerland) (Konno et al., 2013), Äspö Hard Rock Laboratory (HRL, Sweden) (Pedersen, 1997), Chalk Research Laboratories (Canada) (Beaton et al., 2016), Korea Atomic Energy Research Institute (KAERI) Underground Research Tunnel (URT) (Ryu et al., 2012), and Mizunami Underground Research Laboratory (URL; Japan) (Iwatsuki et al., 2005). The large gray triangles indicate the separation between water types. ⋆ = no K^+ data provided for this study.

seismic events caused temporary re-organization of TM-1494's groundwater flow paths, recovering to "baseline" conditions within a matter of weeks.

Although further monitoring is needed to fully describe the connectivity of DELOS and the effect hydraulic stimulation experiments have on the hydrochemical and microbial community diversity patterns, correlated changes between monitored fractures provide new insights into the hydro-biogeological subsurface connectivity of a mountain block in a typical alpine watershed. Recently, a study of the 100,000 km^2 Death Valley Regional Flow System (DVRFS, USA) identified shared taxa in hydrogeologically connected groundwater separated by over 100 km (Merino et al., 2022). At a more local scale, a small number of "core" species (97% OTUs) were reported to increase in relative abundance (from 6% up to 47%) as water flowed downstream of the preferential recharge area in the approximately 5 km Hainich Critical Zone Observatory (HCZO, Germany; Yan et al., 2020). Although the observations and relative proportions of core taxa in the DVRFS, HCZO and DELOS are not directly comparable due to differences in filtration volume and sequencing depth, only 2 ASVs were identified in all DELOS sampling locations from the November and December 2020 time points. These ASVs account for 0.9 ± 0.7% of each samples community with the highest relative abundance of these ASVs (2.5%) in TM-1494. Interestingly, despite exhibiting extremely different hydrochemical compositions, DELOS groundwater sampling location TM-1494 and GTS borehole SB80001 share the most ASVs. These ASVs are "rare", low abundance taxa whose presence in both systems may indicate a similar source of water and microorganisms into these systems. Importantly, neither DELOS TM-1494 or GTS borehole SB80001 have been utilized for hydraulic stimulation experiments; however, these kinds of experiments have been performed in other boreholes within DELOS and GTS (Gischig et al., 2020; Ma et al., 2022) and, therefore, the sampling locations may experience similar changes in hydrochemical and microbiological compositions as a result of the injection procedures associated with hydraulic stimulation (e.g. Zhang et al., 2022). Ultimately, the subsurface fractures that exhibit the highest degrees of microbial community overlap tend to correlate with both hydrochemical and hydrogeologic features in DELOS, providing a new insights into the subsurface connectivity of the Riale di Ronco Alpine catchment.

5 Conclusions

Situated in the Alpine catchment of Riale di Ronco, Switzerland, the BedrettoLab Deep Life Observatory (DELOS) provides a new window into the continental subsurface biosphere by capturing an approximately 1,500 m depth gradient over 5.2 km, largely within the same host rock. Despite the proximity and geologic similarity of subsurface sampling locations within DELOS, a wide range of hydrochemical and microbial community compositions are observed. Despite this variability, broad ecotypes can still be defined. These ecotypes are largely differentiated by the concentration of sulfate, bicarbonate and ultra-small bacteria and archaea. Additional biogeochemical monitoring of DELOS over a one year period further demonstrates the utility

of coupling microbial diversity and hydrochemical studies to help inform hydraulic connectivity and groundwater flow. In particular, hydrochemical responses in TM-1306 and TM-1494 following seismicity suggest that groundwater from these locations experience mixing with warmer, sulfate-rich water but recover to their baseline hydrochemical and biological[1] compositions within three weeks (Figure 2). Taken together, the spatial and temporal heterogeneity of DELOS provide a first look at the hydrochemical and biological diversity within DELOS and provide new insights in the groundwater history, local mineralogy, and hydraulic conductivity of a subsurface Alpine environment.

Data availability statement

The datasets presented in this study can be found in online repositories. The names of the repository/repositories and accession number(s) can be found below: https://www.ncbi.nlm.nih.gov/, PRJNA1181539. The data and code is available via https://github.com/GeobiologyLab/DELOS-2021-time-series.

Author contributions

AA: Conceptualization, Data curation, Formal analysis, Investigation, Methodology, Project administration, Visualization, Writing – original draft, Writing – review & editing. MA: Conceptualization, Data curation, Formal analysis, Investigation, Methodology, Visualization, Writing – original draft, Writing – review & editing. NG: Formal analysis, Investigation, Methodology, Writing – review & editing. AC: Formal Analysis, Investigation, Visualization, Writing – review & editing. PR: Formal analysis, Investigation, Writing – review & editing. HT: Formal analysis, Writing – review & editing. QW: Investigation, Writing – review & editing. EZ: Investigation, Writing – review & editing. MH: Investigation, Writing – review & editing. BB: Conceptualization, Formal analysis, Investigation, Methodology, Supervision, Writing – review & editing. CM: Conceptualization, Data curation, Formal analysis, Funding acquisition, Investigation, Methodology, Project administration, Resources, Software, Supervision, Validation, Visualization, Writing – original draft, Writing – review & editing.

Funding

The author(s) declare financial support was received for the research, authorship, and/or publication of this article. Funding for this project was provided by ETH start-up funding to CM and the Swiss National Science Foundation (Project 215626). Funding for NGD was provided by the Werner Siemens-Stiftung (project 2019-FE-313).

Acknowledgments

We would like to thank Fanny Leuenberger, Simon Loew, Niklaus Kressig, Negar Haghipour, Corey Archer and Thomas Blattmann for assistance with the hydrochemical analyses presented in this study, Erminio Molteni, Bekir Yuece, Lena Bakker, Jasmine Berg and the Bedretto Team for assistance in sampling surface and subsurface locations, Markus Rast for the helpful discussion and insights surrounding the geology of DELOS, and Ingo Blechschmidt and Raphael Schneeberger for access to the Grimsel Test Site.

Conflict of interest

The authors declare that the research was conducted in the absence of any commercial or financial relationships that could be construed as a potential conflict of interest.

Generative AI statement

The author(s) declare that no Gen AI was used in the creation of this manuscript.

Publisher's note

Supplementary material

The Supplementary Material for this article can be found online at: https://www.frontiersin.org/articles/10.3389/fmicb.2025.1522714/full#supplementary-material

SUPPLEMENTARY DATA 1.
Catalog of DELOS sampling sites.

SUPPLEMENTARY DATA 2.
Environmental and sequencing metadata.

SUPPLEMENTARY DATA 3.
16S rRNA gene Amplicon Sequencing Variant and Annotation Table, available on https://github.com/GeobiologyLab/DELOS-2021-time-series.

SUPPLEMENTARY TABLE 1.
A selection of DELOS granitic groundwater trace metal concentrations.

SUPPLEMENTARY FIGURE 1.
The standard curve produced for the qPCR analysis of this study.

SUPPLEMENTARY FIGURE 2.
The melt curve of the qPCR analysis of this study.

SUPPLEMENTARY FIGURE 3.
DELOS 16S rRNA gene amplicon copies per mL.

SUPPLEMENTARY FIGURE 4.
Analysis of Similarities (ANOSIM) of DELOS groundwater 1-year time series samples.

SUPPLEMENTARY FIGURE 5.
Extended version of the water isotope plot of Figure 3.

1 Microbial community data for TM-1306 during the hydraulic stimulation was not collected.

References

Abu-Ashour, J., Joy, D. M., Lee, H., Whiteley, H. R., and Zelin, S. (1994). Transport of microorganisms through soil. *Water, Air, Soil Pollut.* 75, 141–158. doi: 10.1007/BF01100406

Amberg, R. (1983). Design and construction of the Furka Base Tunnel. *Rock Mechanics and Rock Eng.* 16, 215–231. doi: 10.1007/BF01042358

Arnet, M. (2021). *Deep alpine Fluids: Origin, Pathways and Dynamic Remobilisation in Response to Hydraulic Stimulations at the Bedretto Underground Laboratory for Geoenergies (BULGG)* (Master's thesis). Zürich: ETH Zurich.

Bagnoud, A., Chourey, K., Hettich, R. L., De Bruijn, I., Andersson, A. F., Leupin, O. X., et al. (2016). Reconstructing a hydrogen-driven microbial metabolic network in Opalinus clay rock. *Nat. Commun.* 7:12770. doi: 10.1038/ncomms12770

Banwart, S., Tullborg, E.-L., Pedersen, K., Gustafsson, E., Laaksoharju, M., Nilsson, A.-C., et al. (1996). Organic carbon oxidation induced by large-scale shallow water intrusion into a vertical fracture zone at the Äspö Hard Rock Laboratory (Sweden). *J. Contamin. Hydrol.* 21, 115–125. doi: 10.1016/0169-7722(95)00037-2

Bastin, E. S., Greer, F. E., Merritt, C., and Moulton, G. (1926). The presence of sulphate reducing bacteria in oil field waters. *Science* 63, 21–24. doi: 10.1126/science.63.1618.21

Beaton, E., Stevenson, B. S., King-Sharp, K. J., Stamps, B. W., Nunn, H. S., and Stuart, M. (2016). Local and regional diversity reveals dispersal limitation and drift as drivers for groundwater bacterial communities from a fractured granite formation. *Front. Microbiol.* 7:222054. doi: 10.3389/fmicb.2016.01933

Ben Maamar, S., Aquilina, L., Quaiser, A., Pauwels, H., Michon-Coudouel, S., Vergnaud-Ayraud, V., et al. (2015). Groundwater isolation governs chemistry and microbial community structure along hydrologic flowpaths. *Front. Microbiol.* 6:1457. doi: 10.3389/fmicb.2015.01457

Bense, V., Gleeson, T., Loveless, S., Bour, O., and Scibek, J. (2013). Fault zone hydrogeology. *Earth-Sci. Rev.* 127:171–192. doi: 10.1016/j.earscirev.2013.09.008

Blasch, K. W., and Bryson, J. R. (2007). Distinguishing sources of ground water recharge by using δ^2H and δ^{18}O. *Groundwater* 45, 294–308. doi: 10.1111/j.1745-6584.2006.00289.x

Blechschmidt, I., and Vomvoris, S. (2015). "The fourth decade of underground research at the Grimsel Test Site-what we have learned and where we go from here," in *Proc. of WM* (Phoenix), 16–19.

Bochet, O., Bethencourt, L., Dufresne, A., Farasin, J., Pédrot, M., Labasque, T., et al. (2020). Iron-oxidizer hotspots formed by intermittent oxic-anoxic fluid mixing in fractured rocks. *Nature Geosci.* 13, 149–155. doi: 10.1038/s41561-019-0509-1

Bolger, A. M., Lohse, M., and Usadel, B. (2014). Trimmomatic: a flexible trimmer for Illumina sequence data. *Bioinformatics* 30, 2114–2120. doi: 10.1093/bioinformatics/btu170

Borgonie, G., Linage-Alvarez, B., Ojo, A. O., Mundle, S. O., Freese, L. B., Van Rooyen, C., et al. (2015). Eukaryotic opportunists dominate the deep-subsurface biosphere in South Africa. *Nat. Commun.* 6:8952. doi: 10.1038/ncomms9952

Bowen, G. J., and Revenaugh, J. (2003). Interpolating the isotopic composition of modern meteoric precipitation. *Water Resour. Res.* 39:10. doi: 10.1029/2003WR002086

Bucher, K., and Stober, I. (2010). Fluids in the upper continental crust. *Geofluids* 10, 241–253. doi: 10.1002/9781444394900.ch17

Callahan, B. J., McMurdie, P. J., Rosen, M. J., Han, A. W., Johnson, A. J. A., and Holmes, S. P. (2016). DADA2: High-resolution sample inference from Illumina amplicon data. *Nat. Methods* 13, 581–583. doi: 10.1038/nmeth.3869

Casar, C. P., Kruger, B. R., Flynn, T. M., Masterson, A. L., Momper, L. M., and Osburn, M. R. (2020). Mineral-hosted biofilm communities in the continental deep subsurface, Deep Mine Microbial Observatory, SD, USA. *Geobiology* 18, 508–522. doi: 10.1111/gbi.12391

Casar, C. P., Kruger, B. R., and Osburn, M. R. (2021). Rock-hosted subsurface biofilms: mineral selectivity drives hotspots for intraterrestrial life. *Front. Microbiol.* 12:658988. doi: 10.3389/fmicb.2021.658988

Clark, I. D., and Fritz, P. (2013). *Environmental Isotopes in Hydrogeology*. Boca Raton, FL: CRC Press.

Daly, R. A., Borton, M. A., Wilkins, M. J., Hoyt, D. W., Kountz, D. J., Wolfe, R. A., et al. (2016). Microbial metabolisms in a 2.5-km-deep ecosystem created by hydraulic fracturing in shales. *Nat. Microbiol.* 1, 1–9. doi: 10.1038/nmicrobiol.2016.146

Doetsch, J., Gischig, V., Krietsch, H., Villiger, L., Amann, F., Dutler, N., et al. (2018). "Grimsel isc experiment description," in *Technical Report* (Zürich: ETH Zurich).

Dong, Y., Kumar, C. G., Chia, N., Kim, P.-J., Miller, P. A., Price, N. D., et al. (2014). Halomonas sulfidaeris-dominated microbial community inhabits a 1.8 km-deep subsurface Cambrian Sandstone reservoir. *Environm. Microbiol.* 16, 1695–1708. doi: 10.1111/1462-2920.12325

Fukuda, A., Hagiwara, H., Ishimura, T., Kouduka, M., Ioka, S., Amano, Y., et al. (2010). Geomicrobiological properties of ultra-deep granitic groundwater from the Mizunami Underground Research Laboratory (MIU), central Japan. *Microb. Ecol.* 60, 214–225. doi: 10.1007/s00248-010-9683-9

Gannon, J., Mingelgrin, U., Alexander, M., and Wagenet, R. (1991). Bacterial transport through homogeneous soil. *Soil Biol. Biochem.* 23, 1155–1160. doi: 10.1016/0038-0717(91)90028-I

Ginsburg-Karagitscheva, T. L. (1926). "Microbiological research in the sulphurous and salty waters of Apsheron," in *Azerbajdzanskoe Neftjanoe Khozjajstvo*.

Gischig, V. S., Giardini, D., Amann, F., Hertrich, M., Krietsch, H., Loew, S., et al. (2020). Hydraulic stimulation and fluid circulation experiments in underground laboratories: stepping up the scale toward engineered geothermal systems. *Geomech. Energy Environm.* 24:100175. doi: 10.1016/j.gete.2019.100175

Hafner, S. (1958). *Petrographie des südwestlichen Gotthardmassivs zwischen St. Gotthardpass und Nufenenpass* (PhD thesis). Zurich: ETH Zurich.

Hallbeck, L., and Pedersen, K. (2008). Characterization of microbial processes in deep aquifers of the Fennoscandian Shield. *Appl. Geochem.* 23, 1796–1819. doi: 10.1016/j.apgeochem.2008.02.012

Halter, T., Gholizadeh Doonechaly, N., Notzon, A., Rybach, L., Hertrich, M., and Giardini, D. (2024). Exploring the feasibility of energy extraction from the Bedretto Tunnel in Switzerland. *Energies* 17:3669. doi: 10.3390/en17153669

Herrmann, M., Lehmann, K., Totsche, K. U., and Küsel, K. (2023). Seepage-mediated export of bacteria from soil is taxon-specific and driven by seasonal infiltration regimes. *Soil Biol. Biochem.* 187:109192. doi: 10.1016/j.soilbio.2023.109192

Herrmann, M., Wegner, C.-E., Taubert, M., Geesink, P., Lehmann, K., Yan, L., et al. (2019). Predominance of Cand. Patescibacteria in groundwater is caused by their preferential mobilization from soils and flourishing under oligotrophic conditions. *Front. Microbiol.* 10:1407. doi: 10.3389/fmicb.2019.01407

Hosono, T., Yamada, C., Manga, M., Wang, C.-Y., and Tanimizu, M. (2020). Stable isotopes show that earthquakes enhance permeability and release water from mountains. *Nature Commun.* 11, 1–9. doi: 10.1038/s41467-020-16604-y

Hubalek, V., Wu, X., Eiler, A., Buck, M., Heim, C., Dopson, M., et al. (2016). Connectivity to the surface determines diversity patterns in subsurface aquifers of the Fennoscandian Shield. *ISME J.* 10, 2447–2458. doi: 10.1038/ismej.2016.36

Ino, K., Konno, U., Kouduka, M., Hirota, A., Togo, Y. S., Fukuda, A., et al. (2016). Deep microbial life in high-quality granitic groundwater from geochemically and geographically distinct underground boreholes. *Environm. Microbiol. Reports* 8, 285–294. doi: 10.1111/1758-2229.12379

Iwatsuki, T., Furue, R., Mie, H., Ioka, S., and Mizuno, T. (2005). Hydrochemical baseline condition of groundwater at the Mizunami Underground Research Laboratory (MIU). *Appl. Geochem.* 20, 2283–2302. doi: 10.1016/j.apgeochem.2005.09.002

Keller, F., and Schneider, T. (1982). Geologie und geotechnik. *Schweizer Ingenieur und Architekt* 100, 512–520.

Keusen, H., Ganguin, J., Schuler, P., and Buletti, M. (1989). "Grimsel Test Site: geology," in *Technical Report*, *Nationale Genossenschaft fuer die Lagerung Radioaktiver Abfaelle (NAGRA)*. Available at: https://www.osti.gov/etdeweb/biblio/6997735

Konno, U., Kouduka, M., Komatsu, D. D., Ishii, K., Fukuda, A., Tsunogai, U., et al. (2013). Novel microbial populations in deep granitic groundwater from Grimsel Test Site, Switzerland. *Microb. Ecol.* 65, 626–637. doi: 10.1007/s00248-013-0184-5

Kotelnikova, S., and Pedersen, K. (1998). Distribution and activity of methanogens and homoacetogens in deep granitic aquifers at Äspö Hard Rock Laboratory, Sweden. *FEMS Microbiology Ecology* 26:121–134. doi: 10.1016/S0168-6496(98)00028-2

Küsel, K., Totsche, K. U., Trumbore, S. E., Lehmann, R., Steinhäuser, C., and Herrmann, M. (2016). How deep can surface signals be traced in the critical zone? Merging biodiversity with biogeochemistry research in a central German Muschelkalk landscape. *Front. Earth Sci.* 4:32. doi: 10.3389/feart.2016.00032

Kyle, J. E., Eydal, H. S., Ferris, F. G., and Pedersen, K. (2008). Viruses in granitic groundwater from 69 to 450 m depth of the Äspö Hard Rock Laboratory, Sweden. *ISME J.* 2, 571–574. doi: 10.1038/ismej.2008.18

Labhart, T. (2005). *Erläuterungen zum Geologischen Atlas der Schweiz 1: 25000, Val Bedretto, Atlasblatt 68*. Bern-Ittigen: Bundesamt für Wasser und Geologie.

Lipman, C. B. (1928). The discovery of living micro-organisms in ancient rocks. *Science* 68, 272–273. doi: 10.1126/science.68.1760.272.b

Lopez-Fernandez, M., Simone, D., Wu, X., Soler, L., Nilsson, E., Holmfeldt, K., et al. (2018). Metatranscriptomes reveal that all three domains of life are active but are dominated by bacteria in the Fennoscandian crystalline granitic continental deep biosphere. *MBio* 9, 10–1128. doi: 10.1128/mBio.01792-18

Lopez-Fernandez, M., Westmeijer, G., Turner, S., Broman, E., Ståhle, M., Bertilsson, S., et al. (2023). Thiobacillus as a key player for biofilm formation in oligotrophic groundwaters of the Fennoscandian Shield. *NPJ Biofilms Microb.* 9:41. doi: 10.1038/s41522-023-00408-1

Lützenkirchen, V. H. (2002). *Structural Geology and Hydrogeology of Brittle Fault Zones in the Central and Eastern Gotthard Massif, Switzerland* (PhD thesis). Zurich: ETH Zurich.

Ma, X., Hertrich, M., Amann, F., Bröker, K., Gholizadeh Doonechaly, N., Gischig, V., et al. (2022). Multi-disciplinary characterizations of the BedrettoLab-a new underground geoscience research facility. *Solid Earth* 13, 301–322. doi: 10.5194/se-13-301-2022

Magnabosco, C., Biddle, J., Cockell, C., Jungbluth, S., and Twing, K. (2019). "Biogeography, ecology, and evolution of deep life," in *Deep Carbon* (Cambridge: Cambridge University Press), 524–555.

Magnabosco, C., Lin, L.-H., Dong, H., Bomberg, M., Ghiorse, W., Stan-Lotter, H., et al. (2018a). The biomass and biodiversity of the continental subsurface. *Nat. Geosci.* 11, 707–717. doi: 10.1038/s41561-018-0221-6

Magnabosco, C., Timmers, P. H., Lau, M. C., Borgonie, G., Linage-Alvarez, B., Kuloyo, O., et al. (2018b). Fluctuations in populations of subsurface methane oxidizers in coordination with changes in electron acceptor availability. *FEMS Microbiol. Ecol.* 94:fiy089. doi: 10.1093/femsec/fiy089

Masset, O., and Loew, S. (2010). Hydraulic conductivity distribution in crystalline rocks, derived from inflows to tunnels and galleries in the Central Alps, Switzerland. *Hydrogeol. J.* 18, 863–891. doi: 10.1007/s10040-009-0569-1

McNichol, J., Berube, P. M., Biller, S. J., and Fuhrman, J. A. (2021). Evaluating and improving small subunit rRNA PCR primer coverage for bacteria, archaea, and eukaryotes using metagenomes from global ocean surveys. *MSystems* 6, 10–1128. doi: 10.1128/mSystems.00565-21

Merino, N., Jackson, T. R., Campbell, J. H., Kersting, A. B., Sackett, J., Fisher, J. C., et al. (2022). Subsurface microbial communities as a tool for characterizing regional-scale groundwater flow. *Sci. Total Environm.* 842:156768. doi: 10.1016/j.scitotenv.2022.156768

Momper, L., Casar, C. P., and Osburn, M. R. (2023). A metagenomic view of novel microbial and metabolic diversity found within the deep terrestrial biosphere at DeMMO: a microbial observatory in South Dakota, USA. *Environm. Microbiol.* 25, 3719–3737. doi: 10.1111/1462-2920.16543

Ofterdinger, U. S. (2001). *Ground Water Flow Systems in the Rotondo granite, Central Alps (Switzerland)* (PhD thesis). Zurich: ETH Zurich.

Onstott, T. C. (2016). *Deep Life: The Hunt for the Hidden Biology of Earth, Mars, and Beyond*.

Onstott, T. C., Magnabosco, C., Aubrey, A., Burton, A., Dworkin, J., Elsila, J., et al. (2014). Does aspartic acid racemization constrain the depth limit of the subsurface biosphere? *Geobiology* 12, 1–19. doi: 10.1111/gbi.12069

Osburn, M. R., Kruger, B., Masterson, A. L., Casar, C. P., and Amend, J. P. (2019). Establishment of the Deep Mine Microbial Observatory (DeMMO), South Dakota, USA, a geochemically stable portal into the deep subsurface. *Front. Earth Sci.* 7:196. doi: 10.3389/feart.2019.00196

Pedersen, K. (1997). Microbial life in deep granitic rock. *FEMS Microbiol. Rev.* 20, 399–414. doi: 10.1016/S0168-6445(97)00022-3

Poulain, S., Sergeant, C., Simonoff, M., Le Marrec, C., and Altmann, S. (2008). Microbial investigations in Opalinus Clay, an argillaceous formation under evaluation as a potential host rock for a radioactive waste repository. *Geomicrobiol. J.* 25, 240–249. doi: 10.1080/01490450802153314

Quast, C., Pruesse, E., Yilmaz, P., Gerken, J., Schweer, T., Yarza, P., et al. (2012). The SILVA ribosomal RNA gene database project: improved data processing and web-based tools. *Nucleic Acids Res.* 41, D590–D596. doi: 10.1093/nar/gks1219

Quinto, F., Blechschmidt, I., Garcia Perez, C., Geckeis, H., Geyer, F., Golser, R., et al. (2017). Multiactinide analysis with accelerator mass spectrometry for ultratrace determination in small samples: application to an *in situ* radionuclide tracer test within the colloid formation and migration experiment at the Grimsel Test Site (Switzerland). *Analyt. Chem.* 89, 7182–7189. doi: 10.1021/acs.analchem.7b01359

Rast, M., Galli, A., Ruh, J. B., Guillong, M., and Madonna, C. (2022). Geology along the Bedretto Tunnel: kinematic and geochronological constraints on the evolution of the Gotthard Massif (Central Alps). *Swiss J. Geosci.* 115:8. doi: 10.1186/s00015-022-00409-w

Ryu, J.-H., Koh, Y.-K., Park, S.-W., Kim, G.-Y., and Choi, J.-W. (2012). Geochemical characterization of deep groundwater in KURT using geochemical modeling. *J. Environm. Eng.* 138, 351–359. doi: 10.1061/(ASCE)EE.1943-7870.0000492

Schneeberger, R., Mäder, U. K., and Waber, H. N. (2017). Hydrochemical and isotopic (δ^2H, δ^{18}O, ^{3}H) characterization of fracture water in crystalline rock (Grimsel, Switzerland). *Procedia Earth Planet. Sci.* 17, 738–741. doi: 10.1016/j.proeps.2016.12.187

Skelton, A., Liljedahl-Claesson, L., Wästeby, N., Andrén, M., Stockmann, G., Sturkell, E., et al. (2019). Hydrochemical changes before and after earthquakes based on long-term measurements of multiple parameters at two sites in northern Iceland–a review. *J. Geophys. Res.* 124, 2702–2720. doi: 10.1029/2018JB016757

Stroes-Gascoyne, S., Schippers, A., Schwyn, B., Poulain, S., Sergeant, C., Simonoff, M., et al. (2007). Microbial community analysis of Opalinus clay drill core samples from the Mont Terri underground research laboratory, Switzerland. *Geomicrobiol. J.* 24, 1–17. doi: 10.1080/01490450601134275

Walters, W., Hyde, E. R., Berg-Lyons, D., Ackermann, G., Humphrey, G., Parada, A., et al. (2016). Improved bacterial 16S rRNA gene (V4 and V4-5) and fungal internal transcribed spacer marker gene primers for microbial community surveys. *MSystems* 1, 10–1128. doi: 10.1128/mSystems.00009-15

Westmeijer, G., Mehrshad, M., Turner, S., Alakangas, L., Sachpazidou, V., Bunse, C., et al. (2022). Connectivity of Fennoscandian Shield terrestrial deep biosphere microbiomes with surface communities. *Commun. Biol.* 5:37. doi: 10.1038/s42003-021-02980-8

Wu, X., Pedersen, K., Edlund, J., Eriksson, L., Åström, M., Andersson, A. F., et al. (2017). Potential for hydrogen-oxidizing chemolithoautotrophic and diazotrophic populations to initiate biofilm formation in oligotrophic, deep terrestrial subsurface waters. *Microbiome* 5, 1–13. doi: 10.1186/s40168-017-0253-y

Xiao, X.-Y., Wang, M.-W., Zhu, H.-W., Guo, Z.-H., Han, X.-Q., and Zeng, P. (2017). Response of soil microbial activities and microbial community structure to vanadium stress. *Ecotoxicol. Environm. Safety* 142, 200–206. doi: 10.1016/j.ecoenv.2017.03.047

Yan, L., Hermans, S. M., Totsche, K. U., Lehmann, R., Herrmann, M., and Küsel, K. (2021). Groundwater bacterial communities evolve over time in response to recharge. *Water Res.* 201:117290. doi: 10.1016/j.watres.2021.117290

Yan, L., Herrmann, M., Kampe, B., Lehmann, R., Totsche, K. U., and Küsel, K. (2020). Environmental selection shapes the formation of near-surface groundwater microbiomes. *Water Res.* 170:115341. doi: 10.1016/j.watres.2019.115341

Yilmaz, P., Parfrey, L. W., Yarza, P., Gerken, J., Pruesse, E., Quast, C., et al. (2014). The SILVA and "all-species living tree project (LTP)" taxonomic frameworks. *Nucleic Acids Res.* 42, D643–D648. doi: 10.1093/nar/gkt1209

Zhang, B., Wang, S., Diao, M., Fu, J., Xie, M., Shi, J., et al. (2019). Microbial community responses to vanadium distributions in mining geological environments and bioremediation assessment. *J. Geophys. Res.: Biogeosci.* 124, 601–615. doi: 10.1029/2018JG004670

Zhang, H., Zhang, B., Wang, S., Chen, J., Jiang, B., and Xing, Y. (2020a). Spatiotemporal vanadium distribution in soils with microbial community dynamics at vanadium smelting site. *Environm. Pollut.* 265:114782. doi: 10.1016/j.envpol.2020.114782

Zhang, X., Gao, X., Li, C., Luo, W., Wang, Y., and Luo, X. (2023). Seasonal dynamics and interaction of shallow groundwater geochemical properties and microbial community patterns. *Chem. Geol.* 638:121703. doi: 10.1016/j.chemgeo.2023.121703

Zhang, Y., Dekas, A. E., Hawkins, A. J., Parada, A. E., Gorbatenko, O., Li, K., et al. (2020b). Microbial community composition in deep-subsurface reservoir fluids reveals natural interwell connectivity. *Water Resour. Res.* 56:e2019WR025916. doi: 10.1029/2019WR025916

Zhang, Y., Horne, R. N., Hawkins, A. J., Primo, J. C., Gorbatenko, O., and Dekas, A. E. (2022). Geological activity shapes the microbiome in deep-subsurface aquifers by advection. *Proc. Nat. Acad. Sci.* 119:e2113985119. doi: 10.1073/pnas.2113985119

frontiers | Frontiers in Microbiology

TYPE Original Research
PUBLISHED 07 March 2025
DOI 10.3389/fmicb.2025.1504241

OPEN ACCESS

EDITED BY
Jennifer F. Biddle,
University of Delaware, United States

REVIEWED BY
Erin Field,
East Carolina University, United States
Anthony Ranchou-Peyruse,
Université de Pau et des Pays de l'Adour, France

*CORRESPONDENCE
Katrina I. Twing
katrinatwing@weber.edu

RECEIVED 30 September 2024
ACCEPTED 11 February 2025
PUBLISHED 07 March 2025

CITATION
Twing KI, Brazelton WJ, McCollom TM, Schubotz F, Pendleton HL, Harris RL, Brown AR, Richins SM, Kubo MDY, Hoehler TM, Cardace D and Schrenk MO (2025) Heterogeneity of rock-hosted microbial communities in a serpentinizing aquifer of the Coast Range Ophiolite.
Front. Microbiol. 16:1504241.
doi: 10.3389/fmicb.2025.1504241

Heterogeneity of rock-hosted microbial communities in a serpentinizing aquifer of the Coast Range Ophiolite

Katrina I. Twing[1,2,3]*, William J. Brazelton[2], Tom M. McCollom[4], Florence Schubotz[5], H. Lizethe Pendleton[2], Rachel L. Harris[6], Annemarie R. Brown[3], Seth M. Richins[3], Michael D. Y. Kubo[7,8], Tori M. Hoehler[8], Dawn Cardace[9] and Matthew O. Schrenk[1]

[1]Department of Microbiology, Genetics, and Immunology, Michigan State University, East Lansing, MI, United States, [2]School of Biological Sciences, University of Utah, Salt Lake City, UT, United States, [3]Department of Microbiology, Weber State University, Ogden, UT, United States, [4]Laboratory for Atmospheric and Space Physics, University of Colorado, Boulder, CO, United States, [5]MARUM Center for Marine Environmental Sciences, University of Bremen, Bremen, Germany, [6]Department of Organismic and Evolutionary Biology, Harvard University, Cambridge, MA, United States, [7]SETI Institute, Mountain View, CA, United States, [8]Exobiology Branch, NASA Ames Research Center, Moffett Field, CA, United States, [9]Department of Geosciences, University of Rhode Island, Kingston, RI, United States

The movement of groundwater through fractured bedrock provides favorable conditions for subsurface microbial life, characterized by constrained flow pathways and distinctive local environmental conditions. In this study, we examined a subsurface microbial ecosystem associated with serpentinized rocks recovered from the Coast Range Ophiolite in northern California, USA. The distribution and diversity of microbial communities at various depths within two separate cores reaching up to 45 m below the land surface were investigated with microbiological and geochemical approaches. Core samples contained low total organic carbon content, low DNA yields, and low copy numbers of *16S rRNA* genes, yet some samples still yielded amplifiable DNA sequences. The microbial community composition of rock cores was distinct from groundwater, and source tracking of DNA sequences indicated that groundwater is not a significant source of DNA into basement rocks. In contrast, the microbial community of some rock core samples shared similarities with overlying soil samples, which could indicate potential contamination, weathering of shallow serpentinites, or a combination of both. Individual DNA sequences of archaea and bacteria predicted to be endemic to the basement rocks were identified by differential abundance analyses. Core-enriched sequences were distinct from those in groundwater or in the overlying soils and included OTUs related to *Serpentinimonas* as well as putatively anaerobic, deep subsurface-associated taxa such as methanogens and *Bathyarchaeia*. Stable isotope analyses of organic and inorganic carbon did not reveal a chemoautotrophic signal and were instead consistent with a primarily surface vegetation source of organic carbon into the basement. This census of archaeal and bacterial DNA sequences associated with altered ultramafic rocks provides a useful resource for further research into the potential for deep subsurface microbial activity fueled by geochemical reactions associated with serpentinization.

KEYWORDS

16S rRNA, serpentinization, subsurface, low biomass, rock hosted

Introduction

The quantity of liquid water held in bedrock at biologically permissive temperatures (<150°C) beneath the oceans and continents is vast, but our understanding of the varied habitats supported in subsurface environments is still being refined. Most insight into rock-hosted subsurface ecosystems has come through analysis of groundwater from drilled wells or surface seeps, while relatively few studies have directly examined microorganisms attached to rock surfaces (Magnabosco et al., 2018; Templeton and Caro, 2023). In contrast to porous sandstones, the flux of water and materials through altered igneous and metamorphic rocks is dominated by preferential flow occurring along fractures and at interfaces between different lithologies. Although these fractures are of particular biological interest, interfaces are often the most difficult to recover by drilling, and identifying small fractures free of contamination within bulk rocks is challenging. One such type of host material, serpentinites, are observed along continental margins as mantle rock is brought to the near surface through tectonic processes. The formation of serpentinites through oxidation and hydration of ultramafic mantle rocks via the process of serpentinization creates high pH (Crespo-Medina et al., 2017; Brazelton et al., 2012; Suzuki et al., 2013; Tiago and Veríssimo, 2013), oxidant-poor fluids rich in reduced gasses (e.g., hydrogen and methane) (Schrenk et al., 2013; Lang and Brazelton, 2020). When exposed at the surface, serpentinite rocks weather into metal-rich, nutrient-poor soils that host endemic flora, as well as distinct microbial communities (Safford and Miller, 2020).

The microbiology of ultrabasic fluids from serpentinite springs (Brazelton et al., 2013; Brazelton et al., 2017; Woycheese et al., 2015; Crespo-Medina et al., 2017; Brazelton et al., 2012; Suzuki et al., 2013; Tiago and Veríssimo, 2013; Trutschel et al., 2022) and boreholes (Twing et al., 2017; Crespo-Medina et al., 2014; Templeton et al., 2021; Fones et al., 2019; Colman et al., 2022) has been previously studied at a variety of locations around the world. These studies have highlighted the ubiquity of a novel genus of alkaliphiles named *Serpentinimonas* in high pH serpentinizing fluids (Suzuki et al., 2014; Bird et al., 2021). The presence of methanogens, sulfate-reducing bacteria, and fermentative bacteria apparently fueled by the abundance of dihydrogen and low-molecular-weight organic compounds also seems to be a common theme in these fluids (Templeton and Caro, 2023; Schrenk et al., 2013; Templeton et al., 2021). However, microbiological investigations of serpentinite bedrock have proven to be more challenging due to the even lower cell densities per unit volume in rock samples than in fluids and the technical difficulties of isolating and purifying DNA from serpentinized rocks. Shallow cores into seafloor serpentinites revealed a variety of potentially novel, uncultivated archaea and bacteria that did not include any taxa previously identified in continental serpentinite springs or borehole fluids (Motamedi et al., 2020; Goordial et al., 2021). To our knowledge, only one previous census of bacteria and archaea within competent serpentinized bedrock in a continental setting has been reported (Kraus, 2021).

In this study, we report a census of microbial diversity in rock cores from two boreholes (31–45 m deep) in the Coast Range Ophiolite of northern California, along with associated geochemical and geophysical data. We have previously reported on the microbial ecology and geochemistry of fluids from these boreholes, which were characterized by low oxygen (DO 0.03–0.05 mg/L) and extreme high pH (pH 11.5–12.2) and dominated by *Serpentinomonas* and *Clostridia*. Here, our results of the rock core samples include the unexpected discovery of *Bathyarchaeia*, as well as methanogens, in the drill cores and highlight the connectivity among serpentinized bedrock, ultrabasic groundwater, and serpentine soils.

Materials and methods

Site description and sample collection

The Coast Range Ophiolite Microbial Observatory (CROMO) was established in August 2011, when eight wells were drilled into an aquifer hosted in heavily serpentinized peridotite at the UC Davis Donald and Sylvia McLaughlin Natural Reserve near Lower Lake, California. Details of the drilling operations can be found in Cardace et al. (2013). Briefly, two main wells, CSW1.1 and QV1.1, were drilled 1.4 km apart to depths of 31 m and 45 m, respectively, using HQ wireline coring with an inner diameter of 63.5 mm. To mitigate contamination during drilling, purified water (filtered through a 0.1 µm filter and ozonated) was used as the drilling fluid, and 0.5 µm fluorescent microbead tracers (Polysciences Inc.) were included in the drill stream at a concentration of 10^4 beads mL^{-1} (Cardace et al., 2013). Samples for contaminant detection were collected on site from separate interior and exterior sections of whole round cores, preserved in 4% paraformaldehyde, and examined by epifluorescence microscopy. Only samples free of visible fluorescent beads (~85% of the total core samples) were used in downstream microbiological analyses. Fluorescent beads were primarily evident in regions of unconsolidated material, rather than solid rock. Cores were cataloged, and sub-samples were preserved for complimentary mineralogical, geochemical, and microbiological analyses. Microbiological samples were wrapped in combusted aluminum foil, placed into sterile Whirlpak bags, and frozen with liquid nitrogen on-site and subsequently stored at −80°C until DNA extraction.

Additionally, soil samples were collected from the area adjacent to the wells in December 2013 using a sterile micro-coring approach, resulting in approximately 13-cm-long soil cores. Plant and root materials were removed from the cores before they were divided lengthwise to create the replicate soil samples (QV_soil1/QV_soil2 and CSW_soil1/CSW_soil2, respectively) and flash-frozen in the field laboratory. The soil samples were stored frozen until processing with the same DNA extraction methods used for the rock core samples. Groundwater samples from the CSW1.1 and QV1.1 wells were collected in August 2013 by filtration through 0.2 µm Sterivex cartridges and processed following analyses previously described by Twing et al. (2017). During another sampling campaign in 2014, the potential presence of cells and viruses in the 0.2 µm filtrate was explored by concentration of >10 L of filtrate with a VivaFlow 200 concentration cassette (Hydrosart 30k MWCO). The DNA yield of these concentrated filtrates was below detection, and amplicon sequencing of the bacterial *16S rRNA* gene was not successful.

Mineralogical and geochemical analyses

The minerals in the core samples were characterized using a combination of X-ray diffraction (XRD) and scanning electron

microscopy coupled with energy dispersive X-ray spectroscopy (SEM/EDS). Analyses by XRD were used to identify major mineral components of the cores (>5%) and were performed on powdered bulk core samples using a Terra instrument (Olympus, Inc.) with Co Kα radiation. Additional characterization of the minerals, as well as identification of minor components, was performed using SEM/EDS analysis. The analyses were performed using a Hitachi SU3500 SEM equipped with an Oxford Instruments EDS and AZTEC data processing software. Observations were made on crushed core pieces mounted on Al stubs using carbon tape.

Total carbon and total organic carbon analyses

Total carbon (TC) and total organic carbon (TOC) content and stable carbon isotopic composition ($\delta^{13}C$) was measured with a Thermo Scientific Flash 2000 elemental analyzer coupled to a Thermo Delta V Plus isotope ratio mass spectrometer. TOC content and $\delta^{13}C$ was determined following decalcification. For this, ground and homogenized samples were treated with hydrochloric acid (12.5%, aq.), neutralized with deionized water and subsequently freeze-dried. TC and TOC were quantified using a laboratory standard of estuarine sediment and accounting for the weight loss during decalcification. Measured $\delta^{13}C$ values were calibrated with reference CO_2 gas (Air Liquide, 99.99% CO_2). The precision of $\delta^{13}C$ is better than ±0.39‰, and the accuracy is better than ±0.27‰ based on repeated measurements. For analyses with carbon contents <10 µg, the accuracy decreases to ±2‰. Samples with such low carbon contents are reported in Supplementary Table S1 in parentheses. The $\delta^{13}C$ values are expressed relative to VPDB (Vienna Pee Dee Belemnite).

DNA extraction

Thawed core samples and soil material were homogenized using autoclaved and ethanol-sterilized steel percussion mortars and ceramic mortars and pestles. DNA was extracted from two parallel samples of 10 g homogenized core using the PowerMaxSoil Kit (MoBio, Carlsbad, CA, United States), following the manufacturer's instructions. The resulting DNA suspensions were pooled from replicate extractions and concentrated in an Amicon Ultra-2 Centrifugal Filter Unit with Ultracel-30 membrane (Millipore, Darmstadt, Germany) to a volume of 50 µL. DNA was quantified using High Sensitivity reagents for a Qubit® 2.0 Fluorometer (Life Technologies, Grand Island, NY, United States). To conserve DNA for downstream analyses, only 2 µL of the total 50 µL DNA extract was designated for DNA quantification, providing a detection limit of 0.1 ng/µL of the fluorometric quantification method. Since DNA was extracted from approximately 20 g of core material per sample, the limit of detection for DNA quantification was ~0.25 ng of DNA per g of core material.

Quantitative-PCR

The abundances of bacteria and archaea in the DNA extracts were determined by quantitative polymerase chain reaction (q-PCR) using domain-specific primers targeting the V6 hypervariable region of the *16S rRNA* gene for archaea and bacteria, as previously described (Méhay et al., 2013). Primer details can be found in Supplementary Table S2. Samples were analyzed on a BioRad C-1000 Thermo-Cycler with a q-PCR module using the SsoAdvanced SybrGreen Assay (Bio Rad, Hercules, CA, United States). Gene copy numbers were calculated using standard curves generated by amplification of DNA from *Methanocaldococcus jannaschii* for archaea and *Escherichia coli* for bacteria. Amplification efficiencies were 96% for the archaeal and 108% for the bacterial qPCR reactions from cores and soils.

16S rRNA gene sequencing and data analysis

Purified DNA samples from core, soils, and groundwater were submitted to the Josephine Bay Paul Center at the Marine Biological Laboratory (MBL) for sequencing of the V4–V5 region of the *16S rRNA* gene on an Illumina MiSeq instrument as part of the Census of Deep Life project (Morrison et al., 2013) using domain-specific primers to target bacteria and archaea, respectively (Supplementary Table S2). New sequence data from rock cores, soils, and groundwater described here are available via BioProject PRJNA1097798. The paired-end reads were merged and subjected to MBL's post-processing quality control for removal of low-quality reads and chimera checking (Huse et al., 2014). The samples yielded 8,493 to 246,345 and 12,020 to 241,730 merged, quality-filtered sequences with the bacterial and archaeal primers, respectively. Any sample that produced less than 5,000 sequences was considered a failed sequencing attempt and was not included in subsequent analyses.

Amplicon reads were dereplicated into unique sequences using Mothur (Schloss and Westcott, 2011), formed into operational taxonomic units (OTUs) at the 97% sequence similarity level using the Opticlust parameters in Mothur (Westcott and Schloss, 2017), and assigned taxonomy by alignment to the SILVA database (v138; Pruesse et al., 2007; Quast et al., 2013). One thousand four hundred and thirty three OTUs belonging to the genera outlined by Sheik et al. (2018) as putative kit contaminants were removed from the dataset, a detailed list of which can be found in Supplementary Table S3. Additionally, any sequences classified to domain "NA" or "Eukaryota" and all bacteria classified as "Chloroplast" or "Mitochondria" were removed from the dataset. Rarefaction curves were computed in Mothur v1.39.5 (Schloss, 2020; Schloss et al., 2009). Beta diversity was assessed in Mothur using the tree.shared command with the Sørensen dissimilarity index and with an MDS plot with the Bray–Curtis dissimilarity index using the R package Phyloseq v1.26.1 and the plot_ordination command (McMurdie and Holmes, 2013).

SourceTracker2 (Knights et al., 2011) was used to estimate the proportion of the microbial community of each core sample that could be attributed to groundwater or soil. This approach was used to identify samples that contained significant numbers of OTUs associated with groundwater or soil and to remove them from downstream differential abundance analyses. Significant differences in the abundances of OTUs between groups of samples were tested with the aid of the Phyloseq and EdgeR (Robinson et al., 2010) packages in R, which allowed the identification of individual OTUs that were statistically more "enriched" in a given type of sample (i.e.,

core, soil, or groundwater). OTUs that were significantly more abundant in core samples than in soil or fluid samples were identified as "core-enriched." Representative sequences of core-enriched OTUs comprising 1% or more of total sequences in at least one sample were searched against the NCBI non-redundant database using BLAST (Altschul et al., 1997) to identify the environmental source of the best hit.

Phylogenetic analysis of core-enriched *Bathyarchaeia*

A total of 102 "core-enriched" OTUs classified as members of the archaeal phylum *Candidatus* "Bathyarchaeota" (currently recognized in the SILVA database as class *Bathyarchaeia* within phylum Thermoproteota) were aligned with Clustal Omega v.1.2.4 (Sievers and Higgins, 2014) against 498 sequences belonging to 25 Ca. "Bathyarchaeota" subgroups and three outgroups (*Crenarchaeota*, Ca. "Korcharchaeota," and Ca. "YNPFFA"), concatenated in a previous review by Zhou et al. (2018) and appended with additional sequences from Harris (2020) and Harris et al. (2018). Gaps were removed from aligned sequences using Jalview v.2.11.0 (Waterhouse et al., 2009), and a maximum likelihood tree was inferred via IQ-TREE v.1.6.12 (Nguyen et al., 2015) using UFBoot2 (Hoang et al., 2018) for 1,000 bootstrapping iterations of a TIM3e + G4 model determined from ModelFinder (Kalyaanamoorthy et al., 2017).

Statistical analyses

The ANOSIM test using a Bray–Curtis dissimilarity index was used to evaluate whether individual environmental parameters had significant effects on the community composition of core samples using the R package vegan (Oksanen et al., 2020). To statistically determine which combinations of numerical environmental variables best explained the community composition variation within the dataset, the bioenv analysis (Clarke, 1993) was performed.

Results and discussion

Lithological and geochemical changes along the core depth profile

Geochemical and mineralogical analyses of the CROMO cores showed minor lithological variations between the surface and total depth of the borehole (Figure 1). The upper few meters of both the QV and CSW sites were represented by unconsolidated serpentine soils, with a gradation into serpentinized bedrock with varying amounts of magnetite and other accessory minerals at depth. The amount of clay minerals, and therefore the permeability of rock samples, varied significantly along the core, reinforcing the interpretation that closely spaced wells are relatively hydrologically isolated at CROMO both laterally and vertically (Ortiz et al., 2018). In addition, relatively silica-rich layers at certain depths of the core (Table 1), particularly at the QV site, may represent intercalary layers that could be coincident with or post-date ophiolite emplacement. These observations are consistent with the extensive ore mining in the region that also reflects hydrothermal processes (Peters, 1993).

Subsamples of the core material were used for EA-irMS analyses to quantify the total carbon (TC) and total organic carbon (TOC) in solid phases, and to determine their stable carbon isotope compositions. TOC contents decrease with depth, going from 3–7 wt% in the soils to values approaching detection limits in deep sections of the core (Supplementary Table S1). Interestingly, a region relatively enriched in TOC (0.03–0.16 wt%) was observed overlying the silica rich samples of the QV core at approximately 21–26 m depth below the surface. The $\delta^{13}C$ of TOC of the cored section is on average − 25.3‰ ± 0.7‰, and compares to the soil $\delta^{13}C$ (−25.5‰ ± 0.8‰). While TC contents are also low, ranging from 0.04 to 1 wt%, the samples are overall dominated by inorganic carbon phases, which is reflected in the comparably enriched $\delta^{13}C$-TC values ranging from −21.6 to −7.3‰. The ^{13}C-depletion of TOC relative to the calculated inorganic carbon $\delta^{13}C$ values (Ca. −21‰ to −3‰) does not fall into the typical range of isotopic fractionations involved during autotrophy, apart from some methanogens using the reductive acetyl CoA pathway (House et al., 2003). Instead, the consistent isotope values of organic carbon similar to vegetation-associated TOC points to mainly residual surface material encrusted in the rock matrix.

Quantification of DNA yield and *16S rRNA* genes

Environmental DNA yields from most of the rock core samples were below the detection limit of 0.25 ng of DNA per g of core material (Table 1). The exceptions include the shallowest core samples (2–17 m depth) from CSW and two core samples from QV that contain mostly soil-derived OTUs (see below). These results indicate very low biomass in the serpentinite basement rock compared with nearby serpentine soil and groundwater, which is consistent with the TOC measurements reported above. Similarly, bacterial and archaeal *16S rRNA* genes were much more abundant in the top few meters of the cores, as estimated by quantitative PCR, decreasing from 10^7–10^8 gene copies per gram of core in the surface, respectively, down to approximately 10^3 gene copies per gram in core samples below 20 m depth (Figures 1B,E and Table 1). One sample (QV30) at 30.8 m depth had 10^5 gene copies per gram; this sample contained mostly soil-affiliated OTUs, as discussed below. A shallow sample (QV11 at 9.7 m depth) had a low value of 10 gene copies per gram, which we consider to be an outlier. Several samples, including all archaeal *16S rRNA* qPCR reactions from CSW core samples, yielded no detectable signal. In general, bacterial *16S rRNA* genes were more abundant than archaeal *16S rRNA* genes in samples where both were detected (Figures 1B,E and Table 1).

Despite unquantifiable DNA concentrations, many of the core samples were amplifiable via domain-specific qPCR and successfully yielded *16S rRNA* gene sequences (Table 1). Therefore, amplifiability, as opposed to DNA concentration, was used to determine whether a sample was fit for submission to the sequencing facility. Low levels of input DNA for amplicon sequencing are known to cause biases in alpha and beta diversity statistics (e.g., Multinu et al., 2018), but such PCR biases among species are unlikely to alter the general conclusions of this initial, exploration-oriented study. For example, the exact relative abundance of a given individual species in low-biomass rocks

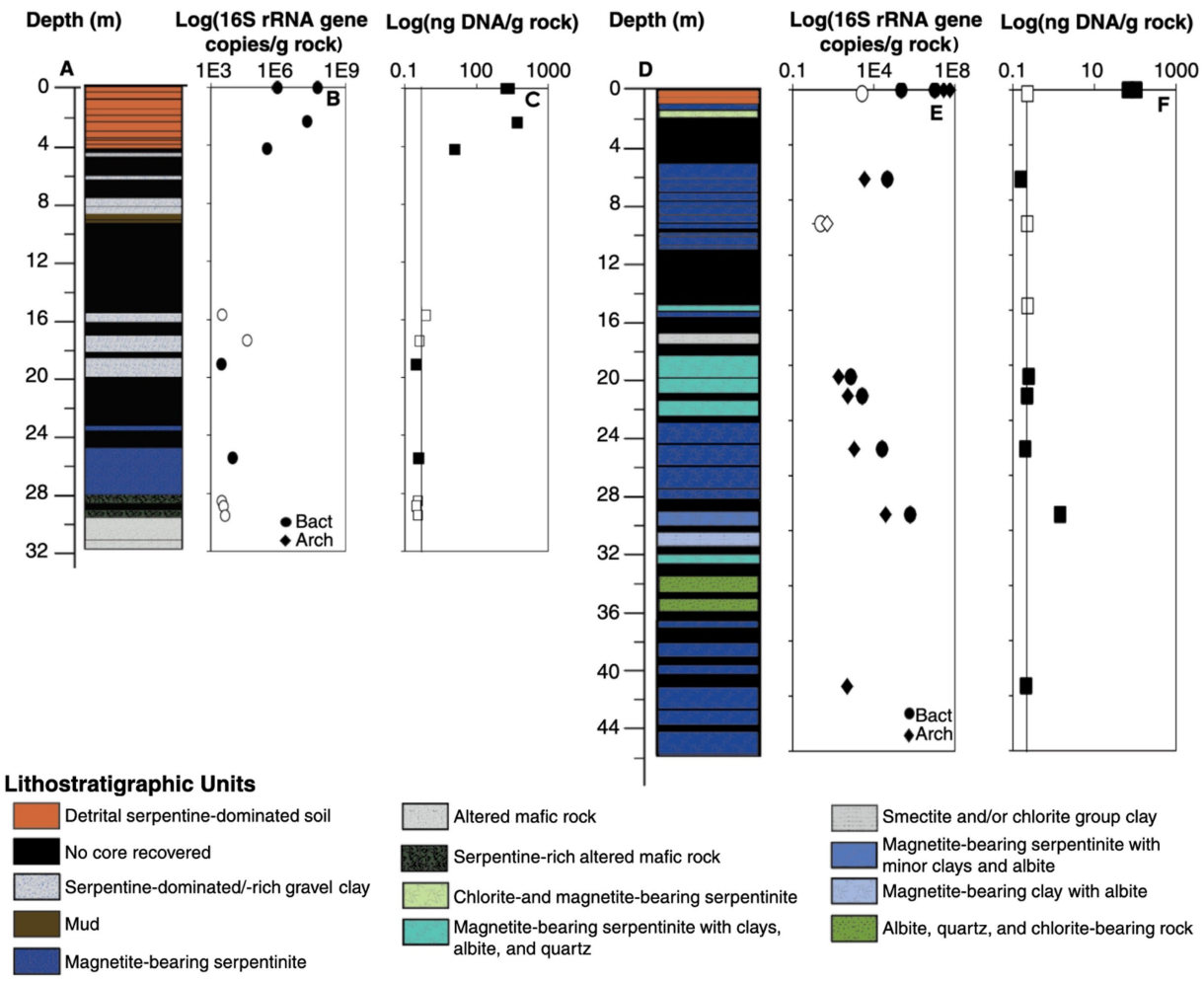

FIGURE 1
Distribution of microbial biomarkers relative to lithostratigraphic variations. Total genomic DNA was extracted and quantified from subsamples from different lithostratigraphic regions of the CROMO cores at both the CSW **(A)** and QV **(D)** sites. Quantitative-PCR was used to measure the abundance of archaeal (diamonds) and bacterial (circles) amplicons across the samples **(B,E)**. DNA yield was quantified by fluorometric methods **(C,F)**. Filled symbols represent samples that yielded *16S rRNA* gene sequences, samples represented by closed symbols failed sequencing. This figure has been adapted from Cardace et al. (2013), licensed under CC BY 3.0 and Ortiz et al. (2018) with permission from John Wiley & Sons.

should be treated with caution, but its presence in the rocks can be nevertheless validated with the contamination-tracing procedures described here. Due to the potential for contamination in very low biomass samples, blank control samples were run at every step of the DNA extraction and purification process. The control samples were neither quantifiable by fluorometric methods nor amplifiable via domain-specific qPCR; therefore, they were not sequenced.

Bacterial compositions of rock core, groundwater, and soil

Bacterial *16S rRNA* gene amplicon sequences from all rock core, groundwater, and soil samples were clustered into operational taxonomic units (OTUs) and ranged from 2,618–14,160 OTUs in core samples, 165–200 OTUs in groundwater samples, and 4,085–7,615 OTUs in soil samples. The number of OTUs in core and soil samples were roughly correlated with sequencing yield (Supplementary Figure S1), but much lower in groundwater samples even at comparable sequencing depths, consistent with our previous study (Twing et al., 2017).

The overall bacterial community compositions of core, groundwater, and soil samples were distinct (Supplementary Figure S1); i.e., the bacterial communities of core samples from different boreholes (CSW and QV, which are 1.4 km apart) are more similar to each other than to groundwater and soil samples from the same borehole, with two exceptions (QV7R and QV30R) discussed below. CSW cores contained more Chloroflexi and *Gammaproteobacteria* and fewer Actinobacteriota sequences compared to the soil samples and QV cores (Supplementary Figure S2). The presence of Acidobacteria, Actinobacteria, Bacteroidota, Chloroflexi, Planctomycetes, Proteobacteria and Verrucomicrobia in serpentine soil is consistent with previous studies (Supplementary Table S4). Groundwater samples were dominated by Comamonadaceae (previously of the Betaproteobacteria, classified within class *Gammaproteobacteria* in SILVA v138) and Firmicutes, as reported previously (Twing et al., 2017).

10.3389/fmicb.2025.1504241

TABLE 1 Mineralogical and microbiological data for each core, soil, and fluid sample.

Sample	Depth (mbs)	Mineralogy	DNA yield (ng/g)	Bacterial *16S rRNA* gene			Archaeal *16S rRNA* gene		
				qPCR (copies/g)	qPCR Std. Dev.	Sequence reads[a]	qPCR (copies/g)	qPCR Std. Dev.	Sequence reads[a]
CSW1.1A	31.1	Fluids	5.29	—	—	**31,054**	—	—	0
CSW1.1B	31.1		2.92	—	—	**23,413**	—	—	0
CSW1.1C	31.1		5.18	—	—	**28,051**	—	—	0
CSWsoil1	0	Serpentine soil	67.0	5.73×10^7	2.07×10^7	**42,570**	2.87×10^7	2.10×10^6	**151,538**
CSWsoil2	0		82.1	9.09×10^5	2.64×10^5	**82,363**	3.00×10^8	3.64×10^7	**236,134**
CSW1R	2.4	Mostly quartz, minor albite, unknown phyllosilicate, trace serpentine minerals	138.1	1.96×10^7	1.82×10^6	**246,412**	ND	ND	**89,017**
CSW2R	4.2	Serpentine, quartz, minor albite, unknown phyllosilicate	2.4	3.28×10^5	1.11×10^5	**147,623**	ND	ND	**105,289**
CSW16R	15.7	Serpentine, minor unknown phyllosilicate	0.4	3.20×10^3	1.91×10^2	18	ND	ND	0
CSW17R	17.4	Chlorite, saponite, unknown minerals	0.3	4.17×10^4	4.13×10^3	16	ND	ND	0
CSW10R	19.1	Unknown phyllosilicate, chlorite	<0.2	2.95×10^3	5.71×10^2	**185,703**	ND	ND	**12,020**
CSW14R	25.6	Pure serpentine minerals	<0.2	9.40×10^3	7.87×10^2	**225,988**	ND	ND	0
CSW22R	28.5	Serpentine, saponite, minor actinolite, talc	<0.2	3.08×10^3	5.81×10^2	9	ND	ND	0
CSW23R	28.9	Serpentine, minor talc, saponite	<0.2	3.70×10^3	2.93×10^2	9	ND	ND	0
CSW24R	29.5	Chlorite, actinolite, minor saponite, unknown minerals	<0.2	4.33×10^3	8.30×10^2	11	ND	ND	0
QV1.1A	45.7	Fluids	13.7	—	—	**36,790**	—	—	0
QV1.1B	45.7		7.31	—	—	**35,185**	—	—	0
QV1.1C	45.7		19.5	—	—	**38,145**	—	—	0
QVsoil1	0	Serpentine soil	66.4	2.27×10^5	3.52×10^4	**44,333**	2.81×10^7	3.72×10^6	**193,560**
QVsoil2	0		106.0	1.02×10^7	4.05×10^6	**83,590**	5.69×10^7	2.50×10^6	**242,101**
QV3R	0.3	Pure serpentine minerals	<0.2	2.62×10^3	8.31×10^2	1,919	ND	ND	2,806
QV7R	6.5	Pure serpentine minerals	0.2	4.67×10^4	3.63×10^3	**78,108**	3.52×10^3	4.63×10^2	4,683

(Continued)

TABLE 1 (Continued)

Sample	Depth (mbs)	Mineralogy	DNA yield (ng/g)	Bacterial *16S rRNA* gene			Archaeal *16S rRNA* gene		
				qPCR (copies/g)	qPCR Std. Dev.	Sequence reads[a]	qPCR (copies/g)	qPCR Std. Dev.	Sequence reads[a]
QV11R	9.7	Pure serpentine minerals	<0.2	2.37×10^{1}	1.45×10^{1}	4,635	5.04×10^{1}	2.85×10^{0}	266
QV13R	15.7	Pure serpentine minerals	<0.2	ND	ND	4,568	ND	ND	1,440
QV18R	20.8	Mostly saponite, trace clinochlore, no serpentine	<0.2	7.30×10^{2}	2.03×10^{2}	**9,225**	1.84×10^{2}	4.22×10^{1}	504
QV21R	22.2	Nearly pure serpentine, minor unknown minerals	<0.2	2.68×10^{3}	1.45×10^{3}	**10,827**	5.17×10^{2}	3.75×10^{1}	998
QV25R	26.1	Mostly saponite, trace clinochlore, no serpentine	<0.2	2.55×10^{4}	1.01×10^{3}	**8,495**	1.09×10^{3}	2.62×10^{2}	2,486
QV30R	30.8	Quartz, albite, trace unknown phyllosilicates	1.4	6.21×10^{5}	3.58×10^{4}	**25,322**	3.85×10^{4}	2.38×10^{3}	**103,561**
QV42R	43.3	Pure serpentine minerals	<0.2	ND	ND	**11,414**	4.85×10^{2}	2.04×10^{1}	**130,842**

ND, not detected; —indicates that sample was not tested.
[a]Sequence counts in bold were successfully sequenced, while those in regular font failed sequencing (i.e., produced <5,000 sequence reads).

Archaeal compositions of rock core, groundwater, and soil

Numbers of archaeal OTUs in rock core and soil samples ranged from 1,238–24,985 OTUs and correlated with sequencing depth (Supplementary Figure S3). No archaeal sequences were recovered from groundwater samples in this study or by Twing et al. (2017) (Table 1). Archaeal DNA sequences identified in serpentine soil samples consisted exclusively of *Nitrososphaeria* (Supplementary Figure S4), which have been identified among additional archaeal taxa in another report of serpentine soils (Solano-Arguedas et al., 2022) (Supplementary Table S4). In contrast, core samples collected from both boreholes contained a remarkable diversity of archaeal DNA sequences, including *Bathyarchaeia*, *Methanococci*, *Methanosarcinia*, and ANME-1. Core sample QV30R, however, consisted almost entirely of *Nitrososphaeria*, suggesting a strong similarity to overlying soil communities.

Source-tracking of core microbes to soil and groundwater

We employed a source tracking approach to identify archaeal and bacterial DNA sequences that were most likely to have originated in the rock cores, rather than in the soil or groundwater. It is expected that the basement rock, soil, and groundwater in this system are in communication with each other over geologically short time scales (consistent with the isotope signatures of TOC reported here), so we expect the rock core samples to contain some contribution of microbes derived from soil or groundwater. Therefore, we applied multiple statistical methods to identify sequences that were significantly more abundant in a particular sample type (i.e., core, soils, or groundwater), and therefore, from where they were most likely to have originated.

First, SourceTracker2 (Knights et al., 2011) was used to identify any core samples that have a majority of OTUs derived from groundwater or soil, since such samples would confuse the downstream identification of core-enriched sequences. The "source" samples were grouped: all four soil samples were grouped as the source "soil," and all s groundwater samples were grouped as the source "fluid." Each core sample was assessed individually to determine what percentage of the core sample OTUs could be attributed to one of the given sources. The percentage of OTUs identified as "unknown" represents sequences that could not be attributed to one of our known sources (i.e., soil or groundwater) and are therefore potentially endemic to the rock core.

Very few core OTUs were traced to groundwater samples (Figure 2), indicating that groundwater is not a significant source of OTUs into the rock core samples. This finding is consistent with a similar study where microbial DNA source tracking indicated a surprisingly small contribution of seawater-derived microbes into seafloor serpentinite rock core samples (Motamedi et al., 2020). In contrast, many rock core OTUs were traced to soil samples, particularly with regard to the bacterial sequences from QV cores (Figure 2A). Dispersal of microbes from soil into basement rocks could occur naturally in the environment or during field sampling or laboratory handling of these low-biomass samples. In the case of the shallowest core samples, it is likely this community overlap represents

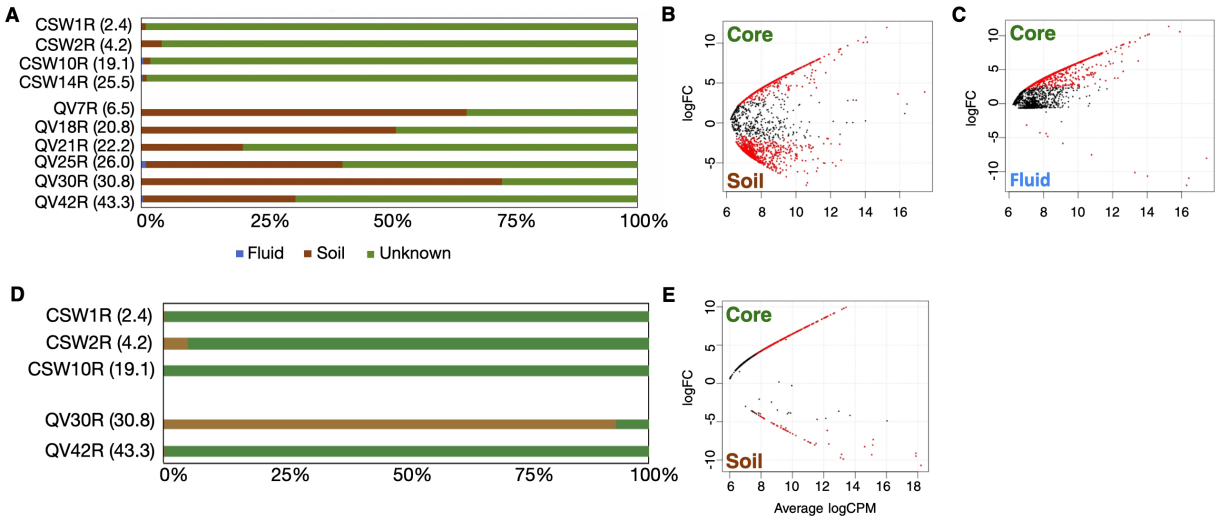

FIGURE 2
Statistical methods were used to identify endemic core microbes. SourceTracker2 was used to identify the percent of each core community that likely came from either soils (brown) or fluids (blue) for bacteria **(A)** and archaea **(D)**. Samples with greater than 50% contribution of OTUs from soils and fluids (QV7R, QV18R, and QV30R for bacteria; QV30R for archaea) were removed from the "core" classification for downstream differential expression analysis in EdgeR, used to identify core-enriched sequences (red). Comparisons were performed for bacterial data between core and soil samples **(B)** and core and fluid samples **(C)** and archaea between core and soil samples **(E)**.

a transition between the soil layers and basement rock. Soil-associated OTUs in deeper core samples could reflect weathering of basement rock into soil, or potential contamination of deeper core samples with soil material. In order to identify archaea and bacteria that are endemic to relatively unweathered basement rock, core samples with greater than 50% of OTUs traced to soil (i.e., QV7R and QV30R for bacteria; QV30R for archaea) were removed from the "core" category for downstream differential expression analyses (Figures 3A,D). The similarity of these samples to soils is further supported by beta-diversity analyses, in which QV7R and QV30R cluster with soil samples rather than with other core samples (Supplementary Figures S1, S3). Although these samples were not included in the pooled core data for the differential abundance analyses, the relative abundances of "core-enriched" OTUs are still reported for these samples in tables and figures.

Differential abundance

We used a differential abundance approach to identify specific OTUs that are significantly enriched in rock cores and therefore likely to be endemic to unweathered basement rock. This approach was chosen instead of a "simple overlap" approach, in which all OTUs that occur in both a control sample and a sample of interest are identified as contaminants (e.g., Salter et al., 2014), because such an approach would not be suitable for the present study, where we expect some degree of environmental mixing between the habitats (Motamedi et al., 2020). Instead, we identified OTUs that were significantly enriched in core samples (called "core-enriched") by comparing the distributions of OTU relative abundances in pooled core samples with their relative abundances in pooled groundwater and soil samples with a differential abundance approach (McMurdie and Holmes, 2013; Robinson et al., 2010). A total of 1,087 bacterial OTUs and 282 archaeal OTUs were identified as core-enriched (Figure 2 and Supplementary Table S5). Of those, 48 bacterial and 36 archaeal OTUs had a relative abundance of ≥1% in at least one core sample (Supplementary Table S6).

Core-enriched bacteria

A total of 1,087 bacterial core-enriched OTUs were identified across the dataset (Supplementary Table S5), but only 48 of those were >1% relative abundance in any given core sample (Supplementary Table S6). The bacterial OTUs identified as core-enriched in each core sample comprised 14–92% of the total bacterial community (Figure 3). Those on the lower end were QV7R and QV30R, which contain mostly soil-derived OTUs (Figure 2A). The majority of OTUs in samples from the CSW core were identified as core-enriched; therefore, the overall taxonomic distribution of OTUs in these samples did not differ greatly from the bulk dataset, especially at the phylum level (Supplementary Figure S2). As expected from the differential abundance procedure, OTUs that are abundant in soil and groundwater do not appear in the set of core-enriched OTUs (Supplementary Table S5).

However, the same taxonomic classification may be represented by distinct OTUs in multiple sample types. For example, a single OTU classified as family Comamonadaceae and 100% identical to *Serpentinimonas maccroryi* (Suzuki et al., 2014; Bird et al., 2021) represents 86–88% of all sequencing reads in the CSW groundwater samples, consistent with previous work at this site (Twing et al., 2017). This OTU is detected at low levels in core samples but is not included in the final set of core-enriched OTUs. Instead, family Comamonadaceae is represented in the core-enriched set by other OTUs that are significantly more abundant in core samples than in groundwater. There are four core-enriched Comamonadaceae OTUs

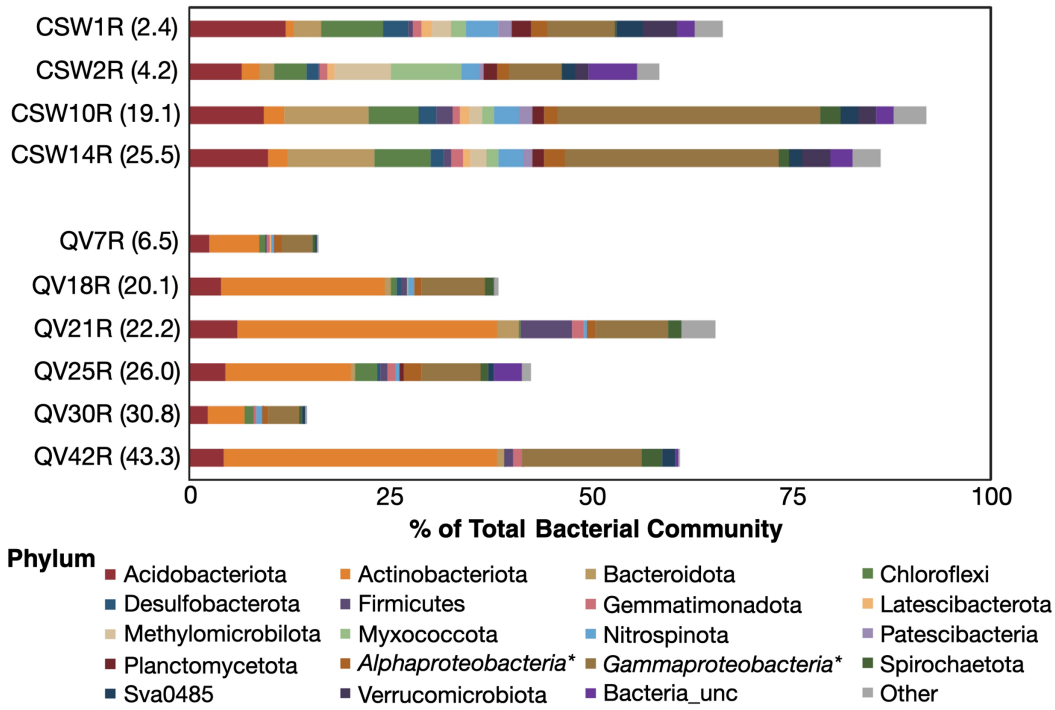

FIGURE 3
Relative abundance of core-enriched bacterial taxa. The sizes of the bars represent the percent of the bacterial community composed of core-enriched bacterial taxa, with white space beyond the bar representing the portion of the microbial community that could not be attributed to core-enriched taxa (as defined by the differential abundance metrics). The core-enriched taxa are identified at the phylum level, except for the Proteobacteria, which are represented at the class level (*Alphaproteobacteria* and *Gammaproteobacteria*).

(OTU00003-B, OTU00010-B, OTU00016-B, and OTU00058-B), and the closest relatives of these, assessed as best hits in the NCBI nr database via BLAST analysis, belong to the genera *Acidovorax*, *Diaphorobacter*, and *Variovorax* (Supplementary Table S6). These core-enriched *Comamonadaceae* OTUs share only 93–96% *16S rRNA* gene sequence similarity with the fluid-enriched *Serpentinomonas maccroryi* (NCBI accession MW411452).

Other notable core-enriched OTUs include those classified as *Nitrosomonadaceae* and iron-oxidizing *Gallionellaceae*, which are most abundant in the shallowest core sample (CSW1R; 2.4 mbs) and fall within the *Gammaproteobacteria* bar in Figure 3. Core sample CSW2R (4.2 mbs) had the most diverse array of core-enriched phyla, including Acidobacteria, *Methylomicrobia*, *Myxococcota*, *Verrucomicrobia*, and *Gammaproteobacteria* (Figure 3), the latter of which was composed of the sulfur-oxidizing *Sulfurifustis* (Kojima et al., 2015) and the uncultivated group TRA3-20 (Kim et al., 2021). The deeper CSW cores, CSW10R (19.1 mbs) and CSW14R (25.5 mbs), contained much higher relative abundances of two particular OTUs, the previously mentioned *Acidovorax* OTU (OTU0003-B) and the other classified as *Dechloromonas* (Achenbach et al., 2001).

The same core-enriched *Comamonadaceae* OTU (OTU0003-B) was also abundant in samples of the QV core, but the *Dechloromonas* OTU that is abundant in CSW core samples was absent in QV core samples. The most abundant core-enriched OTU in QV core samples was OTU00019-B, which was classified as *Mycobacteriaceae* and had best hits in the NCBI nr database to *Mycolicibacterium* sp. from a limestone cave (Niyomvong et al., 2012) and hydrocarbon-rich samples (Yu et al., 2015). This single OTU accounts for the majority of Actinobacteria in QV core samples and was also present at low levels in CSW core samples (0.01–0.4% of the total community; Supplementary Table S6). Additionally, the deepest QV core sample (QV42R, 43.3 mbs) also contained two abundant *Burkholderiaceae* OTUs. The first, OTU00234-B, had multiple best hit results belonging to the genus *Polynucleobacter*, which is typically found in freshwater lakes and streams (Hahn et al., 2017; Hahn et al., 2022). The other was OTU00494-B, classified only to the family level, but with best hit results from hydrocarbon-rich samples (Ros et al., 2014; Salam et al., 2018) and rocks (Elser et al., 2015). Neither of these groups were found in other core or groundwater samples, but were present at low levels in soil samples.

Core-enriched archaea

There were a total of 282 archaeal core-enriched OTUs identified across the dataset (Supplementary Table S5), but only 36 of those were >1% in any given core sample (Supplementary Table S6). The percentage of archaeal OTUs identified as core-enriched ranged from 23–52% in the four core samples for which archaeal sequencing was successful (Figure 4). This excludes core sample QV30R because most of its archaeal OTUs were traced to soil (Figure 2D), and only 1% were identified as core-enriched. The core-enriched archaea of the two shallowest core samples, CSW1R (2.3 mbs) and CSW2R (4.2 mbs), belonged to the *Bathyarchaeia*, *Nitrososphaeria*, *Thermoplasmata*, and unclassified members of the Euryarchaeota (Figure 4). While CSW10R (19.1 mbs) also contained these taxa, it also had much higher relative

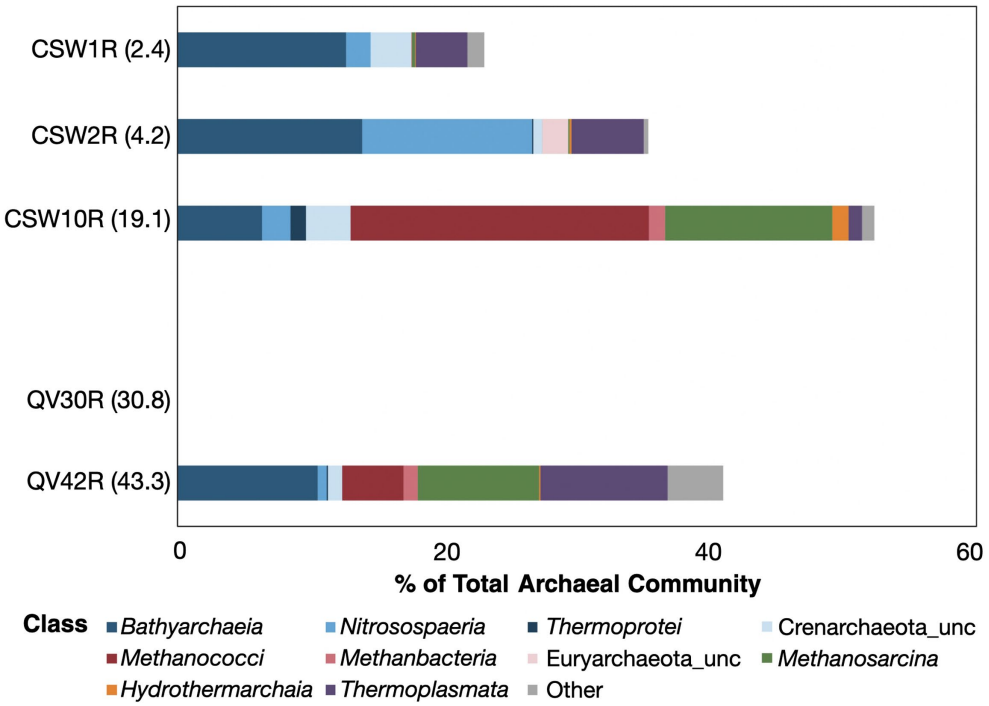

FIGURE 4
Relative abundance of core-enriched archaeal taxa. The sizes of the bars represent the percent of the archaeal community composed of core-enriched taxa, with white space beyond the bar representing the portion of the archaeal community that could not be attributed to core-enriched taxa (as defined by the differential abundance metrics). The core-enriched taxa are identified at the class level. Archaea were only able to be sequenced from five core samples. All the archaeal taxa identified in QV30R were identical to soil-enriched taxa; therefore, there are no core-enriched taxa in this sample to be represented here.

abundances of *Methanococci*, *Methanobacteria*, *Methanosarcinia*, and *Hydrothermarchaeia*, all groups known to contain methane-cycling archaea. CSW10R was dominated by *Methanoferividicoccus*, a single OTU which comprised 15% of the sample, and three additional OTUs all belonging to the same species comprised another 7% cumulative relative abundance. Similarly, the deepest core in the study, QV42R (43.3 mbs) contained *Bathyarchaeia*, *Nitrososphaeria*, *Thermoplasmata*, *Methanococci*, and *Methanosarcinia*. Additional rare taxa in QV42R (classified as "other" in Figure 4) included *Aenigmarchaeia*, *Lokiarchaeia*, *Archaeoglobi*, *Methanocellia*, *Nanoarchaeia*, and unclassified archaea.

Earlier studies assessing the microbial diversity of serpentine rocks detected only archaea belonging to the *Nitrososphaeria* and *Thermoplasmata* (Supplementary Table S6; Motamedi et al., 2020; Goordial et al., 2021; Daae et al., 2013; Khilyas et al., 2019). Recently, potential methanogens classified as *Methanobacteria* and *Methanosarcina* were reported in serpentinite cores from the Oman Drilling Project (Supplementary Table S6; Kraus, 2021), and highly reducing, high-pH fluids from boreholes established by the Oman Drilling Project contain *Methanobacteria* (Kraus et al., 2021; Thieringer et al., 2023). *Methanococci*, which make up 22% of CSW10R, and *Bathyarchaeia*, which are discussed in detail below, were not detected in any previous studies of serpentinized rocks (Supplementary Table S6).

Abundant core-enriched *Bathyarchaeia* OTUs were found in all four archaea-bearing core samples, ranging from 6–13% of the samples' archaeal sequencing reads (Figure 4). A total of 102 *Bathyarchaeia* OTUs were "core-enriched" (Supplementary Table S5), and of those, 13 OTUs had relative abundances as high as 1–3% in a given core sample (Supplementary Table S6).

We constructed a phylogeny with these core-enriched *Bathyarchaeia* OTU sequences and reference sequences obtained from public databases. Most of the core-enriched *Bathyarchaeia* OTUs identified here were assigned to subgroups 5a, 6, or 12 (Supplementary Figure S5). These clades have been found in a variety of environments around the world, where they are expected to thrive in variable environmental conditions with metabolic flexibility (Zhou et al., 2018; Fillol et al., 2016; Wang et al., 2020; Hou et al., 2023; Yin et al., 2022; Devereux et al., 2015). Subgroup 6 is a large and diverse clade known for its variety of metabolic pathways, including the ability to synthesize vitamin B_{12} (Hou et al., 2023). This unique capability suggests subgroup-6 may act as an ecological keystone species by supplying this essential cofactor to the surrounding members of their microbial communities (Fillol et al., 2016). Given the limited hydrological circulation in the cores compared to groundwater samples, *Bathyarchaeia* subgroup-6 may play a critical role in sustaining endolithic, nutrient-limited microbial ecosystems by locally producing and supplying vitamin B12.

One OTU from this study was assigned to subgroup 17, which has been found previously in sulfide-rich and reducing environments (Hou et al., 2023; Anantharaman et al., 2016). Metagenome-assembled genomes assigned to subgroup 17 include genes associated with the

reductive glycine pathway (Hou et al., 2023) and carbohydrate degradation via the Embden-Meyerhof glycolysis pathway (Lazar et al., 2016). Genes for nitrite reduction (*nirB* and *nirD*) indicate *Bathyarchaeia* subgroup-17's potential involvement in nitrogen cycling via dissimilatory nitrite reduction to ammonia (Lazar et al., 2016).

Another *Bathyarchaeia* OTU was assigned to subgroup 15, which has been linked to protein degradation in marine sediments (Yin et al., 2022). In addition, key genes for the reductive glycine pathway are also found in this subgroup (Hou et al., 2023), suggesting a capacity for carbon fixation and metabolic flexibility in nutrient-limited environments.

In summary, these results suggest that *Bathyarchaeia* and methanogens could be mediating carbon fixation within subsurface serpentinites, although this hypothesis remains to be tested with metagenomic and metabolic studies. The presence of potentially autotrophic archaea is a new finding for serpentinites and is consistent with similar studies in other geologic settings, where multiple taxonomic groups of archaea attached to subsurface rocks appear to be autotrophic (Lazar et al., 2017).

Habitats of best hits to core-enriched OTUs

To investigate where the closest matches to the core-enriched OTUs have been found in other studies, we looked up the habitat of the best BLAST hit to each core-enriched OTU. This analysis demonstrated a clear difference between deep rock core samples (19–43 mbs) and shallower samples (2–4 mbs). The best hits of the most abundant core-enriched OTUs in deeper samples were much more likely to be from seafloor hydrothermal vents (deep CSW core samples) and hydrocarbon-rich systems (deep QV core samples) (Figure 5). Meanwhile, the sequences from the shallower samples had best hits that were found in environments such as caves, sinkholes, and sediments from aquatic and contaminated environments (Figure 5).

Correlations between core-enriched OTUs and mineralogy

The compositions of core-enriched bacterial (but not archaeal) OTUs were significantly correlated with the presence of quartz, albite, and phyllosilicate in core samples (Supplementary Table S7). No significant correlations were evident between the distribution of core-enriched OTUs and the presence of serpentine. Quartz and albite were characteristic of the shallowest CSW core samples, while phyllosilicates were associated with deeper samples. The presence of quartz and albite in both the soils and in some regions of the deeper core at QV may reflect the involvement of non-serpentine rocks, impacted by hydrothermalism. These silica-enriched minerals may represent a relatively more permissive environment, with moderate pH and relatively abundant organic carbon and nitrogen. Alternatively, the interface between the silica-enriched layer and the serpentinites may represent a zone of relatively high hydrological connectivity—a supply of energy and nutrients that is more readily available than the surrounding material. In contrast, the phyllosilicate (clay) minerals in the core material likely represent low permeability regions with little connectivity, and thus a relatively harsh region for microbial activity.

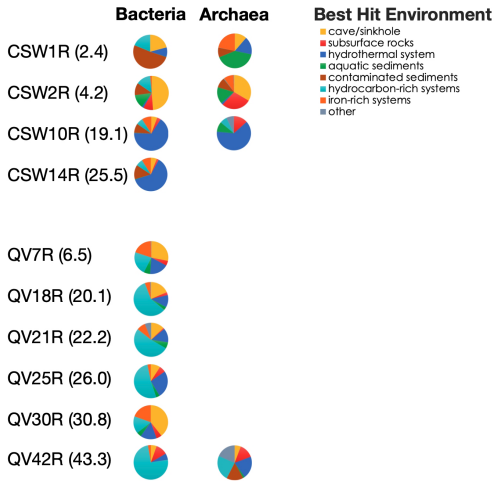

FIGURE 5
Environment of best hit to core-enriched sequences. Representative sequences from abundant core-enriched OTUs (>1% in any sample) were BLASTed to identify the best hit. The environmental origin of each best hit was identified from the literature and classified into an environmental category. The cumulative relative abundances of core-enriched OTUs are plotted according to the environmental category of their best hit. Note this is only the percentage of the core-enriched OTUs, which constitute a subset of the whole community.

Conclusion

The results of this study demonstrate that subsurface serpentinite rocks in a continental setting host archaeal and bacterial species that are distinct from those in groundwater and overlying soil. Although the levels of biomass and organic carbon were very low in rock cores, distinct archaeal and bacterial taxa associated with subsurface serpentinites were identified. Notable rock-associated taxa include *Bathyarchaeia*, *Methanococci*, *Methanobacteria*, *Methanosarcinia*, *Sulfurifustis*, and *Dechloromonas*, all of which are expected to be anaerobic and potentially utilizing reduced inorganic compounds (e.g., hydrogen and hydrogen sulfide) that are expected to be abundant in a subsurface, serpentinite-hosted environment. The subsurface rock-associated taxa were identified with a multifaceted statistical approach designed to control for the high risk of contamination in low-biomass samples while acknowledging the inherent heterogeneity and natural mixing of habitat types that occurs in a dynamic environmental system. Future studies should experimentally test the metabolic capabilities of these putative inhabitants of serpentinites and their unique adaptations for life in a high-pH and highly reducing subsurface habitat.

Data availability statement

The datasets presented in this study can be found in online repositories. The names of the repository/repositories and accession

number(s) can be found at: https://www.ncbi.nlm.nih.gov/, PRJNA289273, PRJNA1097798.

Author contributions

KT: Conceptualization, Formal analysis, Investigation, Methodology, Writing – original draft, Writing – review & editing. WB: Conceptualization, Formal analysis, Investigation, Methodology, Supervision, Writing – original draft, Writing – review & editing, Data curation, Resources. TM: Data curation, Formal analysis, Investigation, Writing – review & editing, Resources. FS: Formal analysis, Writing – review & editing, Investigation, Methodology, Resources. HP: Formal analysis, Writing – review & editing, Investigation, Methodology. RH: Methodology, Writing – review & editing, Formal analysis, Investigation, Writing – original draft. AB: Formal analysis, Writing – review & editing, Resources. SR: Writing – review & editing, Formal analysis, Investigation, Methodology. MK: Investigation, Writing – review & editing, Data curation, Formal analysis, Methodology, Resources. TH: Conceptualization, Formal analysis, Project administration, Resources, Writing – review & editing. DC: Conceptualization, Funding acquisition, Project administration, Resources, Supervision, Writing – review & editing. MS: Conceptualization, Funding acquisition, Investigation, Project administration, Supervision, Writing – original draft, Writing – review & editing.

Funding

The author(s) declare that financial support was received for the research, authorship, and/or publication of this article. The establishment of CROMO was funded by the NASA Astrobiology Institute (Director's Discretionary Fund and CAN-7 Rock-Powered Life #NNA15BB02A), and the research reported here was funded by the Alfred P. Sloan Foundation's Deep Carbon Observatory (2011-12-01) and supported by the Census of Deep Life. Funding support by the Deutsche Forschungsgemeinschaft (DFG, German Research Foundation) is acknowledged (EXC-2077 - 390741603).

Acknowledgments

This work would not have been possible without the support staff at the UC-Davis McLaughlin Natural Reserve, particularly Co-Directors Catherine Koehler and Paul Aigner. Thank you to Melitza Crespo-Medina and Danielle Morgan-Smith for their assistance with field sampling and quantitative-PCR analyses. Thanks to Christopher Thornton and Alex Hyer for computational and bioinformatic support. Thank you to Branson Fonnesbeck and Graeme Beatie for support with background research and to Jenny Wendt for laboratory assistance.

Conflict of interest

The authors declare that the research was conducted in the absence of any commercial or financial relationships that could be construed as a potential conflict of interest.

The author(s) declared that they were an editorial board member of Frontiers, at the time of submission. This had no impact on the peer review process and the final decision.

Publisher's note

Supplementary material

The Supplementary material for this article can be found online at: https://www.frontiersin.org/articles/10.3389/fmicb.2025.1504241/full#supplementary-material

References

Achenbach, L. A., Michaelidou, U., Bruce, R. A., Fryman, J., and Coates, J. D. (2001). *Dechloromonas agitata* gen. nov., sp. nov. and *Dechlorosoma suillum* gen. nov., sp. nov., two novel environmentally dominant (per)chlorate-reducing bacteria and their phylogenetic position. *Int. J. Syst. Evol. Microbiol.* 51, 527–533. doi: 10.1099/00207713-51-2-527

Altschul, S. F., Madden, T. L., Schäffer, A. A., Zhang, J., Zhang, Z., Miller, W., et al. (1997). Gapped BLAST and PSI-BLAST: a new generation of protein database search programs. *Nucleic Acids Res.* 25, 3389–3402. doi: 10.1093/nar/25.17.3389

Anantharaman, K., Brown, C. T., Hug, L. A., Sharon, I., Castelle, C. J., Probst, A. J., et al. (2016). Thousands of microbial genomes shed light on interconnected biogeochemical processes in an aquifer system. *Nat. Commun.* 7:13219. doi: 10.1038/ncomms13219

Bird, L. J., Kuenen, J. G., Osburn, M. R., Tomioka, N., Ishii, S., Barr, C., et al. (2021). Hyperalkaliphilic and facultative autotrophic bacteria isolated from terrestrial serpentinizing springs. *Int. J. Syst. Evol. Microbiol.* 71:004945. doi: 10.1099/ijsem.0.004945

Brazelton, W. J., Morrill, P. L., Szponar, N., and Schrenk, M. O. (2013). Bacterial communities associated with subsurface geochemical processes in continental serpentinite springs. *Appl. Environ. Microbiol.* 79, 3906–3916. doi: 10.1128/AEM.00330-13

Brazelton, W. J., Nelson, B., and Schrenk, M. O. (2012). Metagenomic evidence for H2 oxidation and H2 production by serpentinite-hosted subsurface microbial communities. *Front. Microbiol.* 2:268. doi: 10.3389/fmicb.2011.00268

Brazelton, W. J., Thornton, C. N., Hyer, A., Twing, K. I., Longino, A. A., Lang, S. Q., et al. (2017). Metagenomic identification of active methanogens and methanotrophs in serpentinite springs of the Voltri Massif, Italy. *PeerJ* 5:e2945. doi: 10.7717/peerj.2945

Cardace, D., Hoehler, T., McCollom, T., Schrenk, M., Carnevale, D., Kubo, M., et al. (2013). Establishment of the Coast Range Ophiolite Microbial Observatory (CROMO): drilling objectives and preliminary outcomes. *Sci. Dril.* 16, 45–55. doi: 10.5194/sd-16-45-2013

Clarke, K. R. (1993). Non-parametric multivariate analyses of changes in community structure. *Aust. J. Ecol.* 18, 117–143. doi: 10.1111/j.1442-9993.1993.tb00438.x

Colman, D. R., Kraus, E. A., Thieringer, P. H., Rempfert, K., Templeton, A. S., Spear, J. R., et al. (2022). Deep-branching acetogens in serpentinized subsurface fluids of Oman. *Proc. Natl. Acad. Sci. U.S.A.* 119:e2206845119. doi: 10.1073/pnas.2206845119

Crespo-Medina, M., Twing, K. I., Kubo, M. D. Y., Hoehler, T. M., Cardace, D., McCollom, T., et al. (2014). Insights into environmental controls on microbial communities in a continental serpentinite aquifer using a microcosm-based approach. *Front. Microbiol.* 5:604. doi: 10.3389/fmicb.2014.00604

Crespo-Medina, M., Twing, K. I., Sánchez-Murillo, R., Brazelton, W. J., McCollom, T. M., and Schrenk, M. O. (2017). Methane dynamics in a tropical serpentinizing environment: the Santa Elena Ophiolite, Costa Rica. *Front. Microbiol.* 8:916. doi: 10.3389/fmicb.2017.00916

Daae, F. L., Økland, I., Dahle, H., Jørgensen, S. L., Thorseth, I. H., and Pedersen, R. B. (2013). Microbial life associated with low-temperature alteration of ultramafic rocks in the Leka ophiolite complex. *Geobiology* 11, 318–339. doi: 10.1111/gbi.12035

Devereux, R., Mosher, J. J., Vishnivetskaya, T. A., Brown, S. D., Beddick, D. L. Jr., Yates, D. F., et al. (2015). Changes in northern Gulf of Mexico sediment bacterial and archaeal communities exposed to hypoxia. *Geobiology* 13, 478–493. doi: 10.1111/gbi.12142

Elser, J. J., Navarro, M. B., Corman, J. R., Emick, H., Kellom, M., Laspoumaderes, C., et al. (2015). Community structure and biogeochemical impacts of microbial life on floating pumice. *Appl. Environ. Microbiol.* 81, 1542–1549. doi: 10.1128/AEM.03160-14

Fillol, M., Auguet, J. C., Casamayor, E. O., and Borrego, C. M. (2016). Insights in the ecology and evolutionary history of the *Miscellaneous Crenarchaeotic Group* lineage. *ISME J.* 10, 665–677. doi: 10.1038/ismej.2015.143

Fones, E. M., Colman, D. R., Kraus, E. A., Nothaft, D. B., Poudel, S., Rempfert, K. R., et al. (2019). Physiological adaptations to serpentinization in the Samail Ophiolite, Oman. *ISME J.* 13, 1750–1762. doi: 10.1038/s41396-019-0391-2

Goordial, J., D'Angelo, T., Labonté, J. M., Poulton, N. J., Brown, J. M., Stepanauskas, R., et al. (2021). Microbial diversity and function in shallow subsurface sediment and oceanic lithosphere of the Atlantis Massif. *mBio* 12:e0049021. doi: 10.1128/mBio.00490-21

Hahn, M. W., Pitt, A., Schmidt, J., and Camacho, A. (2022). Fourteen new *Polynucleobacter* species: *P. brandtiae* sp. nov., *P. kasalickyi* sp. nov., *P. antarcticus* sp. nov., *P. arcticus* sp. nov., *P. tropicus* sp. nov., *P. bastaniensis* sp. nov., *P. corsicus* sp. nov., *P. finlandensis* sp. nov., *P. ibericus* sp. nov., *P. hallstattensis* sp. nov., *P. alcilacus* sp. nov., *P. nymphae* sp. nov., *P. paludilacus* sp. nov. and *P. parvulilacunae* sp. nov. *Int. J. Syst. Evol. Microbiol.* 72:005408. doi: 10.1099/ijsem.0.005408

Hahn, M. W., Schmidt, J., Asiyo, G. S., Kyrpides, N. C., Woyke, T., and Whitman, W. B. (2017). Reclassification of a *Polynucleobacter cosmopolitanus* strain isolated from tropical Lake Victoria as *Polynucleobacter victoriensis* sp. nov. *Int. J. Syst. Evol. Microbiol.* 67, 5087–5093. doi: 10.1099/ijsem.0.002421

Harris, R. L. (2020). "Life on the fringe: surveying the ecophysiological tenacity of methanogens and anaerobic methanotrophs in the oligotrophic deep subsurface biosphere" in Dissertations & Theses (Princeton, NJ: Princeton University), 27955474.

Harris, R. L., Lau, M. C. Y., Cadar, A., Bartlett, D. H., Cason, E., van Heerden, E., et al. (2018). Draft genome sequence of "Candidatus Bathyarchaeota" archaeon BE326-BA-RLH, an uncultured denitrifier and putative anaerobic methanotroph from South Africa's deep continental biosphere. *Microbiol. Resour. Announc.* 7:e01295. doi: 10.1128/MRA.01295-18

Hoang, D. T., Chernomor, O., von Haeseler, A., Minh, B. Q., and Vinh, L. S. (2018). UFBoot2: improving the ultrafast bootstrap approximation. *Mol. Biol. Evol.* 35, 518–522. doi: 10.1093/molbev/msx281

Hou, J., Wang, Y., Zhu, P., Yang, N., Liang, L., Yu, T., et al. (2023). Taxonomic and carbon metabolic diversification of Bathyarchaeia during its coevolution history with early earth surface environment. *Sci. Adv.* 9:eadf5069. doi: 10.1126/sciadv.adf5069

House, C. H., Schopf, J. W., and Stetter, K. O. (2003). Carbon isotopic fractionation by archaeans and other thermophilic prokaryotes. *Org. Geochem.* 34, 345–356. doi: 10.1016/S0146-6380(02)00237-1

Huse, S. M., Mark Welch, D. B., Voorhis, A., Shipunova, A., Morrison, H. G., Eren, A. M., et al. (2014). VAMPS: a website for visualization and analysis of microbial population structures. *BMC Bioinformatics* 15:41. doi: 10.1186/1471-2105-15-41

Kalyaanamoorthy, S., Minh, B. Q., Wong, T. K. F., von Haeseler, A., and Jermiin, L. S. (2017). ModelFinder: fast model selection for accurate phylogenetic estimates. *Nat. Methods* 14, 587–589. doi: 10.1038/nmeth.4285

Khilyas, I. V., Sorokina, A. V., Elistratova, A. A., Markelova, M. I., Siniagina, M. N., Sharipova, M. R., et al. (2019). Microbial diversity and mineral composition of weathered serpentine rock of the Khalilovsky Massif. *PLoS One* 14:e0225929. doi: 10.1371/journal.pone.0225929

Kim, S., Islam, M. R., Kang, I., and Cho, J. C. (2021). Cultivation of dominant freshwater bacterioplankton lineages using a high-throughput dilution-to-extinction culturing approach over a 1-year period. *Front. Microbiol.* 12:700637. doi: 10.3389/fmicb.2021.700637

Knights, D., Kuczynski, J., Charlson, E. S., Zaneveld, J., Mozer, M. C., Collman, R. G., et al. (2011). Bayesian community-wide culture-independent microbial source tracking. *Nat. Methods* 8, 761–763. doi: 10.1038/nmeth.1650

Kojima, H., Shinohara, A., and Fukui, M. (2015). *Sulfurifustis variabilis* gen. nov., sp. nov., a sulfur oxidizer isolated from a lake, and proposal of *Acidiferrobacteraceae* fam. nov. and *Acidiferrobacterales* ord. nov. *Int. J. Syst. Evol. Microbiol.* 65, 3709–3713. doi: 10.1099/ijsem.0.000479

Kraus, E. A. (2021). "The endolithic and planktonic subsurface microbiome within zones of active low-temperature serpentinization in the Samail Ophiolite of Oman" in Dissertations & Theses (Golden, CO: Faculty and Board of Trustees of the Colorado School of Mines), 28413788.

Kraus, E. A., Nothaft, D., Stamps, B. W., Rempfert, K. R., Ellison, E. T., Matter, J. M., et al. (2021). Molecular evidence for an active microbial methane cycle in subsurface serpentinite-hosted groundwaters in the Samail Ophiolite, Oman. *Appl. Environ. Microbiol.* 87:e02068. doi: 10.1128/AEM.02068-20

Lang, S. Q., and Brazelton, W. J. (2020). Habitability of the marine serpentinite subsurface: a case study of the lost city hydrothermal field. *Phil. Trans. R. Soc. A* 378:20180429. doi: 10.1098/rsta.2018.0429

Lazar, C. S., Baker, B. J., Seitz, K., Hyde, A. S., Dick, G. J., Hinrichs, K. U., et al. (2016). Genomic evidence for distinct carbon substrate preferences and ecological niches of Bathyarchaeota in estuarine sediments. *Environ. Microbiol.* 18, 1200–1211. doi: 10.1111/1462-2920.13142

Lazar, C. S., Stoll, W., Lehmann, R., Herrmann, M., Schwab, V. F., Akob, D. M., et al. (2017). Archaeal diversity and CO_2 fixers in carbonate-/siliciclastic-rock groundwater ecosystems. *Archaea* 2017:2136287. doi: 10.1155/2017/2136287

Magnabosco, C., Lin, L. H., Dong, H., Bomberg, M., Ghiorse, W., Stan-Lotter, H., et al. (2018). The biomass and biodiversity of the continental subsurface. *Nat. Geosci.* 11, 707–717. doi: 10.1038/s41561-018-0221-6

McMurdie, P. J., and Holmes, S. (2013). Phyloseq: an R package for reproducible interactive analysis and graphics of microbiome census data. *PLoS One* 8:e61217. doi: 10.1371/journal.pone.0061217

Méhay, S., Früh-Green, G. L., Lang, S. Q., Bernasconi, S. M., Brazelton, W. J., Schrenk, M. O., et al. (2013). Record of archaeal activity at the serpentinite-hosted lost city hydrothermal field. *Geobiology* 11, 570–592. doi: 10.1111/gbi.12062

Morrison, H. G., Grim, S. L., Vineis, J. H., and Sogin, M. L. (2013). 16S amplicon fusion primers and protocol for Illumina platform sequencing. Available at: https://figshare.com/articles/dataset/16S_amplicon_fusion_primers_and_protocol_for_Illumina_platform_sequencing/833944/1. (Accessed October 17, 2021)

Motamedi, S., Orcutt, B. N., Früh-Green, G. L., Twing, K. I., Pendleton, H. L., and Brazelton, W. J. (2020). Microbial residents of the Atlantis Massif's shallow serpentinite subsurface. *Appl. Environ. Microbiol.* 86:15. doi: 10.1128/AEM.00356-20

Multinu, F., Harrington, S. C., Chen, J., Jeraldo, P. R., Johnson, S., Chia, N., et al. (2018). Systematic bias introduced by genomic DNA template dilution in *16S rRNA* gene-targeted microbiota profiling in human stool homogenates. *mSphere* 3:e00560. doi: 10.1128/mSphere.00560-17

Nguyen, L. T., Schmidt, H. A., von Haeseler, A., and Minh, B. Q. (2015). IQ-TREE: a fast and effective stochastic algorithm for estimating maximum-likelihood phylogenies. *Mol. Biol. Evol.* 32, 268–274. doi: 10.1093/molbev/msu300

Niyomvong, N., Pathom-Aree, W., Thamchaipenet, A., and Duangmal, K. (2012). Actinomycetes from tropical limestone caves. Available at: https://hero.epa.gov/hero/index.cfm/reference/details/reference_id/2646985. (Accessed September 30, 2024)

Oksanen, J., Blanchet, F. G., Friendly, M., Kindt, R., Legendre, P., McGlinn, D., et al. (2020). vegan: community ecology package. Available at: https://CRAN.R-project.org/package=vegan. (Accessed October 18, 2021)

Ortiz, E., Tominaga, M., Cardace, D., Schrenk, M. O., Hoehler, T. M., Kubo, M. D., et al. (2018). Geophysical characterization of serpentinite hosted hydrogeology at the McLaughlin Natural Reserve, Coast Range Ophiolite. *Geochem. Geophys. Geosyst.* 19, 114–131. doi: 10.1002/2017GC007001

Peters, E. K. (1993). D-18O enriched waters of the Coast Range Mountains, northern California: connate and ore-forming fluids. *Geochim. Cosmochim. Acta* 57, 1093–1104. doi: 10.1016/0016-7037(93)90043-V

Pruesse, E., Quast, C., Knittel, K., Fuchs, B. M., Ludwig, W., Peplies, J., et al. (2007). SILVA: a comprehensive online resource for quality checked and aligned ribosomal RNA sequence data compatible with ARB. *Nucleic Acids Res.* 35, 7188–7196. doi: 10.1093/nar/gkm864

Quast, C., Pruesse, E., Yilmaz, P., Gerken, J., Schweer, T., Yarza, P., et al. (2013). The SILVA ribosomal RNA gene database project: improved data processing and web-based tools. *Nucleic Acids Res.* 41, D590–D596. doi: 10.1093/nar/gks1219

Robinson, M. D., McCarthy, D. J., and Smyth, G. K. (2010). edgeR: a bioconductor package for differential expression analysis of digital gene expression data. *Bioinformatics* 26, 139–140. doi: 10.1093/bioinformatics/btp616

Ros, M., Rodríguez, I., García, C., and Hernández, M. T. (2014). Bacterial community in semiarid hydrocarbon contaminated soils treated by aeration and organic amendments. *Int. Biodeterior. Biodegrad.* 94, 200–206. doi: 10.1016/j.ibiod.2014.07.018

Safford, H., and Miller, J. E. D. (2020). An updated database of serpentine endemism in the California flora. *Madrono* 67, 85–104. doi: 10.3120/0024-9637-67.2.85

Salam, L. B., Ilori, M. O., Amund, O. O., LiiMien, Y., and Nojiri, H. (2018). Characterization of bacterial community structure in a hydrocarbon-contaminated tropical African soil. *Environ. Technol.* 39, 939–951. doi: 10.1080/09593330.2017.1317838

Salter, S. J., Cox, M. J., Turek, E. M., Calus, S. T., Cookson, W. O., Moffatt, M. F., et al. (2014). Reagent and laboratory contamination can critically impact sequence-based microbiome analyses. *BMC Biol.* 12:87. doi: 10.1186/s12915-014-0087-z

Schloss, P. D. (2020). Reintroducing mothur: 10 years later. *Appl. Environ. Microbiol.* 86, e02343–e02319. doi: 10.1128/AEM.02343-19

Schloss, P. D., and Westcott, S. L. (2011). Assessing and improving methods used in operational taxonomic unit-based approaches for *16S rRNA* gene sequence analysis. *Appl. Environ. Microbiol.* 77, 3219–3226. doi: 10.1128/AEM.02810-10

Schloss, P. D., Westcott, S. L., Ryabin, T., Hall, J. R., Hartmann, M., Hollister, E. B., et al. (2009). Introducing mothur: open-source, platform-independent, community-

supported software for describing and comparing microbial communities. *Appl. Environ. Microbiol.* 75, 7537–7541. doi: 10.1128/AEM.01541-09

Schrenk, M. O., Brazelton, W. J., and Lang, S. Q. (2013). Serpentinization, carbon, and deep life. *Rev. Mineral. Geochem.* 75, 575–606. doi: 10.2138/rmg.2013.75.18

Sheik, C. S., Reese, B. K., Twing, K. I., Sylvan, J. B., Grim, S. L., Schrenk, M. O., et al. (2018). Identification and removal of contaminant sequences from ribosomal gene databases: lessons from the census of deep life. *Front. Microbiol.* 9:840. doi: 10.3389/fmicb.2018.00840

Sievers, F., and Higgins, D. G. (2014). Clustal omega. *Curr. Protoc. Bioinformatics* 48, 3.13.1–3.13.16. doi: 10.1002/0471250953.bi0313s48

Solano-Arguedas, A. F., Boothman, C., Newsome, L., Pattrick, R. A. D., Arguedas-Quesada, D., Robinson, C. H., et al. (2022). Geochemistry and microbiology of tropical serpentine soils in the Santa Elena Ophiolite, a landscape-biogeographical approach. *Geochem. Trans.* 23:2. doi: 10.1186/s12932-022-00079-5

Suzuki, S., Ishii, S., Wu, A., Cheung, A., Tenney, A., Wanger, G., et al. (2013). Microbial diversity in the cedars, an ultrabasic, ultrareducing, and low salinity serpentinizing ecosystem. *Proc. Natl. Acad. Sci. U.S.A.* 110, 15336–15341. doi: 10.1073/pnas.1302426110

Suzuki, S., Kuenen, J. G., Schipper, K., van der Velde, S., Ishii, S., Wu, A., et al. (2014). Physiological and genomic features of highly alkaliphilic hydrogen-utilizing *Betaproteobacteria* from a continental serpentinizing site. *Nat. Commun.* 5:3900. doi: 10.1038/ncomms4900

Templeton, A. S., and Caro, T. A. (2023). The rock-hosted biosphere. *Annu. Rev. Earth Planet. Sci.* 51, 493–519. doi: 10.1146/annurev-earth-031920-081957

Templeton, A. S., Ellison, E. T., Glombitza, C., Morono, Y., Rempfert, K. R., Hoehler, T. M., et al. (2021). Accessing the subsurface biosphere within rocks undergoing active low-temperature serpentinization in the Samail Ophiolite (Oman Drilling Project). *J. Geophys. Res. Biogeosci.* 126:e2021JG006315. doi: 10.1029/2021JG006315

Thieringer, P. H., Boyd, E. S., Templeton, A. S., and Spear, J. R. (2023). Metapangenomic investigation provides insight into niche differentiation of methanogenic populations from the subsurface serpentinizing environment, Samail Ophiolite, Oman. *Front. Microbiol.* 14:1205558. doi: 10.3389/fmicb.2023.1205558

Tiago, I., and Veríssimo, A. (2013). Microbial and functional diversity of a subterrestrial high pH groundwater associated to serpentinization. *Environ. Microbiol.* 15, 1687–1706. doi: 10.1111/1462-2920.12034

Trutschel, L. R., Chadwick, G. L., Kruger, B., Blank, J. G., Brazelton, W. J., Dart, E. R., et al. (2022). Investigation of microbial metabolisms in an extremely high pH marine-like terrestrial serpentinizing system: ney springs. *Sci. Total Environ.* 836:155492. doi: 10.1016/j.scitotenv.2022.155492

Twing, K. I., Brazelton, W. J., Kubo, M. D. Y., Hyer, A. J., Cardace, D., Hoehler, T. M., et al. (2017). Serpentinization-influenced groundwater harbors extremely low diversity microbial communities adapted to high pH. *Front. Microbiol.* 8:308. doi: 10.3389/fmicb.2017.00308

Wang, P., Zhang, T., Chen, S., Li, X., Lai, D., Gao, S., et al. (2020). Niche specificity and potential terrestrial organic carbon utilization of benthic *Bathyarchaeota* in a eutrophic subtropic estuarine system. *Chem. Geol.* 556:119839. doi: 10.1016/j.chemgeo.2020.119839

Waterhouse, A. M., Procter, J. B., Martin, D. M. A., Clamp, M., and Barton, G. J. (2009). Jalview version 2—a multiple sequence alignment editor and analysis workbench. *Bioinformatics* 25, 1189–1191. doi: 10.1093/bioinformatics/btp033

Westcott, S. L., and Schloss, P. D. (2017). OptiClust, an improved method for assigning amplicon-based sequence data to operational taxonomic units. *mSphere* 2:e00073. doi: 10.1128/mSphereDirect.00073-17

Woycheese, K. M., Meyer-Dombard, D. R., Cardace, D., Argayosa, A. M., and Arcilla, C. A. (2015). Out of the dark: transitional subsurface-to-surface microbial diversity in a terrestrial serpentinizing seep (Manleluag, Pangasinan, the Philippines). *Front. Microbiol.* 6:44. doi: 10.3389/fmicb.2015.00044

Yin, X., Zhou, G., Cai, M., Zhu, Q. Z., Richter-Heitmann, T., Aromokeye, D. A., et al. (2022). Catabolic protein degradation in marine sediments confined to distinct archaea. *ISME J.* 16, 1617–1626. doi: 10.1038/s41396-022-01210-1

Yu, B., Tao, F., Li, F., Hou, J., Tang, H., Ma, C., et al. (2015). Complete genome sequence of *Mycobacterium goodii* X7B, a facultative thermophilic biodesulfurizing bacterium with industrial potential. *J. Biotechnol.* 212, 56–57. doi: 10.1016/j.jbiotec.2015.08.004

Zhou, Z., Pan, J., Wang, F., Gu, J. D., and Li, M. (2018). Bathyarchaeota: globally distributed metabolic generalists in anoxic environments. *FEMS Microbiol. Rev.* 42, 639–655. doi: 10.1093/femsre/fuy023

frontiers | Frontiers in Microbiology

TYPE Original Research
PUBLISHED 21 March 2025
DOI 10.3389/fmicb.2025.1511421

OPEN ACCESS

EDITED BY
Philippe M. Oger,
UMR5240 Microbiologie, Adaptation et Pathogenie (MAP), France

REVIEWED BY
Satya P. Singh,
Saurashtra University, India
Wei-Jia Zhang,
Chinese Academy of Sciences (CAS), China

*CORRESPONDENCE
Steven E. Finkel
✉ sfinkel@usc.edu

†PRESENT ADDRESSES
Alberto Robador,
Marine and Environmental Biology Section, Department of Biological Sciences, University of Southern California, Los Angeles, CA, United States
Dawson Ray,
Brightseed, Inc., South San Francisco, CA, United States

RECEIVED 15 October 2024
ACCEPTED 07 February 2025
PUBLISHED 21 March 2025

CITATION
Sebastian H, Robador A, Ray D, Angermeyer A, D'Hondt S, Huber JA and Finkel SE (2025) Identifying potential nutrient acquisition mechanisms for long-term survival: adaptive evolution of *Halomonas* isolated from subseafloor crustal fluids. *Front. Microbiol.* 16:1511421. doi: 10.3389/fmicb.2025.1511421

Identifying potential nutrient acquisition mechanisms for long-term survival: adaptive evolution of *Halomonas* isolated from subseafloor crustal fluids

Hans Sebastian[1], Alberto Robador[1†], Dawson Ray[1†], Angus Angermeyer[2], Steven D'Hondt[3], Julie A. Huber[4] and Steven E. Finkel[1*]

[1]Molecular and Computational Biology Section, Department of Biological Sciences, University of Southern California, Los Angeles, CA, United States, [2]Marine Biological Laboratory, Woods Hole, MA, United States, [3]Graduate School of Oceanography, University of Rhode Island, Narragansett, RI, United States, [4]Marine Chemistry and Geochemistry, Woods Hole Oceanographic Institution, Woods Hole, MA, United States

In nature, microbes must often survive for long periods of time under conditions of nutrient and carbon limitation while also facing extremes in temperature, pressure, and competition with other microbes. One low-carbon, cold, and high pressure environment is the subseafloor crustal aquifer, where fluids circulate through old ocean crust. While microbial communities are known to be present in these fluids and contribute to biogeochemical cycling, the survival strategies of microbes in these communities is poorly constrained. In this study, multiple *Halomonas* strains were isolated from subseafloor crustal fluids of North Pond, a site located on the western flank of the Mid-Atlantic Ridge. These organisms are able to grow under laboratory conditions in minimal medium without the addition of carbon sources, as well as in rich nutrient conditions. We found that these *Halomonas* strains are highly related to each other in genomic content, but each strain has acquired unique mutations and/or undergone genomic rearrangements, suggesting that the strains were all derived from a single ancestral *Halomonas* progenitor. After serial passage of isolates from this *Halomonas* population under rich nutrient conditions in the laboratory, we identified mutants that can no longer scavenge scarce nutrients in minimal medium with no added carbon. Genomic analysis identified several genes that appear to be essential for survival under extremely low-nutrient condition, including several hypothetical proteins predicted to function as lipases, peptidases, or nutrient transporters. One of these genes was mutated in six out of the eight lineages studied, indicating that this hypothetical lipase protein is selected against during growth in rich medium, but may be required for growth under low-nutrient conditions. The application of an adaptive evolution platform selecting for survival and growth under one environmental condition that simultaneously selects against survival in different environments may prove to be a very useful tool for identifying genes and metabolic pathways in a wide variety of complex environments.

KEYWORDS

long-term survival, bacterial evolution, deep biosphere, nutrient acquisition, low nutrient environment

Highlights

- Bacteria occupy every life-sustaining niche on Earth, yet frequently the mechanisms allowing organisms to succeed are difficult to determine.
- New tools are needed to identify mechanisms of survival and the genes upon which these mechanisms rely.
- We have developed a novel strategy for identifying genes essential to low-nutrient environments by selecting for cells adapted to high-nutrient conditions.
- These evolved cells have "forgotten" how to thrive in the extremely nutrient-restricted environments from which they were isolated.
- Since many organisms sampled from these extreme environments are recalcitrant to laboratory manipulation, this approach has the potential to identify important molecular biomarkers that can be used to study microbial communities, furthering our knowledge of which genes and metabolic pathways contribute to evolutionary fitness.

Introduction

Microbial life thrives within the fluids of the subseafloor oceanic igneous crust, which spans 70% of Earth's surface, and plays a critical role in shaping the planet's biogeochemistry on a global scale (Orcutt et al., 2020; Orcutt et al., 2013; Meyer et al., 2016; Robador, 2024). Circulation of crustal waters begins and ends as fluids enter and exit the subsurface through exposed rocks at the seafloor and interact with both the minerals and microbes within the rock to change the chemistry of the fluids (Orcutt et al., 2020; Trembath-Reichert et al., 2021). Since the retention of these fluids during transit from one outcrop to another spans a wide range of distances and time (Price et al., 2022), microbes in transit often do not encounter an influx of fresh nutrients, but must instead rely on nutrients and carbon trapped in the crustal fluids, which can be carbon-poor with limited reduced substrates available for growth (Shah Walter et al., 2018). Understanding survival mechanisms in such extreme environments allows us to address the question of how microbes can survive for long periods of time under conditions of nutrient and carbon limitation and competition with other microbes.

To facilitate the study of crustal fluid environments, CORK (Circulation Obviation Retrofit Kit) subseafloor observatories were used to extract fluids from beneath the seafloor with minimal contamination (Edwards et al., 2012b). Samples in this study were obtained from North Pond (22°45′N, 46°05′W), located at ~4,450 meters on the western flank of the Mid-Atlantic Ridge, where multiple boreholes were drilled, and CORKs were installed during IODP Expedition 336 in 2011 (Edwards et al., 2012b; Edwards et al., 2012a). By studying these crustal fluids, many insights into the chemistry and microbial activity of these waters have been obtained, including a better understanding of specific respiration processes that occur, rates of carbon uptake and metabolic activity, changes in microbial composition and gene expression over time, and organic carbon composition of the fluids (Trembath-Reichert et al., 2021; Orcutt et al., 2013; Seyler et al., 2021; Robador et al., 2016; Tully et al., 2018; LaRowe et al., 2017; Zhang et al., 2016; Anderson et al., 2022). However, to date, these studies have not defined the specific adaptations that may be responsible for allowing bacterial species to survive and compete within this low-carbon environment for long periods of time.

Long-term survival of bacterial populations has been well investigated in the laboratory with the goal of modeling aspects of natural systems (Finkel, 2006; Ratib et al., 2021; Kram and Finkel, 2015; Kram and Finkel, 2014). Under laboratory conditions, bacteria typically experience five phases of growth and survival (Finkel, 2006). The three most commonly studied phases are lag phase, log or exponential phase, and stationary phase. Briefly, lag phase is the period where cells enter a new environment and sense available nutrients without appreciable increase in the number of cells. Then, cells retool their metabolism prior to initiating growth in log phase where cells proliferate (Rolfe et al., 2012). Cells then transition into a period of logarithmic or exponential growth where within hours or days, the number of cells increase by many orders-of-magnitude. After reaching maximum cell density, cells enter stationary phase where the number of viable cells remains constant. During stationary phase many cellular stress responses are activated and, for some species, cell morphology and physiological changes results in a more protected state (Farrell and Finkel, 2003; Navarro Llorens et al., 2010; Nystrom, 2004). While the length of stationary phase varies by strain and specific growth conditions, the population will eventually enter death phase, usually after 1–2 days of incubation in a rich medium, where ~99% of cells lose viability (Kram and Finkel, 2015). However, not all cells die, and surviving cells enter long-term stationary phase (LTSP), where they continue to survive for long periods of time without addition of nutrients to the culture. During LTSP, microbes survive utilizing detrital nutrients, which continuously modifies the habitable environment, requiring the community to continuously adapt and evolve to survive (Ratib et al., 2021). This fifth phase of LTSP in batch culture most resembles natural environments, where cells must survive and adapt to conditions of starvation, changing environments, and other environmentally induced stresses (Finkel, 2006). While we can learn much through *in vitro* experimentation, the need exists to study microbes from the natural world, under conditions that better simulate their extreme environments.

Here, we exposed multiple bacterial strains isolated from North Pond crustal fluids to an adaptive evolution protocol designed to select for mutants that may have lost the ability to scavenge and metabolize scarce nutrients. It is important to note that these *Halomonas* strains were the only species of bacteria that formed colonies on plates incubated without the addition of carbon. After evolving these strains for approximately 300 generations in the rich medium Luria-Bertani (LB) broth, their ability to grow in a culture medium with no added carbon was compared to the parental strains. Mutations that reduced their ability to grow under conditions of nutrient stress, including mutations in catabolic enzymes, nutrient transporters, and putative exoenzymes, were observed following adaptive evolution. Together, these mutations provide insight into possible mechanisms that allow these microbes to survive for long periods of time with relatively low carbon availability, such as the crustal subseafloor habitat. While we understand that the conditions of selection and fitness determination used here do not fully reflect those found *in situ* in

crustal fluids, the conditions and media used provide a launching identify important functions and adaptations.

Materials and methods

Sample collection

In 2014, crustal fluids were collected from a subseafloor borehole fitted with a Circulation Obviation Retrofit Kit (CORK), designated as 'U1383C' and located at the North Pond site (22°45′N, 46°05′W) along the western flank of the Mid-Atlantic Ridge (Edwards et al., 2012a). Samples were collected at two depth horizons beneath the seafloor: a 'shallow' (58–142 m) horizon and 'deep' (200–330 m) horizon, as described in (Meyer et al., 2016).

Enrichment and isolation

Fluid samples were plated on 10 cm plastic petri dishes containing ~20 mL of a medium modified from DSMZ Medium-113[1] (Kelly and Wood, 2000). A 2X modified media solution (herein referred to as modified DSMZ-113) was made containing (per 500 mL DI-H2O): 2.0 g $KH2PO_4$, 2.0 g KNO_3, 1.0 g NH_4Cl, 0.8 g $MgSO_4 \times 7\ H_2O$, 5.0 g $Na_2S_2O_3 \times 5\ H_2O$, 2.0 mg $FeSO_4 \times 7\ H_2O$ (solubilized in 0.1 N 102 H_2SO_4), 1.0 g $NaHCO_3$, and 2 mL MC-TMS trace element solution (ATCC, Manassas, VA, USA). The medium was adjusted to pH 7.0 with NaOH and filter sterilized into carbon-free glassware (combusted at 400°C for 5 h). Prior to filtration, each 0.2 µm filter was washed twice with sterile water to prevent potential carbon-source carry over from filter paper "wetting agents" (believed to be glycerol or other utilizable organic compounds). To solidify the medium for plates, 15 g of agar (Fisher Scientific, Fair Lawn, NJ, USA) was autoclaved in 500 mL DI-H_2O and combined with 500 mL of 2X modified DSMZ-113 when cooled below ~50°C. After plating, replicate dishes were incubated at 4°C and 20°C aerobically and at 20°C anaerobically until individual colonies were visible. Distinct colonies that grew on the plates were transferred to combusted carbon-free glass culture tubes containing 5 mL of 1X modified DSMZ-113 and incubated at 20°C while shaking at 180 rpm. A sample from each culture that grew turbid was stored in 15% glycerol at −80°C. The isolation details including the specific fluid sample origin for each of the 46 strains can be found at doi: 10.26300/6f5k-za64.

16S rRNA gene sequencing

DNA was extracted from each isolated culture using the Biostic bacteremia DNA Isolation Kit (MoBio, Carlsbad, CA, USA) and stored at −20°C. Extracted DNA was PCR amplified with universal 16S rRNA primers 8F (5'-AGAGTTTGATCC TGGCTCAG) and 1492R (5'-GGTTACCTTGTTACGACTT) [3 min at 94°C, 35 cycles of, 40 s at 94°C, 1.5 min at 55°C, 2 min at 72°C and a final extension for 10 min at 72C]. PCR products were purified with MinElute PCR purification kit (Qiagen, Valencia, CA, USA). Bidirectional Sanger sequencing was performed at the Marine Biological Laboratory (Woods Hole, MA, USA) on an AB 3730XL Genetic Analyzer (Thermo Fisher Scientific, Waltham, MA, USA) using AB BigDye3.1 chemistry. Quality scoring and merging into full-length 16S rRNA gene sequences was performed with Phred and Phrap (Ewing et al., 1998). Taxonomy at the genus level was determined with NCBI BLASTn. Sequence alignment was performed using mothur (Schloss et al., 2009) and a neighbor-joining phylogenetic tree was generated with ClustalX (Larkin et al., 2007) using 1,000 bootstrap trials.

Experimental culture conditions and titering assays

Forty-six strains identified as *Halomonas* were outgrown from glycerol stocks in modified DMSZ medium 113 at 30°C in 5 mL cultures containing Luria Bertani (LB) broth (Lennox; 10 g Tryptone, 5 g Yeast Extract, 5 g NaCl, components from BD) until turbid, and stored in LB with 20% glycerol at −80°C.

For testing growth and survival dynamics at high-nutrient conditions, strains were incubated in 5 mL LB broth in 18 × 150 mm borosilicate tubes, at 30°C rolling in a TC-7 roller drum (New Brunswick Scientific). For testing survival under low-nutrient conditions, strains were incubated in the modified DSMZ-113 medium in 18 × 150 mm borosilicate tubes, at room temperature (18°C) rolling in a TC-7 roller drum (New Brunswick Scientific). All starter cultures were first inoculated into modified DSMZ-113 medium for 5 days to allow carry-over carbon to be depleted. These 'carbon-depleted' cultures were then used to initiate all low-nutrient growth and survival experiments in fresh, no-carbon-added, modified DSMZ-113 medium. All viable cell counts were measured using the spot titering assay plated on LB agar (Kraigsley and Finkel, 2009) with a limit of detection of <1,000 CFU/mL.

Adaptive evolution by serial passage

Nine representative strains were incubated in triplicate in 5 mL LB broth, as described above. Every 2 days, 5 µL of these 27 cultures (nine representative strains in triplicate) were re-inoculated into a fresh 5 mL LB culture and propagated for a total of 30 passages (Kram et al., 2017). After 30 passages, evolved populations were stored in LB with 20% glycerol in −80°C.

Clone isolation from evolved populations

The growth and survival patterns of each of the strains were compared to their respective parental strains when incubated in DSMZ-113 medium, with no addition of carbon or energy sources. However, it is clear that some form of bioavailable organic compounds exist that support low levels of microbial growth under these conditions. Evolved strains that grew significantly worse overall compared to their parental strain, as reflected by either demonstrating a reduced relative cell yield after 5 days, a slower growth rate, and/or

1 https://www.dsmz.de/microorganisms/medium/pdf/DSMZ_Medium113.pdf

entering death phase earlier, were chosen for further analysis. Each candidate population was plated on LB agar. Twelve clones were then picked from individual colonies on each plate, grown overnight in LB medium, and stored in LB with 20% glycerol at −80°C.

Genomic DNA isolation and DNA sequencing

DNA from each parental strain and the corresponding 12 evolved clones from each strain was extracted from ~10^9 cells using the ZymoBIOMICS DNA Miniprep Kit. To obtain the reference genome of the parental strains, a combination of long reads using Nanopore (Wang et al., 2021) and short reads using NextSeq (Illumina) were used to assemble the whole genome. Whole-genome sequencing-library preparation and short-read sequencing of the clones were performed using the NextSeq2000 platform. All sequencing, genome assemblies, and gene annotations were performed by the Microbial Genome Sequencing Center (MiGS), Pittsburgh, PA. Briefly, post sequencing, quality control and adapter trimming was performed with bcl2fastq (Illumina, Inc., n.d.) and porechop (GitHub, Inc., n.d.) for Illumina and ONT sequencing, respectively. Hybrid assembly with Illumina and ONT reads was performed with Unicycler (Wick et al., 2017). Assembly annotation was performed with Prokka (Seemann, 2014).

Identifying mutations

Genomic sequences of evolved clones were aligned to each respective parental genome using BreSeq version 0.36.0 (Deatherage and Barrick, 2014) in consensus mode to identify SNPs, small indels, deletions, and mobile genetic elements. The comparison of presence or absence of genes was analyzed using Roary (Page et al., 2015). Each genome was visualized through Geneious R8.1.9 software and genomic rearrangement analysis was done using the progressiveMauve algorithm (Darling et al., 2004).

Results

Enrichment, isolation, and identification of isolates

Fluids from the deep and shallow horizons of CORK observatory U1383C that were plated on autotrophic minimal media (modified DSMZ-113) generated distinct, uniform colonies. These colonies were small (~1–2 mm), whitish tan in appearance, and relatively slow growing. The plates incubated at 20°C aerobically exhibited barely visible colony growth after 7 days and distinguishable colonies at ~10 days. Those incubated at the same temperature anaerobically did not show growth, nor did those inoculated aerobically at 4°C. Therefore, all further cultured strains originated from the 20°C aerobic colonies and were given a North Pond diversity identification number (NPDiv#). NPDiv1-34 ($n = 32$) were from the 1383C deep horizon and NPDiv35-52 ($n = 14$) were from 1383C Shallow (Supplementary Table 1).

Sanger sequencing of cultures revealed that the majority (46/52) belonged to the genus *Halomonas* and were closely related to one another. Isolates NPDiv37, 43, and 50 were identified as Pseudomonas and not used in further experiments. NPDiv8, 10, and 49 failed to sequence well enough to determine taxonomy and were not used in further experiments. Phylogenetic analysis of North Pond *Halomonas* sequences indicated that all the North Pond isolates grouped with other isolates from cold deep seawater samples ('Ecotype 2B') (Kaye et al., 2011; Supplementary Figure 3).

Halomonas strains sampled from crustal fluids can each be assigned to one of nine different growth phenotype groups

All 46 isolated *Halomonas* strains were incubated in LB medium, and their growth and survival patterns were determined. Nine different phenotypic groups were observed after incubating in batch culture at 30°C in LB for 4 days (Figure 1). The features used to distinguish each group are described in detail below. They include: (i) initial growth yield at the end of log phase, (ii) duration of stationary phase, (iii) time of entry into and duration of death phase, (iv) severity of loss of cell viability during death phase, and (v) the post-death phase dynamics of each strain.

The overnight growth yields were determined for each culture. Groups 1 through 6 (Figures 1A–F) had an average overnight yield of ~2.5×10^9 CFU/mL while Groups 7 through 9 (Figures 1G–I) displayed yields that were ~ 10-fold lower, at ~5.8×10^8 CFU/mL. Comparing the lengths of stationary phase, strains in Groups 1 through 6 (Figures 1A–F) exhibited a 1-day stationary phase, compared to Groups 7 through 9 (Figures 1G–I) whose stationary phase was twice as long lasting for 2 days.

The timing of entry and duration of death phase also varied considerably between each strain. Of the strains that reached a maximum cell yield of ~10^9 CFU/mL upon entry into stationary phase, Group 1 (Figure 1A), Group 3 (Figure 1C), and Group 4 (Figure 1D) strains have death phases that last for 2 days. However, among these strains, there were differences in the degree to which cells died: strains in Groups 1 and 4 showed a reduction in viability of ~100-fold, while Group 3 strains showed a more modest 10-fold loss in viability. While Group 2 (Figure 1B), Group 5 (Figure 1E), and Group 6 (Figure 1F) strains also reached ~10^9 CFU/ml on day 1, their death phases continued through day 4 of the experiment, with populations never entering Long-Term Stationary Phase(). However, the magnitude of the extent of death phase also varied with these three groups, where Group 2 and 6 strains showed a 10-fold decrease in viability, compared to Group 5 strains that suffered up to 1,000-fold decreases in cell viability. Among the strains that reached ~10^8 CFU/mL at the end of log phase, Group 7 strains (Figure 1G) had a death phase that lasted 2 days, while Group 8 and 9 strains (Figures 1H,I) had a 1-day death phase. Group 7 and 9 strains exhibited ~100-fold decreases in cell yield, while Group 8 strains showed 10-fold losses in viability. Lastly, the post-death-phase dynamics of these groups also differed. Specifically, Group 1 exhibited noticeable re-growth after death phase where cell counts increased ~8-fold, while Group 2, 5, 6, and 7 strains were still declining in cell yield by the end of the experiment. This is in contrast to Groups 3, 4, 8 and 9 strains, which maintained viability at a constant cell density after death phase.

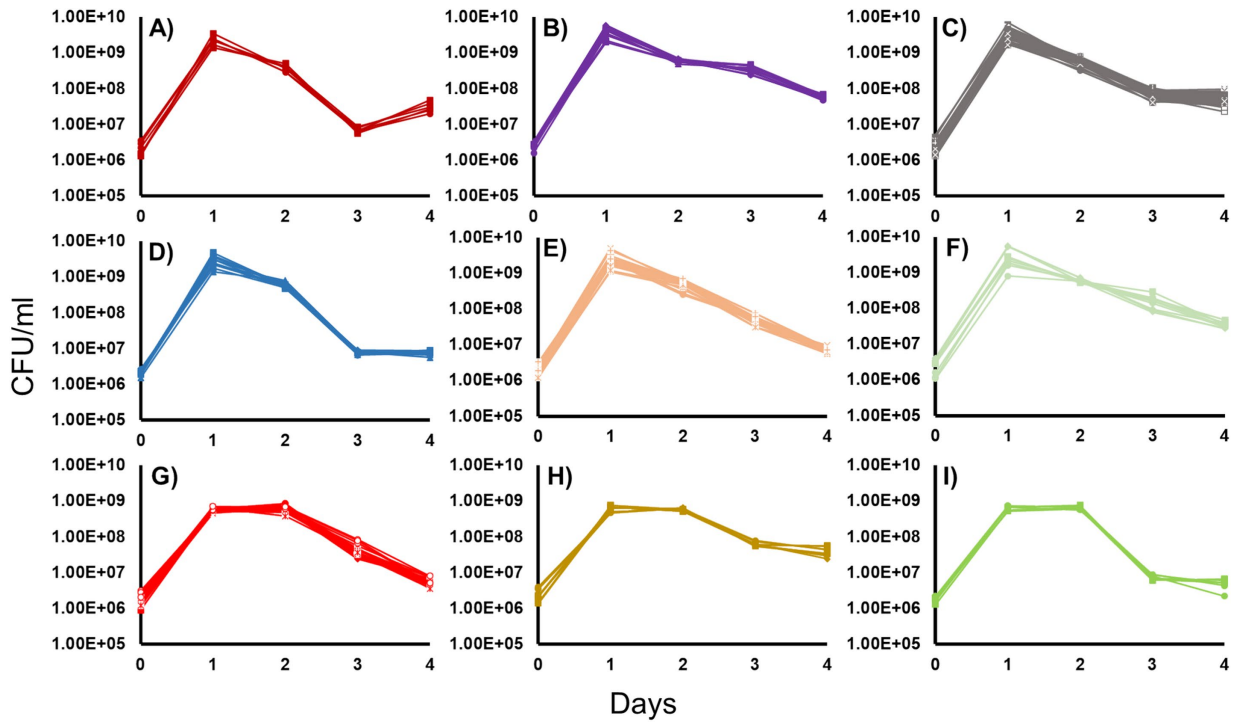

FIGURE 1
Growth and survival of the 46 *Halomonas* isolates incubated in Luria-Bertani Broth. Forty-six *Halomonas* strains isolated from the crustal fluids of North Pond were grown in LB and separated into phenotypic classes, based on growth and survival dynamics of each strain (6). **(A)** Group 1 (2 strains: A1, **A2**), **(B)** Group 2 (4 strains: A8, **B1**, B5, B6), **(C)** Group 3 (14 strains: A3, B3, B4, B7, B8, C7, D2, D6, E1, E4, F6, G4, H2, **H6**), **(D)** Group 4 (4 strains: E2, **E3**, G6, H3), **(E)** Group 5 (7 strains: A4, D3, D4, D7, E7, F7, **G1**), **(F)** Group 6 (3 strains: A5, A6, G2), **(G)** Group 7 (7 strains: C1, **C2**, **D1,** C3, E6, F2, F3), **(H)** Group 8 (3 strains: **C4**, F4, G3), **(I)** Group 9 (2 strains: **F1**, H4). Strains chosen for further study are indicated in bold.

Adaptive evolution selects for mutants with reduced fitness under low-nutrient conditions

We selected 9 strains and serially passaged them in triplicate, creating a total of 27 individual cultures, for 30 passages in LB (~300 generations) (see Materials and Methods; Supplementary Figure 1). Following the opportunity for adaptive evolution in rich medium, we compared the survivability of each of the 27 cultures in low-nutrient DSMZ-113 medium to its original parental strain and ultimately selected 8 cultures, described below, that exhibited significant growth differences for further study (Supplementary Figure 1). We refer to these 8 cultures as populations A through H (Figure 2). Population A originated from a single parental strain within Group 1. Population B originated from a single parental strain within Group 2. Population C originated from a single parental strain within Group 3. Populations D and E originated from different replicates of the same parental strain within Group 4. Populations F and G originated from different parental strains within Group 7. Lastly, population H originated from a parental strain within Group 8. Therefore, the eight populations, A through H, originated from seven parental strains. In the following sections of this study, parental strains are referred to using their Group number.

For each of the populations that exhibited changes in growth or survival patterns when incubated in minimal medium without additional carbon, cultures were streaked to single colonies and 12 individual clones from each population were selected at random. The growth and survival of each of these "evolved" clones were then compared to their respective parental strains. Overall, the majority of the clones isolated from the evolved populations were less fit than their parent without any addition of carbon (Figure 2). In population A (Figure 2A), 4 clones had reduced Day-5 yields, ranging from ~7×10^3 CFU/ml to ~3×10^5 CFU/mL. The yields of the 8 remaining population A clones were below the limit of detection by day 5, compared to the parental strain with a final yield of ~8×10^5 CFU/mL (Figure 2A). For population B, only two clones were detectable by day 5 (Figure 2B). For population C, all clones were overall less fit in comparison to the parental strain (Figure 2C). For population D, all 12 clones were less fit, with final yields above the limit of detection by day 5 (Figure 2D), ranging from 5×10^3 CFU/ml to 1×10^6 CFU/mL. However, population E, though derived from the same parental strain as population D, produced clones with significantly worse growth yields, resulting in only one clone able to survive at ~$4x10^4$CFU/mL yield by day 5 (Figure 2E). For population F, the yields of 3 clones were below the limit of detection and 9 clones had measurable yields, ranging from 4×10^3 CFU/ml to 1×10^6 CFU/mL, by the end of the experiment on day 5, compared to parental average yields of ~9×10^5 CFU/mL (Figure 2F). The clones taken from population G also grew poorly, with no growth detected throughout the experiment (Figure 2G). Finally, population H yielded no clones that exhibited yields above the detection limit, except for a single clone on day 1, compared to its parental strain that was able to grow in our experimental condition (Figure 2H).

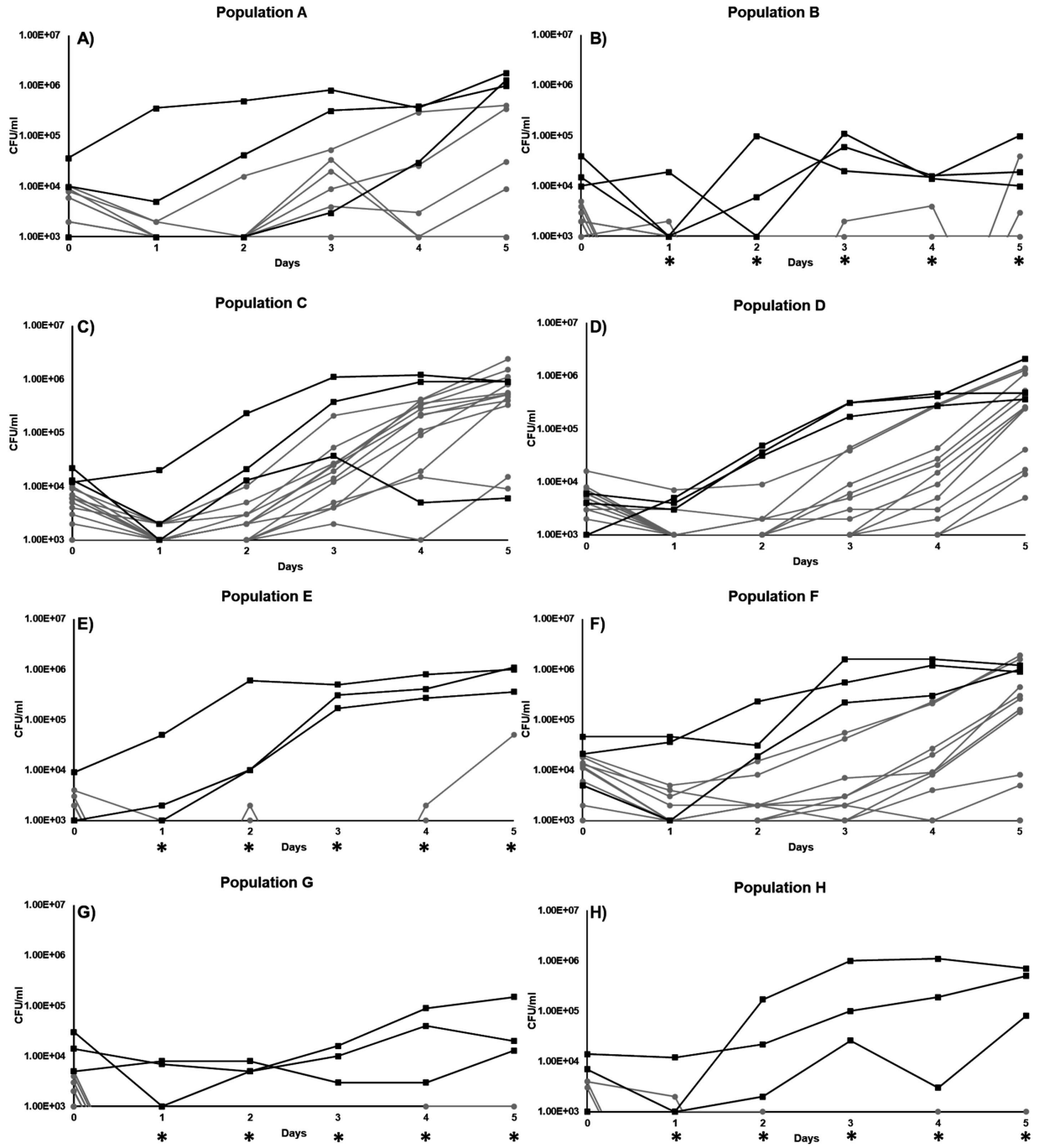

FIGURE 2
Growth curve of individual clones isolated from 8 different populations incubated in minimal DSM-113 low-carbon media: **(A)** Population A, **(B)** Population B, **(C)** Population C, **(D)** Population D, **(E)** Population E, **(F)** Population F, **(G)** Population G, and **(H)** Population H.

Genomic characterization of the parental strains

Genomic sequencing revealed that all seven parental strains (one each from Groups 1, 2, 3, 4, and 8, and two from Group 7) are closely related to each other, with genomes ranging in size from 5,411,111 to 5,411,303 bp, and G + C content of 54.8% (Table 1). Each strain contains from 4,947–4,950 predicted protein coding genes, with a coding density of 89.9%. Though highly isogenic, there are notable differences between strains. First, several major chromosomal inversions exist between strains. Four parental strains from Groups 1, 2, 3, and 8 (referred to as Arrangement I), are fully syntenic with the same arrangement of genes (Figure 3). The parental strain from Group 4 and one of the strains from Group 7, henceforth 7–1, has a different arrangement from Arrangement I (referred to as Arrangement II) due to an inversion between two homologous copies of an IS91 family transposase gene, ISSod25, located at positions 846,036 and 3,511,426 (Figure 3). The other strain from Group 7, henceforth 7–2, has a third arrangement

TABLE 1 Sequencing statistics on the parental *Halomonas* strains.

	Pop. A	Pop. B	Pop. F	Pop. H	Pop. G	Pop. D/E	Pop. C
Assembly size (bp)	54,11,118	54,11,111	54,11,303	54,11,184	54,11,185	54,11,223	54,11,130
G+C Content %	54.8%	54.8%	54.8%	54.8%	54.8%	54.8%	54.8%
Estimated Illumina genome coverage	120	120	120	120	120	120	120
Contigs	1	6	1	1	1	1	1
Protein-coding Genes	4950	4947	4949	4951	4948	4949	4950
tRNA genes	70	70	70	70	70	70	70
rRNA operons	6	6	6	6	6	6	6
Differences between parental strains							
SNPs Upstream of 16S	I	II	I	II	II	I	I
SNP in 23S - I	I	II	I	II	II	I	I
SNPs Downstream of 23S - I				I	I		
Deletion of 7bp	I						
SNP in *bamA*							C -> T
Insertion in ISsod25 600bp		I		I	I		
SNP in RDD Family Protein			T -> A				
SNPs in *lgrB*		II		I	I		
SNPs in intergenic region		GA -> TT					
SNP in hypothetical glycosyl transferase							C -> T
SNPs in *etfB*		I					
Deletion in *etfB*		I					
SNPs Downstream of 23S - II		I		I	I		
SNP in 16S - I			G -> A				
SNPs in 23S - II	II	I	III	II	III	II	III
SNPs in intergenic region		I		I	I		
SNP in UniProt 10802		A -> G					
SNPs Downstream of 23S - II		I		I	I		
SNPs in 23S - II	II	I	III	II	III	II	III
SNP in 16S - I			G -> A				
SNP in *tctB*			142 A -> C 156 A -> T	147 C -> G	147 C -> G 156 A -> T	147 C -> G	147 C -> G
Insertion of C in *tctB*							I
SNP in *soxZ*							G -> T

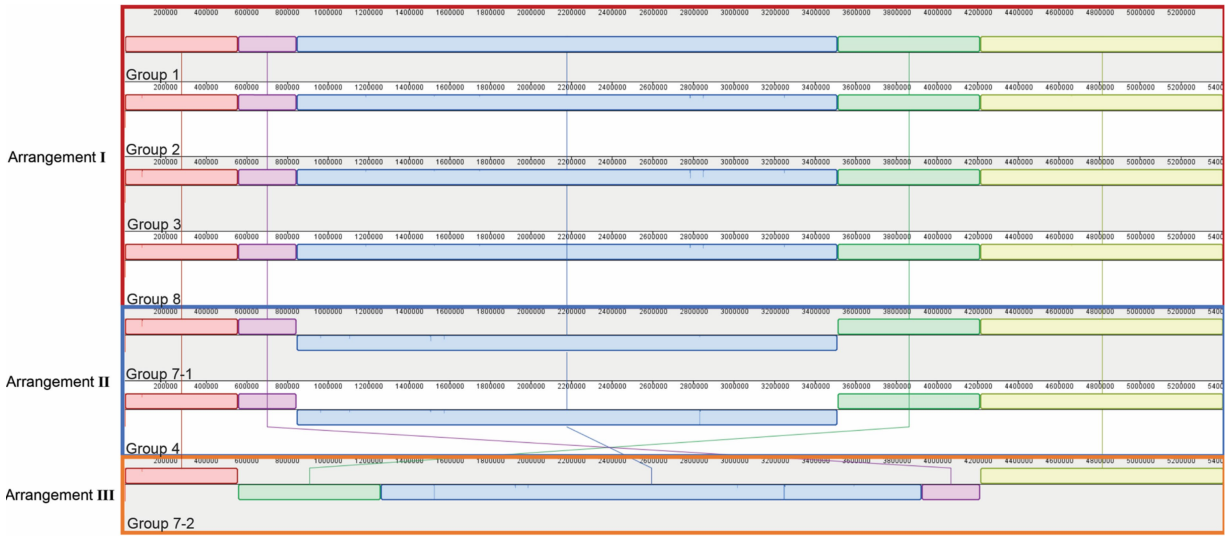

FIGURE 3
Genomic rearrangements of the parental *Halomonas* strains. Parental strains were aligned using progressiveMauve algorithm and resulted in 5 different colored locally collinear blocks (LCB). An LCB is defined as a homologous region of sequence shared by two or more genomes. LCBs above the line represent the top-strand and LCBs below the line represent the bottom strand. Lines spanning across the strains indicate the position of the LCB relative.

(referred to as Arrangement III), with an inversion between the 23S rRNA genes located at positions 556,910 and 4,214,392 compared to Arrangement I. Another difference is in the genomic sequences that primarily differ from one another through insertions of a repeated sequence in the intergenic regions. This causes the difference in genome sizes while the protein-coding regions of the genome are almost entirely

TABLE 2 List of mutations common to more than one in the evolved clone.

	position	mutation	annotation	gene	# of clones with the mutation	description	(putative) function
Population A	17,13,424	Δ8,194 bp		*[A_01630]–[A_01635]*	3	*[A_01630], mshB, A_01632, btuD_6, tagG, [A_01635]*	A_01630 - hypothetical glycosyltransferase *mshB* - N-acetyl-1-D-myo-inosityl-2-amino-2-deoxy-alpha-D-glucopyranoside deacetylase A_01632 - hypothetical GNAT Family N-acetyltransferase *btuD* - Vitamin B12 import ATP-binding protein *tagG* - Teichoic acid translocation permease protein
	17,21,485	Δ5 bp	coding (302–306/3117 nt)	*A_01635 →*	1	hypothetical protein	A_01635 - DUF4214 domain-containing protein
	17,21,613	+GTAG	coding (430/3117 nt)	*A_01635 →*	1	hypothetical protein	A_01635 - DUF4214 domain-containing protein
Population B	41,57,406	$(GAATCGT)_{10\rightarrow11}$	coding (164/330 nt)	*B_03905 ←*	1	hypothetical protein	HAD-IB family hydrolase (truncated)
	42,46,076	G→A	Q259* (CAA→TAA)	*B_03980 ←*	1	hypothetical protein	DUF4214 domain-containing protein
	42,46,364	G→A	Q163* (CAG→TAG)	*B_03980 ←*	4	hypothetical protein	DUF4214 domain-containing protein
	42,46,524	Δ10 bp	coding (318–327/3117 nt)	*B_03980 ←*	6	hypothetical protein	DUF4214 domain-containing protein
	42,46,596	Δ289 bp		*[B_03980]*	1	*[B_03980]*	DUF4214 domain-containing protein
Population F	34,41,978	G→A	L8L (CTG→CTA)	*C2_03293 →*	1	hypothetical protein	hypothetical metallopeptidase
	34,42,610	G→T	G219V (GGC→GTC)	*C2_03293 →*	1	hypothetical protein	hypothetical metallopeptidase
Population H	17,21,215	G→A	intergenic (−439/−14)	*tagG ← / → C4_01636*	1	Teichoic acid translocation permease protein TagG/hypothetical protein	C4_01636 - DUF4214-containing-protein
	17,21,247	C→T	Q7* (CAA→TAA)	*C4_01636 →*	1	hypothetical protein	DUF4214 domain-containing protein
	17,21,305	+G	coding (77/3117 nt)	*C4_01636 →*	1	hypothetical protein	DUF4214 domain-containing protein
	17,21,480	C→G	Y64* (TAC→TAG)	*C4_01636 →*	2	hypothetical protein	DUF4214 domain-containing protein
	17,21,840	+TG	coding (612/3117 nt)	*C4_01636 →*	1	hypothetical protein	DUF4214 domain-containing protein
	17,21,867	+C	coding (639/3117 nt)	*C4_01636 →*	1	hypothetical protein	DUF4214 domain-containing protein
Population G	26,33,807	Δ848 bp	coding (431–1278/3117 nt)	*D_02501 ←*	3	hypothetical protein	DUF4214 domain-containing protein
	30,28,071	A→C	T383P (ACA→CCA)	*D_02899 →*	3	hypothetical protein	hypothetical metallopeptidase
Population D	26,34,679	Δ305 bp	coding (40–344/3117 nt)	*E_02501 ←*	1	hypothetical protein	DUF4214 domain-containing protein
	26,34,683	G→A	Q114* (CAA→TAA)	*E_02501 ←*	2	hypothetical protein	DUF4214 domain-containing protein
	26,34,787	+T	coding (236/3117 nt)	*E_02501 ←*	2	hypothetical protein	DUF4214 domain-containing protein
	26,34,932	Δ223 bp		*[E_02501]*	3	*[E_02501]*	DUF4214 domain-containing protein
	26,34,958	Δ1 bp	coding (65/3117 nt)	*E_02501 ←*	2	hypothetical protein	DUF4214 domain-containing protein
	26,34,959	C→T	A22T (GCC→ACC)	*E_02501 ←*	2	hypothetical protein	DUF4214 domain-containing protein
	46,62,573	A→T	I52N (ATC→AAC)	*E_04370 ←*	3	hypothetical protein	tripartite tricarboxylate transporter TctB
	46,62,581	G→C	A49A (GCC→GCG)	*E_04370 ←*	2	hypothetical protein	tripartite tricarboxylate transporter TctB
Population E	25,45,578	$(GAATCGT)_{10\rightarrow11}$	coding (164/330 nt)	*E_02426 ←*	2	hypothetical protein	HAD-IB family hydrolase (truncated)
	26,33,429	Δ1 bp	coding (1594/3117 nt)	*E_02501 ←*	1	hypothetical protein	DUF4214 domain-containing protein
	26,34,787	+T	coding (236/3117 nt)	*E_02501 ←*	5	hypothetical protein	DUF4214 domain-containing protein
Population C	17,21,104	Δ407 bp		*[H_01634]*	1	*[H_01634]*	DUF4214 domain-containing protein
	17,21,314	$(T)_{5\rightarrow4}$	coding (124/3117 nt)	*H_01634 →*	2	hypothetical protein	DUF4214 domain-containing protein
	46,62,479	A→T	D52E (GAC→GAA)	*H_04371 ←*	3	hypothetical protein	tripartite tricarboxylate transporter TctB
	46,62,488	G→C	A49A (GCC→GCG)	*H_04371 ←*	2	hypothetical protein	tripartite tricarboxylate transporter TctB

Color Scheme (Orange = Deletions; Blue = Insertions; Green = Nonsense mutations; Gray = nonsynonymous mutations; Yellow = synonymous mutations; Purple = Mutations in intergenic region). *Corresponds to a Stop Codon.

identical. The most notable differences within the protein coding genes are differences in length and sequence of a hypothetical protein that is predicted to be a homolog of *tctB*, a tricarboxylate transporter (Rosa et al., 2018); a SNP in another hypothetical protein that is predicted to be a quinoprotein dehydrogenase-associated SoxYZ-like carrier, which is a carrier complex involved in sulfur oxidation; and a SNP in the gene *lgrB*, which codes for gramicidin synthase, a protein involved in the biosynthesis of a pentadecapeptide antibiotic (Table 1). Of these mutations, *tctB* had the highest variability, where the majority of the strains contain different SNPs in this gene. Finally, there are differences in the 23S rRNA sequences of these strains. While the sizes of the 23S rRNA genes are almost identical, parental strains from Group 3 and Group 7 (both 7–1, and 7–2), have two copies of their 23S rRNA genes that differ from the rest of the strains. This difference is found from position 1,464 bp to 1,510 bp, which is located in the V3 region (Helix 58) of the *Escherichia coli* 23S rRNA gene.

Individual evolved clones contain mutations in nutrient transporter, metal and glycosyl transferases, catabolic enzymes, and other fundamental metabolic activity genes

To further understand the possible mechanisms that enable *Halomonas* to scavenge scarce nutrients in unsupplemented minimal medium in the laboratory, and possibly the natural world, we sequenced the aforementioned 12 clones from each of the 8 evolved populations (A through H), giving a total of 96 independent clones. In total, there were 32 loci with unique mutations across the 96 clones (Tables 2, 3). Four of those loci had been mutated in more than one independently evolved population. It is important to note that, where the same locus has been mutated, the molecular basis of the mutations differs in each of the cultures, supporting an independent origin for each of these mutations. Each of the four genes with multiple mutations encode hypothetical proteins, and using blastx,[2] were identified as: (i) a putative tripartite tricarboxylate transporter (*tctB*) family protein, (ii) a DUF4214 domain-containing protein (DUF stands for Domain of Unassigned Function), (iii) a putative metallopeptidase, and (iv) a HAD-IB family hydrolase. Surprisingly, the DUF4214 domain-containing protein was mutated in 7 out of the 8 evolved populations (A, B, C, D, E, G, and H). Each of the mutations in this coding region were unique and include nonsynonymous mutations, frame-shift mutations, small and large indels, nonsense mutations, and mutations in putative regulatory regions upstream of the gene (Tables 2, 3). In addition, the 3 other protein coding genes were mutated in 2 different strains. As shown in Table 2, populations B and E had mutations in a gene that encodes a putative HAD-IB family hydrolase; in this case, the same insertion mutation occurred in the same location in both strains. Populations C and D had mutations in the gene that codes for a hypothetical tripartite tricarboxylate transporter. In both strains, the codons for amino acids 49 and 52 of the protein were mutated. While both strains have the identical mutation of A49A, a synonymous mutation of GCC to GCG, amino acid 52 in population D had the mutation I52N, while population C had the mutation D52E (Table 2). Lastly, populations F and G had mutations in the gene that encodes a hypothetical metallopeptidase. In addition to these mutations, all evolved populations contained unique mutations. Among these genes were those involved in the biosynthesis of sugars and amino acids, transcriptional regulation, transport of metals across membranes,

2 blast.ncbi.nlm.nih.gov

TABLE 3 List of all mutations group by GO classification in all evolved clones.

Population	Function	position	mutation	annotation	gene	# of clones with mutation	description
A	Biosynthesis	17,60,636	A→T	E299D (GAA→GAT)	*ribD* →	1	Riboflavin biosynthesis protein RibD
G		34,41,958	G→A	A862V (GCA→GTA)	*alaS* ←	1	Alanine--tRNA ligase
H		12,65,860	C→T	R160R (CGC→CGT)	*ilvG* →	1	Acetolactate synthase isozyme 2 large subunit
G		31,71,160	T→C	T5217A (ACA→GCA)	*lgrB* ←	8	Linear gramicidin synthase subunit B
E		23,26,144	G→A	H277H (CAC→CAT)	*hisZ* ←	1	ATP phosphoribosyltransferase regulatory subunit
E		25,13,918	A→T	Y970* (TAT→TAA)	*mshA_5* ←	1	D-inositol-3-phosphate glycosyltransferase
A	Regulation	50,97,743	$(ATAG)_{2\rightarrow1}$	coding (260-263/606 nt)	*glaR_4* ←	1	HTH-type transcriptional repressor GlaR
B		23,39,779	Δ10 bp	coding (447-456/894 nt)	*rhaS_2* ←	1	HTH-type transcriptional activator RhaS
C		11,05,226	G→C	V133V (GTC→GTG)	*dmlR_6* ←	1	HTH-type transcriptional regulator DmlR
G		28,43,337	C→A	E170* (GAG→TAG)	*eryD* ←	1	Erythritol catabolism regulatory protein EryD
B	Transport	3,75,929	T→A	C21S (TGT→AGT)	*B_00400* →	1	hypothetical nuclear transport factor 2 family protein
F		40,55,924	T→A	R142W (AGG→TGG)	*C2_03820* ←	5	hypothetical RDD family protein
F		4,23,206	$(CCACGA)_{11\rightarrow10}$	coding (186-191/726 nt)	*C2_00416* →	1	hypothetical metal binding protein ZinT
H		6,65,841	C→T	A544V (GCC→GTC)	*bamA* →	11	Outer membrane protein assembly factor BamA
H		50,79,369	G→A	D240N (GAC→AAC)	*phnE_3* →	1	Phosphate-import permease protein PhnE
D		47,80,476	$(CGACCA)_{9\rightarrow8}$	coding (462-467/1044 nt)	*znuA* →	1	High-affinity zinc uptake system protein ZnuA
C		25,05,127	C→T	P356P (CCC→CCT)	*H_02348* →	1	hypothetical NnrS family protein [Halomonas]
B	Metabolism	19,61,707	G→A	V179V (GTG→GTA)	*B_01835* →	1	hypothetical allantoinase PuuE
C		9,21,021	C→T	F277F (TTC→TTT)	*oadB* →	1	Oxaloacetate decarboxylase beta chain
E		24,82,809	G→T	R1769L (CGC→CTC)	*tdh_1* →	1	L-threonine 3-dehydrogenase
C		52,19,131	+G	coding (192/933 nt)	*C1-hpah* ←	1	p-hydroxyphenylacetate 3-hydroxylase, reductase component
A	Stress Response	8,69,965	C→T	D230D (GAC→GAT)	*dinB* →	1	DNA polymerase IV
H		9,10,121	G→C	G44A (GGT→GCT)	*recA* →	1	Protein RecA
H		28,94,205	A→T	K54N (AAA→AAT)	*lexA_3* →	1	LexA repressor
E	Unknown Function	3,76,946	G→T	L141M (CTG→ATG)	*E_00367* ←	1	Copper resistance protein CopD family protein
E		7,40,161	G→C	T24T (ACC→ACG)	*E_00732* ←	1	TIGR03643 Family Protein
F	Intergenic	19,22,726	$(GCCTCAC)_{8\rightarrow6}$	intergenic (+201/+3)	*C2_01852* → / ← *guaD*	1	5S ribosomal RNA/Guanine deaminase
G		3,65,749	G→T	intergenic (-44/-204)	*D_00355* ← / → *dipZ_2*	3	Peroxiredoxin/Protein DipZ
G		28,32,133	+TT	intergenic (-41/+47)	*D_02698* ← / ← *talB_1*	2	putative ketoamine kinase/Transaldolase B
C		18,59,703	$(GATTCAC)_{11\rightarrow10}$	intergenic (+445/+8)	*pgm* → / ← *H_01750*	1	Phosphoglucomutase/hypothetical SLC13 family permease
C		18,59,709	$(GATTCAC)_{11\rightarrow12}$	intergenic (+451/+8)	*pgm* → / ← *H_01750*	1	Phosphoglucomutase/hypothetical SLC13 family permease
C		28,48,445	$(TGAGGCG)_{8\rightarrow9}$	intergenic (+59/+158)	*guaD* → / ← *H_02679*	1	Guanine deaminase/5S ribosomal RNA

*Corresponds to a Stop Codon.

purine metabolism, and the starvation and SOS stress responses. In particular, there were 7 unique mutations that were found in genes encoding known or putative transport functions, two of which are Zinc binding proteins. The detailed descriptions of all mutations identified are listed in Table 3.

Potential functions of the predicted DUF4214 domain protein

One particular gene, encoding a DUF4214 domain, was mutated in all but one evolved population, suggesting that its function was under negative selection during adaptation to rich medium. To begin determining the unknown function of the DUF4214 domain-containing-protein (referred to as Halo4214 henceforth), we used Phyre2, SWISS-MODEL, and PredictProtein to identify potential functional regions. The predicted gene product consists of 1,038 amino acids (and is likely to contain multiple domains). Phyre2 identified 19 different protein alignment templates and mapped the hypothetical protein onto these templates with >90% confidence. Out of the 19 proteins identified, 6 indicated similarity with a hydrolase. Two templates matched this protein with the highest confidence (99.2%), and both encode a lipase: the extracellular lipase, *lipA,* from *Serratia marcescens* and a lipase from a *Pseudomonas* sp. organism. For the extracellular lipase, 32% coverage was aligned from residues 598–936 and, for the *Pseudomonas* lipase, 38% coverage was aligned from residues 565–966, significantly overlapping the enzyme from *Serratia*. Further, the PredictProtein algorithm associated the hypothetical protein to Gene Ontology terms related to S-layer surface proteins, extracellular protein regions, cell wall components, and calcium ion binding domain. The SWISS-MODEL software aligned 88 amino acids (S16-V104) to the S-layer protein from *Caulobacter crescentus*. From these results, we hypothesize that this large protein is likely to have multiple domains, where one domain anchors itself to the outer membrane of the cell, while another domain functions as an extracellular lipase.

Discussion

The diversity of mechanisms that allow bacteria to survive in low-carbon, low-energy natural environments is not well understood (Flint, 1987). In the subseafloor, this question is of particular interest due to the challenging nature of its environments, spanning wide gradients in temperature, pressure, and carbon and nutrient availability (Cario et al., 2019). Microbes inhabiting these environments often need to survive and/or grow with scarce nutrient availability, constantly changing environments, and competition with other organisms, while maintaining cellular repair, homeostasis, and replication machinery (Haruta and Kanno, 2015; Orcutt et al., 2013). The *Halomonas* strains isolated from the crustal fluids of North Pond in the Atlantic Ocean were subjected to experimental adaptive evolution selection to enrich for mutants that have lost their ability to scavenge for scarce nutrients, with the goal of identifying genes potentially responsible for the ability to grow under low nutrient conditions.

As gammaproteobacteria, *Halomonas* strains are ubiquitous and found in ocean waters, lakes, fermented foods, hydrothermal vents, as animal symbionts, and many other environments that span a range of both pH and temperature (Kaye et al., 2011; de la Haba et al., 2014).

The *Halomonas* strains we studied here can grow in rich medium at elevated temperature (30°C), which is a growth condition in stark contrast to the cold (4–15°C), oligotrophic environment where they originated. *Halomonas* isolated from deep-sea environments, lakes, estuaries, and coastal waters are known to be able to grow on a wide range of carbon sources including glucose, galactose, arabinose, ethanol, and amino acids, among others (Kaye et al., 2011). However, this characteristic ability to consume a wide range of carbon sources is not unique to the *Halomonas*. Among many marine bacteria adapted to oligotrophic environments, *Sphingomonas* sp. strain RB2256 and *Marinobacter* strains also exhibit the ability to grow in rich medium (Kaye et al., 2011; Eguchi et al., 1996). For RB2256, growth rate does not alter when inoculated using various amounts of carbon source, differed in growth characteristics depending on whether or not carbon was present in the media.

The genomic rearrangements observed between the parental strains (Figure 3) raises several important questions. The extremely similar genomic content and DNA sequences that are shared between all seven parental strains (one each from Groups 1, 2, 3, 4, and 8, and two from Group 7) strongly support a model where all sequenced strains share an ancestral parental genotype. Whether this ancestor is one of the isolates studied here or from prior generations, the similarity that is shared between these strains suggests two possibilities for the colonization of these waters: (i) either there was substantial selection for the genomic content of these *Halomonas* strains among the myriad of other *Halomonas* sp. that could occupy the crustal fluids, or (ii) a single ancestor strain was the founder strain of all the *Halomonas* that entered this crustal fluid environment. Further, the intraspecies diversity of 23S rRNA genes that is observed within the strains studied here suggests that several mutational events have occurred during the colonization of this environment. Among the six rRNA gene clusters, parental strains from Group 3 and Group 7 (Strains 7–1 and 7–2) share 2 copies of a different 23S ribosomal RNA gene compared to the rest of the parental strains.

We observe that homologous rRNA exists in different genomic arrangements, and the opposite, where heterologous rRNA existing in the same genomic arrangements (Figures 3, 4). For example, parental strains from Group 1 and 4 have different genomic arrangements, but consists of essentially the same rRNA sequences. In contrast, the parental strains from Group 1 and 8 share the same genomic arrangement but have different copies of rRNAs within their genomes. This observation may give insight into the origins of the strains' diversity. For example, one ancestral strain might have undergone an inversion and gave rise to another arrangement, which was then followed by mutations in different 23S ribosomal RNA genes, giving rise to what we now call a different parental strain Group. The reverse could also be true, where mutations were first gained (i.e., parental strains from Arrangement I) and an inversion mutation may have occurred later. A graphical illustration of one potential pattern of events, based on the observed rRNA gene sequences, is shown in Figure 4.

To begin to address whether the similarities in the strains studied here are due to a potential "founder effect," we examined the genomes of other *Halomonas* species obtained from open-ocean and coastal environments that contain at least two different strains within the same species. When comparing their aligned genomes, significantly

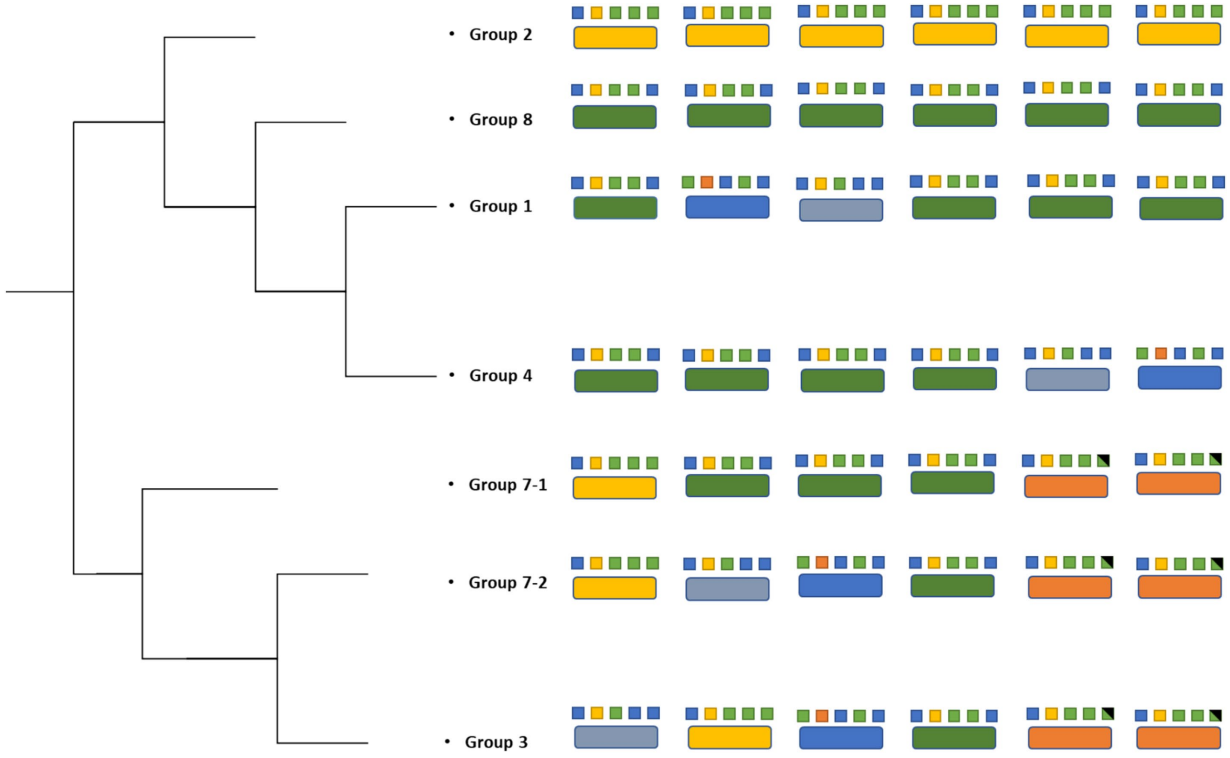

FIGURE 4
Strain phylogenetic tree based on the 23S rRNA. Different colors in large boxes represent unique rRNA sequences. Colors in the small boxes represent combinations of SNPs that constitute each unique rRNA.

less similarity is observed in these intraspecies genomes compared to the North Pond samples. For example, three different strains were analyzed from the species *Halomonas titanicae* (ANRCS81, GPM3, and SOB56), and three from *Halomonas meridiana* (Slthf1, Eplume2, and SCSIO 43005). An analysis of those genomes shows a lower degree of synteny of strains within each species (while sharing genomic content; Supplementary Figure 2), compared to the *Halomonas* strains studied here. This analysis further supports a model where the *Halomonas* strains isolated from the North Pond site were likely to have been founded by a single strain that became the source of all the subsequent diversity identified.

Despite the high degree of similarity of their genomes, the growth dynamics of the seven parental strains (one each from Groups 1, 2, 3, 4, and 8, and two from Group 7) differed from each other when incubated in LB medium at 30°C (Figure 1). The differences that are observed may be due to the small number of genomic differences observed within each population. For example, the differences in tripartite tricarboxylate transporter between 5 of the populations may lead to variance in the ability of the microbes to transport carboxylate groups across the membrane, which in turn may cause differences in the observed growth and survival patterns.

As each population underwent serial passage and adaptive evolution in LB, the evolved cells began to achieve maximum cell density in rich medium very quickly compared to the parental strains, indicating that the populations were experiencing adaptive evolution. From these evolved populations, a total of 96 clones were sequenced, with the objective of identifying mutations that resulted in these populations performing less well than their parental strains in minimal medium with no added carbon (Figure 2). The isolation of individual clones from each population, instead of a metagenomic population sample, allowed us to pinpoint specific genotypes that may drive the overall growth phenotype of the population, as well as those specific mutant loci resulting in reduced fitness under nutrient stress (Ratib et al., 2021).

A compelling observation in this study is the identification of many different mutations affecting same gene (which we refer to as Halo4214) in different populations, corresponding with a significant loss of fitness under low-nutrient conditions. Protein structure/function prediction algorithms indicate that the N-terminus region of Halo4214 most closely resembles an S-layer (surface layer) protein domain, suggesting that the protein is likely on the extracellular side of the outer membrane, and may be anchored to the peptidoglycan (Yang et al., 2016). The C-terminus region aligns with the gene *lipA*, an extracellular lipase found in *Serratia marcescens* and other species (Chen et al., 2021). While *S. marcescens* contains several genes encoding lipases (Tully et al., 2018), *lipA* is relatively large at 613 amino acid residues, producing a 64.9 kDa protein and is involved in catalysis of esters, including membrane-derived glycerides (Akatsuka et al., 1994; Adetunji and Olaniran, 2021). In another organism, *Candidatus* Dechloromonas occultata, DUF4214 surface proteins are thought to assemble into an S-layer protein-anchored enzyme that reduces manganese nodules (Wang et al., 2009; Szeinbaum et al., 2020; Sleytr et al., 2014). Together these data suggest that Halo4214 is possibly an anchored extracellular enzyme that helps breakdown extracellular lipids prior to transfer into the cell.

In our experimental approach, following ~300 generations of laboratory adaptive evolution, growth in LB led to the selection of mutants with little to no activity of the Halo4214 gene (the mutations are predominantly deletions, early stop codons, and frameshifts; Table 2) and consequently decreased the strains' viability in the low nutrient DSMZ-113 medium with no added carbon. This is consistent with our hypothesis, in which cells that have adapted to LB will experience an antagonistic pleiotropy toward the genes that are relied on in the crustal fluid environments. In nature, it is known that exoenzymes play an important role for prokaryotes in degrading surrounding organic matter, especially in nutrient-limited settings (Boetius and Lochte, 1996; Engelen et al., 2008). These same exoenzymes may be counter-selective under the rich nutrient conditions of LB-medium cultures.

Another gene that was mutated across several populations is the gene encoding a hypothetical Tripartite Tricarboxylate Transporter, TctB family protein, identified as E_04370 in populations D and E, and H_04371 in population C (Table 2). Tripartite Tricarboxylate Transporters (TTT) are one of the three families of Solute-Binding Protein-dependent systems that are known to be important for high-affinity uptake of substrates including tricarboxylic acids and dicarboxylic acids, even allowing uptake of substrates at very low concentrations (Rosa et al., 2018). The best known of the TTT system proteins is the citrate transporter TctC that is commonly found in proteobacteria (Rosa et al., 2018). TctB is part of the TctABC system that is believed to be a symporter that uses an electrochemical ion-gradient for solute transport; TctB itself, however, is a polymorphic protein that has a putative transmembrane-spanning α-helix, but otherwise unknown function (Rosa et al., 2018; Winnen et al., 2003).

Genes involved in metal binding, primarily zinc, are also mutated frequently in our experiment (Tables 2, 3). A notable gene that had mutations in two different populations is the hypothetical metallopeptidase found in populations F and G. Metallopeptidases are typically secreted enzymes used to break down peptides up to 40 residues in length, such as bradykinin (Page et al., 2015). These enzymes are widespread among bacteria, and have been found in deep-sea microbes, including deep-sea *Shewanella* sp. E525-6 (Weissman et al., 2021). Other genes that involve metal binding properties where mutations were found include *zinT* and *znu*A (Table 3), both of which are involved in the transport of zinc into the cell (Graham et al., 2009; Yatsunyk et al., 2008).

Finally, the gene encoding a hypothetical HAD-IB family hydrolase, a family of enzymes known to catalyze bond cleavages through reaction with water (Table 2), was also mutated in more than one population. These mutations in the same gene in multiple populations indicate that the gene is selected against in rich medium. This result indicates that it may be costly to maintain this gene function in this environment, but perhaps necessary for survival under low nutrient conditions such as the crustal fluids. The genes where mutations arise across multiple populations all appear to encode activities directly related to the acquisition of nutrients: surface proteins, extracellular enzymes, and transport systems for metals and peptides. This pattern is consistent with the mutated genes that are unique to individual clones as well (Table 2), such as the aforementioned *zinT* and *znuA* genes involved in the recruitment of zinc (Graham et al., 2009), the surface proteins gene for outer membrane assembly *bamA*, and enzymes involved in catabolism such as threonine dehydrogenase.

This study shows that crustal fluid microbes are capable of adaptive evolution under laboratory conditions, and this nutrient-rich laboratory environment can select for mutants that have lost the ability to grow in a low-nutrient medium, more similar to crustal fluid environments from which they were originally isolated. Following ~300 generations of incubation in rich medium, these

microbes accumulated mutations in catabolic enzymes, transporters, and transcriptional regulators. One hypothetical protein that is shared among these populations was independently mutated multiple times, and we hypothesize it to be a cell-associated extracellular lipase. The selection against this hypothetical protein is evidence that its activity may be deleterious in nutrient-rich environments, while essential for growth and survival in low-nutrient environments, based on the poor growth in that environment post-evolution. Future work including experiments controlling gene expression to directly monitor fitness in different environments, along with determination of the crystal structure of the protein, may help to elucidate the function of this protein further. Together, these data provide first clues into the types of activities that may be essential for long-term survival of microbes isolated from crustal fluid environments. In doing so, these data also demonstrate the potential utility of using laboratory adaptive evolution-based techniques to gain insight into these mechanism of scavenging for scarce nutrients.

Data availability statement

The original contributions presented in the study are publicly available. This data can be found here: PRJNA1224213.

Author contributions

HS: Conceptualization, Data curation, Formal analysis, Investigation, Methodology, Resources, Software, Validation, Visualization, Writing – original draft, Writing – review & editing. AR: Conceptualization, Formal analysis, Methodology, Writing – review & editing. DR: Conceptualization, Data curation, Investigation, Methodology, Resources, Writing – review & editing. AA: Data curation, Formal analysis, Investigation, Methodology, Resources, Validation, Visualization, Writing – review & editing. SD'H: Conceptualization, Formal analysis, Funding acquisition, Investigation, Methodology, Writing – review & editing. JH: Conceptualization, Data curation, Formal analysis, Funding acquisition, Investigation, Methodology, Resources, Validation, Writing – review & editing. SF: Conceptualization, Formal analysis, Funding acquisition, Methodology, Project administration, Resources, Supervision, Validation, Visualization, Writing – original draft, Writing – review & editing.

Funding

The author(s) declare financial support was received for the research and/or publication of this article. The Gordon and Betty Moore Foundation sponsored most of the observatory components at North Pond through grant GBMF1609. This work was supported by NSF OCE-1062006, OCE-1745589 and OCE-1635208 to JH. The Center for Dark Energy Biosphere Investigations (C-DEBI OCE-0939564) also supported the participation of all authors.

Acknowledgments

We thank the captain and crew of the R/V Merian, the pilots and engineers of the ROV Jason II, and the shipboard science party of MSM37 for sample collection, especially Chief Scientist Heinrich Villinger and the fluid collection team including J-P Baquiran, K. Becker, S. Carr, B. Glazer S. Hulme, B. Kraft, A. Sturm, and C. G. Wheat for their work in accomplishing the field programs and returning precious samples to Woods Hole. J. Delaney, H-T. Lin, B. Orcutt, M. Rappe, and E. Reddington provided critical shoreside support as well. Ship time was provided by the German Science Foundation (DFG). We thank Douglas Bartlett for providing both additional *Halomonas* strains. Both Katrina Edwards's and James Cowen's efforts were critical to the field component and success of the North Pond project; Jan Amend led C-DEBI for over a decade and this collaboration grew out of his exceptional leadership. They are all missed. This is C-DEBI contribution number 620. S. D'Hondt is a CIFAR Fellow in the Earth 4D: Subsurface Science and Exploration Program.

Conflict of interest

The authors declare that the research was conducted in the absence of any commercial or financial relationships that could be construed as a potential conflict of interest.

Generative AI statement

The authors declare that no Gen AI was used in the creation of this manuscript.

Publisher's note

Supplementary material

The Supplementary Material for this article can be found online at: https://www.frontiersin.org/articles/10.3389/fmicb.2025.1511421/full#supplementary-material

References

Adetunji, A. I., and Olaniran, A. O. (2021). Production strategies and biotechnological relevance of microbial lipases: a review. *Braz. J. Microbiol.* 52, 1257–1269. doi: 10.1007/s42770-021-00503-5

Akatsuka, H., Kawai, E., Omori, K., Komatsubara, S., Shibatani, T., and Tosa, T. (1994). The *lipA* gene of *Serratia marcescens* which encodes an extracellular lipase having no N-terminal signal peptide. *J. Bacteriol.* 176, 1949–1956. doi: 10.1128/jb.176.7.1949-1956.1994

Anderson, R. E., Graham, E. D., Huber, J. A., and Tully, B. J. (2022). Microbial populations are shaped by dispersal and recombination in a low biomass subseafloor habitat. *Environ. Microbiol.* 13:e0035422. doi: 10.1128/mbio.00354-22

Boetius, A., and Lochte, K. (1996). Effect of organic enrichments on hydrolytic potentials and growth of bacteria in deep-sea sediments. *Mar. Ecol. Prog. Ser.* 140, 239–250. doi: 10.3354/meps140239

Cario, A., Oliver, G. C., and Rogers, K. L. (2019). Exploring the deep marine biosphere: challenges, innovations, and opportunities. *Front. Earth Sci.* 7:225. doi: 10.3389/feart.2019.00225

Chen, H., Yu, F., Shi, N., Du, P., Liu, S., Zhang, X., et al. (2021). Overexpression and mutation of a novel lipase from *Serratia marcescens* L1 in *Escherichia coli*. *Process Biochem.* 111, 233–240. doi: 10.1016/j.procbio.2021.11.001

Darling, A. C. E., Mau, B., Blattner, F. R., and Perna, N. T. (2004). Mauve: multiple alignment of conserved genomic sequence with rearrangements. *Genome Res.* 14, 1394–1403. doi: 10.1101/gr.2289704

Deatherage, D. E., and Barrick, J. E. (2014). Identification of mutations in laboratory-evolved microbes from next generation sequencing data using breseq. *Methods Mol. Biol.* 1151, 165–188. doi: 10.1007/978-1-4939-0554-6_12

de la Haba, R. R., Arahal, D. R., Sánchez-Porro, C., and Ventosa, A. (2014). "The family *Halomonadaceae*" in *The prokaryotes*. eds. E. Rosenberg, E. F. DeLong, S. Lory, E. Stackebrandt and F. Thompson (Berlin, Heidelberg: Springer).

Edwards, K. J., Bach, W., Klaus, A., and the Expedition 336 Scientists (2012a). Proceedings of the Integrated Ocean Drilling Program Volume 336 Expedition Reports Mid-Atlantic ridge microbiology: initiation of long-term coupled microbiological, geochemical, and hydrological experimentation within the seafloor at north pond, western flank of the mid-Atlantic ridge. *IODP Sci. Prosp.* 336. doi: 10.2204/iodp.sp.336.2010

Edwards, K. J., Wheat, C. G., Orcutt, B., Hulme, S., Becker, K., Jannasch, H., et al. (2012b). "Design and deployment of borehole observatories and experiments during IODP expedition 336, mid-Atlantic ridge flank at north pond" in *And the expedition 336 scientists, proc. IODP*. eds. K. J. Edwards, W. Bach and A. Klaus, vol. *336* (Tokyo: Integrated Ocean Drilling Program).

Eguchi, M., Nishikawa, T., Macdonald, K., Cavicchioli, R., Gottschal, J. C., and Kjelleberg, S. (1996). Responses to stress and nutrient availability by the marine Ultramicrobacterium Sphingomonas sp. strain RB2256. *Appl. Environ. Microbiol.* 62, 1287–1294. doi: 10.1128/aem.62.4.1287-1294.1996

Engelen, B., Ziegelmüller, K., Wolf, L., Köpke, B., Gittel, A., Cypionka, H., et al. (2008). Fluids from the oceanic crust support microbial activities within the deep biosphere. *Geomicrobiol J.* 25, 56–66. doi: 10.1080/01490450701829006

Ewing, B., Hillier, L., Wendl, M. C., and Green, P. (1998). Base-calling of automated sequencer traces usingPhred. *I. Accuracy assessment. Genome Res.* 8, 175–185. doi: 10.1101/gr.8.3.175

Farrell, M. J., and Finkel, S. E. (2003). The growth advantage in stationary-phase phenotype conferred by rpoS mutations is dependent on the pH and nutrient environment. *J. Bacteriol.* 185, 7044–7052. doi: 10.1128/JB.185.24.7044-7052.2003

Finkel, S. (2006). Long-term survival during stationary phase: evolution and the GASP phenotype. *Nat. Rev. Microbiol.* 4, 113–120. doi: 10.1038/nrmicro1340

Flint, K. P. (1987). The long-term survival of *Escherichia coli* in river water. *J. Appl. Bacteriol.* 63, 261–270. doi: 10.1111/j.1365-2672.1987.tb04945.x

GitHub, Inc. An open source software for the QC and adapter trimming of ONT technologies. Available at: https://github.com/rrwick/Porechop

Graham, A. I., Hunt, S., Stokes, S. L., Bramall, N., Bunch, J., Cox, A. G., et al. (2009). Severe zinc depletion of *Escherichia coli* roles for high affinity zinc binding by zinT, zinc transport and zinc-independent proteins. *J. Biol. Chem.* 284, 18377–18389. doi: 10.1074/jbc.M109.001503

Haruta, S., and Kanno, N. (2015). Survivability of microbes in natural environments and their ecological impacts. *Microbes Environ.* 30, 123–125. doi: 10.1264/jsme2.ME3002rh

Illumina, Inc. bcl2fastq: a proprietary Illumina software for the conversion of bcl files to basecalls. Available at: https://support.illumina.com/sequencing/sequencing_software/bcl2fastq-conversion-software.html

Kaye, J. Z., Sylvan, J. B., Edwards, K. J., and Baross, J. A. (2011). *Halomonas* and *Marinobacter* ecotypes from hydrothermal vent, subseafloor and deep-sea environments. *FEMS Microbiol. Ecol.* 75, 123–133. doi: 10.1111/j.1574-6941.2010.00984.x

Kelly, D. P., and Wood, A. P. (2000). Reclassification of some species of Thiobacillus to the newly designated genera Acidithiobacillus gen. nov., Halothiobacillus gen. nov. and Thermithiobacillus gen. nov. *Int. J. Syst. Evol. Microbiol.* 50, 511–516. doi: 10.1099/00207713-50-2-511

Kraigsley, A. M., and Finkel, S. E. (2009). Adaptive evolution in single species bacterial biofilms. *FEMS Microbiol. Lett.* 293, 135–140. doi: 10.1111/j.1574-6968.2009.01526.x

Kram, K. E., and Finkel, S. E. (2014). Culture volume and vessel affect long-term survival, mutation frequency, and oxidative stress of *Escherichia coli*. *Appl. Environ. Microbiol.* 80, 1732–1738. doi: 10.1128/AEM.03150-13

Kram, K. E., and Finkel, S. E. (2015). Rich medium composition affects *Escherichia coli* survival, glycation, and mutation frequency during long-term batch culture. *Appl. Environ. Microbiol.* 81, 4442–4450. doi: 10.1128/AEM.00722-15

Kram, K. E., Geiger, C., Ismail, W. M., Lee, H., Tang, H., Foster, P. L., et al. (2017). Adaptation of *Escherichia coli* to long-term serial passage in complex medium: evidence of parallel evolution. *mSystems* 2:e00192-16. doi: 10.1128/mSystems.00192-16

Larkin, M. A., Blackshields, G., Brown, N. P., Chenna, R., McGettigan, P. A., McWilliam, H., et al. (2007). Clustal W and Clustal X version 2.0. *bioinformatics* 23, 2947–2948. doi: 10.1093/bioinformatics/btm404

LaRowe, D. E., Koch, B. P., Robador, A., Witt, M., Ksionzek, K., and Amend, J. (2017). Identification of organic compounds in ocean basement fluids. *Org. Geochem.* 113, 124–127. doi: 10.1016/j.orggeochem.2017.07.017

Meyer, J. L., Jaekel, U., Tully, B. J., Glazer, B. T., Wheat, C. G., Lin, H., et al. (2016). A distinct and active bacterial community in cold oxygenated fluids circulating beneath the western flank of the mid-Atlantic ridge. *Sci. Rep.* 6:22541. doi: 10.1038/srep22541

Navarro Llorens, J. M., Tormo, A., and Martinez-Garcia, E. (2010). Stationary phase in gram-negative bacteria. *FEMS Microbiol. Rev.* 34, 476–495. doi: 10.1111/j.1574-6976.2010.00213.x

Nystrom, T. (2004). Stationary-phase physiology. *Ann. Rev. Microbiol.* 58, 161–181. doi: 10.1146/annurev.micro.58.030603.123818

Orcutt, B. N., D'Angelo, T., Jungbluth, S. P., Huber, J. A., and Sylvan, J. B. (2020). Microbial life in oceanic crust. *OSF [Preprints]*. doi: 10.31219/osf.io/2wxe6

Orcutt, B. N., LaRowe, D. E., Biddle, J. F., Colwell, F. S., Glazer, B. T., Reese, B. K., et al. (2013). Microbial activity in the marine deep biosphere: progress and prospects. *Front. Microbiol.* 4:189. doi: 10.3389/fmicb.2013.00189

Orcutt, B. N., Wheat, C. G., Rouxel, O., Hulme, S., Edwards, K. J., and Bach, W. (2013). Oxygen consumption rates in subseafloor basaltic crust derived from a reaction transport model. *Nat. Commun.* 4:2539. doi: 10.1038/ncomms3539

Page, A. J., Cummins, C. A., Hunt, M., Wong, V. K., Reuter, S., Holden, M. T. G., et al. (2015). Roary: rapid large-scale prokaryote pan genome analysis. *Bioinformatics* 31, 3691–3693. doi: 10.1093/bioinformatics/btv421

Price, A. N., Fisher, A. T., Stauffer, P. H., and Gable, C. W. (2022). Numerical simulation of cool hydrothermal processes in the upper volcanic crust beneath a marine sediment pond: north pond, North Atlantic Ocean. *JGR Solid Earth* 127:e2021JB023158. doi: 10.1029/2021JB023158

Ratib, N. R., Seidl, F., Ehrenreich, I. M., and Finkel, S. E. (2021). Evolution in long-term stationary-phase batch culture: emergence of divergent *Escherichia coli* lineages over 1, 200 days. *mBio* 12:123. doi: 10.1128/mBio.03337-20

Robador, A. (2024). The subseafloor crustal biosphere: Ocean's hidden biogeochemical reactor. *Front. Microbiol.* 15:1495895. doi: 10.3389/fmicb.2024.1495895

Robador, A., Jungbluth, S. P., LaRowe, D., Bowers, R., Rappé, M., Amend, J., et al. (2015). Activity and phylogenetic diversity of sulfate-reducing microorganisms in low-temperature subsurface fluids within the upper oceanic crust. *Front. Microbiol.* 5:748. doi: 10.3389/fmicb.2014.00748

Robador, A., LaRowe, D. E., Jungbluth, S. P., Lin, H., Rappe, M. S., Nealson, K. H., et al. (2016). Nanocalorimetric characterization of microbial activity in deep subsurface oceanic crustal fluids. *Front. Microbiol.* 7:454. doi: 10.3389/fmicb.2016.00454

Rolfe, M. D., Rice, C. J., Lucchini, S., Pin, C., Thompson, A., Cameron, A. D., et al. (2012). Lag phase is a distinct growth phase that prepares bacteria for exponential growth and involves transient metal accumulation. *J. Bacteriol.* 194, 686–701. doi: 10.1128/JB.06112-11

Rosa, L. T., Bianconi, M. E., Thomas, G. H., and Kelly, D. J. (2018). Tripartite ATP-independent periplasmic (TRAP) transporters and tripartite Tricarboxylate transporters (TTT): from uptake to pathogenicity. *Front. Cell. Infect. Microbiol.* 8:33. doi: 10.3389/fcimb.2018.00033

Schloss, P. D., Westcott, S. L., Ryabin, T., Hall, J. R., Hartmann, M., Hollister, E. B., et al. (2009). Introducing mothur: open-source, platform-independent, community-supported software for describing and comparing microbial communities. *Appl. Environ. Microbiol.* 75, 7537–7541. doi: 10.1128/AEM.01541-09

Seemann, T. (2014). Prokka: rapid prokaryotic genome annotation. *Bioinformatics* 30, 2068–2069. doi: 10.1093/bioinformatics/btu153

Seyler, L. M., Trembath-Reichert, E., Tully, B. J., and Huber, J. A. (2021). Time-series transcriptomics from cold, oxic subseafloor crustal fluids reveals a motile, mixotrophic microbial community. *ISME J.* 15, 1192–1206. doi: 10.1038/s41396-020-00843-4

Shah Walter, S. R., Jaekel, U., Osterholz, H., Fisher, A. T., Huber, J. A., Pearson, A., et al. (2018). Microbial decomposition of marine dissolved organic matter in cool oceanic crust. *Nat. Geosci.* 11, 334–339. doi: 10.1038/s41561-018-0109-5

Sleytr, U. B., Schuster, B., Egelseer, E., and Pum, D. (2014). S-layers: principles and applications. *FEMS Micro Rev.* 38, 823–864. doi: 10.1111/1574-6976.12063

Szeinbaum, N., Nunn, B. L., Cavazos, A. R., Crowe, S. A., Stewart, F. J., DiChristina, T. J., et al. (2020). Novel insights into the taxonomic diversity and molecular mechanisms of bacterial Mn (III) reduction. *Environ. Microbiol.* 12, 583–593. doi: 10.1111/1758-2229.12867

Trembath-Reichert, E., Shah Walter, S. R., Ortiz, M. A. F., Carter, P. D., Girguis, P. R., and Huber, J. A. (2021). Multiple carbon incorporation strategies support microbial survival in cold subseafloor crustal fluids. *Sci. Adv.* 7:18. doi: 10.1126/sciadv.abg0153

Tully, B. J., Wheat, C. G., Glazer, B. T., and Huber, J. A. (2018). A dynamic microbial community with high functional redundancy inhabits the cold, oxic subseafloor aquifer. *ISME J.* 12, 1–16. doi: 10.1038/ismej.2017.187

Wang, X., Schroder, H. C., Schlobmacher, U., and Muller, W. E. G. (2009). Organized bacterial assemblies in manganese nodules: evidence for a role of S-layers in metal deposition. *Geo Mar. Lett.* 29, 85–91. doi: 10.1007/s00367-008-0125-3

Wang, Y., Zhao, Y., Bollas, A., Wang, Y., and Fai-Au, K. (2021). Nanopore sequencing technology, bioinformatics and applications. *Nat. Biotechnol.* 39, 1348–1365. doi: 10.1038/s41587-021-01108-x

Weissman, J. L., Hou, S., and Fuhrman, J. A. (2021). Estimating maximal microbial growth rates from cultures, metagenomes, and single cells via codon usage patterns. *Proc. Natl. Acad. Sci.* 118:e2016810118. doi: 10.1073/pnas.2016810118

Wick, R. R., Judd, L. M., Gorrie, C. L., and Holt, K. E. (2017). Unicycler: resolving bacterial genome assemblies from short and long sequencing reads. *PLoS Comput. Biol.* 13:e1005595. doi: 10.1371/journal.pcbi.1005595

Winnen, B., Hvorup, R. N., and Saier, M. H. Jr. (2003). The tripartite tricarboxylate transporter (TTT) family. *Res. Microbiol.* 154, 457–465. doi: 10.1016/S0923-2508(03)00126-8

Yang, J. Y., Wang, P., Li, C. Y., Dong, S., Song, X. Y., Zhang, X. Y., et al. (2016). Characterization of a new M13 metallopeptidase from Deep-Sea *Shewanella* sp. E525-6 and mechanistic insight into its catalysis. *Front. Microbiol.* 6:1498. doi: 10.3389/fmicb.2015.01498

Yatsunyk, L. A., Easton, J. A., Kim, L. R., Sugarbaker, S. A., Bennett, B., Breece, R. M., et al. (2008). Structure and metal binding properties of Znu A, a periplasmic zinc transporter from *Escherichia coli*. *J. Biol. Inorg. Chem.* 13, 271–288. doi: 10.1007/s00775-007-0320-0

Zhang, X., Feng, X., and Wang, F. (2016). Diversity and metabolic potentials of subsurface crustal microorganisms from the Western flank of the mid-Atlantic ridge. *Front. Microbiol.* 7:363. doi: 10.3389/fmicb.2016.00363

frontiers | Frontiers in Microbiology

TYPE Perspective
PUBLISHED 29 April 2025
DOI 10.3389/fmicb.2025.1524057

OPEN ACCESS

EDITED BY
Alberto Robador,
University of Southern California,
United States

REVIEWED BY
Luigi Jovane,
University of São Paulo, Brazil

*CORRESPONDENCE
Elva Escobar-Briones
✉ escobri@cmarl.unam.mx

RECEIVED 07 November 2024
ACCEPTED 14 April 2025
PUBLISHED 29 April 2025

CITATION
Montoya L and Escobar-Briones E (2025) Unveiling the significance of prokaryotic composition from ferromanganese crusts regarding the interlink between cobalt and vitamin B_{12} in deep-sea ecosystems. *Front. Microbiol.* 16:1524057. doi: 10.3389/fmicb.2025.1524057

Unveiling the significance of prokaryotic composition from ferromanganese crusts regarding the interlink between cobalt and vitamin B_{12} in deep-sea ecosystems

Lilia Montoya[1] and Elva Escobar-Briones[2]*

[1]Consejo Nacional de Humanidades, Ciencias y Tecnologías, Mexico City, Mexico, [2]Instituto de Ciencias del Mar y Limnología, Universidad Nacional Autonoma de Mexico, Mexico City, Mexico

The intricate relationship between prokaryotic vitamin B_{12} (cobalamin) producers and metazoans in deep-sea ecosystems, particularly within ferromanganese crusts and polymetallic nodules, is critical for understanding oceanic biogeochemical cycling of cobalt. Microbial communities are key regulators of essential biogeochemical cycles, with cobalt serving as a vital component in the synthesis of cobalamin, a metallocofactor indispensable for numerous metabolic processes. We analyzed the significance of cobalamin biosynthetic pathways confined to prokaryotes and emphasized the ecological importance of auxotrophic organisms that rely on exogenous sources of vitamin B_{12}. Additionally, we recognize recent research regarding the spatial distribution of dissolved cobalt and its consequential effects on cobalamin production and bioavailability, indicating the scarcity of cobalt and cobalamin in marine environments. We propose that cobalt-rich environments may foster unique interactions between prokaryotic and eukaryotic organisms, potentially altering the food web dynamics owing to the localized abundance of this element. By investigating the roles of cobalt and cobalamin in nutrient cycling and interspecies interactions, we outlined key criteria for future research on deep-sea microbial communities and their contributions to the cobalt biogeochemical cycle.

KEYWORDS

food web, meiofauna, prokaryotes, biogeochemical cycling, auxotrophy

1 Introduction

Microbial communities represent most of the ocean's diversity and are of fundamental importance in maintaining the functionality and stability of global ocean ecosystems. Microorganisms, while not strictly essential for survival, play a pivotal role in regulating marine C, N, P, and S biogeochemical cycles. However, trace elements (<0.1 μM) are also required for growth and are interlinked with the global biogeochemical cycles of macro and microelements (Giovannelli, 2023). One such example is cobalt (Co), as cobalt and iron cycles are co-regulated by phytoplankton, as they require both nutrients for optimal growth, and the availability of one can influence the utilization of the other (Chmiel et al., 2022).

In addition, Co is used for numerous metabolic functions, including non-corrin Co-containing enzymes such as methionine aminopeptidase, prolidase, nitrile hydratase, glucose isomerase, methylmalonyl-CoA carboxytransferase, aldehyde decarbonylase, lysine-2,3-aminomutase, and bromoperoxidase (Okamoto and Eltis, 2011).

We focused on cobalt as a central constituent of the corrin cofactor cobalamin or vitamin B_{12} present in early life as methanogenesis (Buan, 2018) and globally as phytoplankton, particularly cyanobacteria, which have an absolute requirement for cobalamin (Chmiel et al., 2022). Cobalamin has been demonstrated to be of crucial importance in trophic networks from several environments, including marine systems. Consequently, Co can limit certain metabolic pathways, potentially restricting the metabolic niches of cobalamin synthesis and auxotrophy, and incentivizing ecological relationships linked to the acquisition of vitamin B_{12}, such as predation and symbiosis.

The sensitivity of trophic networks to Co has been studied in Co-depleted systems with nutrient amendments. In this regard, we propose to study sites naturally characterized by a high abundance of cobalt. We specifically refer to ferromanganese nodules and cobalt-rich crusts, which are mineral deposits found on the deep ocean floor that are enriched in metals, such as manganese, iron, copper, nickel, and cobalt. These mineral concretions are recognized as important habitats that support a unique deep-sea biodiversity (Rabone et al., 2023).

We review the importance of understanding the sources and delivery pathways of vitamin B_{12} in marine ecosystems, particularly those linked to polymetallic nodules and cobalt crusts, considering that the bioavailability of cobalt may regulate its use in different life forms. This allowed us to gain new insights into the biogeochemical cycling of Co in deep-sea ecosystems.

2 Cobalamin: structure, biosynthesis and ecological significance

2.1 Cobalamin is a corrinoid with cobalt

Coenzyme B_{12} is the only vitamin that contains metal ions; therefore, it is an organometallic cofactor. It also has the most complex structure and largest formula weight, with a chemical structure characterized by a tetrapyrrole with a central Co atom (Figure 1). Cobalamin is derived from the same porphyrin precursor as heme and chlorophyll and the F_{420} coenzyme. It has the most complex structure of any biological cofactor (Bryant et al., 2020) and contains a tetrapyrrole corrin ring surrounding a central Co atom with an oxidation state of 3+. The fifth coordinated position of Co is occupied by a dimethyl-benzimidazole nucleotide loop, and the sixth catalytic upper ligand position is occupied by either a methyl group or deoxyadenosine, leading to methylcobalamin (MeCbl) or deoxyadenosylcobalamin (AdoCbl), respectively (Doxey et al., 2015; Figure 1).

The main driving force for the utilization of Co is the chemistry of this transition metal. The essential ability of Co is to form metal-carbon bonds, which is facilitated by its powerful nucleophilicity. Three cobalt oxidation states participate in the functioning of the B_{12} coenzyme: Co^{+}, Co^{2+}, and Co^{3+} (Okamoto and Eltis, 2011), each in a coordinated manner and a spatial arrangement facilitated by conformational rearrangements in the corrin ring (Osman et al., 2021).

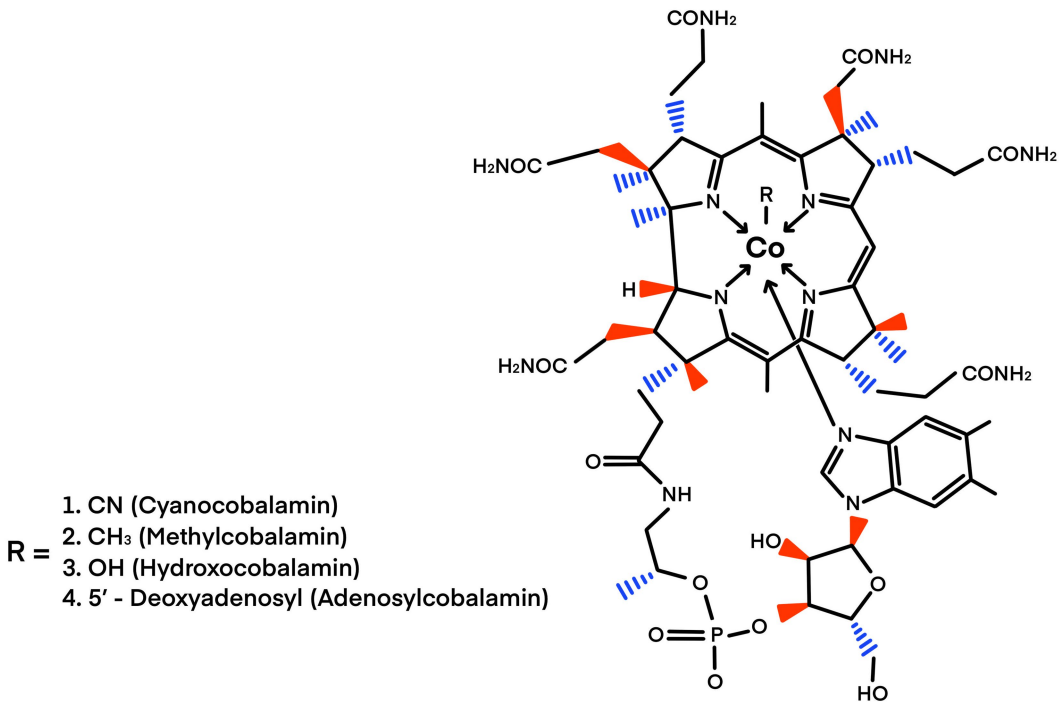

FIGURE 1
Structure of cobalamin. The cobalt ion is coordinated equally to the four pyrrolic nitrogen atoms of the corrin macrocycle. Cobalamines differ in their sixth ligand (R –). The sixth ligand differentiates between the cofactors cyanocobalamin, methylcobalamin, hydroxocobalamin, and adenosylcobalamin. Modified from Buckel (2007). Credit design: L. Montoya and C. F. Franco-Rodríguez.

2.2 Biosynthetic pathways for cobalamin

There are essentially two alternative cobalamin biosynthetic routes in bacteria and archaea, aerobic and anaerobic. These routes differ primarily in the contraction stage of the macrocycle: (a) the late insertion pathway is an aerobic pathway because cobalt is inserted into the tetrapyrrole macrocycle after ring contraction, where molecular oxygen is a prerequisite; and (b) the early insertion pathway can operate under anaerobic conditions, where cobalt is chelated before ring contraction (Scott and Roessner, 2002). Despite the differences in the timing of cobalt insertion and the mechanism of ring contraction, many other enzymes associated with methylation and amidations operate in the same order along the pathway (Osman et al., 2021).

In natural ecosystems, B_{12} biosynthesis is energetically expensive and imposes a high metabolic burden on the B_{12} producers. The cobalamin biosynthetic pathway (aerobic or anaerobic) is one of the most complex pathways in nature, requiring approximately 20 enzymes for complete *de novo* synthesis, starting with cobalt (Co^{2+}) (Warren et al., 2002). Cofactors are often imported by cobalamin producers, a strategy that is energetically more favorable than biosynthesis (Nijland et al., 2022).

2.3 Metabolic processes dependent on cobalamin

Coenzyme B_{12} or cobalamin-dependent enzymes are mainly included in the following groups: (a) transferases (E.C. 2.x.x.x), such as methylcobalamin (MeCbl)-dependent transferases and (b) isomerases (E.C. 5.x.x.x), such as adenosylcobalamin (AdoCbl) deoxyadenosyl cobalamin-dependent isomerase (Table 1). These catalysts are present in both prokaryotes and eukaryotes and reductive dehalogenases (E.C. 1.x.x.x) are found only in organohalide-respiring bacteria (Giedyk et al., 2015).

TABLE 1 Metabolism processes linked to cobalamin are denoted as cobalamin-dependent enzymes (Buckel, 2007; Degnan et al., 2014).

MTR	Methyltetrahydromethanopterin:coenzyme M methyltransferase	2.1.1.86
Mta/Mtt	Methanol/methylamine/trimethylamine methyltransferases	2.1.1.247
Lyases		
PduCDE	Propanediol dehydratase/Glycerol dehydratase	4.2.1.28/4.2.1.30
EutBC	Ethanolamine ammonia-lyase	4.1.3.7
Isomerases		
MCM/SpcA/MutAB	Methylmalonyl-CoA mutase	5.4.99.2
Mgm	2-methyleneglutarate mutase	5.4.99.4
GlmES	Glutamate mutase, metylaspartate mutase	5.4.99.1
IcmAB	Isobutyryl-CoA mutase	5.4.99.13
KamED	b-Lysine 5,6-aminomutase	5.4.3.3
OraSE	D-ornithine 4,5-aminomutase	5.4.3.5

MeCbl serves as the intermediate carrier of activated methyl groups. During the catalytic cycle, the coenzyme shuttles between MeCbl and the highly nucleophilic cobalamin form (Giedyk et al., 2015). Examples of MeCbl-dependent enzymes include methionine synthase, which is a cytosolic methionine synthase (formation of methionine) (Balabanova et al., 2021) that reacts with cobalamin-dependent methionine synthesis and DNA synthesis through the conversion of ribonucleotides to deoxyribonucleotides and tRNA biosynthesis (Banerjee and Ragsdale, 2003).

AdoCbl functions as a source of carbon-based free radicals that are unmasked by homolysis of the cobalt-carbon bond of the coenzyme. Free radicals are subsequently used to remove non-acidic hydrogen atoms from substrates to facilitate a variety of reactions involving cleavage of carbon–carbon, carbon–oxygen, and carbon–nitrogen bonds. Most of these reactions involve the migration of hydroxy-, amino-, and carbon-containing groups. In addition, one class of ribonucleotide reductases uses AdoCbl (Giedyk et al., 2015).

2.4 Ecological interactions between cobalamin producers and auxotrophs in marine ecosystems

The natural forms of vitamin B_{12}, MeCbl, and AdoCbl are synthesized only by prokaryotes via aerobic and anaerobic pathways (Balabanova et al., 2021). Cyanobacteria and key taxa within α- and γ-Proteobacteria (Sañudo-Wilhelmy et al., 2014), Actinobacteria, and Bacteroidetes Thaumarchaeota (Doxey et al., 2015; Shelton et al., 2019) are included among the cobalamin producers. The involvement of archaea in cobalamin production is poorly understood; thus, the insight into the cobalamin biosynthesis have mainly focused on bacteria (Table 2). The ability to synthesize cobalamin has neither been inherited by eukaryotes nor has it been subjected to lateral gene transfer (Croft et al., 2005). In eukaryotes, vitamin B_{12} is acquired in two ways:

a Directly from a metabolite pool released by prokaryotes, either through cell lysis of the producers or via passive transport (Romine et al., 2017), benefiting cobalamin-dependent eukaryotic consumers, such as the diatom *Thalassiosira pseudonana* (Sultana et al., 2023). Several experimental amendments support this, showing that dissolved cobalamin in the ocean stimulates the growth of eukaryotic phytoplankton (Bonnet et al., 2013) and heterotrophic protists (Wienhausen et al., 2022).

b Indirectly through interactions with prokaryotes, such as mutualism, symbiosis, or predation (Joglar et al., 2021). Among marine cultures, symbiosis and mutualism are the most studied interactions. For example, symbiosis has been explored in co-cultures such as *Ostreococcus tauri* and the alphaproteobacterium *Dinoroseobacter shibae* (Cooper et al., 2018). Additionally, it has been hypothesized that marine sponges obtain cobalamin through symbiotic relationships with associated microbes (Degnan et al., 2014).

These mechanisms of eukaryotic acquisition of cobalamin from external sources have shaped ecosystems. In all ecosystems, auxotrophs are organisms that depend on cobalamin, but lack the ability to synthesize these cofactors, including both prokaryotes and eukaryotes

TABLE 2 Cobalamin producers in marine ecosystems (Sañudo-Wilhelmy et al., 2014; Wang J. et al., 2024; Wang L. et al., 2024).

Phylum[1]	Order	Described at polymetallic nodules/cobalt crusts
Cyanobacteria	Chroococcales	No
Cyanobacteria	Prochlorales	No
Cyanobacteria	Nostocales	No
Cyanobacteria	Oscillatoriales	No
α-Proteobacteria	*Mycoplana* (Hyphomicrobiales)	No
α-Proteobacteria	Magnetococcales[2]	Yes (Liu et al., 2024)
α-Proteobacteria	*Rhodobacter* (Rhodobacterales)	Yes (Shulga et al., 2022)
β-Proteobacteria	*Achromobacter* (Burkholderiales)	Yes (Zhang et al., 2023)
γ-Proteobacteria[3]	*Pseudomonas* (Pseudomonadales)	Yes (Zhang et al., 2015)
γ-Proteobacteria	*Halomonas* (Oceanospirillales)	Yes (Zhang et al., 2015)
γ-Proteobacteria	*Marinomonas* (Oceanospirillales)	Yes (Zhang et al., 2015)
γ-Proteobacteria	*Neptuniibacter* (Oceanospirillales)	No
Bacteroidetes	*Flavobacterium* (Flavobacteriales)	Yes (Huo et al., 2015)
Actinobacteria	*Micrococcus* (Micrococcales)	Yes (Bergo et al., 2022)
Actinobacteria	*Corynebacterium*, *Nocardia* (Mycobacteriales)	No
Actinobacteria	*Streptomyces* (Kitasatosporales)	No
Firmicutes	*Bacillus* (Caryophanales)	Yes (Liao et al., 2011)
Thaumarchaeota	Nitrosopumilales	Yes (Hollingsworth et al., 2021)
Thaumarchaeota	Nitrososphaerales	Yes (Hollingsworth et al., 2021)

[1]Proteobacteria were divided into classes.
[2]Magnetococcales have been implicated in the occurrence of biogenic magnetotactic bacteria in polymetallic nodules (Liu et al., 2024).
[3]With the exception of Pseudomonas, Halomonas, Marinomonas, and Neptuniibacter, marine γ-Proteobacteria lack genes for B_{12} synthesis (Sañudo-Wilhelmy et al., 2014).

(Nijland et al., 2022). Examples of auxotrophs are organohalide-respiring bacteria and several eukaryotic lineages, such as vertebrates, most protists, and invertebrates, but not plants, insects, or fungi (Degnan et al., 2014). Intriguingly, higher plants have no cobalamin-dependent enzymes and so do not utilize or synthesize cobalamin (Croft et al., 2006); in comparison, nearly half of marine species are cobalamin auxotrophs (Croft et al., 2005). Eukaryotic auxotrophy has evolved several times, resulting in close and intricate ecological relationships. For example, algae can be influenced by their symbionts, which supply fixed carbon in return for vitamin B_{12} (Grant et al., 2014).

As one of the highly limited nutrients and growth factors controlled by a minority of microbes, B_{12} can be considered as "hard currency" in the global ocean ecosystem (Zhou et al., 2023). Therefore, cobamide sharing creates a network of cobamide-dependent interactions, providing a useful system for studying mechanisms that influence community composition and function (Sokolovskaya et al., 2020). Evidence of this shaping of B vitamins in the photic zone, including vitamin B_{12}, has been studied in the Mediterranean Sea and the Eastern Atlantic Ocean, exploring picoplankton and suggesting that cobalamin is crucial for determining the structure and function of microbial ecosystems (Suffridge et al., 2018).

3 Cobalt and cobalamin in the water column

3.1 Distribution and dynamics of cobalt

Cobalt (Co) is required for the *de novo* synthesis of vitamin B_{12} (Panzeca et al., 2008), as this trace metal serves as the central coordinating ion within the molecule. However, the total dissolved Co concentrations (mainly Co^{2+} and Co^{3+}) are relatively low, ranging from 3 to 120 picomolar (pM) in the open ocean (Saito and Moffett, 2002), and only a small fraction of this Co pool is thought to exist in the bioavailable dissolved form as Co^{2+} (Panzeca et al., 2009). Generally, dissolved metals, including Co, increase with depth because of the release associated with the decomposition of organic matter (Gerringa et al., 2021). In comparison, at the surface, dissolved cobalt exhibits low concentrations and high variability, whereas in the ocean interior, cobalt concentrations increase from the surface to intermediate waters and decline in the deep ocean (Tagliabue et al., 2018). Considering the low cobalt concentrations and chemical speciation, the total dissolved cobalt pool of redox state 2+, suitable for B_{12} synthesis, is very low, within the femtomolar (fM) range (Panzeca et al., 2008). This low Co (II) content is consistent with the proportional distribution of dissolved B_{12} in the North Atlantic Ocean according to the abundance of total dissolved Co availability (Panzeca et al., 2009). A similar conclusion was reported by Hawco et al. (2020), who found that Co could limit the growth of the cyanobacterium, *Prochlorococcus*, in the Pacific Ocean.

3.2 Cobalamin availability

Vitamin B_{12} is an energetically costly metabolite, which may explain why less than 40% of prokaryotes encode the genes required for its complete biosynthesis (Shelton et al., 2019). In the open ocean, vitamin B_{12} concentrations range from sub-picomolar to picomolar (Sañudo-Wilhelmy et al., 2012). This distribution is influenced by Co availability (Moore et al., 2013), which plays a role in shaping the ecological structure. Sañudo-Wilhelmy et al. (2006) conducted field-based vitamin B_{12} amendment experiments and observed an increase in phytoplankton biomass, leading to the recognition of this metallocofactor as a limiting factor in some marine ecosystems (Wang L. et al., 2024). Additionally, cobalt has been identified as playing a secondary role in biogeochemical interactions, such as phosphorus, whereas nitrogen and iron remain the primary limiting nutrients (Valiela, 2015).

The concentration of vitamin B_{12} in seawater varies significantly across marine regions. For instance, in coastal areas, cobalamin levels range from undetectable to 30 pM (Sañudo-Wilhelmy et al., 2012). Additionally, it has been reported that coastal waters generally contain higher concentrations of vitamin B_{12} compared to open ocean waters (Sañudo-Wilhelmy et al., 2012; Heal et al., 2017). A similar trend was observed when comparing water depths, with lower vitamin B_{12} concentrations found in deeper waters (100–200 m) than in surface and subsurface waters (0–100 m) (Bonnet et al., 2013).

Cobalamin *de novo* synthesis in surface waters has been linked to heterotrophic Proteobacteria bacteria, mainly Rhodobacterales (Gómez-Consarnau et al., 2018), and to photoautotrophic Cyanobacteria synthesizing pseudocobalamin with a peak concentration within the euphotic zone (Heal et al., 2017). These cobalamin providers are related to different biogeographic settings, including the Mediterranean Sea and Eastern Atlantic Ocean (Suffridge et al., 2018), Northwest Atlantic Ocean (Soto et al., 2023), subtropical, equatorial, polar frontal Pacific Ocean (Wienhausen et al., 2022), and North Pacific Ocean (Heal et al., 2017).

Cobalamin compounds (cyanocobalamin, methylcobalamin, and hydroxycobalamin; Figure 1) are labile after aerobic light exposure, even in various aqueous solutions (Vaid et al., 2018). The photosensitivity of cobalamin is attributed to the dissociation of covalent cobalt-carbon bonds upon exposure to light, resulting in its photolabile characteristics (Vaid et al., 2018; Bannon et al., 2024). Consequently, enzymatic reactions involving cobalamin must be conducted under dim light (Giedyk et al., 2015).

4 Polymetallic nodules and cobalt crusts: key study sites in cobalt biogeochemistry

4.1 Generalities of polymetallic nodules and cobalt crusts

Polymetallic nodules and cobalt-rich crusts are classified in the same paragenetic group (Hazen and Morrison, 2022). Their formation involves complex interactions among geological, chemical, and biological processes that occurr over millions of years (Wang and Müller, 2009). Nodules develop through three main types of precipitation: hydrogenesis refers to the growth of nodules through the direct precipitation of metals from the water column, whereas diagenesis involves the growth of nodules through the precipitation of metals from the sediment pore water. Mixed-type nodules contain layers formed by both hydrogenesis and diagenesis (Benites et al., 2018; Hein et al., 2020). Hydrogenetic nodules form on the sediment surface in well-oxygenated environments where sedimentation rates are low because of the direct supply and precipitation of metallic elements from seawater and diagenetically unenriched sediment pore water (Sujith and Gonsalves, 2021). These nodules are mainly composed of manganese, iron, and trace metals such as nickel (Ni), copper (Cu), cobalt, molybdenum (Mo), and rare earth elements (REE) (Mukhopadhyay et al., 2008). Cobalt crusts are found globally on the ocean floor, generally adjacent to the oxygen minimum zone (OMZ), where less oxidizing conditions prevail (Verlaan and Cronan, 2022). The exposed rock surfaces of the seamounts and ridges are the most concentrated areas. Cobalt-rich crusts occur at shallower depths (<2,500 m) in the deep sea, whereas nodules are formed at much deeper depths (up to 5,500 m) (Verlaan and Cronan, 2022). Initially, it was hypothesized that cobalt precipitates formed solely through inorganic precipitation; however, increasing evidence suggests the involvement of certain bacteria found within nodules and crusts that can oxidize both Mn and Co (Moffett and Ho, 1996; Murray et al., 2007).

4.2 Cobalt enrichment in deep-sea minerals

Both polymetallic nodules and cobalt-rich crusts are enriched in cobalt, Ni, Cd, Zn, and REE, relative to their lower concentrations in seawater (Hawco et al., 2018; Hein et al., 2020). Oxidized cobalt (Co^{3+}) precipitates in the water column and eventually precipitates via hydrogenesis. Cobalt enrichment in nodules can be up to 100-fold higher than its elemental abundance in Earth's crust. Cobalt (II) in seawater can undergo surface oxidation to Co (III) via adsorption onto iron and manganese oxyhydroxides (Koschinsky and Hein, 2003; Wang et al., 2009) in minerals, such as birnessite (Wu et al., 2019). Factors such as sedimentation, oxygen concentration, temperature, and growth rate influence Co enrichment in crusts. Slower rates lead to greater Co accumulation, resulting in an average Co content of up to 0.77% in the crust (Verlaan and Cronan, 2022). These factors explain the higher Co concentration in cobalt crusts than in nodules (Mukhopadhyay et al., 2008). Hydrogenetic-type nodules are characterized by higher Co/Mn ratios (Hein et al., 2020). In cobalt-rich crusts, the Co content ranges from 0.3 to 1.2% (Halbach et al., 2017). Nodules from the Clarion-Clipperton Zone (CCZ) have higher Co concentrations, with an average content of 0.21%, compared to other locations (Hein et al., 2020). The Co oxidation state predominantly exists as +3 and a minor fraction as +2 in these deposits (Wegorzewski et al., 2020).

4.3 Cobalt crusts: a reliable system for comparative studies

Experiments on cobalt limitation or co-limitation of cobalamin availability have shown that B_{12} synthesis can be restricted by cobalt concentrations in certain ocean regions. For example, amendment experiments conducted in waters with low dissolved cobalt (approximately 20 pM) resulted in a two-fold increase in B_{12} production compared to unamended controls (Panzeca et al., 2008). Furthermore, in amendment experiments conducted in the South Atlantic gyre, the addition of cobalt after nitrogen and iron limitation was alleviated, leading to a significant increase in phytoplankton growth (Browning et al., 2017). It has been proposed that cobalamin availability is regulated not only by photodegradation, alteration, and the supply/demand ratio but also by cobalt availability (Bannon et al., 2022). This suggests that, in surface waters, cobalt and light frequently modulate and limit cobalamin availability, as phytoplankton, especially cyanobacteria, are the main sources of this metallocofactor (Heal et al., 2017). However, this scenario is not equivalent to an increase in depth, considering that anoxic ecosystems favor cobalt dissolution, leading to a long residence time for cobalt (Tagliabue et al., 2018).

Therefore, different conditions of cobalamin availability, such as light, phytoplankton distribution, and oxygen concentration, provoke distinctive ecological networks in the deep sea. In this regard, sites enriched in ferromanganese (Fe-Mn) nodules and cobalt crusts are useful for resolving these ecological questions and testing hypotheses. As mentioned earlier, these deposits are broadly characterized by high levels of Mn oxides, where cobalt is incorporated into the octahedral sheets of phyllomanganates, particularly vernadite (δ-MnO_2) (Wegorzewski et al., 2020). A relevant question arises regarding whether cobalamin synthesizers in these regions play a role in supporting local auxotrophic organisms, or whether and to what extent the communities depend on surface sources, such as cyanobacteria, given that previous studies have shown phytodetritus contributes to particulate organic carbon in sediments within the Clarion Clipperton Zone (Cecchetto et al., 2023).

4.4 Thaumarchaeota as potential key players in cobalamin biosynthesis

Thaumarchaeota, formerly known as Crenarchaeota, is a phylum that is frequently found in the deeper waters of the ocean (Heal et al., 2017; Qin et al., 2020). Their distribution is likely due to the sensitivity of ammonia oxidation to light (Merbt et al., 2012). Ammonia-oxidizing archaea (AOA) or Thaumarchaeota strains are typically isolated under dark conditions (Stieglmeier et al., 2014). Indeed, the initial steps of both ammonia-oxidizing pathways, archaeal and bacterial (AOA and AOB, respectively), are inhibited by light (Merbt et al., 2012). In this sense, ammonia-oxidizing archaea are abundant in sediments (coastal and estuarine) (Francis et al., 2005). These archaea are the major cobalamin sources in the oxygen-deficient zone (ODZ) of coastal productive ecosystems (Heal et al., 2017), and as suggested by their genomic potential, they could potentially inhabit bathypelagic habitats (Doxey et al., 2015). Interestingly, Thaumarchaeota, formerly known as Crenarchaeota, is a significant source of vitamin B_{12} in these environments (Heal et al., 2017).

Isolation of the non-cyanobacterial and cobalamin synthesizers *Nitrosopumilus* spp. (Thaumarchaeota), *Sulfitobacter* sp. SA11, and *Ruegeria pomeroyi* DSS-3 (α-Proteobacteria) from deep water support the hypothesis of vertical niche differentiation (Heal et al., 2017). This is particularly noteworthy given that cobalamin itself is photosensitive (Bannon et al., 2024), suggesting an interplay between the light environment and cobalamin dynamics in the ocean. The growth of Thaumarchaeota, also known as AOA, can be promoted by ammonia provided by auxotrophs (Heal et al., 2017; Hollibaugh, 2017). Therefore, in mesophotic ecosystems, only selected cobalamin auxotrophic hosts (bacteria and eukaryotes) provide this essential nutrient for AOA. This contrasts with Cyanobacteria, which have a distinct euphotic ecological niche.

The presence of the cobalamin biosynthetic pathway in an ecosystem implies a level of sustainability at which auxotrophic organisms can thrive only in communities that provide this essential vitamin. In this context, we hypothesized that certain taxa characteristic of these aquatic environments play key roles in cobalamin biosynthesis. In this regard, we highlight the abundance of Thaumarchaeota associated with these concretions, as recognized by the clone library (Shulse et al., 2017) and metagenomic approaches (Zhang et al., 2023). Notably, analysis of bacterial and archaeal 16S rRNA gene sequences from deep-sea polymetallic nodules and sediment extracted from the South Pacific Gyre revealed that the phylum Thaumarchaeota was more abundant in the nodules than in the surrounding sediments (Shiraishi et al., 2016). Based on this, we suggest that members of this archaeal phylum may serve as a source of cobalamin for both prokaryotes and eukaryotes. Furthermore, considering the high cobalt content in cobalt crusts and some polymetallic nodules, it is plausible that, in these habitats, a cobalt-cobalamin connection exists along the food web and involves prokaryotes and metazoans (Figure 2).

Therefore, cobalamin-producing prokaryotes, including Thaumarchaeota, play key roles in linking cobalt and cobalamin. Furthermore, the availability of cobalt, a critical element in the organometallic metabolite cobalamin, may explain the sustainability of auxotrophs in these deep-sea regions. To examine this claim, it is essential to study organisms, such as Thaumarchaeota and other cobalamin producers, as they provide this vital metabolite to auxotrophic bacteria and metazoans. This study aimed to explore the relative abundance of these prokaryotes, and the genetic repertoire associated with cobalamin synthesis in the metazoan microbiome thriving on cobalt crusts and polymetallic nodules and compare them with other deep-sea regions. The relationship between metazoans and their cobalamin-producing symbionts or mutualists may be particularly relevant for bacterivorous meiofauna.

4.5 Proposed ecological networks driven by cobalt and cobalamin availability

Prokaryotic B_{12} sources in some unicellular eukaryotes and metazoans may occur through symbiosis, predation, or commensalism. Within the nodule and cobalt crust communities, some prokaryotes, such as α- and γ-Proteobacteria and Thaumarchaeota, may benefit to other populations with essential vitamin B_{12}. An ecological example to argue this is the commensalism between the auxotrophic algal species *Porphyridium purpureum*, which obtains cobalamin from marine *Halomonas* sp. In return, algae provide γ-Proteobacteria with carbon sources (Croft et al., 2005) and and also acquire cobalamin through particulate organic carbon (POC) and dissolved organic carbon (DOC) (Moran et al., 2022). The implications of cobalt availability modulation on cobalamin synthesis have been demonstrated in surface water samples from the North Atlantic Ocean (Panzeca et al., 2008). Therefore, we propose that contrary to the cobalt limitation prevailing in the North Atlantic Ocean, as reported by Panzeca et al. (2008), cobalt crusts and polymetallic nodules support an abundance of cobalamin synthesizers in the absence of light.

Polymetallic nodules provide crucial hard surfaces for deep-sea benthic life with organisms such as stalked and encrusting sponges (Stratmann et al., 2021). An example is *Plenaster craigi*, an abundant sponge frequently attached to nodules that relies on particulate organic matter, bacteria, and other microbes (Taboada et al., 2018). Some annelids like the polychaeta *Neanthes goodayi* reside inside polymetallic nodules highlight the importance of the mineral itself as microhabitat (Drennan et al., 2021; Neal et al., 2022). In this sense, nodules and crusts represent a cobalt micro-oasis to sessile life that is likely to provide metal content that is beneficial to the synthesis of

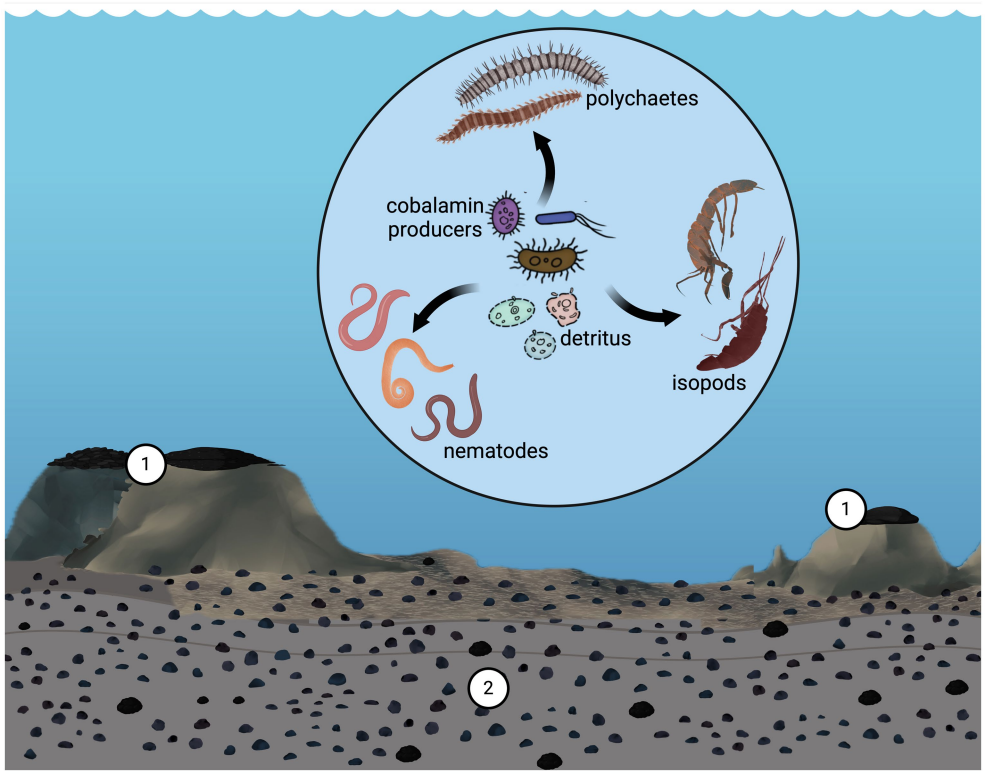

FIGURE 2
Scheme illustrates the proposed interrelationship between cobalt found in cobalt crusts (1) and polymetallic nodules (2), and cobalamin and trophic interactions within the community in these systems, mediated through synthesizers (prokaryotes) and bacterivores. Credit design: L. Montoya and C. F. Franco-Rodríguez.

cobalamine. The experimental extraction of nodules from the Clarion-Clipperton Fracture Zone (CCZ) in the central Pacific has recorded impacts on biodiversity loss and changes in deep-sea water-sediment processes (Bonifácio et al., 2024; Stratmann, 2023; Stratmann et al., 2021). Bacterivores, such as Bryozoa, Cnidaria, Platyhelminthes, and Porifera, are among the most affected ecological groups (Stratmann et al., 2021). Other studies have experimentally focused on Nematoda and found that this taxon does not recover after extraction (Miljutin et al., 2011). These taxa, together with the rotifers and polychaetes present in nodules and crusts, represent a trophic link between bacteria and larger fauna (Stratmann, 2023; Uhlenkott et al., 2023). In this context, we propose a role for cobalt in the loss of taxa induced by nodule extraction. This proposal arises from keeping in mind that model species for some of the phyla described in the CCZ metazoan organisms acquire vitamin B_{12} from bacteria directly by ingestion or commensalism, as cobalamin-producing bacteria are abundant resident gut microbes (Degnan et al., 2014), such as α-, γ-Proteobacteria and Thaumarchaeota (Shulse et al., 2017). Nematodes are noteworthy in this context as they are the most abundant meiobenthic taxon in the ecosystems of nodule-bearing deep-sea sediments (Hauquier et al., 2019). Experimental work with the laboratory nematode *Caenorhabditis elegans* highlights cobalamin limitation, resulting in reduced fertility and longevity (Degnan et al., 2014) and predatory behavior, such as *Pristionchus pacificus*, where vitamin B_{12} is an important inducer (Lo and Sommer, 2022). Additional experimental work has shown symbiotic synthesis of cobalamin in a microbial co-culture of the bacteria *Colwellia* sp. and *Roseovarius* sp. (Wienhausen et al., 2024). Shallow water *Aplysina aerophoba* sponges show B_{12} synthesis dependency on Poribacteria (Siegl et al., 2011). Similar ecological interactions can occur in the mesophotic water columns and seafloor ecosystems.

5 Future research questions for understanding cobalt-cobalamin dynamics in deep-sea ecosystems

The ecological significance of cobalamin (vitamin B_{12}) in other ecosystems remains largely unexplored. Future field studies should clarify the physiological requirements of organisms for cobalamin, particularly the minimum concentration required for growth and survival in the absence of light and oxygen. Laboratory evidence demonstrating the effects of B vitamins, specifically cobalamin, on microplankton has shed light on how marine bacteria fulfill the cobalamin requirements of auxotrophic organisms. For example, key research, such as the co-culture of Ostreococcus tauri with the bacterium *Dinoroseobacter shibae* (Cooper et al., 2018), provides a foundation for analyzing cobalt-rich crust prokaryotic and eukaryotic isolates. In addition, the co-culture approach employed by Wienhausen et al. (2024) further enhances research on prokaryote-prokaryote interactions,

revealing a closer ecological connection where a symbiosis of two bacteria (Colwellia sp. and Roseovarius sp.) is required for complete cobalamin synthesis.

It is crucial to determine whether metazoans living in the absence of light selectively or preferentially ingest cobalamin directly or rely on symbiotic microbes (endo- or exosymbionts) to synthesize and provide cobalamin. Furthermore, investigating whether cobalamin-dependent metabolism offers an advantage to organisms living in environments with high concentrations of cobalt despite the absence of light or oxygen is essential for understanding the occurrence of microbial species that use cobalt and their adaptations.

The potential influence of cobalt availability on deep-sea metazoan distribution owing to cobalamin requirements highlights the urgent need for further research on the ecological implications of cobalt. In this regard, cobalt crusts and nodule habitats are sites for study. Advancements in genomics and metagenomics, particularly regarding the microbiome of metazoans, will be instrumental in characterizing their potential role as vitamin B12 auxotrophs. A valuable strategy for understanding the importance of cobalamin in ocean microbial communities and their integration along the food web will lead to new discoveries (Wang L. et al., 2024).

However, the chemical profile of Co in areas containing Co crusts and polymetallic nodules remains poorly characterized. A thorough investigation of cobalt distribution, particularly its redox speciation, is needed, as is research on abiotic and biotic cobalt oxidation from Co^{2+} to Co^{3+} within these systems, where microorganisms interact with the global cobalt biogeochemical cycle (Swanner et al., 2014). Some approaches already used in this context have involved cobalt amendment experiments (Bannon et al., 2022) and characterization of cobalamin-dependent enzymes (Hawco et al., 2020). This review provides a synthesis for future research determining whether cobalt limits or co-limits ecosystems in the absence of light and/or oxygen.

Studies focused on this topic will not only provide a clearer understanding of this subset of prokaryotes in the global ocean but will also shed light on its function (Zhou et al., 2023). As stated by Moore et al. (2013) and Giovannelli (2023), the distribution and availability of trace elements in the environment are required to understand the diversity of life on the planet.

Data availability statement

The original contributions presented in the study are included in the article/supplementary material, further inquiries can be directed to the corresponding authors.

Author contributions

LM: Conceptualization, Formal analysis, Investigation, Methodology, Visualization, Writing – original draft, Writing – review & editing. EE-B: Formal analysis, Funding acquisition, Project administration, Resources, Supervision, Validation, Writing – review & editing.

Funding

The author(s) declare that financial support was received for the research and/or publication of this article. LM and EE-B acknowledge Instituto de Ciencias del Mar y Limnología, UNAM, Mexico for full coverage of the article processing fee through the yearly budget of EE-B. LM received support from the Consejo Nacional de Humanidades, Ciencias y Tecnologías, Mexico, under grant number 3838403.

Acknowledgments

Credit design for Figures 1, 2: L. Montoya and C. F. Franco-Rodríguez.

Conflict of interest

The authors declare that the research was conducted in the absence of any commercial or financial relationships that could be construed as a potential conflict of interest.

Generative AI statement

The authors declare that no Gen AI was used in the creation of this manuscript.

Publisher's note

References

Balabanova, L., Averianova, L., Marchenok, M., Son, O., and Tekutyeva, L. (2021). Microbial and genetic resources for cobalamin (Vitamin B_{12}) biosynthesis: from ecosystems to industrial biotechnology. *Int. J. Mol. Sci.* 22:4522. doi: 10.3390/ijms22094522

Banerjee, R., and Ragsdale, S. W. (2003). The many faces of vitamin B_{12}: catalysis by cobalamin-dependent enzymes. *Annu. Rev. Biochem.* 72, 209–247. doi: 10.1146/annurev.biochem.72.121801.161828

Bannon, C. C., Mudge, E. M., and Bertrand, E. M. (2024). Shedding light on cobalamin photodegradation in the ocean. *Limnol. Oceanogr. Lett.* 9, 135–144. doi: 10.1002/lol2.10371

Bannon, C., Rapp, I., and Bertrand, E. M. (2022). Community interaction co-limitation: nutrient limitation in a marine microbial community context. *Front. Microbiol.* 13:846890. doi: 10.3389/fmicb.2022.846890

Benites, M., Millo, C., Hein, J., Nath, B. N., Murton, B., Galante, D., et al. (2018). Integrated geochemical and morphological data provide insights into the genesis of ferromanganese nodules. *Fortschr. Mineral.* 8:488. doi: 10.3390/min8110488

Bergo, N. M., Torres-Ballesteros, A., Signori, C. N., Benites, M., Jovane, L., Murton, B. J., et al. (2022). Spatial patterns of microbial diversity in Fe-Mn deposits and associated sediments in the Atlantic and Pacific oceans. *Sci. Total Environ.* 837:155792. doi: 10.1016/j.scitotenv.2022.155792

Bonifácio, P., Kaiser, S., Washburn, T. W., Smith, C. R., Vink, A., and Arbizu, P. M. (2024). Biodiversity of the clarion-Clipperton fracture zone: a worm perspective. *Mar. Biodivers.* 54:5. doi: 10.1007/s12526-023-01396-3

Bonnet, S., Tovar-Sanchez, A., Panzeca, C., Ortega-Retuerta, E., Duarte, C., and Sanudo-Wilhelmy, S. (2013). Geographical gradients of dissolved vitamin B_{12} in the Mediterranean Sea. *Front. Microbiol.* 4:126. doi: 10.3389/fmicb.2013.00126

Browning, T. J., Achterberg, E. P., Rapp, I., Engel, A., Bertrand, E. M., Tagliabue, A., et al. (2017). Nutrient co-limitation at the boundary of an oceanic gyre. *Nature* 551, 242–246. doi: 10.1038/nature24063

Bryant, D. A., Hunter, C. N., and Warren, M. J. (2020). Biosynthesis of the modified tetrapyrroles—the pigments of life. *J. Biol. Chem.* 295, 6888–6925. doi: 10.1074/jbc.REV120.006194

Buan, N. R. (2018). Methanogens: pushing the boundaries of biology. *Emerg. Top. Life Sci.* 2, 629–646. doi: 10.1042/ETLS20180031

Buckel, W. (2007). "Cobalamin coenzymes and vitamin B_{12}" in *eLS*. ed. M. Maccarrone (Chichester: John Wiley & Sons Ltd.).

Cecchetto, M. M., Moser, A., Smith, C. R., Van Oevelen, D., and Sweetman, A. K. (2023). Abyssal seafloor response to fresh phytodetrital input in three areas of particular environmental interest (APEIs) in the western clarion-Clipperton zone (CCZ). *Deep-Sea Res. I Oceanogr. Res. Pap.* 195:103970. doi: 10.1016/j.dsr.2023.103970

Chmiel, R., Lanning, N., Laubach, A., Lee, J. M., Fitzsimmons, J., Hatta, M., et al. (2022). Major processes of the dissolved cobalt cycle in the north and equatorial Pacific Ocean. *Biogeosciences* 19, 2365–2395. doi: 10.5194/bg-19-2365-2022

Cooper, M. B., Kazamia, E., Helliwell, K. E., Kudahl, U. J., Sayer, A., Wheeler, G. L., et al. (2018). Cross-exchange of B-vitamins underpins a mutualistic interaction between Ostreococcus tauri and *Dinoroseobacter shibae*. *ISME J.* 13, 334–345. doi: 10.1038/s41396-018-0274-y

Croft, M. T., Lawrence, A. D., Raux-Deery, E., Warren, M. J., and Smith, A. G. (2005). Algae acquire vitamin B_{12} through a symbiotic relationship with bacteria. *Nature* 438, 90–93. doi: 10.1038/nature04056

Croft, M. T., Warren, M. J., and Smith, A. G. (2006). Algae need their vitamins. *Eukaryot. Cell* 5, 1175–1183. doi: 10.1128/EC.00097-06

Degnan, P. H., Taga, M. E., and Goodman, A. L. (2014). Vitamin B_{12} as a modulator of gut microbial ecology. *Cell Metab.* 20, 769–778. doi: 10.1016/j.cmet.2014.10.002

Doxey, A. C., Kurtz, D. A., Lynch, M. D. J., Sauder, L. A., and Neufeld, J. D. (2015). Aquatic metagenomes implicate Thaumarchaeota in global cobalamin production. *ISME J.* 9, 461–471. doi: 10.1038/ismej.2014.142

Drennan, R., Wiklund, H., Rabone, M., Georgieva, M. N., Dahlgren, T. G., and Glover, A. G. (2021). *Neanthes goodayi* sp. nov. (Annelida, Nereididae), a remarkable new annelid species living inside deep-sea polymetallic nodules. *Eur. J. Taxon.* 760, 160–185. doi: 10.5852/ejt.2021.760.1447

Francis, C. A., Roberts, K. J., Beman, J. M., Santoro, A. E., and Oakley, B. B. (2005). Ubiquity and diversity of ammonia-oxidizing archaea in water columns and sediments of the ocean. *Proc. Natl. Acad. Sci.* 102, 14683–14688. doi: 10.1073/pnas.0506625102

Gerringa, L. J. A., Rijkenberg, M. J. A., Slagter, H. A., Laan, P., Paffrath, R., Bauch, D., et al. (2021). Dissolved Cd, Co, Cu, Fe, Mn, Ni, and Zn in the Arctic Ocean. *J. Geophys. Res. Oceans* 126:e2021JC017323. doi: 10.1029/2021JC017323

Giedyk, M., Goliszewska, K., and Gryko, D. (2015). Vitamin B_{12} catalysed reactions. *Chem. Soc. Rev.* 44, 3391–3404. doi: 10.1039/C5CS00165J

Giovannelli, D. (2023). Trace metal availability and the evolution of biogeochemistry. *Nat. Rev. Earth Environ.* 4, 597–598. doi: 10.1038/s43017-023-00477-y

Gómez-Consarnau, L., Sachdeva, R., Gifford, S. M., Cutter, L. S., Fuhrman, J. A., Sañudo-Wilhelmy, S. A., et al. (2018). Mosaic patterns of B-vitamin synthesis and utilization in a natural marine microbial community. *Environ. Microbiol.* 20, 2809–2823. doi: 10.1111/1462-2920.14133

Grant, M. A. A., Kazamia, E., Cicuta, P., and Smith, A. G. (2014). Direct exchange of vitamin B_{12} is demonstrated by modelling the growth dynamics of algal–bacterial co-cultures. *ISME J.* 8, 1418–1427. doi: 10.1038/ismej.2014.9

Halbach, P. E., Jahn, A., and Cherkashov, G. (2017). "Marine co-rich ferromanganese crust deposits: description and formation, occurrences and distribution, estimated world-wide resources" in Deep-Sea mining: Resource potential, technical and environmental considerations. ed. R. Sharma (Cham: Springer International Publishing), 65–141.

Hauquier, F., Macheriotou, L., Bezerra, T. N., Egho, G., Martínez Arbizu, P., and Vanreusel, A. (2019). Distribution of free-living marine nematodes in the clarion–Clipperton zone: implications for future deep-sea mining scenarios. *Biogeosciences* 16, 3475–3489. doi: 10.5194/bg-16-3475-2019

Hawco, N. J., Lam, P. J., Lee, J.-M., Ohnemus, D. C., Noble, A. E., Wyatt, N. J., et al. (2018). Cobalt scavenging in the mesopelagic ocean and its influence on global mass balance: synthesizing water column and sedimentary fluxes. *Mar. Chem.* 201, 151–166. doi: 10.1016/j.marchem.2017.09.001

Hawco, N. J., Mcilvin, M. M., Bundy, R. M., Tagliabue, A., Goepfert, T. J., Moran, D. M., et al. (2020). Minimal cobalt metabolism in the marine cyanobacterium *Prochlorococcus*. *Proc. Natl. Acad. Sci.* 117, 15740–15747. doi: 10.1073/pnas.2001393117

Hazen, R. M., and Morrison, S. M. (2022). On the paragenetic modes of minerals: a mineral evolution perspective. *Am. Mineral.* 107, 1262–1287. doi: 10.2138/am-2022-8099

Heal, K. R., Qin, W., Ribalet, F., Bertagnolli, A. D., Coyote-Maestas, W., Hmelo, L. R., et al. (2017). Two distinct pools of B_{12} analogs reveal community interdependencies in the ocean. *Proc. Natl. Acad. Sci.* 114, 364–369. doi: 10.1073/pnas.1608462114

Hein, J. R., Koschinsky, A., and Kuhn, T. (2020). Deep-ocean polymetallic nodules as a resource for critical materials. *Nat. Rev. Earth Environ.* 1, 158–169. doi: 10.1038/s43017-020-0027-0

Hollibaugh, J. T. (2017). Oxygen and the activity and distribution of marine Thaumarchaeota. *Environ. Microbiol. Rep.* 9, 186–188. doi: 10.1111/1758-2229.12534

Hollingsworth, A. L., Jones, D. O. B., and Young, C. R. (2021). Spatial vriability of abyssal nitrifying microbes in the north-eastern clarion-clipperton zone. *Front. Mar. Sci.* 8:663420. doi: 10.3389/fmars.2021.663420

Huo, Y., Cheng, H., Post, A. F., Wang, C., Jiang, X., Pan, J., et al. (2015). Ecological functions of uncultured microorganisms in the cobalt-rich ferromanganese crust of a seamount in the Central Pacific are elucidated by fosmid sequencing. *Acta Oceanol. Sin.* 34, 92–113. doi: 10.1007/s13131-015-0650-7

Joglar, V., Pontiller, B., Martínez-García, S., Fuentes-Lema, A., Pérez-Lorenzo, M., Lundin, D., et al. (2021). Microbial plankton community structure and function responses to vitamin B_{12} and B_{12} amendments in an uwelling system. *Appl. Environ. Microbiol.* 87:e01525-21. doi: 10.1128/AEM.01525-21

Koschinsky, A., and Hein, J. R. (2003). Uptake of elements from seawater by ferromanganese crusts: solid-phase associations and seawater speciation. *Mar. Geol.* 198, 331–351. doi: 10.1016/S0025-3227(03)00122-1

Liao, L., Xu, X.-W., Jiang, X.-W., Wang, C.-S., Zhang, D.-S., Ni, J.-Y., et al. (2011). Microbial diversity in deep-sea sediment from the cobalt-rich crust deposit region in the Pacific Ocean. *FEMS Microbiol. Ecol.* 78, 565–585. doi: 10.1111/j.1574-6941.2011.01186.x

Liu, Y., Liu, S., Piedrahita, V. A., Liu, P., He, S., Pan, H., et al. (2024). Insights into a correlation between magnetotactic bacteria and polymetallic nodule distribution in the Eastern Central Pacific Ocean. *J. Geophys. Res.* 129:e2024JB029062. doi: 10.1029/2024JB029062

Lo, W.-S., and Sommer, R. J. (2022). Vitamin B12 and predatory behavior in nematodes. *Vitam. Horm.* 119, 471–89. doi: 10.1016/bs.vh.2022.01.006

Merbt, S. N., Stahl, D. A., Casamayor, E. O., Martí, E., Nicol, G. W., and Prosser, J. I. (2012). Differential photoinhibition of bacterial and archaeal ammonia oxidation. *FEMS Microbiol. Lett.* 327, 41–46. doi: 10.1111/j.1574-6968.2011.02457.x

Miljutin, D. M., Miljutina, M. A., Arbizu, P. M., and Galéron, J. (2011). Deep-sea nematode assemblage has not recovered 26 years after experimental mining of polymetallic nodules (clarion-Clipperton fracture zone, tropical eastern Pacific). *Deep-Sea Res. I Oceanogr. Res. Pap.* 58, 885–897. doi: 10.1016/j.dsr.2011.06.003

Moffett, J. W., and Ho, J. (1996). Oxidation of cobalt and manganese in seawater via a common microbially catalyzed pathway. *Geochim. Cosmochim. Acta* 60, 3415–3424. doi: 10.1016/0016-7037(96)00176-7

Moore, C. M., Mills, M. M., Arrigo, K. R., Berman-Frank, I., Bopp, L., Boyd, P. W., et al. (2013). Processes and patterns of oceanic nutrient limitation. *Nat. Geosci.* 6, 701–710. doi: 10.1038/ngeo1765

Moran, M. A., Kujawinski, E. B., Schroer, W. F., Amin, S. A., Bates, N. R., Bertrand, E. M., et al. (2022). Microbial metabolites in the marine carbon cycle. *Nat. Microbiol.* 7, 508–523. doi: 10.1038/s41564-022-01090-3

Mukhopadhyay, R., Ghosh, A. K., and Iyer, S. D. (2008). "Ferromanganese deposits" in Handbook of exploration and environmental geochemistry. eds. R. Mukhopadhyay, A. K. Ghosh and S. D. Iyer (Netherlands: Elsevier Science BV), 155–224.

Murray, K. J., Webb, S. M., Bargar, J. R., and Tebo, B. M. (2007). Indirect oxidation of co(II) in the presence of the marine Mn(II)-oxidizing bacterium *Bacillus* sp. strain SG-1. *Appl. Environ. Microbiol.* 73, 6905–6909. doi: 10.1128/AEM.00971-07

Neal, L., Wiklund, H., Rabone, M., Dahlgren, T. G., and Glover, A. G. (2022). Abyssal fauna of polymetallic nodule exploration areas, eastern clarion-Clipperton zone, Central Pacific Ocean: Annelida: Spionidae and Poecilochaetidae. *Mar. Biodivers.* 52:51. doi: 10.1007/s12526-022-01277-1

Nijland, M., Martínez Felices, J. M., Slotboom, D. J., and Thangaratnarajah, C. (2022). Membrane transport of cobalamin. *Vitam. Horm.* 119, 121–148. doi: 10.1016/bs.vh.2022.01.008

Okamoto, S., and Eltis, L. D. (2011). The biological occurrence and trafficking of cobalt. *Metallomics* 3, 963–970. doi: 10.1039/c1mt00056j

Osman, D., Cooke, A., Young, T. R., Deery, E., Robinson, N. J., and Warren, M. J. (2021). The requirement for cobalt in vitamin B_{12}: a paradigm for protein metalation. *Biochim. Biophys. Acta* 1868:118896. doi: 10.1016/j.bbamcr.2020.118896

Panzeca, C., Beck, A. J., Leblanc, K., Taylor, G. T., Hutchins, D. A., and Sañudo-Wilhelmy, S. A. (2008). Potential cobalt limitation of vitamin B_{12} synthesis in the North Atlantic Ocean. *Glob. Biogeochem. Cycles* 22:GB2029. doi: 10.1029/2007GB003124

Panzeca, C., Beck, A. J., Tovar-Sanchez, A., Segovia-Zavala, J., Taylor, G. T., Gobler, C. J., et al. (2009). Distributions of dissolved vitamin B_{12} and Co in coastal and open-ocean environments. *Estuar. Coast. Shelf Sci.* 85, 223–230. doi: 10.1016/j.ecss.2009.08.016

Qin, W., Zheng, Y., Zhao, F., Wang, Y., Urakawa, H., Martens-Habbena, W., et al. (2020). Alternative strategies of nutrient acquisition and energy conservation map to the biogeography of marine ammonia-oxidizing archaea. *ISME J.* 14, 2595–2609. doi: 10.1038/s41396-020-0710-7

Rabone, M., Wiethase, J. H., Simon-Lledó, E., Emery, A. M., Jones, D. O. B., Dahlgren, T. G., et al. (2023). How many metazoan species live in the world's largest mineral exploration region? *Curr. Biol.* 33, 2383–2396.e5. doi: 10.1016/j.cub.2023.04.052

Romine, M. F., Rodionov, D. A., Maezato, Y., Osterman, A. L., and Nelson, W. C. (2017). Underlying mechanisms for syntrophic metabolism of essential enzyme cofactors in microbial communities. *ISME J.* 11, 1434–1446. doi: 10.1038/ismej.2017.2

Saito, M. A., and Moffett, J. W. (2002). Temporal and spatial variability of cobalt in the Atlantic Ocean. *Geochim. Cosmochim. Acta* 66, 1943–1953. doi: 10.1016/S0016-7037(02)00829-3

Sañudo-Wilhelmy, S. A., Cutter, L. S., Durazo, R., Smail, E. A., Gómez-Consarnau, L., Webb, E. A., et al. (2012). Multiple B-vitamin depletion in large areas of the coastal ocean. *Proc. Natl. Acad. Sci.* 109, 14041–14045. doi: 10.1073/pnas.1208755109

Sañudo-Wilhelmy, S. A., Gobler, C. J., Okbamichael, M., and Taylor, G. T. (2006). Regulation of phytoplankton dynamics by vitamin B_{12}. *Geophys. Res. Lett.* 33:L04604. doi: 10.1029/2005GL025046

Sañudo-Wilhelmy, S. A., Gómez-Consarnau, L., Suffridge, C., and Webb, E. A. (2014). The role of B vitamins in marine biogeochemistry. *Annu. Rev. Mar. Sci.* 6, 339–367. doi: 10.1146/annurev-marine-120710-100912

Scott, A. I., and Roessner, C. A. (2002). Biosynthesis of cobalamin (vitamin B_{12}). *Biochem. Soc. Trans.* 30, 613–620. doi: 10.1042/bst0300613

Shelton, A. N., Seth, E. C., Mok, K. C., Han, A. W., Jackson, S. N., Haft, D. R., et al. (2019). Uneven distribution of cobamide biosynthesis and dependence in bacteria predicted by comparative genomics. *ISME J.* 13, 789–804. doi: 10.1038/s41396-018-0304-9

Shiraishi, F., Mitsunobu, S., Suzuki, K., Hoshino, T., Morono, Y., and Inagaki, F. (2016). Dense microbial community on a ferromanganese nodule from the ultra-oligotrophic South Pacific gyre: implications for biogeochemical cycles. *Earth Planet. Sci. Lett.* 447, 10–20. doi: 10.1016/j.epsl.2016.04.021

Shulga, N., Abramov, S., Klyukina, A., Ryazantsev, K., and Gavrilov, S. (2022). Fast-growing Arctic Fe–Mn deposits from the Kara Sea as the refuges for cosmopolitan marine microorganisms. *Sci. Rep.* 12:21967. doi: 10.1038/s41598-022-23449-6

Shulse, C. N., Maillot, B., Smith, C. R., and Church, M. J. (2017). Polymetallic nodules, sediments, and deep waters in the equatorial North Pacific exhibit highly diverse and distinct bacterial, archaeal, and microeukaryotic communities. *Microbiol. Open* 6:e00428. doi: 10.1002/mbo3.428

Siegl, A., Kamke, J., Hochmuth, T., Piel, J., Richter, M., Liang, C., et al. (2011). Single-cell genomics reveals the lifestyle of Poribacteria, a candidate phylum symbiotically associated with marine sponges. *ISME J.* 5, 61–70. doi: 10.1038/ismej.2010.95

Sokolovskaya, O. M., Shelton, A. N., and Taga, M. E. (2020). Sharing vitamins: cobamides unveil microbial interactions. *Science* 369:eaba0165. doi: 10.1126/science.aba0165

Soto, M. A., Desai, D., Bannon, C., Laroche, J., and Bertrand, E. M. (2023). Cobalamin producers and prokaryotic consumers in the Northwest Atlantic. *Environ. Microbiol.* 25, 1300–1313. doi: 10.1111/1462-2920.16363

Stieglmeier, M., Klingl, A., Alves, R. J. E., Rittmann, S. K.-M. R., Melcher, M., Leisch, N., et al. (2014). *Nitrososphaera viennensis* gen. nov., sp. nov., an aerobic and mesophilic, ammonia-oxidizing archaeon from soil and a member of the archaeal phylum Thaumarchaeota. *Int. J. Syst. Evol. Microbiol.* 64, 2738–2752. doi: 10.1099/ijs.0.063172-0

Stratmann, T. (2023). Role of polymetallic-nodule dependent fauna on carbon cycling in the eastern clarion-Clipperton fracture zone (Pacific). *Front. Marine Sci.* 10:1151442. doi: 10.3389/fmars.2023.1151442

Stratmann, T., Soetaert, K., Kersken, D., and Van Oevelen, D. (2021). Polymetallic nodules are essential for food-web integrity of a prospective deep-seabed mining area in Pacific abyssal plains. *Sci. Rep.* 11:12238. doi: 10.1038/s41598-021-91703-4

Suffridge, C. P., Gómez-Consarnau, L., Monteverde, D. R., Cutter, L., Arístegui, J., Alvarez-Salgado, X. A., et al. (2018). B vitamins and their congeners as potential drivers of microbial community composition in an oligotrophic marine ecosystem. *J. Geophys. Res. Biogeo.* 123, 2890–2907. doi: 10.1029/2018JG004554

Sujith, P. P., and Gonsalves, M. J. B. D. (2021). Ferromanganese oxide deposits: geochemical and microbiological perspectives of interactions of cobalt and nickel. *Ore Geol. Rev.* 139:104458. doi: 10.1016/j.oregeorev.2021.104458

Sultana, S., Bruns, S., Wilkes, H., Simon, M., and Wienhausen, G. (2023). Vitamin B_{12} is not shared by all marine prototrophic bacteria with their environment. *ISME J.* 17, 836–845. doi: 10.1038/s41396-023-01391-3

Swanner, E. D., Planavsky, N. J., Lalonde, S. V., Robbins, L. J., Bekker, A., Rouxel, O. J., et al. (2014). Cobalt and marine redox evolution. *Earth Planet. Sci. Lett.* 390, 253–263. doi: 10.1016/j.epsl.2014.01.001

Taboada, S., Riesgo, A., Wiklund, H., Paterson, G. L. J., Koutsouveli, V., Santodomingo, N., et al. (2018). Implications of population connectivity studies for the design of marine protected areas in the deep sea: an example of a demosponge from the clarion-Clipperton zone. *Mol. Ecol.* 27, 4657–4679. doi: 10.1111/mec.14888

Tagliabue, A., Hawco, N. J., Bundy, R. M., Landing, W. M., Milne, A., Morton, P. L., et al. (2018). The role of external inputs and internal cycling in shaping the global ocean cobalt distribution: insights from the first cobalt biogeochemical model. *Glob. Biogeochem. Cycles* 32, 594–616. doi: 10.1002/2017GB005830

Uhlenkott, K., Meyn, K., Vink, A., and Martínez Arbizu, P. (2023). A review of megafauna diversity and abundance in an exploration area for polymetallic nodules in the eastern part of the clarion Clipperton fracture zone (North East Pacific), and implications for potential future deep-sea mining in this area. *Mar. Biodivers.* 53:22. doi: 10.1007/s12526-022-01326-9

Vaid, F. H. M., Zahid, S., Faiyaz, A., Qadeer, K., Gul, W., Anwar, Z., et al. (2018). Photolysis of methylcobalamin in aqueous solution: a kinetic study. *J. Photochem. Photobiol. A Chem.* 362, 40–48. doi: 10.1016/j.jphotochem.2018.05.011

Valiela, I. (2015). "Controls of primary production" in Marine ecological processes. ed. I. Valiela (New York, NY: Springer New York), 61–112.

Verlaan, P. A., and Cronan, D. S. (2022). Origin and variability of resource-grade marine ferromanganese nodules and crusts in the Pacific Ocean: a review of biogeochemical and physical controls. *Geochemistry* 82:125741. doi: 10.1016/j.chemer.2021.125741

Wang, X., and Müller, W. E. (2009). Marine biominerals: Perspectives and challenges for polymetallic nodules and crusts. *Trends Biotechnol.* 27, 375–383. doi: 10.1016/j.tibtech.2009.03.004

Wang, X.-H., Schloßmacher, U., Natalio, F., Schröder, H. C., Wolf, S. E., Tremel, W., et al. (2009). Evidence for biogenic processes during formation of ferromanganese crusts from the Pacific Ocean: implications of biologically induced mineralization. *Micron* 40, 526–535. doi: 10.1016/j.micron.2009.04.005

Wang, L., Zhao, H., Bi, R., Chen, X., Lyu, Z., and Liu, W. (2024). Roles and sources of B vitamins in the marine ecosystem. *Rev. Fish Biol. Fish.* 34, 111–130. doi: 10.1007/s11160-023-09818-y

Wang, J., Zhu, Y.-G., Tiedje, J. M., and Ge, Y. (2024). Global biogeography and ecological implications of cobamide-producing prokaryotes. *ISME J.* 18:wrae009. doi: 10.1093/ismejo/wrae009

Warren, M. J., Raux, E., Schubert, H. L., and Escalante-Semerena, J. C. (2002). The biosynthesis of adenosylcobalamin (vitamin B_{12}). *Nat. Prod. Rep.* 19, 390–412. doi: 10.1039/b108967f

Wegorzewski, A. V., Grangeon, S., Webb, S. M., Heller, C., and Kuhn, T. (2020). Mineralogical transformations in polymetallic nodules and the change of Ni, Cu and Co crystal-chemistry upon burial in sediments. *Geochim. Cosmochim. Acta* 282, 19–37. doi: 10.1016/j.gca.2020.04.012

Wienhausen, G., Dlugosch, L., Jarling, R., Wilkes, H., Giebel, H.-A., and Simon, M. (2022). Availability of vitamin B_{12} and its lower ligand intermediate α-ribazole impact prokaryotic and protist communities in oceanic systems. *ISME J.* 16, 2002–2014. doi: 10.1038/s41396-022-01250-7

Wienhausen, G., Moraru, C., Bruns, S., Tran, D. Q., Sultana, S., Wilkes, H., et al. (2024). Ligand cross-feeding resolves bacterial vitamin B_{12} auxotrophies. *Nature* 629, 886–892. doi: 10.1038/s41586-024-07396-y

Wu, Z., Peacock, C. L., Lanson, B., Yin, H., Zheng, L., Chen, Z., et al. (2019). Transformation of co-containing birnessite to todorokite: effect of co on the transformation and implications for co mobility. *Geochim. Cosmochim. Acta* 246, 21–40. doi: 10.1016/j.gca.2018.11.001

Zhang, D., Li, X., Wu, Y., Xu, X., Liu, Y., Shi, B., et al. (2023). Microbe-driven elemental cycling enables microbial adaptation to deep-sea ferromanganese nodule sediment fields. *Microbiome* 11:160. doi: 10.1186/s40168-023-01601-2

Zhang, D.-C., Liu, Y.-X., and Li, X.-Z. (2015). Characterization of bacterial diversity associated with deep sea ferromanganese nodules from the South China Sea. *J. Microbiol.* 53, 598–605. doi: 10.1007/s12275-015-5217-y

Zhou, J., Qin, W., Lu, X., Yang, Y., Stahl, D., Jiao, N., et al. (2023). The diversity and ecological significance of microbial traits potentially involved in B_{12} biosynthesis in the global ocean. *mLife* 2, 416–427. doi: 10.1002/mlf2.12095

Frontiers in Microbiology

Explores the habitable world and the potential of microbial life

The largest and most cited microbiology journal which advances our understanding of the role microbes play in addressing global challenges such as healthcare, food security, and climate change.

Discover the latest Research Topics

See more →

Frontiers

Avenue du Tribunal-Fédéral 34
1005 Lausanne, Switzerland
frontiersin.org

Contact us

+41 (0)21 510 17 00
frontiersin.org/about/contact